



ATLAS Note

ATL-COM-PHYS-2018-794

9th July 2019



Draft version 0.21

Search for flavour-changing neutral currents in single-top quark production processes in association with a photon at $\sqrt{s} = 13 \text{ TeV}$ with the ATLAS experiment

Johannes Erdmann^a, Gregor Geßner^a, Kevin Kröninger^a

^a*Technische Universität Dortmund, Germany*

In this note, the search for flavour-changing neutral currents is presented in processes where a single-top quark is produced in association with a photon. The analysis uses pp collisions at $\sqrt{s} = 13 \text{ TeV}$ collected by the ATLAS detector during 2015, 2016 and 2017, corresponding to an integrated luminosity of 81 fb^{-1} . The top quark is assumed to decay into a b quark and a W boson that itself decays leptonically. Selected events contain an isolated high- p_T photon, an isolated charged lepton, a b -tagged jet and missing transverse momentum. Data-driven techniques are used to estimate the background contributions stemming from events with a photon from the hard scattering or with a photon faked by an electron or a jet. A neural network is used to classify events into signal-like and background-like candidates. Since there is no sensitivity for an observation with the current dataset, upper limits on the branching ratio $\mathcal{B}(t \rightarrow q\gamma)$ are set with $q = u, c$ for left- and right-handed coupling in the context of an effective field theory. The observed (expected) 95 % C.L. limits on the branching ratio are $\mathcal{B}(t \rightarrow u\gamma, \text{left-handed}) < 2.8 \times 10^{-5}$ (4.0×10^{-5}), $\mathcal{B}(t \rightarrow u\gamma, \text{right-handed}) < 6.1 \times 10^{-5}$ (5.9×10^{-5}), $\mathcal{B}(t \rightarrow c\gamma, \text{left-handed}) < 21.8 \times 10^{-5}$ (26.6×10^{-5}), and $\mathcal{B}(t \rightarrow c\gamma, \text{right-handed}) < 18.3 \times 10^{-5}$ (28.4×10^{-5}). These limits translate into limits on the cross section $\sigma(pp \rightarrow t\gamma)$ and into limits on the Wilson coefficients $|C_{uW}^{ij} + C_{uB}^{ij}|$.

23 **Contents**

24	1 Changes w.r.t previous version	6
25	2 Introduction	13
26	3 Analysis strategy	16
27	4 Data and Monte Carlo samples	18
28	4.1 Data	18
29	4.2 Monte Carlo samples	18
30	4.2.1 Removal of duplicate events in $X+\gamma+jets$ samples	20
31	5 Object definition	21
32	5.1 Photons	21
33	5.2 Electrons	21
34	5.3 Muons	21
35	5.4 Jets	22
36	5.5 Missing transverse momentum	22
37	5.6 Object overlap removal	22
38	6 Event selection	23
39	6.1 Preselection of events	23
40	6.2 Signal region	23
41	6.2.1 Signal efficiencies	24
42	6.2.2 Kinematic differences of assumed signal couplings and modes	26
43	6.2.3 Scaling of the production and decay mode signals	29
44	6.2.4 Background events	32
45	6.3 Control and validation regions	36
46	6.3.1 Control region for the process $W+\gamma+jets$	36
47	6.3.2 Control region for the process $Z+\gamma$	37
48	6.3.3 Other regions	38
49	6.4 Photon p_T reweighting	40
50	7 Background estimation	45
51	7.1 Electron-to-photon fakes	45
52	7.1.1 Control regions	45
53	7.1.2 Fit of invariant mass distributions	46
54	7.1.3 Fake rate and scale factor	47
55	7.1.4 Validation of $SF(e \rightarrow \gamma)$	50
56	7.2 Hadron-to-photon fakes	51
57	7.2.1 Control regions	51
58	7.2.2 ABCD method	52
59	7.2.3 Distributions in control regions	55
60	7.2.4 Validation of $SF(j \rightarrow \gamma)$	61
61	8 Separation of signal from background events	62
62	8.1 Input variables	62

Not reviewed, for internal circulation only

63	8.2	Architecture of neural network	68
64	8.3	Training and validation	68
65	8.4	Optimal number of input variables and hidden layers	69
66	8.5	Output of neural network	74
67	8.6	Comparison of signal in production and decay mode	77
68	8.7	Comparison of different training setups	77
69	9	Estimation of systematic uncertainties	86
70	9.1	Symmetrisation, smoothing and pruning	86
71	9.2	Theory uncertainties	86
72	9.2.1	Signal modelling	87
73	9.2.2	Background modelling	87
74	9.3	Experimental uncertainties	88
75	10	Statistical analysis	90
76	10.1	Fit strategy	90
77	10.2	Nuisance parameters	91
78	10.3	Fit result with Asimov data	93
79	10.4	Signal injection test using Asimov data	99
80	10.5	Ranking plots using Asimov data	99
81	10.6	Fit result with data in control regions	100
82	10.7	Fit result with data	106
83	10.8	Ranking plots using data in all regions	114
84	10.9	Validation of fit result	115
85	10.9.1	Input variables of the neural network in the signal region	115
86	10.9.2	Validation regions	119
87	11	Interpretation of results	123
88	11.1	Limits on signal strength	123
89	11.2	Limits on cross section	123
90	11.3	Limits on Wilson coefficients	123
91	11.4	Limits on branching ratio	124
92	11.5	Limits for Asimov data	124
93	12	Conclusion	126
94	Appendices		133
95	A	List of MC samples	133
96	B	Studies for left- and right-handedness in decay mode	137
97	C	Estimation of non-available samples for the SM process single top + photon	138
98	D	Studies for parameter $\Delta R(\gamma^{\text{reco}}, e^{\text{truth}})$ for event overlap removal	140
99	E	Studies for different b-tagging working points	142

Not reviewed, for internal circulation only

100	F Cutflow for the SR separated by lepton flavour	143
101	G Distribution of kinematic variables in the SR separated by lepton flavour	144
102	H Check for fit of MC with signal+background function for SF($e \rightarrow \gamma$)	146
103	I Fit functions and parameters for $e \rightarrow \gamma$ fake estimation	147
104	J Plots for $e \rightarrow \gamma$ fake estimation in linear scale	150
105	K Photon p_T independence of scale factor SF($e \rightarrow \gamma$)	153
106	L Input variables for neural network for different signal samples	154
107	M Correlation of NN input variables in CR $W+\gamma+jets$	160
108	N Studies for neural network output	165
109	N.1 Neural network output separated by lepton flavour	165
110	N.2 Neural network output before and after the photon reweighting	166
111	O Plots for systematic uncertainties	169
112	O.1 Plots for the left-handed $t\gamma$ coupling	170
113	O.1.1 SR (left-handed $t\gamma$ coupling)	170
114	O.1.2 CR $W+\gamma+jets$ (left-handed $t\gamma$ coupling)	184
115	O.1.3 CR $Z+\gamma$ (left-handed $t\gamma$ coupling)	198
116	O.2 Plots for the right-handed $t\gamma$ coupling	209
117	O.2.1 SR (right-handed $t\gamma$ coupling)	209
118	O.2.2 CR $W+\gamma+jets$ (right-handed $t\gamma$ coupling)	223
119	O.2.3 CR $Z+\gamma$ (right-handed $t\gamma$ coupling)	237
120	O.3 Plots for the left-handed $t\gamma$ coupling	251
121	O.3.1 SR (left-handed $t\gamma$ coupling)	251
122	O.3.2 CR $W+\gamma+jets$ (left-handed $t\gamma$ coupling)	265
123	O.3.3 CR $Z+\gamma$ (left-handed $t\gamma$ coupling)	279
124	O.4 Plots for the right-handed $t\gamma$ coupling	290
125	O.4.1 SR (right-handed $t\gamma$ coupling)	290
126	O.4.2 CR $W+\gamma+jets$ (right-handed $t\gamma$ coupling)	300
127	O.4.3 CR $Z+\gamma$ (right-handed $t\gamma$ coupling)	310
128	P Studies for an increased uncertainty of the cross section for the $t\bar{t} + \gamma$ process	320
129	Q Studies of a fit with a changed setup for the scale uncertainties	325
130	R Studies for the default uncertainty on the SF($e \rightarrow \gamma$)	334
131	S Studies with photon p_T as discriminating variable	339
132	T Pruning of the nuisance parameters for the different signal couplings	340
133	U Composition of physics processes of the photon fake categories	343

134	V Statistical fit for different signal samples using Asimov data	344
135	V.1 Statistical fit using Asimov data for the right-handed $t\gamma\gamma$ coupling	344
136	V.2 Statistical fit using Asimov data for the left-handed $t\gamma\gamma$ coupling	350
137	V.3 Statistical fit using Asimov data for the right-handed $t\gamma\gamma$ coupling	356
138	W Statistical fit for different signal samples using data in control regions	362
139	W.1 Statistical fit using data in the control regions for the right-handed $t\gamma\gamma$ coupling	362
140	W.2 Statistical fit using data in the control regions for the left-handed $t\gamma\gamma$ coupling	367
141	W.3 Statistical fit using data in the control regions for the right-handed $t\gamma\gamma$ coupling	372
142	X Tables with systematic uncertainties	377
143	Y Studies of a fit when separating the MC uncertainties	402
144	Z Statistical fit for different signal samples using data in all regions	407
145	Z.1 Statistical fit using data in all regions for the right-handed $t\gamma\gamma$ coupling	407
146	Z.1.1 Validation of fit result	414
147	Z.2 Statistical fit using data in all regions for the left-handed $t\gamma\gamma$ coupling	421
148	Z.2.1 Validation of fit result	428
149	Z.3 Statistical fit using data in all regions for the right-handed $t\gamma\gamma$ coupling	435
150	Z.3.1 Validation of fit result	442

151 1 Changes w.r.t previous version

152 Version 0.21

- 153 • removing uncertainty for LF normalisation
 154 – limits changed by maximally 1.3 %

155 Version 0.20

- 156 • including uncertainty for HF and LF normalisation, description added in Section 9.3
 157 – limits changed by maximally 2 %

158 Version 0.19

- 159 • redefine value proportional to fake rate: $F_{e \rightarrow \gamma} = N(e\gamma)/2N(ee)$, as both electrons from the Z boson
 160 may fake a photon. Scale factor stays the same as the factor 2 cancels out, $SF(e \rightarrow \gamma) = \frac{F_{e \rightarrow \gamma}^{\text{data}}}{F_{e \rightarrow \gamma}^{\text{MC}}}$

161 Version 0.18

- 162 • adding Appendix N.1 for the NN output distribution separated by lepton flavour
 163 • adding Appendix N.2 to illustrated the impact of the photon p_T reweighting on the NN output

164 Version 0.17

- 165 • increasing uncertainty on $SF(e \rightarrow \gamma)$ to $\sim 10\%$
 166 – change of expected and observed limits in the order of $O(1\%)$
 167 • including follow-up comments on version 0.16 by Lisa and Wolfgang (top approval)

168 Version 0.16

- 169 • reduction of total uncertainty in VR $SF(e \rightarrow \gamma)$ caused by missing files for some systematic
 170 uncertainties
 171 • including follow-up comments on version 0.15 by Lisa and Wolfgang (top approval)

172 Version 0.15

- 173 • removing scale uncertainties for $t\bar{t}$ process, as it is already taken into account by ISR uncertainty.
- 174 Minor changes of limits:
 - 175 – expected limit on cross section for right-handed $t\gamma$ coupling: $75 \rightarrow 74$
 - 176 – observed and expected limit on signal strength for left-handed $t\gamma$ coupling $[10^{-2}]$:
 177 $21.8 (26.4^{+10.9}_{-7.4}) \rightarrow 21.9 (26.2^{+10.8}_{-7.3})$
 - 178 – observed and expected limit on Wilson coefficients for left-handed $t\gamma$ coupling:
 179 $0.519 (0.571^{+0.108}_{-0.086}) \rightarrow 0.521 (0.569^{+0.107}_{-0.086})$
 - 180 – observed and expected limit on branching ratio for left-handed $t\gamma$ coupling $[10^{-5}]$:
 181 $21.8 (26.4^{+10.9}_{-7.4}) \rightarrow 21.9 (26.2^{+10.8}_{-7.3})$
 - 182 – expected limit on signal strength for right-handed $t\gamma$ coupling $[10^{-2}]$:
 183 $(28.1^{+12.2}_{-7.8}) \rightarrow (27.9^{+12.1}_{-7.8})$
 - 184 – observed and expected limit on Wilson coefficients for right-handed $t\gamma$ coupling:
 185 $0.476 (0.589^{+0.116}_{-0.089}) \rightarrow 0.477 (0.587^{+0.116}_{-0.089})$
 - 186 – expected limit on branching ratio for right-handed $t\gamma$ coupling $[10^{-5}]$:
 187 $(28.1^{+12.2}_{-7.8}) \rightarrow (27.9^{+12.1}_{-7.8})$
- 188 • including answers by Lisa and Wolfgang on v0.14 (follow-up on top approval)
- 189 • including comments by Marc on v0.14

190 Version 0.14

- 191 • subleading digits of some limits changed caused by previous issues with eos when filling histograms
 192 (improved protection against it implemented)
 - 193 – observed limit on branching ratio for left-handed $t\gamma$ coupling: $21.9 \times 10^{-5} \rightarrow 21.8 \times 10^{-5}$
 - 194 – $+1\sigma$ on expected limit on branching ratio for left-handed $t\gamma$ coupling: $26.4^{+10.8}_{-7.4} \rightarrow 26.4^{+10.9}_{-7.4}$
 - 195 – observed limit on Wilson coefficients for left-handed $t\gamma$ coupling: $0.520 \rightarrow 0.519$
 - 196 – expected limit on branching ratio for right-handed $t\gamma$ coupling: $28.0 \times 10^{-5} \rightarrow 28.1 \times 10^{-5}$
 - 197 – observed limit on Wilson coefficients for right-handed $t\gamma$ coupling: $0.477 \rightarrow 0.476$
- 198 • adding $\pm 1\sigma$ ranges for expected limits in Section 11
- 199 • adding information about the scale of new physics $\Lambda = 1$ TeV for interpretation of Wilson coefficients
- 200 • adding tables for pre- and post-fit yields in Section 10
- 201 • providing post-fit validation plots in Section 10.9
- 202 • renamed region CR $Z \rightarrow \ell\ell\gamma$ to CR $Z+\gamma$, as the photon is not explicitly required to originate from
 203 the Z boson decay

- 204 • answering Wolfgang's comments on v0.13
- 205 • answering Catrin's comments on v0.13
- 206 • answering Yichen's comments on v0.13
- 207 • answering Romain's comments on v0.13
- 208 • answering Andrea's comments on v0.13
- 209 • answering comments by Lisa and Wolfgang on v0.13 (top approval comments)

210 **Version 0.13**

- 211 • Fixing some typos: GRL for 2017, Table 6, Table 19

212 **Version 0.12**

- 213 • Change how to estimate PDF uncertainties: from NNPDF error sets to correlated PDF4LHC15
214 error sets.
- 215 • Full unblinding of signal region
 - 216 – updating plots and tables
 - 217 – setting observed limits

218 **Version 0.11**

- 219 • bug fix for uncertainty on photon p_T reweighting: normalisation now preserved

220 **Version 0.10**

- 221 • using the photon p_T reweighting as default
- 222 • revisiting definition of ISR and FSR uncertainty
- 223 • removing PDF($W/Z+\gamma+jets$) uncertainty from fit
- 224 • illustration in pruning plot: JES flavour composition/response uncertainties separately shown for
225 each region (previously, decorrelated, but with same name -> one line in pruning plot)

226 Version 0.9

- 227 • switching to n-tuples produced with AnalysisTop, 21.2.55 (all numbers updated)
- 228 • updating k-factor for ttgamma sample 410389 from 1.16 to 1.24
- 229 • switching b -tagging WP to 60 %, before 77 %
- 230 • revisiting scaling of signal processes
- 231 • introducing photon p_T reweighting for $W/Z+\gamma+jets$ contributions, described in Section 6.4
- 232 • using data in CRs for statistical fit, Section 10.7
- 233 • adding studies for another estimation of the SM single top + photon contribution in Appendix C
- 234 • including back-propagation of prompt photon scale factor to VRs in Appendix ??
- 235 • answering comments by Marc on version 0.8.
- 236 • answering comments by Yichen on version 0.8.
- 237 • answering comments by Lidia and Regions on version 0.8.
- 238 • answering comments done during the pre-approval on December 22.

239 Version 0.8

- 240 • renamed region CR $Z+\gamma+jets$ to CR $Z \rightarrow \ell\ell\gamma$ to avoid confusion (no requirements on jets in this
241 region)
- 242 • adding description of top and single top variation samples in Section 4.2 (not yet included in fit,
243 n-tuples for these samples currently in production)
- 244 • optimisation of statistical fit
- 245 • adding discussion about correlation coefficients
- 246 • signal injection tests for all couplings
- 247 • adding negative log-likelihood scans in Figure ??
- 248 • adding ranking plots in Section ??
- 249 • testing photon p_T distribution as discriminating variable in all regions in statistical fit, shown in
250 Appendix S
- 251 • adding tables with relative effect of each systematic uncertainty (post-fit) on yields in Appendix X
- 252 • answering comments by Yichen on version 0.6.
- 253 • answering comments by Marc on version 0.7.

254 **Version 0.7**

- 255 • adding signal from decay mode
 - 256 – Section 6.2.1 largely modified and partially rearranged
 - 257 – shape comparison of different kinematic distributions in Sections 8.1 and 8.6
 - 258 – modified interpretation in Section 11
- 259 • including all systematic uncertainties in fit in Section 10
- 260 • adding injection test in Section 10.4
- 261 • adding Appendix E with studies for different b -tagging WP
- 262 • answering comments by Marc on version 0.6.
- 263 • answering comments by Catrin on version 0.6.

264 **Version 0.6**

- 265 • new n-tuples arrived: AT21.2.44. Numbers updated. **DRAWBACK: Couldn't make it to re-run**
266 **fit. Plots in Section 10 from previous version.**
- 267 • including Table 15 with signal efficiencies and S/B ratio for all regions in Section 6
- 268 • including Section 6.2.3 about signal in decay mode
- 269 • clarification for electron-fake-rate: I measure a quantity proportional to the fake rate, but not the
270 fake rate itself since I ignore reconstruction efficiencies etc.
- 271 • largely extending Section 8 about signal-background separation
 - 272 – describing different training scenarios with different number of input variables and hidden
273 layers
 - 274 – including ROC curves
- 275 • explaining symmetrisation, smoothing and pruning for uncertainties in Section 9.1
- 276 • adding description of PDF, scale variation and jet flavour composition uncertainty
- 277 • Table ?? fitted signal strength (before limits by TRexFitter on cross section were shown)
- 278 • including W decay to tau leptons in interpretation of results
- 279 • adding Appendix D w/ $\Delta R(\gamma^{\text{reco}}, e^{\text{truth}})$ studies for $e \rightarrow \gamma$ definition
- 280 • adding Appendix J w/ linear plots for fit of $e \rightarrow \gamma$ estimation
- 281 • adding Appendix M w/ plots for input variable correlation in CR $W + \gamma + \text{jets}$
- 282 • answering re-comments by Catrin on version 0.4
- 283 • answering comments by Marc on version 0.4 and version 0.5
- 284 • answering comments by Yichen on version 0.5

- 285 • harmonising table layout

286 **Version 0.5**

- 287 • extending section for systematic uncertainties
 288 • list of results in abstract updated: only quoting observed and expected limits on branching ratio for
 289 all four assumed couplings. To be discussed!
 290 • adding table with explanations of cuts for cutflow histogram
 291 • finalising systematic uncertainty of fit function variation for $e \rightarrow \gamma$ fake estimation (not yet propag-
 292 ated to statistical analysis)
 293 • fixing bug on uncertainty on number of events in VR SF($e \rightarrow \gamma$) and VR SF($j \rightarrow \gamma$)
 294 • reordering of Section 9: statistical analysis
 295 • adding plots for kinematic distributions in SR separately for electron and muon channel in appendix
 296 • adding table with information about MC samples in appendix
 297 • adding fit functions and fit parameters for e->gamma fake estimation in appendix
 298 • adding plots for systematic uncertainties used in the fit in appendix
 299 • harmonising naming, plot layout, descriptions, etc.
 300 • answering comments by Lidia and Regina on version 0.2 posted on August 7, 2018
 301 • answering comments by Marc on version 0.4 posted on August 25, 2018
 302 • answering comments by Catrin on version 0.4 posted on August 26, 2018
 303 • answering comments by Yichen on version 0.4 posted on August 29, 2018
 304 • answering comments by Lidia and Regina on version 0.4 posted on August 31, 2018

305 **Version 0.4**

- 306 • including statistical analysis for all four single couplings
 307 • including limits for all four single couplings

308 **Version 0.3**

- 309 • adding separation power S and ranking for input variables of neural network
- 310 • including Asimov fit
- 311 • adding interpretation of results
 - 312 – limit on pairs of Wilson coefficients
 - 313 – limit on branching ratio

314 **Version 0.2**

- 315 • adding description of $t\bar{t}$ and single-top MC samples
- 316 • adding plots for cutflows in SR
- 317 • bug fix: selection (veto) of photon in EFR $Z \rightarrow e\gamma$ (EFR $Z \rightarrow ee$) with correct $p_T = 20 \text{ GeV}$
 318 (before: $p_T = 27 \text{ GeV}$)
 - 319 – impact not large
 - 320 – updating scale factors, plots and number of events
- 321 • new definition of validation region for $\text{SF}(j \rightarrow \gamma)$, Table 14
- 322 • extending section 8 about separation of signal from background
 - 323 – reducing number of input parameters
 - 324 – grid search for hyper-parameter optimisation
 - 325 – including plots for correlation coefficients of input and output variables
- 326 • adding plots for statistical analysis
- 327 • adding chapter for interpretation of results
- 328 • adding tables with expected number of events for CR $W+\gamma+\text{jets}$ and CR $Z+\gamma+\text{jets}$ in appendix

329 **Version 0.1**

- 330 • First version!

331 2 Introduction

332 The Standard Model (SM) of particle physics describes the current knowledge about particle physics in
 333 a minimal theory. Over the past years, many measurements confirmed the predictions done by the SM.
 334 Since the SM may be the lower energy limit of a larger theory, searches for physics beyond the SM (BSM)
 335 were and are performed at various experiments. As the top quark is the heaviest known particle and has
 336 unique properties like existing as bare quark due to its short lifetime, it often serves as physics object to
 337 probe the SM and to look for BSM physics.

338 The top quark was discovered at the Tevatron in 1995 [1, 2] and is predominantly produced in pairs via
 339 the strong interaction at the LHC. In addition, it can be singly produced via the electroweak interaction in
 340 three different channels: the dominant t -channel, the tW -channel and the s -channel. The top quark almost
 341 exclusively decays into a W boson and a b quark due to the close to unity value of the V_{tb} element in the
 342 Cabibbo-Kobayashi-Maskawa (CKM) unitary matrix. A transition changing the flavour of the quark, but
 343 not the electric charge by a neutral gauge boson, Z , g , γ , or the Higgs boson H is called flavour-changing
 344 neutral current (FCNC). Such a process is forbidden at tree-level in the SM and highly suppressed at higher
 345 orders by the Glashow-Iliopoulos-Maiani (GIM) mechanism [3]. However, extensions to the SM predict
 346 higher cross sections of processes including an FCNC and higher branching ratios of a quark decaying
 347 via an FCNC. In Figure 1, the branching ratios of the top quark decay via an FCNC are shown for the
 348 SM, several BSM scenarios and the current experimental limits by ATLAS and CMS. It can be seen that
 349 the SM predictions are far below the experimental limits, while experimental searches may reach regions
 350 where they are sensitive to BSM theories.

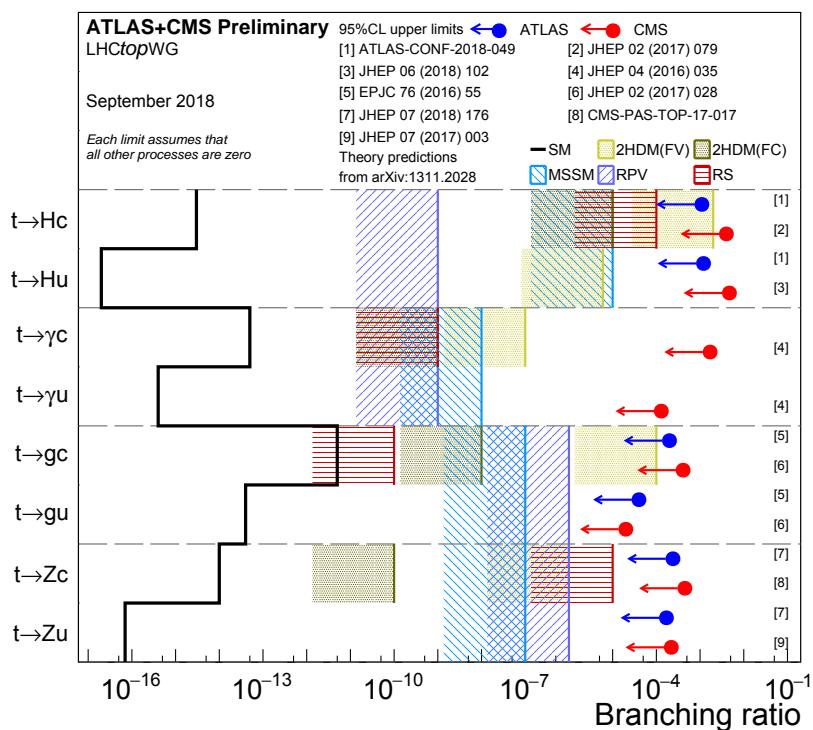


Figure 1: Summary of the current 95 % confidence level observed limits on the branching ratios of the top quark decay via flavour-changing neutral currents to a quark and a neutral boson $t \rightarrow Xq$ ($X = g, Z, \gamma$ or H ; $q = u, c$) by the ATLAS and CMS Collaborations compared to the Standard Model and several new physics models [4].

Not reviewed, for internal circulation only

In this note, the first search by ATLAS for FCNCs with a single-top quark produced in association with a photon is presented. An example Feynman diagram is shown in Figure 2(a) depicting the process¹ $qg \rightarrow t\gamma \rightarrow \ell^+ \nu b\gamma$ with $q = u, c$, also referred to as *production mode*. The anomalous coupling is marked as red circle. It may also appear in the so called *decay mode* where a $t\bar{t}$ system is produced with one top quark decaying SM-like and the other via an FCNC. An example diagram for the decay mode is shown in Figure 2(b) depicting the process $gg \rightarrow t\bar{t} \rightarrow \ell\bar{\nu}b q\gamma$ with $q = u, c$.

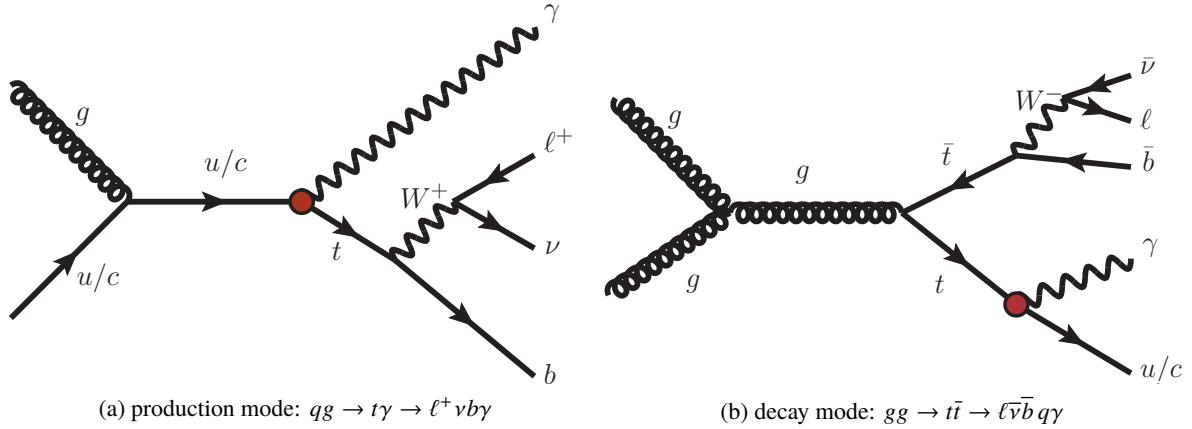


Figure 2: Example Feynman diagrams for processes containing an FCNC with the anomalous $tq\gamma$ ($q = u, c$) vertex (red circle) under study. On the left side, the production mode process is shown where an incoming up-type quark interacts with a gluon. As a result, a single-top quark is produced in association with a photon. The top quark decays into a b quark and a W boson that decays leptonically. On the right side, the decay mode process is shown where a $t\bar{t}$ system is produced with one top quark decaying SM-like and the other via an FCNC.

The anomalous coupling can be described model-independently in a so called effective field theory (EFT). In this theory, the SM Lagrangian \mathcal{L}_{SM} is extended by operators in higher-dimensions of the mass suppressed by the scale of new physics Λ as shown in Equation (1). Dimension-5 operators introduce lepton-flavour violating processes and consequently, are not considered in this analysis. The anomalous coupling at hand can be approximated with dimension-6 operators $O_i^{(6)}$ whose strength is given by the Wilson coefficients $C_i^{(6)}$.

$$\mathcal{L} = \mathcal{L}_{SM} + \frac{1}{\Lambda^2} \sum_i C_i^{(6)} O_i^{(6)} \quad (1)$$

The relevant operators for an FCNC with a top quark and a photon, following the notation in Ref. [5], are the operators O_{uB}^{ij} and O_{uW}^{ij} with $i \neq j$ and either $i = 3$ or $j = 3$, respectively, defined as follows:

$$O_{uB}^{(ij)} = (\bar{q}_i \sigma^{\mu\nu} r_j) \bar{\varphi} B_{\mu\nu}, \quad (2)$$

$$O_{uW}^{(ij)} = (\bar{q}_i \sigma^{\mu\nu} \tau^I r_j) \bar{\varphi} W_{\mu\nu}^I, \quad (3)$$

¹ Charge conjugate production and decay modes are implied throughout the note.

365 where \bar{q}_i describes the left-handed quark doublet and r_j the right-handed quark singlet, $\sigma^{\mu\nu} = \frac{1}{2}[\gamma^\mu, \gamma^\nu]$
 366 with the gamma matrix γ^α , τ^I are the Pauli matrices, $\tilde{\varphi}$ is the complex conjugate of the Higgs field
 367 doublet with $(\tilde{\varphi})^j = \varepsilon_{jk}(\varphi^k)^*$ and $\varepsilon_{12} = 1$ being totally antisymmetric, and $B_{\mu\nu}$ and $W_{\mu\nu}^I$ are the $U(1)_Y$
 368 and $SU(2)_L$ field tensors, respectively. The indices i and j of the spinors refer to the flavour indices of
 369 the quark generations. One index always equals to 3 as a top quark must be involved, while the other one
 370 is either 1 or 2 corresponding to an up or charm quark. These operators introduce an FCNC with a $tq\gamma$
 371 vertex.

372 In this analysis, the search is performed independently for four different coupling scenarios described by
 373 the flavour of the up-type quark, u or c quark, and by the handedness of the coupling, left- or right handed.
 374 Both the production and decay mode are considered as shown in Figure 2, while the analysis is optimised
 375 for the production mode. Each scenario features different kinematic properties of physics objects in the
 376 final state in a phase space accessible by the ATLAS detector. For each coupling, a 95 % confidence level
 377 (C.L.) limit on the signal strength is derived that is interpreted in terms of EFT giving a limit on the cross
 378 section $\sigma(pp \rightarrow t\gamma)$. Furthermore, the limit on the sum of a pair of Wilson coefficients C_{uB}^{ij} and C_{uW}^{ij} and
 379 on the branching ratio $\mathcal{B}(t \rightarrow q\gamma)$ are computed. The currently most stringent experimental limits are set
 380 by the CMS collaboration to $\mathcal{B}(t \rightarrow u\gamma) < 1.3 \times 10^{-4}$ and $\mathcal{B}(t \rightarrow c\gamma) < 1.7 \times 10^{-3}$ [6], assuming the
 381 same strength for left- and right-handed coupling.

382 The note is organised as follows. In Section 3 the analysis strategy is presented. In Section 4, the
 383 data and Monte-Carlo (MC) samples are described. The definitions of objects are given in Section 5
 384 and the event selection is reported in Section 6. In Section 7, the background estimation is presented
 385 and the separation of signal from background is described in Section 8. In Section 9, the estimation of
 386 systematic uncertainties is explained. The statistical analysis is explicated in Section 10. The results and
 387 the interpretation are given in Section 11. Conclusions are made in Section 12.

388 3 Analysis strategy

389 A brief overview of the analysis strategy is given here. Details about each step can be found in the
 390 respective section.

391 **Definition of common objects** In this analysis, the physics objects used are photons, electrons, muons,
 392 (b -tagged) jets, and missing transverse momentum. Common cuts and working points are used as
 393 recommended by different CP groups.

394 **Event classification** Each simulated event is classified as either an event with a prompt photon when the
 395 photon stems from the hard scattering, or an event with an electron faking a photon ($e \rightarrow \gamma$ fake), or
 396 an event with a hadron/jet faking a photon ($j \rightarrow \gamma$ fake). For classifying an event, the information
 397 of the truth particle associated to the reconstructed photon is used.

398 **Definition of signal and control regions** In this analysis, the signal region (SR) is defined by requiring
 399 a photon, a charged lepton being either an electron or a muon, a b -jet and $E_T^{\text{miss}} > 30 \text{ GeV}$. In order
 400 to handle the background contributions, control regions (CR) orthogonal, but close to the SR are
 401 defined. The main background arises from events with an electron-to-photon fake and $W+\gamma+\text{jets}$
 402 events. For the latter background, a CR is defined by reversing the b -tagging requirement on the jet.
 403 Another CR is enriched with $Z+\gamma$ events by requiring two same flavour, opposite charged leptons
 404 and a photon. The purpose of these two CRs is to estimate the normalisation of the respective
 405 processes that is done in a combined fit to data where their normalisations are treated as free
 406 parameters.

407 **Estimation of fake-photon backgrounds** For the fake photon contributions, data-driven methods are
 408 used to derive scale factors to correct simulation for any deviation from data. For the $e \rightarrow \gamma$ fake
 409 contribution, a quantity proportional to the electron-to-photon fake rate is measured in both data
 410 and simulation and their ratio is taken as scale factor $\text{SF}(e \rightarrow \gamma)$. For the $j \rightarrow \gamma$ fake contribution,
 411 the ABCD method is used where the isolation and the identification criteria on the photon are used
 412 to construct the four regions A, B, C and D. The ratio of number of events with a hadronic fake in
 413 data over that in simulation is defined as scale factor $\text{SF}(j \rightarrow \gamma)$.

414 **Agreement between data and simulation** The agreement between data and simulation is checked in
 415 dedicated validation regions (VR) for the scale factor $\text{SF}(e \rightarrow \gamma)$ and for the combined background
 416 including hadronic fakes. In addition, the CR $W+\gamma+\text{jets}$ and $Z+\gamma$ before and after the fit of the
 417 statistical analysis give an idea for the agreement.

418 The next steps of the analysis are performed independently for each assumed signal coupling: tuy left-
 419 handed, tuy right-handed, tcy left-handed, and tcy right-handed

420 **Signal-background separation** As the signal region is not pure in signal events, a neural network (NN)
 421 is used to construct a variable to better discriminate signal from background. Signal-like events are
 422 assigned a value close to unity, while background-like events get an output value close to zero. Only
 423 the signal from the production mode is trained against SM contributions, while the decay mode
 424 signal is ignored here. The distribution of this discriminating variable is used for the statistical
 425 analysis in the SR and CR $W+\gamma+\text{jets}$. In the CR $Z+\gamma$, the photon p_T spectrum is used because some
 426 input variables for the NN are not defined in this region.

427 **Statistical analysis** In the statistical analysis, a profile likelihood fit of the discriminating variable is
428 performed simultaneously in the SR and CRs taking into account all sources of uncertainties as
429 nuisance parameters. As a result, the signal strength for the assumed signal is obtained.

430 **Interpretation of results** Based on the fit outcome of the statistical analysis, a 95 % C.L. upper limit on
431 the signal strength is computed. This limit is interpreted in the context of EFT that gives limits on
432 the cross section $\sigma(pp \rightarrow t\gamma)$, pairs of Wilson coefficients $|C_{uW}^{ij} + C_{uB}^{ij}|$, and the branching ratio
433 $\mathcal{B}(t \rightarrow q\gamma)$.

4 Data and Monte Carlo samples

In this section, details about the data used and the different MC samples are given.

4.1 Data

The data² used in this analysis were recorded by the ATLAS detector at $\sqrt{s} = 13$ TeV in 2015, 2016 and 2017 and correspond to an integrated luminosity of 81 fb^{-1} . Only events where the ATLAS experiment was fully operational are considered. The uncertainty on the integrated luminosity is 2.0 % [7]. It is derived, following a methodology similar to that detailed in Ref. [8], from a preliminary calibration of the luminosity scale using x-y beam-separation scans performed in May 2016 and July 2017.

4.2 Monte Carlo samples

MC samples are used to describe the signal and background contribution of the various processes. After event generation, the ATLAS detector response is simulated by the toolkit **GEANT 4** [9] with the full simulation of the ATLAS detector [10] or with the fast-simulation package *AtfastII* (AFII) [11]. The AFII package simulates the Inner Detector using **GEANT 4**. For muons, the other parts of the detector are also simulated using **GEANT 4**, while for all other particles, only the calorimeter systems are simulated using a parameterisation included in *FastCaloSim* in order to reduce CPU time. A discussion about AFII versus full-sim for samples with prompt photons can be found here: [ATLMCPROD-5558](#). The simulation of pile-up events is included in the digitisation step. The setup for each MC sample is explained below. A list of all MC samples used is found in Appendix A.

The signal in the production mode ($pp \rightarrow t\gamma \rightarrow b\bar{t}\nu\gamma$) and in the decay mode ($pp \rightarrow t\bar{t} \rightarrow b\bar{t}\nu\bar{q}\gamma$) is simulated with the **MADGRAPH5_aMC@NLO** 2.4.3 generator [12] with the **UFO** model **TopFCNC** [13, 14] at next-to-leading order (NLO) in QCD, using the **NNPDF3.0NLO** parton distribution function (PDF) set [15]. The scale of new physics is set to $\Lambda = 1$ TeV and the top mass equals to 172.5 GeV. For the decay of the top quark decaying SM-like, the spin correlation is preserved using **MADSPIN** [16]. The parton showering is simulated using **PYTHIA 8.212** [17] with the A14 tune [18] and the **NNPDF2.3LO** PDF set [19]. The **EvtGen 1.2.0** programme [20] is used for the decay of *B* and *D* hadrons. After event generation, the samples are processed with the AFII package. In the production mode, four samples are generated with different couplings turned on: *tuy* left-handed, *tuy* right-handed, *tcy* left-handed, and *tcy* right-handed. In the decay mode, four samples are generated: two samples with left-handed *tuy* coupling turned on where once the top quark decays via FCNC and once the anti-top quark decays via FCNC. The other two samples simulate the left-handed *tcy* coupling, again differing in the decay of the top and anti-top quarks. It shall be mentioned that no difference between left- and right-handed coupling was found at truth level in the decay mode as seen in Appendix B and thus, only the processes with left-handed coupling were simulated. In Table 1, the number of simulated events for the different signal samples for the production and decay mode are shown.

For the following simulated samples, only the SM is assumed.

² `data15_13TeV.periodAllYear_DetStatus-v89-pro21-02_Unknown_PHYS_StandardGRL_All_Good_25ns.xml`,
`data16_13TeV.periodAllYear_DetStatus-v89-pro21-01_DQDefects-00-02-04_PHYS_StandardGRL_All_Good_25ns.xml`,
`data17_13TeV.periodAllYear_DetStatus-v99-pro22-01_Unknown_PHYS_StandardGRL_All_Good_25ns_Triggerno17e33prim.xml`

Table 1: Number of simulated events for the signal samples for the production and decay mode for both MC campaigns.

Mode	MC DSID	Coupling	# sim. events	
			MC16a	MC16d
Production	410650	$t\gamma$, LH	115 000	370 000
	410651	$t\gamma$, RH	125 000	370 000
	410652	$t\gamma$, LH	135 000	370 000
	410653	$t\gamma$, RH	150 000	370 000
Decay	410980	$t\gamma$, anti-top	170 000	210 000
	410981	$t\gamma$, top	170 000	210 000
	410984	$t\gamma$, anti-top	170 000	210 000
	410985	$t\gamma$, top	170 000	210 000

469 The $t\bar{t}+\gamma$ sample is simulated with the `MADGRAPH5_aMC@NLO` 2.3.3 generator using the NNPDF2.3LO
 470 PDF set at leading order (LO) in QCD. The top mass is set to 172.5 GeV. A k -factor of 1.24 is used to
 471 extrapolate to NLO [21, 22]. The parton showering is performed with `PYTHIA` 8.212 with the A14 tune
 472 and the NNPDF2.3LO PDF set. The `EvtGen` 1.6.0 programme [20] is used for the decay of B and D
 473 hadrons. The full simulation package for the ATLAS response is used.

474 For the generation of $t\bar{t}$ and electroweak t -, s - and tW -channel single top-quark events, `PowHEG-Box` 2 [23–
 475 31] is used with the NNPDF3.0NLO PDF set in the matrix element calculations at NLO in QCD. For the
 476 samples with single top events in the tW -channel, the diagram subtraction (DS) scheme is used to remove
 477 overlap with $t\bar{t}$ events [32, 33]. Different k -factors are used to extrapolate to next-to-next-to-leading order
 478 (NNLO) [34]. Top-quark spin correlations are preserved (for t -channel, top quarks are decayed using
 479 `MADSPIN`). The parton shower, hadronisation, and the underlying event are simulated using `PYTHIA` 8.230
 480 with the A14 tune and the NNPDF2.3LO PDF set. The top mass is set to 172.5 GeV and the factor h_{damp}
 481 is set to $1.5m_{\text{top}}$. The `EvtGen` 1.6.0 programme is used for the decay of B and D hadrons. The full
 482 simulation package for the ATLAS response is used.

483 For systematic variations of the matrix element and shower generators used for the $t\bar{t}$ and single top
 484 processes, samples using `MADGRAPH5_aMC@NLO` 2.6.0 (`MADGRAPH5_aMC@NLO` 2.6.2 for single
 485 top processes) and the NNPDF3.0NLO PDF set interfaced to `PYTHIA` 8.230 with the A14 tune and
 486 the NNPDF2.3LO PDF set, and `PowHEG-Box` 2 with the NNPDF3.0NLO PDF set interfaced to `HER-`
 487 `WIG` 7.0.4 [35, 36] with the H7UE set of tuned parameters and the MMHT2014lo68cl PDF set [37] are
 488 produced. For the estimation of the initial state radiation for the $t\bar{t}$ process, a sample with a varied factor
 489 of $h_{\text{damp}} = 3m_{\text{top}}$ is produced. The fast-simulation package for the ATLAS response is used. All other
 490 options are kept as described above. Additionally, samples with single top events in the tW -channel are
 491 produced using the diagram removal (DR) scheme instead of the DS scheme, while keeping all other
 492 options as before. All these samples are normalised to a cross section at NNLO in QCD.

493 Since there is no dedicated single top + photon MC sample available, the contribution of the SM single
 494 top + photon is estimated using the single top samples. Another estimation for this process is given in
 495 Appendix C. It is found that the single top samples are sufficient.

496 Events containing a W or Z boson decaying into a pair of leptons and a photon, and diboson processes with

497 4 charged leptons, 3 charged leptons and 1 neutrino or 2 charged leptons and 2 neutrinos are simulated with
 498 the SHERPA 2.2.2 event generator [38]. Diboson processes with one of the bosons decaying hadronically
 499 and the other leptonically are simulated with the SHERPA 2.2.1 event generator. Matrix elements contain
 500 all diagrams with four electroweak vertices. They are calculated for up to 1 parton at NLO and up to 3
 501 partons at LO. Events containing a W or Z boson with associated jets are simulated using the SHERPA 2.2.1
 502 event generator. Matrix elements are calculated for up to 2 partons at next-to-leading order and up to 4
 503 partons at leading-order. All matrix elements are matched and merged with the SHERPA parton shower
 504 based on Catani-Seymour dipole [39, 40] using the MEPS@NLO prescription [41–44]. The virtual QCD
 505 correction for matrix elements at NLO accuracy are provided by the OpenLoops library [45, 46]. Samples
 506 are generated using the NNPDF3.0NNLO PDF set, along with the dedicated set of tuned parton-shower
 507 parameters developed by the SHERPA authors. The full simulation package for the ATLAS response is
 508 used.

509 4.2.1 Removal of duplicate events in $X+\text{jets}$ and $X+\gamma+\text{jets}$ samples

510 For samples containing processes with $X+\text{jets}$ and $X+\gamma+\text{jets}$ ($X = W, Z, t\bar{t}$), there might be duplicate
 511 events when a photon is radiated in an event in the $X+\text{jets}$ sample. To account for this double counting, an
 512 overlap removal is performed. It is based on information of the associated truth particle to the reconstructed
 513 photon (cf. Section 5.1). The association is performed by the *Truth to Cluster* matching algorithm of the
 514 *MCTruthClassifier* package [47] and is based on the distance³ ΔR in the η - ϕ -plane. From the truth record,
 515 the truth particle ID, the truth type and the truth origin are used where the latter two variables are based
 516 on the parent particles. A photon may be faked by an electron ($e \rightarrow \gamma$ fake) or a jet ($j \rightarrow \gamma$ fake). The
 517 decision of the fake type of the photon follows:

518 **$e \rightarrow \gamma$ fake** A photon is considered as electron fake if (a) the truth particle ID is equal to the PDG ID of
 519 an electron or (b) the truth particle ID is equal to the PDG ID of a photon and a truth electron is
 520 within a distance of $\Delta R < 0.05$. The impact of different distance parameters was studied as shown
 521 in Appendix D and found to be negligible.

522 **$j \rightarrow \gamma$ fake** A photon is considered as hadronic fake when the truth particle originates from a hadron,
 523 i.e. any meson or baryon, or when the truth particle is a hadron.

524 All events with a photon from the hard scattering (technically not matching the fake definitions) are
 525 removed from $X+\text{jets}$ samples, while all events with a fake photon are removed from the $X+\gamma+\text{jets}$
 526 samples. This overlap removal ensures that events of the $X+\gamma+\text{jets}$ samples only contribute to events with a
 527 a photon from hard scattering process, while events from $X+\text{jets}$ samples only contribute to events with a
 528 photon faked by an electron or a jet.

³ ATLAS uses a right-handed coordinate system with its origin at the nominal interaction point (IP) in the centre of the detector and the z -axis along the beam pipe. The x -axis points from the IP to the centre of the LHC ring, and the y -axis points upward. Cylindrical coordinates (r, ϕ) are used in the transverse plane, ϕ being the azimuthal angle around the z -axis. The pseudorapidity is defined in terms of the polar angle θ as $\eta = -\ln \tan(\theta/2)$.

529 5 Object definition

530 In this section, the reconstruction and identification of the physics objects used in this analysis are
 531 explained. The objects considered here are photons, electrons, muons, jets, and missing transverse
 532 momentum. The reconstruction of these objects follows the standard methods used in the ATLAS
 533 collaboration. Recommended calibrations and corrections are applied as implemented in the AnalysisTop
 534 framework [48], version 21.2.55.

535 **5.1 Photons**

536 The photons are reconstructed from energy depositions in the Electromagnetic Calorimeter (ECAL). If the
 537 cluster is not matched to a reconstructed track in the Inner Detector or a conversion vertex, an unconverted
 538 photon candidate is reconstructed. If the cluster is matched to at least one reconstructed track consistent
 539 with originating from a reconstructed conversion vertex, a converted photon candidate is reconstructed.
 540 Both kind of photons are considered. The photons are required to satisfy the *tight* ID criteria and the
 541 *FixedCutTight* isolation working point. Scale factors based on comparisons between data and simulation
 542 are used to correct the simulation. Only photons with $p_T > 20 \text{ GeV}$ and $|\eta_{\text{clus}}| < 2.37$, excluding the crack
 543 region $1.37 < |\eta_{\text{clus}}| < 1.52$, are selected (η_{clus} is the pseudorapidity of the calorimeter cluster associated
 544 to the photon). The reconstruction, ID and scale factor extraction methods are described in Ref. [49], the
 545 isolation is described in Ref. [50], and the calibration is described in Ref. [51].

546 **5.2 Electrons**

547 Electrons are reconstructed from energy deposits in the central region of the ECAL associated with
 548 reconstructed tracks from the Inner Detector, and are required to satisfy the *tightLH* ID criteria and
 549 the *Gradient* isolation criteria. Scale factors based on comparison between data and simulation are
 550 used to correct the simulation for any discrepancy. Only electrons with calibrated $E_T > 27 \text{ GeV}$ and
 551 $|\eta_{\text{clus}}| < 2.47$, excluding the crack region, are considered. The recommended requirements on the impact
 552 parameter variables are also applied: the transverse impact parameter with respect to the beam line
 553 $|d_0|/\sigma(d_0)$ is required to be lower than 5 and the difference in the z -axis between the track origin and the
 554 primary vertex⁴ when expressed at the beam line $|\Delta z_0 \sin(\theta)|$ is required to be lower than 0.5 mm. The
 555 reconstruction, ID and scale factor extraction methods are described in Ref. [52], the isolation is described
 556 in Ref. [50], and the calibration is described in Ref. [51].

557 **5.3 Muons**

558 Muons are reconstructed with the combined algorithm, using the track segments in the various layers of the
 559 Muon Spectrometer and the tracks in the Inner Detector. They are required to fulfil the *Medium* ID criteria
 560 and the *Gradient* isolation criteria. Scale factors based on comparisons between data and simulation are
 561 used to correct the simulation for any discrepancy. Only muons with calibrated $p_T > 27 \text{ GeV}$ and $|\eta| < 2.5$
 562 are considered. The recommended requirements on the impact parameter variables are also applied: the
 563 transverse impact parameter with respect to the beam line $|d_0|/\sigma(d_0)$ is required to be lower than 3 and

⁴ The primary vertex is defined as the vertex with the largest $\sum p_T$ of the associated tracks.

564 the difference in the z -axis between the track origin and the primary vertex when expressed at the beam
 565 line $\Delta z_0 \sin(\theta)$ is required to be lower than 0.5 mm. The reconstruction, ID, calibrations and scale factor
 566 extraction methods are described in Ref. [53], the isolation is described in Ref. [50].

567 5.4 Jets

568 Jets are reconstructed using the anti- k_t algorithm [54] with a distance parameter $R = 0.4$ in $\eta - \phi$ space
 569 and are reconstructed from topological calorimeter clusters [55]. The jet energy scale and jet energy
 570 resolution are computed as described in Ref. [56]. Jets are required to have $p_T > 25$ GeV and $|\eta| < 2.5$.
 571 In order to reject jets from pile-up or other primary vertices, jets with $p_T < 120$ GeV and $|\eta| < 2.4$ are
 572 required to have a Jet Vertex Tagger (JVT) discriminant [57] larger than 0.59. The efficiency of this JVT
 573 cut is corrected by a scale factor extracted when comparing data to simulation.

574 The b -tagging algorithm to identify jets from b quark hadronisation is the MV2c10 algorithm [58], which
 575 is based on a boosted decision tree using the output weights of the JetFitter, IP3D and SV1 algorithms as
 576 input. The 60 % working point is used, calibrated as recommended⁵. In Appendix E, studies for different
 577 working points are presented. A scale factor to correct the flavour-tagging efficiency (b , c and light jet) in
 578 simulation is used [59].

579 5.5 Missing transverse momentum

580 The reconstructed missing transverse momentum \vec{E}_T^{miss} [60] is computed as the negative vector sum over all
 581 reconstructed, fully calibrated physics objects and remaining unclustered energy, also called soft energy.
 582 This soft energy is estimated from low- p_T tracks associated with the primary vertex not being assigned to
 583 any reconstructed object.

584 5.6 Object overlap removal

585 An overlap removal procedure is applied to avoid that a same deposit in the calorimeter systems or track
 586 is used to reconstruct two different objects. The followed overlap removal procedure corresponds to the
 587 procedure recommended for Moriond 2017 based on the distance⁶ ΔR between two objects. At first,
 588 electrons sharing their track with a muon candidate are removed. Then, all jets being close to an electron
 589 with $\Delta R < 0.2$ are removed. Next, all electrons that are within $\Delta R < 0.4$ to a remaining jet are removed.
 590 For muons and jets being close $\Delta R < 0.4$ to each other, the muon is removed if the jet has more than two
 591 associated tracks, otherwise the jet is removed. All the photons that are within $\Delta R < 0.4$ to a remaining
 592 electron or muon are removed. Finally, all the jets being close with $\Delta R < 0.4$ to a remaining photon are
 593 removed⁷.

⁵ 2017-21-13TeV-MC16-CDI-2018-10-19_v1.root

⁶ In case of jets, the rapidity is used for the computation of ΔR , while it is the pseudorapidity otherwise.

⁷ For technical reasons, these photons are slightly different than the one considered in the analysis: no ID and isolation criteria, and $p_T > 15$ GeV.

594 6 Event selection

595 In this section, the event selection of the signal, control and validation regions is presented. In Tables 3, 13
 596 and 14, an overview of all regions used in this analysis is given. Generally, events are classified into the
 597 electron or muon channel depending on which lepton is present in the final state. The *electron+muon*
 598 channel is the combination of both channels. The τ lepton is not explicitly reconstructed and selected.

599 6.1 Preselection of events

600 Each event is required to have at least one reconstructed primary vertex with at least two reconstructed
 601 tracks. Furthermore, every event has to have fired at least one lepton trigger listed in Table 2. Depending
 602 on the year, a different set of triggers was in use. Since the instantaneous luminosity increased, higher
 603 trigger thresholds were implemented in 2016 and 2017 compared to those in 2015. In addition, at least
 604 one of the selected leptons must be matched to a lepton that fired one of the triggers.

Table 2: List of lepton triggers used in this analysis.

Year	Electron trigger	Muon trigger
2015	HLT_e24_lhmedium_L1EM20VH	HLT_mu20_iloose_L1MU15
	HLT_e60_lhmedium	HLT_mu50
	HLT_e120_lhloose	
2016 + 2017	HLT_e26_lhtight_nod0_ivarloose	HLT_mu26_ivarmedium
	HLT_e60_lhmedium_nod0	HLT_mu50
	HLT_e140_lhloose_nod0	

605 6.2 Signal region

606 The signal region (SR) contains events with a topology as shown in the Feynman diagram in Figure 2(a)
 607 in order to select events with a top quark singly produced in association with a photon. Selected events
 608 are required to have exactly one tightly identified and isolated photon ($p_T > 20 \text{ GeV}$ and $|\eta| < 2.37$,
 609 excluding the crack region), exactly one charged and isolated lepton being either an electron ($p_T > 27 \text{ GeV}$
 610 and $|\eta| < 2.47$, excluding the crack region) or a muon ($p_T > 27 \text{ GeV}$ and $|\eta| < 2.5$) passing dedicated
 611 ID requirements, exactly one jet⁸ being *b*-tagged ($p_T > 25 \text{ GeV}$ and $|\eta| < 2.5$) and missing transverse
 612 momentum $E_T^{\text{miss}} \geq 30 \text{ GeV}$. In Table 3, an overview of the cuts in the SR is given.

⁸ There is also a decay mode analysis ongoing that requires at least two jets. In order to not unblind its SR, only one jet is required in the final state here.

Table 3: Overview of the definition of the signal and some control regions used in this analysis. A hyphen means that no requirement is applied. The abbreviation *SFOS* stands for same flavor with opposite electric charge.

Object	SR	CR $W + \gamma + \text{jets}$	CR $Z + \gamma$
Photons	= 1 w/ $p_T > 20 \text{ GeV}$	= 1 w/ $p_T > 20 \text{ GeV}$	= 1 w/ $p_T > 20 \text{ GeV}$
Leptons	= 1 w/ $p_T > 27 \text{ GeV}$	= 1 w/ $p_T > 27 \text{ GeV}$	= 2 (SFOS) w/ $p_T > 27 \text{ GeV}$
Jets	= 1 w/ $p_T > 25 \text{ GeV}$	= 1 w/ $p_T > 25 \text{ GeV}$	-
being <i>b</i> -tagged	= 1	= 0	-
E_T^{miss}	$\geq 30 \text{ GeV}$	$\geq 30 \text{ GeV}$	-
$m(\ell\gamma)$	-	not in $[60 \text{ GeV}, 100 \text{ GeV}]$	-

613 6.2.1 Signal efficiencies

614 In Figure 3, the signal efficiency in the electron+muon channel is depicted after each cut for all four types
 615 of coupling in the production mode and for both $tq\gamma$ couplings in the decay mode. The explanation of
 616 cuts is given in Table 4. The signal efficiency per lepton flavour is shown in Appendix F. The cuts on
 617 the lepton requirements are mostly covered by the initial requirement of having exactly one reconstructed
 618 and identified lepton giving flat efficiencies. The signal efficiencies in the production mode are similar
 619 and exceed those in the decay mode by an order of magnitude. This difference is mainly driven by the
 620 requirements on the jets since in the decay mode, a high jet multiplicity is expected. Taking into account
 621 all cuts including the preselection cuts, in the production mode, the signal efficiency for the left-handed
 622 tuy coupling is $3.03\% \pm 0.03\%$, for the right-handed tuy coupling $2.45\% \pm 0.03\%$, for the left-handed
 623 $tc\gamma$ coupling $3.79\% \pm 0.03\%$, and for the right-handed $tc\gamma$ coupling $3.14\% \pm 0.03\%$. In the decay mode,
 624 the signal efficiency for the tuy coupling is $0.45\% \pm 0.01\%$ and for the $tc\gamma$ coupling $0.51\% \pm 0.01\%$.
 625 Generally, all applied cuts equally impact the different signal samples, ignoring the jet requirements. Note
 626 that the signal region is not optimised for the signal at hand. In order to separate signal from background,
 627 a neural network is used to construct a discriminating variable as described in Section 8.

Not reviewed, for internal circulation only

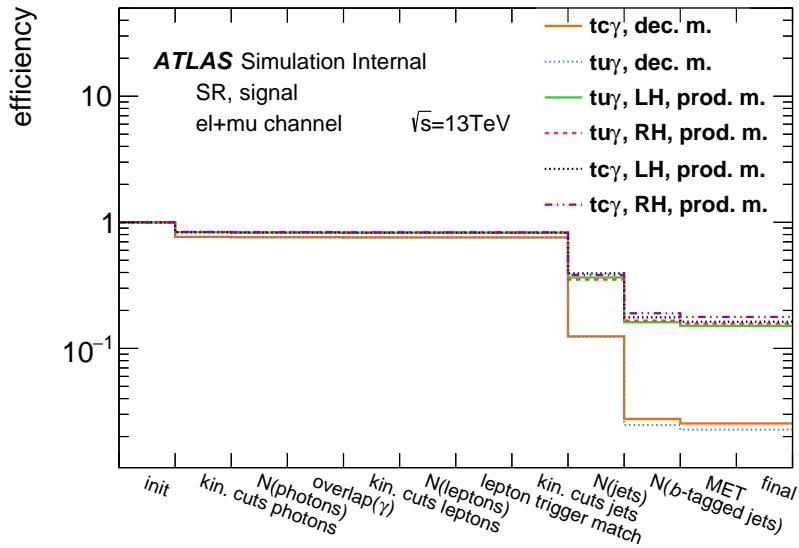


Figure 3: Signal efficiency in dependence of the cuts in the SR for all signal coupling types w.r.t the preselection.

Table 4: Explanation of the cuts in the SR.

Cut	Explanation
Init	Initial number of events with exactly one reconstructed lepton being trigger matched
Kin. cuts photons	At least one photon passing the photon requirements
N(photons)	Exactly one photon passing the photon requirements
Overlap(γ)	Overlap removal between $X+jets$ and $X+\gamma+jets$ samples as described in Section 4.2.1
Kin. cuts leptons	At least one lepton being an electron or muon passing its dedicated requirements
N(leptons)	Exactly one lepton passing its dedicated requirements
Lepton trigger match	Selected lepton matches the lepton that fired a trigger
Kin. cuts jets	At least one jet passing the jet requirements
N(jets)	Exactly one jet passing the jet requirements
N(b -tagged jets)	Exactly one jet being b -tagging
MET	$E_T^{\text{miss}} \geq 30 \text{ GeV}$
Final	Final number of events passing the selection

628 6.2.2 Kinematic differences of assumed signal couplings and modes

629 Signal events feature different kinematic properties depending on the mode and coupling. In both modes,
630 it can be differentiated between $t\gamma$ and $t\gamma$ couplings. In the production mode, differences between right-
631 and left-handed couplings show up. Generally, in the production mode, the spectrum of energy per event
632 tends to higher values than that in the decay mode where the energy range is limited by twice the top quark
633 mass. Subsequently, the average energy of the final state objects differs and angular distances between
634 particles feature different properties.

635 In the production mode, the u quark takes in average more of the proton's energy than the c quark due to
636 the PDF of a proton. Consequently, the final state objects tend to be more energetic which in particular is
637 the case for the photon. The handedness of the coupling affects the state of the top quark and subsequently,
638 its electroweak decay into a W boson and a b quark. If the coupling is right-handed, the p_T spectrum
639 of the b -tagged jet tends to higher values compared to that with left-handed coupling due to the $V - A$
640 structure of the electroweak coupling.

641 In Figures 4 and 5, normalised distributions for the different signal couplings in the production and decay
642 modes are shown where all the effects mentioned above are displayed.

Not reviewed, for internal circulation only

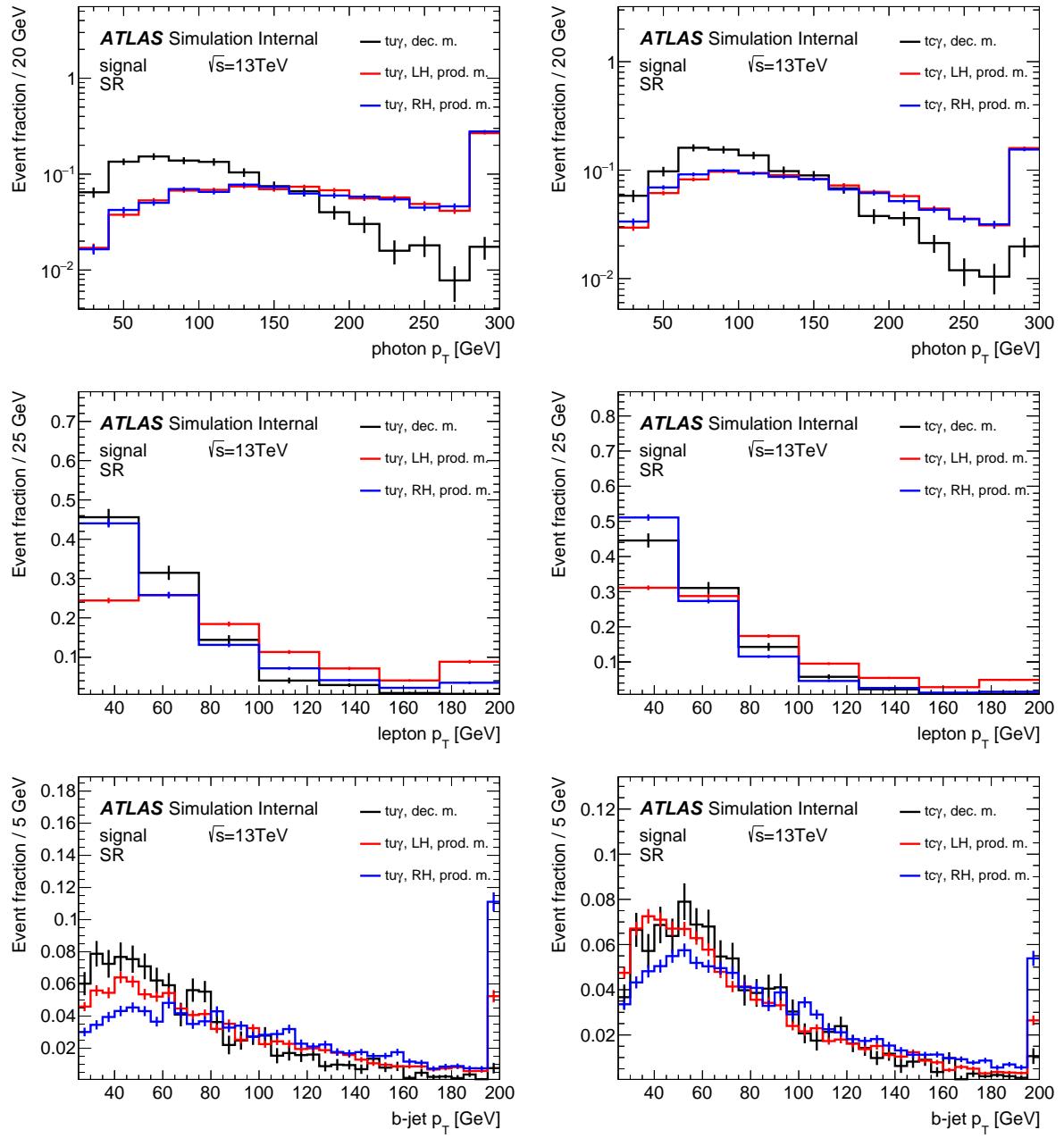


Figure 4: Distributions of different kinematic variables for the tuy (left) and $tc\gamma$ couplings (right) in the production and decay modes in the SR: photon p_T spectrum (top), lepton p_T spectrum (middle), and b -jet p_T spectrum (bottom). All distributions are normalised to unity and the over- and underflow bins are shown.

Not reviewed, for internal circulation only

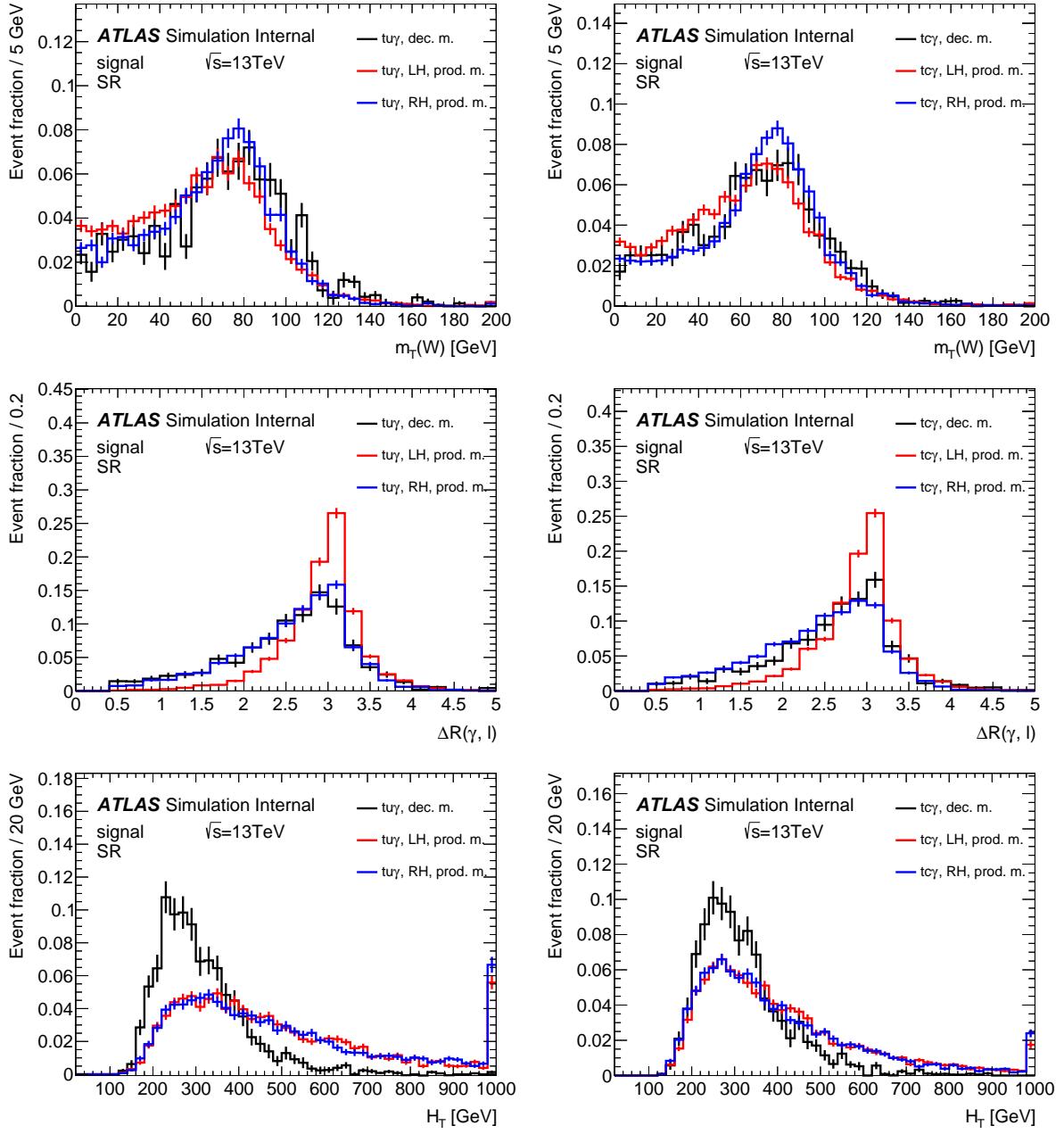


Figure 5: Distributions of different kinematic variables for the tuy (left) and $tc\gamma$ couplings (right) in the production and decay modes in the SR: transverse mass of the W boson (top), distance ΔR between the photon and lepton (middle), and sum of the p_T of all reconstructed objects H_T (bottom). All distributions are normalised to unity and the over- and underflow bins are shown.

6.2.3 Scaling of the production and decay mode signals

For both modes and all couplings, the event yields are scaled to an effective cross section $\sigma_{\text{eff}}^{\text{coup}}$ that is computed by the total cross section of that process and all relevant branching ratios. For the scaling, the branching ratio $\mathcal{B}(t \rightarrow q\gamma)$ with $q = u, c$ is assumed to be 10^{-3} , a value close to the current experimental limit.

In the production mode, in order to connect the branching ratio $\mathcal{B}(t \rightarrow q\gamma)$ to the effective cross section, both values are expressed in terms of the Wilson coefficients $C_{uW}^{(ij)}$ and $C_{uB}^{(ij)}$. The effective cross section in the production mode $\sigma_{\text{eff}}^{\text{prod. m.}}$ equals to

$$\sigma_{\text{eff}}^{\text{prod. m.}} = \sigma(pp \rightarrow t\gamma) \times \mathcal{B}(t \rightarrow Wb) \times \mathcal{B}(W \rightarrow \ell\nu). \quad (4)$$

with the branching ratios $\mathcal{B}(t \rightarrow Wb) \approx 1$, and $\mathcal{B}(W \rightarrow \ell\nu) = 32.58\%$ [61]. The cross section $\sigma(pp \rightarrow t\gamma)$ is computed in the context of the EFT, neglecting any SM contribution. Therefore, the Lagrangian as implemented in the UFO model TopFCNC [62] is looked at. This model is also used in the generation of the signal events. It is defined as

$$\mathcal{L}_{\text{TopFCNC}} = \frac{ev}{\sqrt{2}\Lambda^2} \sum_{a \in \{1,2\}} \bar{q} \sigma^{\mu\nu} \left[\left(C_{uW}^{(a3)*} + C_{uB}^{(a3)*} \right) P_L + \left(C_{uW}^{(3a)} + C_{uB}^{(3a)} \right) P_R \right] t A_{\mu\nu} + h.c., \quad (5)$$

with the electric charge e , the vacuum expectation value v , the scale of new physics Λ , the left-handed quark doublet \bar{q} , the tensor $\sigma^{\mu\nu} = \frac{1}{2}[\gamma^\mu, \gamma^\nu]$ with the gamma matrix γ^α , the Wilson coefficients $C_{uW}^{(ij)}$ and $C_{uB}^{(ij)}$, the left-/right-handed projection P_L (P_R), the right-handed top quark singlet t , and the electromagnetic field tensor $A_{\mu\nu}$. The index a runs over the first two quark generations. Since the cross section depends on the square of the absolute value of the matrix element being proportional to the Lagrangian in Equation (5), it shows a quadratic dependence on the sum of the Wilson coefficients $C_{\text{sum}} = C_{uW}^{(ij)} + C_{uB}^{(ij)}$ as shown in Equation (6). Since any SM contribution is neglected, the constant term c and the coefficient b introducing interference effects between the SM and EFT are zero. Consequently, the ratio of the cross section over the square of the sum of Wilson coefficients is constant as shown in Equation 8. In Table 5, the value for the coefficient a , the cross section and the sum of Wilson coefficients used in the simulation of the signal process are shown for the different couplings. Note that in simulation, the sum of Wilson coefficients is chosen to be large and far from the excluded region since otherwise, MADSPIN could not be executed for the decay mode.

$$\sigma(C_{\text{sum}}) = aC_{\text{sum}}^2 + bC_{\text{sum}} + c \quad (6)$$

$$\implies \sigma(C_{\text{sum}}) = aC_{\text{sum}}^2 \quad (7)$$

$$\implies \frac{\sigma(C_{\text{sum}})}{C_{\text{sum}}^2} = a = \text{const.} \quad (8)$$

Not reviewed, for internal circulation only

Table 5: The coefficient a , sum of Wilson coefficients $C_{\text{sum},\text{MC}}$ and cross section $\sigma_{\text{MC}}^{\text{prod. m.}}$ used in the simulation of the signal process of in the production mode for the different assumed couplings.

Coupling	Coefficient a [pb]	$C_{\text{sum},\text{MC}}$	$\sigma_{\text{MC}}^{\text{prod. m.}} [\text{pb}]$
$t u \gamma$, left-handed	1.0348	12	149.018
$t u \gamma$, right-handed	1.0341	12	148.910
$t c \gamma$, left-handed	0.1477	12	21.2664
$t c \gamma$, right-handed	0.1478	12	21.2762

668 The branching ratio in LO is defined as

$$\mathcal{B}(t \rightarrow q\gamma) = \frac{\Gamma(t \rightarrow q\gamma)}{\Gamma(t \rightarrow Wb) + \Gamma(t \rightarrow q\gamma)} \approx \frac{\Gamma(t \rightarrow q\gamma)}{\Gamma(t \rightarrow Wb)} \quad \text{for } \Gamma(t \rightarrow q\gamma) \ll \Gamma(t \rightarrow Wb) \quad (9)$$

669 with the partial decay width [14]

$$\Gamma(t \rightarrow q\gamma) = \frac{\alpha m_{\text{top}}^5}{\Lambda^4} \sum_{a \in \{1,2\}} \left(|C_{uB}^{(a3)*} + C_{uW}^{(a3)*}|^2 + |C_{uB}^{(3a)} + C_{uW}^{(3a)}|^2 \right) \quad (10)$$

670 and the total decay width of the top quark [63] being

$$\Gamma(t \rightarrow Wb) = \frac{\alpha}{16 \sin^2 \theta_W} |V_{tb}|^2 \frac{m_{\text{top}}^3}{m_W^2} \left(1 - 3 \frac{m_W^4}{m_{\text{top}}^4} + 2 \frac{m_W^6}{m_{\text{top}}^6} \right) = 1.378 \text{ GeV}, \quad (11)$$

671 with the fine-structure constant α , the mass of the top quark m_{top} , the weak mixing angle θ_W , the CKM
672 matrix element V_{tb} , and the W boson mass m_W assuming the following values for them:

$$\alpha = \frac{1}{137}, \quad (12)$$

$$v = 246 \text{ GeV}, \quad (13)$$

$$m_{\text{top}} = 172.5 \text{ GeV}, \quad (14)$$

$$\Lambda = 1000 \text{ GeV}, \quad (15)$$

$$m_W = 80.379 \text{ GeV}, \quad (16)$$

$$\sin^2(\theta_W) = 0.23122, \quad (17)$$

$$V_{tb} = 1. \quad (18)$$

673 Note that the approximation in Equation (9) is not valid for the sum of Wilson coefficients $C_{\text{sum},\text{MC}}$ used
674 in the generation of signal events enforcing a reweighting to a proper value. Assuming that only one
675 coupling is present at once, the sum of Wilson coefficients for the branching ratio is

$$\mathcal{B}(t \rightarrow q\gamma) = 10^{-3} \implies C_{\text{sum,eff}} = 1.11. \quad (19)$$

⁶⁷⁶ Using Equation (8), the cross section and sum of Wilson coefficients used for simulating the process as
⁶⁷⁷ shown in Table 5, the effective cross section in the production mode can be computed as follows:

$$\sigma_{\text{eff}}^{\text{prod. m.}} = \frac{\sigma_{\text{MC}}^{\text{prod. m.}} \cdot C_{\text{sum,eff}}^2}{C_{\text{sum,MC}}^2}. \quad (20)$$

⁶⁷⁸ In the decay mode, the effective cross section $\sigma_{\text{eff}}^{\text{dec. m.}}$ is given by

$$\sigma_{\text{eff}}^{\text{dec. m.}} = 2 \times \sigma(pp \rightarrow t\bar{t}) \times \mathcal{B}(t \rightarrow Wb) \times \mathcal{B}(W \rightarrow \ell\nu) \times \mathcal{B}(t \rightarrow q\gamma), \quad (21)$$

⁶⁷⁹ with $\sigma(pp \rightarrow t\bar{t}) = 831.76 \text{ pb}$ [34]. It can be seen that the effective cross section $\sigma_{\text{eff}}^{\text{dec. m.}}$ is the same for
⁶⁸⁰ both tuy and $tc\gamma$ coupling assuming the same branching ratios $\mathcal{B}(t \rightarrow u\gamma) = \mathcal{B}(t \rightarrow c\gamma)$.

⁶⁸¹ In Table 6, the effective cross sections for both modes and all couplings and the expected number of events
⁶⁸² in the SR are shown assuming the branching ratio $\mathcal{B}(t \rightarrow q\gamma) = 10^{-3}$ for $q = u, c$.

Table 6: Effective cross sections $\sigma_{\text{eff}}^{\text{coup}}$ and numbers of signal events for both the production and decay modes in the SR for each channel assuming pair of Wilson coefficients of $C_{\text{sum,eff}} = 1.11$ at a scale of new physics $\Lambda = 1 \text{ TeV}$ for all couplings. The statistical uncertainty is also shown.

Mode	Coupling	$\sigma_{\text{eff}}^{\text{coup}} [\text{fb}]$	Number of events		
			Electron channel	Muon channel	Electron+muon channel
production	$tuy, \text{ LH}$	416.70	532 ± 11	480.0 ± 9.9	1012 ± 15
	$tuy, \text{ RH}$	416.40	412.6 ± 9.5	397.8 ± 8.8	810 ± 13
	$tc\gamma, \text{ LH}$	59.47	95.6 ± 1.6	84.0 ± 1.5	179.5 ± 2.2
	$tc\gamma, \text{ RH}$	59.49	74.7 ± 1.4	73.6 ± 1.3	148.3 ± 1.9
	tuy	541.97	100.4 ± 4.5	91.9 ± 4.1	192.3 ± 6.1
	$tc\gamma$	541.97	112.0 ± 4.8	104.7 ± 4.5	216.7 ± 6.5

⁶⁸³ Note that these effective cross sections are used in all regions. In different studies⁹, it was shown that
⁶⁸⁴ interference effects between the production and decay mode for $tq\gamma$ and tqZ coupling seem to be negligible
⁶⁸⁵ for events taken at the LHC at $\sqrt{s} = 13 \text{ TeV}$.

⁹ cf. poster @ TOP 2018, M. Barros, N. Castro, J. Erdmann, G. Geßner, K. Kröninger, S. La Cagnina, A. Peixoto

686 6.2.4 Background events

687 There are a number of different SM processes with the same or similar signature as the signal searched
 688 for in the detector. Due to mis-reconstruction and/or mis-identification of one or more objects, e.g.
 689 the photon and/or a jet flavour, it may happen that an event with an actual different final state passes
 690 the SR requirements. The SM processes that are present in the SR are processes with a single top, $t\bar{t}$,
 691 $W+jets$, $Z+jets$, or dibosons, passing the photon requirement via either a prompt photon radiation or a
 692 mis-reconstructed fake photon. In Table 7, the expected number of SM background events are shown for
 693 the electron, muon and electron+muon channels, respectively.

694 A contribution arising from fake leptons is not considered since they are expected at low photon p_T and
 695 consequently, would get a low score for the discriminating variable introduced in Section 8 that is covered
 696 by the E_T^{miss} uncertainties. In Figure 70, the pre- and post-fit E_T^{miss} distributions are shown where no
 697 disagreement at low E_T^{miss} values, but rather a broad normalisation difference for a large E_T^{miss} range (and
 698 then there is disagreement between data and prediction at values up to 110 GeV, likely coming from the
 699 mis-modelling of the top p_T). Moreover, in the cross section measurement of the $t\bar{t} + \gamma$ process [22], that
 700 uses the same lepton definitions as in this search, but does not cut on E_T^{miss} , the fake lepton contribution
 701 is only 3 % at pre-fit stage and 1.5 % at post-fit stage, present at a photon p_T below 50 GeV. Thus, it is
 702 concluded that the lepton fake contribution is small for this analysis and covered by uncertainties.

703 In the combined electron+muon channels, the main background stems from $t\bar{t}$ events where (a) both W
 704 bosons decay into leptons and one of the lepton is an electron faking a photon, or (b) a W boson decays
 705 leptonically and the other one into jets and one of any jet in such an event is mis-reconstructed as photon.
 706 87.2 % of all $t\bar{t}$ events in the SR contain an electron faking a photon, and 12.8 % contain a hadron faking a
 707 photon. The second main background arises from the $W+\gamma+jets$ process that shows the same final state as
 708 the signal. Another large background contribution stems from events including a Z boson decaying into
 709 electrons where one of these electrons fakes a photon. This background is almost exclusively present in the
 710 electron channel. Events with a single top quark may pass the SR selection when either a photon is radiated
 711 in the hard scattering or a jet is mis-reconstructed as photon (t -channel or tW -channel) or an electron is
 712 mis-reconstructed as photon (tW -channel); events involving a radiative Z boson decay are selected when
 713 a lepton is not reconstructed which happens more often in the muon than in the electron channel. Events
 714 from the $t\bar{t} + \gamma$ process are selected when some final state objects are not reconstructed. $W+jets$ events
 715 pass the SR selection mainly when a jet fakes a photon. Diboson events enter the signal region when an
 716 electron fakes a photon, or a jet is mis-reconstructed as photon or a prompt photon is radiated in the hard
 717 scattering. The cutflow for each background process and the pie chart of all SM processes being present in
 718 the SR are shown in the electron+muon channel in Figure 6 and in Appendix F separately for the electron
 719 and muon channels. It can be seen that the photon requirement and the b -tagging condition significantly
 720 reduce the expected number of background events.

721 Background events in the signal region can be categorised into three classes depending on the source of
 722 the photon as described in Section 4.2.1: (a) an electron fakes a photon; (b) a jet is mis-reconstructed as
 723 photon; or (c) the photon stems from the hard scattering. The numbers of events for this classification are
 724 shown in Table 8. In Figure 7, various kinematic distributions for signal as well as background processes
 725 in the SR are shown in the electron+muon channel¹⁰. The same plots are shown separately for the electron
 726 and muon channels in Appendix G. In these and all other plots, events with left-handed $t\gamma$ coupling

¹⁰ The transverse W boson mass is defined as $m_T(W) = \sqrt{2(p_T(\ell)E_T^{\text{miss}} - \vec{p}_T(\ell) \cdot \vec{E}_T^{\text{miss}})}$ with $\vec{p}_T(\ell)$ describing the momentum of the lepton.

Not reviewed, for internal circulation only

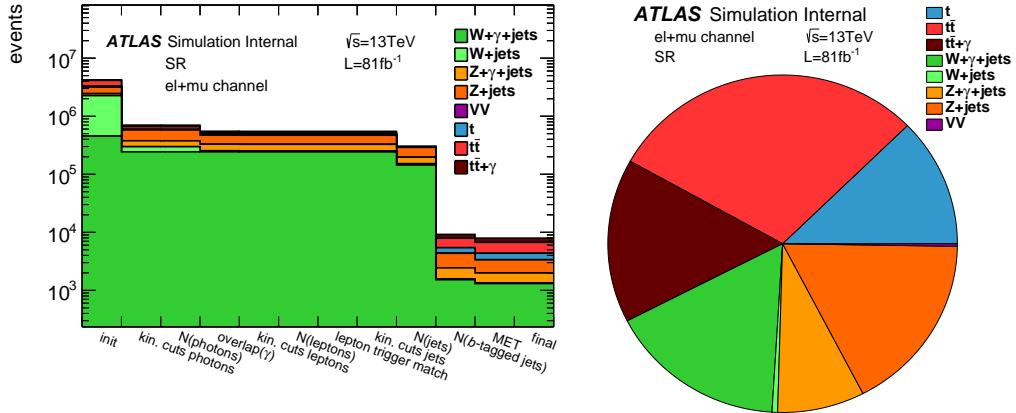


Figure 6: Cutflow in the SR showing the expected number of events for all background processes (left) and pie chart of all SM processes being present in the SR (right).

Table 7: Observed and expected number of events in the signal region per process, separately for the electron, muon and electron+muon channels. For the combined channel, the relative fraction of events is also given. The data-driven scale factors for the photon fake estimations are already considered. Only the statistical uncertainty is shown.

Process	Electron channel	Muon channel	Electron+muon channel	Fraction [%]
Single top	491 \pm 12	479 \pm 12	969 \pm 17	11.7 \pm 0.2
t <bar>t</bar>	1 204 \pm 17	1 107 \pm 16	2 311 \pm 32	27.8 \pm 0.4
t <bar>t + γ</bar>	619.5 \pm 5.1	579.8 \pm 4.9	1 199.4 \pm 7.1	14.4 \pm 0.1
W+jets	51 \pm 17	6.0 \pm 48	57 \pm 51	0.6 \pm 0.6
W+ γ +jets	805 \pm 35	844 \pm 40	1 648 \pm 53	19.8 \pm 0.6
Z+jets	1 412 \pm 77	11.4 \pm 5.4	1 423 \pm 77	17.1 \pm 0.9
Z+ γ +jets	241 \pm 30	430 \pm 45	671 \pm 54	8.1 \pm 0.6
Diboson	15.3 \pm 1.3	6.9 \pm 1.4	22.2 \pm 1.9	0.3 \pm <0.1
Total SM	4 838 \pm 94	3 463 \pm 80	8 300 \pm 120	
Data	5 716	3 841	9 557	

are shown as signal, when not stated otherwise. The data-driven scale factors for electron-to-photon and hadronic fakes, as described in Section 7, are already considered for the number of events shown and in the plots, and the photon p_T reweighting is applied being introduced in Section 6.4. As only statistical uncertainties are included in the plots, the agreement between data and prediction will improve when adding all systematic uncertainties and performing a fit to a discriminating variable as described in Section 10 with the normalisation of the prompt photon contribution of the $W+\gamma+\text{jets}$ and $Z+\gamma+\text{jets}$ being free parameters.

Table 8: Expected number of background events in the signal region per photon origin, separately for the electron, muon and electron+muon channels. The data-driven scale factors for the photon fake estimations are already considered. Only the statistical uncertainty is shown.

Photon origin	Electron channel	Muon channel	Electron+muon channel
$e \rightarrow \gamma$ fake	$2\,676 \pm 78$	$1\,164 \pm 16$	$3\,840 \pm 80$
$j \rightarrow \gamma$ fake	285 ± 22	226 ± 49	511 ± 54
Prompt photon	$1\,877 \pm 47$	$2\,073 \pm 61$	$3\,950 \pm 77$

Not reviewed, for internal circulation only

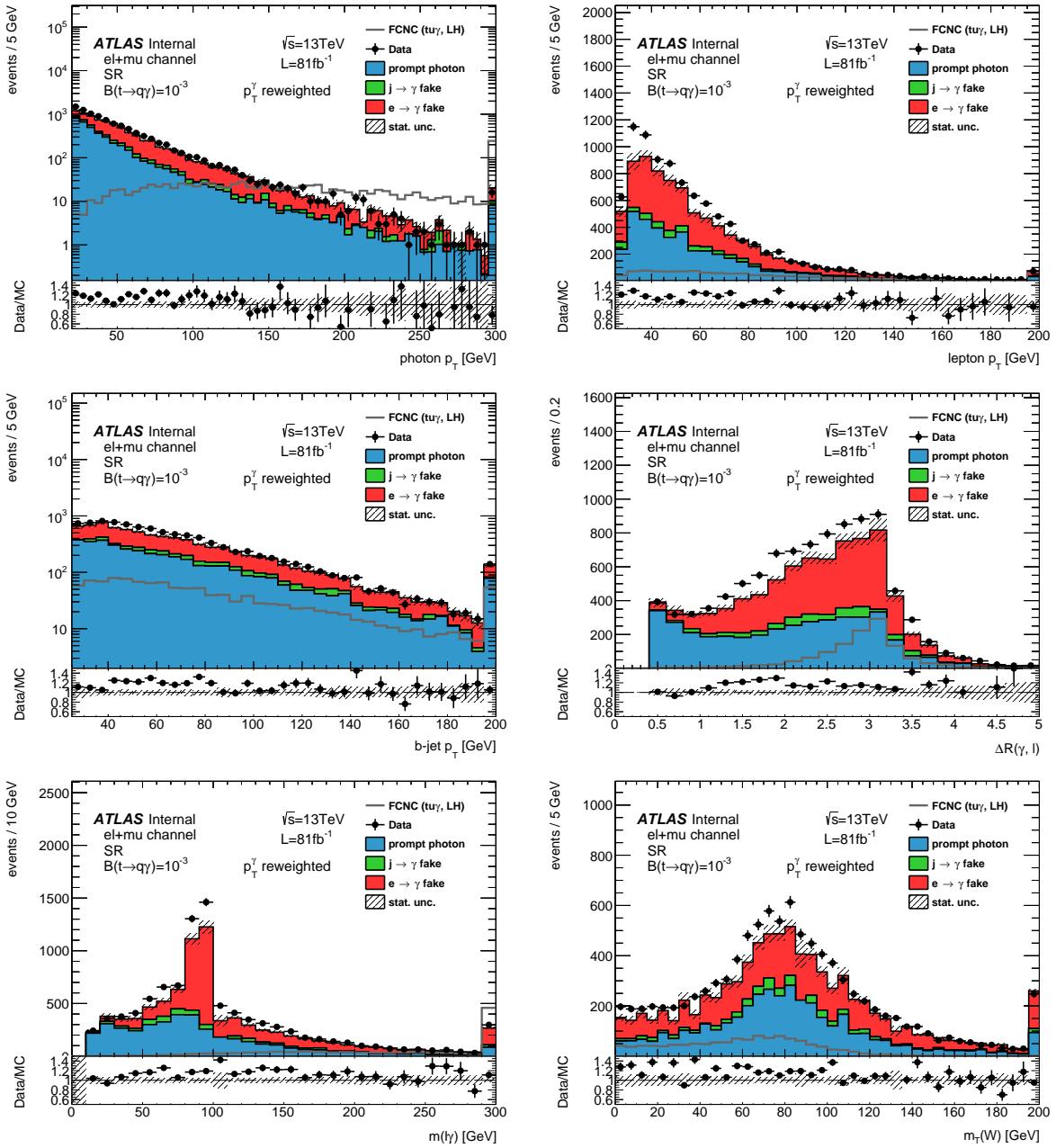


Figure 7: Distributions of different kinematic variables in the SR for signal as well as background processes: photon p_T spectrum (top left), lepton p_T spectrum (top right), b -jet p_T spectrum (middle left), distance ΔR between the photon and lepton (middle right), invariant mass $m(\ell\gamma)$ of the lepton and photon (bottom left), and transverse W boson mass $m_T(W)$ (bottom right). The data-driven scale factors for electron and jet fakes are already included. Only the statistical uncertainty is shown and the over- and underflow bins are plotted.

734 6.3 Control and validation regions

735 Several control (CR) and validation regions (VR) orthogonal to the SR and each other are defined in order
 736 to estimate background contributions and to check the agreement between data and simulation.

737 6.3.1 Control region for the process $W+\gamma+\text{jets}$

738 The CR $W+\gamma+\text{jets}$ mentioned in Table 3 is enriched with events involving a W boson and a prompt photon.
 739 In this region, the b -tagging requirement is reversed with respect to the SR. In addition, the invariant mass
 740 of the photon and lepton $m(\ell\gamma)$ is required to not lie in the range of 60 GeV to 100 GeV to reject events
 741 with an electron faking a photon from a Z boson decay. The purity of this region in $W+\gamma+\text{jets}$ events is
 742 equal to 74 % in the electron+muon channel. The observed and expected numbers of events are shown in
 743 Table 9 for the different physics processes and in Table 10 based on the photon origin. In Figure 8, the
 744 composition of physics processes in this region is illustrated.

Table 9: Expected number of events in the CR $W+\gamma+\text{jets}$ per process, separately for the electron, muon and electron+muon channels. The data-driven scale factors for the photon fake estimations are already considered. Only the statistical uncertainty is shown.

Process	Electron channel	Muon channel	Electron+muon channel
Single top	436 \pm 11	432 \pm 11	867 \pm 16
$t\bar{t}$	894 \pm 15	830 \pm 14	1 724 \pm 20
$t\bar{t} + \gamma$	594.0 \pm 5.1	560.0 \pm 4.9	1 154.4 \pm 7.1
$W+\text{jets}$	3 340 \pm 470	3 660 \pm 450	7 000 \pm 650
$W+\gamma+\text{jets}$	41 100 \pm 210	41 260 \pm 210	82 360 \pm 300
$Z+\text{jets}$	4 820 \pm 240	485 \pm 81	5 310 \pm 260
$Z+\gamma+\text{jets}$	6 000 \pm 140	5 730 \pm 130	11 730 \pm 190
Diboson	421.8 \pm 8.6	381.0 \pm 6.8	803 \pm 11
Total SM	57 610 \pm 590	53 340 \pm 520	111 000 \pm 790
Data	67 375	60 489	127 864

Table 10: Expected and observed number of events in the CR $W+\gamma+\text{jets}$ per photon origin, separately for the electron, muon and electron+muon channels. Scale factors of the data-driven background estimations are already considered. Only the statistical uncertainty is shown.

Photon origin	Electron channel	Muon channel	Electron+muon channel
$e \rightarrow \gamma$ fake	5 610 \pm 230	1 225 \pm 31	6 830 \pm 230
$j \rightarrow \gamma$ fake	3 980 \pm 480	4 250 \pm 450	8 230 \pm 860
Prompt photon	48 020 \pm 250	47 870 \pm 250	95 890 \pm 360
Total SM	57 610 \pm 590	53 340 \pm 520	110 950 \pm 790
Data	67 375	60 489	127 864

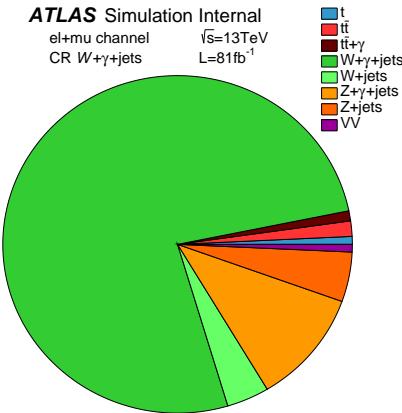


Figure 8: Pie chart showing the composition of physics processes in the CR $W+\gamma+jets$.

Not reviewed, for internal circulation only

745 6.3.2 Control region for the process $Z+\gamma$

746 The CR $Z+\gamma$ mentioned in Table 3 are enriched with events involving a Z boson and a prompt photon. In
 747 this region, two leptons with the same flavour and opposite electric charge (SFOS) are required instead
 748 of only one as in the SR. The requirements on the jets and E_T^{miss} are dropped. The purity of $Z+\gamma$ events
 749 is 93 %. The observed and expected numbers of events are shown in Table 11 for the different physics
 750 processes and in Table 12 based on the photon origin. In Figure 9, the composition of physics processes
 751 in this region is illustrated.

Table 11: Expected number of events in the CR $Z+\gamma$ per process, separately for the electron, muon and electron+muon channels. The data-driven scale factors for the photon fake estimations are already considered. Only the statistical uncertainty is shown.

Process	Electron channel	Muon channel	Electron+muon channel
Single top	75.5 ± 4.5	83.3 ± 4.7	158.9 ± 6.5
$t\bar{t}$	54.5 ± 4.4	47.6 ± 4.1	102.1 ± 6.1
$t\bar{t} + \gamma$	774.0 ± 5.7	934.7 ± 6.2	$1\,708.7 \pm 8.4$
$W+jets$	$< 0.1 \pm < 0.1$	$< 0.1 \pm < 0.1$	$< 0.1 \pm < 0.1$
$W+\gamma+jets$	3.2 ± 1.8	1.9 ± 1.3	5.1 ± 2.2
$Z+jets$	$1\,210 \pm 190$	$1\,430 \pm 200$	$2\,640 \pm 280$
$Z+\gamma+jets$	$31\,130 \pm 290$	$42\,190 \pm 380$	$73\,320 \pm 480$
Diboson	249.0 ± 3.3	243.2 ± 4.1	492.2 ± 5.3
Total SM	$33\,490 \pm 340$	$44\,940 \pm 430$	$78\,430 \pm 550$
Data	35 647	49 700	85 347

Table 12: Expected and observed number of events in the CR $Z+\gamma$ per photon origin, separately for the electron, muon and electron+muon channels. Scale factors of the data-driven background estimations are already considered. Only the statistical uncertainty is shown.

Photon origin	Electron channel	Muon channel	Electron+muon channel
$e \rightarrow \gamma$ fake	137.0 ± 3.5	89.8 ± 3.4	226.8 ± 4.9
$j \rightarrow \gamma$ fake	$1\,270 \pm 190$	$1\,500 \pm 200$	$2\,760 \pm 280$
Prompt photon	$32\,080 \pm 290$	$43\,350 \pm 380$	$75\,430 \pm 480$
Total SM	$33\,490 \pm 340$	$44\,940 \pm 430$	$78\,430 \pm 550$
Data	$35\,647$	$49\,700$	$85\,347$

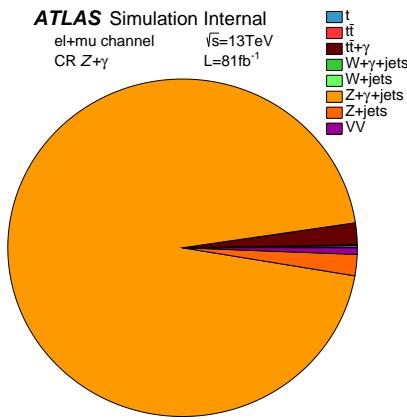


Figure 9: Pie chart showing the composition of physics processes in the CR $Z+\gamma$.

752 6.3.3 Other regions

753 The *electron fake regions* (EFR) are used to derive a scale factor for the $e \rightarrow \gamma$ fakes. Their selection is
 754 listed in Table 13 as well as the VR for the scale factor. For all these regions, only the electron channel is
 755 considered. In these regions, the requirement on E_T^{miss} is inverted compared to the SR. The EFR $Z \rightarrow ee$
 756 is enriched with events including a Z boson decaying into two electrons with opposite electric charge. In
 757 the EFR $Z \rightarrow e\gamma$, the contribution of events containing a Z boson decaying into two electrons is enhanced
 758 where one of the electrons is mis-reconstructed as photon. In both regions, no jet is allowed to be present
 759 in order to be able to build an orthogonal VR including jets for the electron-to-photon fake estimation. An
 760 event passes the selection for the VR SF($e \rightarrow \gamma$) when one electron and one photon are reconstructed and
 761 has at least one jet. This region is enriched with events containing a Z boson decaying into two electrons
 762 where one of them is mis-reconstructed as photon. The purity of electron-to-photon fakes is equal to
 763 91 %.

764 The *hadronic fake regions* (HFR) are used to compute a scale factor for the $j \rightarrow \gamma$ fakes. In Table 14, an
 765 overview of these regions and the VR for combined background is given. Three HFRs are constructed by
 766 changing the isolation and ID criteria on the photon, while all other cuts are kept with respect to the SR.
 767 A detailed description is given in Section 7.2.1. The combined background VR is constructed in a way
 768 that it is close to the SR with similar requirements on the photon, i.e. being tightly identified and isolated.

Table 13: Overview of the definition of control and validation regions used for the electron-to-photon fake estimation. Here, EFR stands for *electron fake region* and VR for *validation region*. The abbreviation *SFOS* stands for same flavour with opposite electric charge.

Object	EFR $Z \rightarrow ee$	EFR $Z \rightarrow e\gamma$	VR SF($e \rightarrow \gamma$)
Photons	$= 0$ w/ $p_T > 20$ GeV	$= 1$ w/ $p_T > 20$ GeV	$= 1$ w/ $p_T > 20$ GeV
Electrons	$= 2$ (SFOS) w/ $p_T > 27$ GeV	$= 1$ w/ $p_T > 27$ GeV	$= 1$ w/ $p_T > 27$ GeV
Jets	$= 0$ w/ $p_T > 25$ GeV	$= 0$ w/ $p_T > 25$ GeV	≥ 1 w/ $p_T > 25$ GeV
E_T^{miss}	< 30 GeV	< 30 GeV	< 30 GeV
$m(\ell\gamma)$	-	[60 GeV, 120 GeV]	[70 GeV, 110 GeV]
$m(\ell\ell)$	[60 GeV, 120 GeV]	-	-

- ⁷⁶⁹ An upper cut on the transverse photon momentum of 100 GeV is set to reduce the signal contamination.
⁷⁷⁰ To be orthogonal to the SR, at least 2 jets must be reconstructed with none being *b*-tagged ensuring a low
⁷⁷¹ signal contamination from the decay mode.

Table 14: Overview of the definition of control and validation regions used for the hadron-to-photon fake estimation. Here, HFR stands for *hadronic fake region* and VR for *validation region*. The definition of photon ID' is given in Section 7.2.1.

Object	HFR region A	HFR region B
Photons	$= 1$ w/ $p_T > 20$ GeV isolated fail ID'	$= 1$ w/ $p_T > 20$ GeV not isolated fail ID'
Leptons	$= 1$ w/ $p_T > 27$ GeV	$= 1$ w/ $p_T > 27$ GeV
Jets	$= 1$ w/ $p_T > 25$ GeV being <i>b</i> -tagged	$= 1$ w/ $p_T > 25$ GeV $= 1$
E_T^{miss}	≥ 30 GeV	≥ 30 GeV

	HFR region C	combined background VR
Photons	$= 1$ w/ $p_T > 20$ GeV not isolated ID	$= 1$ w/ $20 \text{ GeV} < p_T < 100 \text{ GeV}$ isolated ID
Leptons	$= 1$ w/ $p_T > 27$ GeV	$= 1$ w/ $p_T > 27$ GeV
Jets	$= 1$ w/ $p_T > 25$ GeV being <i>b</i> -tagged	≥ 2 w/ $p_T > 25$ GeV $= 0$
E_T^{miss}	≥ 30 GeV	≥ 30 GeV

- ⁷⁷² For all regions, the signal leakage is checked. In Table 15, the signal-to-background ratio S/B and the
⁷⁷³ significance S/\sqrt{B} are listed for each region. The highest signal-to-background ratio and significance are
⁷⁷⁴ achieved in the SR. Generally, all regions except for the SR do not contain much signal and can be safely
⁷⁷⁵ used for fake estimation or as validation region. Note that nevertheless, the signal contributions in all

Not reviewed, for internal circulation only

776 regions are taken into account.

Table 15: Ratio S/B and significance S/\sqrt{B} in all regions assuming the left-handed $t\gamma\gamma$ coupling and a branching ratio $\mathcal{B}(t \rightarrow u\gamma) = 10^{-3}$.

Region	$S/B [\%]$	S/\sqrt{B}
SR	9.3	8.31
CR $W+\gamma+jets$	1.2	4.04
CR $Z+\gamma$	< 0.01	< 0.01
EFR $Z \rightarrow ee$	< 0.01	< 0.01
EFR $Z \rightarrow e\gamma$	< 0.01	0.01
VR SF($e \rightarrow \gamma$)	< 0.01	0.25
HFR region A	3.2	1.05
HFR region B	< 0.01	0.15
HFR region C	1.2	1.07
combined background VR	1.5	6.63

777 6.4 Photon p_T reweighting

778 In both CRs $W+\gamma+jets$ and $Z + \gamma$, that are enriched with events with a prompt photon, the ratio of data to
 779 simulation of the photon p_T spectrum shows a systematic slope, as shown in Figure 10 including the data-
 780 driven scale factors for fake estimations as described in Section 7. This effect stems from the imperfectly
 781 simulated processes $W+\gamma+jets$ and $Z+\gamma+jets$, respectively, and is also visible in p_T distributions of other
 782 physics objects.

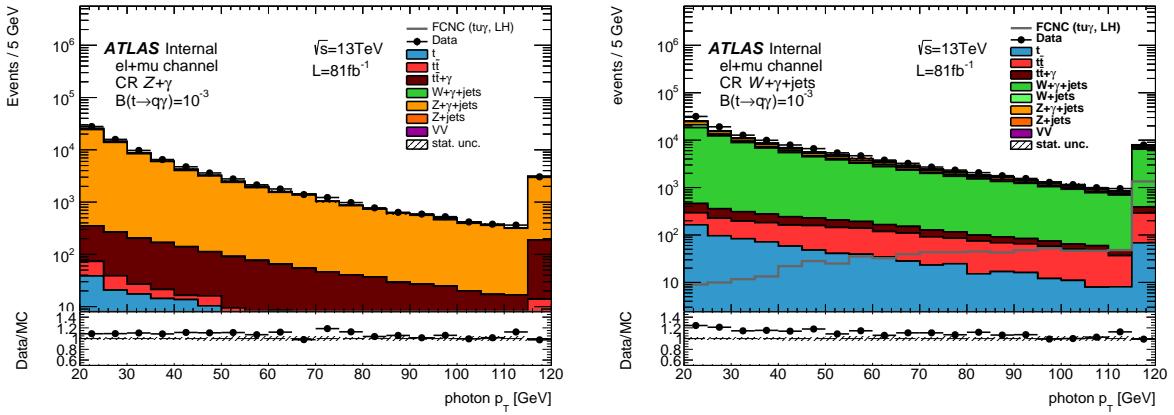


Figure 10: Photon p_T distributions in the CRs $Z + \gamma$ (left) and $W+\gamma+jets$ (right). The data-driven scale factors for fake estimations are included. The ratio between data and simulation shows a systematic slope. Only the statistical uncertainty is included.

783 In order to correct for this effect, a reweighting procedure is applied. First, the photon p_T of the $Z+\gamma+jets$
 784 process is reweighted using the CR $Z+\gamma$ where the $W+\gamma+jets$ contribution is negligible. Then, the photon

p_T of the $W+\gamma+\text{jets}$ process is corrected for in the CR $W+\gamma+\text{jets}$, taking into account the reweighted $Z+\gamma+\text{jets}$ contribution. The reweighting for both processes happens as follows:

- 787 1. From data, all contributions not stemming from the $Z+\gamma+\text{jets}$ ($W+\gamma+\text{jets}$) in the CR $Z+\gamma$ (CR
788 $W+\gamma+\text{jets}$) are subtracted.
- 789 2. The ratio of the corrected data and the contribution $Z+\gamma+\text{jets}$ ($W+\gamma+\text{jets}$) is computed.
- 790 3. The ratio is fitted by a linear function of the form $w(p_T) = a \cdot p_T + b$.
- 791 4. The functional weight $w(p_T)$ is bin-wise used for the corresponding process to correct the shape,
792 while the normalisation is preserved.

793 In Figure 11, plots for the reweighting procedure are shown. In order not to be sensitive to statistical
 794 fluctuations, a coarse binning is chosen. Since this procedure does not take into account any other source
 795 of uncertainty that might change the shape, an uncertainty of 100 % is assigned to it.

796 Note that the correction is only applied in the SR, CRs $Z + \gamma$ and $W+\gamma+\text{jets}$, and VRs $SF(e \rightarrow \gamma)$ and
 797 $SF(j \rightarrow \gamma)$. In the other regions for the background estimation, only the total expected number of events
 798 in simulation is used, i.e. shape effects do not contribute. In Figures 12 and 13, the photon, lepton, and
 799 jet p_T are shown before and after using the reweighting in the CRs $Z + \gamma$ and $W+\gamma+\text{jets}$, respectively.
 800 It can be seen that the simulated shapes are in good agreement with those found in data. Note that the
 801 normalisation is not corrected for and enters the final fit as nuisance parameter as described in Section 9.

Not reviewed, for internal circulation only

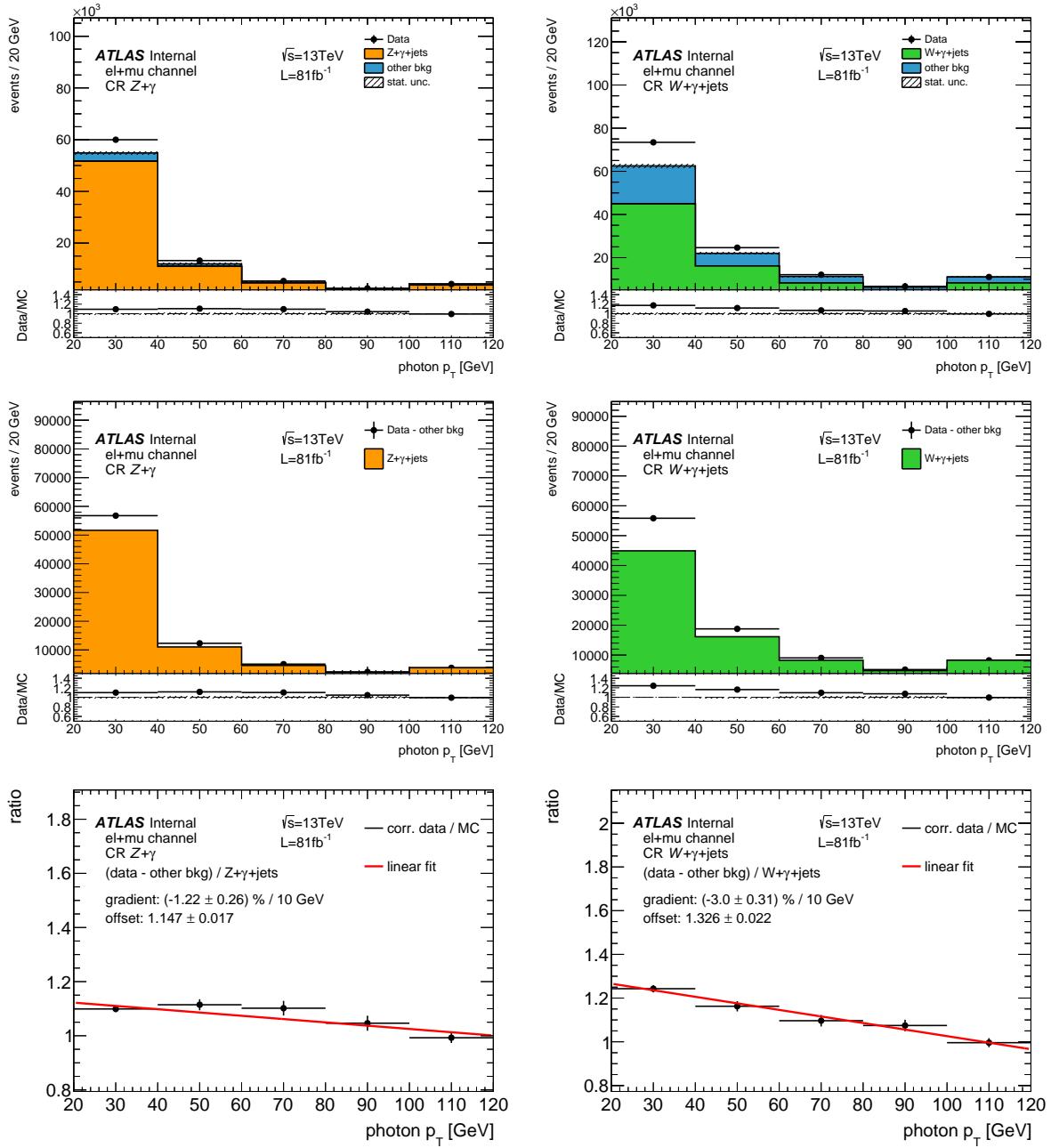


Figure 11: Illustration of the reweighting procedure in the CR $Z + \gamma$ (left) and CR $W + \gamma + \text{jets}$ (right): comparison of data to simulation (top), comparison of data minus all other background contributions to the $Z + \gamma + \text{jets}$ or $W + \gamma + \text{jets}$ contribution, respectively, (middle), and the fit of ratio between the corrected data and the contribution of the $Z + \gamma + \text{jets}$ or $W + \gamma + \text{jets}$ process (bottom). Only the statistical uncertainty is included.

Not reviewed, for internal circulation only

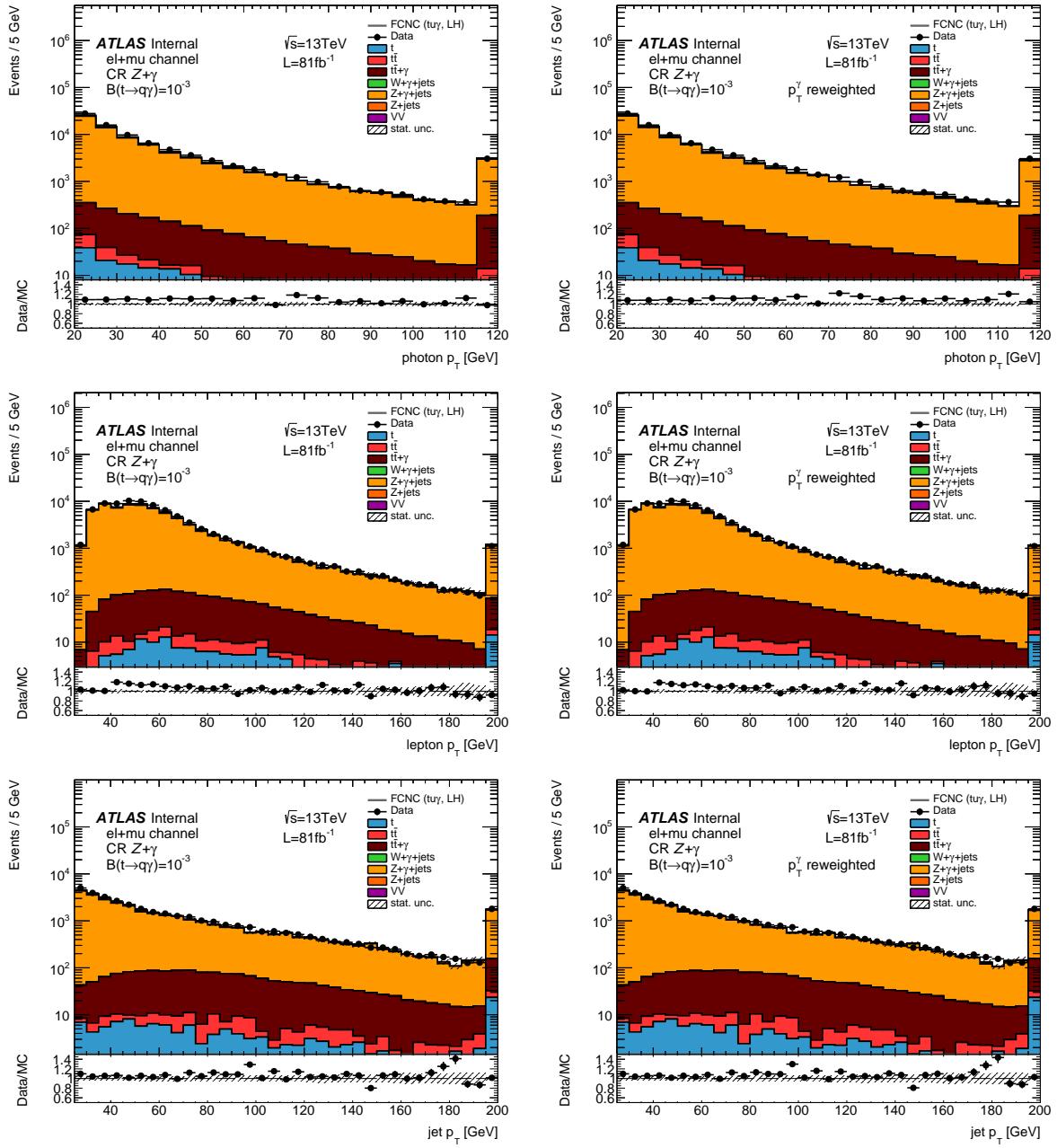


Figure 12: Plots for the validation of the photon p_T reweighting in the CR $Z + \gamma$ before (left) and after applying the reweighting (right): photon p_T distributions (top), lepton p_T distribution (middle), and jet p_T distribution (bottom). Only the statistical uncertainty is included.

Not reviewed, for internal circulation only

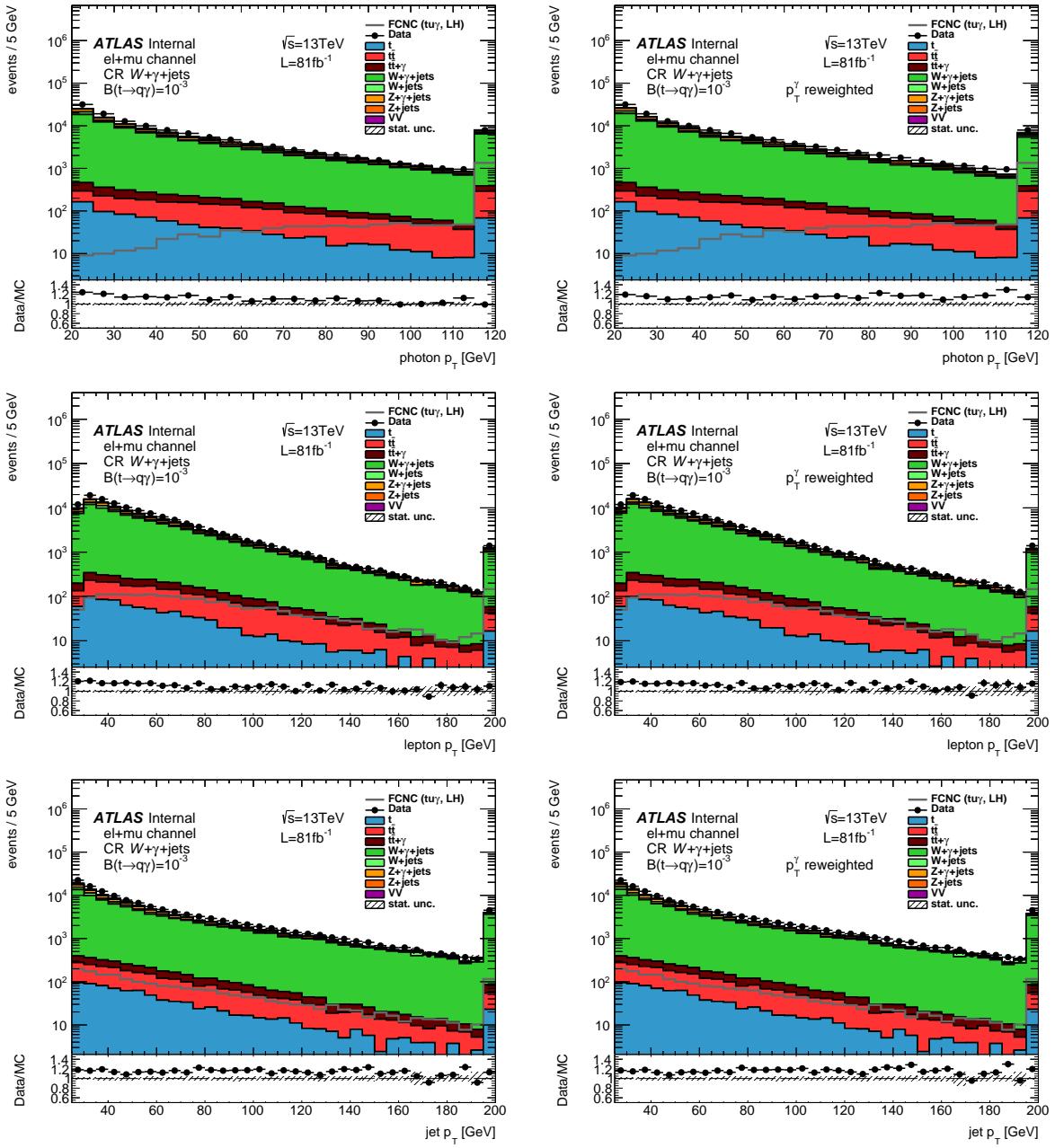


Figure 13: Plots for the validation of the photon p_T reweighting in the CRs $W+\gamma+jets$ before (left) and after applying the reweighting (right): photon p_T distributions (top), lepton p_T distribution (middle), and jet p_T distribution (bottom). Only the statistical uncertainty is included.

802 7 Background estimation

803 In this analysis, all events from SM processes are denoted as background. Three kinds of background
 804 are defined depending on the source of the photon, analogously to the overlap removal presented in
 805 Section 4.2.1. The different categories of background events are events with an $e \rightarrow \gamma$ fake, events with
 806 a $j \rightarrow \gamma$ fake, and events with a photon from the hard scattering process. For the fake contributions,
 807 individual techniques are used to derive data-driven scale factors to correct simulation for any deviation
 808 from data. The estimation of the prompt photon contribution is part of the statistical analysis described in
 809 Section 10.

810 7.1 Electron-to-photon fakes

811 Since electrons and photons are reconstructed very similarly in the ATLAS experiment, an electron faking
 812 a photon may happen. A quantity proportional to the fake rate is measured in data and simulation and a
 813 scale factor is determined from their ratio. The general idea is to count all events including a Z boson that
 814 decays into two electrons. Those events may originate from $Z+jets$ events and also from diboson events.
 815 Two regions are constructed where either both electrons are correctly reconstructed or one of the electrons
 816 is correctly reconstructed and the other is mis-reconstructed at photon.

817 7.1.1 Control regions

818 To estimate the impact of $e \rightarrow \gamma$ fakes, two regions are constructed enriched in events where a Z boson
 819 decays into two electrons. In the electron fake region (EFR) $Z \rightarrow ee$, events with two reconstructed
 820 electrons are selected, while in EFR $Z \rightarrow e\gamma$ events are required to have a reconstructed electron and
 821 a reconstructed photon. This reconstructed photon is assumed to be a mis-reconstructed electron. The
 822 region selection is given in Table 13. To be orthogonal to the SR, the requirement on the missing transverse
 823 momentum is inverted. For both regions, the distribution of the invariant mass of the two physics objects
 824 $m(ee)$ or $m(e\gamma)$, respectively, are shown in Figure 14. The agreement between data and MC of the
 825 invariant mass distribution $m(ee)$ in the EFR $Z \rightarrow ee$ is good, while there are discrepancies in the tails
 826 for the invariant mass distribution $m(e\gamma)$ in the EFR $Z \rightarrow e\gamma$. As only the normalisation of the simulated
 827 samples is used in this region, the deviations in the tails of the distributions can be neglected.

828 In order to distinguish between real prompt photons and faked photons in the EFR $Z \rightarrow e\gamma$ in simulation,
 829 each event is categorised based on the source of the photon into four groups as follows:

830 **type I** The reconstructed photon is matched to a truth electron. These photons are mis-reconstructed
 831 electrons.

832 **type II** The reconstructed photon is matched to a truth photon and a truth electron is present within a
 833 cone of $\Delta R < 0.05$ around the reconstructed photon. The absolute difference¹¹ between the p_T of
 834 the reconstructed photon and the p_T of the truth photon over the p_T of the reconstructed photon is
 835 greater than or equal to 0.1. These photons are mis-matched electrons.

¹¹ Since the value of this parameter does not take influence on the computation of the scale factor, no further studies on its value were done.

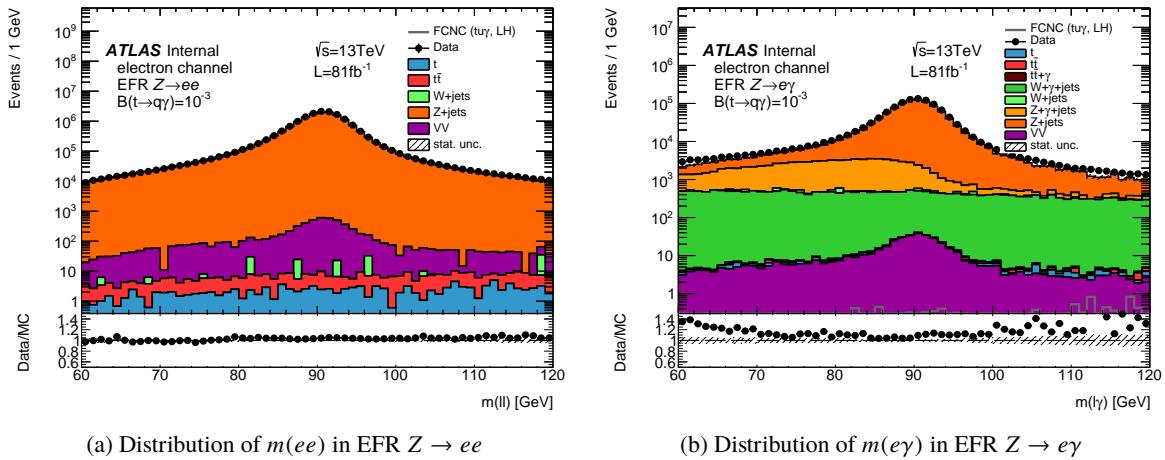


Figure 14: Distribution of the invariant mass $m(ee)$ in the EFR $Z \rightarrow ee$ (left) and $m(e\gamma)$ in the EFR $Z \rightarrow e\gamma$ (right). In the bottom plot, the ratio between data and MC is shown. Only statistical uncertainties are shown and the over- and underflow bins are plotted.

type III The reconstructed photon is matched to a truth photon and a truth electron is present within a cone of $\Delta R < 0.05$ around the reconstructed photon. The absolute difference between the p_T of the reconstructed photon and the p_T of the truth photon over the p_T of the reconstructed photon is smaller than 0.1. These photons stem from non-prompt QED.

type IV The reconstructed photon is matched to a truth photon and no truth electron is present within a cone of $\Delta R < 0.05$. These photons are real prompt photons and called prompt QED.

In Figure 15, the categorisation of events is illustrated and the percentages are shown. For the SR and other regions, a similar composition of electron fakes is observed.

7.1.2 Fit of invariant mass distributions

The distributions of the invariant masses are parametrized by two functions representing the signal and background. In the EFR $Z \rightarrow ee$ the signal function is supposed to model all events with a Z boson decaying into two electrons. Any other event is covered by the background function, e.g. an event with a mis-reconstructed jet. In the EFR $Z \rightarrow e\gamma$, the signal function also models all Z boson decays, i.e. $Z \rightarrow ee$ with a mis-reconstructed photon and radiative Z boson decays $Z \rightarrow ee\gamma$ where an electron is not reconstructed. Since the last process contains a real prompt photon (type IV), but no photon fake, its contribution will be subtracted as described in more detail in Section 7.1.3. The background function is supposed to account for other mis-reconstructed objects than photons, i.e. electrons or jets. Note that in MC, the expected number of events are used instead of the fit functions. A consistency check is presented in Appendix H where also the simulated distributions are fitted, giving a similar scale factor as the nominal one.

In both regions, the same functions are used. As signal function, a double-sided Crystal Ball function is used and as background function, a Bernstein polynomial of order 4. The analytic expressions and the fit results are shown in Appendix I. The choice of these functions is based on the $e \rightarrow \gamma$ fake study of the

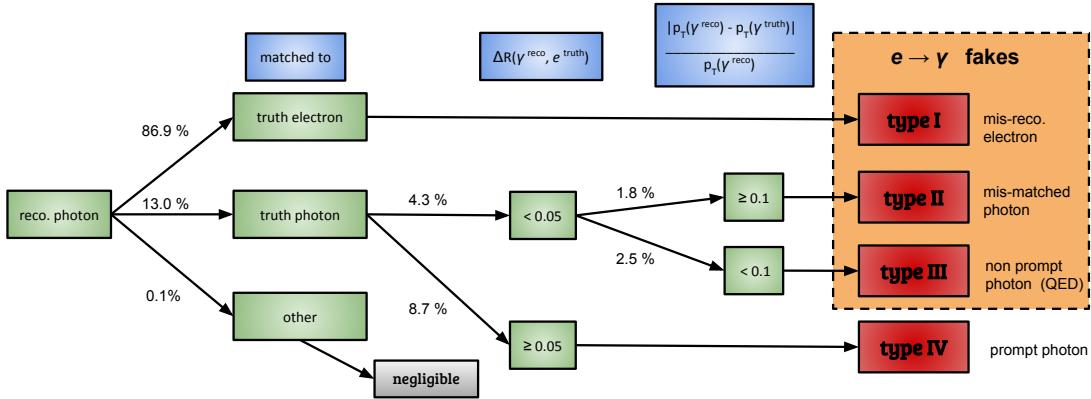


Figure 15: Classification of events in the EFR $Z \rightarrow e\gamma$ based on truth information of the reconstructed photon.

859 photon ID group [49]. To estimate the impact of the choice of the functions, the parameters of the signal
 860 function fitted with MC are propagated and fixed when fitting data except for the normalisation, and at the
 861 same time the background function is changed to a Gaussian function. The fit range is set to 60 GeV to
 862 120 GeV and varied to 65 GeV to 115 GeV to estimate the systematic impact. The fitted distributions for
 863 both data and simulation as cross-check are shown in Figures 16 and 17 for both regions. The fit result in
 864 data when varying the functions is shown in Figure 18. The tail of the distribution in the EFR $Z \rightarrow e\gamma$
 865 shows a mis-agreement of the fit to data. As only 4 % of the data are present there, the effect is negligible.
 866 The result when varying the fit range is shown in Figures 19 and 20 for both regions. Both the signal
 867 and background functions are added as well. It can be seen that the sum of the signal and background
 868 functions reasonably describes the invariant mass distributions. All plots are shown in linear scale in
 869 Appendix J.

870 7.1.3 Fake rate and scale factor

871 In the EFR $Z \rightarrow ee$, the number of signal events in data $N^{\text{data}}(ee)$ is given by the integral of the signal
 872 function. In the EFR $Z \rightarrow e\gamma$, the number of signal events $N^{\text{data}}(e\gamma)$ is given by the integral of the signal
 873 function $N_{\text{fitted signal}}^{\text{data}}(e\gamma)$, while subtracting the impact of events with a real prompt photon (type IV in
 874 Figure 15). Their impact is estimated by applying the fraction κ^{MC} of prompt photons events $N_{\text{prompt-}\gamma}^{\text{MC}}(e\gamma)$
 875 over all events $N_{\text{total}}^{\text{MC}}(e\gamma)$ as found in simulation, as given in Equation (22).

$$\kappa^{\text{MC}} = \frac{N_{\text{prompt-}\gamma}^{\text{MC}}(e\gamma)}{N_{\text{total}}^{\text{MC}}(e\gamma)} = (8.827 \pm 0.058) \times 10^{-2} \quad (22)$$

$$N^{\text{data}}(e\gamma) = (1 - \kappa^{\text{MC}}) N_{\text{fitted signal}}^{\text{data}}(e\gamma) \quad (23)$$

Not reviewed, for internal circulation only

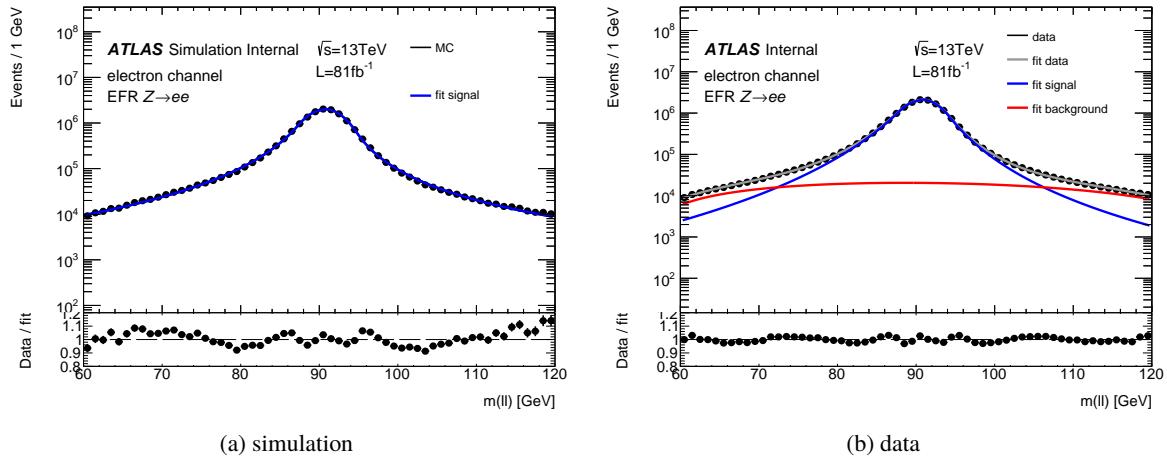


Figure 16: Fitted distribution of the invariant mass $m(ee)$ in the EFR $Z \rightarrow ee$ for simulation (left) and data (right). In the bottom plot, the ratio between simulation/data and the fit function is shown.

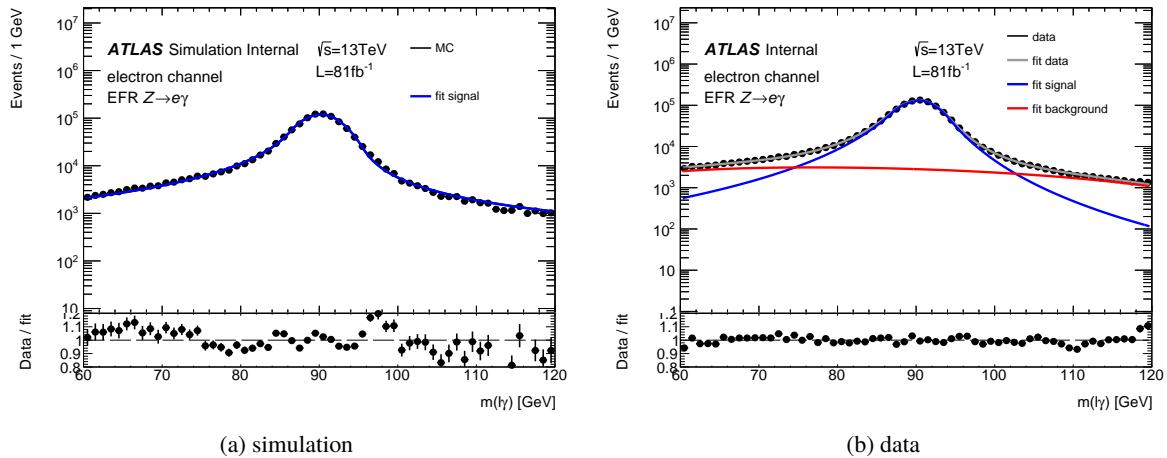


Figure 17: Fitted distribution of the invariant mass $m(ey)$ in the EFR $Z \rightarrow ey$ for simulation (left) and data (right). In the bottom plot, the ratio between simulation/data and the fit function is shown.

Not reviewed, for internal circulation only

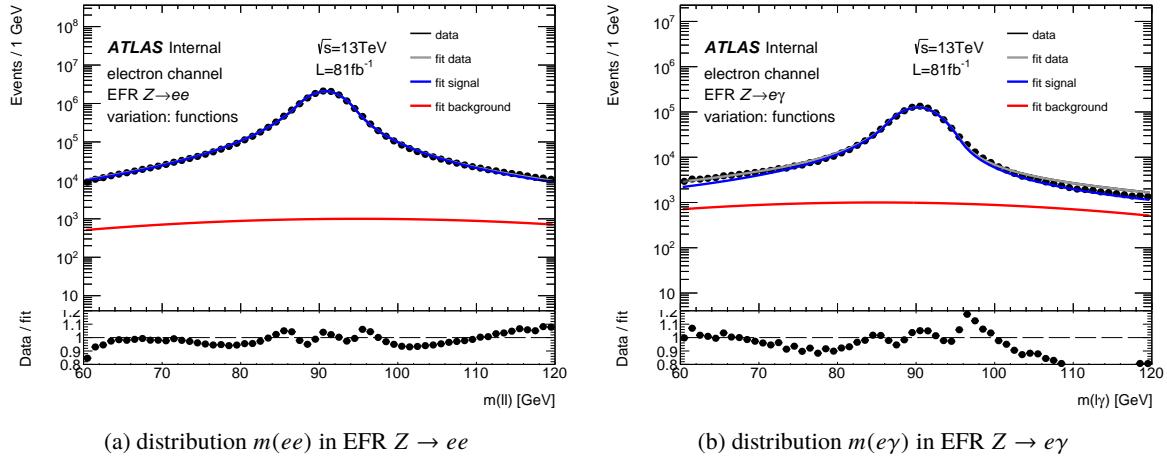


Figure 18: Fitted distribution of the invariant mass $m(ee)$ in the EFR $Z \rightarrow ee$ (left) and the invariant mass $m(e\gamma)$ in the EFR $Z \rightarrow e\gamma$ (right) in data when varying the setup of the functions. For the signal function, the parameters fitted in simulation except for the normalisation are propagated and fixed when fitting data, and the background function is changed to a Gaussian function. In the bottom plot, the ratio between data and the fit function is shown.

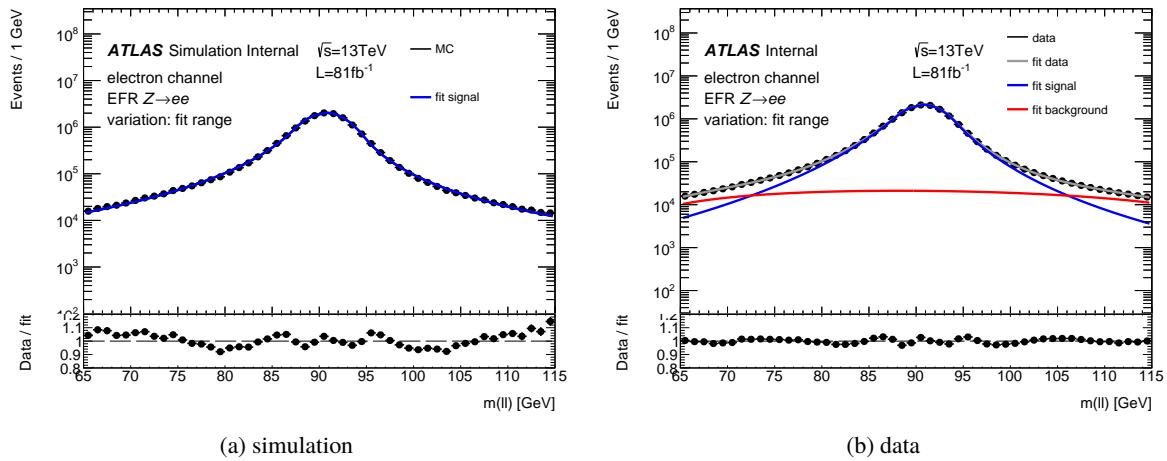


Figure 19: Fitted distribution of the invariant mass $m(ee)$ in the EFR $Z \rightarrow ee$ for simulation (left) and data (right) when varying the fit range. In the bottom plot, the ratio between simulation/data and the fit function is shown.

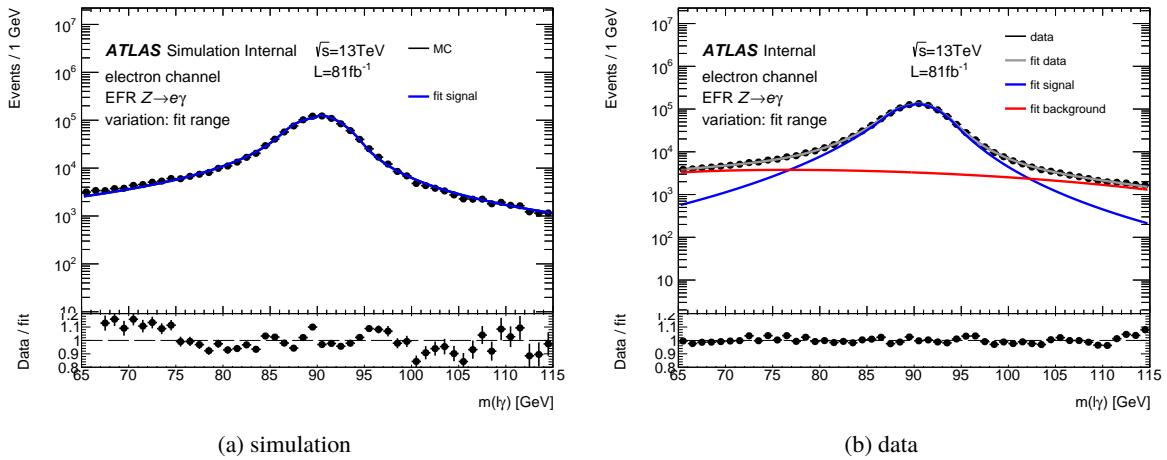


Figure 20: Fitted distribution of the invariant mass $m(e\gamma)$ in the EFR $Z \rightarrow e\gamma$ for simulation (left) and data (right) when varying the fit range. In the bottom plot, the ratio between simulation/data and the fit function is shown.

In order to estimate the systematic effect of the subtraction, the expected number of events $N_{\text{prompt-}\gamma}^{\text{MC}}(e\gamma)$ with a prompt photon is directly subtracted from data instead of using the fraction κ^{MC} . Since isolation and identification efficiencies are not considered, the quantity proportional to the fake rate $F_{e \rightarrow \gamma}^{\text{data}} (F_{e \rightarrow \gamma}^{\text{MC}})$ is defined as the number of signal events in the EFR $Z \rightarrow e\gamma$ over twice the number of signal events in the EFR $Z \rightarrow ee$ region, as both electrons may fake the photon. The electron-to-photon scale factor $SF(e \rightarrow \gamma)$ is the ratio of the fake rate in data $F_{e \rightarrow \gamma}^{\text{data,true}}$ over that in simulation $F_{e \rightarrow \gamma}^{\text{MC,true}}$. Both measures are defined as follows:

$$F_{e \rightarrow \gamma}^{\text{data(MC)}} = \frac{N^{\text{data(MC)}}(e\gamma)}{2 \cdot N^{\text{data(MC)}}(ee)}, \quad (24)$$

$$SF(e \rightarrow \gamma) = \frac{F_{e \rightarrow \gamma}^{\text{data,true}}}{F_{e \rightarrow \gamma}^{\text{MC,true}}} = \frac{F_{e \rightarrow \gamma}^{\text{data}}}{F_{e \rightarrow \gamma}^{\text{MC}}}. \quad (25)$$

The expected and observed event yields for the signal $N^{\text{data(MC)}}(e\gamma)$ after prompt photon subtraction and $N^{\text{data(MC)}}(ee)$, the quantities proportional to the fake rate and the scale factor are shown in Table 16 for different variations. It can be seen that each scale factor is close to unity.

The final scale factor $SF(e \rightarrow \gamma)$ with statistical and systematic uncertainty is measured as

$$SF(e \rightarrow \gamma) = \frac{F_{e \rightarrow \gamma}^{\text{data}}}{F_{e \rightarrow \gamma}^{\text{MC}}} = 0.978 \pm 0.004 \text{ (stat.)} \pm 0.040 \text{ (syst.)}. \quad (26)$$

7.1.4 Validation of $SF(e \rightarrow \gamma)$

The scale factor for the electron-to-photon fakes $SF(e \rightarrow \gamma)$ is validated in the VR $SF(e \rightarrow \gamma)$ as defined in Table 13. This region is enriched in events with a reconstructed photon being faked by an electron

Table 16: Number of expected (observed) signal events $N^{\text{data(MC)}}(e\gamma)$ and $N^{\text{data(MC)}}(ee)$ in the EFR $Z \rightarrow e\gamma$ after prompt photon subtraction and EFR $Z \rightarrow ee$, respectively, for the nominal setup and systematic variations. The quantities proportional to the fake rate and the scale factors are also shown. Only the statistical uncertainty is included.

Fit setup	$N^{\text{data(MC)}}(e\gamma)$	$N^{\text{data(MC)}}(ee)$	$F_{e \rightarrow \gamma}^{\text{data(MC)}} [\%]$	$SF(e \rightarrow \gamma)$
MC	$1\,010\,900 \pm 3\,600$	$15\,912\,000 \pm 14\,000$	3.176 ± 0.012	
Data	Nominal	$970\,200 \pm 2\,400$	$15\,617\,800 \pm 4\,700$	3.1059 ± 0.0078
	Functions	$1\,062\,600 \pm 1\,200$	$16\,510\,400 \pm 4\,100$	3.2180 ± 0.0037
	Bkg subtraction	$966\,200 \pm 2\,600$	$15\,617\,800 \pm 4\,700$	3.0933 ± 0.0084
	Fit range	$949\,000 \pm 2\,900$	$15\,568\,500 \pm 4\,700$	3.0480 ± 0.0092
				0.9595 ± 0.0046

achieved by the requirement on the invariant mass of $70 \text{ GeV} < m(\ell\gamma) < 110 \text{ GeV}$. Tables and plots are shown in Section 10.9.2 after the statistical fit is performed. In Appendix K, studies on the dependence of the scale factor on the photon p_T are shown that is found to be negligible.

7.2 Hadron-to-photon fakes

Since ATLAS records proton-proton collisions, many jets and hadrons occur after a collision. Hence, it may happen that a jet is mistakenly reconstructed as photon or a photon is radiated in a hadron decay. The number of events with a jet mis-reconstructed as a photon is measured in data using the ABCD method and compared to the expected number of events with a hadronic fake in order to obtain a data-driven scale factor. This scale factor is only valid in regions with a tightly identified and isolated photon.

7.2.1 Control regions

The definition of the regions is given in Table 14 and illustrated in Figure 21. It is exploited that the photon isolation and the photon ID variables measured in the first layer of the ECAL are only weakly correlated within a few percent. These variables are f_{side} , ΔE , E_{ratio} and ω_{s3} and called *narrow-strip* variables. If a photon passes the criteria on the narrow-strip variables, it fulfils the so called ID' requirement. Since the first layer of the ECAL is very finely granulated, only the inner core of the photon shower is measured by the narrow-strip variables resulting in the weak correlation to the isolation that takes into account energy deposits in the outer part of the shower. The group of the other ID variables R_{had} , R_{had1} , R_η , R_φ , ω_{s2} and $\omega_{s,\text{tot}}$ is referred to as *relaxed-tight*. Details about the photon ID variables can be found in Ref. [49]. For an event being classified in region A, its photon must pass the isolation criterion and the relaxed-tight criteria, but fails at least one criterion on the narrow-strip variables. An event is categorised in region B when its photon passes the relaxed-tight criteria, but fails both the isolation and the ID' criteria. In region C, events with a photon failing the isolation requirement, but passing both the relaxed-tight and narrow-strip criteria, i.e. this photon passes the nominal ID criteria. Region D is the SR of this analysis with photons being isolated and tightly identified. Consequently, no data in this region are used for the fake estimation.

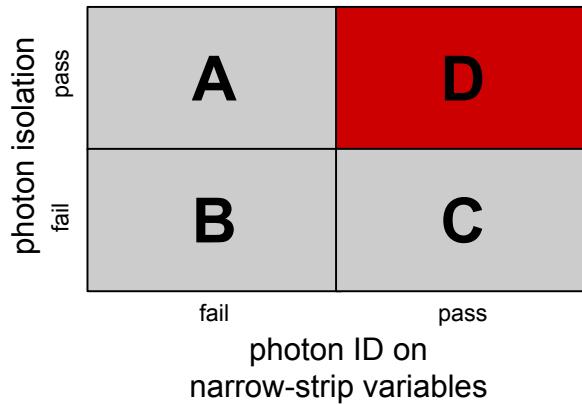


Figure 21: Sketch to illustrate the regions used in the ABCD method for the hadronic fake estimation. The horizontal axis represents the ID' criteria based on the narrow-strip variables, and the vertical axis represents the photon isolation requirement.

915 In Figure 22, the composition of events in dependence on the origin of the photon is shown for all regions.
 916 The event yields for hadronic fakes $N(i)^{h\text{-fake}}_{MC}$ found in simulation for each region $i = A, B, C, D$ are given
 917 in Table 17 and visualised in Figure 23.

Table 17: Expected number of events with a jet faking a photon in regions A, B, C, and D (SR) for the hadronic fake estimation, separately for the electron, muon and electron+muon channel. Only statistical uncertainty is shown.

	Electron channel	Muon channel	Electron+muon channel
$N(A)^{h\text{-fake}}_{MC}$	246 ± 42	239 ± 41	495 ± 58
$N(B)^{h\text{-fake}}_{MC}$	2187 ± 59	2177 ± 93	4360 ± 110
$N(C)^{h\text{-fake}}_{MC}$	1609 ± 36	1530 ± 48	3139 ± 59
$N(D)^{h\text{-fake}}_{MC}$	169 ± 13	134 ± 29	303 ± 32

918 7.2.2 ABCD method

919 The ABCD method is based on the assumption that two classes of variables are uncorrelated, or at least
 920 only weakly correlated. Here, for events with a photon faked by a hadron, denoted as $N(i)^{h\text{-fake}}$ in region
 921 $i = A, B, C, D$, the photon isolation and ID criteria on the narrow-strip variables are only weakly correlated
 922 of a few percent. Consequently, Equation (27) holds for events containing a photon faked by a hadron.

$$N(D)^{h\text{-fake}} \approx \frac{N(A)^{h\text{-fake}} \cdot N(C)^{h\text{-fake}}}{N(B)^{h\text{-fake}}} \quad (27)$$

923 As a closure test, the expected numbers of events with a hadronic fake are put in Equation (27). The
 924 expected ratios are shown in Table 18. It can be seen that the ratios agree within a standard deviation
 925 w.r.t to the statistical uncertainty, and the ratios of the different channels are compatible to each other.

Not reviewed, for internal circulation only

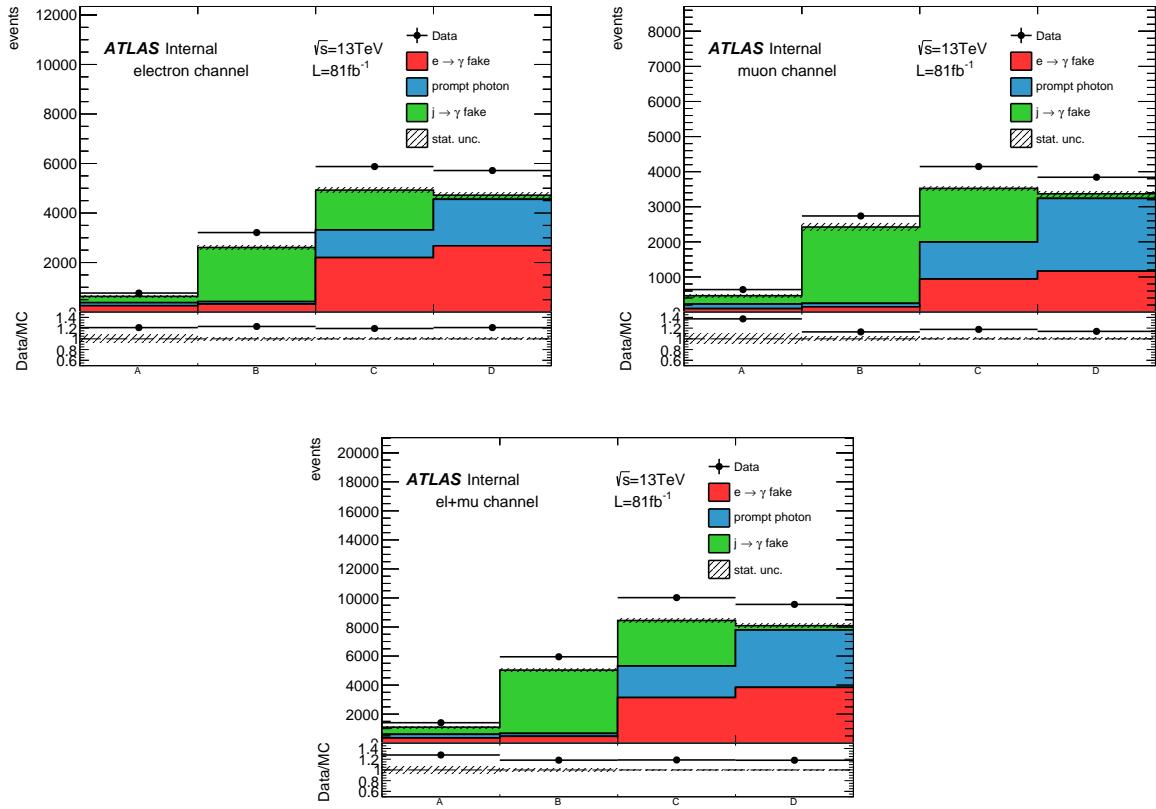


Figure 22: Plots of the observed and expected number of events in all regions in the ABCD method for the electron (top left), muon (top right) and the electron+muon channels (bottom). Only the statistical uncertainty is plotted.

926 The non-perfect closure is caused by imperfect simulation of fake photons in MC. In order to take this
 927 imperfection into account, a correction factor θ_{MC} is computed in simulation as given in Equation (28)
 928 and also listed in Table 18. To account for any imperfect MC modelling, a systematic uncertainty of 50 %
 929 is set on the correction factor.

$$\theta_{\text{MC}} = \frac{N(D)_{\text{MC}}^{\text{h-fake}} \cdot N(B)_{\text{MC}}^{\text{h-fake}}}{N(C)_{\text{MC}}^{\text{h-fake}} \cdot N(A)_{\text{MC}}^{\text{h-fake}}} \quad (28)$$

930 In data, the number of events with a hadronic fake $N(i)_{\text{data}}^{\text{h-fake}}$ in region $i = A, B, C$ is obtained by
 931 subtracting the contributions of events with an electron fake and of events with a prompt photon as given
 932 in Equation (29). The events with an electron fake are estimated by the expected number of events with
 933 an electron fake $N(i)_{\text{MC}}^{e \rightarrow \gamma}$ corrected by the scale factor $SF(e \rightarrow \gamma)$. As systematic uncertainty, the scale
 934 factor $SF(e \rightarrow \gamma)$ is varied up and down by one standard deviation and the maximal difference between
 935 the nominal and the up and down variations is taken as systematic uncertainty. The number of events
 936 with a prompt photon $N(i)_{\text{data}}^{\text{prompt-}\gamma}$ is estimated by multiplying the observed number of events $N(i)_{\text{data}}$ by
 937 the fraction of the expected number of events with a prompt photon $N(i)_{\text{MC}}^{\text{prompt-}\gamma}$ over the total expected

Not reviewed, for internal circulation only

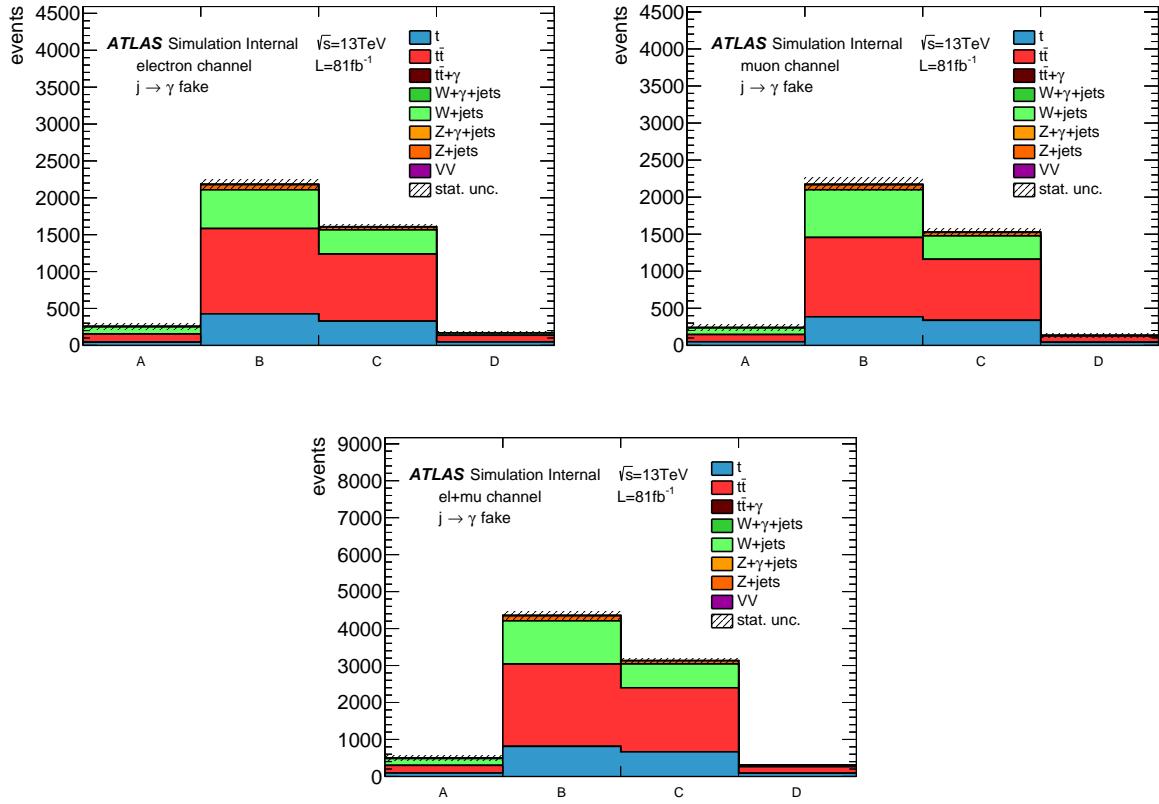


Figure 23: Plots of the expected number of events with an hadronic fake in all regions in the ABCD method for the electron (top left), muon (top right) and the electron+muon channels (bottom). Only the statistical uncertainty is plotted.

Table 18: Closure test and resulting correction factor θ_{MC} for all channels for the hadronic fake estimation using Equation (27). Only the statistical uncertainties are included

Channel	$\frac{N_{MC}^{h-fake}(A)}{N_{MC}^{h-fake}(B)} [\%]$	$\frac{N_{MC}^{h-fake}(D)}{N_{MC}^{h-fake}(C)} [\%]$	θ_{MC}
Electron channel	11.2 ± 1.9	10.50 ± 0.84	0.90 ± 0.16
Muon channel	11.0 ± 1.9	8.8 ± 1.9	0.80 ± 0.22
Electron+muon channel	11.4 ± 1.3	9.7 ± 1.0	0.85 ± 0.14

number of events $N(i)_{\text{MC}}^{\text{total}}$. As systematic uncertainty, the multiplication is replaced by direct subtraction of the expected number of events $N(i)_{\text{MC}}^{\text{prompt-}\gamma}$.

$$N(i)_{\text{data}}^{\text{h-fake}} = N(i)_{\text{data}}^{\text{total}} \cdot \left(1 - \frac{N(i)_{\text{MC}}^{\text{prompt-}\gamma}}{N(i)_{\text{MC}}^{\text{total}}} \right) - N(i)_{\text{MC}}^{e \rightarrow \gamma} \cdot SF(e \rightarrow \gamma) \quad \text{with } i = \text{A, B, C} \quad (29)$$

The number of events in data in region D is derived by using Equation (27) and the correction factor θ_{MC} as written in Equation (30). In Table 19, the events with a hadronic fake in all regions A, B, C and D determined in data are shown for all channels.

$$N(D)_{\text{data}}^{\text{h-fake}} = \frac{N(\text{A})_{\text{data}}^{\text{h-fake}} \cdot N(\text{C})_{\text{data}}^{\text{h-fake}}}{N(\text{B})_{\text{data}}^{\text{h-fake}}} \cdot \theta_{\text{MC}} \quad (30)$$

Table 19: Events in data with a hadronic fake in regions A, B, C, and D (SR) for all channels using Equations (29) and (30). Only the statistical uncertainty is shown.

	Electron channel	Muon channel	Electron+muon channel
$N(\text{A})_{\text{data}}^{\text{h-fake}}$	363 ± 32	364 ± 19	731 ± 37
$N(\text{B})_{\text{data}}^{\text{h-fake}}$	2766 ± 59	2479 ± 51	5246 ± 78
$N(\text{C})_{\text{data}}^{\text{h-fake}}$	2345 ± 95	1965 ± 47	4310 ± 110
$N(\text{D})_{\text{data}}^{\text{h-fake}}$	276 ± 58	231 ± 66	511 ± 87

The scale factor $SF(j \rightarrow \gamma)$ is defined as the ratio of the events with a hadronic fake determined in data over the events with a hadronic fake found in simulation as given in Equation (31).

$$SF(j \rightarrow \gamma) = \frac{N(D)_{\text{data}}^{\text{h-fake}}}{N(D)_{\text{MC}}^{\text{h-fake}}} \quad (31)$$

In Table 20, the data-driven hadron scale factor $SF(j \rightarrow \gamma)$ is shown for all three channels with statistical and systematic uncertainty. The systematic uncertainty due to the correction factor is the dominant uncertainty on the scale factor. In each channel, the very same scale factor is obtained and the systematic uncertainty dominates over the statistical one. In the further analysis, the scale factor determined in the electron+muon channel is exclusively used, unless stated otherwise.

7.2.3 Distributions in control regions

In order to validate the hadronic scale factor, the distributions of the photon p_T , isolation and ID variables are looked at in the HFR regions B and C. For both regions, the isolation requirements are dropped. For the HFR region B, the ID requirements must be failed, and for HFR region C, the ID' requirements must be fulfilled. In Figure 24, the photon p_T and isolation variables are shown after applying the hadronic

Table 20: Hadron scale factor $SF(j \rightarrow \gamma)$ determined in data for all three channels. Both statistical and systematic uncertainties are shown.

	Electron channel	Muon channel	Electron+muon channel
$SF(j \rightarrow \gamma)$ (stat. + syst.)	$1.63 \pm 0.36 \pm 0.86$	$1.72 \pm 0.61 \pm 0.95$	$1.69 \pm 0.33 \pm 0.96$

Not reviewed, for internal circulation only

955 scale factor. The photon ID variables after applying the hadronic scale factor are shown in Figures 25,
956 26, 27, and 28. Only the statistical and the uncertainty on the hadronic scale factor are included. It can
957 be seen that the data and MC already agree within those uncertainties.

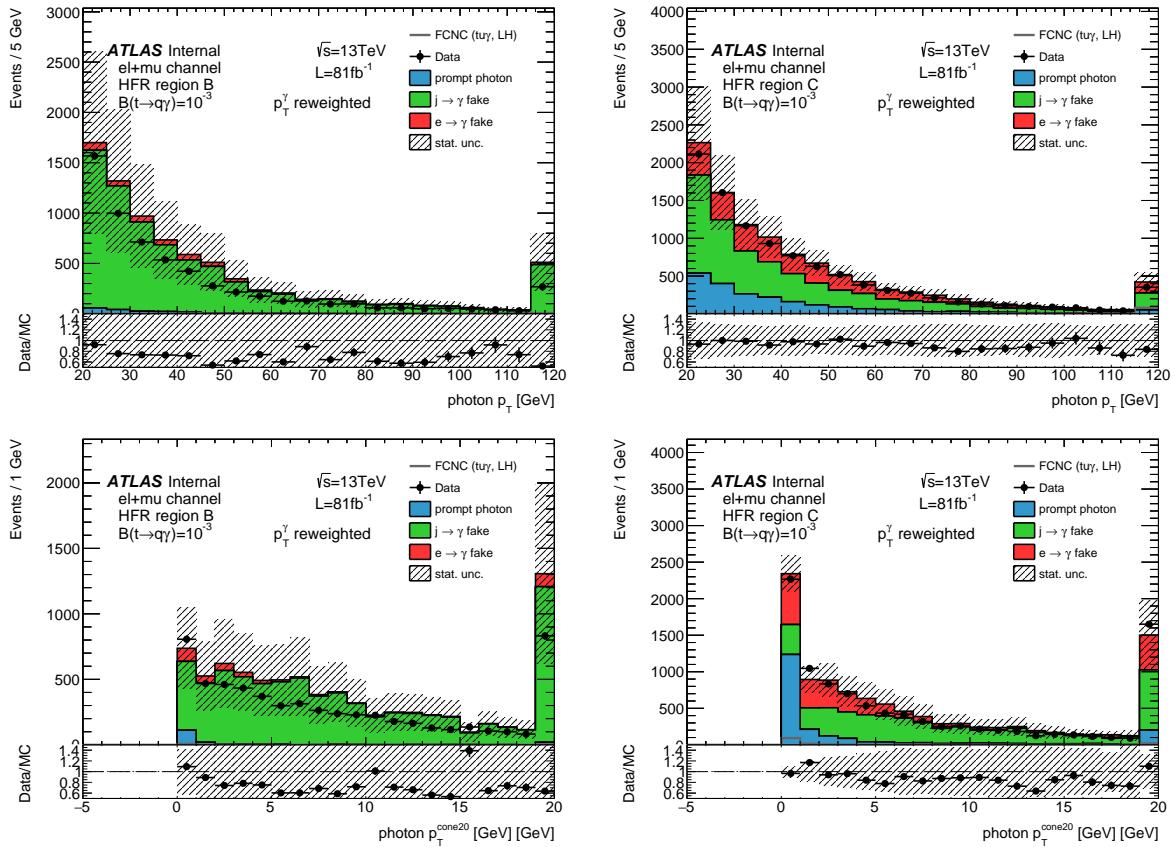


Figure 24: Distributions of different kinematic variables in the HFR region B (left) and HFR region C (right): photon p_T (top), and photon isolation variable $p_T^{\text{cone}20}$ (bottom). Only the statistical uncertainty and the uncertainty for the scale factor $SF(j \rightarrow \gamma)$ are shown and the over- and underflow bins are plotted.

Not reviewed, for internal circulation only

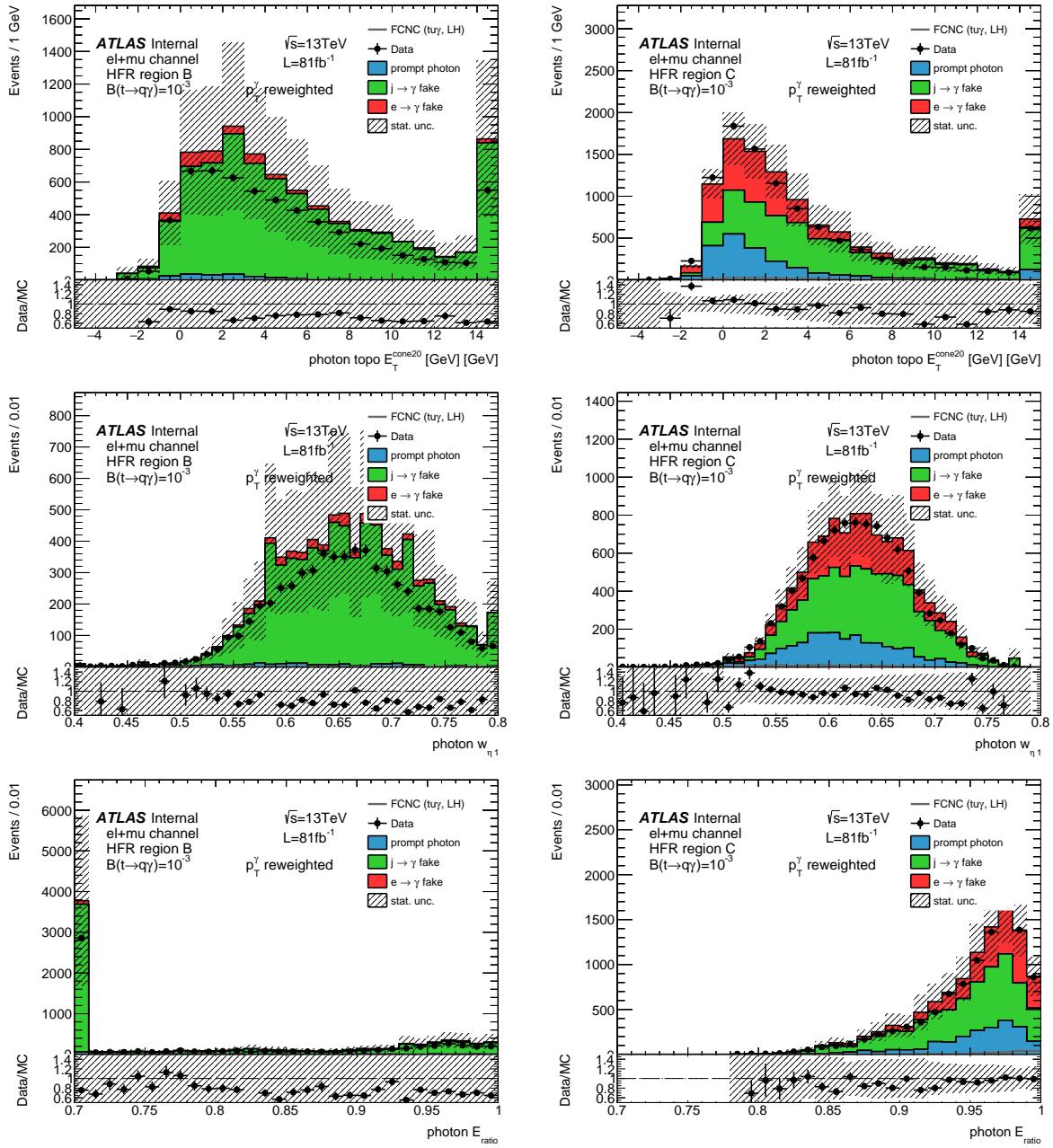


Figure 25: Distributions of the photon ID variables in the HFR region B (left) and HFR region C (right): photon isolation variable topo $E_T^{\text{cone}20}$ (top), ω_{s3} (middle), and E_{ratio} (bottom). Only the statistical uncertainty and the uncertainty for the scale factor $SF(j \rightarrow \gamma)$ are shown and the over- and underflow bins are plotted.

Not reviewed, for internal circulation only

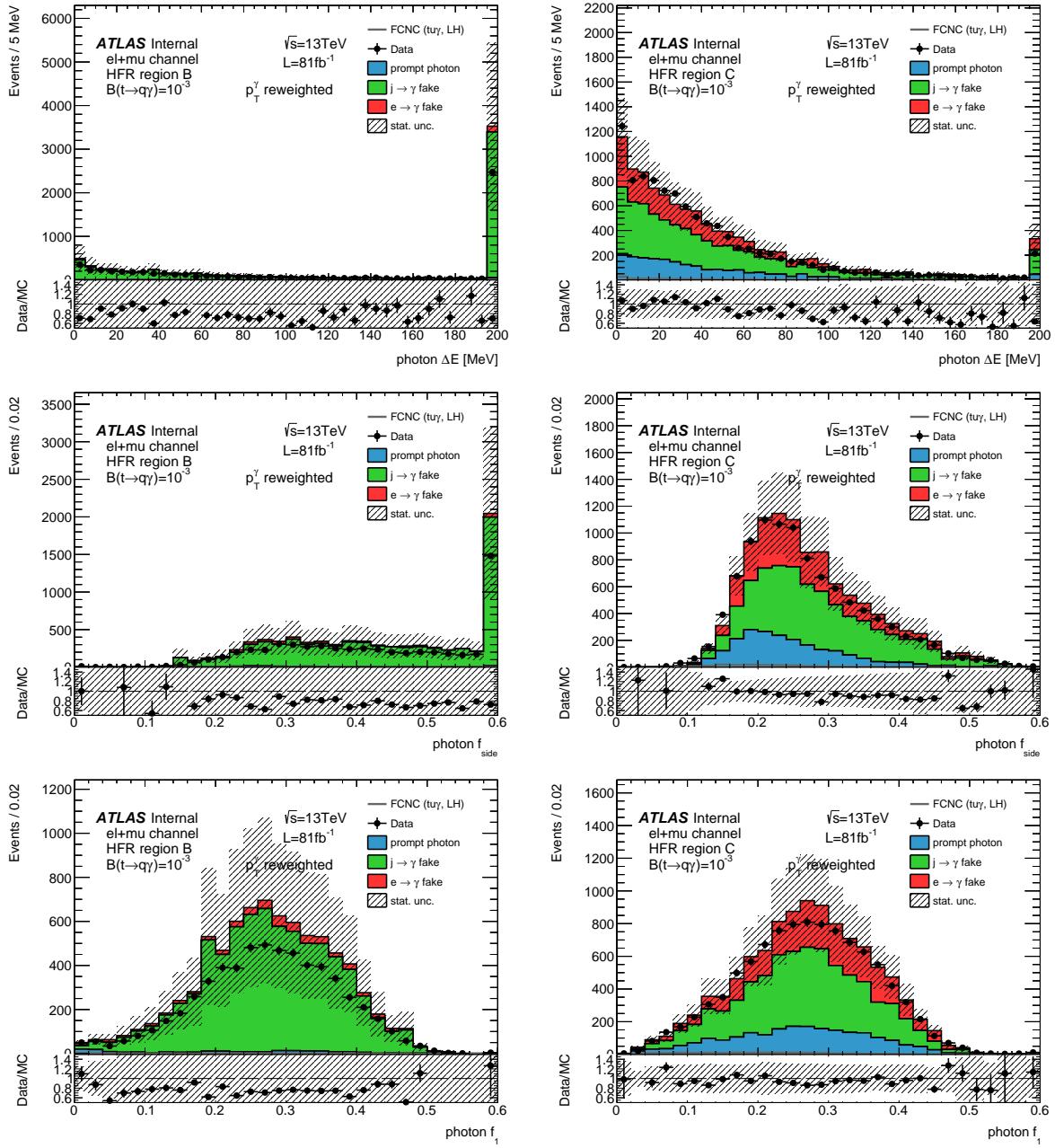


Figure 26: Distributions of the photon ID variables in the HFR region B (left) and HFR region C (right): ΔE (top), f_{side} (middle), and f_1 (bottom). Only the statistical uncertainty and the uncertainty for the scale factor $SF(j \rightarrow \gamma)$ are shown and the over- and underflow bins are plotted.

Not reviewed, for internal circulation only

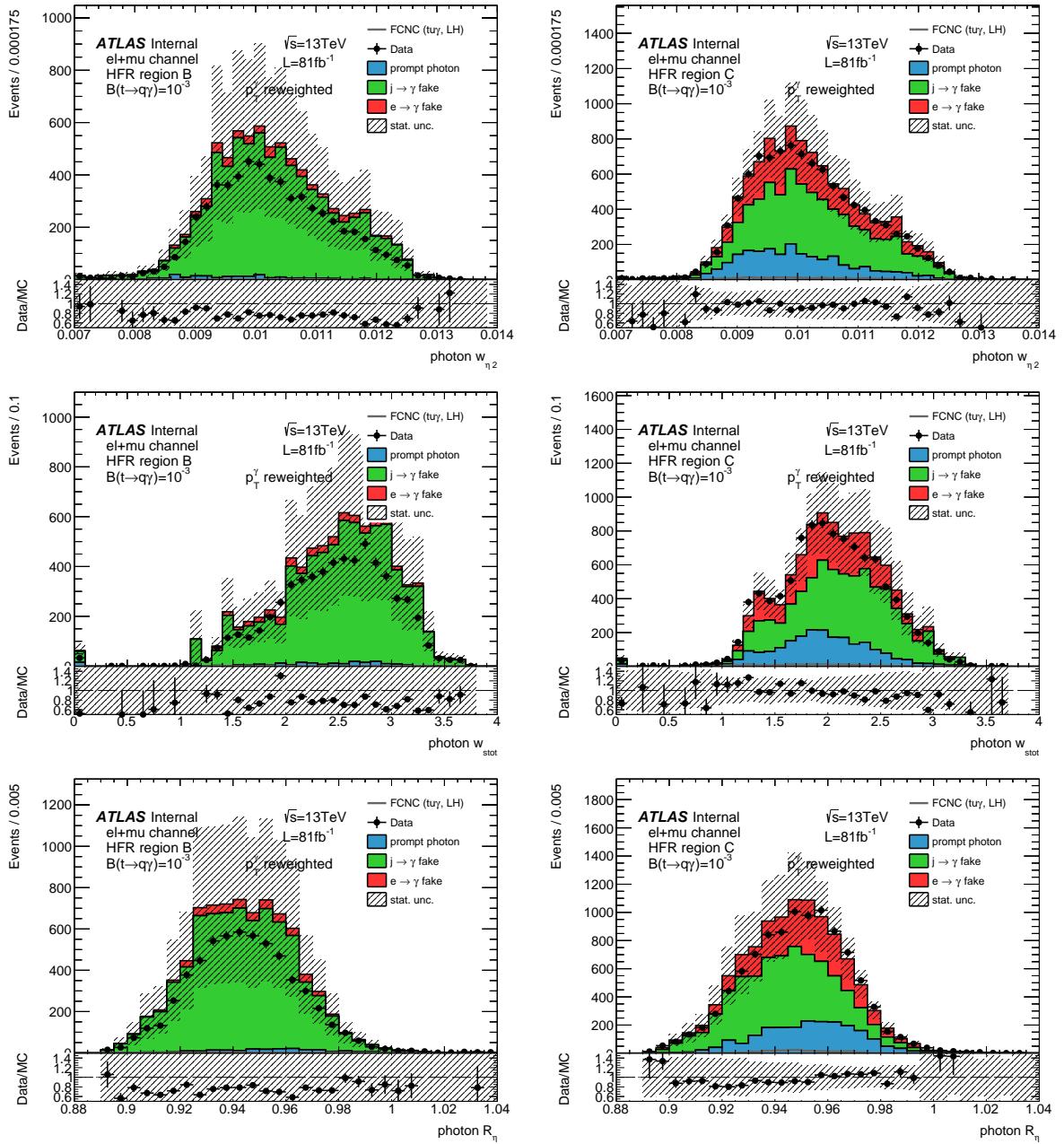


Figure 27: Distributions of the photon ID variables in the HFR region B (left) and HFR region C (right): $\omega_{\eta 2}$ (top), $\omega_{s,\text{tot}}$ (middle), and R_η (bottom). Only the statistical uncertainty and the uncertainty for the scale factor $SF(j \rightarrow \gamma)$ are shown and the over- and underflow bins are plotted.

Not reviewed, for internal circulation only

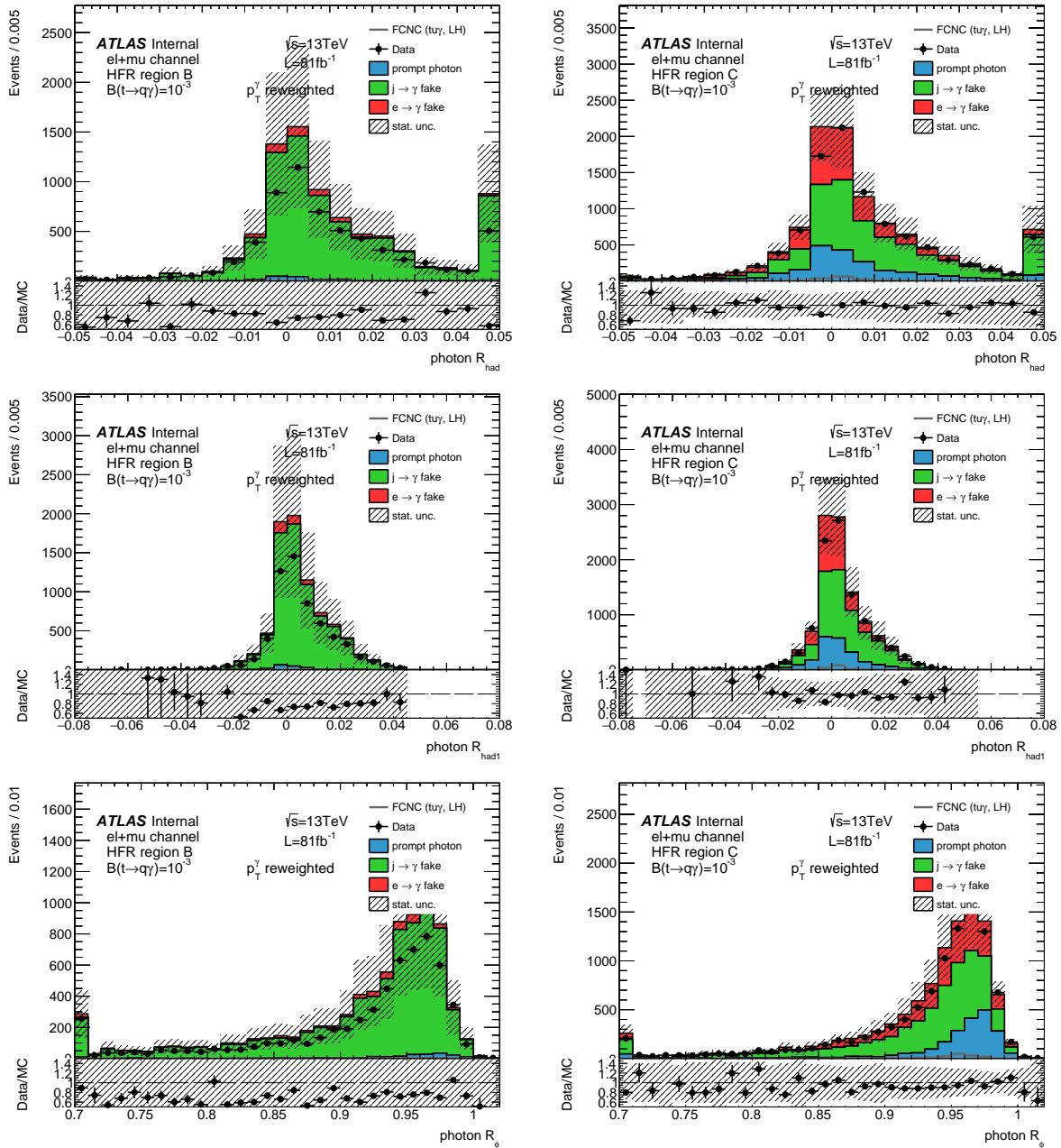


Figure 28: Distributions of the photon ID variables in the HFR region B (left) and HFR region C (right): R_{had} (top), $R_{\text{had}1}$ (middle), and R_φ (bottom). Only the statistical uncertainty and the uncertainty for the scale factor $SF(j \rightarrow \gamma)$ are shown and the over- and underflow bins are plotted.

958 7.2.4 Validation of $SF(j \rightarrow \gamma)$

959 The hadron-to-photon scale factor $SF(j \rightarrow \gamma)$ is validated in the combined background VR as defined in
960 Table 14. This region contains a tightly identified and isolated photon and a higher jet multiplicity than
961 the SR which the scale factor is actually exclusively determined for. However, this region is assumed to
962 be close enough to the SR to serve as validation region. Tables and plots are shown in Section 10.9.2 after
963 the statistical fit is performed.

Not reviewed, for internal circulation only

964 8 Separation of signal from background events

965 In order to distinguish between signal and background events, a multivariate method is used. Since this
 966 analysis focuses on top quarks singly produced associated with a photon, only signal from the production
 967 mode is considered in the evaluation of a separation. In this analysis, a neural network is built to
 968 construct a discriminating variable for the later analysis step. This variable ranges from 0 to 1. Signal
 969 events accumulate at 1, while background events obtain values close to zero. In the following, the input
 970 variables, the architecture for the neural network, its training and validation and the output distribution
 971 are described. In total, four different networks are trained accounting for the four types of coupling of the
 972 signal. All studies are done in the combined electron+muon channel.

973 8.1 Input variables

974 As input, 12 different variables are studied in detail¹²¹³. They describe either properties of the reconstructed
 975 physics objects or event variables and are categorised as follows:

976 **properties of physics objects** $p_T(\gamma)$, $p_T(\ell)$, lepton charge, $p_T(\text{jet})$, E_T^{miss}

977 **event variables** $m(\ell, \gamma)$, $m(\ell, \text{jet})$, $m_T(W)$, $\Delta R(\text{jet}, \ell)$, $\Delta R(\text{jet}, \gamma)$, $\Delta R(\gamma, \ell)$, H_T (sum of all reconstructed
 978 object's p_T).

979 In Table 21, the variables are ranked by their separation power S computed by

$$S = \sum_i^{N_{\text{bins}}} \frac{(s_i - b_i)^2}{s_i + b_i}. \quad (32)$$

980 Hereby, the value $s_i = N_i^s / N_{\text{total}}^s$ ($b_i = N_i^b / N_{\text{total}}^b$) is the fraction of the number of expected signal
 981 (background) events N_i^s (N_i^b) in bin i over the total number of expected signal (background) events N_{total}^s
 982 (N_{total}^b).

983 Generally, the separation depends on the up-type quark being present: for both $t\gamma\gamma$ couplings, the
 984 separation for all variables is mostly higher than that of $t\gamma\gamma$ coupling since such events tends to be more
 985 energetic. For all four signal samples, the photon p_T , the invariant mass $m(\ell\gamma)$, and the sum of all
 986 reconstructed physics objects H_T come along with the highest separation. The separation power of the
 987 remaining variables shows dependencies on the type of coupling. In the case of left-handed couplings, the
 988 distance $\Delta R(\gamma, \ell)$ is important since the particles fly back-to-back. Furthermore, couple of variables show
 989 dependencies on the involved up-type quark. E.g. when an up quark is involved, the lepton charge gives
 990 some separation power between signal and background, while it is not the case for the coupling involving
 991 a charm quark.

¹² More variables were tested, but no improvement was found.

¹³ Note that the photon p_T reweighting is not considered in the training of the neural network.

Table 21: Input variables for the neural network with its separation power S including the statistical uncertainty and ranking for all four signal couplings.

Variable	$t\gamma$, LH		$t\gamma$, RH		$t\gamma$, LH		$t\gamma$, RH	
	S [%]	rank						
$p_T(\gamma)$	62 ± 16	(1)	61 ± 16	(1)	52 ± 15	(1)	50 ± 15	(1)
$m(\ell, \gamma)$	49 ± 17	(2)	36 ± 17	(3)	41 ± 17	(2)	24 ± 14	(3)
H_T	40 ± 20	(3)	40 ± 20	(2)	29 ± 17	(3)	27 ± 17	(2)
$\Delta R(\text{jet}, \ell)$	32 ± 17	(4)	22 ± 16	(4)	25 ± 15	(4)	14 ± 13	(5)
$\Delta R(\gamma, \ell)$	22 ± 15	(5)	6.1 ± 9.2	(11)	19 ± 13	(5)	3.3 ± 7.2	(10)
$m(\ell, \text{jet})$	15 ± 13	(6)	15 ± 12	(5)	16 ± 13	(6)	16 ± 12	(4)
$m_T(W)$	10 ± 13	(7)	10 ± 13	(10)	9.5 ± 13	(7)	8.0 ± 11	(7)
$p_T(\ell)$	10 ± 11	(8)	1.2 ± 5.0	(12)	4.6 ± 7.9	(8)	0.5 ± 3.3	(11)
Lepton charge	9.8 ± 5.4	(9)	10.4 ± 5.8	(9)	< 0.1 ± < 0.0	(12)	< 0.1 ± 0.2	(12)
E_T^{miss}	7.5 ± 8.8	(10)	11 ± 11	(7)	3.9 ± 6.7	(9)	5.3 ± 7.4	(9)
$\Delta R(\text{jet}, \gamma)$	5.2 ± 9.3	(11)	13 ± 13	(6)	3.6 ± 8.2	(10)	9.2 ± 11	(6)
$p_T(\text{jet})$	3.8 ± 7.3	(12)	11 ± 12	(7)	1.3 ± 4.4	(11)	5.5 ± 8.4	(8)

Not reviewed, for internal circulation only

992 The shapes of possible input variables are shown in Figures 29 and 30 for signal (here: $t\gamma$, left-handed
993 coupling) and background events. The integral of each distributions equals to unity. The numbers of
994 MC events in the signal and background samples are also shown. It can be seen that all these variables
995 have a good separation power between signal and background. The plots for the input variables for the
996 other signal couplings can be found in Appendix L. In Section 10.9.1, the data-MC agreement for the
997 input variables is shown after the statistical fit. The correlation coefficients of all variables to each other
998 for the signal samples in the production mode are depicted in Figure 31, and for the signal in the decay
999 mode and the background samples in Figure 32. In Appendix M, the comparison of the average of
1000 each input variable against every other input variable between data and simulation is shown in the CR
1001 $W+\gamma+\text{jets}$ whose definition is given in Section 6.3. It can be found that the correlations are well modelled
1002 in simulation.

Not reviewed, for internal circulation only

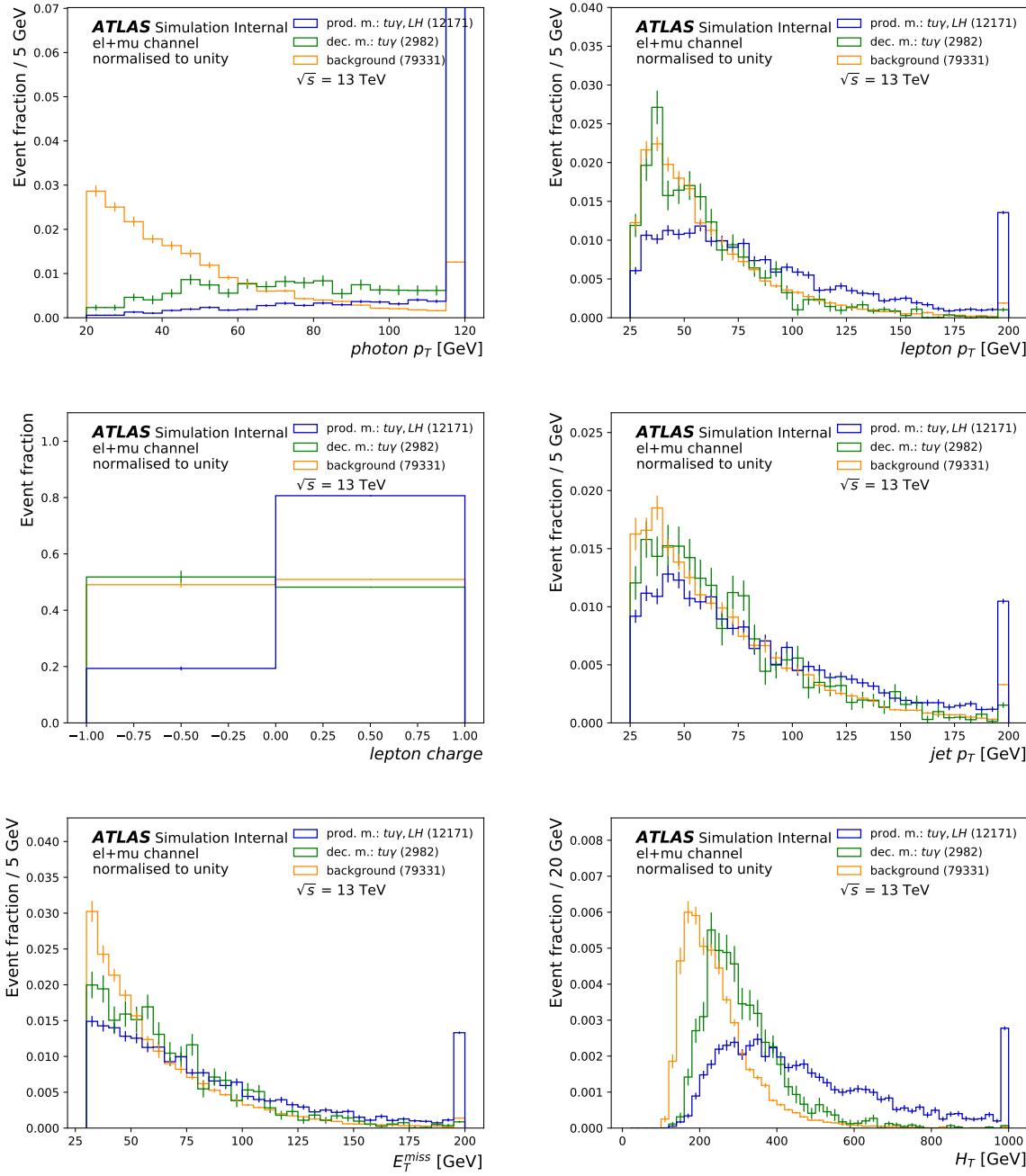


Figure 29: Comparison of shapes of kinematic distributions between signal (here: *tuy*, left-handed coupling) and background in the SR: photon p_T spectrum (top left), lepton p_T spectrum (top right), lepton charge (middle left), jet p_T spectrum (middle right), missing transverse momentum E_T^{miss} (bottom left), and H_T (bottom right). The number of MC events in the signal and background samples and the over- and underflow bins are also shown. Only the statistical uncertainty is shown.

Not reviewed, for internal circulation only

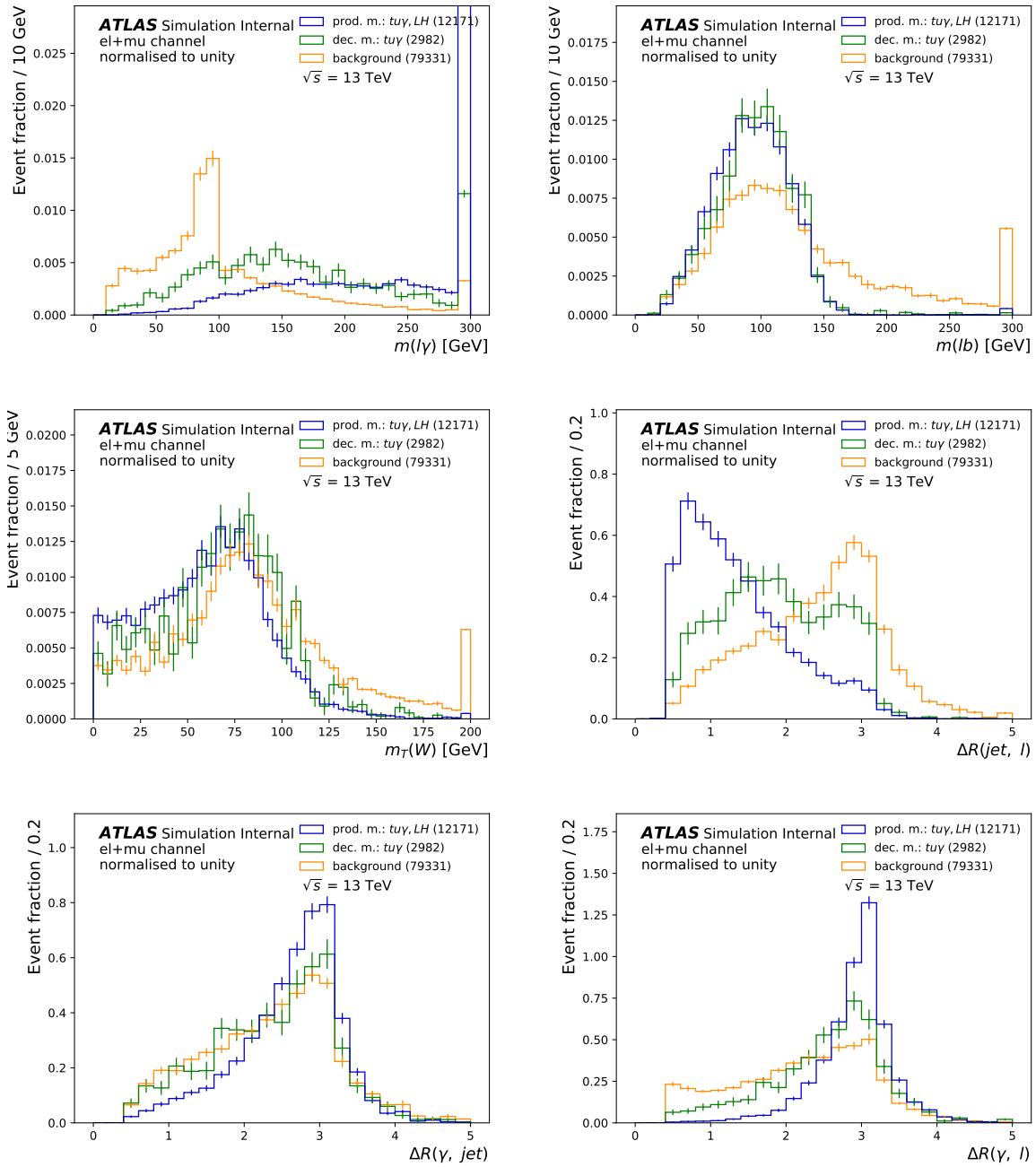


Figure 30: Comparison of shapes of kinematic distributions between signal (here: *tuy*, left-handed coupling) and background in the SR: invariant mass of the lepton and photon $m(\ell, \gamma)$ (top left), invariant mass of the lepton and b -jet $m(\ell, b\text{-jet})$ (top right), the transverse mass of the W boson $m_T(W)$ (middle left), distance ΔR between the b -jet and lepton (middle right), distance ΔR between the b -jet and photon (bottom left), and distance ΔR between the lepton and photon (bottom right). The number of MC events in the signal and background samples and the over- and underflow bins are also shown. Only the statistical uncertainty is shown.

Not reviewed, for internal circulation only

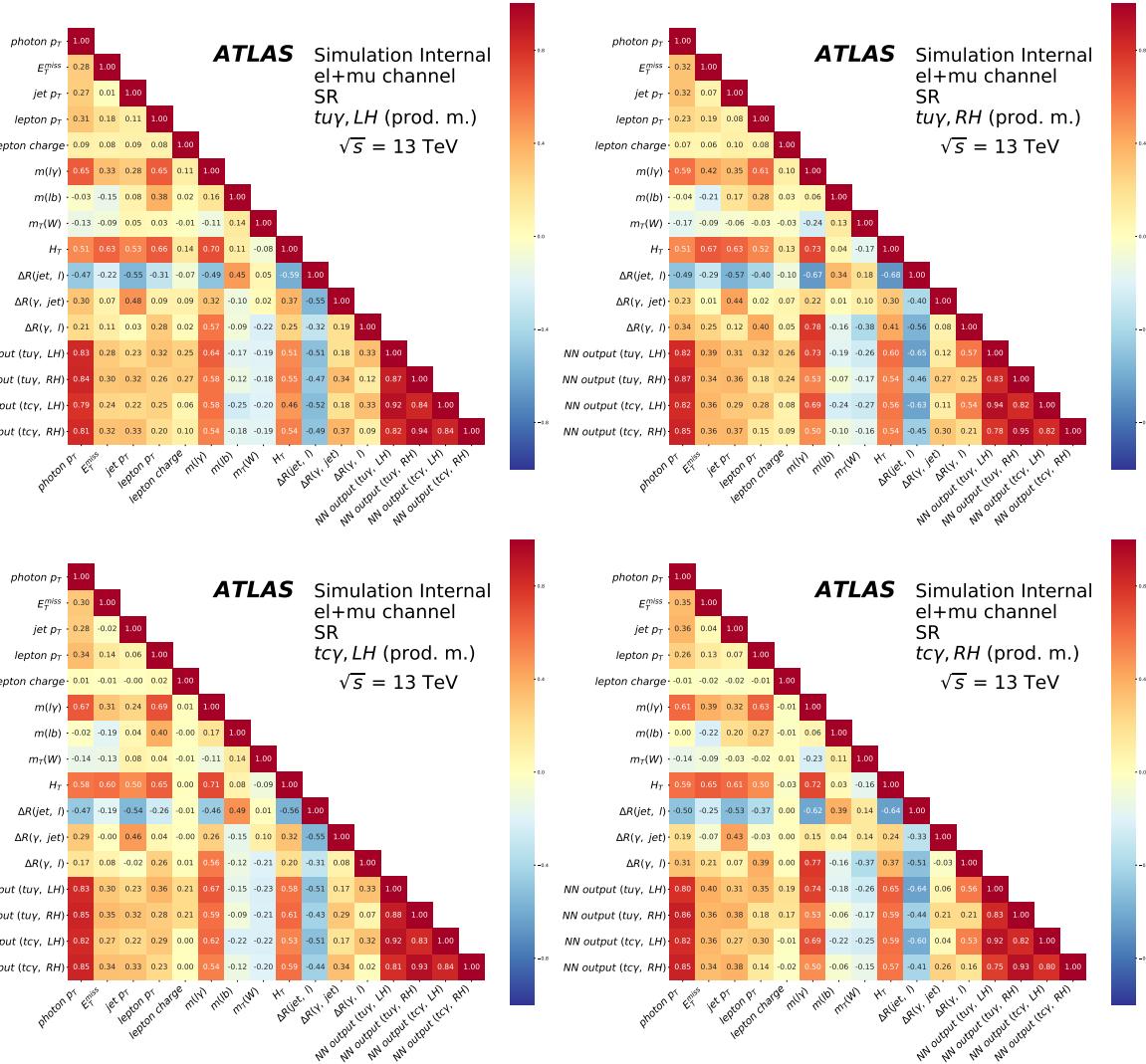


Figure 31: Visualisation of the correlation coefficients of all input variables and the output of the neural networks to each other for all signal couplings in the production mode in the SR.

Not reviewed, for internal circulation only

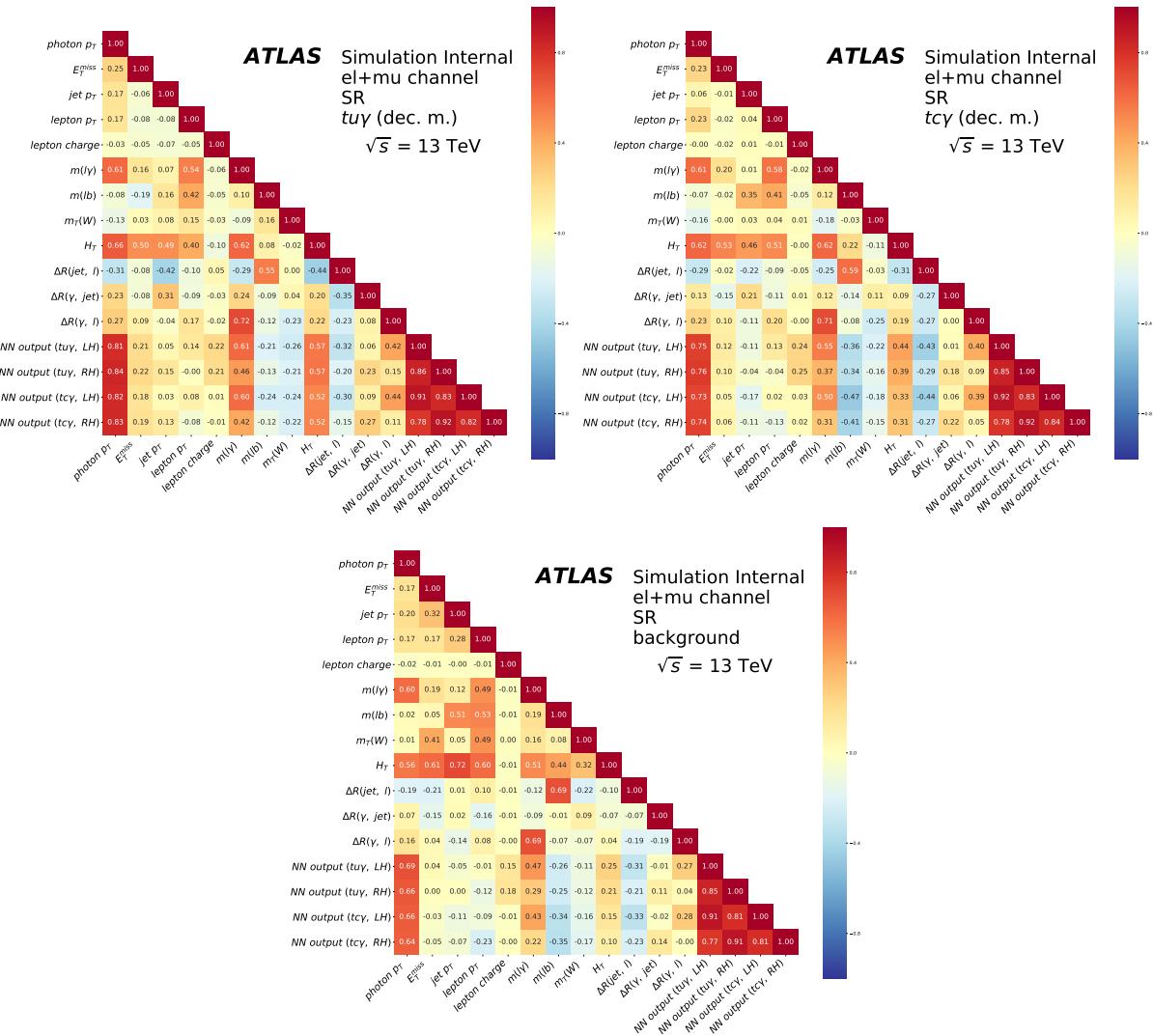


Figure 32: Visualisation of the correlation coefficients of all input variables and the output of the neural networks to each other for all signal couplings in the decay mode (top) and the background (bottom) in the SR.

1003 **8.2 Architecture of neural network**

1004 As neural network implementation, the TensorFlow system [64] implemented in Keras [65] is used.
 1005 Different architectures are tested. The tested neural network consists either of three or four layers: one
 1006 input layer where the input variables are fed in, one or two hidden layer/s and one output layer. The input
 1007 layer has n nodes with n equal to the number of input variables. The first hidden layer is composed of
 1008 $n + 1$ nodes referring to the number of input variables plus a bias node. The potential second hidden layer
 1009 consists of $n + 1$ nodes. The output layer consists of a single node. Each node in a layer is connected to
 1010 all nodes of the previous and next layer. Every connection is assigned a weight that is optimised in the
 1011 training. For every node, an output value is computed using the weights and input values of the previous
 1012 node by an activation function. This value indicates how 'activated' or 'important' it is. As activation
 1013 function in the input and hidden layers, the Rectified Linear Unit activation function $R(x)$ is in use that is
 1014 defined as follows:

$$R(x) = \begin{cases} x, & \text{if } x \geq 0 \\ 0, & \text{if } x < 0. \end{cases} \quad (33)$$

1015 For the output layer, the sigmoid function $\sigma(x)$ is used as activation function:

$$\sigma(x) = \frac{1}{1 + e^{-x}}. \quad (34)$$

1016 As optimiser that updates the weight of a node, the Adam algorithm [66] is used. It follows the steepest
 1017 gradient to reach the minimum of the parameter of interest called loss function. In this neural network,
 1018 the binary cross entropy is minimised that considers the true label $p(i)$ and the estimate $q(i)$ for each
 1019 event i :

$$loss = - \sum_i^{N_{\text{events}}} \left[p(i) \log q(i) + (1 - p(i)) \log (1 - q(i)) \right]. \quad (35)$$

1020 The cross entropy assigns small values for correctly assigned events, but punishes wrongly assigned
 1021 events.

1022 **8.3 Training and validation**

1023 Before the input variables are fed into the network, they are preprocessed. Therefore, the RobustScaler
 1024 implemented in scikit-learn [67] is used which is robust against outliers. It transforms each variable
 1025 x as given by the following equation:

$$z = \frac{x - m}{q_3 - q_1}, \quad (36)$$

1026 where m is the median of the distribution of the variable and q_1 (q_3) is the first (third) quartile. Thus, the
 1027 preprocessed distributions are centred around zero.

1028 The number of MC events in the signal¹⁴ and background samples are given in Table 22 for the training
 1029 and test set. The training set is used in the training of the neural network and contains 80 % of all MC
 1030 events, while the test set is used after the training to check the output of the network containing 20 % of
 1031 all MC events.

Table 22: Number of MC events for the four signal samples and the background samples used in the training and for testing.

Samples	Training set	Test set
Signal $t\gamma$, LH	9 737	2 434
Signal $t\gamma$, RH	7 958	1 989
Signal $t\gamma$, LH	13 142	3 285
Signal $t\gamma$, RH	10 870	2 717
Background	63 465	15 866

1032 Further parameters of the training are the learning rate, the number of epochs and the batch size. The
 1033 learning rate limits the step size a weight may be changed. The number of epochs states how many iterations
 1034 with the full training set are done. The batch size is the number of MC events that are simultaneously
 1035 used in the training. After each batch, the weights are updated. These hyper-parameters are optimised in
 1036 a grid search where the neural network is trained with different combinations of hyper-parameter values.
 1037 The performance of the network is estimated by the accuracy *accur* as defined as follows:

$$\text{accur} = \frac{N(\text{NN output} \geq 0.5|\text{signal}) + N(\text{NN output} < 0.5|\text{background})}{N(\text{signal}) + N(\text{background})}. \quad (37)$$

1038 Here, the number $N(\text{NN output} \geq 0.5|\text{signal})$ ($N(\text{NN output} < 0.5|\text{background})$) is the number of sig-
 1039 nal (background) MC events classified as signal (background) by the neural network and $N(\text{signal})$
 1040 ($N(\text{background})$) is the number of all signal (background) MC events. Hereby, a default cut on the output
 1041 of 0.5 is assumed.

1042 To avoid overtraining, a 3-fold cross validation is done: the training set is randomly split into three
 1043 independent sets. Then, two sets are used for the training and the third one is used to compute the
 1044 performance of the trained neural network.

1045 8.4 Optimal number of input variables and hidden layers

1046 Different numbers of input variables and numbers of hidden layers are tested and compared to each other.
 1047 The following four scenarios are presented here:

1048 **scenario 1** all 12 input variables are used with one hidden layer;

¹⁴ The different numbers of MC events for signal are caused by the different total number of simulated events in the MC samples.

Not reviewed, for internal circulation only

- 1049 **scenario 2** all 12 input variables are used with two hidden layers;
 1050 **scenario 3** 10 input variables are used with one hidden layer;
 1051 **scenario 4** 10 input variables are used with two hidden layers.

1052 For the subset of 10 input variables, the variables H_T and $m_W(T)$ are removed. The variable H_T is highly
 1053 correlated to the single transverse momentum of the different reconstructed physics objects. The variable
 1054 $m_W(T)$ gives not enough information to help separating signal from background as the main background
 1055 also contains a W boson. For each scenario, the hyper-parameters are optimised in the grid search. The
 1056 *Receiver Operating Characteristic* (ROC) curves are shown in Figure 33 for each coupling as well as the
 1057 *Area Under Curve* (AUC). The ROC curve shows the value ($1 - \text{background efficiency}$) versus the signal
 1058 efficiency, while the AUC is a measure of how close the result is to the optimal area of unity. In Table 23,
 1059 the AUC and separation power S of the test dataset are given for all scenarios and couplings. Generally
 1060 for each coupling, the AUC and the separation power only show small fluctuations between the scenarios.
 1061 Therefore, scenario 4 with the minimal set of variables and two hidden layers is taken as baseline in the
 1062 further analysis.

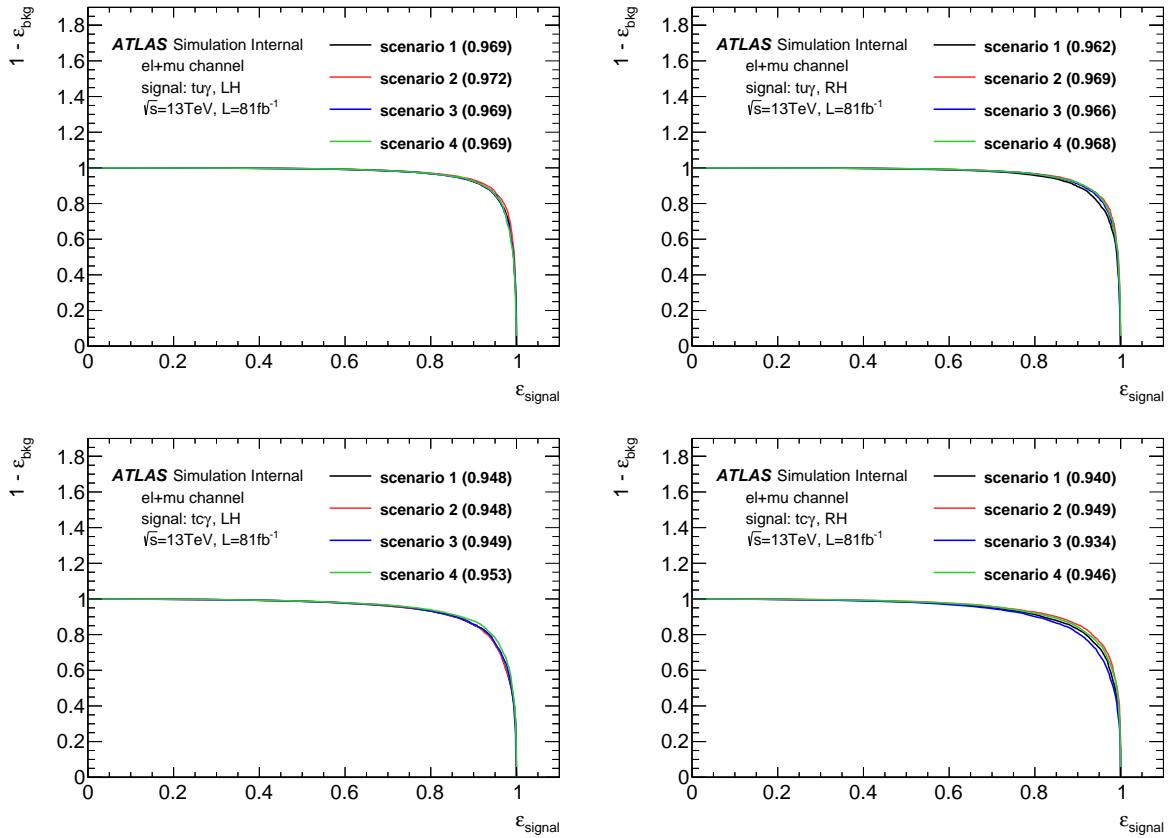


Figure 33: ROC curves and AUC for the four scenarios for each signal coupling: left-handed tuy coupling (top left), right-handed tuy coupling (top right), left-handed $tc\gamma$ coupling (bottom left), and right-handed $tc\gamma$ coupling (bottom right).

Table 23: AUC and separation power S of the test dataset for all four scenarios tested for each coupling.

Scenario	$t\gamma$, LH		$t\gamma$, RH	
	AUC	S [%]	AUC	S [%]
1	0.969	74.4 ± 1.9	0.962	65.2 ± 2.0
2	0.972	75.6 ± 1.9	0.969	67.8 ± 2.0
3	0.969	74.5 ± 1.9	0.966	66.5 ± 2.0
4	0.969	73.7 ± 1.9	0.968	67.4 ± 2.0

Scenario	$t\gamma$, LH		$t\gamma$, RH	
	AUC	S [%]	AUC	S [%]
1	0.948	65.8 ± 1.6	0.940	61.3 ± 1.6
2	0.948	66.7 ± 1.6	0.949	64.0 ± 1.6
3	0.949	66.7 ± 1.6	0.934	59.3 ± 1.6
4	0.953	68.7 ± 1.6	0.946	63.0 ± 1.6

Not reviewed, for internal circulation only

¹⁰⁶³ The best combination of hyper-parameters for scenario 4 for the different signal couplings is listed in
¹⁰⁶⁴ Table 24.

Table 24: Best combination of hyper-parameters for the different signal samples.

Hyper-parameter	$t\gamma$ LH	$t\gamma$ RH	$t\gamma$ LH	$t\gamma$ RH
Learning rate	0.001	0.001	0.001	0.001
Number of epochs	30	50	45	25
Batch size	200	300	200	200

¹⁰⁶⁵ The loss function for scenario 4 for each training with a different coupling is depicted in Figure 34. The
¹⁰⁶⁶ accuracy of this training is shown in Figure 35. Both quantities show an increasing (decreasing) behaviour
¹⁰⁶⁷ as expected.

Not reviewed, for internal circulation only

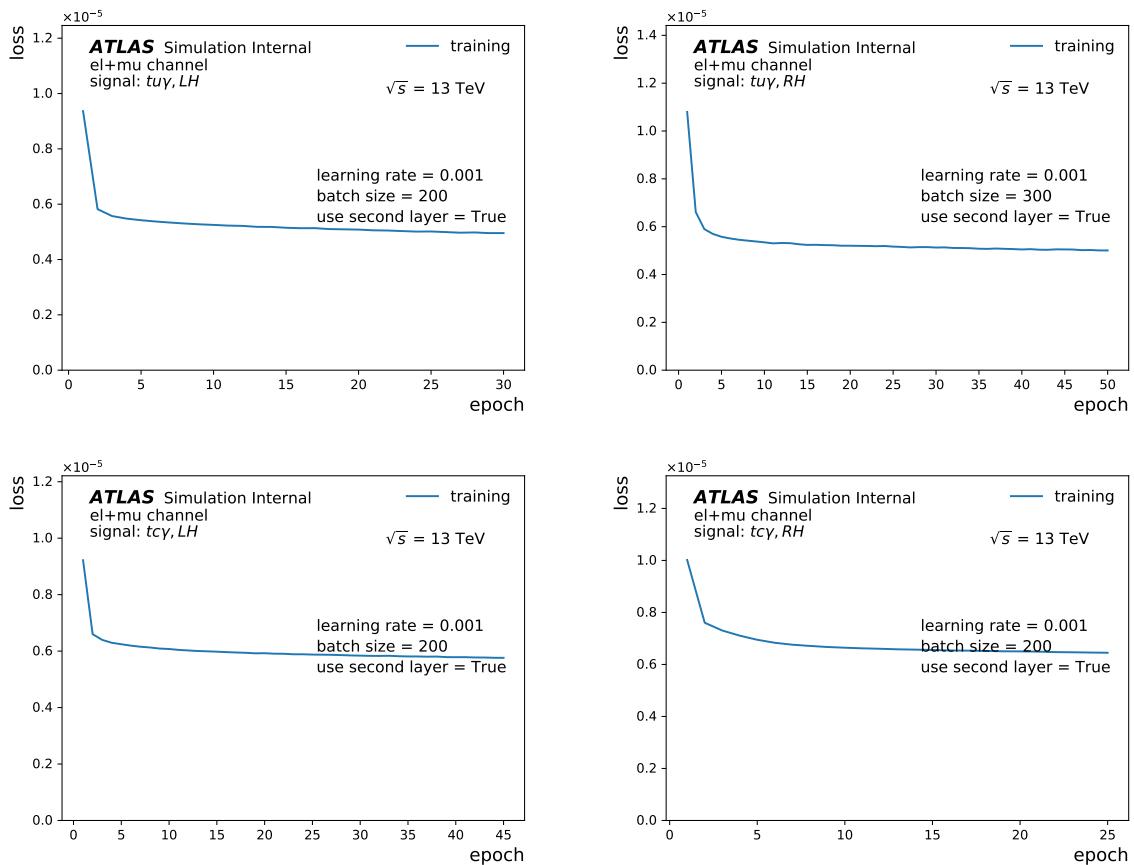


Figure 34: Loss functions for the different signal samples: FCNC sample with left-handed tuy coupling (top left), FCNC sample with right-handed tuy coupling (top right), FCNC sample with left-handed $tc\gamma$ coupling (bottom left), and FCNC sample with right-handed $tc\gamma$ coupling (bottom right).

Not reviewed, for internal circulation only

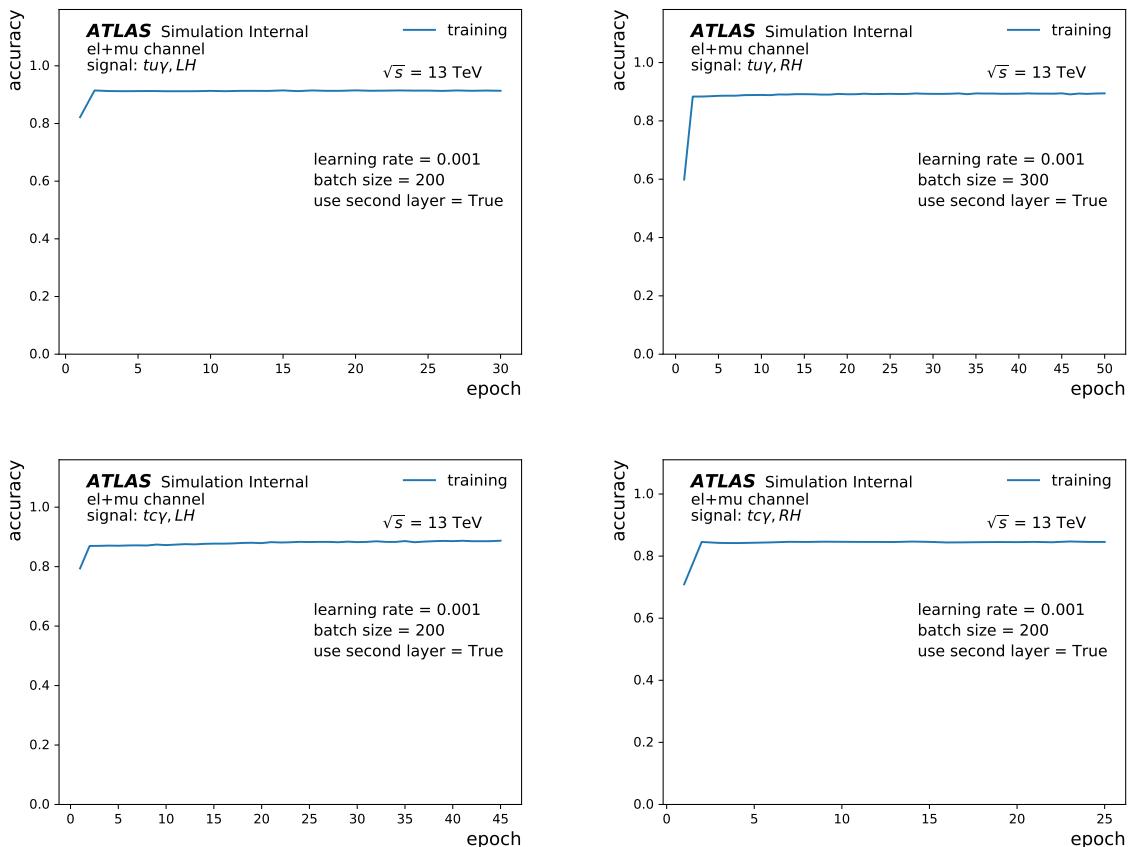


Figure 35: Accuracy A for the different signal samples: FCNC sample with left-handed $t\gamma y$ coupling (top left), FCNC sample with right-handed $t\gamma y$ coupling (top right), FCNC sample with left-handed $t c\gamma$ coupling (bottom left), and FCNC sample with right-handed $t c\gamma$ coupling (bottom right).

1068 8.5 Output of neural network

1069 The output distributions of the neural network for scenario 4 are shown for the training and test sets and
 1070 the different couplings in Figures 36 and 37. It can be seen that output distributions for both the training
 1071 and test set agree with each other for each training. The separation power for the distributions are given
 1072 in Table 23. Compared to the highest separation of the input variable being the photon p_T in Table 21,
 1073 the separation of the output distribution increased by more than 10 percentage points for each coupling.
 1074 In Figure 38, the output distributions obtained in the CR $W+\gamma+jets$ by the neural network trained for
 1075 the different signal samples are shown. In Appendix N.1, the NN output distributions in the SR for the
 1076 different couplings are shown separated by lepton flavour. In Appendix N.2, the impact of the photon p_T
 1077 reweighting on the NN output distribution is illustrated.

Not reviewed, for internal circulation only

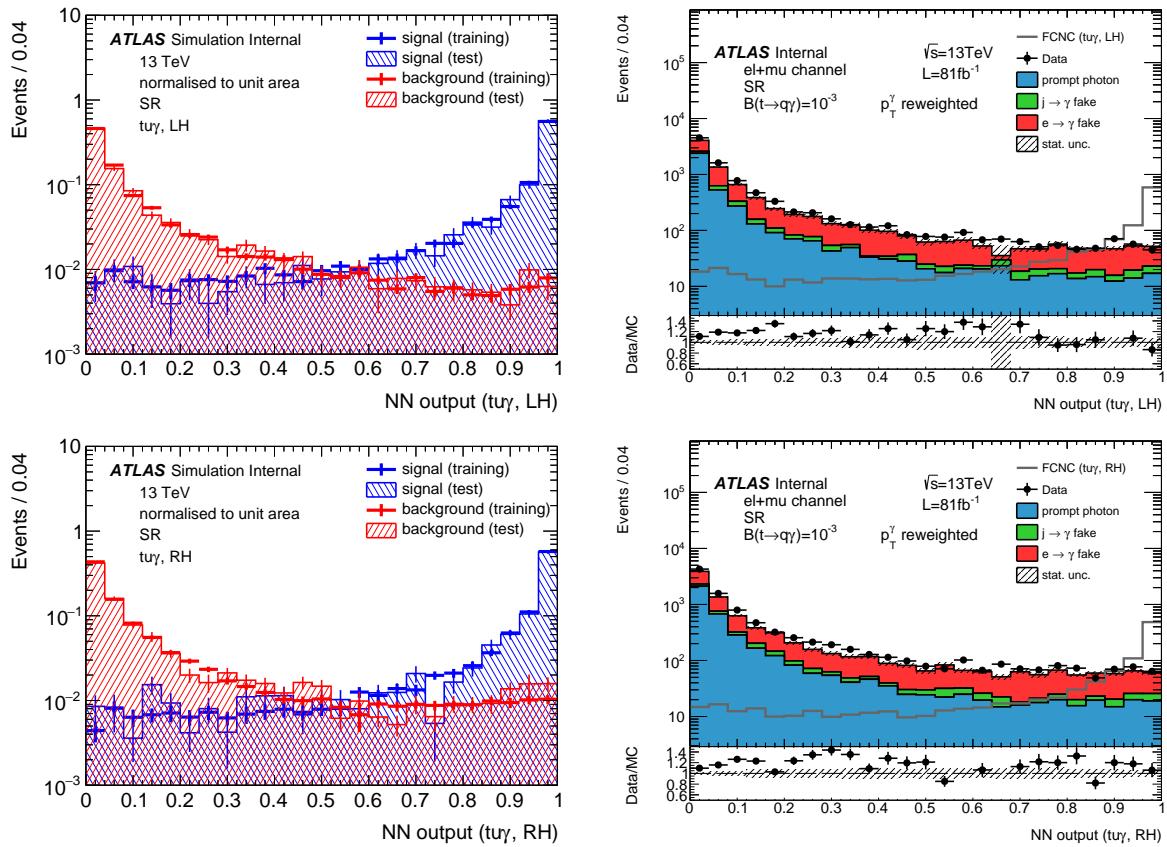


Figure 36: Output distributions of the neural network trained with the $t\bar{u}\gamma$ coupling, left-handed (top) and right-handed (bottom). Both the training and test set are evaluated for signal and background (left). The number of MC events in the signal and background samples used is also shown. The distribution of the expected number of events per photon origin is shown on the right side, including both signal modes. Only the statistical uncertainty is shown.

Not reviewed, for internal circulation only

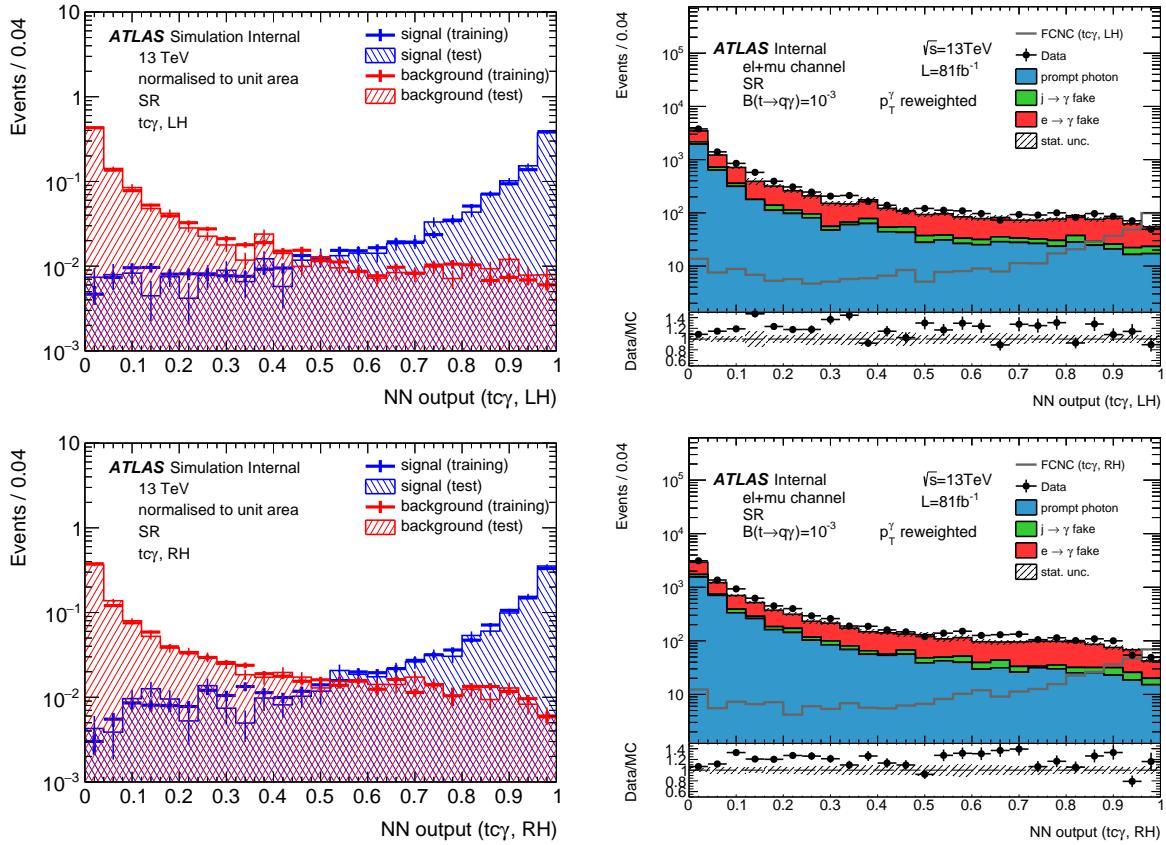


Figure 37: Output distributions of the neural network trained with the $tc\gamma$ coupling, left-handed (top) and right-handed (bottom). Both the training and test set are evaluated for signal and background (left). The number of MC events in the signal and background samples used is also shown. The distribution of the expected number of events per photon origin is shown on the right side, including both modes. Only the statistical uncertainty is shown.

Not reviewed, for internal circulation only

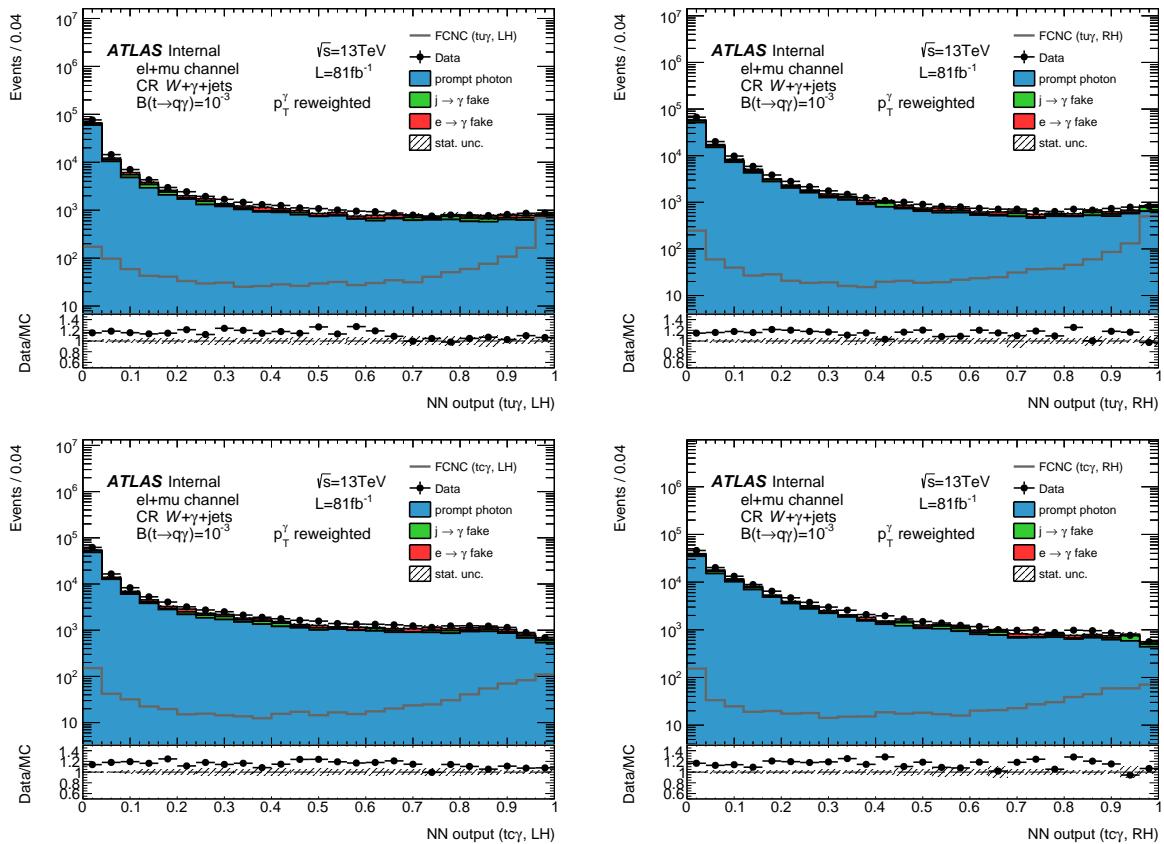


Figure 38: Output distributions of the neural network in the CR $W+\gamma+jets$ trained with the different couplings: $t\bar{u}\gamma$, left-handed (top left), $t\bar{u}\gamma$, right-handed (top right), $t\bar{c}\gamma$, left-handed (bottom left), and $t\bar{c}\gamma$, right-handed (bottom right). Both signal modes are included. Only statistical uncertainties are shown.

1078 8.6 Comparison of signal in production and decay mode

1079 The input variables for the signal in the production and decay mode feature different kinematic properties
 1080 as shown in Figures 29 and 30. Consequently, the output distribution for both types of signal differ.
 1081 In Figure 39, the signal is plotted separately for both types. While the signal of the production mode
 1082 accumulates around unity, the signal from the decay mode is rather flat distributed with a tendency to
 1083 higher values. This behaviour is expected since the energy per events in the decay mode is limited by
 1084 twice the top mass affecting the kinematic properties of the final state particles, while for the production
 1085 mode, no limitation exists.

Not reviewed, for internal circulation only

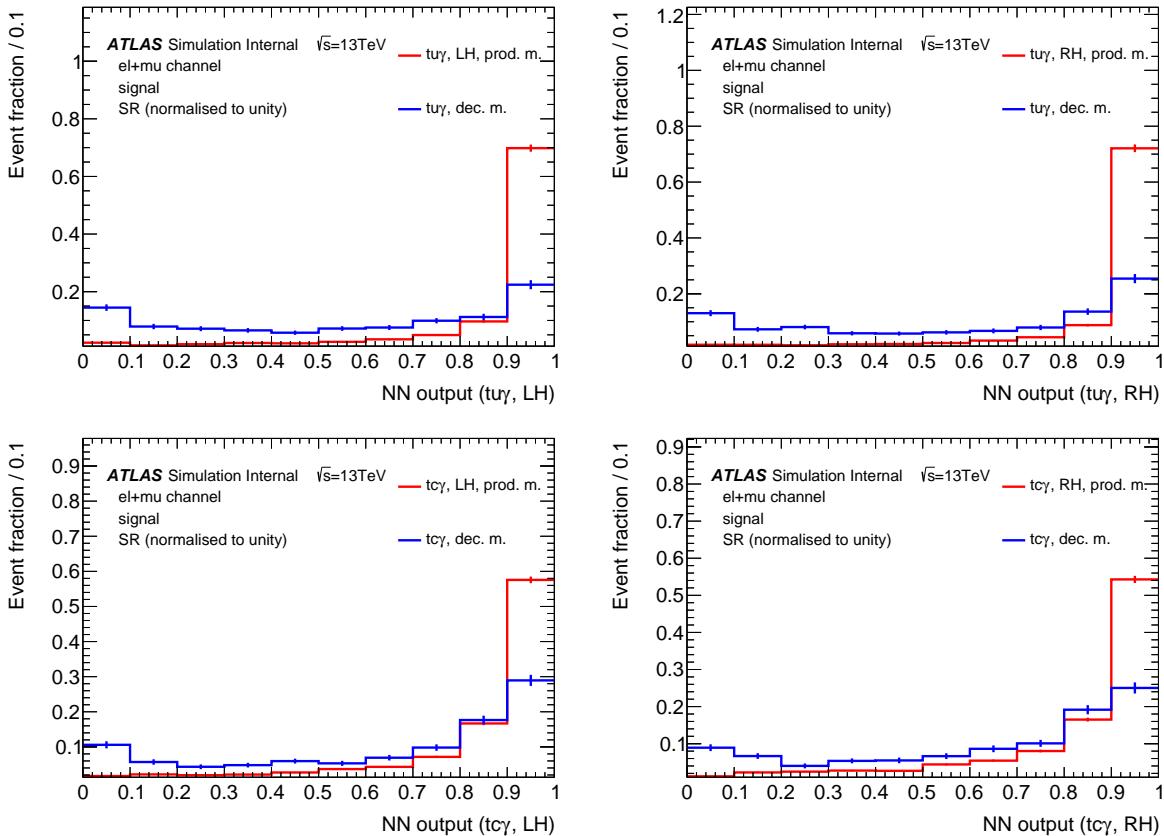


Figure 39: Output distributions of the neural network in the SR for the different signal couplings normalised to unity: $tuya$, left-handed (top left), $tuya$, right-handed (top right), tcy , left-handed (bottom left), and tcy , right-handed (bottom right). Only statistical uncertainties are shown.

1086 8.7 Comparison of different training setups

1087 The four neural network outcome, one for each signal coupling, are compared to each other. In Figure 40,
 1088 the shape of the distributions of the signal including both production and decay mode, data and the
 1089 total background are compared to each other in the SR and CR $W+\gamma+jets$. In general, all shapes are
 1090 comparable to each other. For the signal of both $tuya$ couplings, the score in the last bin of the NN output
 1091 distributions exceed that of the tcy couplings as the kinematic properties are different as discussed above.

1092 The total background and the data shapes in both regions are similar to each other. Note that there are
1093 more background events at the high tail of the NN output distribution for the right-handed $t\gamma$ coupling
1094 compared to the case of the left-handed $t\gamma$ coupling. In Figures 41, 42 and 43, the shape distributions in
1095 the SR are shown for the physics processes and split by the photon origin, respectively. In Figures 44, 45
1096 and 46, the shape distributions in the CR $W+\gamma+\text{jets}$ are shown for the physics processes and split by the
1097 photon origin, respectively. It can be seen that the shape of the different neural networks for the various
1098 background classes are similar. Generally, the networks trained for the $t\gamma$ coupling separates better signal
1099 from background due to the kinematic properties of the signal.

Not reviewed, for internal circulation only

Not reviewed, for internal circulation only

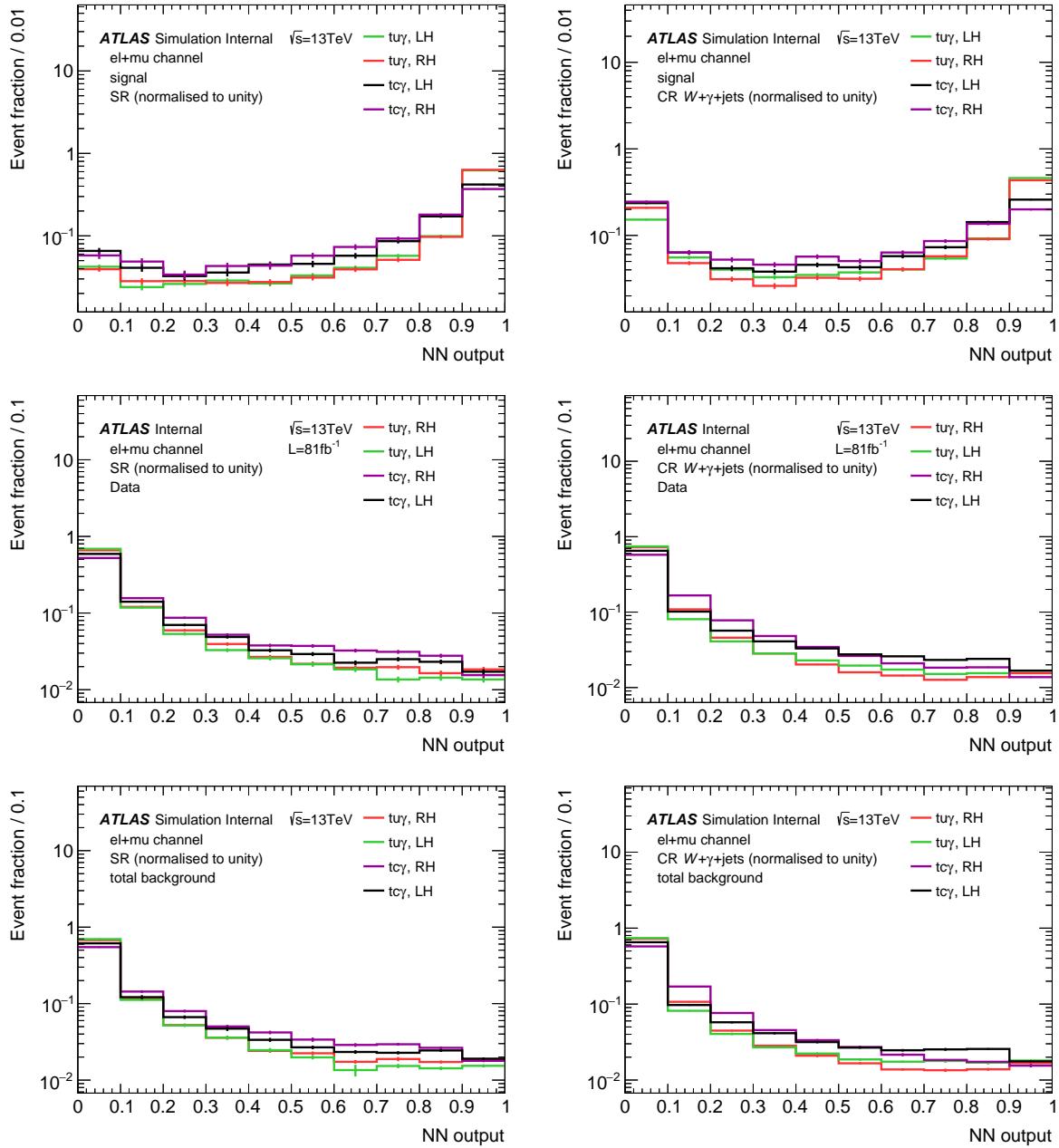


Figure 40: Output distributions of the neural network trained for the four signal couplings normalised to unity in the SR (left) and CR $W+\gamma+jets$ (right): signal including both production and decay mode (top), data (middle), and total background (bottom). Only statistical uncertainties are shown.

Not reviewed, for internal circulation only

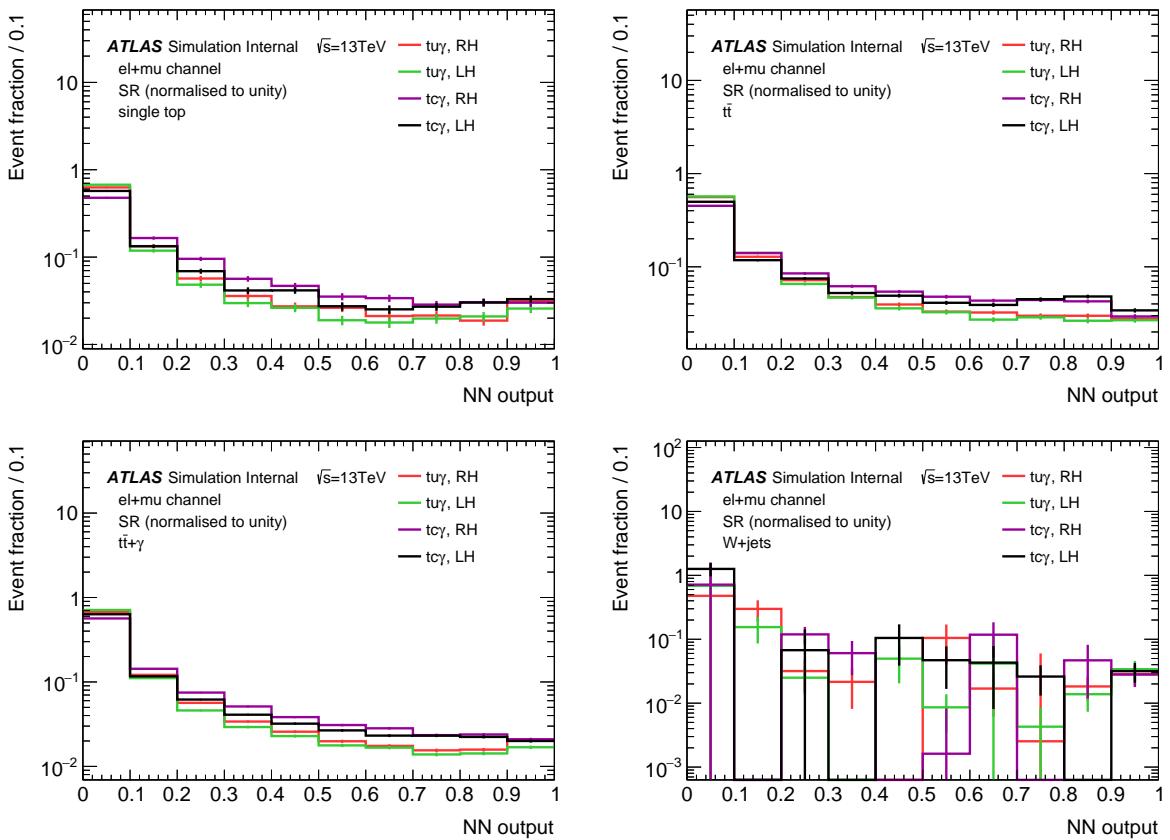


Figure 41: Output distributions of the neural network trained for the four signal couplings for the different physics processes normalised to unity in the SR: single top (top left), $t\bar{t}$ (top right), $t\bar{t} + \gamma$ (bottom left), and $W+jets$ (bottom right). Only statistical uncertainties are shown.

Not reviewed, for internal circulation only

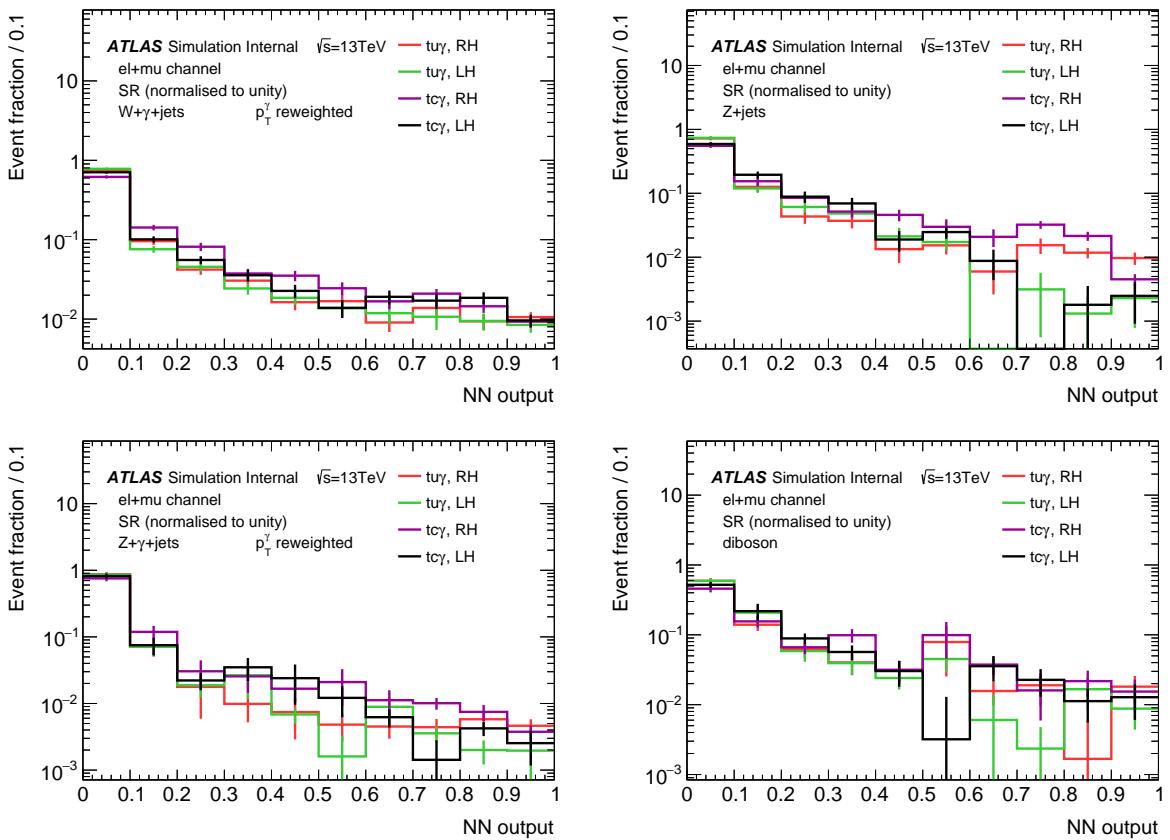


Figure 42: Output distributions of the neural network trained for the four signal couplings for the different physics processes normalised to unity in the SR: $W+\gamma+jets$ (top left), $Z+jets$ (top right), $Z+\gamma+jets$ (bottom left), and diboson (bottom right). Only statistical uncertainties are shown.

Not reviewed, for internal circulation only

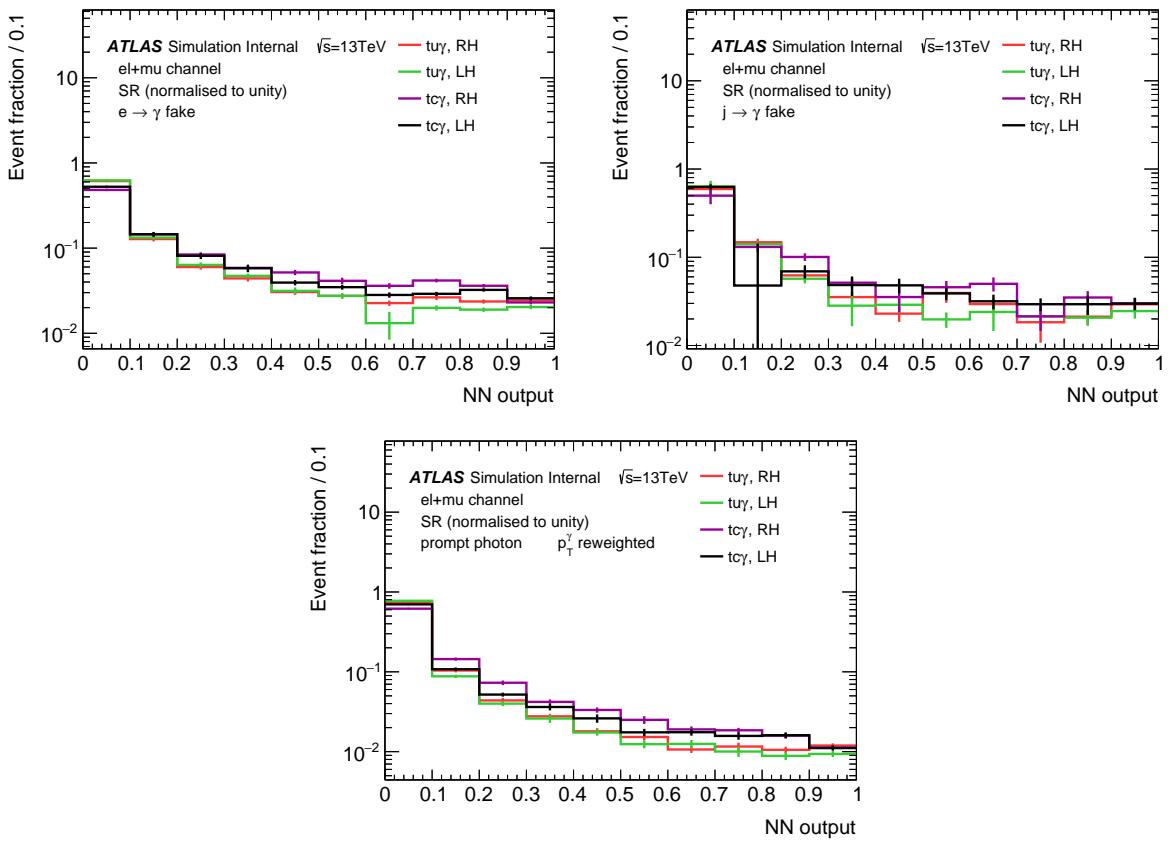


Figure 43: Output distributions of the neural network trained for the four signal couplings for the photon sources normalised to unity in the SR: $e \rightarrow \gamma$ fakes (top left), $j \rightarrow \gamma$ fakes (top right), and prompt photons (bottom). Only statistical uncertainties are shown.

Not reviewed, for internal circulation only

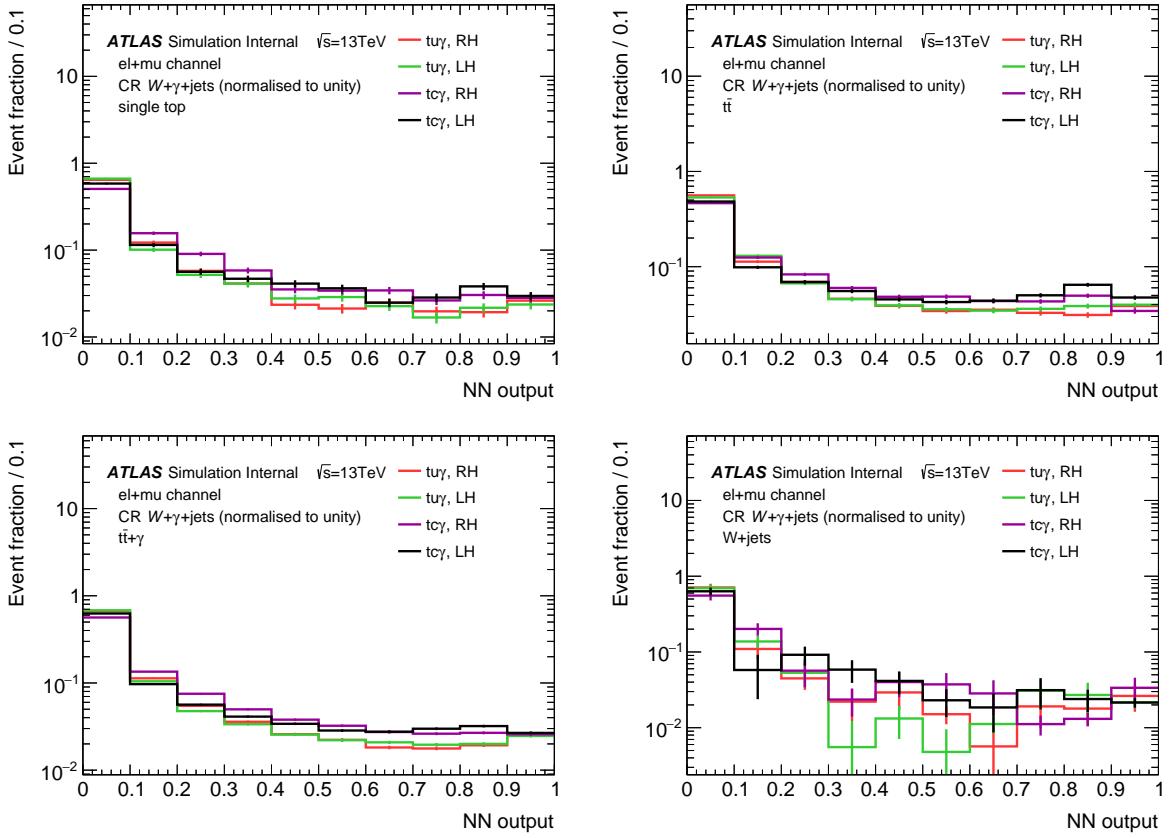


Figure 44: Output distributions of the neural network trained for the four signal couplings for the different physics processes normalised to unity in the CR $W+\gamma+jets$: single top (top left), $t\bar{t}$ (top right), $t\bar{t} + \gamma$ (bottom left), and $W+jets$ (bottom right). Only statistical uncertainties are shown.

Not reviewed, for internal circulation only

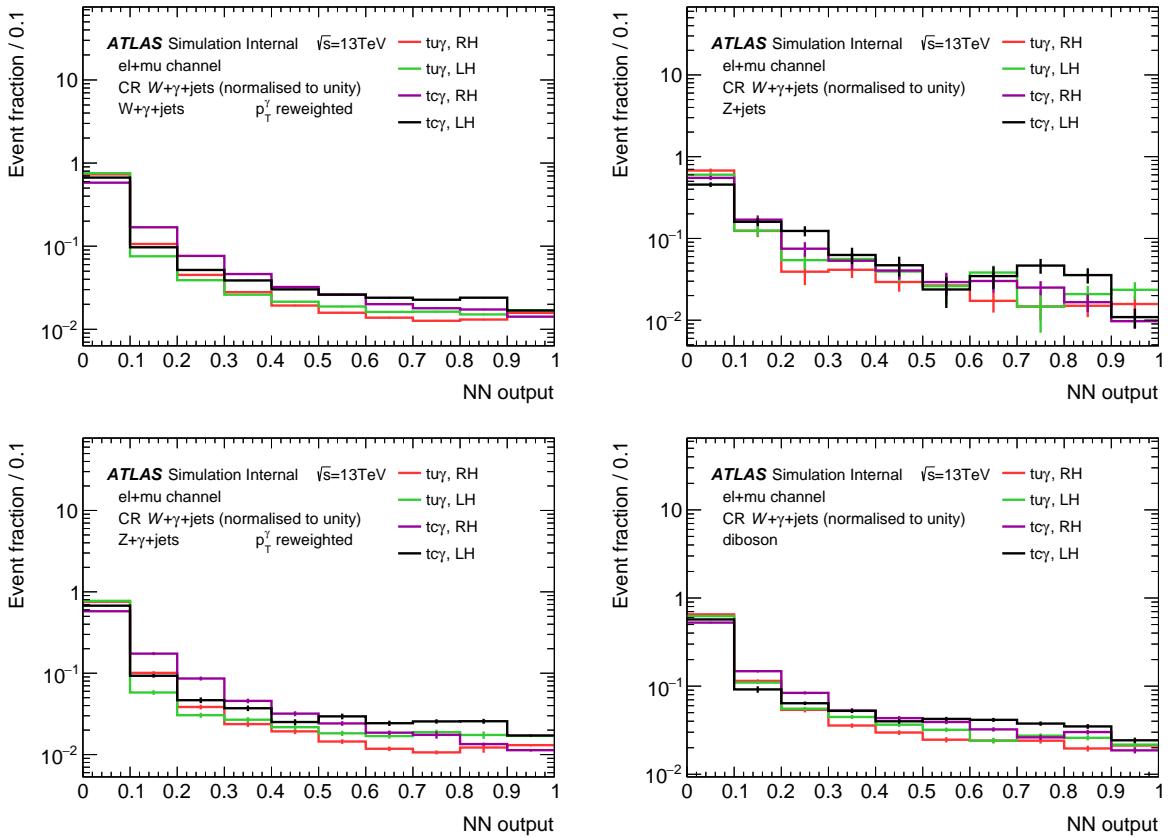


Figure 45: Output distributions of the neural network trained for the four signal couplings for the different physics processes normalised to unity in the CR $W+\gamma+jets$: $W+\gamma+jets$ (top left), $Z+jets$ (top right), $Z+\gamma+jets$ (bottom left), and diboson (bottom right). Only statistical uncertainties are shown.

Not reviewed, for internal circulation only

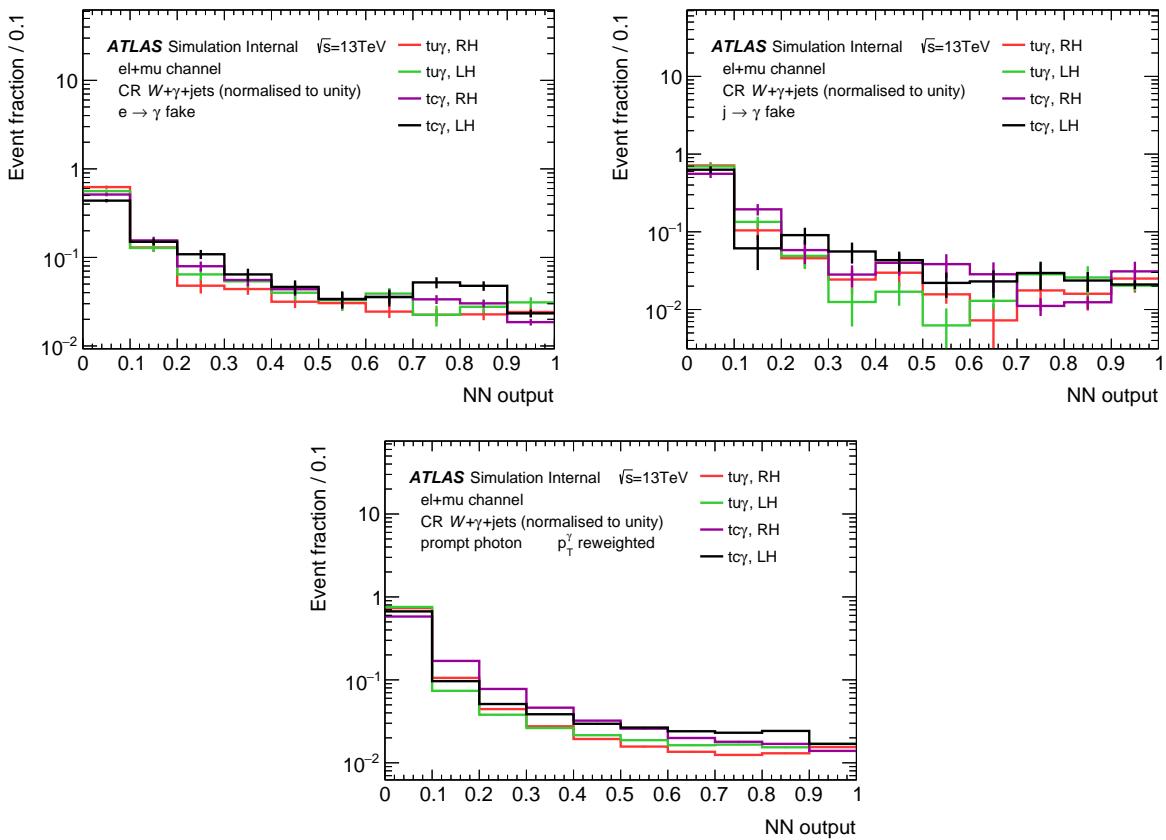


Figure 46: Output distributions of the neural network trained for the four signal couplings for the photon sources normalised to unity in the CR $W+\gamma+jets$: $e \rightarrow \gamma$ fakes (top left), $j \rightarrow \gamma$ fakes (top right), and prompt photons (bottom). Only statistical uncertainties are shown.

1100 9 Estimation of systematic uncertainties

1101 Each analysis deals with a number of different sources of uncertainties being either of statistical or
 1102 systematic nature. This analysis is affected by various sources of systematic effects. Each of them
 1103 is individually estimated and fed into the statistical analysis as nuisance parameter (NP) as described
 1104 in Section 10. In the following, techniques to deal with uncertainties and each source of systematic
 1105 effects including its estimation are briefly described. In Appendix O, the distributions of the systematic
 1106 uncertainties compared to the nominal distribution are shown for all regions and all couplings.

1107 9.1 Symmetrisation, smoothing and pruning

1108 When symmetrising an uncertainty, it is centred around the nominal value. Note that all uncertainties are
 1109 symmetrised, if not stated otherwise. *Two-sided* symmetrisation is performed when both the up and down
 1110 variation of an uncertainty are available, e.g. photon ID scale factor. Then, the half sum of two absolute
 1111 deviations from the nominal value is taken as symmetric variation as shown in Equation (38). Now, the
 1112 nominal value is varied up and down by this symmetrised value.

$$\text{symmetric variation} = \frac{|\text{up} - \text{nominal}| + |\text{down} - \text{nominal}|}{2} \quad (38)$$

1113 *One-sided* symmetrisation means that only an up or a down variation is available. For the missing
 1114 variation, the varied distribution is mirrored on the nominal distribution.

1115 The technique of *smoothing* an uncertainty is used to average the expected number of events across bins in
 1116 order to remove statistical fluctuations. Otherwise, the statistical uncertainty would be double-counted for.
 1117 The algorithm used depends on two parameters: the tolerance and the maximal number of slope changes.
 1118 First, the distribution is rebinned until the statistical uncertainty of each bin is below the tolerance, here
 1119 set to 8 %. Next, the number of slope changes in this new distribution is checked. If it is smaller than
 1120 the threshold of four, the distribution is kept. Otherwise, the first step is performed with halved tolerance.
 1121 This iterative procedure is done until the number of slopes is equal to or below the threshold. Lastly, the
 1122 smoothing algorithm 353QH [68] is run to avoid artificially flat uncertainties introduced by steps 1 and 2.
 1123 Note that all uncertainties are smoothed, if not stated otherwise.

1124 *Pruning* means removing uncertainties that would only have a small impact on the result in order to reduce
 1125 the number of NP. This procedure stabilises the fit. Each uncertainty is split into a normalisation and shape
 1126 part. The shape of an uncertainty is dropped when in each bin, the ratio of the varied distribution over
 1127 the nominal distribution minus one is smaller than 1 %. The normalisation of an uncertainty is dropped
 1128 when the overall ratio minus one is smaller than 1 %. A reduced pruning parameter of 0.5 % was tested
 1129 and gave similar results deviating less than 1 %.

1130 9.2 Theory uncertainties

1131 **Cross section** The cross sections for the MC samples are separately varied up and down by one standard
 1132 deviation for each type of process, i.e. $t\bar{t}$ ($\pm 5.6\%$ [34]), $t\bar{t} + \gamma$ ($\pm 8.0\%$ [69]), single top (t -channel,

1133 top: $^{+4.0\%}_{-3.4\%}$, t -channel, anti-top: $^{+5.0\%}_{-4.5\%}$, s -channel, top: $^{+3.6\%}_{-3.1\%}$, s -channel, anti-top: $^{+4.8\%}_{-4.3\%}$, tW -
 1134 channel: $\pm 5.3\%$) [70], $V+\text{jets}$ ($\pm 5\%$ [71]), and diboson ($\pm 6\%$ [72]). Each variation enters the
 1135 fit. Note that for the prompt photon contributions $W/Z+\gamma+\text{jets}$ the cross section uncertainty is
 1136 dismissed since their normalisation enters the fit as other NPs. In Appendix P, studies with an
 1137 increased cross section uncertainty for the $t\bar{t} + \gamma$ process are shown giving the same results as the
 1138 default setup.

1139 9.2.1 Signal modelling

1140 **Renormalisation and factorisation scale** The effect of the choice of the renormalisation scale μ_r and
 1141 factorisation scale μ_f is estimated by varying the scales independently or simultaneously up and
 1142 down by a factor of 2 with respect to the nominal sample value, excluding simultaneous up and
 1143 down variations (off-diagonal elements). The variation is done by using event weights. For each
 1144 bin, the maximal (minimal) deviation from the nominal value is taken as up (down) variation.

1145 **PDF uncertainty** The PDF uncertainty is estimated by using the PDF4LHC15 error set, containing 30
 1146 eigen variations. Each variation enters the fit as NP.

1147 9.2.2 Background modelling

1148 **Renormalisation and factorisation scale** For each background process except for the $t\bar{t}$ process, the
 1149 uncertainty on the choice of the renormalisation and factorisation scales are individually estimated.
 1150 The same procedure as for the signal is performed. The scale uncertainties for the $t\bar{t}$ process are
 1151 part of the uncertainty of the initial state radiation. In Appendix Q, a fit setup with three variations
 1152 of the scales for selected processes are shown giving the same results as the default setup.

1153 **PDF uncertainty** For the PDF uncertainty, the same procedure as for the signal is performed.

1154 **Initial state radiation** The effects of the initial state radiation (ISR) are estimated by decreasing and
 1155 increasing the QCD radiation activity in an event and are only available for single top and $t\bar{t}$
 1156 processes. For single top events, the A14 tune is varied up (down) using event weights (Var3cUp
 1157 and Var3cDown) and at the same time dividing (multiplying) the renormalisation and factorisation
 1158 scale by a factor of 2. For the up variation of the ISR uncertainty for $t\bar{t}$ processes, the sample with
 1159 $h_{\text{damp}} = 3m_{\text{top}}$ is used with event weights referring to the varied A14 tune Var3cUp and dividing
 1160 the renormalisation and factorisation scale by a factor of 2. For the down variation, the A14 tune
 1161 Var3cDown is used and the renormalisation and factorisation scale are doubled, by using event
 1162 weights in the nominal sample.

1163 **Final state radiation** The effects of the final state radiation (FSR) are estimated by varying parameters
 1164 used in the initial and final state showers in an event and are only available for single top and $t\bar{t}$
 1165 processes. Therefore, the A14 tune is varied up and down using event weights (Var2).

1166 **Normalisation of prompt photon contribution** The normalisation of the prompt photon contributions
 1167 stemming from $W+\gamma+\text{jets}$ and $Z+\gamma+\text{jets}$ enter the fit as free floating NPs.

1168 **Photon p_T reweighting** An uncertainty of 100 % is assigned to the reweighting of the photon p_T of
 1169 the prompt photon contributions $W+\gamma+\text{jets}$ and $Z+\gamma+\text{jets}$. Note that the reweighting is applied as
 1170 default in the fit. Hence, an up variation of 100 % doubles the correction, while the down variation
 1171 switches it off.

1172 **$t\bar{t}$ matrix element and shower generator** To estimate the influence of the generators used for the $t\bar{t}$ pro-
 1173 cess, the matrix element and the shower generators are replaced. Once, the nominal sample produced
 1174 with POWHEG-Box + PYTHIA is replaced by the sample generated by MADGRAPH5_aMC@NLO +
 1175 PYTHIA, and another time by the samples produced by POWHEG-Box + HERWIG.

1176 **Single top matrix element and shower generator** To estimate the influence of the generators used for
 1177 the single top processes, the matrix element and the shower generators are replaced. Once, the
 1178 nominal samples produced with POWHEG-Box + PYTHIA are replaced by the samples generated by
 1179 MADGRAPH5_aMC@NLO + PYTHIA, and another time by the samples produced by POWHEG-Box
 1180 + HERWIG.

1181 9.3 Experimental uncertainties

1182 **Lepton efficiency** The lepton efficiency contains the trigger, reconstruction, ID and isolation efficiencies.
 1183 In simulation, scale factors are used to correct for deviations between efficiencies measured in data
 1184 and found in simulation. The scale factors are measured using the *tag-and-probe* method with
 1185 $Z \rightarrow \ell\ell$ and $J/\Psi \rightarrow \ell\ell$ decays for both electrons [52] and muons [53]. The scale factors are varied
 1186 up and down by one standard deviation.

1187 **Lepton energy (momentum) scale and resolution** The lepton energy (momentum) is calibrated using
 1188 MC-based techniques. Correction factors, which are derived from the study of dileptonic decay
 1189 of the Z boson are applied to correct possible detector mis-modelings in the calibration. These
 1190 correction factors are varied up and down by one standard deviation. For electrons, the energy scale
 1191 and resolution are calculated together with photons as EGamma scale and resolution.

1192 **Photon efficiencies** The scale factor for the photon ID efficiency is derived from three measurements:
 1193 the radiative Z boson method using a sample enriched in events with radiative Z boson decays, the
 1194 electron extrapolation technique using a sample enriched in $Z \rightarrow ee$ events where the similarity
 1195 between electrons and photons in the detector is exploited, and the matrix method using a sample
 1196 enriched with isolated, high- p_T photons and exploiting that the narrow-strip variables are only
 1197 weakly correlated to the isolation. The scale factor is computed as the ratio of the efficiency
 1198 measured in data and that determined in simulation. The sets of scale factors of all measurements
 1199 are combined into one single set that is applied to simulation to correct for deviations between
 1200 efficiencies measured in data and found in simulation. The scale factors for photon isolation are
 1201 measured as described in Ref. [50]. The scale factors are varied up and down by one standard
 1202 deviation.

1203 **Photon energy (momentum) scale and resolution** The uncertainties on the photon energy (momentum)
 1204 scale and resolution are calculated together with the electrons as EGamma scale and resolution.

1205 **Jet energy scale** The jet energy scale (JES) and its uncertainty are derived by combining measurements
 1206 in simulation and in data. In this analysis, the *CategoryReduction* parameter set (30 NPs) is used
 1207 that can be classified into categories for the η inter-calibration, b -jet energy scale, pile-up, single-
 1208 hadron high- p_T , flavour composition and response, and *in-situ* jet energy corrections. Each NP is

1209 independently varied up and down. The NPs for the jet flavour composition and response are treated
 1210 as uncorrelated between the regions.

1211 **Jet flavour fraction** For an uncertainty due to the jet flavour composition, the ratio of light-quark- to
 1212 gluon-initiated jets is varied. Hereby, light jets include jets initiated by a charm quark. A 50:50
 1213 ratio is nominally assumed with an uncertainty of 100 %. Moreover in the SR, the shape of the
 1214 b -quark-initiated jet contribution is replaced by that of the light flavour contribution while keeping
 1215 the normalisation, and vice versa, called *heavy flavour fraction* uncertainty. In the CR $W+\gamma+jets$,
 1216 the b -quark initiated jet contribution is negligible.

1217 **Heavy flavour normalisation** The normalisation of the heavy flavour contribution of the $W+\gamma+jets$
 1218 process is assigned a conservative uncertainty of 50 % to account for imperfect modelling in
 1219 simulation.

1220 **Jet energy resolution** The jet energy resolution (JER) is measured separately for data and simulation
 1221 using two *in-situ* techniques [73], resulting in 8 NPs. As the techniques only measure one-sided
 1222 variations, the uncertainties are symmetrised.

1223 **Jet vertex tagging** In order to derive an uncertainty on the JVT scale factor, the cut on the JVT dis-
 1224 criminant is varied up and down [57]. This uncertainty on the scale factor is propagated in this
 1225 analysis.

1226 **b -tagging** The efficiency of the b -tagging working point is measured in data and scale factors are derived
 1227 for simulation depending on the jet flavour. Uncertainties on the scale factors are obtained by using
 1228 the uncertainties on the calibration scale factors provided by the Flavour Tagging group for b -, c -
 1229 and light jets. Those uncertainties are independently used in this analysis.

1230 **E_T^{miss}** The uncertainties on the lepton, photon and jet scale and resolution are propagated to the E_T^{miss}
 1231 calculation. Consequently, their impact is estimated when evaluating their shifts. The effects of
 1232 the energy scale and resolution uncertainties on soft-terms are estimated by varying the scales and
 1233 resolutions up and down by one standard deviation.

1234 **Pile-up** The uncertainty on the pile-up is estimated by changing the nominal rescale factor of 1.03 for the
 1235 expected number of interactions $\langle\mu\rangle$ and varying it up and down by 0.09.

1236 **Luminosity** The uncertainty on the integrated luminosity is 2.0 % [7]. It is derived, following a methodo-
 1237 logy similar to that detailed in Ref. [8], from a preliminary calibration of the luminosity scale using
 1238 x-y beam-separation scans performed in May 2016 and July 2017. This uncertainty is dismissed
 1239 for the $W/Z+\gamma+jets$ contributions that is superseded by their normalisation factors.

1240 **Background estimation** The uncertainties on the scale factors $SF(e \rightarrow \gamma)$ and $SF(j \rightarrow \gamma)$ determined by
 1241 data-driven techniques as explained in Section 7 are used to vary the scale factors independently up
 1242 and down by one standard deviation. The uncertainty on the $SF(e \rightarrow \gamma)$ is increased to 10 %, closer
 1243 to the uncertainty as seen in other analyses. In Appendix R, the fit is redone without increasing the
 1244 uncertainty.

1245 10 Statistical analysis

1246 As statistical analysis, a profile likelihood fit is performed simultaneously in the SR and the CR $W+\gamma+\text{jets}$
 1247 and CR $Z+\gamma$ whose definitions are given in Table 3. The **TRExFitter** framework version 3.26 [74] is
 1248 used. The discriminating distribution built by the neural network described in Section 8 is taken as input
 1249 for the SR and CR $W+\gamma+\text{jets}$. In the CR $Z+\gamma$, the photon p_{T} spectrum is taken as input since in most
 1250 events, no jet is present and consequently, not all input variables can be properly filled. The two CRs
 1251 are used to estimate the normalisations of the $W+\gamma+\text{jets}$ and the $W+\gamma+\text{jets}$ contribution. In Appendix S,
 1252 studies are shown when using the photon p_{T} distribution in all regions giving weaker limits.

1253 10.1 Fit strategy

1254 The fit is preformed with a likelihood function \mathcal{L} that is generally defined as follows:

$$\mathcal{L} = \mathcal{L}(\mu, \theta | \text{NN output}, p_{\text{T}}(\gamma)). \quad (39)$$

1255 where the parameter μ is the signal strength, θ is the set of NPs for the systematic uncertainties, NN
 1256 output is the output value of the neural network, and the photon p_{T} . In this analysis, a binned maximum
 1257 likelihood fit is performed. The likelihood is computed as follows:

$$\mathcal{L} = \prod_r^{N_{\text{regions}}} \prod_i^{N_{r,\text{bins}}} P\left(N_{r,i} \middle| N_{r,i}^s + \sum_b^{N_{\text{bkg}}} N_{r,i}^b\right) \cdot \prod_j^{N_{\text{NP}}} G(\vartheta | 1, \theta_j) \quad (40)$$

1258 with the following parameters:

- 1259 • $P(x|\lambda)$ is the Poisson function with mean λ ;
- 1260 • N_{regions} is the number of regions;
- 1261 • $N_{r,\text{bins}}$ is the number of bins of the distribution in region r ;
- 1262 • index r runs over the different regions;
- 1263 • index i runs over the number of bins;
- 1264 • $N_{r,i}$ is the observed number of events in bin i in region r ;
- 1265 • $N_{r,i}^s$ is the expected number of signal events in bin i in region r ;
- 1266 • N_{bkg} is the number of background processes considered in the fit;
- 1267 • index b runs over all categories of background events;
- 1268 • $N_{r,i}^b$ is the expected number of events of background b in bin i in region r ;
- 1269 • N_{NP} is number of NPs considered in the fit;
- 1270 • j runs over the number of NPs;

- 1271 • $G(x|\mu, \sigma)$ is the Gaussian function with mean μ and width σ (in the case of the uncertainty due to
 1272 the MC statistics, a Poisson function replaces the Gaussian function);
 1273 • θ_j is the NP for the source of systematic effect j .

1274 The signal strength μ enters the likelihood as follows:

$$N_{r,i}^s = \mu \cdot N_{\text{input},r}^s \cdot \rho_{r,i} \quad (41)$$

1275 with $N_{\text{input},r}^s$ being the number of signal events in region r scaled using the effective cross section $\sigma_{\text{eff}}^{\text{coup}}$
 1276 and $\rho_{r,i}$ being the fraction of signal events in the respective bin i in region r . In terms of physics, the
 1277 signal strength can be interpreted as

$$\mu = \frac{N_{\text{fit}}^{\text{prod. m.}} + N_{\text{fit}}^{\text{dec. m.}}}{N_{\text{in}}^{\text{prod. m.}} + N_{\text{in}}^{\text{dec. m.}}} \quad (42)$$

$$= \frac{\varepsilon^{\text{prod. m.}} \times \mathcal{A}^{\text{prod. m.}} \times \sigma_{\text{eff,fit}}^{\text{prod. m.}} \times L + \varepsilon^{\text{dec. m.}} \times \mathcal{A}^{\text{dec. m.}} \times \sigma_{\text{eff,fit}}^{\text{dec. m.}} \times L}{\varepsilon^{\text{prod. m.}} \times \mathcal{A}^{\text{prod. m.}} \times \sigma_{\text{eff,in}}^{\text{prod. m.}} \times L + \varepsilon^{\text{dec. m.}} \times \mathcal{A}^{\text{dec. m.}} \times \sigma_{\text{eff,in}}^{\text{dec. m.}} \times L} \quad (43)$$

1278 with the fitted (input) numbers of signal events per coupling $N_{\text{fit}}^{\text{coup}}$ ($N_{\text{in}}^{\text{coup}}$), the signal efficiencies $\varepsilon^{\text{coup}}$, the
 1279 detector acceptances $\mathcal{A}^{\text{coup}}$, the fitted (input) effective cross sections $\sigma_{\text{eff,fit}}^{\text{coup}}$ ($\sigma_{\text{eff,in}}^{\text{coup}}$), and the luminosity
 1280 L . Exploiting that both effective cross sections show the same dependence on the coupling strength
 1281 ($\sigma_{\text{eff}}^{\text{dec. m.}}/\sigma_{\text{eff}}^{\text{prod. m.}} = \text{const.}$), and assuming that the detector acceptances $\mathcal{A}^{\text{coup}}$ and the signal efficiencies
 1282 $\varepsilon^{\text{coup}}$ are independent from the coupling strength, the mathematical expression for the signal strength μ
 1283 can be simplified to

$$\mu = \frac{\sigma_{\text{eff,fit}}^{\text{prod. m.}}}{\sigma_{\text{eff,in}}^{\text{prod. m.}}} = \frac{\sigma_{\text{eff,fit}}^{\text{dec. m.}}}{\sigma_{\text{eff,in}}^{\text{dec. m.}}} \quad (44)$$

1284 Note that shape effects and higher order corrections in EFT are neglected here.

1285 10.2 Nuisance parameters

1286 For the statistical analysis, several uncertainties enter the fit as NPs that are described in Section 9. For
 1287 each uncertainty, the pruning algorithm as described in Section 9.1 is applied. In Figure 47, an overview
 1288 of all NPs in all regions and their considerations in the fit are shown for the left-handed signal coupling
 1289 *tuy*. It can be seen that many parameters are dropped. For some, only the normalisation is accounted
 1290 for in the fit, i.e. the shape impact is dropped, or vice versa. In Appendix T, the outcome of the pruning
 1291 is shown for the other signal couplings. The input distributions for each systematic uncertainty for all
 1292 regions and all couplings are shown in Appendix O.

Not reviewed, for internal circulation only

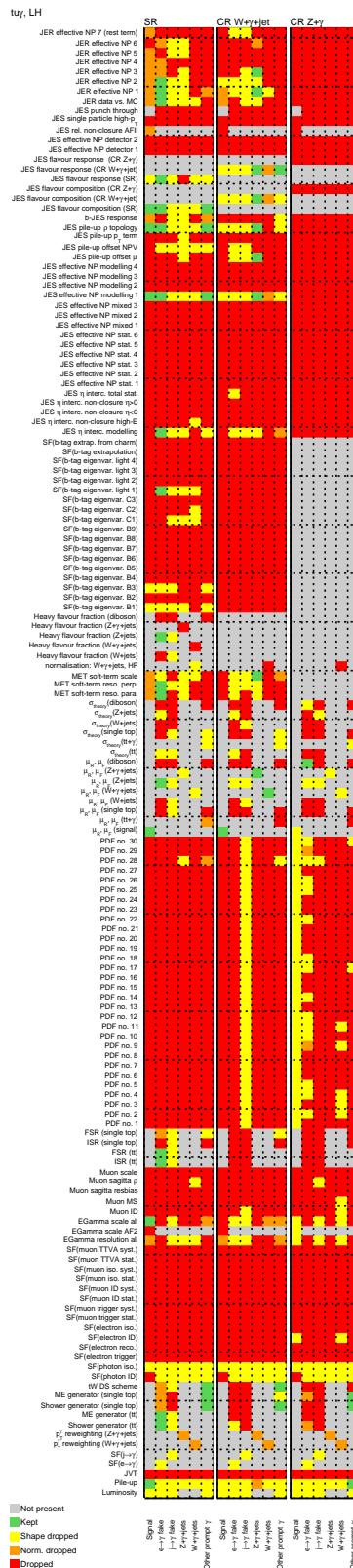


Figure 47: Overview of all nuisance parameters after pruning for the left-handed tuy coupling: if the shape and/or normalisation impacts are smaller than 1 %, the normalisation and/or shape of the parameter will be dropped, shown as orange, yellow or red square.

1293 10.3 Fit result with Asimov data

1294 For the fit of Asimov data, the signal strength μ is set to zero. The correlation coefficients of the NPs to each
 1295 other are given in Figure 48 for the left-handed signal coupling $t\gamma$. Here, only systematic sources with at
 1296 least one correlation coefficient above 10 % are drawn. It can be seen that most of the correlations are of
 1297 a few percent. The normalisation factors for the prompt photon contributions are highly anti-correlated to
 1298 the respective scale uncertainties and to the pile-up uncertainty since all these uncertainties mainly impact
 1299 the normalisation of the prompt photon contributions. The pre-fit yields for the different processes in the
 1300 different regions considered in the fit are shown in Table 25. Since the normalisation of the $W+\gamma+jets$ and
 1301 $Z + \gamma$ contributions enters the fit as free normalisation factors, their contributions are shown separately.
 1302 All other events with a prompt photon are referred to as *other prompt* γ . In Appendix U, the composition
 1303 of the physics processes for the photon fake categories and the *other prompt* γ class is shown for all
 1304 regions. The distributions in the different regions before and after the fit are shown for the left-handed
 1305 $t\gamma$ coupling in Figure 49. In the bottom plots, the ratio of data to prediction including all uncertainties
 1306 is shown. The signal contribution is set to zero at pre-fit stage. In the post-fit distributions, the total
 1307 uncertainty in each bin is strongly reduced. In Figure 50, the normalisation factors for the $W+\gamma+jets$ and
 1308 $Z+\gamma+jets$ process are shown.

1309 The pull and its uncertainty for the NPs is defined as

$$pull = \frac{\theta_{\text{fit}} - \theta_{\text{in}}}{\sigma_{\text{in}}}, \quad (45)$$

$$\Delta_{\text{pull}} = \frac{\sigma_{\text{fit}}}{\sigma_{\text{in}}} \quad (46)$$

1310 with the fitted (input) NP θ_{fit} (θ_{in}) and its uncertainty σ_{fit} (σ_{in}). The pull values for the systematic NPs
 1311 are shown for the left-handed $t\gamma$ coupling in Figure 51. All pulls are centred at zero. Most of the
 1312 uncertainties are at unity, while some can be constrained even with Asimov data as those NPs come along
 1313 with a large pre-fit uncertainty. In Figure 52, the normalisation factors γ for the bins in each region are
 1314 presented that are centred around one.

1315 The distribution of the negative-log likelihood is shown in Figure 53. It can be seen that the fitted signal
 1316 strength is below one standard deviation meaning that no signal could be found. The distributions for the
 1317 right-handed $t\gamma$, left-handed $t\gamma$, and right-handed $t\gamma$ coupling couplings are shown in Appendix V.

Not reviewed, for internal circulation only

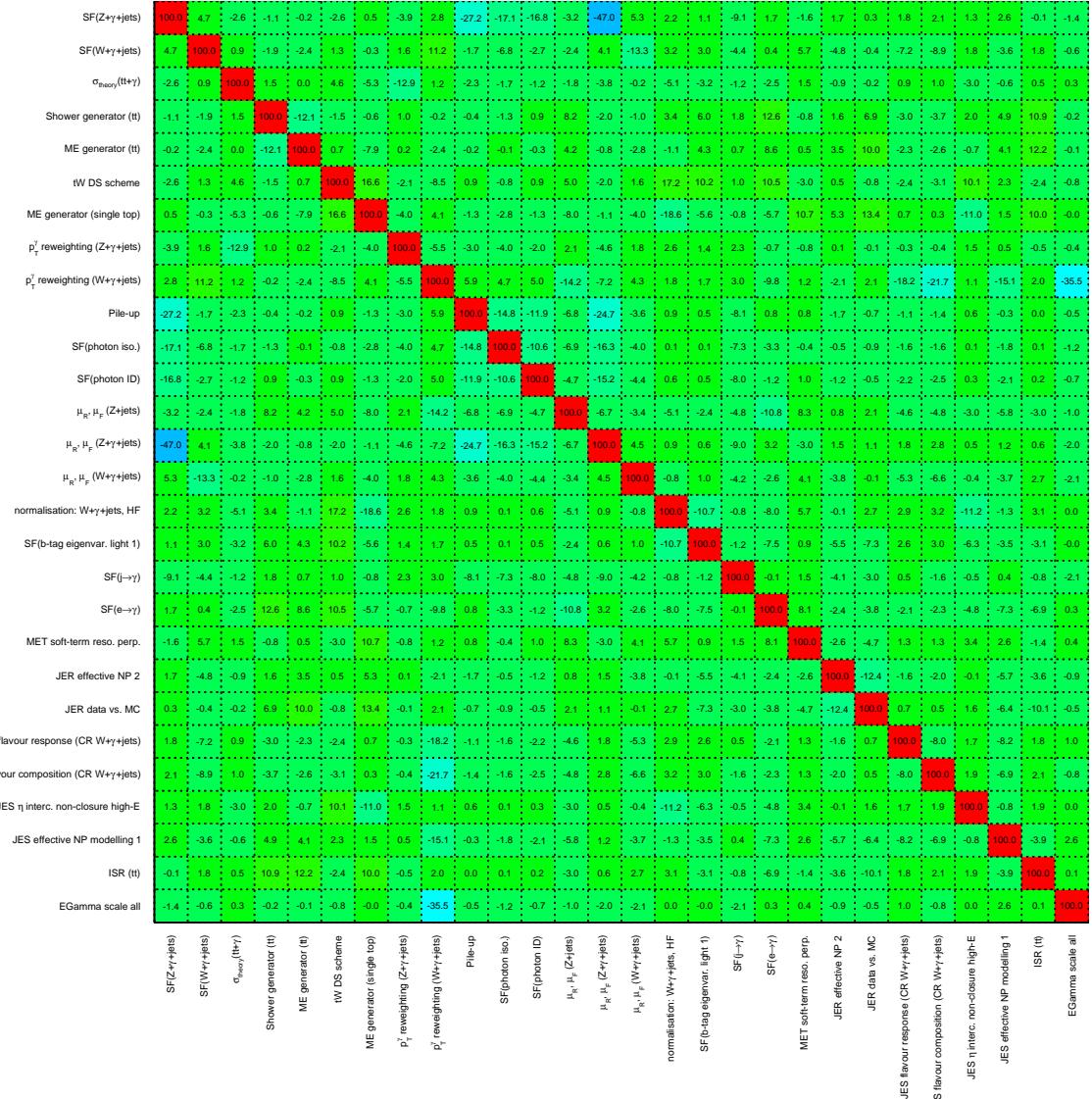


Figure 48: Correlation coefficients of all parameters with at least one coefficient above 10 % for the left-handed $t\gamma\gamma$ coupling considered in the fit using Asimov data.

Not reviewed, for internal circulation only

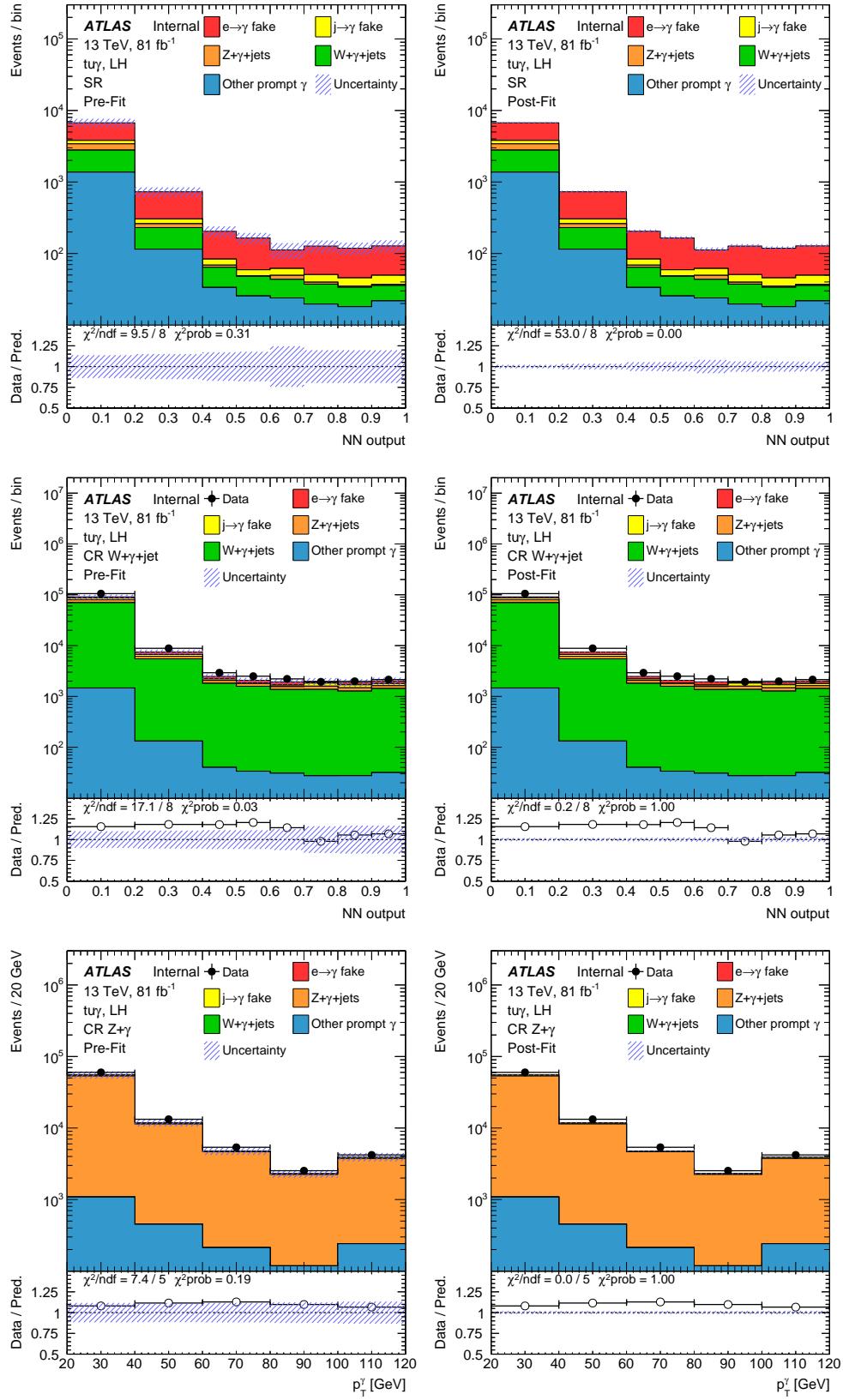


Figure 49: Pre- (left) and post-fit (right) distributions for the left-handed signal coupling tuy using Asimov data: NN output distribution in the SR (top) and in the CR $W+\gamma+jets$ (middle), and the photon p_T spectrum in the CR $Z+\gamma$ (bottom). Statistical and systematic uncertainties are included.

Table 25: Yields for the different contributions in the different regions before the fit. The statistical uncertainty and all systematic uncertainties are included.

Photon origin	SR			CR $W+\gamma+\text{jets}$			CR $Z+\gamma$		
$e \rightarrow \gamma$	3 840	\pm	660	6 800	\pm	1 500	227	\pm	34
$j \rightarrow \gamma$	510	\pm	340	8 200	\pm	6 300	2 800	\pm	1 700
$Z+\gamma+\text{jets}$	670	\pm	160	11 700	\pm	1 600	73 300	\pm	8 700
$W+\gamma+\text{jets}$	1 650	\pm	480	82 400	\pm	6 700	5.1	\pm	3.1
Other prompt photon	1 630	\pm	430	1 790	\pm	470	2 110	\pm	220
Total SM	8 300	\pm	1 100	111 000	\pm	11 000	78 400	\pm	9 000
Data	9 557			127 864			85 347		

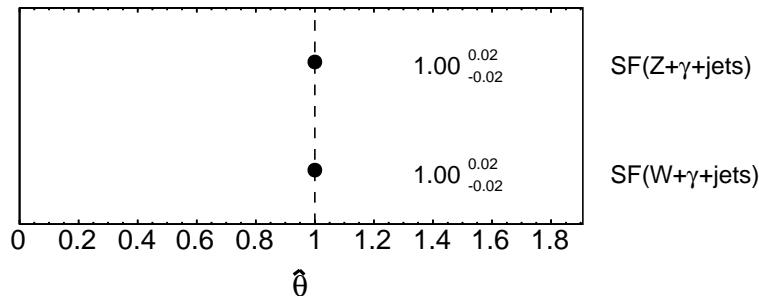


Figure 50: Normalisation factors for the $W+\gamma+\text{jets}$ and $Z+\gamma+\text{jets}$ process using the left-handed tuy coupling and Asimov data.

Not reviewed, for internal circulation only

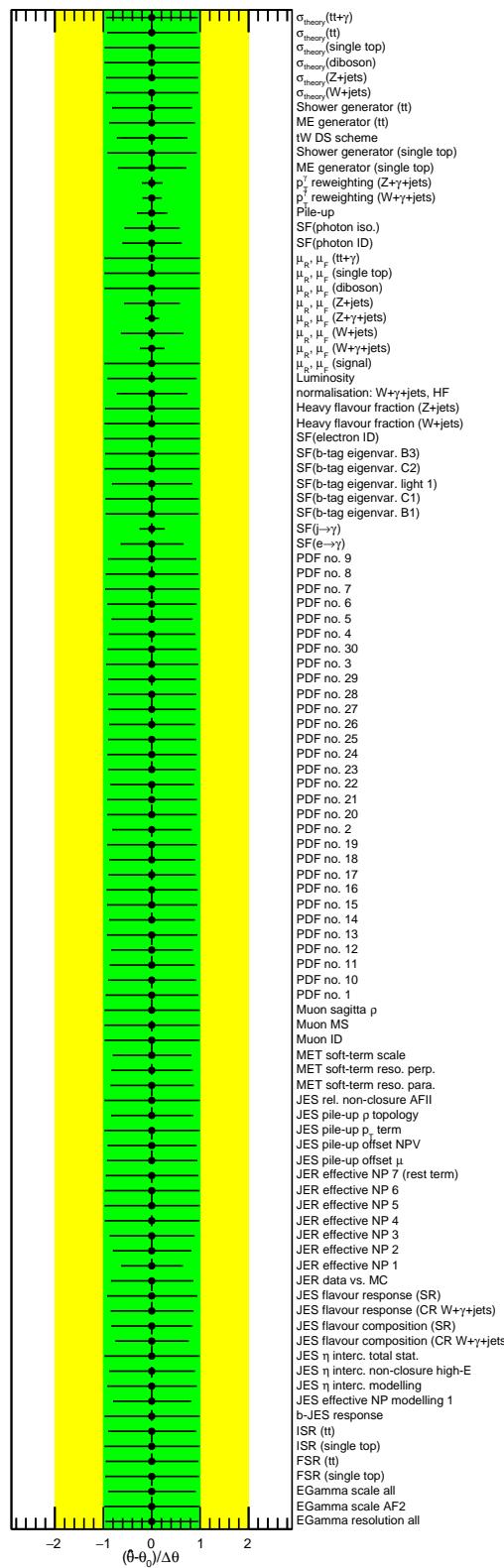


Figure 51: Pull values for the left-handed $t\bar{u}\gamma$ coupling for the different nuisance parameters considered in the fit using Asimov data.

Not reviewed, for internal circulation only

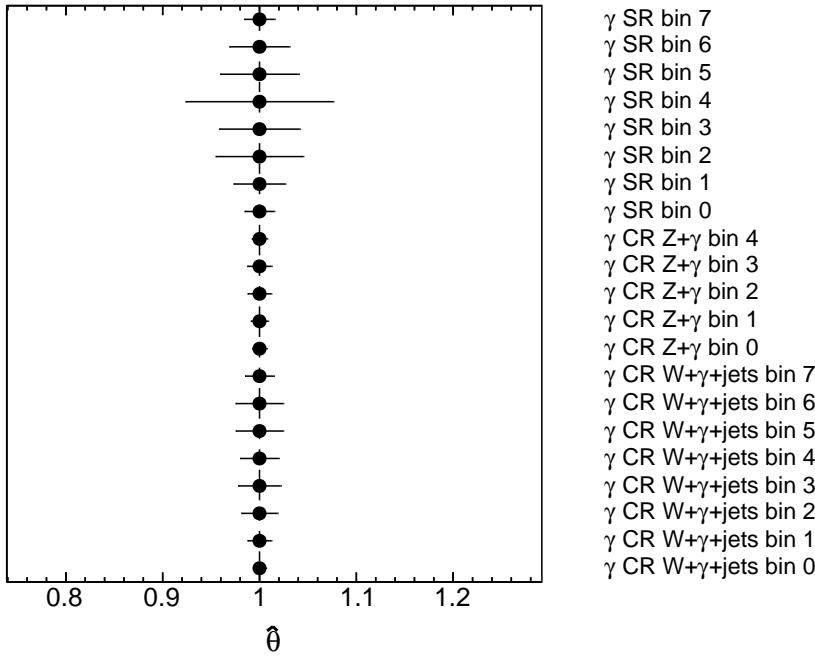


Figure 52: Normalisation factors γ for each bin in each region for the left-handed tuy coupling using Asimov data.

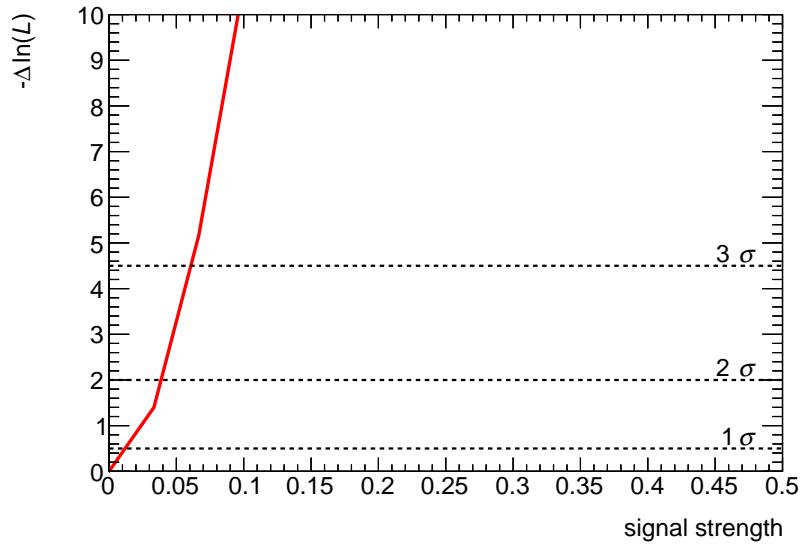


Figure 53: Distributions of the negative-log likelihood for the signal strength using Asimov data for the left-handed tuy coupling. The one, two and three standard deviations are marked.

1318 10.4 Signal injection test using Asimov data

1319 In order to test the model implemented in the statistical fit, signal is artificially added to the background and
 1320 the fit is re-run. The test is done for all couplings and a signal strength of 1 is assumed using Asimov data
 1321 in all regions. All systematic uncertainties are included. As result, the fit also determines a normalisation
 1322 factor of 1 for the signal as seen in Table 26.

Table 26: Measured signal strength μ for the different assumed signal couplings with Asimov data using $\mu = 1.0$.

Signal coupling	tuy , left-handed	tuy , right-handed	$tc\gamma$, left-handed	$tc\gamma$, right-handed
μ	$1.00^{+0.06}_{-0.06}$	$1.00^{+0.08}_{-0.08}$	$1.00^{+0.15}_{-0.15}$	$1.00^{+0.17}_{-0.17}$

1323 10.5 Ranking plots using Asimov data

1324 In order to estimate what uncertainty has the largest impact on the signal strength, ranking plots are
 1325 built using Asimov data and a signal strength of 1. For each NP, four fits are performed with a fixed
 1326 value and the resulting signal strength is compared to the nominal one. The four variations are: pre-fit
 1327 value \pm pre-fit uncertainty, and post-fit value \pm post-fit uncertainty. In Figure 54, the 20 NPs with the
 1328 largest impact on the signal strength are shown for the left-handed tuy coupling. The ranking plots for
 1329 the other couplings can be found in Appendix V. Note that for illustrating purposes of the pull values
 1330 in the ranking plots, both the pre-fit value and uncertainty of the normalisation factors γ are set to one.
 1331 Note that for all variations, the impact on the signal strength is small in the order of $O(1\%)$. For both
 1332 the left- and right-handed tuy coupling, the signal scale uncertainty has the largest impact on the signal
 1333 strength. For the left-handed $tc\gamma$ coupling, the statistical uncertainty of the last bin in the SR comes
 1334 along the largest impact on the signal strength, and for the right-handed $tc\gamma$ coupling, the jet flavour
 1335 composition in the SR of the JES uncertainty is the most important uncertainty. Generally, different JES,
 1336 JER, E_T^{miss} and E/Gamma components, statistical uncertainties in the different regions and the photon
 1337 p_T reweighting for the $W+\gamma+\text{jets}$ process are highly ranked. Moreover, generator uncertainties for the
 1338 single top and $t\bar{t}$ process appear in the ranking plots. The normalisation factors for the prompt photon
 1339 contributions do not show up in the ranking plots for each coupling as they are highly correlated to the
 1340 scale uncertainties of the respective process compensating large variations. Since both the signal and
 1341 background input distributions, the correlations of the NPs and the impacts of the various uncertainties
 1342 differ for the different signal couplings in the fit, the impact of the NPs differ among the signal couplings.

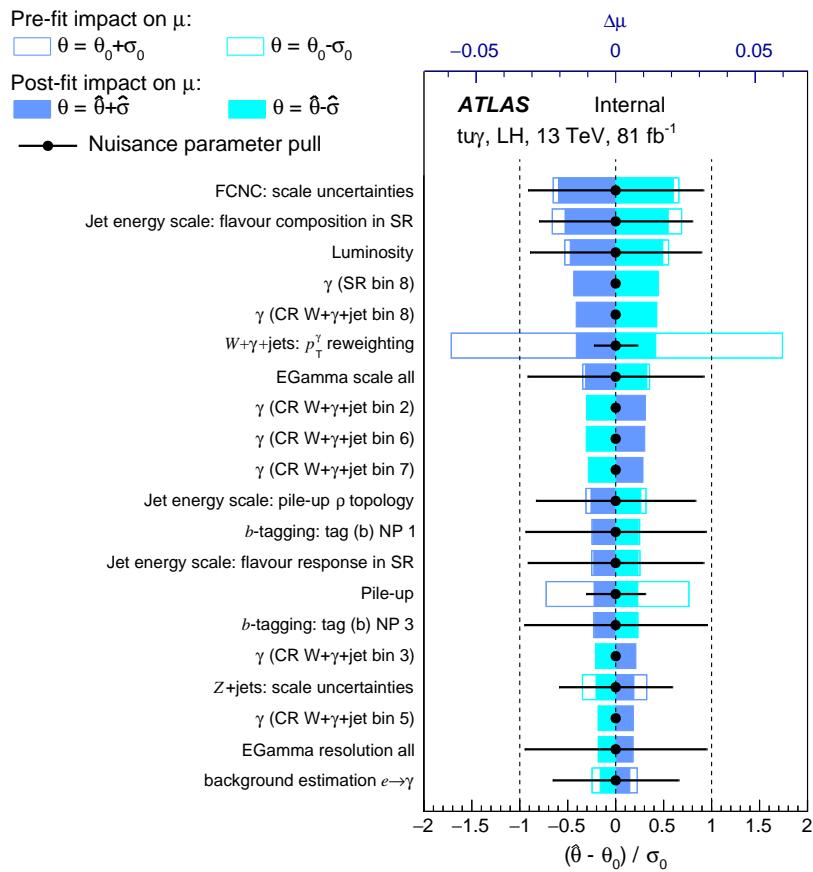


Figure 54: Ranking plot for the 20 nuisance parameters with the largest impact on the signal strength for the left-handed tuy coupling using Asimov data.

10.6 Fit result with data in control regions

The correlation coefficients of the NPs to each other are given in Figure 55 for the left-handed signal coupling tuy . Here, only systematic sources with at least one correlation coefficient above 10 % are drawn. It can be seen that most of the correlations are of a few percent. The normalisation factors for the prompt photon contributions are highly anti-correlated to the respective scale uncertainties and to the pile-up uncertainty since all these uncertainties mainly impact the normalisation of the prompt photon contributions. Furthermore, the NP for the photon p_T reweighting shows some medium correlations to other NPs. Those NPs also introduce a slope as the photon p_T reweighting. The pre-fit and post-fit yields for the different processes in the different regions considered in the fit are shown in Tables 25 and 27, respectively. The distributions in the different regions before and after the fit are shown for the left-handed tuy coupling in Figures 49 and 56. In the bottom plots, the ratio of data to prediction including all uncertainties is shown. It can be seen that the data and MC are in good agreement in the CRs. In Figure 57, the normalisation factors for the $W+\gamma+jets$ and $Z+\gamma+jets$ process are shown. The pull values for the NPs representing the systematic uncertainties are shown for the left-handed tuy coupling in Figure 58 and the normalisation factors γ in Figure 59. It can be seen that the NPs for the photon p_T reweighting are tightly constrained and slightly pulled in the case for the $W+\gamma+jets$ process, as they come along with a large uncertainty. Moreover, some of the scale uncertainties are pulled, as they have a large impact on the

normalisation of the respective process and also impact the shape of the distributions. The uncertainty for the hadronic fake scale factor is also pulled which is not surprising since its estimation comes along with a large uncertainty. In addition, this background only plays a minor role in all regions. All other pull values look reasonable. The distribution of the negative-log likelihood is shown in Figure 60. It can be seen that the fitted signal strength is below one standard deviation meaning that no signal could be found. The distributions for the right-handed $t\gamma\gamma$, left-handed $t\gamma\gamma$, and right-handed $t\gamma\gamma$ coupling couplings are shown in Appendix W.

Not reviewed, for internal circulation only

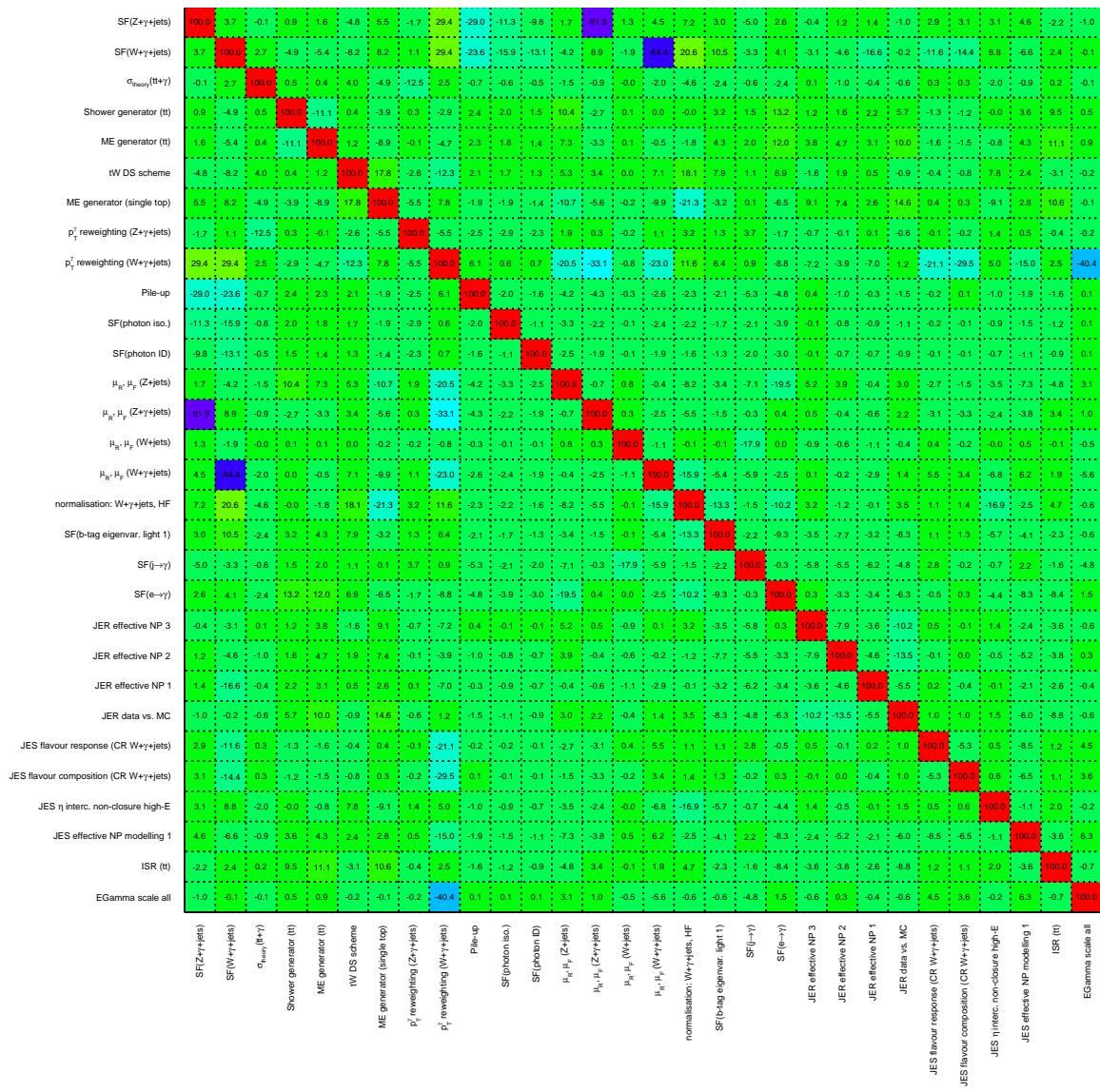


Figure 55: Correlation coefficients of all parameters with at least one coefficient above 10 % for the left-handed $t\gamma\gamma$ coupling considered in the fit using data in the CRs.

Not reviewed, for internal circulation only

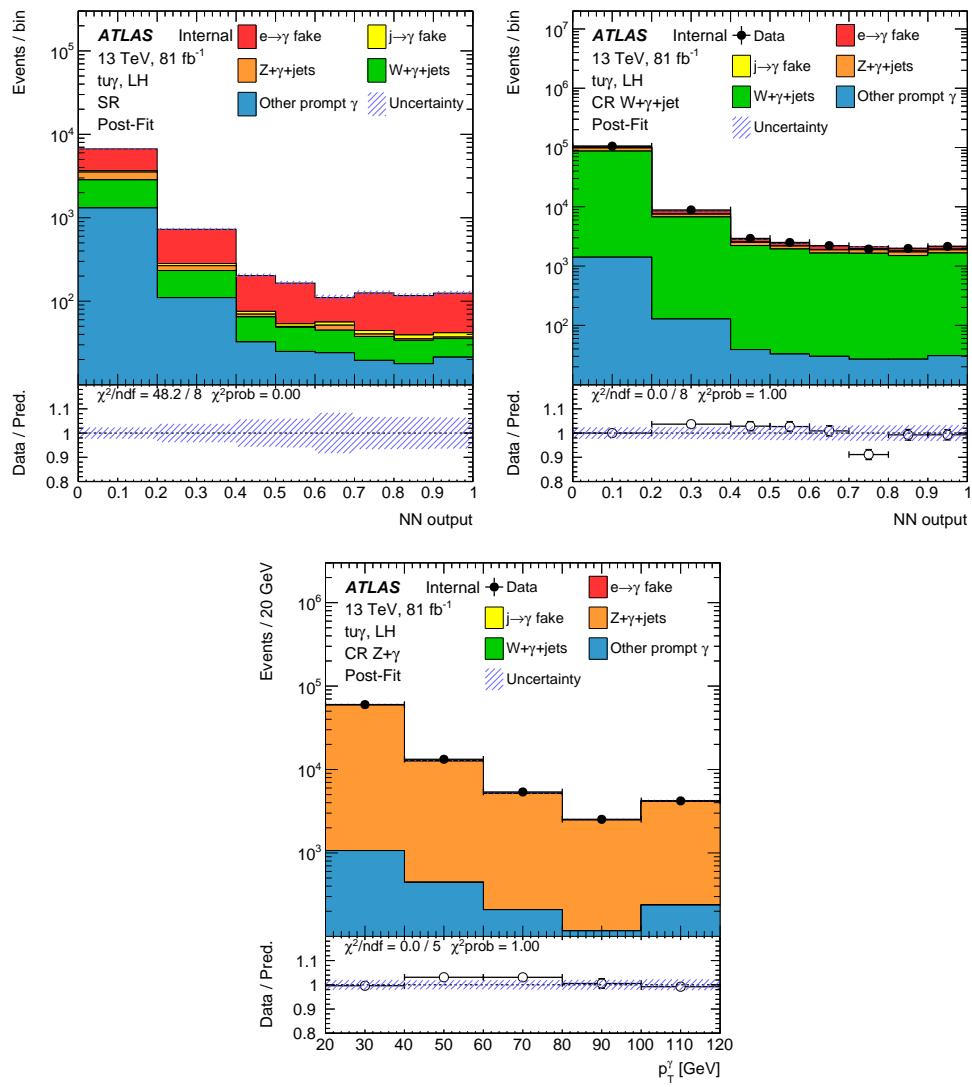


Figure 56: Post-fit distributions for the left-handed signal coupling tuy using data in the CRs: NN output distribution in the SR (top left) and the CR $W+\gamma+jets$ (top right) and the photon p_T spectrum in the CR $Z+\gamma$ (bottom). Statistical and systematic uncertainties are included.

Table 27: Yields for the different contributions in the different regions after the fit using data in the CRs for the left-handed $t\gamma\gamma$ coupling. The statistical uncertainty and all systematic uncertainties are included.

Photon origin	SR			CR $W+\gamma+\text{jets}$			CR $Z+\gamma$	
$e \rightarrow \gamma$	4 000	\pm	360	7 400	\pm	1 200	227	\pm 30
$j \rightarrow \gamma$	190	\pm	140	2 700	\pm	1 900	1 100	\pm 800
$Z+\gamma+\text{jets}$	733	\pm	96	13 300	\pm	1 300	81 600	\pm 1 800
$W+\gamma+\text{jets}$	1 780	\pm	360	102 500	\pm	2 700	5.1	\pm 1.7
Other prompt photon	1 560	\pm	330	1 700	\pm	370	2 070	\pm 200
Total SM	8 270	\pm	200	127 600	\pm	3 000	85 000	\pm 1 600
Data	9 557			127 864			85 347	

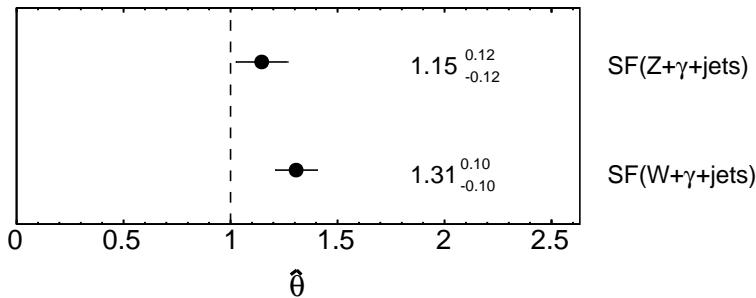


Figure 57: Normalisation factors for the $W+\gamma+\text{jets}$ and $Z+\gamma+\text{jets}$ process using the left-handed $t\gamma\gamma$ coupling using data in the CRs.

Not reviewed, for internal circulation only

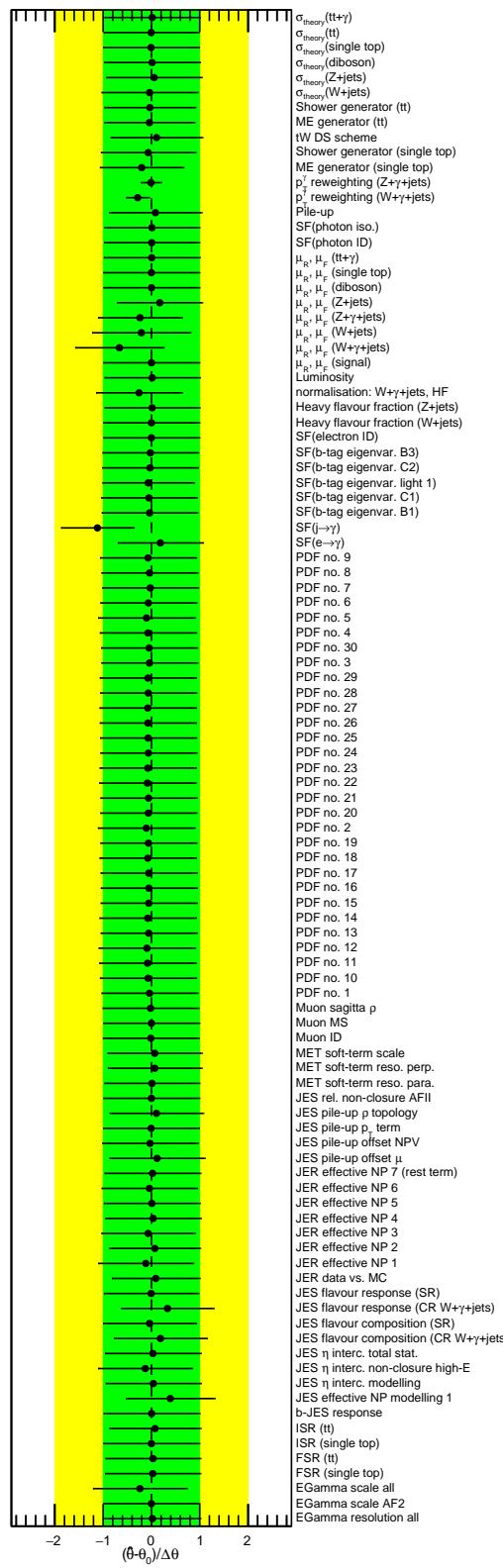


Figure 58: Pull values for the left-handed tuy coupling for the different nuisance parameters considered in the fit using data in the CRs.

Not reviewed, for internal circulation only

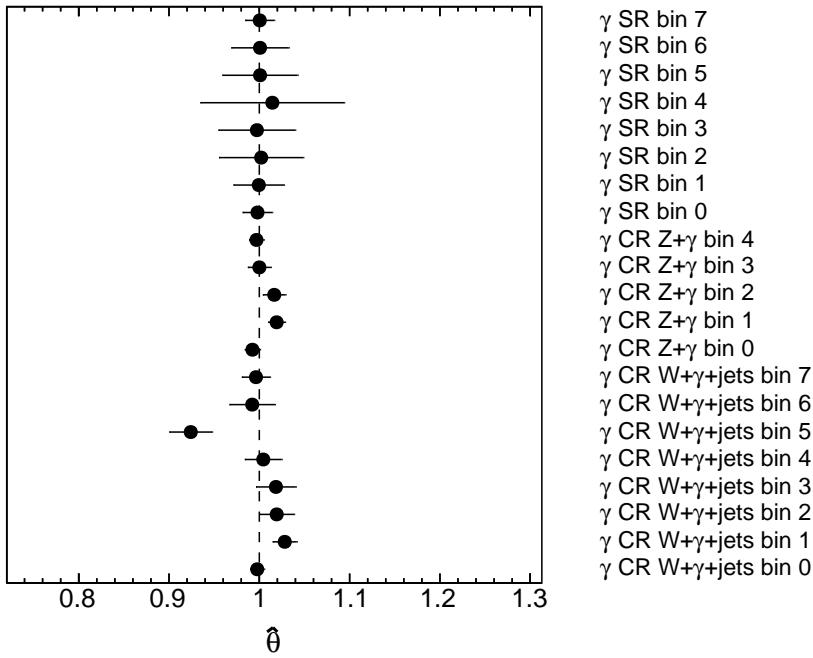


Figure 59: Normalisation factors γ for each bin in each region for the left-handed $t\bar{u}\gamma$ coupling using data in the CRs.

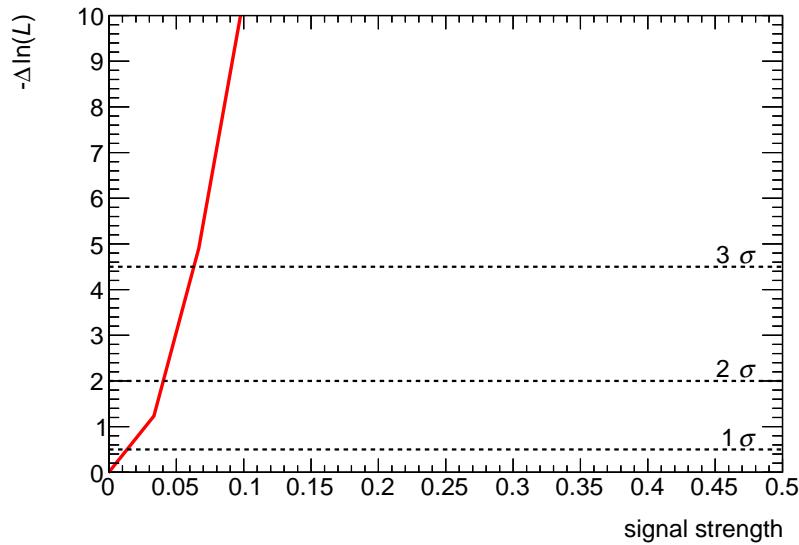


Figure 60: Distributions of the negative-log likelihood for the signal strength using data in the CRs for the left-handed $t\bar{u}\gamma$ coupling. The one, two and three standard deviations are marked.

1367 10.7 Fit result with data

1368 The correlation coefficients of the NPs to each other are given in Figure 61 for the left-handed signal
 1369 coupling tuy . Here, only systematic sources with at least one correlation coefficient above 10 % are
 1370 drawn. It can be seen that most of the correlations are of a few percent. The normalisation factors for
 1371 the prompt photon contributions are highly anti-correlated to the respective scale uncertainties and to the
 1372 pile-up uncertainty since all these uncertainties mainly impact the normalisation of the prompt photon
 1373 contributions. Furthermore, the NP for the photon p_T reweighting shows some medium correlations to
 1374 other NPs. Those NPs also introduce a slope as the photon p_T reweighting. The pre-fit and post-fit yields
 1375 for the different processes in the different regions considered in the fit are shown in Tables 28 and 29,
 1376 respectively, and illustrated in Figure 62. The impact of each systematic uncertainty on the yield in each
 1377 region for all couplings is shown in Appendix X. In Appendix U, the composition of the physics processes
 1378 for the photon fake categories and the *other prompt γ* class is shown for all regions. The distributions in
 1379 the different regions before and after the fit are shown for the left-handed tuy coupling in Figure 63. In
 1380 the bottom plots, the ratio of data to prediction including all uncertainties is shown. It can be seen that the
 1381 data and MC are in good agreement in the CRs. In Figure 64, the normalisation factors for the $W+\gamma+jets$
 1382 and $Z+\gamma+jets$ process are shown. The pull values for the NPs representing the systematic uncertainties
 1383 are shown for the left-handed tuy coupling in Figure 65. It can be seen that the NPs for the photon p_T
 1384 reweighting are tightly constrained and slightly pulled in the case for the $W+\gamma+jets$ process, as they come
 1385 along with a large uncertainty. Moreover, some of the scale uncertainties are pulled, as they have a large
 1386 impact on the normalisation of the respective process and also impact the shape of the distributions. The
 1387 uncertainty for the hadronic fake scale factor is also pulled which is not surprisingly since its estimation
 1388 comes along with a large uncertainty. This also holds for the scale factor $SF(e \rightarrow \gamma)$. In addition, this
 1389 background only plays a minor role in all regions. In Figure 66, the normalisation factors γ are shown for
 1390 each bin in each region. The γ value of bin 5 in the SR γ SR bin 4 is caused by a down fluctuation of
 1391 the $e \rightarrow \gamma$ fake contribution, as studies in Appendix Y confirmed. All other pull values look reasonable.
 1392 The distribution of the negative-log likelihood is shown in Figure 60. It can be seen that the fitted signal
 1393 strength is below one standard deviation meaning that no signal could be found. The distributions for the
 1394 right-handed tuy , left-handed $t\gamma\gamma$, and right-handed $t\gamma\gamma$ coupling couplings are shown in Appendix Z.
 1395 The validation of the fit result is discussed in Section 10.9.

Not reviewed, for internal circulation only

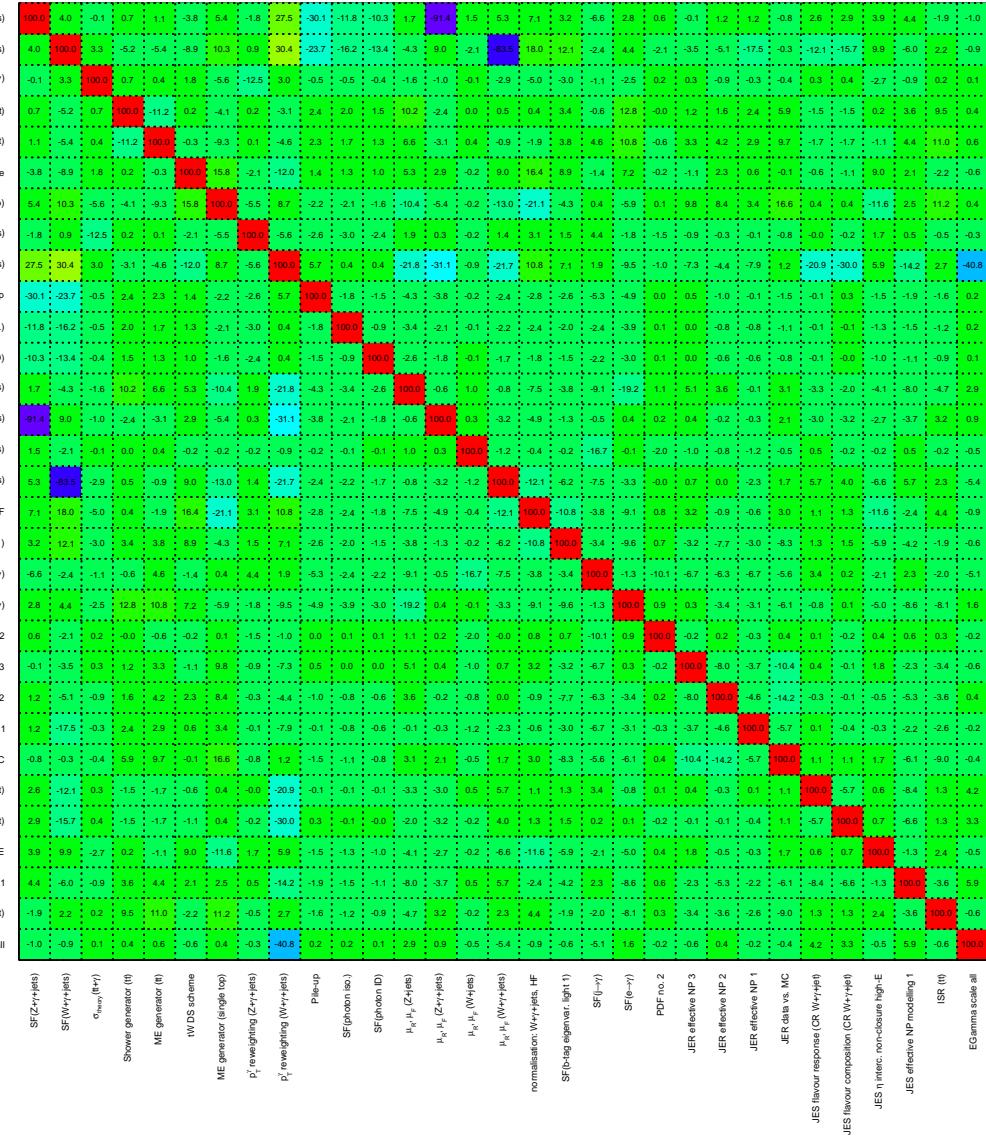


Figure 61: Correlation coefficients of all parameters with at least one coefficient above 10 % for the left-handed $t\gamma\gamma$ coupling considered in the fit using data in all regions.

Table 28: Yields for the different contributions in the different regions before the fit. The statistical uncertainty and all systematic uncertainties are included.

Photon origin	SR		CR $W+\gamma+\text{jets}$			CR $Z+\gamma$		
$e \rightarrow \gamma$	3 840	\pm	660	6 800	\pm	1 500	227	\pm
$j \rightarrow \gamma$	510	\pm	340	8 200	\pm	6 300	2 800	\pm
$Z+\gamma+\text{jets}$	670	\pm	160	11 700	\pm	1 600	73 300	\pm
$W+\gamma+\text{jets}$	1 650	\pm	480	82 400	\pm	6 700	5.1	\pm
Other prompt photon	1 630	\pm	430	1 790	\pm	470	2 110	\pm
Total SM	8 300	\pm	1 100	111 000	\pm	11 000	78 400	\pm
Data	9 557			127 864			85 347	

Table 29: Yields for the different contributions in the different regions after the fit for the left-handed $t\bar{u}y$ coupling. The statistical uncertainty and all systematic uncertainties are included.

Photon origin	SR			CR $W+\gamma+\text{jets}$			CR $Z+\gamma$		
$e \rightarrow \gamma$	4 470	\pm	410	8 200	\pm	1 300	236	\pm	32
$j \rightarrow \gamma$	260	\pm	200	2 900	\pm	2 000	1 300	\pm	970
$Z+\gamma+\text{jets}$	780	\pm	100	13 400	\pm	1 300	81 400	\pm	1 900
$W+\gamma+\text{jets}$	2 200	\pm	440	101 200	\pm	2 800	5.8	\pm	1.8
Other prompt photon	1 790	\pm	380	1 900	\pm	420	2 140	\pm	200
Total SM	9 500	\pm	220	127 700	\pm	3 000	85 100	\pm	1 600
Data	9 557			127 864			85 347		

Not reviewed, for internal circulation only

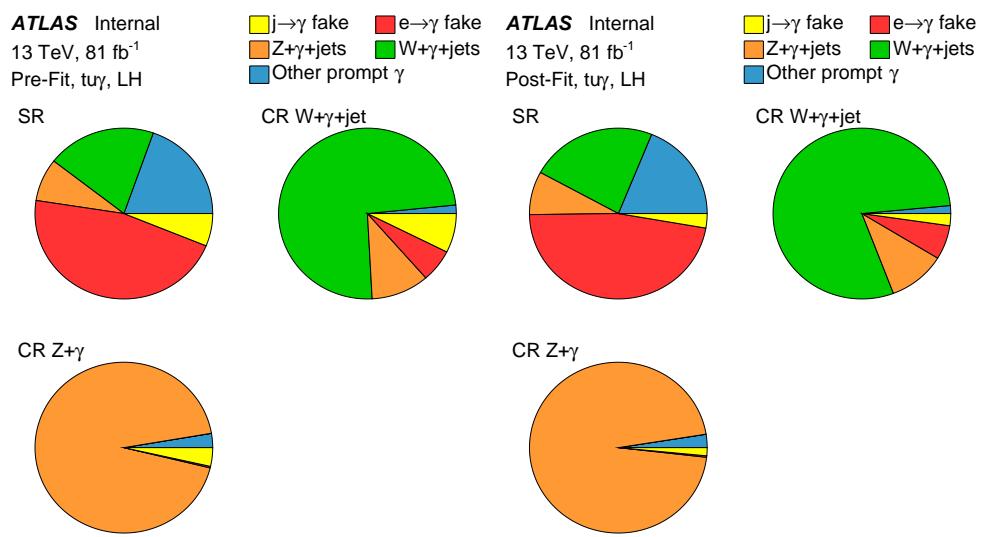


Figure 62: Pie charts showing the composition of the processes before (left) and after the fit using data in all regions (right) in the SR, CR $W+\gamma+\text{jets}$, and CR $Z+\gamma$.

Not reviewed, for internal circulation only

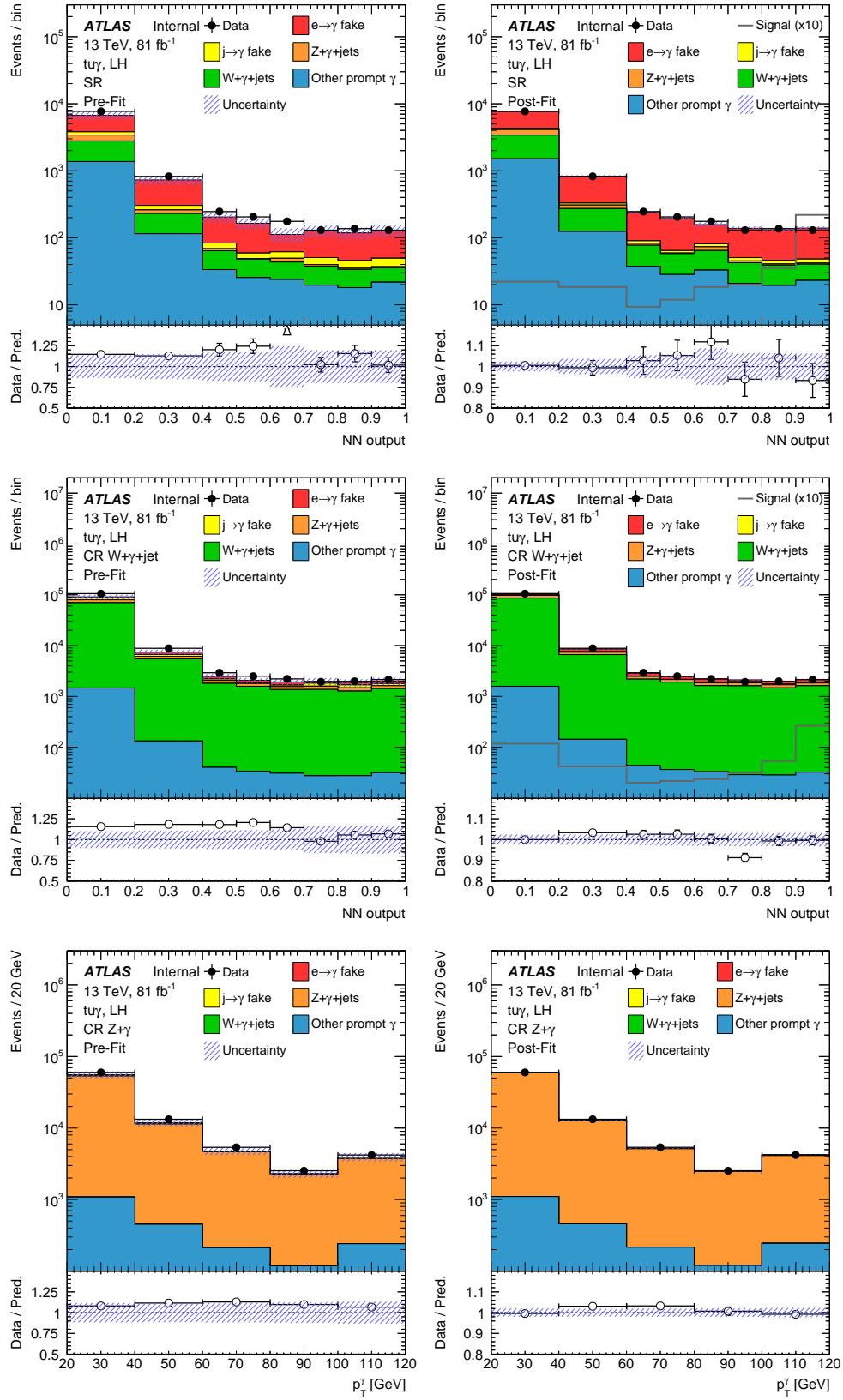


Figure 63: Pre- (left) and post-fit (right) distributions for the left-handed signal coupling $t\gamma$ using data in all regions: NN output distribution in the SR (top), CR $W + \gamma + \text{jets}$ (middle) and the photon p_T spectrum in the CR $Z + \gamma$ (bottom). In the SR and CR $W + \gamma + \text{jets}$, the signal distribution scaled to the observed limit multiplied by 10 is included for the post-fit plots. Statistical and systematic uncertainties are included.
9th July 2019 - 11:54

Not reviewed, for internal circulation only

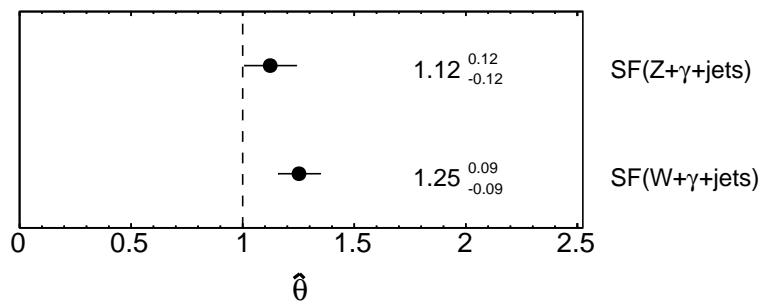


Figure 64: Normalisation factors for the $W + \gamma + \text{jets}$ and $Z + \gamma + \text{jets}$ process using the left-handed $t u \gamma$ coupling using data in all regions.

Not reviewed, for internal circulation only

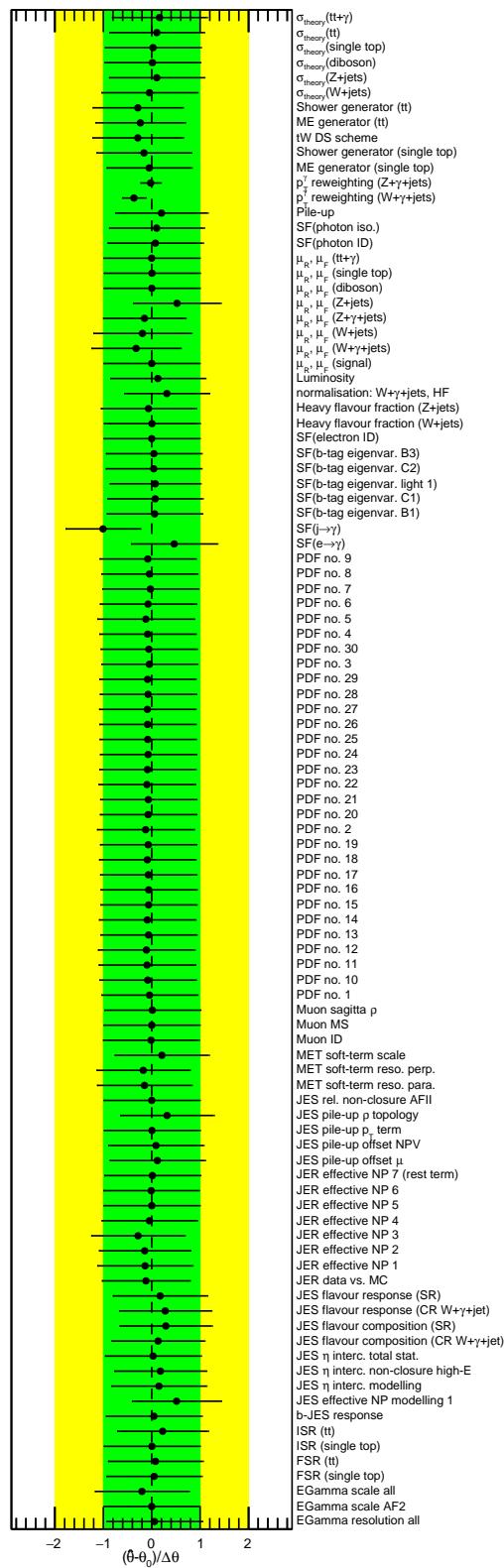


Figure 65: Pull values for the left-handed tuy coupling for the different nuisance parameters considered in the fit using data in all regions.

Not reviewed, for internal circulation only

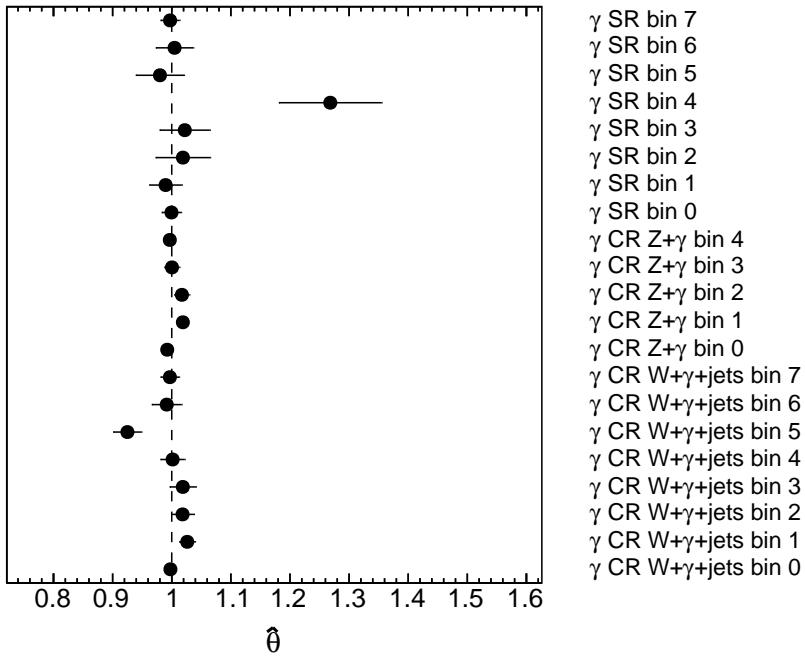


Figure 66: Normalisation factors γ for each bin in each region for the left-handed tuy coupling using data in all regions.

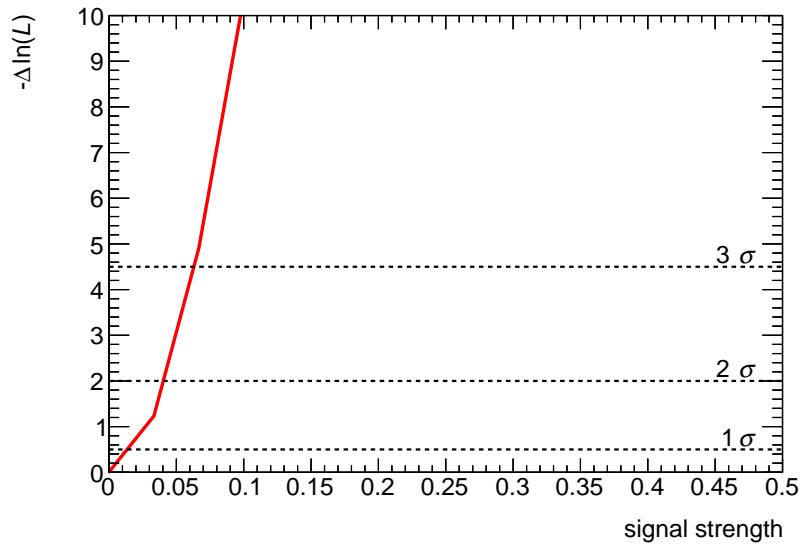


Figure 67: Distributions of the negative-log likelihood for the signal strength using data in all regions for the left-handed tuy coupling. The one, two and three standard deviations are marked.

1396 10.8 Ranking plots using data in all regions

1397 In order to estimate what uncertainty has the largest impact on the signal strength, ranking plots are built
1398 using data in all regions. In Figure 68, the 20 NPs with the largest impact on the signal strength are shown
1399 for the left-handed $t\gamma\gamma$ coupling. The ranking plots for the other couplings can be found in Appendix Z.
1400 For the left-handed $t\gamma\gamma$ coupling, the JER component data vs. MC has the largest impact on the signal
1401 strength, while the variation of the diagram overlap removal scheme for the single top tW process impacts
1402 the most in the case of the right-handed $t\gamma\gamma$ coupling. For the left-handed $t\gamma\gamma$ coupling, the uncertainty
1403 due to the heavy flavour fraction of the $Z+jets$ process comes along the largest impact on the signal
1404 strength, and for the right-handed $t\gamma\gamma$ coupling, the uncertainty on hadronic scale factor represents the
1405 most important uncertainty. Generally, different JES, JER, E_T^{miss} and E/Gamma components, statistical
1406 uncertainties in the different regions and the photon p_T reweighting for the $W+\gamma+jets$ process are highly
1407 ranked. Moreover, generator uncertainties for the single top and $t\bar{t}$ process and the uncertainty on the
1408 hadronic scale factor appear in the ranking plots. For both $t\gamma\gamma$ couplings, the electron-to-photon scale
1409 factor is under the top ranked uncertainties. Since both the signal and background input distributions, the
1410 correlations of the NPs and the impacts of the various uncertainties differ for the different signal couplings
1411 in the fit, the impact of the NPs differ among the signal couplings. Moreover, when comparing the ranking
1412 plots for the Asimov fit in Figure 54, it can be seen that NPs affecting the shape become more important
1413 for the fit to data as more pieces of shape information are available in this case.

Not reviewed, for internal circulation only

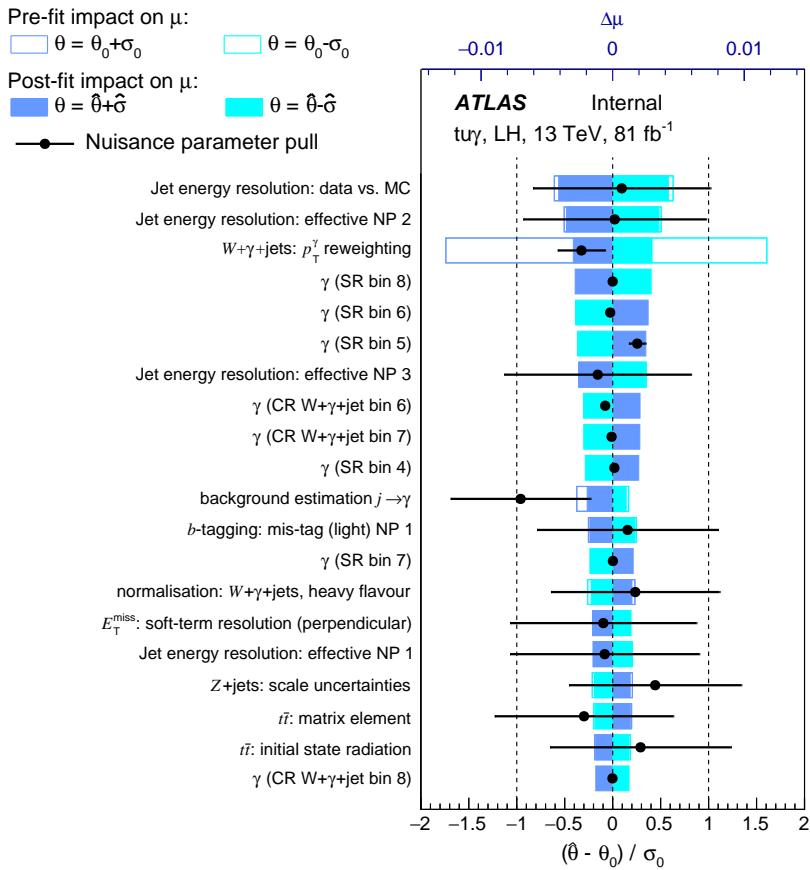


Figure 68: Ranking plot for the 20 nuisance parameters with the largest impact on the signal strength for the left-handed tuy coupling using data in all regions and performing an S+B fit.

1414 10.9 Validation of fit result

1415 In order to validate the fit outcome, different distributions are looked at. On the one hand, the input
 1416 variables for the NN in the SR are plotted, and on the other hand, distributions in the VRs for the electron-
 1417 to-photon scale factor $SF(e \rightarrow \gamma)$ and for the combined background are shown. In Appendix Z, the same
 1418 plots are shown for the other signal couplings.

1419 10.9.1 Input variables of the neural network in the signal region

1420 The input variables for the NN as described in Section 8.1 are used to validate the fit result. In Fig-
 1421 ures 69, 70, 71, and 72 the distributions are shown before and after the fit. It can be seen that the prediction
 1422 agrees well with data after the fit is performed.

Not reviewed, for internal circulation only

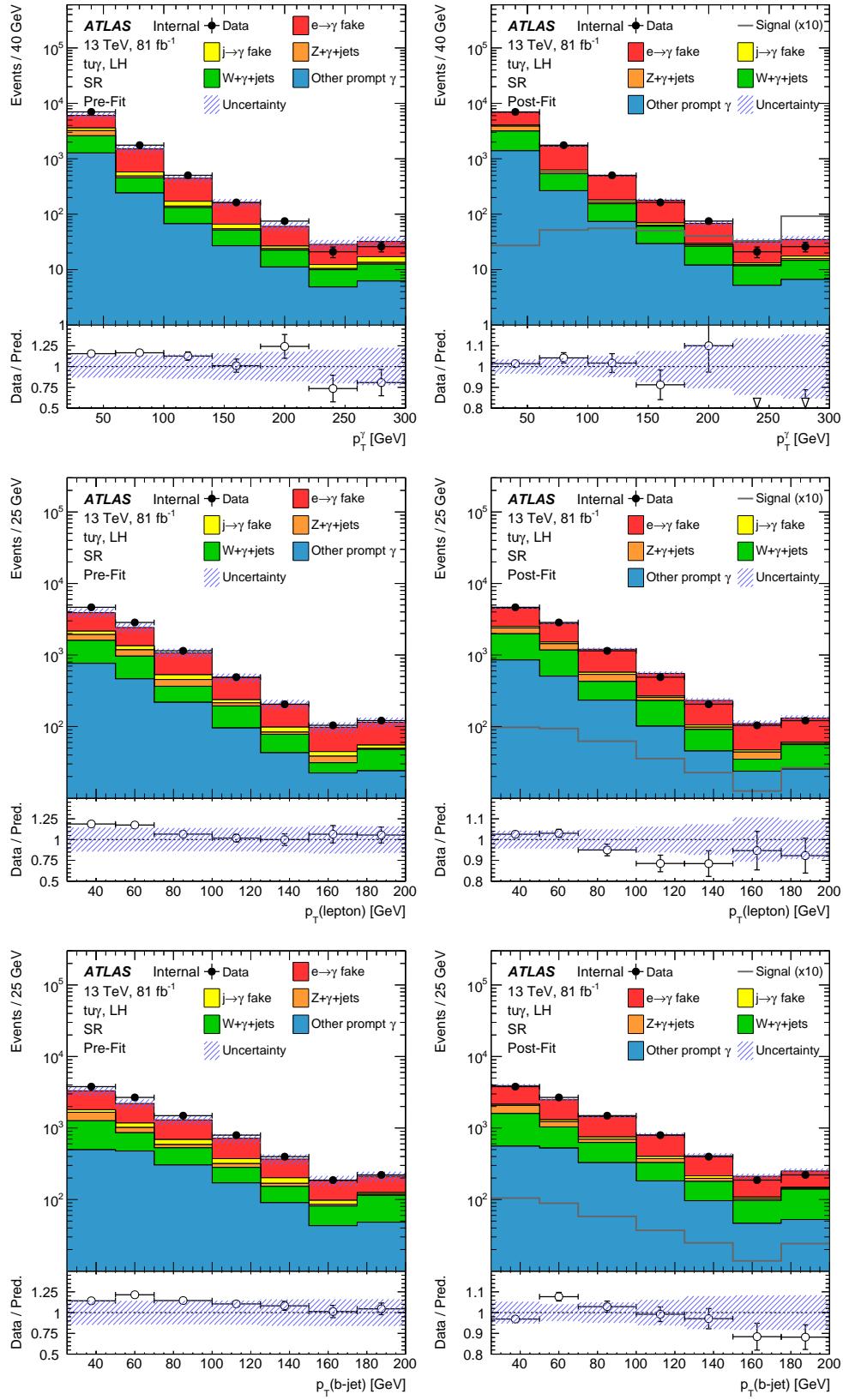


Figure 69: Pre- (left) and post-fit (right) distributions for the left-handed signal coupling tuy using data in the SR: photon p_T (top), lepton p_T (middle), and jet p_T (bottom). In the post-fit distributions, the signal distribution scaled to the observed limit multiplied by 10 is included. Statistical and systematic uncertainties are included.

Not reviewed, for internal circulation only

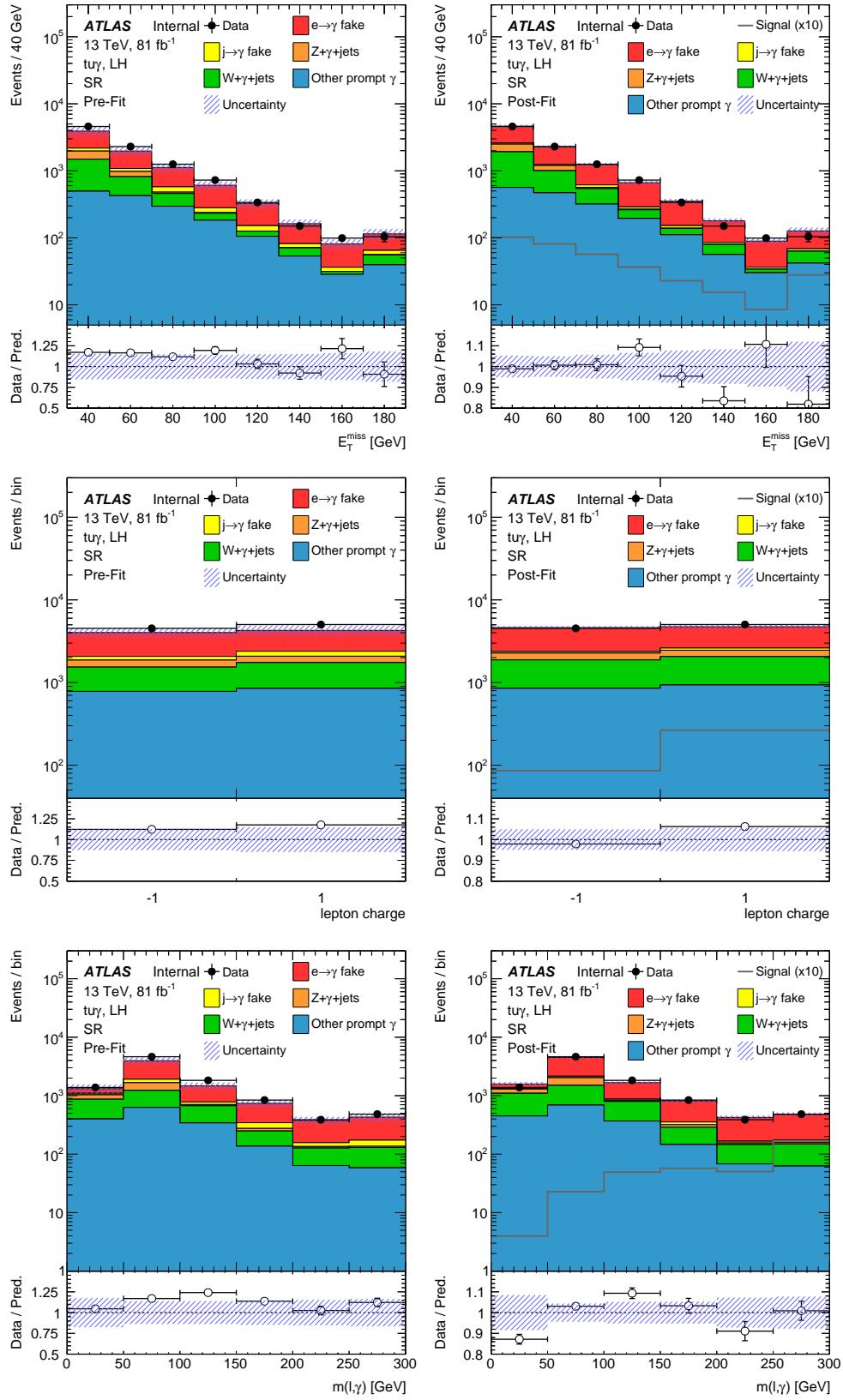


Figure 70: Pre- (left) and post-fit (right) distributions for the left-handed signal coupling tuy using data in the SR: missing transverse momentum E_T^{miss} (top), lepton charge (middle), and invariant mass of the lepton-photon system $m(l\gamma)$ (bottom). In the post-fit distributions, the signal distribution scaled to the observed limit multiplied by 10 is included. Statistical and systematic uncertainties are included.

Not reviewed, for internal circulation only

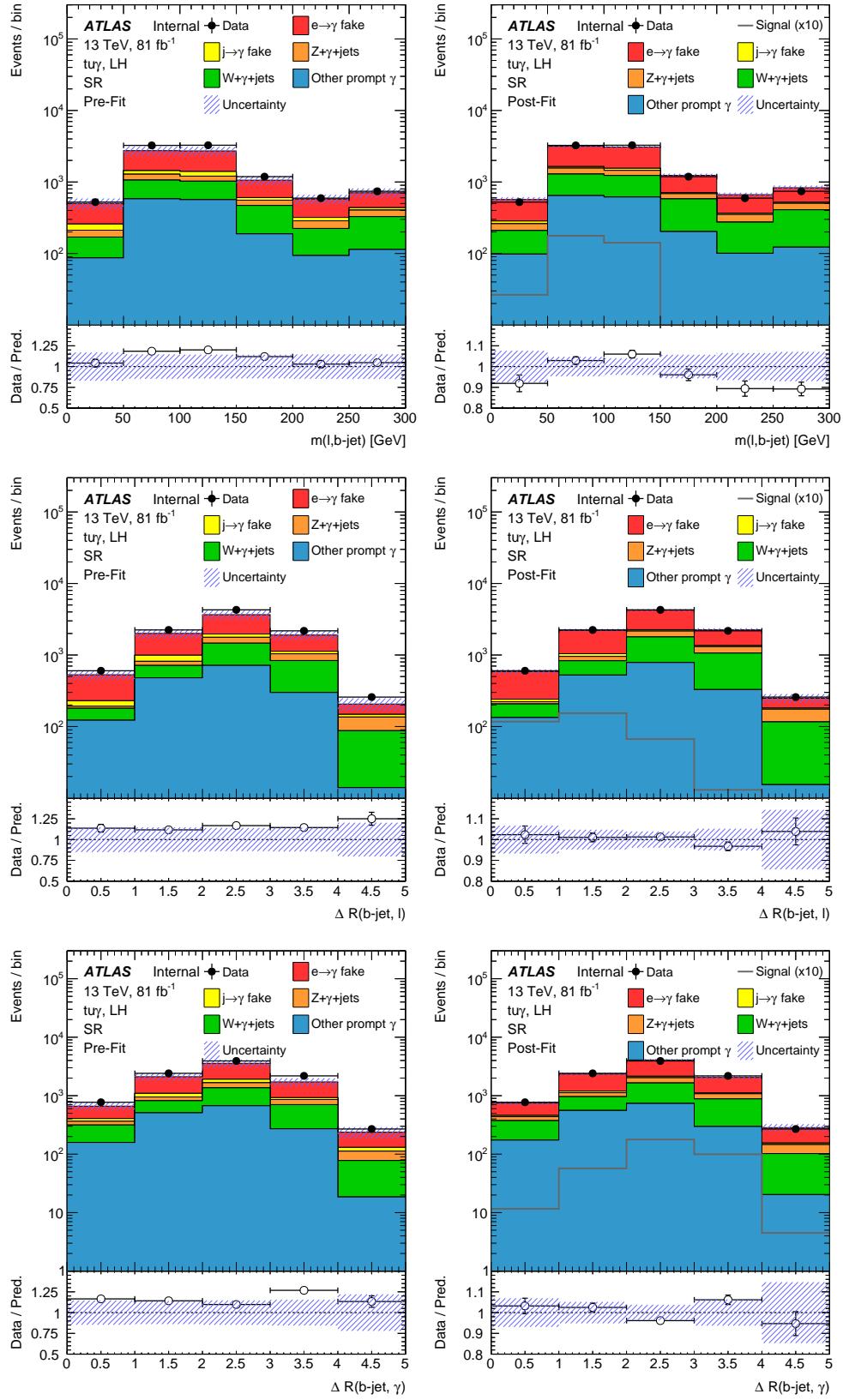


Figure 71: Pre- (left) and post-fit (right) distributions for the left-handed signal coupling tuy using data in the SR: invariant mass of the jet-lepton system $m(lj)$ (top), distance between the jet and lepton $\Delta R(j, \ell)$ (middle), and distance between the jet and photon $\Delta R(j, \gamma)$ (bottom). In the post-fit distributions, the signal distribution scaled to the observed limit multiplied by 10 is included. Statistical and systematic uncertainties are included.

9th July 2019 – 11:54

118

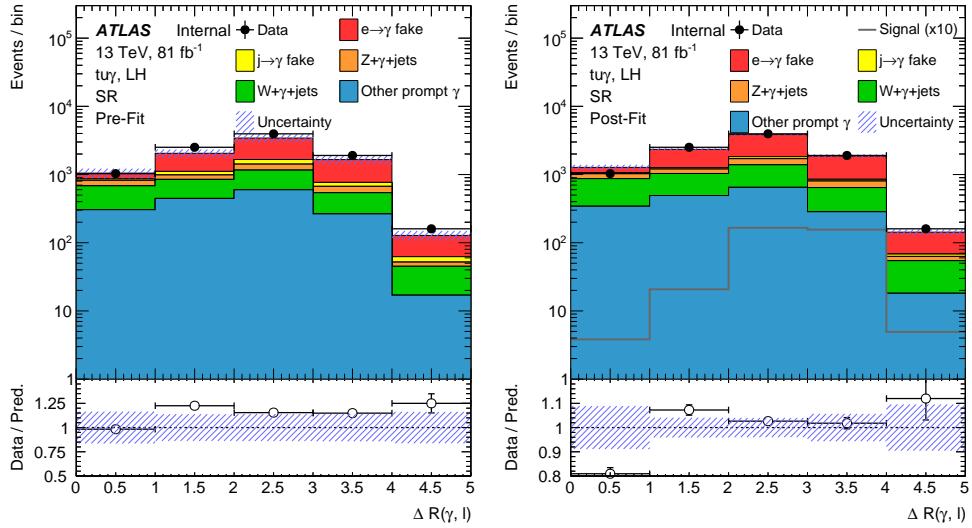


Figure 72: Pre- (left) and post-fit (right) distribution for the left-handed signal coupling tuy using data in the SR: distance between the lepton and photon $\Delta R(\ell, \gamma)$. In the post-fit distributions, the signal distribution scaled to the observed limit multiplied by 10 is included. Statistical and systematic uncertainties are included.

1423 10.9.2 Validation regions

1424 In order to validate the fit outcome in regions enriched with photon fakes, kinematic properties in the
 1425 validation regions for the data-driven background scale factor $SF(e \rightarrow \gamma)$ and the combined background
 1426 are investigated whose definitions are given in Tables 13 and 14. In Tables 30 and 31, the pre- and post-fit
 1427 yields, respectively, are shown for the VR $SF(e \rightarrow \gamma)$ and combined background VR. In Figures 353
 1428 and 354, plots are shown for the VR $SF(e \rightarrow \gamma)$ and combined background VR, respectively. In both
 1429 regions, a good agreement between prediction and data can be observed.

Table 30: Yields for the different contributions before the fit using the left-handed tuy coupling in the VRs $SF(e \rightarrow \gamma)$ and combined background. The statistical uncertainty and all systematic uncertainties are included.

Photon origin	VR $SF(e \rightarrow \gamma)$	combined background VR		
$e \rightarrow \gamma$	237 000	\pm	31 000	36 500
$j \rightarrow \gamma$	540	\pm	220	9 100
$Z + \gamma + \text{jets}$	24 000	\pm	2 200	19 200
$W + \gamma + \text{jets}$	9 030	\pm	950	70 000
Other prompt photon	1 040	\pm	170	21 700
Total SM	271 000	\pm	32 000	157 000
Data	312 550			180 804

Table 31: Yields for the different contributions after the fit using the left-handed $t\gamma\gamma$ coupling in the VRs $SF(e \rightarrow \gamma)$ and combined background. The statistical uncertainty and all systematic uncertainties are included.

Photon origin	VR $SF(e \rightarrow \gamma)$		combined background VR	
$e \rightarrow \gamma$	260 000	\pm	28 000	40 500
$j \rightarrow \gamma$	620	\pm	200	4 100
$Z + \gamma + \text{jets}$	27 000	\pm	2 000	21 800
$W + \gamma + \text{jets}$	11 100	\pm	610	84 000
Other prompt photon	1 090	\pm	150	22 400
Total SM	299 000	\pm	29 000	173 000
Data	312 550			180 804

Not reviewed, for internal circulation only

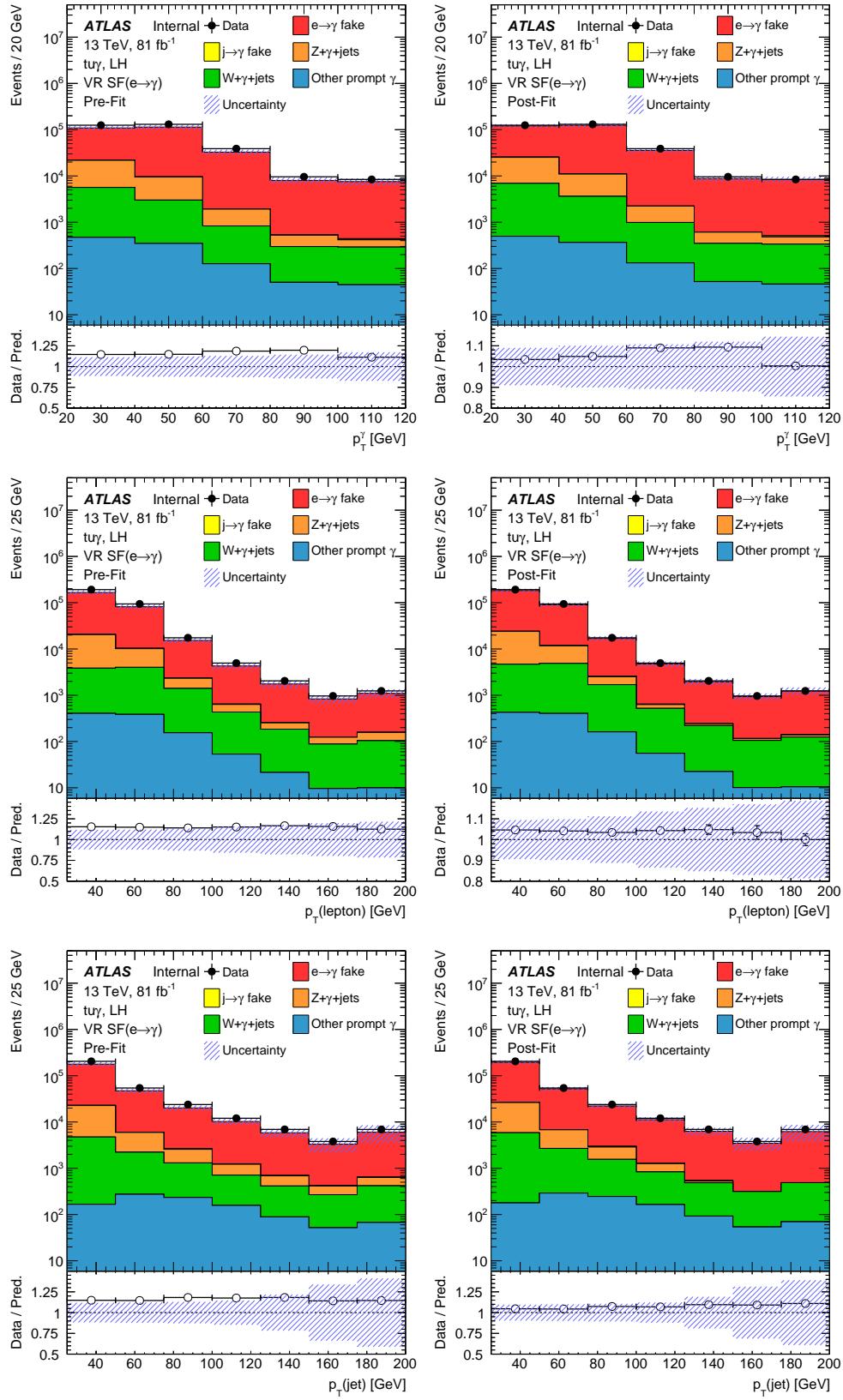


Figure 73: Pre- (left) and post-fit (right) distributions for the left-handed signal coupling tuy using data in the VR $SF(e \rightarrow \gamma)$: photon p_T (top), lepton p_T (middle), and jet p_T (bottom). Statistical and systematic uncertainties are included.

Not reviewed, for internal circulation only

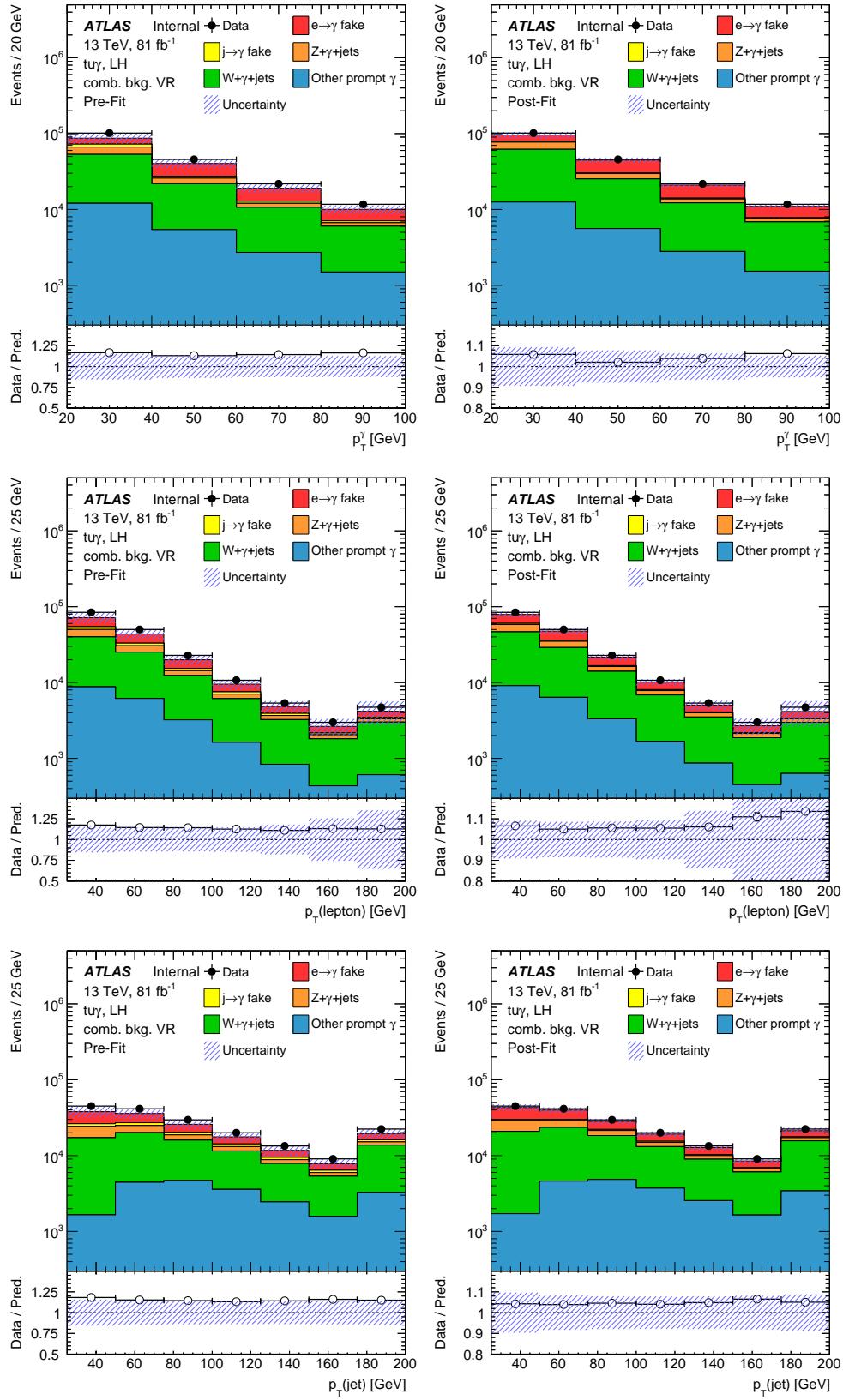


Figure 74: Pre- (left) and post-fit (right) distributions for the left-handed signal coupling tuy using data in the combined background VR: photon p_T (top), lepton p_T (middle), and jet p_T (bottom). Statistical and systematic uncertainties are included.

1430 11 Interpretation of results

1431 In this chapter, the fit results are interpreted and 95 % C.L. limits are set on different measures using the
 1432 CL_s method. The interpretation follows the description as given in Ref. [14]. For all limits, it is assumed
 1433 that only one coupling is present at once in both production and decay mode. For the computation of the
 1434 expected limits, all fitted NPs and normalisation factors are taken into account.

1435 11.1 Limits on signal strength

1436 Limits on the signal strength are derived by using the CL_s method. In Table 32, the 95 % C.L. observed
 1437 (expected) upper limits on the signal strength are shown for all couplings using data in all regions.

Table 32: 95 % C.L. observed (expected) upper limits on the signal strength for the different assumed signal couplings.

Signal coupling	$t\gamma$, left-handed	$t\gamma$, right-handed	$t\gamma$, left-handed	$t\gamma$, right-handed
$\mu [10^{-2}]$	$2.8 (4.0^{+1.6}_{-1.1})$	$6.1 (5.9^{+2.4}_{-1.6})$	$21.8 (26.6^{+11.0}_{-7.4})$	$18.3 (28.4^{+12.3}_{-7.9})$

1438 11.2 Limits on cross section

1439 The limits on the signal strength are used to compute limits on the cross section $\sigma(pp \rightarrow t\gamma)$ for the
 1440 different couplings using Equations (4), (44) and the values $\sigma_{\text{eff,in}}^{\text{coup}}$ given in Table 6 as $\sigma_{\text{eff}}^{\text{coup}}$. The 95 %
 1441 C.L. observed (expected) upper limits on the cross section are displayed in Table 33.

Table 33: 95 % C.L. observed (expected) upper limits on the cross section for the different assumed signal couplings.

Signal coupling	$t\gamma$, left-handed	$t\gamma$, right-handed	$t\gamma$, left-handed	$t\gamma$, right-handed
$\sigma(pp \rightarrow t\gamma) [\text{fb}]$	$36 (52^{+21}_{-14})$	$78 (75^{+31}_{-21})$	$40 (49^{+20}_{-14})$	$33 (52^{+22}_{-14})$

1442 11.3 Limits on Wilson coefficients

1443 In order to derive limits on the Wilson coefficients, Equations (8) and (44) are combined giving

$$\mu = \frac{C_{\text{sum,fit}}^2}{C_{\text{sum,eff}}^2}. \quad (47)$$

1444 The 95 % C.L. observed (expected) upper limits on the absolute sum of the Wilson coefficients assuming
 1445 a scale of new physics of $\Lambda = 1 \text{ TeV}$ for the different signal couplings are shown in Table 34.

Not reviewed, for internal circulation only

Table 34: 95 % C.L. observed (expected) upper limits on the absolute sum of the Wilson coefficients for the different assumed signal couplings assuming a scale of new physics of $\Lambda = 1$ TeV.

Signal coupling	Sum of Wilson coefficients	95 % C.L. upper limit
$t\gamma u\gamma$, left-handed	$ C_{uW}^{(13)*} + C_{uB}^{(13)*} $	$0.186 \left(0.224^{+0.042}_{-0.034}\right)$
$t\gamma u\gamma$, right-handed	$ C_{uW}^{(31)} + C_{uB}^{(31)} $	$0.274 \left(0.270^{+0.050}_{-0.041}\right)$
$t\gamma c\gamma$, left-handed	$ C_{uW}^{(23)*} + C_{uB}^{(23)*} $	$0.519 \left(0.574^{+0.108}_{-0.087}\right)$
$t\gamma c\gamma$, right-handed	$ C_{uW}^{(32)} + C_{uB}^{(32)} $	$0.475 \left(0.592^{+0.117}_{-0.090}\right)$

1446 11.4 Limits on branching ratio

1447 For the limits on the branching ratio, Equations (21) and (44) are connected giving

$$\mu = \frac{\mathcal{B}(t \rightarrow q\gamma)_{\text{fit}}}{\mathcal{B}(t \rightarrow q\gamma)_{\text{eff}}} . \quad (48)$$

1448 The 95 % C.L. observed (expected) upper limits on the branching ratio are displayed in Table 35.

Table 35: 95 % C.L. observed (expected) upper limits on the branching ratio for the different assumed signal couplings.

Signal coupling	$t\gamma u\gamma$, left-handed	$t\gamma u\gamma$, right-handed	$t\gamma c\gamma$, left-handed	$t\gamma c\gamma$, right-handed
$\mathcal{B}(t \rightarrow q\gamma) [10^{-5}]$	$2.8 \left(4.0^{+1.6}_{-1.1}\right)$	$6.1 \left(5.9^{+2.4}_{-1.6}\right)$	$21.8 \left(26.6^{+11.0}_{-7.4}\right)$	$18.3 \left(28.4^{+12.3}_{-7.9}\right)$

1449 11.5 Limits for Asimov data

1450 The 95 % C.L. limits on the different measures discussed above when using Asimov data are shown in
1451 Table 36.

Table 36: Expected 95 % C.L. upper limits on the cross sections $\sigma(pp \rightarrow t\gamma)$, sum of pairs of Wilson coefficients $|C_{uB}^{ij} + C_{uW}^{ij}|$ assuming a scale of new physics of $\Lambda = 1$ TeV and branching ratios $\mathcal{B}(t \rightarrow q\gamma)$ for the four different assumed signal couplings using Asimov data.

Coupling	$\mu [10^{-2}]$	$\sigma(pp \rightarrow t\gamma) [\text{fb}]$	$ C_{uB}^{ij} + C_{uW}^{ij} $	$\mathcal{B}(t \rightarrow q\gamma) [10^{-5}]$
$t \rightarrow u\gamma$, left-handed	$3.9^{+1.6}_{-1.1}$	50^{+21}_{-14}	$0.221^{+0.041}_{-0.033}$	$3.9^{+1.6}_{-1.1}$
$t \rightarrow u\gamma$, right-handed	$5.5^{+2.3}_{-1.5}$	71^{+29}_{-20}	$0.262^{+0.049}_{-0.040}$	$5.5^{+2.3}_{-1.5}$
$t \rightarrow c\gamma$, left-handed	$25.0^{+10.3}_{-7.0}$	46^{+19}_{-13}	$0.556^{+0.104}_{-0.084}$	$25.0^{+10.3}_{-7.0}$
$t \rightarrow c\gamma$, right-handed	$27.3^{+11.7}_{-7.6}$	50^{+21}_{-14}	$0.581^{+0.113}_{-0.088}$	$27.3^{+11.7}_{-7.6}$

1452 12 Conclusion

1453 In this note, the first search by ATLAS for flavour-changing neutral currents with a single-top quark
 1454 produced in association with a photon has been presented. The data were collected at $\sqrt{s} = 13$ TeV
 1455 corresponding to an integrated luminosity of 81 fb^{-1} recorded in 2015, 2016 and 2017. Four different
 1456 signal couplings differing in kinematic properties have been tested, namely $t u \gamma$ left-handed, $t u \gamma$ right-
 1457 handed, $t c \gamma$ left-handed, and $t c \gamma$ right-handed. Both the production and decay mode have been considered.
 1458 The top quark has been assumed to decay into a b quark and a W boson that itself decays leptonically.
 1459 Events have been required to contain an isolated high- p_T photon, an isolated charged lepton, a b -tagged jet
 1460 and missing transverse momentum and classified into events with an electron-to-photon fake, a hadronic
 1461 fake, or a prompt photon. The main background arises from events with an electron-to-photon fake and
 1462 with a prompt photon stemming from $W + \gamma + \text{jets}$ process. The backgrounds with a fake photon have
 1463 been estimated using data-driven techniques. A neural network has been used to separate signal-like
 1464 events from background-like candidates. The output distribution of the neural network has been studied
 1465 in the statistical analysis where a binned maximum likelihood fit has been performed. The fit has been
 1466 simultaneously done in the signal region and two control regions enriched with $W/Z + \gamma + \text{jets}$ events. Since
 1467 there is no sensitivity for a real observation with the current dataset, 95 % C.L. upper limits on the cross
 1468 section $\sigma(pp \rightarrow t\gamma)$ have been set for each signal coupling. These limits have been interpreted in terms of
 1469 effective field theory and limits on the absolute sum of pairs of Wilson coefficients $C_{uB}^{ij} + C_{uW}^{ij}$ assuming
 1470 a scale of new physics of $\Lambda = 1$ TeV and the branching ratio $\mathcal{B}(t \rightarrow q\gamma)$ have been derived. All observed
 1471 and expected limits are summarised in Table 37.

Table 37: 95 % C.L. upper limits on the cross sections $\sigma(pp \rightarrow t\gamma)$, sum of pairs of Wilson coefficients $|C_{uB}^{ij} + C_{uW}^{ij}|$ assuming a scale of new physics of $\Lambda = 1$ TeV and branching ratios $\mathcal{B}(t \rightarrow q\gamma)$ for the four different assumed signal couplings.

Coupling	$\sigma(pp \rightarrow t\gamma) [\text{fb}]$		$ C_{uB}^{ij} + C_{uW}^{ij} $		$\mathcal{B}(t \rightarrow q\gamma) [10^{-5}]$	
	Observed	Expected	Observed	Expected	Observed	Expected
$t \rightarrow u\gamma$, left-handed	36	52	0.186	0.224	2.8	4.0
$t \rightarrow u\gamma$, right-handed	78	75	0.274	0.270	6.1	5.9
$t \rightarrow c\gamma$, left-handed	40	49	0.519	0.574	21.8	26.6
$t \rightarrow c\gamma$, right-handed	33	52	0.475	0.592	18.3	28.4

1472 References

- 1473 [1] CDF Collaboration, *Observation of top quark production in $\bar{p}p$ collisions*,
 1474 Phys. Rev. Lett. **74** (1995) 2626, arXiv: [hep-ex/9503002](#) [hep-ex].
- 1475 [2] D0 Collaboration, *Observation of the top quark*, Phys. Rev. Lett. **74** (1995) 2632,
 1476 arXiv: [hep-ex/9503003](#) [hep-ex].
- 1477 [3] S. L. Glashow, J. Iliopoulos, L. Maiani, *Weak Interactions with Lepton-Hadron Symmetry*,
 1478 Phys. Rev. **D2** (1970) 1285.
- 1479 [4] LHCtopWG, *FCNC summary*, Web page, Retrieved from
 1480 https://atlas.web.cern.ch/Atlas/GROUPS/PHYSICS/CombinedSummaryPlots/TOP/fcnc_summarybsm/fcnc_summarybsm.pdf on December 6, 2018, 2018.
- 1481 [5] B. Grzadkowski, M. Iskrzynski, M. Misiak, J. Rosiek,
 1482 *Dimension-Six Terms in the Standard Model Lagrangian*, JHEP **10** (2010) 085,
 1483 arXiv: [1008.4884](#) [hep-ph].
- 1484 [6] CMS Collaboration, *Search for anomalous single top quark production in association with a
 1485 photon in pp collisions at $\sqrt{s} = 8$ TeV*, JHEP **04** (2016) 035, arXiv: [1511.03951](#) [hep-ex].
- 1486 [7] ATLAS collaboration, *Luminosity For Physics (restricted)*, Web page,
 1487 <https://twiki.cern.ch/twiki/bin/viewauth/Atlas/LuminosityForPhysics>, 2018.
- 1488 [8] ATLAS Collaboration,
 1489 *Luminosity determination in pp collisions at $\sqrt{s} = 8$ TeV using the ATLAS detector at the LHC*,
 1490 Eur. Phys. J. C **76** (2016) 653, arXiv: [1608.03953](#) [hep-ex].
- 1491 [9] GEANT4 Collaboration, *GEANT4: A Simulation toolkit*, Nucl. Instrum. Meth. A **506** (2003) 250.
- 1492 [10] ATLAS Collaboration, *The ATLAS Simulation Infrastructure*, Eur. Phys. J. C **70** (2010) 823,
 1493 arXiv: [1005.4568](#) [physics.ins-det].
- 1494 [11] ATLAS Collaboration,
 1495 *The simulation principle and performance of the ATLAS fast calorimeter simulation FastCaloSim*,
 1496 ATL-PHYS-PUB-2010-013, 2010, URL: <https://cds.cern.ch/record/1300517>.
- 1497 [12] J. Alwall et al., *The automated computation of tree-level and next-to-leading order differential
 1498 cross sections, and their matching to parton shower simulations*, JHEP **07** (2014) 79,
 1499 arXiv: [1405.0301](#) [hep-ph].
- 1500 [13] C. Degrande, F. Maltoni, J. Wang, C. Zhang, *Automatic computations at next-to-leading order in
 1501 QCD for top-quark flavor-changing neutral processes*, Phys. Rev. D **91** (2015) 034024,
 1502 arXiv: [1412.5594](#) [hep-ph].
- 1503 [14] G. Durieux, F. Maltoni, C. Zhang, *A global approach to top-quark flavor-changing interactions*,
 1504 Phys. Rev. D **91** (2015) 074017, arXiv: [1412.7166](#) [hep-ph].
- 1505 [15] NNPDF Collaboration, *Parton distributions for the LHC Run II*, JHEP **04** (2015) 040,
 1506 arXiv: [1410.8849](#) [hep-ph].
- 1507 [16] P. Artoisenet, R. Frederix, O. Mattelaer, R. Rietkerk,
 1508 *Automatic spin-entangled decays of heavy resonances in Monte Carlo simulations*,
 1509 JHEP **03** (2013) 015, arXiv: [1212.3460](#) [hep-ph].
- 1510 [17] T. Sjöstrand et al., *An Introduction to PYTHIA 8.2*, Comput. Phys. Commun. **191** (2015) 159,
 1511 arXiv: [1410.3012](#) [hep-ph].

- 1513 [18] ATLAS Collaboration, *ATLAS Run 1 Pythia8 tunes*, ATL-PHYS-PUB-2014-021, 2014,
 1514 URL: <https://cds.cern.ch/record/1966419>.
- 1515 [19] J. Pumplin et al.,
 1516 *New generation of parton distributions with uncertainties from global QCD analysis*,
 1517 **JHEP** **07** (2002) 012, arXiv: [hep-ph/0201195](https://arxiv.org/abs/hep-ph/0201195) [hep-ph].
- 1518 [20] D. J. Lange, *The EvtGen particle decay simulation package*,
 1519 **Nucl. Instrum. Meth. A** **462** (2001) 152.
- 1520 [21] K. Melnikov, M. Schulze, A. Scharf,
 1521 *QCD corrections to top quark pair production in association with a photon at hadron colliders*,
 1522 **Phys. Rev. D** **83** (2011) 074013, arXiv: [1102.1967](https://arxiv.org/abs/1102.1967) [hep-ph].
- 1523 [22] ATLAS Collaboration, *Measurements of inclusive and differential fiducial cross-sections of $t\bar{t}\gamma$ production in leptonic final states at $\sqrt{s} = 13$ TeV in ATLAS*, Submitted to: Eur. Phys. J. (2018),
 1524 arXiv: [1812.01697](https://arxiv.org/abs/1812.01697) [hep-ex].
- 1526 [23] P. Nason, *A New method for combining NLO QCD with shower Monte Carlo algorithms*,
 1527 **JHEP** **11** (2004) 040, arXiv: [hep-ph/0409146](https://arxiv.org/abs/hep-ph/0409146) [hep-ph].
- 1528 [24] S. Frixione, P. Nason, C. Oleari,
 1529 *Matching NLO QCD computations with Parton Shower simulations: the POWHEG method*,
 1530 **JHEP** **11** (2007) 070, arXiv: [0709.2092](https://arxiv.org/abs/0709.2092) [hep-ph].
- 1531 [25] J. M. Campbell, R. K. Ellis, P. Nason, E. Re,
 1532 *Top-Pair Production and Decay at NLO Matched with Parton Showers*, **JHEP** **04** (2015) 114,
 1533 arXiv: [1412.1828](https://arxiv.org/abs/1412.1828) [hep-ph].
- 1534 [26] S. Alioli, P. Nason, C. Oleari, E. Re, *A general framework for implementing NLO calculations in*
 1535 *shower Monte Carlo programs: the POWHEG BOX*, **JHEP** **06** (2010) 043,
 1536 arXiv: [1002.2581](https://arxiv.org/abs/1002.2581) [hep-ph].
- 1537 [27] S. Frixione, G. Ridolfi, P. Nason,
 1538 *A positive-weight next-to-leading-order Monte Carlo for heavy flavour hadroproduction*,
 1539 **JHEP** **0709** (2007) 126, arXiv: [0707.3088](https://arxiv.org/abs/0707.3088) [hep-ph].
- 1540 [28] ATLAS Collaboration,
 1541 *Improvements in $t\bar{t}$ modelling using NLO+PS Monte Carlo generators for Run2*,
 1542 ATL-PHYS-PUB-2018-009, 2018, URL: <https://cds.cern.ch/record/2630327>.
- 1543 [29] R. Frederix, E. Re, P. Torrielli,
 1544 *Single-top t-channel hadroproduction in the four-flavour scheme with POWHEG and aMC@NLO*,
 1545 **JHEP** **09** (2012) 130, arXiv: [1207.5391](https://arxiv.org/abs/1207.5391) [hep-ph].
- 1546 [30] S. Alioli et al.,
 1547 *NLO single-top production matched with shower in POWHEG: s- and t-channel contributions*,
 1548 **JHEP** **09** (2009) 111, [Erratum: **JHEP**02,011(2010)], arXiv: [0907.4076](https://arxiv.org/abs/0907.4076) [hep-ph].
- 1549 [31] E. Re,
 1550 *Single-top Wt-channel production matched with parton showers using the POWHEG method*,
 1551 **Eur. Phys. J. C** **71** (2011) 1547, arXiv: [1009.2450](https://arxiv.org/abs/1009.2450) [hep-ph].
- 1552 [32] ATLAS Collaboration, *Studies on top-quark Monte Carlo modelling for Top2016*,
 1553 ATL-PHYS-PUB-2016-020, 2016, URL: <https://cds.cern.ch/record/2216168>.

- 1554 [33] S. Frixione et al., *Single-top hadroproduction in association with a W boson*,
 1555 JHEP **07** (2008) 029, arXiv: [0805.3067 \[hep-ph\]](#).
- 1556 [34] LHCPhysics, *NNLO+NNLL top-quark-pair cross sections*, Web page,
 1557 <https://twiki.cern.ch/twiki/bin/view/LHCPhysics/TtbarNNLO>, 2015.
- 1558 [35] M. Bahr et al., *Herwig++ Physics and Manual*, Eur. Phys. J. C **58** (2008) 639,
 1559 arXiv: [0803.0883 \[hep-ph\]](#).
- 1560 [36] J. Bellm et al., *Herwig 7.0/Herwig++ 3.0 release note*, Eur. Phys. J. C **76** (2016) 196,
 1561 arXiv: [1512.01178 \[hep-ph\]](#).
- 1562 [37] L. A. Harland-Lang et al., *Parton distributions in the LHC era: MMHT 2014 PDFs*,
 1563 Eur. Phys. J. C **75** (2015) 204, arXiv: [1412.3989 \[hep-ph\]](#).
- 1564 [38] T. Gleisberg et al., *Event generation with SHERPA 1.1*, JHEP **02** (2009) 007,
 1565 arXiv: [0811.4622 \[hep-ph\]](#).
- 1566 [39] T. Gleisberg, S. Höche, *Comix, a new matrix element generator*, JHEP **12** (2008) 039,
 1567 arXiv: [0808.3674 \[hep-ph\]](#).
- 1568 [40] S. Schumann, F. Krauss,
 1569 *A Parton shower algorithm based on Catani-Seymour dipole factorisation*, JHEP **03** (2008) 038,
 1570 arXiv: [0709.1027 \[hep-ph\]](#).
- 1571 [41] S. Höche, F. Krauss, M. Schönher, F. Siegert, *A critical appraisal of NLO+PS matching methods*,
 1572 JHEP **09** (2012) 049, arXiv: [1111.1220 \[hep-ph\]](#).
- 1573 [42] S. Höche, F. Krauss, M. Schönher, F. Siegert,
 1574 *QCD matrix elements + parton showers: The NLO case*, JHEP **04** (2013) 027,
 1575 arXiv: [1207.5030 \[hep-ph\]](#).
- 1576 [43] S. Catani, F. Krauss, R. Kuhn, B. R. Webber, *QCD matrix elements + parton showers*,
 1577 JHEP **11** (2001) 063, arXiv: [hep-ph/0109231](#).
- 1578 [44] S. Höche, F. Krauss, M. Schönher, F. Siegert, *QCD matrix elements and truncated showers*,
 1579 JHEP **05** (2009) 053, arXiv: [0903.1219 \[hep-ph\]](#).
- 1580 [45] F. Cascioli, P. Maierhofer, S. Pozzorini, *Scattering Amplitudes with Open Loops*,
 1581 Phys. Rev. Lett. **108** (2012) 111601, arXiv: [1111.5206 \[hep-ph\]](#).
- 1582 [46] A. Denner, S. Dittmaier, L. Hofer,
 1583 *Collier: a fortran-based Complex One-Loop Library in Extended Regularizations*,
 1584 Comput. Phys. Commun. **212** (2017) 220, arXiv: [1604.06792 \[hep-ph\]](#).
- 1585 [47] ATLAS collaboration, *MCTruthClassifier (restricted)*, Web page,
 1586 <https://twiki.cern.ch/twiki/bin/view/AtlasProtected/MCTruthClassifier>,
 1587 2016.
- 1588 [48] ATLAS collaboration, *AnalysisTop21 (restricted)*, Web page,
 1589 <https://twiki.cern.ch/twiki/bin/view/AtlasProtected/AnalysisTop21>, 2018.
- 1590 [49] ATLAS Collaboration, *Measurement of the photon identification efficiencies with the ATLAS*
 1591 *detector using LHC Run 2 data collected in 2015 and 2016*, Eur. Phys. J. C **79** (2019),
 1592 arXiv: [1810.05087 \[hep-ex\]](#).
- 1593 [50] ATLAS Collaboration, *ATLAS electron, photon and muon isolation in Run 2*,
 1594 ATL-COM-PHYS-2017-290, 2017, URL: <https://cds.cern.ch/record/2256658>.

- 1595 [51] ATLAS Collaboration, *Electron and photon energy calibration with the ATLAS detector using*
 1596 *2015-2016 LHC proton-proton collision data*, ATL-COM-PHYS-2018-062, 2018,
 1597 URL: <https://cds.cern.ch/record/2302477>.
- 1598 [52] ATLAS Collaboration, *Electron Reconstruction and Identification in the ATLAS Experiment using*
 1599 *the 2015 and 2016 LHC proton-proton collision data*, ATL-COM-PHYS-2018-436, 2018,
 1600 URL: <https://cds.cern.ch/record/2315291>.
- 1601 [53] ATLAS Collaboration, *Muon reconstruction performance of the ATLAS detector in proton–proton*
 1602 *collision data at $\sqrt{s} = 13$ TeV*, Eur. Phys. J. C **76** (2016) 292, arXiv: [1603.05598](https://arxiv.org/abs/1603.05598) [hep-ex].
- 1603 [54] M. Cacciari, G. P. Salam, G. Soyez, *The anti- k_t jet clustering algorithm*, JHEP **04** (2008) 063,
 1604 arXiv: [0802.1189](https://arxiv.org/abs/0802.1189) [hep-ph].
- 1605 [55] ATLAS Collaboration, *Properties of jets and inputs to jet reconstruction and calibration with the*
 1606 *ATLAS detector using proton–proton collisions at $\sqrt{s} = 13$ TeV*, ATL-PHYS-PUB-2015-036,
 1607 2015, URL: <https://cds.cern.ch/record/2044564>.
- 1608 [56] ATLAS Collaboration, *Jet energy scale measurements and their systematic uncertainties in*
 1609 *proton–proton collisions at $\sqrt{s} = 13$ TeV with the ATLAS detector*,
 1610 Phys. Rev. D **96** (2017) 072002, arXiv: [1703.09665](https://arxiv.org/abs/1703.09665) [hep-ex].
- 1611 [57] ATLAS Collaboration, *Tagging and suppression of pileup jets with the ATLAS detector*,
 1612 ATLAS-CONF-2014-018, 2014, URL: <https://cds.cern.ch/record/1700870>.
- 1613 [58] ATLAS Collaboration, *Optimisation and performance studies of the ATLAS b-tagging algorithms*
 1614 *for the 2017-18 LHC run*, ATL-PHYS-PUB-2017-013, 2017,
 1615 URL: <https://cds.cern.ch/record/2273281>.
- 1616 [59] ATLAS Collaboration,
 1617 *Measurements of b-jet tagging efficiency with the ATLAS detector using $t\bar{t}$ events at $\sqrt{s} = 13$ TeV*,
 1618 CERN-EP-2018-047, 2018, URL: <https://cds.cern.ch/record/2316380>.
- 1619 [60] ATLAS Collaboration,
 1620 E_T^{miss} *performance in the ATLAS detector using 2015-2016 LHC p-p Collisions*,
 1621 ATL-COM-PHYS-2017-1732, 2017, URL: <https://cds.cern.ch/record/2294891>.
- 1622 [61] M. Tanabashi et al. (Particle Data Group), *Review of Particle Physics*,
 1623 Phys. Rev. D **98** (3 2018) 030001,
 1624 URL: <https://link.aps.org/doi/10.1103/PhysRevD.98.030001>.
- 1625 [62] A. Amorim, *GeneralFCNTop*, Web page,
 1626 <http://feynrules.irmp.ucl.ac.be/wiki/GeneralFCNTop>, 2015.
- 1627 [63] J. A. Aguilar-Saavedra,
 1628 *Top flavor-changing neutral interactions: Theoretical expectations and experimental detection*,
 1629 Acta Phys. Polon. B **35** (2004) 2695, arXiv: [hep-ph/0409342](https://arxiv.org/abs/hep-ph/0409342) [hep-ph].
- 1630 [64] M. Abadi et al., *TensorFlow: Large-Scale Machine Learning on Heterogeneous Systems*,
 1631 Software available from tensorflow.org, 2015, URL: <https://www.tensorflow.org/>.
- 1632 [65] F. Chollet et al., *Keras*, <https://keras.io>, 2015.
- 1633 [66] D. P. Kingma, J. Ba, *Adam: A Method for Stochastic Optimization*, CoRR **abs/1412.6980** (2014),
 1634 arXiv: [1412.6980](https://arxiv.org/abs/1412.6980).
- 1635 [67] F. Pedregosa et al., *Scikit-learn: Machine Learning in Python*, JMLR **12** (2011) 2825.

- [68] J. H. Friedman,
1974 CERN School of Computing, Godoysund, Norway, 11-24 Aug 1974: Proceedings, CERN, 1974, URL: <https://cds.cern.ch/record/186223>.
- [69] ATLAS Collaboration, *Measurement of the $t\bar{t}\gamma$ production cross-section in leptonic final states using 36.1 fb^{-1} pp collisions at $\sqrt{s} = 13 \text{ TeV}$ with the ATLAS detector*, 2018, URL: <https://cds.cern.ch/record/2621490>.
- [70] LHCPhysics, *NLO single-top channel cross sections*, Web page, <https://twiki.cern.ch/twiki/bin/view/LHCPhysics/SingleTopRefXsec>, 2017.
- [71] ATLAS Collaboration, *BosonJetsFocusGroup*, Web page, <https://twiki.cern.ch/twiki/bin/viewauth/AtlasProtected/BosonJetsFocusGroup>, 2018.
- [72] ATLAS Collaboration, *MultibosonFocusGroup*, Web page, <https://twiki.cern.ch/twiki/bin/viewauth/AtlasProtected/MultibosonFocusGroup>, 2018.
- [73] ATLAS Collaboration, *Jet Calibration and Systematic Uncertainties for Jets Reconstructed in the ATLAS Detector at $\sqrt{s} = 13 \text{ TeV}$* , (2015), URL: <https://cds.cern.ch/record/2037613>.
- [74] ATLAS Collaboration, *TRExFitter (previously known as TtHFitter)*, 2018, URL: <https://twiki.cern.ch/twiki/bin/viewauth/AtlasProtected/TtHFitter>.

Not reviewed, for internal circulation only

1653 List of contributions

1653	Johannes Erdmann	Supervisor of Gregor Geßner and paper editor.
1654	Gregor Geßner	Main analyzer and editor of the supporting note.
1655	Kevin Kröninger	Supervisor of the Dortmund activities and paper editor.

[Not reviewed, for internal circulation only]

1656 Appendices

1657 A List of MC samples

Table 38: List for MC16a samples (r-tag 9364) used to simulate top and diboson processes. All samples are also available for MC16d with r-tag 10201, if not stated otherwise.

Process	MC DSID	Generator	Generator tune	AMI-tag	$\sigma \times$ filter eff. \times k-factor [pb]
signal samples for FCNC in production mode: $p\bar{p} \rightarrow t\gamma \rightarrow b\bar{t}\nu\gamma$, NLO, AFII					
$t\bar{u}\gamma$, left-handed	410650	MADGRAPH5_aMC@NLO + PYTHIA 8 + EvtGen	A14 NNPDF23LO	e6054_a875_r9364_p3629	48.550
$t\bar{u}\gamma$, left-handed	410651	MADGRAPH5_aMC@NLO + PYTHIA 8 + EvtGen	A14 NNPDF23LO	e6054_a875_r9364_p3629	48.515
$t\bar{u}\gamma$, left-handed	410652	MADGRAPH5_aMC@NLO + PYTHIA 8 + EvtGen	A14 NNPDF23LO	e6054_a875_r9364_p3629	6.9286
$t\bar{u}\gamma$, left-handed	410653	MADGRAPH5_aMC@NLO + PYTHIA 8 + EvtGen	A14 NNPDF23LO	e6054_a875_r9364_p3629	6.9318
signal samples for FCNC in decay mode: $p\bar{p} \rightarrow t\bar{t} \rightarrow b\bar{t}\nu\bar{q}\gamma$, NLO, AFII					
$t\bar{c}\gamma$, anti-top	410980	MADGRAPH5_aMC@NLO + PYTHIA 8 + EvtGen	A14 NNPDF23LO	e6908_a875_r9364_p3629	21.608
$t\bar{c}\gamma$, top	410981	MADGRAPH5_aMC@NLO + PYTHIA 8 + EvtGen	A14 NNPDF23LO	e6908_a875_r9364_p3629	21.609
$t\bar{u}\gamma$, anti-top	410984	MADGRAPH5_aMC@NLO + PYTHIA 8 + EvtGen	A14 NNPDF23LO	e6908_a875_r9364_p3629	21.609
$t\bar{u}\gamma$, top	410985	MADGRAPH5_aMC@NLO + PYTHIA 8 + EvtGen	A14 NNPDF23LO	e6908_a875_r9364_p3629	21.611
$t\bar{t}$ processes (full simulation)					
$t\bar{t}$ (NLO)	410470	POWHEG-BOX + PYTHIA 8 + EvtGen	A14 NNPDF23LO	e6337_s3126_r9364_p3629	452.344358399
$t\bar{t} + \gamma$ (LO)	410389	POWHEG-BOX + PYTHIA 8 + EvtGen	A14 NNPDF23LO	e6155_s3126_r9364_p3629	5.734008
$t\bar{t}$ processes (variation samples, NLO, AFII)					
$t\bar{t}$ (single lepton)	410557	POWHEG-BOX + HERWIG7 + EvtGen	MMHT2014lo68cl	e6366_a875_r9364_p3629	364.6715904
$t\bar{t}$ (di-lepton)	410558	POWHEG-BOX + HERWIG7 + EvtGen	MMHT2014lo68cl	e6366_a875_r9364_p3629	87.7107
$t\bar{t}$ (single lepton)	410464	MADGRAPH5_aMC@NLO + PYTHIA 8 + EvtGen	A14 NNPDF23LO	e6762_a875_r9364_p3629	366.2498025
$t\bar{t}$ (di-lepton)	410465	MADGRAPH5_aMC@NLO + PYTHIA 8 + EvtGen	A14 NNPDF23LO	e6762_a875_r9364_p3629	89.1447196
$t\bar{t}$ (single lepton, $h_{\text{damp}} = 3m_{\text{top}}$)	410480	POWHEG-BOX + PYTHIA 8 + EvtGen	A14 NNPDF23LO	e6454_a875_r9364_p3629	364.7428388
$t\bar{t}$ (di-lepton, $h_{\text{damp}} = 3m_{\text{top}}$)	410482	POWHEG-BOX + PYTHIA 8 + EvtGen	A14 NNPDF23LO	e6454_a875_r9364_p3629	87.70054324
single-top processes (NLO, full simulation)					
t -channel, top	410658	POWHEG-BOX + PYTHIA 8 + EvtGen	A14 NNPDF23LO	e6671_s3126_r9364_p3629	44.154726
t -channel, anti-top	410659	POWHEG-BOX + PYTHIA 8 + EvtGen	A14 NNPDF23LO	e6671_s3126_r9364_p3629	26.2751575
s -channel, top	410644	POWHEG-BOX + PYTHIA 8 + EvtGen	A14 NNPDF23LO	e6527_s3126_r9364_p3629	2.061459
s -channel, anti-top	410645	POWHEG-BOX + PYTHIA 8 + EvtGen	A14 NNPDF23LO	e6527_s3126_r9364_p3629	1.28856558
WW -channel, top	410646	POWHEG-BOX + PYTHIA 8 + EvtGen	A14 NNPDF23LO	e6552_s3126_r9364_p3629	35.84952
WW -channel, anti-top	410647	POWHEG-BOX + PYTHIA 8 + EvtGen	A14 NNPDF23LO	e6552_s3126_r9364_p3629	35.8467585
single-top processes (variation samples, NLO)					
t -channel, anti-top, AFII	411032	POWHEG-BOX + HERWIG7 + EvtGen	MMHT2014lo68cl	e6719_a875_r9364_p3629	26.27888
t -channel, top, AFII	411033	POWHEG-BOX + HERWIG7 + EvtGen	MMHT2014lo68cl	e6719_a875_r9364_p3629	44.153754
t -channel, AFII	412004	MADGRAPH5_aMC@NLO + PYTHIA 8 + EvtGen	A14 NNPDF23LO	e6888_a875_r9364_p3629	70.43697
s -channel, anti-top, AFII	411034	POWHEG-BOX + HERWIG7 + EvtGen	MMHT2014lo68cl	e6734_a875_r9364_p3629	2.0612592
s -channel, top, AFII	411035	POWHEG-BOX + HERWIG7 + EvtGen	MMHT2014lo68cl	e6734_a875_r9364_p3629	1.28851702
s -channel, AFII	412005	MADGRAPH5_aMC@NLO + PYTHIA 8 + EvtGen	A14 NNPDF23LO	e6867_a875_r9364_p3629	3.3499983
WW -channel, anti-top, AFII	411036	POWHEG-BOX + HERWIG7 + EvtGen	MMHT2014lo68cl	e6702_a875_r9364_p3629	35.8503865
WW -channel, top, AFII	411037	POWHEG-BOX + HERWIG7 + EvtGen	MMHT2014lo68cl	e6702_a875_r9364_p3629	35.84671
WW -channel, AFII	412002	MADGRAPH5_aMC@NLO + PYTHIA 8 + EvtGen	A14 NNPDF23LO	e6867_a875_r9364_p3629	71.7001974
WW -channel, DR, anti-top, full simulation	410654	POWHEG-BOX + HERWIG7 + EvtGen	MMHT2014lo68cl	e6552_s3126_r9364_p3629	35.8549542
WW -channel, DR, top, full simulation	410655	POWHEG-BOX + HERWIG7 + EvtGen	MMHT2014lo68cl	e6552_s3126_r9364_p3629	35.863618
diboson processes (0,1p @ NLO, 2,3p @ LO, full simulation)					
$ZZ \rightarrow \ell\ell\ell\ell$	364250	SHERPA	NNPDF3.0 NNLO	e5894_s3126_r9364_p3629	1.252
$ZW \rightarrow \ell\ell\ell\nu$	364253	SHERPA	NNPDF3.0 NNLO	e5916_s3126_r9364_p3629	4.5765
$WW/ZZ \rightarrow \ell\ell\nu\nu$	364254	SHERPA	NNPDF3.0 NNLO	e5916_s3126_r9364_p3629	12.501
$WZ \rightarrow \ell\nu\nu\nu$	364255	SHERPA	NNPDF3.0 NNLO	e5916_s3126_r9364_p3629	3.2344
$ZZ \rightarrow qq\nu\nu$	363355	SHERPA	NNPDF3.0 NNLO	e5525_s3126_r9364_p3629	4.3079416
$ZZ \rightarrow qq\ell\ell$	363356	SHERPA	NNPDF3.0 NNLO	e5525_s3126_r9364_p3629	2.19983005
$WZ \rightarrow qq\nu\nu$	363357	SHERPA	NNPDF3.0 NNLO	e5525_s3126_r9364_p3629	6.7951
$WZ \rightarrow qq\ell\ell$	363358	SHERPA	NNPDF3.0 NNLO	e5525_s3126_r9364_p3629	3.4328
$WW \rightarrow q\bar{q}\ell^-\ell^+$	363359	SHERPA	NNPDF3.0 NNLO	e5583_s3126_r9364_p3629	24.707
$WW \rightarrow q\bar{q}\ell^+\ell^+$	363360	SHERPA	NNPDF3.0 NNLO	e5983_s3126_r9364_p3629	24.726
$WZ \rightarrow qq\ell\nu$	363389	SHERPA	NNPDF3.0 NNLO	e5525_s3126_r9364_p3629	11.419

Not reviewed, for internal circulation only

Table 39: List for MC16a samples (r-tag 9364) used to simulate $W/Z + \gamma + \text{jets}$ processes. All processes are simulated for up to 1 parton at NLO and up to 3 partons at LO. For all samples, the full simulation package is used. All samples are also available for MC16d with r-tag 10201, if not stated otherwise.

Process	MC DSID	Generator	Generator tune	AMI-tag	$\sigma \times \text{filter eff.} \times \text{k-factor [pb]}$
$Z + \gamma + \text{jets}$					
$Z \rightarrow ee, 7 \text{ GeV} < p_T^\gamma < 15 \text{ GeV}$	364500	SHERPA	NNPDF3.0 NNLO	e5928_s3126_r9364_p3629	57.619
$Z \rightarrow ee, 15 \text{ GeV} < p_T^\gamma < 35 \text{ GeV}$	364501	SHERPA	NNPDF3.0 NNLO	e5928_s3126_r9364_p3629	34.59
$Z \rightarrow ee, 35 \text{ GeV} < p_T^\gamma < 70 \text{ GeV}$	364502	SHERPA	NNPDF3.0 NNLO	e5928_s3126_r9364_p3629	6.2856
$Z \rightarrow ee, 70 \text{ GeV} < p_T^\gamma < 140 \text{ GeV}$	364503	SHERPA	NNPDF3.0 NNLO	e5928_s3126_r9364_p3629	0.49186
$Z \rightarrow ee, p_T^\gamma > 140 \text{ GeV}$	364504	SHERPA	NNPDF3.0 NNLO	e5928_s3126_r9364_p3629	0.062987
$Z \rightarrow \mu\mu, 7 \text{ GeV} < p_T^\gamma < 15 \text{ GeV}$	364505	SHERPA	NNPDF3.0 NNLO	e5928_s3126_r9364_p3629	57.701
$Z \rightarrow \mu\mu, 15 \text{ GeV} < p_T^\gamma < 35 \text{ GeV}$	364506	SHERPA	NNPDF3.0 NNLO	e5988_s3126_r9364_p3629 e5928_s3126_r10201_p3629	34.588
$Z \rightarrow \mu\mu, 35 \text{ GeV} < p_T^\gamma < 70 \text{ GeV}$	364507	SHERPA	NNPDF3.0 NNLO	e5928_s3126_r9364_p3629	6.2853
$Z \rightarrow \mu\mu, 70 \text{ GeV} < p_T^\gamma < 140 \text{ GeV}$	364508	SHERPA	NNPDF3.0 NNLO	e5928_s3126_r9364_p3629	0.49392
$Z \rightarrow \mu\mu, p_T^\gamma > 140 \text{ GeV}$	364509	SHERPA	NNPDF3.0 NNLO	e5928_s3126_r9364_p3629	0.06308
$Z \rightarrow \tau\tau, 7 \text{ GeV} < p_T^\gamma < 15 \text{ GeV}$	364510	SHERPA	NNPDF3.0 NNLO	e5928_s3126_r9364_p3629	57.619
$Z \rightarrow \tau\tau, 15 \text{ GeV} < p_T^\gamma < 35 \text{ GeV}$	364511	SHERPA	NNPDF3.0 NNLO	e5928_s3126_r9364_p3629	34.638
$Z \rightarrow \tau\tau, 35 \text{ GeV} < p_T^\gamma < 70 \text{ GeV}$	364512	SHERPA	NNPDF3.0 NNLO	e5928_s3126_r9364_p3629	6.2964
$Z \rightarrow \tau\tau, 70 \text{ GeV} < p_T^\gamma < 140 \text{ GeV}$	364513	SHERPA	NNPDF3.0 NNLO	e5982_s3126_r9364_p3629	0.49501
$Z \rightarrow \tau\tau, p_T^\gamma > 140 \text{ GeV}$	364514	SHERPA	NNPDF3.0 NNLO	e5928_s3126_r9364_p3629	0.063417
$Z \rightarrow \nu\nu, 35 \text{ GeV} < p_T^\gamma < 70 \text{ GeV}$	364517	SHERPA	NNPDF3.0 NNLO	e5928_s3126_r9364_p3629	5.2576
$Z \rightarrow \nu\nu, 70 \text{ GeV} < p_T^\gamma < 140 \text{ GeV}$	364518	SHERPA	NNPDF3.0 NNLO	e5928_s3126_r9364_p3629	1.339
$Z \rightarrow \nu\nu, p_T^\gamma > 140 \text{ GeV}$	364519	SHERPA	NNPDF3.0 NNLO	e5928_s3126_r9364_p3629	0.24448
$W + \gamma + \text{jets}$					
$W \rightarrow ev, 7 \text{ GeV} < p_T^\gamma < 15 \text{ GeV}$	364521	SHERPA	NNPDF3.0 NNLO	e5928_s3126_r9364_p3629	199.27
$W \rightarrow ev, 15 \text{ GeV} < p_T^\gamma < 35 \text{ GeV}$	364522	SHERPA	NNPDF3.0 NNLO	e5928_s3126_r9364_p3629	134.42
$W \rightarrow ev, 35 \text{ GeV} < p_T^\gamma < 70 \text{ GeV}$	364523	SHERPA	NNPDF3.0 NNLO	e5928_s3126_r9364_p3629	19.077
$W \rightarrow ev, 70 \text{ GeV} < p_T^\gamma < 140 \text{ GeV}$	364524	SHERPA	NNPDF3.0 NNLO	e5928_s3126_r9364_p3629	1.9212
$W \rightarrow ev, p_T^\gamma > 140 \text{ GeV}$	364525	SHERPA	NNPDF3.0 NNLO	e5928_s3126_r9364_p3629	0.29742
$W \rightarrow \mu\nu, 7 \text{ GeV} < p_T^\gamma < 15 \text{ GeV}$	364526	SHERPA	NNPDF3.0 NNLO	e5928_s3126_r9364_p3629	199.44
$W \rightarrow \mu\nu, 15 \text{ GeV} < p_T^\gamma < 35 \text{ GeV}$	364527	SHERPA	NNPDF3.0 NNLO	e5928_s3126_r9364_p3629	134.4
$W \rightarrow \mu\nu, 35 \text{ GeV} < p_T^\gamma < 70 \text{ GeV}$	364528	SHERPA	NNPDF3.0 NNLO	e5928_s3126_r9364_p3629	19.133
$W \rightarrow \mu\nu, 70 \text{ GeV} < p_T^\gamma < 140 \text{ GeV}$	364529	SHERPA	NNPDF3.0 NNLO	e5928_s3126_r9364_p3629	1.9221
$W \rightarrow \mu\nu, p_T^\gamma > 140 \text{ GeV}$	364530	SHERPA	NNPDF3.0 NNLO	e5928_s3126_r9364_p3629	0.29763
$W \rightarrow \tau\nu, 7 \text{ GeV} < p_T^\gamma < 15 \text{ GeV}$	364531	SHERPA	NNPDF3.0 NNLO	e5928_s3126_r9364_p3629	199.4
$W \rightarrow \tau\nu, 15 \text{ GeV} < p_T^\gamma < 35 \text{ GeV}$	364532	SHERPA	NNPDF3.0 NNLO	e5928_s3126_r9364_p3629	134.44
$W \rightarrow \tau\nu, 35 \text{ GeV} < p_T^\gamma < 70 \text{ GeV}$	364533	SHERPA	NNPDF3.0 NNLO	e5928_s3126_r9364_p3629	19.126
$W \rightarrow \tau\nu, 70 \text{ GeV} < p_T^\gamma < 140 \text{ GeV}$	364534	SHERPA	NNPDF3.0 NNLO	e5928_s3126_r9364_p3629	1.9283
$W \rightarrow \tau\nu, p_T^\gamma > 140 \text{ GeV}$	364535	SHERPA	NNPDF3.0 NNLO	e5928_s3126_r9364_p3629	0.29736

Table 40: List for MC16a samples (r-tag 9364) used to simulate $Z+jets$ processes. All processes are simulated for up to 2 partons at NLO and up to 4 partons at LO. For all samples, the full simulation package is used. All samples are also available for MC16d with r-tag 10201.

Process	MC DSID	Generator	Generator tune	AMI-tag	$\sigma \times$ filter eff. \times k-factor [pb]
$Z \rightarrow \mu\mu, \max(H_T, p_T^V) < 70 \text{ GeV}, c \text{ veto}, b \text{ veto}$	364100	SHERPA	NNPDF3.0 NNLO	e5271_s3126_r9364_p3629	1588.47417372
$Z \rightarrow \mu\mu, \max(H_T, p_T^V) < 70 \text{ GeV}, c \text{ filter}, b \text{ veto}$	364101	SHERPA	NNPDF3.0 NNLO	e5271_s3126_r9364_p3629	219.521257742
$Z \rightarrow \mu\mu, \max(H_T, p_T^V) < 70 \text{ GeV}, b \text{ filter}$	364102	SHERPA	NNPDF3.0 NNLO	e5271_s3126_r9364_p3629	127.130374288
$Z \rightarrow \mu\mu, 70 \text{ GeV} < \max(H_T, p_T^V) < 140 \text{ GeV}, c \text{ veto}, b \text{ veto}$	364103	SHERPA	NNPDF3.0 NNLO	e5271_s3126_r9364_p3629	73.369402885
$Z \rightarrow \mu\mu, 70 \text{ GeV} < \max(H_T, p_T^V) < 140 \text{ GeV}, c \text{ filter}, b \text{ veto}$	364104	SHERPA	NNPDF3.0 NNLO	e5271_s3126_r9364_p3629	20.906068332
$Z \rightarrow \mu\mu, 70 \text{ GeV} < \max(H_T, p_T^V) < 140 \text{ GeV}, b \text{ filter}$	364105	SHERPA	NNPDF3.0 NNLO	e5271_s3126_r9364_p3629	12.505429717
$Z \rightarrow \mu\mu, 140 \text{ GeV} < \max(H_T, p_T^V) < 280 \text{ GeV}, c \text{ veto}, b \text{ veto}$	364106	SHERPA	NNPDF3.0 NNLO	e5271_s3126_r9364_p3629	23.437350636
$Z \rightarrow \mu\mu, 140 \text{ GeV} < \max(H_T, p_T^V) < 280 \text{ GeV}, c \text{ filter}, b \text{ veto}$	364107	SHERPA	NNPDF3.0 NNLO	e5271_s3126_r9364_p3629	9.145130781
$Z \rightarrow \mu\mu, 140 \text{ GeV} < \max(H_T, p_T^V) < 280 \text{ GeV}, b \text{ filter}$	364108	SHERPA	NNPDF3.0 NNLO	e5271_s3126_r9364_p3629	6.076989874
$Z \rightarrow \mu\mu, 280 \text{ GeV} < \max(H_T, p_T^V) < 500 \text{ GeV}, c \text{ veto}, b \text{ veto}$	364109	SHERPA	NNPDF3.0 NNLO	e5271_s3126_r9364_p3629	4.657367095
$Z \rightarrow \mu\mu, 280 \text{ GeV} < \max(H_T, p_T^V) < 500 \text{ GeV}, c \text{ filter}, b \text{ veto}$	364110	SHERPA	NNPDF3.0 NNLO	e5271_s3126_r9364_p3629	2.214827532
$Z \rightarrow \mu\mu, 280 \text{ GeV} < \max(H_T, p_T^V) < 500 \text{ GeV}, b \text{ filter}$	364111	SHERPA	NNPDF3.0 NNLO	e5271_s3126_r9364_p3629	1.468357812
$Z \rightarrow \mu\mu, 500 \text{ GeV} < \max(H_T, p_T^V) < 1000 \text{ GeV}$	364112	SHERPA	NNPDF3.0 NNLO	e5271_s3126_r9364_p3629	1.74260121
$Z \rightarrow \mu\mu, \max(H_T, p_T^V) > 100 \text{ GeV}$	364113	SHERPA	NNPDF3.0 NNLO	e5271_s3126_r9364_p3629	0.14392476
$Z \rightarrow ee, \max(H_T, p_T^V) < 70 \text{ GeV}, c \text{ veto}, b \text{ veto}$	364114	SHERPA	NNPDF3.0 NNLO	e5299_s3126_r9364_p3629	1587.02159455
$Z \rightarrow ee, \max(H_T, p_T^V) < 70 \text{ GeV}, c \text{ filter}, b \text{ veto}$	364115	SHERPA	NNPDF3.0 NNLO	e5299_s3126_r9364_p3629	219.995811609
$Z \rightarrow ee, \max(H_T, p_T^V) < 70 \text{ GeV}, c \text{ veto}, b \text{ filter}$	364116	SHERPA	NNPDF3.0 NNLO	e5299_s3126_r9364_p3629	127.085761415
$Z \rightarrow ee, 70 \text{ GeV} < \max(H_T, p_T^V) < 140 \text{ GeV}, c \text{ veto}, b \text{ veto}$	364117	SHERPA	NNPDF3.0 NNLO	e5299_s3126_r9364_p3629	74.903817417
$Z \rightarrow ee, 70 \text{ GeV} < \max(H_T, p_T^V) < 140 \text{ GeV}, c \text{ filter}, b \text{ veto}$	364118	SHERPA	NNPDF3.0 NNLO	e5299_s3126_r9364_p3629	20.315989103
$Z \rightarrow ee, 70 \text{ GeV} < \max(H_T, p_T^V) < 140 \text{ GeV}, b \text{ filter}$	364119	SHERPA	NNPDF3.0 NNLO	e5299_s3126_r9364_p3629	12.867331841
$Z \rightarrow ee, 140 \text{ GeV} < \max(H_T, p_T^V) < 280 \text{ GeV}, c \text{ veto}, b \text{ veto}$	364120	SHERPA	NNPDF3.0 NNLO	e5299_s3126_r9364_p3629	24.441849784
$Z \rightarrow ee, 140 \text{ GeV} < \max(H_T, p_T^V) < 280 \text{ GeV}, c \text{ filter}, b \text{ veto}$	364121	SHERPA	NNPDF3.0 NNLO	e5299_s3126_r9364_p3629	9.237605979
$Z \rightarrow ee, 140 \text{ GeV} < \max(H_T, p_T^V) < 280 \text{ GeV}, b \text{ filter}$	364122	SHERPA	NNPDF3.0 NNLO	e5299_s3126_r9364_p3629	6.081254464
$Z \rightarrow ee, 280 \text{ GeV} < \max(H_T, p_T^V) < 500 \text{ GeV}, c \text{ veto}, b \text{ veto}$	364123	SHERPA	NNPDF3.0 NNLO	e5299_s3126_r9364_p3629	4.789669885
$Z \rightarrow ee, 280 \text{ GeV} < \max(H_T, p_T^V) < 500 \text{ GeV}, c \text{ filter}, b \text{ veto}$	364124	SHERPA	NNPDF3.0 NNLO	e5299_s3126_r9364_p3629	2.249186051
$Z \rightarrow ee, 280 \text{ GeV} < \max(H_T, p_T^V) < 500 \text{ GeV}, b \text{ filter}$	364125	SHERPA	NNPDF3.0 NNLO	e5299_s3126_r9364_p3629	1.49219843
$Z \rightarrow ee, 500 \text{ GeV} < \max(H_T, p_T^V) < 1000 \text{ GeV}$	364126	SHERPA	NNPDF3.0 NNLO	e5299_s3126_r9364_p3629	1.76415092
$Z \rightarrow ee, \max(H_T, p_T^V) > 100 \text{ GeV}$	364127	SHERPA	NNPDF3.0 NNLO	e5299_s3126_r9364_p3629	0.145046125
$Z \rightarrow \tau\tau, \max(H_T, p_T^V) < 70 \text{ GeV}, c \text{ veto}, b \text{ veto}$	364128	SHERPA	NNPDF3.0 NNLO	e5307_s3126_r9364_p3629	1612.53148306
$Z \rightarrow \tau\tau, \max(H_T, p_T^V) < 70 \text{ GeV}, c \text{ filter}, b \text{ veto}$	364129	SHERPA	NNPDF3.0 NNLO	e5307_s3126_r9364_p3629	211.708887205
$Z \rightarrow \tau\tau, \max(H_T, p_T^V) < 70 \text{ GeV}, c \text{ veto}, b \text{ filter}$	364130	SHERPA	NNPDF3.0 NNLO	e5307_s3126_r9364_p3629	127.091559652
$Z \rightarrow \tau\tau, 70 \text{ GeV} < \max(H_T, p_T^V) < 140 \text{ GeV}, c \text{ veto}, b \text{ veto}$	364131	SHERPA	NNPDF3.0 NNLO	e5307_s3126_r9364_p3629	74.707406047
$Z \rightarrow \tau\tau, 70 \text{ GeV} < \max(H_T, p_T^V) < 140 \text{ GeV}, c \text{ filter}, b \text{ veto}$	364132	SHERPA	NNPDF3.0 NNLO	e5307_s3126_r9364_p3629	20.508136263
$Z \rightarrow \tau\tau, 70 \text{ GeV} < \max(H_T, p_T^V) < 140 \text{ GeV}, b \text{ filter}$	364133	SHERPA	NNPDF3.0 NNLO	e5307_s3126_r9364_p3629	11.965105705
$Z \rightarrow \tau\tau, 140 \text{ GeV} < \max(H_T, p_T^V) < 280 \text{ GeV}, c \text{ veto}, b \text{ veto}$	364134	SHERPA	NNPDF3.0 NNLO	e5307_s3126_r9364_p3629	24.57266372
$Z \rightarrow \tau\tau, 140 \text{ GeV} < \max(H_T, p_T^V) < 280 \text{ GeV}, c \text{ filter}, b \text{ veto}$	364135	SHERPA	NNPDF3.0 NNLO	e5307_s3126_r9364_p3629	9.301821784
$Z \rightarrow \tau\tau, 140 \text{ GeV} < \max(H_T, p_T^V) < 280 \text{ GeV}, b \text{ filter}$	364136	SHERPA	NNPDF3.0 NNLO	e5307_s3126_r9364_p3629	6.192971739
$Z \rightarrow \tau\tau, 280 \text{ GeV} < \max(H_T, p_T^V) < 500 \text{ GeV}, c \text{ veto}, b \text{ veto}$	364137	SHERPA	NNPDF3.0 NNLO	e5307_s3126_r9364_p3629	4.759698353
$Z \rightarrow \tau\tau, 280 \text{ GeV} < \max(H_T, p_T^V) < 500 \text{ GeV}, c \text{ filter}, b \text{ veto}$	364138	SHERPA	NNPDF3.0 NNLO	e5313_s3126_r9364_p3629	2.236223236
$Z \rightarrow \tau\tau, 280 \text{ GeV} < \max(H_T, p_T^V) < 500 \text{ GeV}, b \text{ filter}$	364139	SHERPA	NNPDF3.0 NNLO	e5313_s3126_r9364_p3629	1.491822884
$Z \rightarrow \tau\tau, 500 \text{ GeV} < \max(H_T, p_T^V) < 1000 \text{ GeV}$	364140	SHERPA	NNPDF3.0 NNLO	e5307_s3126_r9364_p3629	1.76249325
$Z \rightarrow \tau\tau, \max(H_T, p_T^V) > 100 \text{ GeV}$	364141	SHERPA	NNPDF3.0 NNLO	e5307_s3126_r9364_p3629	0.144568326

Table 41: List for MC16a samples (r-tag 9364) used to simulate $W+jets$ processes. All processes are simulated for up to 2 partons at NLO and up to 4 partons at LO. For all samples, the full simulation package is used. All samples are also available for MC16d with r-tag 10201 and p-tag 3554.

Process	MC DSID	Generator	Generator tune	AMI-tag	$\sigma \times$ filter eff. \times k-factor [pb]
$W \rightarrow \mu\nu, \max(H_T, p_T^V) < 70 \text{ GeV}, c \text{ veto}, b \text{ veto}$	364156	SHERPA	NNPDF3.0 NNLO	e5340_s3126_r9364_p3629	15317.8576551
$W \rightarrow \mu\nu, \max(H_T, p_T^V) < 70 \text{ GeV}, c \text{ filter}, b \text{ veto}$	364157	SHERPA	NNPDF3.0 NNLO	e5340_s3126_r9364_p3629	2431.20401924
$W \rightarrow \mu\nu, \max(H_T, p_T^V) < 70 \text{ GeV}, b \text{ filter}$	364158	SHERPA	NNPDF3.0 NNLO	e5340_s3126_r9364_p3629	828.880142152
$W \rightarrow \mu\nu, 70 \text{ GeV} < \max(H_T, p_T^V) < 140 \text{ GeV}, c \text{ veto}, b \text{ veto}$	364159	SHERPA	NNPDF3.0 NNLO	e5340_s3126_r9364_p3629	618.564724747
$W \rightarrow \mu\nu, 70 \text{ GeV} < \max(H_T, p_T^V) < 140 \text{ GeV}, c \text{ filter}, b \text{ veto}$	364160	SHERPA	NNPDF3.0 NNLO	e5340_s3126_r9364_p3629	223.216653845
$W \rightarrow \mu\nu, 70 \text{ GeV} < \max(H_T, p_T^V) < 140 \text{ GeV}, b \text{ filter}$	364161	SHERPA	NNPDF3.0 NNLO	e5340_s3126_r9364_p3629	77.592920029
$W \rightarrow \mu\nu, 140 \text{ GeV} < \max(H_T, p_T^V) < 280 \text{ GeV}, c \text{ veto}, b \text{ veto}$	364162	SHERPA	NNPDF3.0 NNLO	e5340_s3126_r9364_p3629	198.708528665
$W \rightarrow \mu\nu, 140 \text{ GeV} < \max(H_T, p_T^V) < 280 \text{ GeV}, c \text{ filter}, b \text{ veto}$	364163	SHERPA	NNPDF3.0 NNLO	e5340_s3126_r9364_p3629	96.221473591
$W \rightarrow \mu\nu, 140 \text{ GeV} < \max(H_T, p_T^V) < 280 \text{ GeV}, b \text{ filter}$	364164	SHERPA	NNPDF3.0 NNLO	e5340_s3126_r9364_p3629	36.345256661
$W \rightarrow \mu\nu, 280 \text{ GeV} < \max(H_T, p_T^V) < 500 \text{ GeV}, c \text{ veto}, b \text{ veto}$	364165	SHERPA	NNPDF3.0 NNLO	e5340_s3126_r9364_p3629	38.299835164
$W \rightarrow \mu\nu, 280 \text{ GeV} < \max(H_T, p_T^V) < 500 \text{ GeV}, c \text{ filter}, b \text{ veto}$	364166	SHERPA	NNPDF3.0 NNLO	e5340_s3126_r9364_p3629	22.395646627
$W \rightarrow \mu\nu, 280 \text{ GeV} < \max(H_T, p_T^V) < 500 \text{ GeV}, b \text{ filter}$	364167	SHERPA	NNPDF3.0 NNLO	e5340_s3126_r9364_p3629	8.768196432
$W \rightarrow \mu\nu, 500 \text{ GeV} < \max(H_T, p_T^V) < 1000 \text{ GeV}$	364168	SHERPA	NNPDF3.0 NNLO	e5340_s3126_r9364_p3629	14.5588212
$W \rightarrow \mu\nu, \max(H_T, p_T^V) > 100 \text{ GeV}$	364169	SHERPA	NNPDF3.0 NNLO	e5340_s3126_r9364_p3629	1.19800296
$W \rightarrow e\nu, \max(H_T, p_T^V) < 70 \text{ GeV}, c \text{ veto}, b \text{ veto}$	364170	SHERPA	NNPDF3.0 NNLO	e5340_s3126_r9364_p3629	15324.2163556
$W \rightarrow e\nu, \max(H_T, p_T^V) < 70 \text{ GeV}, c \text{ filter}, b \text{ veto}$	364171	SHERPA	NNPDF3.0 NNLO	e5340_s3126_r9364_p3629	2430.65632194
$W \rightarrow e\nu, \max(H_T, p_T^V) < 70 \text{ GeV}, b \text{ filter}$	364172	SHERPA	NNPDF3.0 NNLO	e5340_s3126_r9364_p3629	832.203758232
$W \rightarrow e\nu, 70 \text{ GeV} < \max(H_T, p_T^V) < 140 \text{ GeV}, c \text{ veto}, b \text{ veto}$	364173	SHERPA	NNPDF3.0 NNLO	e5340_s3126_r9364_p3629	618.697367969
$W \rightarrow e\nu, 70 \text{ GeV} < \max(H_T, p_T^V) < 140 \text{ GeV}, c \text{ filter}, b \text{ veto}$	364174	SHERPA	NNPDF3.0 NNLO	e5340_s3126_r9364_p3629	224.003177715
$W \rightarrow e\nu, 70 \text{ GeV} < \max(H_T, p_T^V) < 140 \text{ GeV}, b \text{ filter}$	364175	SHERPA	NNPDF3.0 NNLO	e5340_s3126_r9364_p3629	94.867508168
$W \rightarrow e\nu, 140 \text{ GeV} < \max(H_T, p_T^V) < 280 \text{ GeV}, c \text{ veto}, b \text{ veto}$	364176	SHERPA	NNPDF3.0 NNLO	e5340_s3126_r9364_p3629	197.316765608
$W \rightarrow e\nu, 140 \text{ GeV} < \max(H_T, p_T^V) < 280 \text{ GeV}, c \text{ filter}, b \text{ veto}$	364177	SHERPA	NNPDF3.0 NNLO	e5340_s3126_r9364_p3629	96.328009119
$W \rightarrow e\nu, 140 \text{ GeV} < \max(H_T, p_T^V) < 280 \text{ GeV}, b \text{ filter}$	364178	SHERPA	NNPDF3.0 NNLO	e5340_s3126_r9364_p3629	35.917294921
$W \rightarrow e\nu, 280 \text{ GeV} < \max(H_T, p_T^V) < 500 \text{ GeV}, c \text{ veto}, b \text{ veto}$	364179	SHERPA	NNPDF3.0 NNLO	e5340_s3126_r9364_p3629	38.340532609
$W \rightarrow e\nu, 280 \text{ GeV} < \max(H_T, p_T^V) < 500 \text{ GeV}, c \text{ filter}, b \text{ veto}$	364180	SHERPA	NNPDF3.0 NNLO	e5340_s3126_r9364_p3629	22.364320276
$W \rightarrow e\nu, 280 \text{ GeV} < \max(H_T, p_T^V) < 500 \text{ GeV}, b \text{ filter}$	364181	SHERPA	NNPDF3.0 NNLO	e5340_s3126_r9364_p3629	9.586344845
$W \rightarrow e\nu, 500 \text{ GeV} < \max(H_T, p_T^V) < 1000 \text{ GeV}$	364182	SHERPA	NNPDF3.0 NNLO	e5340_s3126_r9364_p3629	14.5985994
$W \rightarrow e\nu, \max(H_T, p_T^V) > 100 \text{ GeV}$	364183	SHERPA	NNPDF3.0 NNLO	e5340_s3126_r9364_p3629	1.19761488
$W \rightarrow \tau\nu, \max(H_T, p_T^V) < 70 \text{ GeV}, c \text{ veto}, b \text{ veto}$	364184	SHERPA	NNPDF3.0 NNLO	e5340_s3126_r9364_p3629	15324.8873362
$W \rightarrow \tau\nu, \max(H_T, p_T^V) < 70 \text{ GeV}, c \text{ filter}, b \text{ veto}$	364185	SHERPA	NNPDF3.0 NNLO	e5340_s3126_r9364_p3629	2443.4258809
$W \rightarrow \tau\nu, \max(H_T, p_T^V) < 70 \text{ GeV}, b \text{ filter}$	364186	SHERPA	NNPDF3.0 NNLO	e5340_s3126_r9364_p3629	838.044622246
$W \rightarrow \tau\nu, 70 \text{ GeV} < \max(H_T, p_T^V) < 140 \text{ GeV}, c \text{ veto}, b \text{ veto}$	364187	SHERPA	NNPDF3.0 NNLO	e5340_s3126_r9364_p3629	619.44787491
$W \rightarrow \tau\nu, 70 \text{ GeV} < \max(H_T, p_T^V) < 140 \text{ GeV}, c \text{ filter}, b \text{ veto}$	364188	SHERPA	NNPDF3.0 NNLO	e5340_s3126_r9364_p3629	222.595302935
$W \rightarrow \tau\nu, 70 \text{ GeV} < \max(H_T, p_T^V) < 140 \text{ GeV}, b \text{ filter}$	364189	SHERPA	NNPDF3.0 NNLO	e5340_s3126_r9364_p3629	95.340318062
$W \rightarrow \tau\nu, 140 \text{ GeV} < \max(H_T, p_T^V) < 280 \text{ GeV}, c \text{ veto}, b \text{ veto}$	364190	SHERPA	NNPDF3.0 NNLO	e5340_s3126_r9364_p3629	197.370775768
$W \rightarrow \tau\nu, 140 \text{ GeV} < \max(H_T, p_T^V) < 280 \text{ GeV}, c \text{ filter}, b \text{ veto}$	364191	SHERPA	NNPDF3.0 NNLO	e5340_s3126_r9364_p3629	93.84257385
$W \rightarrow \tau\nu, 140 \text{ GeV} < \max(H_T, p_T^V) < 280 \text{ GeV}, b \text{ filter}$	364192	SHERPA	NNPDF3.0 NNLO	e5340_s3126_r9364_p3629	34.895868846
$W \rightarrow \tau\nu, 280 \text{ GeV} < \max(H_T, p_T^V) < 500 \text{ GeV}, c \text{ veto}, b \text{ veto}$	364193	SHERPA	NNPDF3.0 NNLO	e5340_s3126_r9364_p3629	38.354471928
$W \rightarrow \tau\nu, 280 \text{ GeV} < \max(H_T, p_T^V) < 500 \text{ GeV}, c \text{ filter}, b \text{ veto}$	364194	SHERPA	NNPDF3.0 NNLO	e5340_s3126_r9364_p3629	22.268425407
$W \rightarrow \tau\nu, 280 \text{ GeV} < \max(H_T, p_T^V) < 500 \text{ GeV}, b \text{ filter}$	364195	SHERPA	NNPDF3.0 NNLO	e5340_s3126_r9364_p3629	9.490847273
$W \rightarrow \tau\nu, 500 \text{ GeV} < \max(H_T, p_T^V) < 1000 \text{ GeV}$	364196	SHERPA	NNPDF3.0 NNLO	e5340_s3126_r9364_p3629	14.6034504
$W \rightarrow \tau\nu, \max(H_T, p_T^V) > 100 \text{ GeV}$	364197	SHERPA	NNPDF3.0 NNLO	e5340_s3126_r9364_p3629	1.19732382

1658 B Studies for left- and right-handedness in decay mode

1659 For the decay mode signal, only the left-handed coupling is simulated. In Figure 75, the normalised
 1660 distribution of the p_T spectrum of the photon, charm and top quark for left- and right-handed $t\gamma$ coupling
 1661 are compared to each other. It is found that there is no difference.

Not reviewed, for internal circulation only

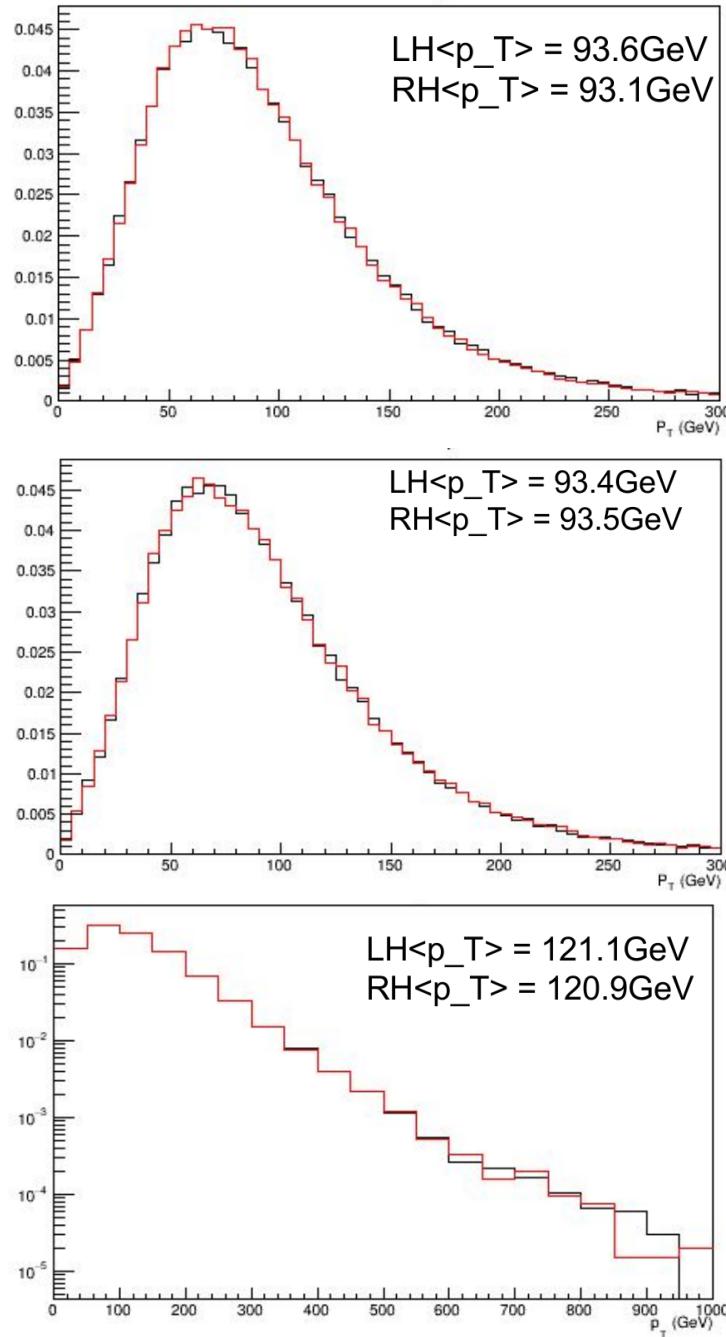


Figure 75: Normalised distribution of the photon p_T (top), charm quark p_T (middle) and top p_T (bottom) for the left- and right-handed $t\gamma$ coupling in the decay mode.

1662 C Estimation of non-available samples for the SM process single top + 1663 photon

1664 Since there are no available samples for the SM process single-top + photon, its contribution is estimated
 1665 from the single top samples. In these samples, the photons are added by the shower generator, already
 1666 giving an estimation of the SM $t + \gamma$ process. Two studies are done in order to test if this estimation covers
 1667 its contribution. In these studies, the single top contribution is compared to that for $t\bar{t}$ processes. First,
 1668 the ratio of cross sections are looked at. Next, the expected number of events in the SR with a prompt and
 1669 fake photon are considered.

1670 Comparison of cross sections

1671 As a rough estimation, the cross sections of the $t\bar{t}$, $t\bar{t} + \gamma$ and single top processes are looked at, as listed in
 1672 Appendix A. Assuming that the ratios for the single top and $t\bar{t}$ processes are comparable, the cross section
 1673 for the single top + photon process can be estimated as

$$\sigma(t + \gamma) \approx \frac{\sigma(t) \cdot \sigma(t\bar{t} + \gamma)}{\sigma(t\bar{t})} \approx 1.84 \text{ pb}. \quad (49)$$

1674 As it is difficult to extract any expected number of events from the cross section, a second approach is
 1675 done.

1676 Comparison of expected number of events

1677 In order to estimate the expected number of events for the single top + photon process, the expected
 1678 number of events for the $t\bar{t}$, $t\bar{t} + \gamma$ and single top processes in the SR are considered using the available
 1679 MC samples and listed in Table 42.

Table 42: Expected number of events with a prompt or fake photon for any $t\bar{t}$ and single top process in the SR.

Process	Events with a prompt photon	Events with a fake photon
Event from any $t\bar{t}$ process	1199.4 ± 7.1	2311 ± 32
Event from any single top process	427 ± 11	542 ± 13

1680 Assumed that the ratios of the processes are the same, although the processes are selected for different
 1681 reasons, the expected number of events for the single + photon process is

$$N(t + \gamma) \approx \frac{N(t) \cdot N(t\bar{t} + \gamma)}{N(t\bar{t})} = \frac{542 \cdot 1199.4}{2311} \approx 281.3 \pm 7.5. \quad (50)$$

1682 Following this assumption, the single + photon contribution would be overestimated by 50 % using the
 1683 single top MC samples. To check the impact of such a deviation, the statistical fit using data in all regions

₁₆₈₄ is re-done assuming a 100 % uncertainty on the expected number of events with a prompt photon coming
₁₆₈₅ from the single top process and the limit on the signal strength is compared. For all couplings, the impact
₁₆₈₆ is in the order of a few permille. Consequently, it is concluded that the current estimation of the SM $t + \gamma$
₁₆₈₇ process is sufficient.

[Not reviewed, for internal circulation only]

1688 D Studies for parameter $\Delta R(\gamma^{\text{reco}}, e^{\text{truth}})$ for event overlap removal

1689 The event overlap between the $V+\text{jets}$ and $V+\gamma+\text{jets}$, and the $t\bar{t}$ and $t\bar{t} + \gamma$ samples is investigated in the SR
 1690 and EFR $S \rightarrow e\gamma$ in the electron channel, where many events with an $e \rightarrow \gamma$ fake are expected. The event
 1691 selections are applied as stated in Tables 3 and 13, except for the event overlap removal cut. Events with
 1692 a photon originating from hadrons are excluded since they are classified as photon fake anyway. Since
 1693 in the object overlap removal, physics objects are considered as being separated at $\Delta R > 0.4$, cut values
 1694 below 0.4 are studied. The studies for the $\Delta R(\gamma^{\text{reco}}, e^{\text{truth}})$ cut, in order to define electron-to-photon fakes,
 1695 have been done in an early stage of the search with an integrated luminosity of 36 fb^{-1} .

1696 In Figure 76, the simulated $\Delta R(\gamma^{\text{reco}}, e^{\text{truth}})$ distributions are shown up to 0.4 in the SR and EFR $Z \rightarrow e\gamma$
 1697 in the electron channel for different processes, excluding events where the photon stems from a hadron.
 1698 The expected number of events for $W+\text{jets}$ processes is negligible compared to that of the other two
 1699 processes. The typical signature for $e \rightarrow \gamma$ fakes is visible for values below 0.05, especially for $Z+\text{jets}$
 1700 and $t\bar{t}$ events. Consequently, the cut value is set to 0.05. Since the expected number of events is very low
 1701 compared to the total expected number of events in these regions, any uncertainty on the impact of this
 1702 cut is negligible.

Not reviewed, for internal circulation only

Not reviewed, for internal circulation only

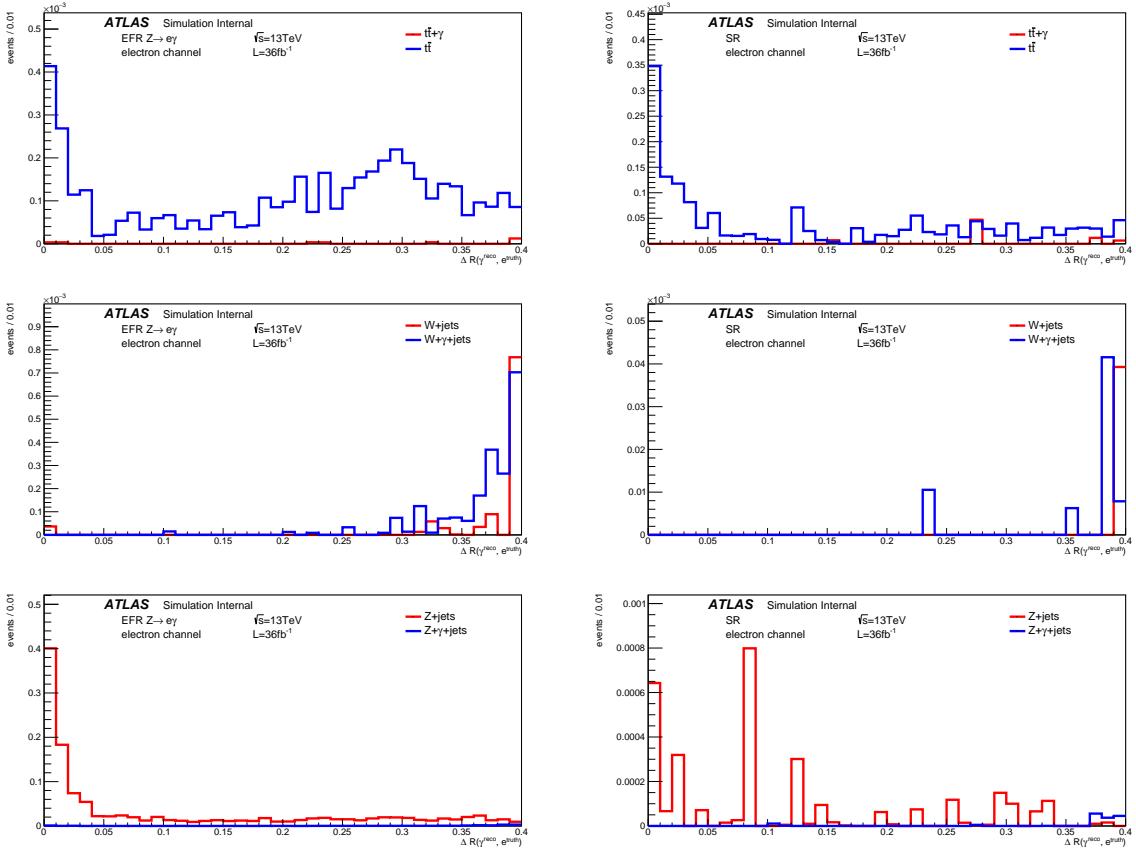


Figure 76: Simulated $\Delta R(\gamma^{\text{reco}}, e^{\text{truth}})$ distributions in the SR (right) and EFR $Z \rightarrow e\gamma$ (left) up to 0.4 without applying the event overlap removal in the electron channel for different processes. Events with a photon stemming from a hadron are excluded. In the top row, the expected $t\bar{t} + \gamma$ and $t\bar{t}$ events are shown. In the middle row, the expected $W + \text{jets}$ and $W + \gamma + \text{jets}$ events are shown, and in the bottom row the expected $Z + \text{jets}$ and $Z + \gamma + \text{jets}$ events are shown.

1703 E Studies for different b -tagging working points

1704 Four different working points for b -tagging are tested and compared to each other: 60 %, 70 %, 77 % and
 1705 85 %. For all of them, the full analysis chain is performed. Since the processing of all systematic is very
 1706 CPU expensive, only a subset of systematic uncertainties is taken in this comparison for all three working
 1707 points. The comparison is done with Asimov data. As parameter of interest, the 95 % C.L. upper limit
 1708 on the branching ratio $\mathcal{B}(t \rightarrow q\gamma)$ with $q = u, c$ is used to compare the working points to each other. In
 1709 Table 43, the branching ratios are printed. All limits are close to each other and lie in the same order of
 1710 magnitude. Since the 60% WP performs best in three out of four cases, it is taken as nominal WP.

Table 43: 95 % C.L. upper limit on the branching ratio $\mathcal{B}(t \rightarrow q\gamma)$ for the different b -tagging working points

b -tagging WP	$t\gamma, LH$	$t\gamma, RH$	$t\gamma, LH$	$tC\gamma, RH$
60 %	3.5	4.9	21.1	22.7
70 %	3.9	4.4	22.3	25.0
77 %	4.2	5.3	25.9	24.9
85 %	6.9	7.7	26.4	28.9

1711 F Cutflow for the SR separated by lepton flavour

Not reviewed, for internal circulation only

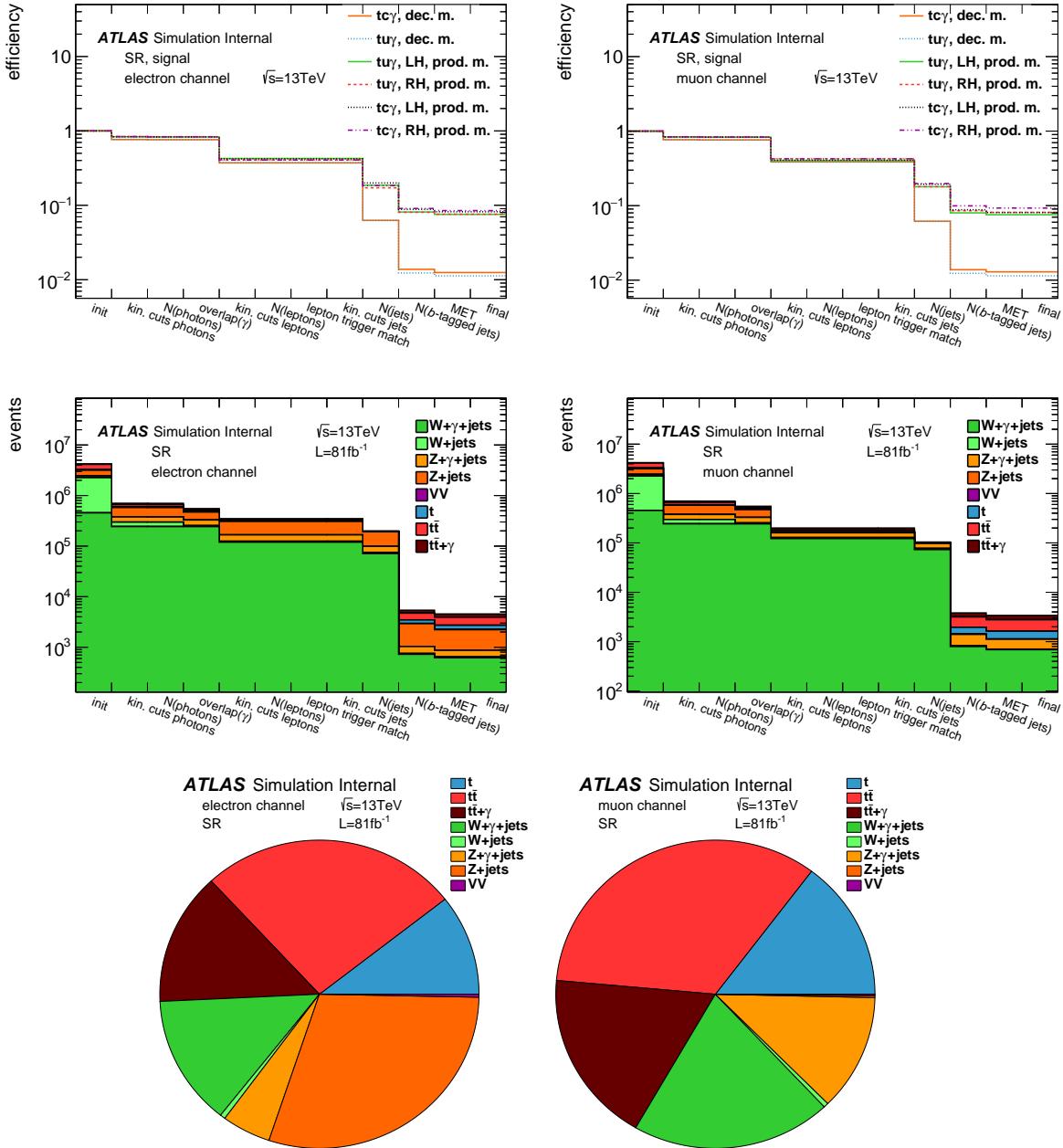


Figure 77: Cutflow in the SR for the electron (left) and muon channel (right): signal efficiencies for all signal coupling types in both the production and decay mode (top), expected numbers of events for all background processes (middle), and the pie charts of all SM processes being present in the SR (bottom).

1712 G Distribution of kinematic variables in the SR separated by lepton flavour

Not reviewed, for internal circulation only

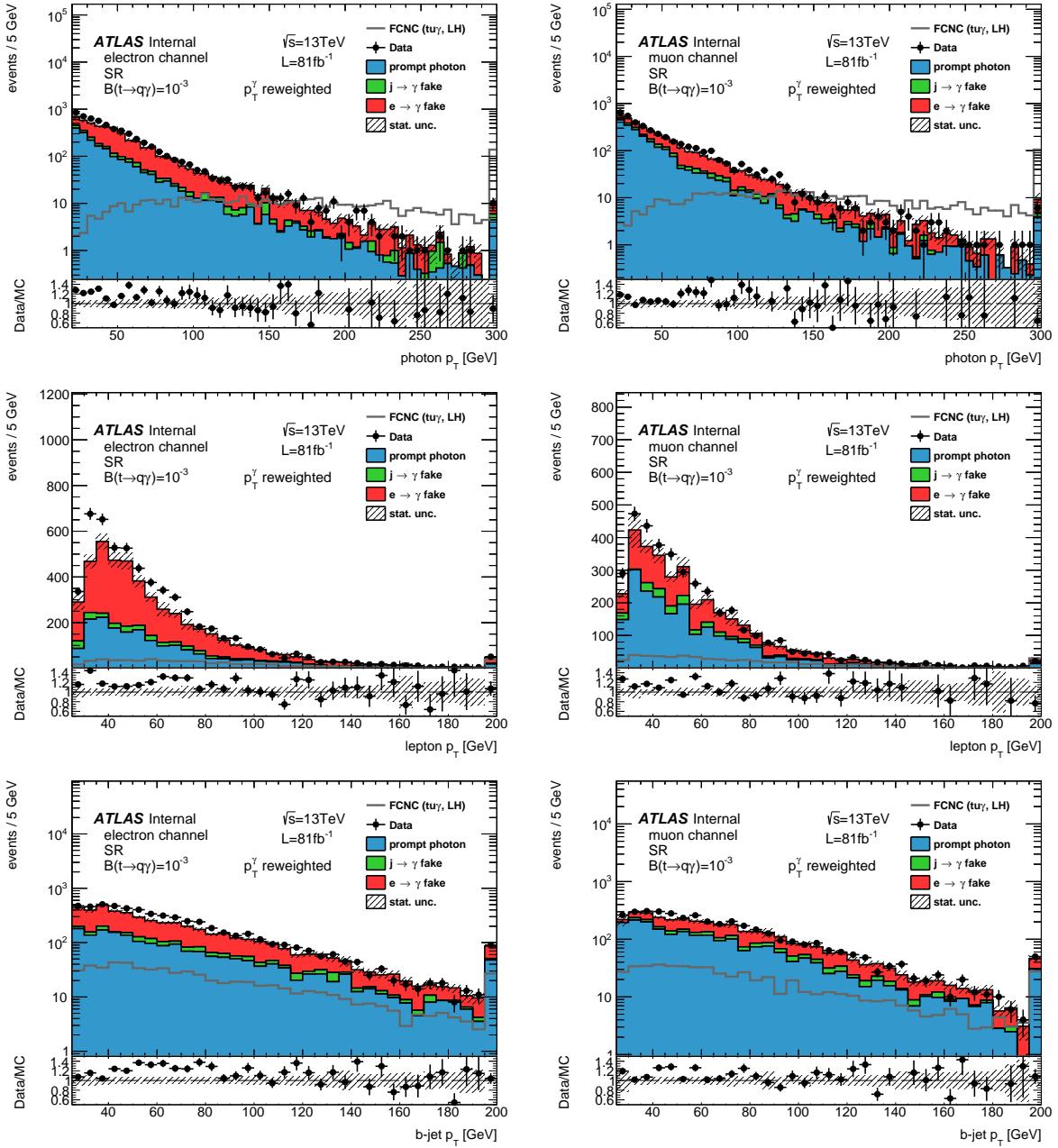


Figure 78: Distributions of different kinematic variables in the SR in the electron (left) and muon channel (right): photon p_T spectrum (top), lepton p_T spectrum (bottom), and b -jet p_T spectrum (bottom). The signal is scaled by a factor 10. The data-driven scale factors for electron and jet fakes are already included. Only the statistical uncertainty is shown and the over- and underflow bins are plotted.

Not reviewed, for internal circulation only

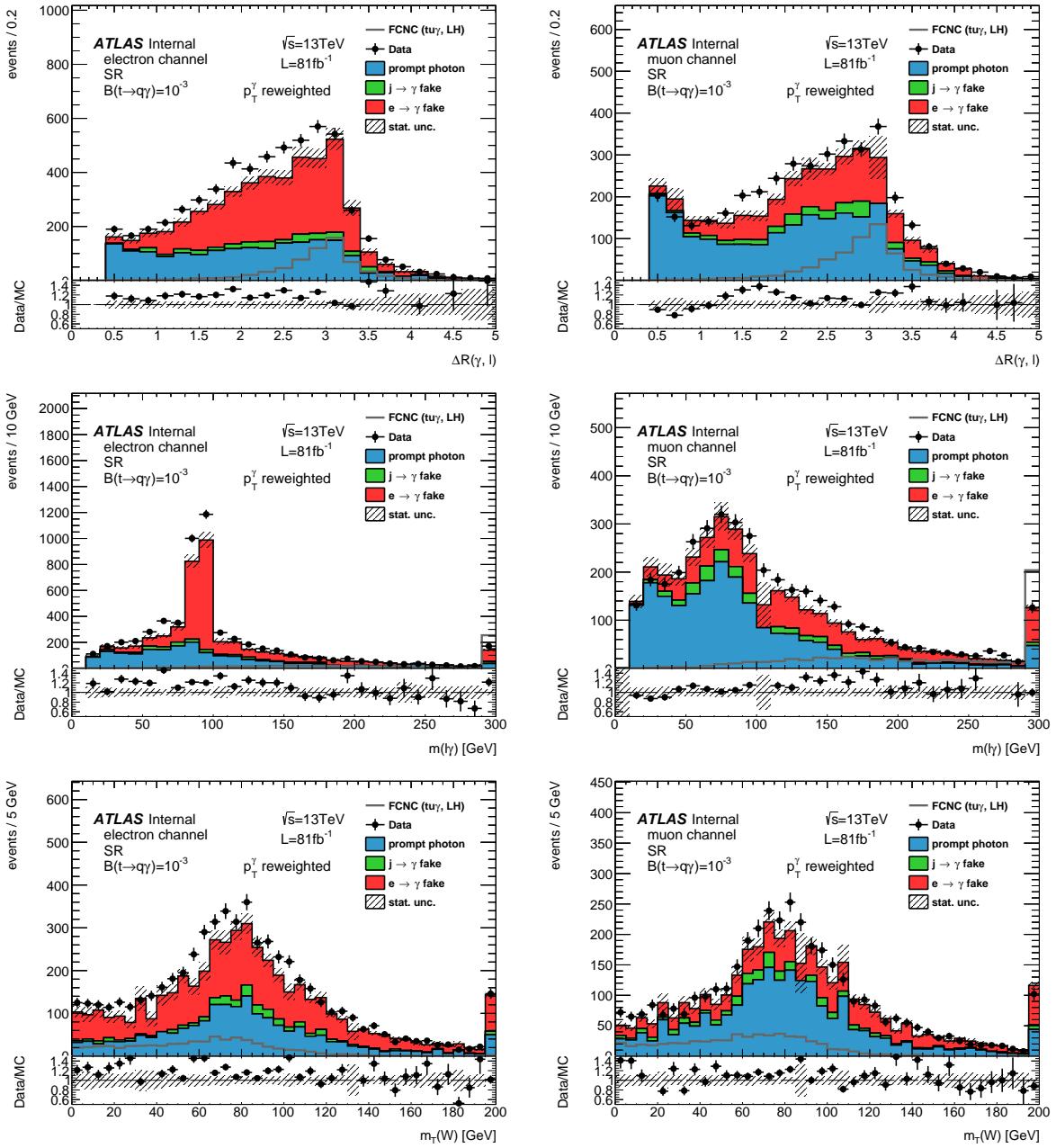


Figure 79: Distributions of different kinematic variables in the SR in the electron (left) and muon channel (right): distance ΔR between the photon and lepton (top), invariant mass $m(\ell\gamma)$ of the lepton and photon (middle), and transverse W boson mass $m_T(W)$ (bottom). The signal is scaled by a factor 10. The data-driven scale factors for electron and jet fakes are already included. Only the statistical uncertainty is shown and the over- and underflow bins are plotted.

1713 H Check for fit of MC with signal+background function for SF($e \rightarrow \gamma$)

1714 As a consistency check, the computation of the scale factor SF($e \rightarrow \gamma$) is redone when also using the
 1715 signal and background function in the fit to MC. For data, the same setup as for the nominal scale factor is
 1716 used, i.e. nothing is changed for fitting data. In Figure 80, the fitted MC distributions for the EFR $Z \rightarrow ee$
 1717 and EFR $Z \rightarrow e\gamma$ are shown. After background and prompt photon subtraction, the expected signal event
 1718 yields are $N^{\text{MC}}(e\gamma) = 957700 \pm 2200$ and $N^{\text{MC}}(ee) = 14968100 \pm 4400$. The scale factor is determined
 1719 to be $SF(e \rightarrow \gamma) = 0.971 \pm 0.003$, deviating less than a percent from the nominal setup. Therefore, it is
 1720 concluded that both approaches are equal to each other.

Not reviewed, for internal circulation only

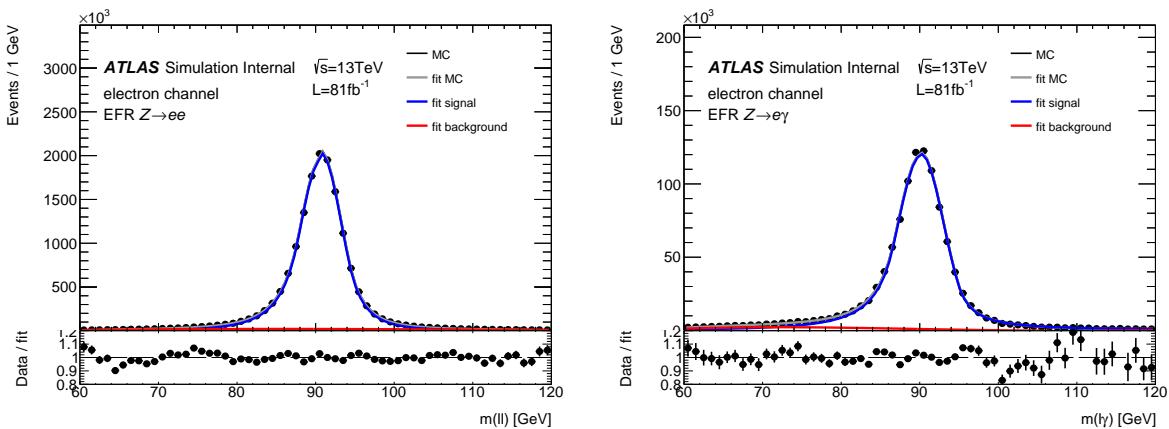


Figure 80: Fitted distribution of the invariant mass $m(ee)$ in the EFR $Z \rightarrow ee$ (left) and EFR $Z \rightarrow e\gamma$ (right) for simulation. In the bottom plot, the ratio between the fit function and prediction is shown.

1721 I Fit functions and parameters for $e \rightarrow \gamma$ fake estimation

- 1722 The double-sided Crystal Ball function $CB(x; N_{CB}, \vec{p})$ has 7 free parameters with the normalisation N_{CB}
 1723 and the parameters $\vec{p} = (n_1, n_2, \alpha_1, \alpha_2, \mu_{CB}, \sigma_{CB})$. Please see https://en.wikipedia.org/wiki/Crystal_Ball_function for the analytic expression.
- 1725 The Bernstein polynomial $B(z; N_B, \vec{\beta})$ of order 4 comes along with 6 free parameters consisting of
 1726 the normalisation N_B and the parameters $\vec{\beta} = (\beta_0, \beta_1, \beta_2, \beta_3, \beta_4)$. Here, the x -value is centred by
 1727 $z = \alpha_B(x - \mu_B) + 0.5$. Please see https://en.wikipedia.org/wiki/Bernstein_polynomial for
 1728 the analytic term.
- 1729 The Gaussian function $G(x; N_G, \mu, \sigma)$ has the normalisation N_G , the mean μ_G and the width σ_G .
- 1730 In Tables 44 and 45, the fitted parameters for the nominal and varied scenarios of the $e \rightarrow \gamma$ fake estimation
 1731 are shown in the EFR $Z \rightarrow ee$ and EFR $Z \rightarrow e\gamma$, respectively.

Not reviewed, for internal circulation only

Not reviewed, for internal circulation only

Table 44: Parameters of the fit in the $e \rightarrow \gamma$ fake estimation for the EFR $Z \rightarrow ee$.

	Nominal		Variation: functions		Variation: fit range	
	Data	MC	Data	MC	Data	MC
N_{CB}	14 526 700 \pm 4400	14 857 300 \pm 4400	15 394 400 \pm 3800	14 516 800 \pm 4400	14 833 200 \pm 4500	
α_1	-1.4155 \pm 0.0016	-1.5576 \pm 0.0016	fixed	-1.4191 \pm 0.0016	-1.5383 \pm 0.0017	
α_2	1.1023 \pm 0.0012	1.2434 \pm 0.0014	fixed	1.1060 \pm 0.0012	1.2418 \pm 0.0014	
n_1	4.0000 \pm 0.0037	2.0008 \pm 0.0048	fixed	4.0000 \pm 0.0034	2.0902 \pm 0.0059	
n_2	5.0000 \pm 0.0013	2.5335 \pm 0.0054	fixed	5.0000 \pm 0.0010	2.5327 \pm 0.0063	
σ_{CB}	2.5594 \pm 0.0015	2.6619 \pm 0.0014	fixed	2.5609 \pm 0.0014	2.6572 \pm 0.0014	
μ_{CB}	90.69146 \pm 0.00091	90.6580 \pm 0.0010	fixed	90.69146 \pm 0.00087	90.6527 \pm 0.0010	
N_B	11 320 \pm 640	-	-	-	16 230 \pm 300	-
β_0	-3.93 \pm 0.12	-	-	-	-4.709 \pm 0.074	-
β_1	1.61 \pm 0.42	-	-	-	3.36 \pm 0.13	-
β_2	4.9983 \pm 0.0057	-	-	-	2.08 \pm 0.18	-
β_3	-0.7956 \pm 0.0016	-	-	-	0.21 \pm 0.17	-
β_4	-0.48 \pm 0.13	-	-	-	-2.01 \pm 0.23	-
μ_B	90.4 \pm 1.1	-	-	-	94.942 \pm 0.050	-
α_B	0.008017 \pm 0.000077	-	-	-	0.007442 \pm 0.000058	-
N_G	-	-	-	-	-	-
μ_G	-	-	-	-	-	-
σ_G	-	-	-	-	-	-
					1000 \pm 0.77	
					95 \pm 0.026	
					30 \pm 0.058	

Table 45: Parameters of the fit in the $e \rightarrow \gamma$ fake estimation for the EFR $Z \rightarrow e\gamma$.

	Nominal		Variation: functions		Variation: fit range	
	Data	MC	Data	MC	Data	MC
N_{CB}	99350 ± 2400	1160900 ± 2700	1217500 ± 1100	976100 ± 2900	1067900 ± 2300	
α_1	-1.5142 ± 0.0073	-1.8340 ± 0.0029	fixed	-1.5227 ± 0.0080	-1.656 ± 0.011	
α_2	1.1590 ± 0.0083	1.2878 ± 0.0020	fixed	1.1183 ± 0.0084	1.2451 ± 0.0043	
n_1	4.000 ± 0.012	1.1483 ± 0.0037	fixed	3.992 ± 0.022	1.616 ± 0.033	
n_2	3.19 ± 0.11	1.50000 ± 0.00073	fixed	4.34 ± 0.18	1.603 ± 0.010	
σ_{CB}	2.8402 ± 0.0062	3.0020 ± 0.0048	fixed	2.8171 ± 0.0064	2.9710 ± 0.0061	
μ_{CB}	901234 ± 0.0058	901244 ± 0.0091	fixed	901601 ± 0.0061	899012 ± 0.0073	
N_B	2272 ± 64	-	-	2780 ± 110	110	-
β_0	-4.969 ± 0.077	-	-	-3.82 ± 0.20	0.20	-
β_1	4.137 ± 0.081	-	-	4.683 ± 0.066	-	-
β_2	1.787 ± 0.034	-	-	0.756 ± 0.012	-	-
β_3	-0.334 ± 0.018	-	-	-0.170 ± 0.072	-	-
β_4	-0.2273 ± 0.0091	-	-	-0.006 ± 0.014	-	-
μ_B	86.69 ± 0.21	-	-	90.478 ± 0.070	-	-
α_B	0.00658 ± 0.00011	-	-	0.00804 ± 0.00031	-	-
N_G	-	-	1000 ± 0.19	-	-	-
μ_G	-	-	85 ± 0.0093	-	-	-
σ_G	-	-	30 ± 0.0086	-	-	-

1732 **J Plots for $e \rightarrow \gamma$ fake estimation in linear scale**

Not reviewed, for internal circulation only

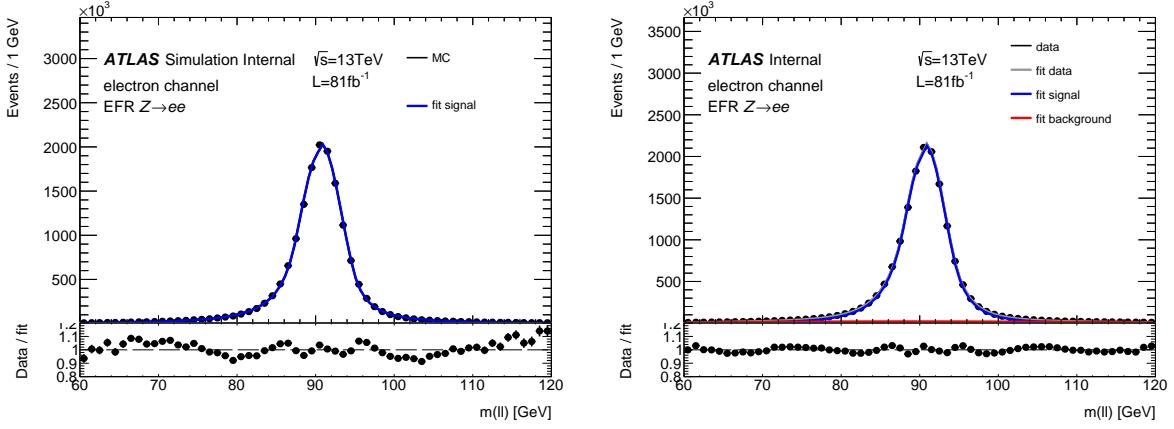


Figure 81: Fitted distribution of the invariant mass $m(ee)$ in the EFR $Z \rightarrow ee$ for simulation (left) and data (right) in linear scale. In the bottom plot, the ratio between simulation/data and the fit function is shown.

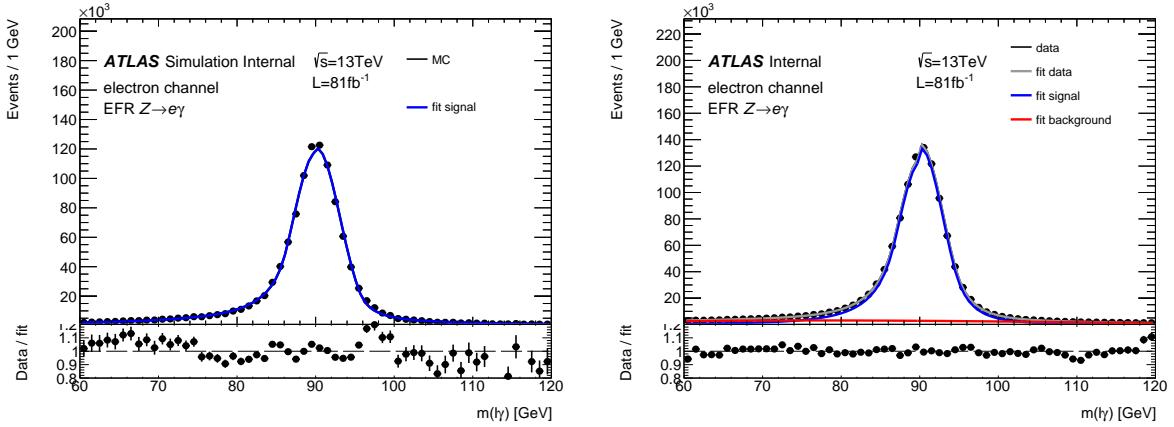


Figure 82: Fitted distribution of the invariant mass $m(e\gamma)$ in the EFR $Z \rightarrow e\gamma$ for simulation (left) and data (right) in linear scale. In the bottom plot, the ratio between simulation/data and the fit function is shown.

Not reviewed, for internal circulation only

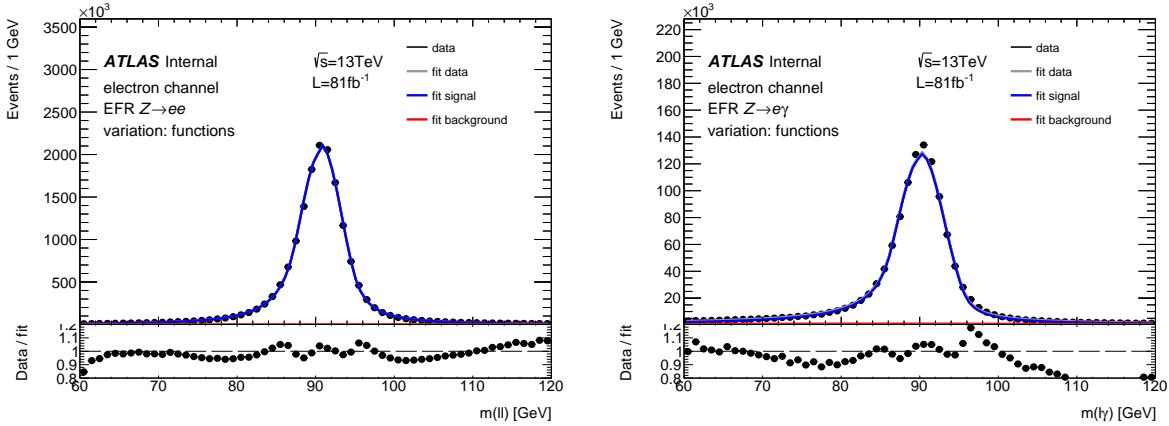


Figure 83: Fitted distribution of the invariant mass $m(ee)$ in the EFR $Z \rightarrow ee$ (left) and the invariant mass $m(e\gamma)$ in the EFR $Z \rightarrow e\gamma$ (right) in data when varying the setup of the functions in linear scale. For the signal function, the parameters fitted in simulation are propagated and fixed when fitting data, and the background function is changed to a Gaussian function. In the bottom plot, the ratio between data and the fit function is shown.

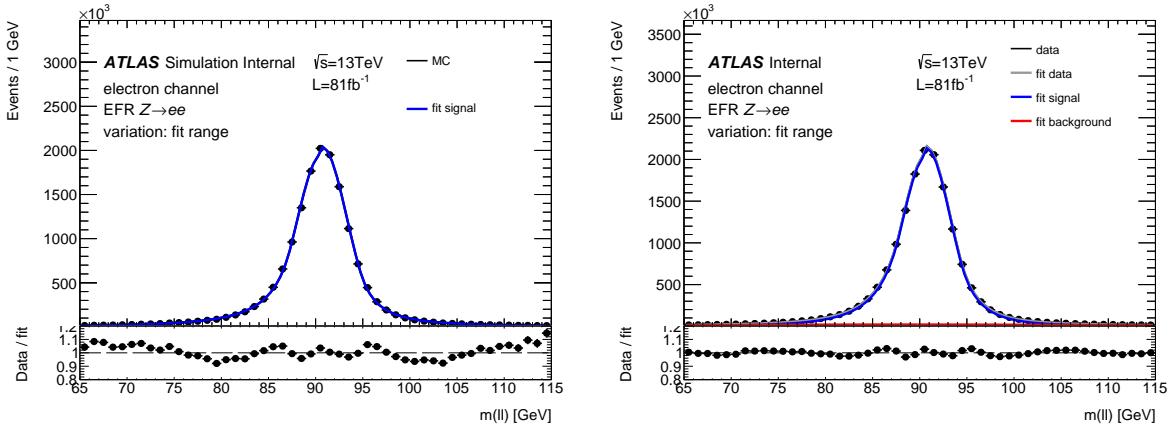


Figure 84: Fitted distribution of the invariant mass $m(ee)$ in the EFR $Z \rightarrow ee$ for simulation (left) and data (right) when varying the fit range in linear scale. In the bottom plot, the ratio between simulation/data and the fit function is shown.

Not reviewed, for internal circulation only

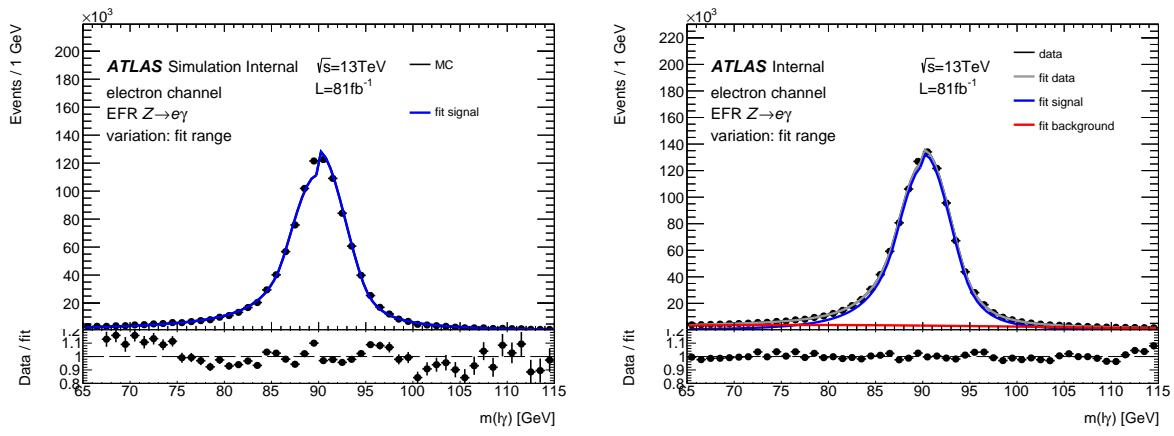


Figure 85: Fitted distribution of the invariant mass $m(e\gamma)$ in the EFR $Z \rightarrow e\gamma$ for simulation (left) and data (right) when varying the fit range in linear scale. In the bottom plot, the ratio between simulation/data and the fit function is shown.

1733 K Photon p_T independence of scale factor $SF(e \rightarrow \gamma)$

1734 In order to check if the scale factor $SF(e \rightarrow \gamma)$ shows dependencies on the photon p_T , the photon p_T
 1735 spectrum of the $e \rightarrow \gamma$ fakes in the EFR $Z \rightarrow e\gamma$, SR and VR $SF(e \rightarrow \gamma)$ is looked at, as shown in
 1736 Figure 86. The photon p_T spectrum of the $e \rightarrow \gamma$ fakes coming from the $Z+jets$ events in the EFR
 1737 $Z \rightarrow e\gamma$ and SR are very similar. As the spectra in the VR $SF(e \rightarrow \gamma)$ and SR are alike and the agreement
 1738 between data and MC is good in the VR $SF(e \rightarrow \gamma)$ as also shown in the validation of the fit outcome in
 1739 Section 10.9.2, it is concluded that an inclusive scale factor for the electron-to-photon fakes is sufficient.

Not reviewed, for internal circulation only

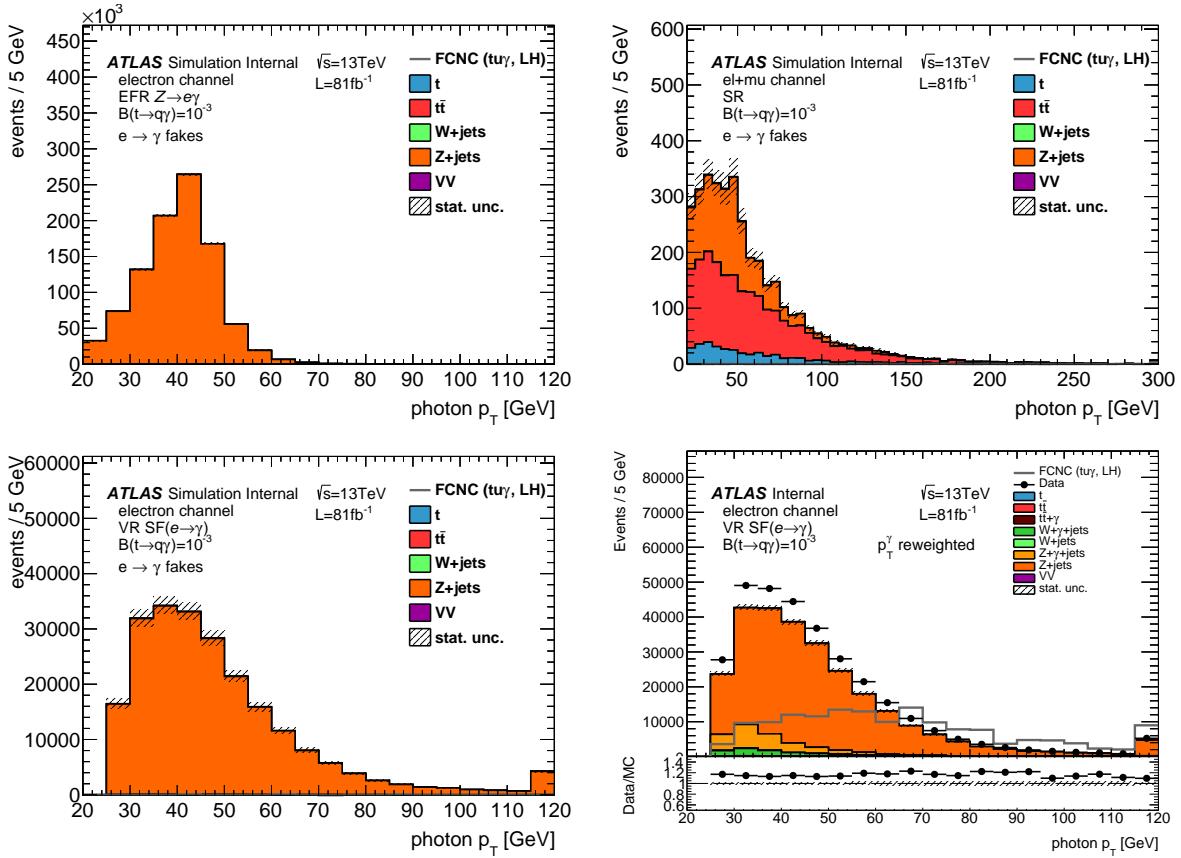


Figure 86: Photon p_T spectrum of the $e \rightarrow \gamma$ fakes in the EFR $Z \rightarrow e\gamma$ (top left), SR (top right), and VR $SF(e \rightarrow \gamma)$ (bottom left), and the photon p_T spectrum of all backgrounds in the VR $SF(e \rightarrow \gamma)$ (bottom right). Only the statistical uncertainties are included.

1740 L Input variables for neural network for different signal samples

Not reviewed, for internal circulation only

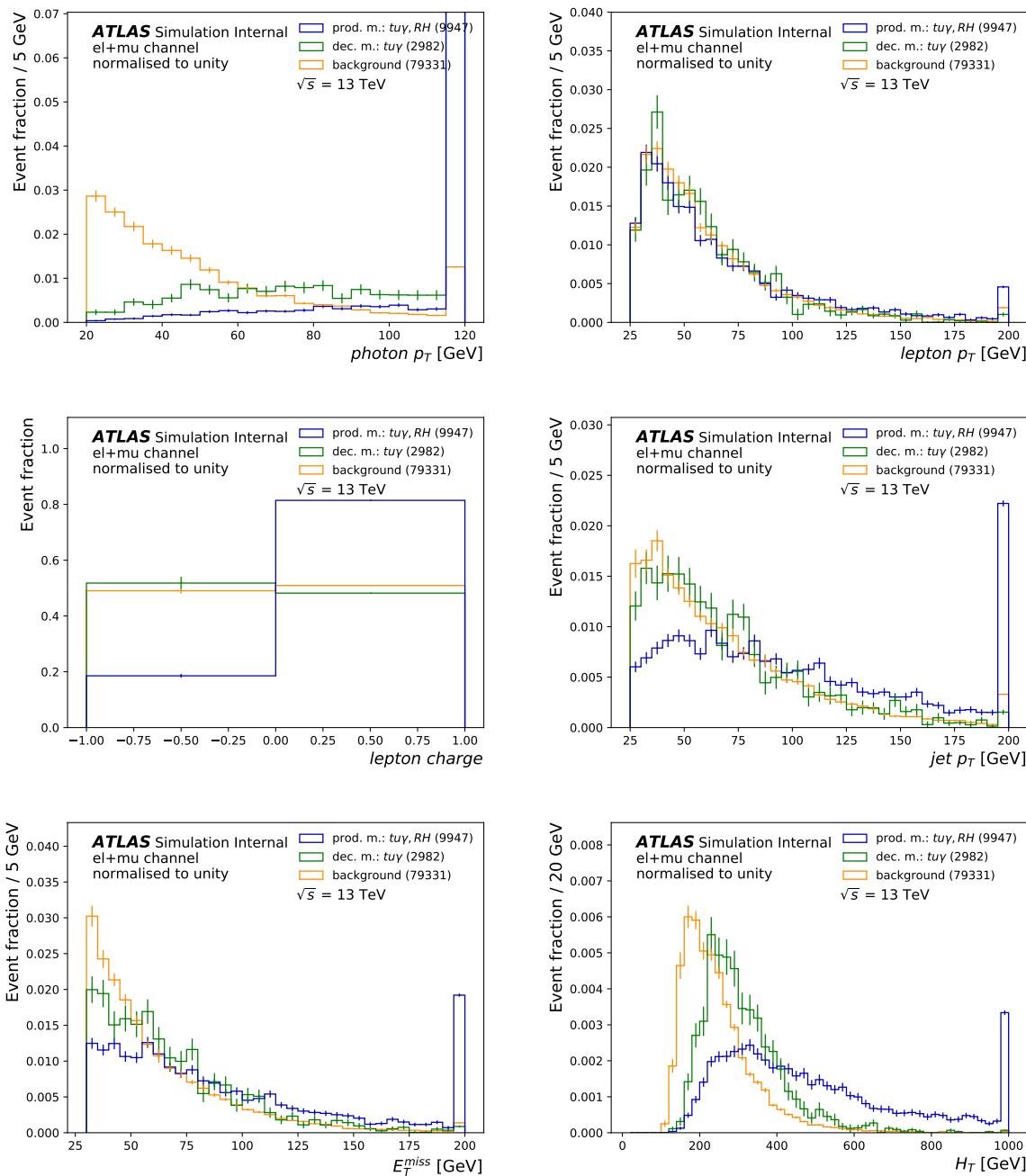


Figure 87: Comparison of shapes of kinematic distributions between signal (here: *tuy*, right-handed coupling) and background in the SR: photon p_T spectrum (top left), lepton p_T spectrum (top right), lepton charge (middle left), jet p_T spectrum (middle right), missing transverse momentum E_T^{miss} (bottom left), and H_T (bottom right). The number of MC events in the signal and background samples and the over- and underflow bins are also shown. Only the statistical uncertainty is shown.

Not reviewed, for internal circulation only

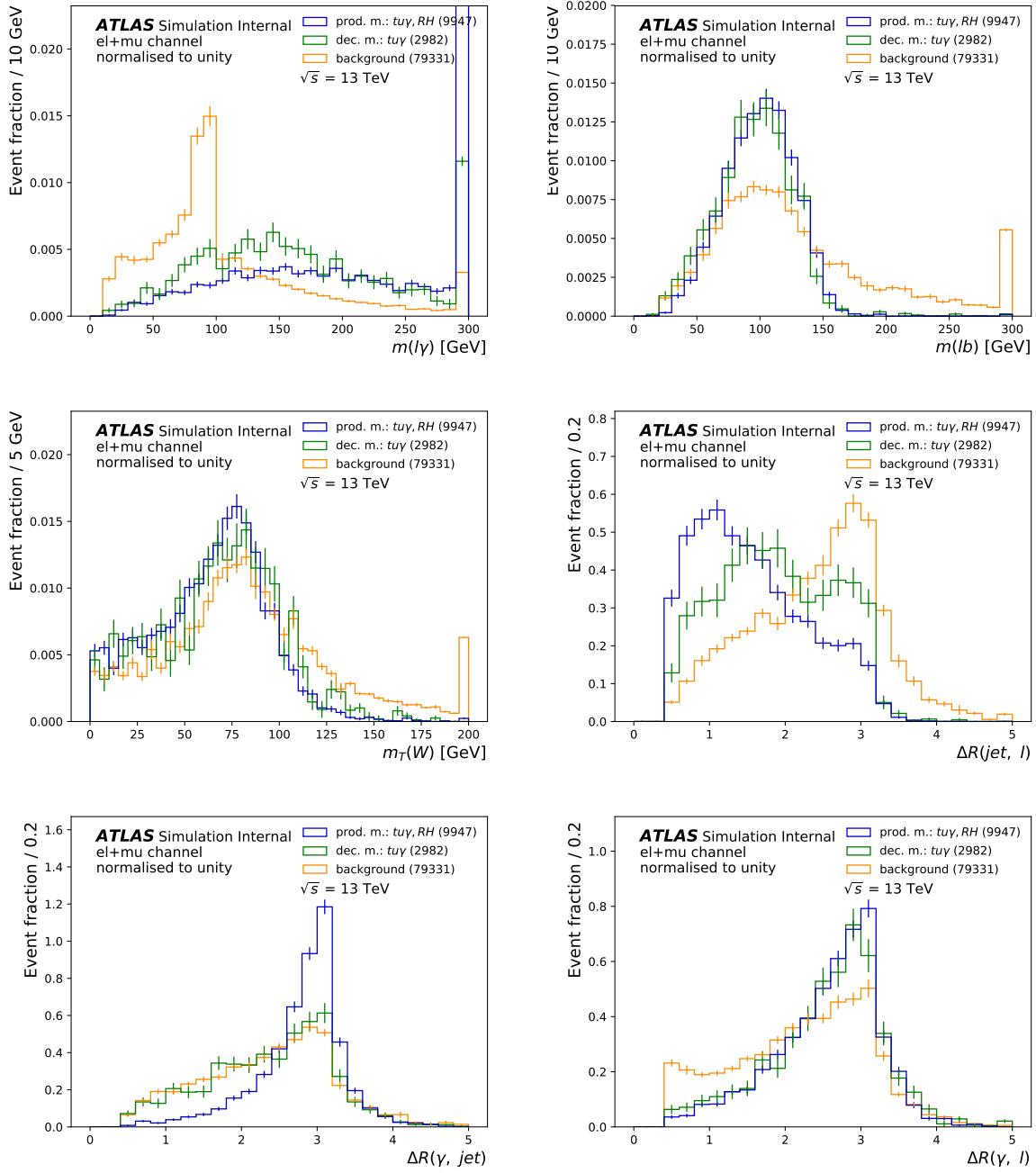


Figure 88: Comparison of shapes of kinematic distributions between signal (here: *tuy*, right-handed coupling) and background in the SR: invariant mass of the lepton and photon $m(\ell, \gamma)$ (top left), invariant mass of the lepton and b -jet $m(\ell, b\text{-jet})$ (top right), the transverse mass of the W boson $m_T(W)$ (middle left), distance ΔR between the b -jet and lepton (middle right), distance ΔR between the b -jet and photon (bottom left), and distance ΔR between the lepton and photon (bottom right). The number of MC events in the signal and background samples and the over- and underflow bins are also shown. Only the statistical uncertainty is shown.

Not reviewed, for internal circulation only

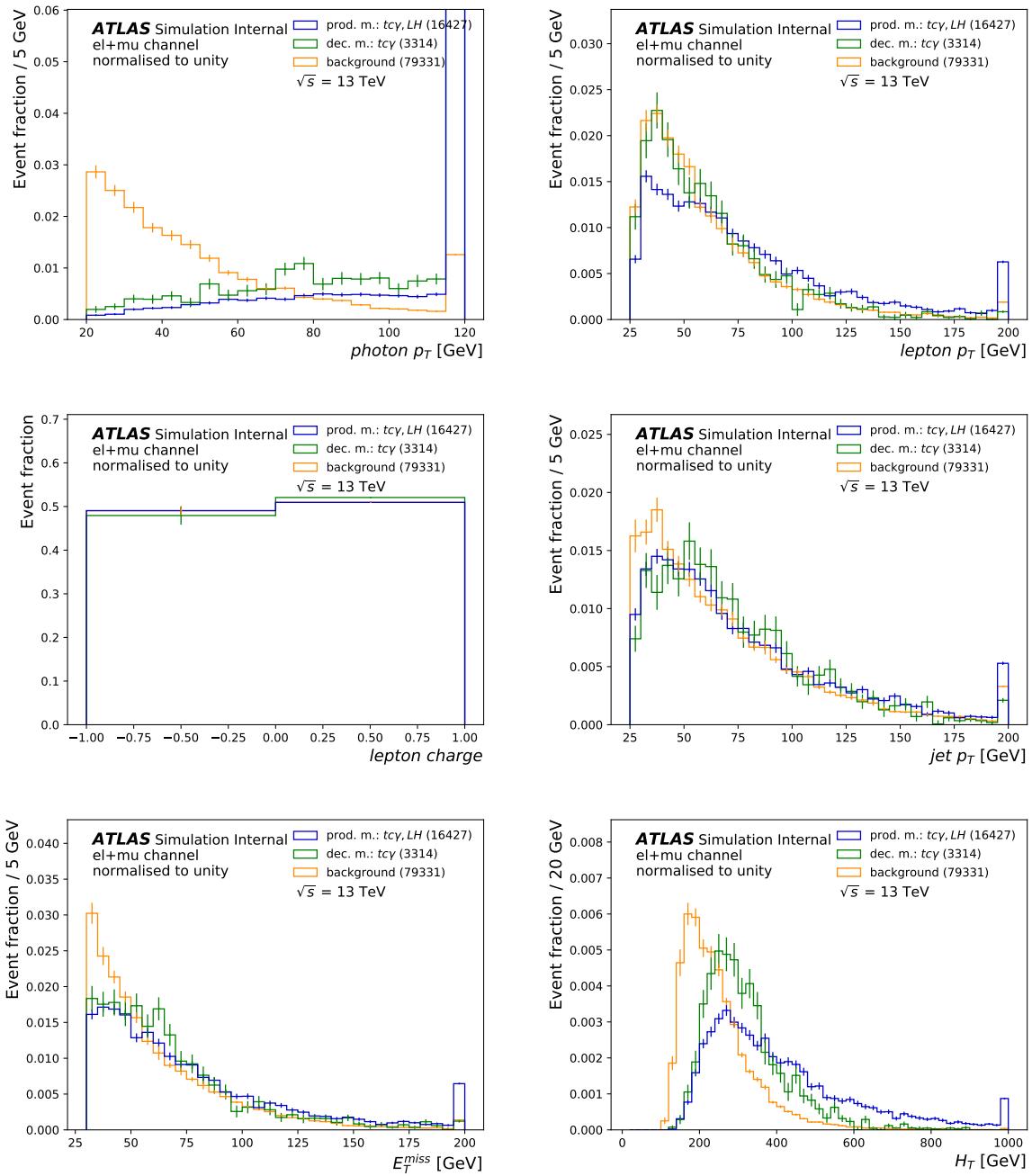


Figure 89: Comparison of shapes of kinematic distributions between signal (here: $tc\gamma$, left-handed coupling) and background in the SR: photon p_T spectrum (top left), lepton p_T spectrum (top right), lepton charge (middle left), jet p_T spectrum (middle right), missing transverse momentum E_T^{miss} (bottom left), and H_T (bottom right). The number of MC events in the signal and background samples and the over- and underflow bins are also shown. Only the statistical uncertainty is shown.

Not reviewed, for internal circulation only

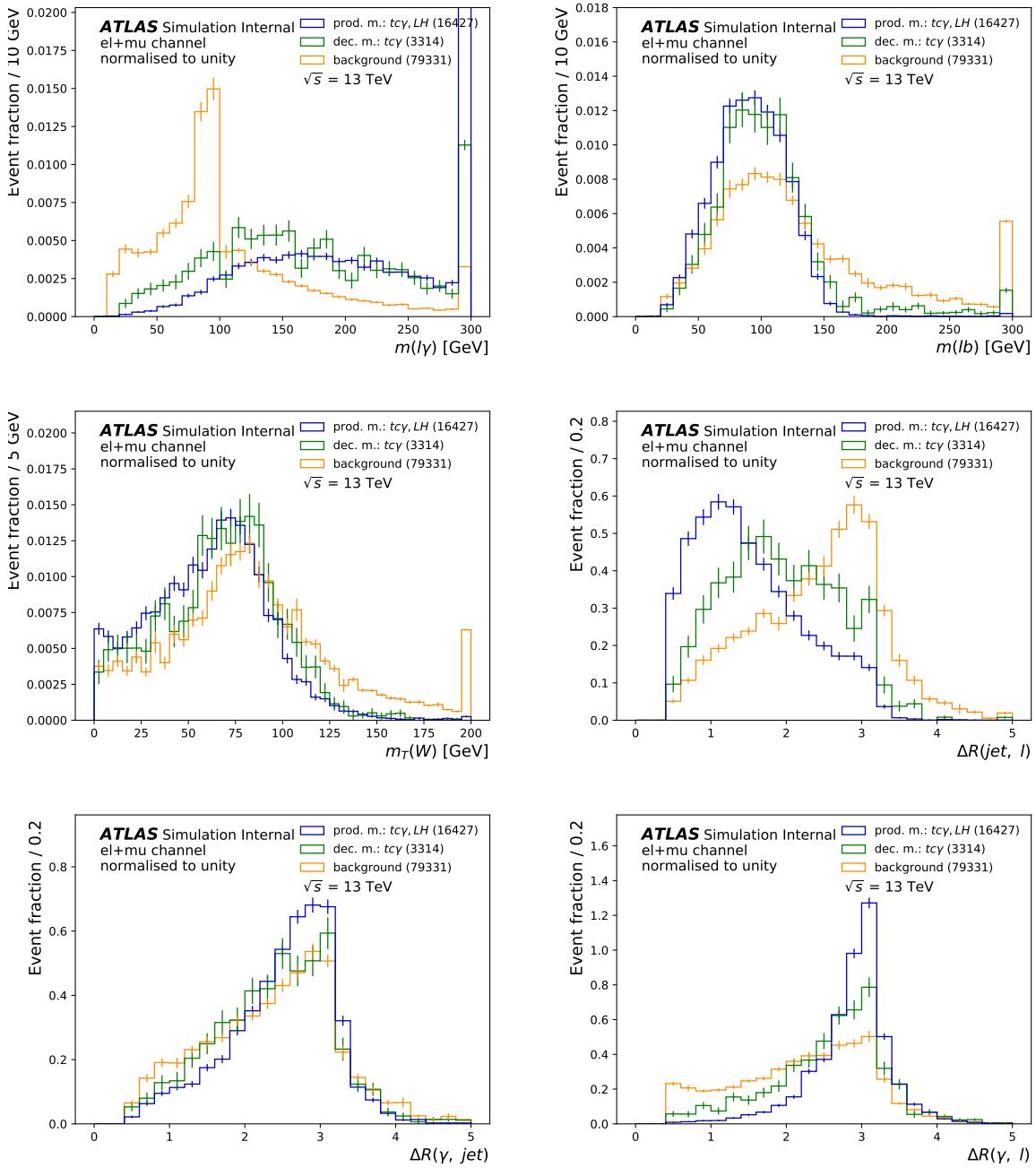


Figure 90: Comparison of shapes of kinematic distributions between signal (here: $tc\gamma$, left-handed coupling) and background in the SR: invariant mass of the lepton and photon $m(\ell, \gamma)$ (top left), invariant mass of the lepton and b -jet $m(\ell, b\text{-jet})$ (top right), the transverse mass of the W boson $m_T(W)$ (middle left), distance ΔR between the b -jet and lepton (middle right), distance ΔR between the b -jet and photon (bottom left), and distance ΔR between the lepton and photon (bottom right). The number of MC events in the signal and background samples and the over- and underflow bins are also shown. Only the statistical uncertainty is shown.

Not reviewed, for internal circulation only

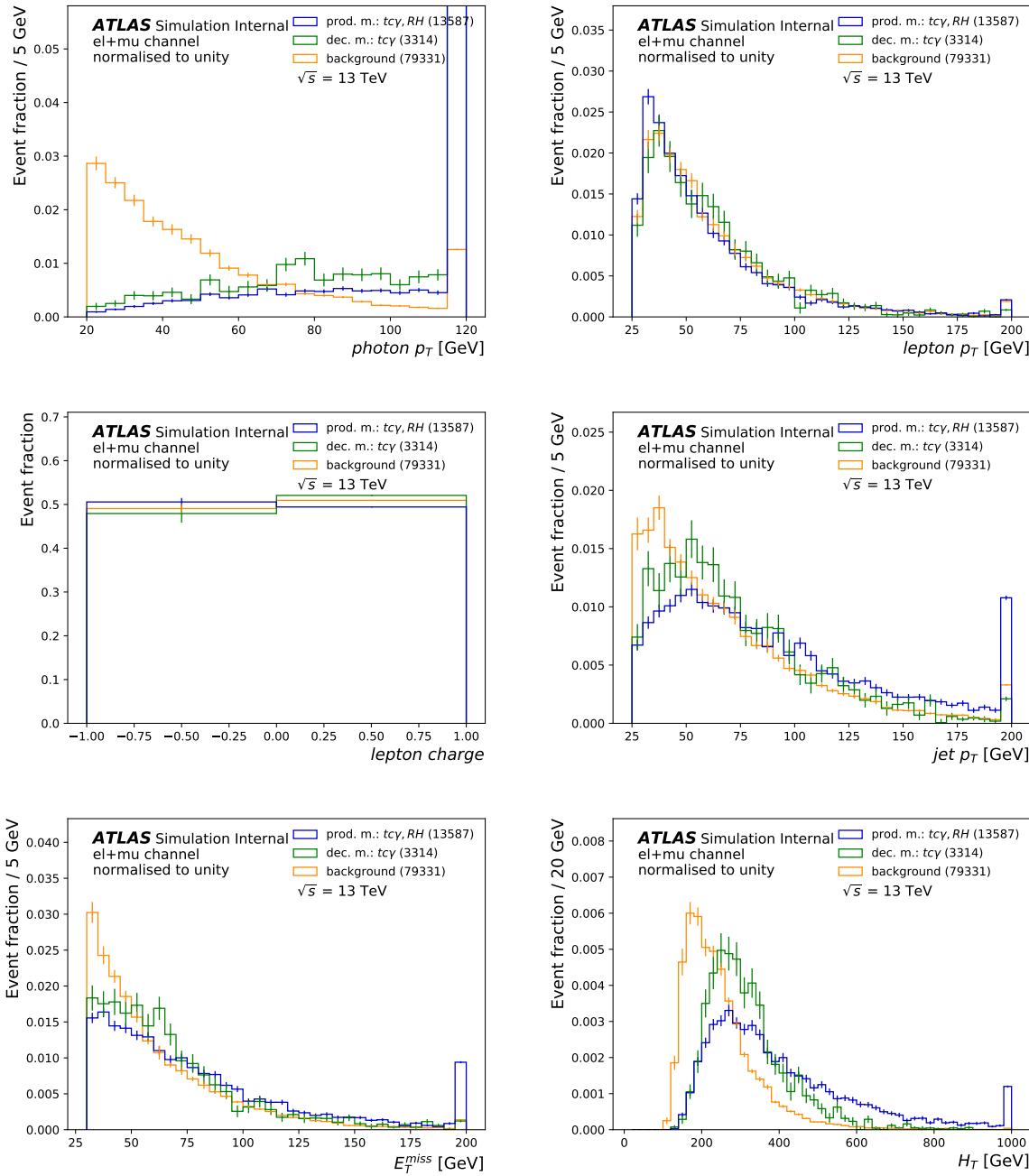


Figure 91: Comparison of shapes of kinematic distributions between signal (here: $tc\gamma$, right-handed coupling) and background in the SR: photon p_T spectrum (top left), lepton p_T spectrum (top right), lepton charge (middle left), jet p_T spectrum (middle right), missing transverse momentum E_T^{miss} (bottom left), and H_T (bottom right). The number of MC events in the signal and background samples and the over- and underflow bins are also shown. Only the statistical uncertainty is shown.

Not reviewed, for internal circulation only

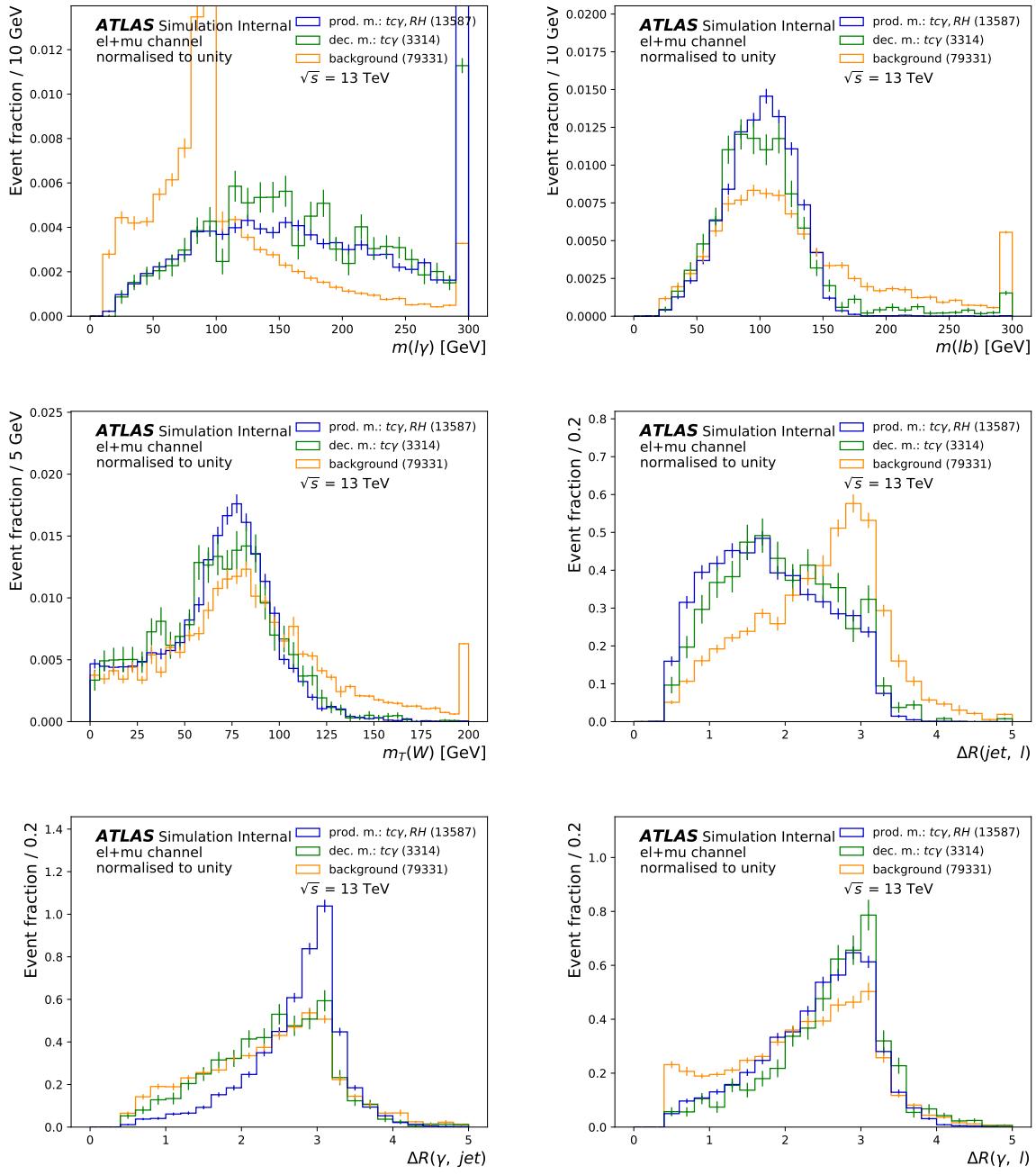


Figure 92: Comparison of shapes of kinematic distributions between signal (here: $tc\gamma$, right-handed coupling) and background in the SR: invariant mass of the lepton and photon $m(\ell, \gamma)$ (top left), invariant mass of the lepton and b -jet $m(\ell, b\text{-jet})$ (top right), the transverse mass of the W boson $m_T(W)$ (middle left), distance ΔR between the b -jet and lepton (middle right), distance ΔR between the b -jet and photon (bottom left), and distance ΔR between the lepton and photon (bottom right). The number of MC events in the signal and background samples and the over- and underflow bins are also shown. Only the statistical uncertainty is shown.

1741 **M Correlation of NN input variables in CR $W+\gamma+\text{jets}$**

[Not reviewed, for internal circulation only]

Not reviewed, for internal circulation only

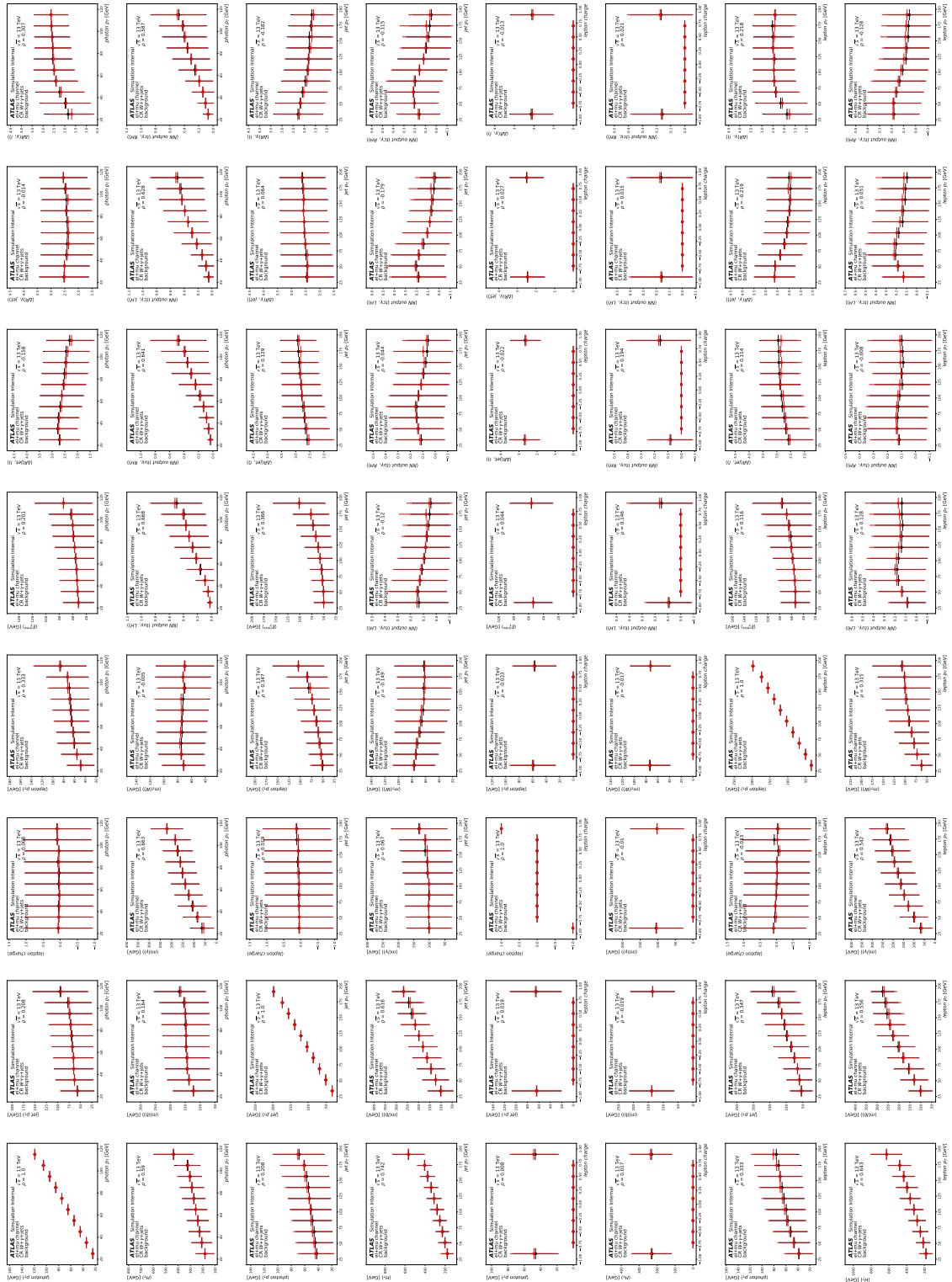


Figure 93: Distributions of the average of variable $\langle z_i \rangle$ against variable $\langle z_i \rangle$ in CR $W+\gamma+jets$ (part I). Data is shown as black dots and simulation is shown as red dots.

Not reviewed, for internal circulation only

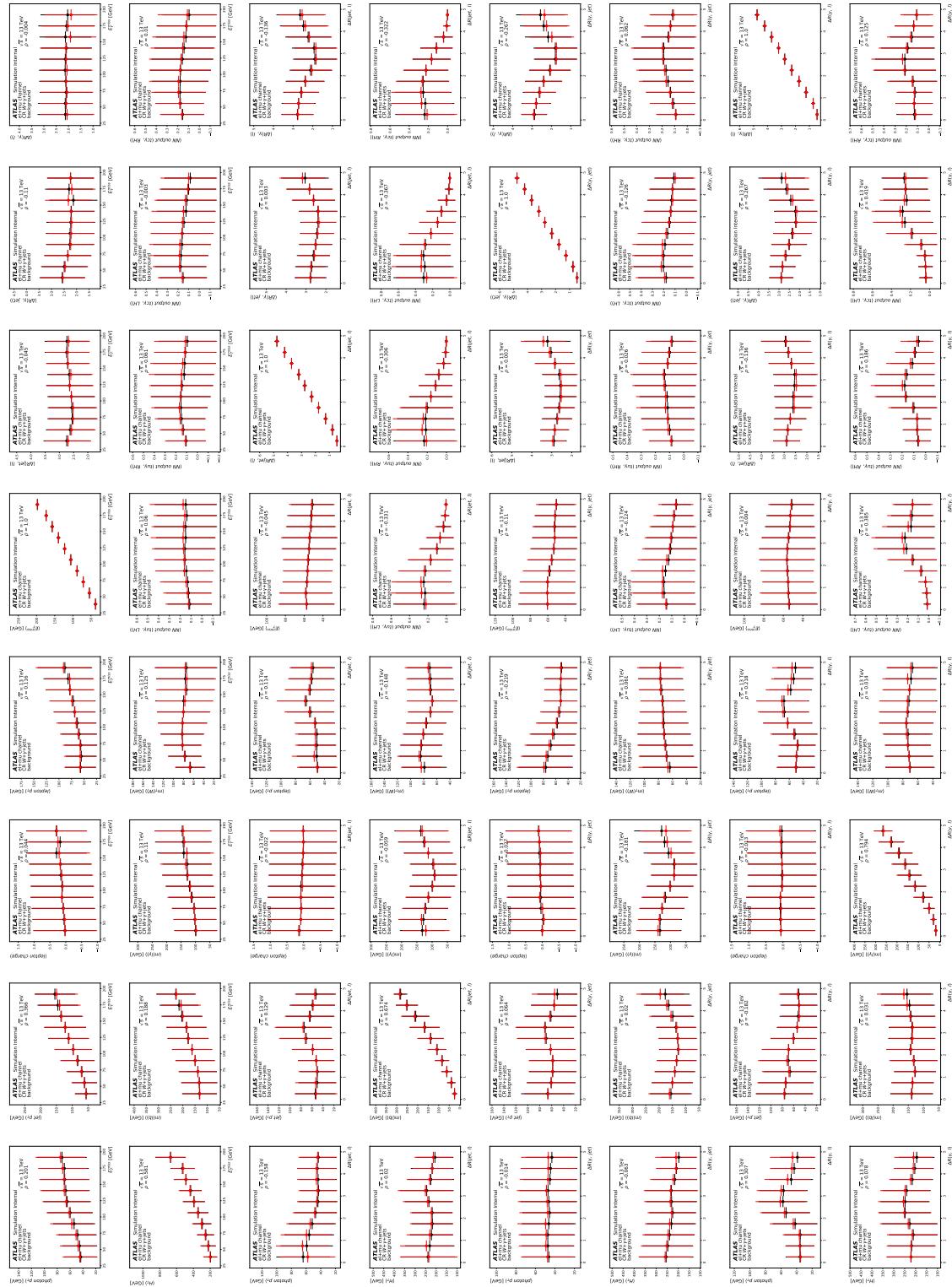


Figure 94: Distributions of the average of variable $\langle z_i \rangle$ against variable $\langle z_i \rangle$ in CR $W+\gamma+jets$ (part II). Data is shown as black dots and simulation is shown as red dots.

Not reviewed, for internal circulation only

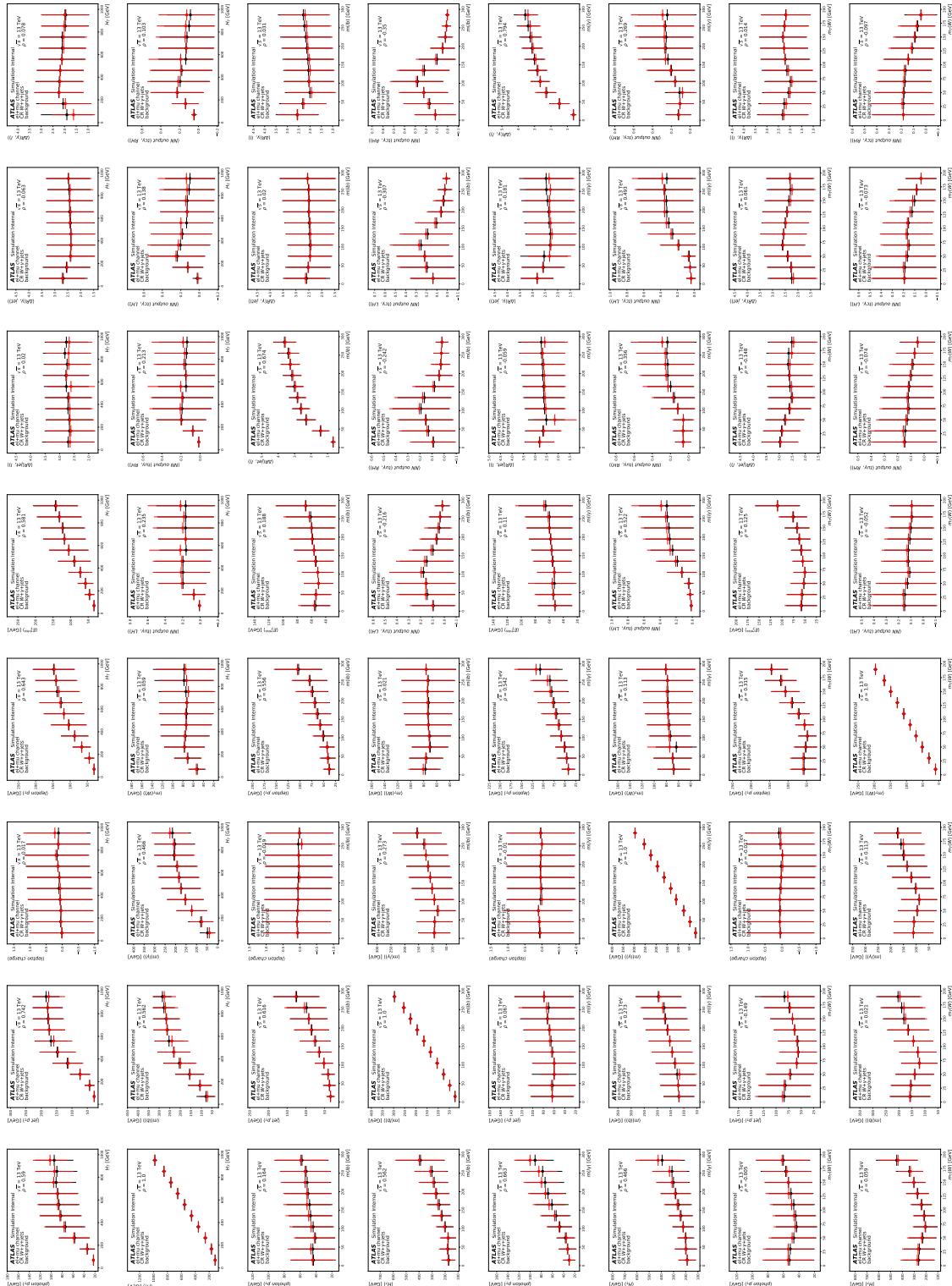


Figure 95: Distributions of the average of variable $\langle z_i \rangle$ against variable $\langle z_i \rangle$ in CR $W + \gamma + \text{jets}$ (part III). Data is shown as black dots and simulation is shown as red dots.

Not reviewed, for internal circulation only

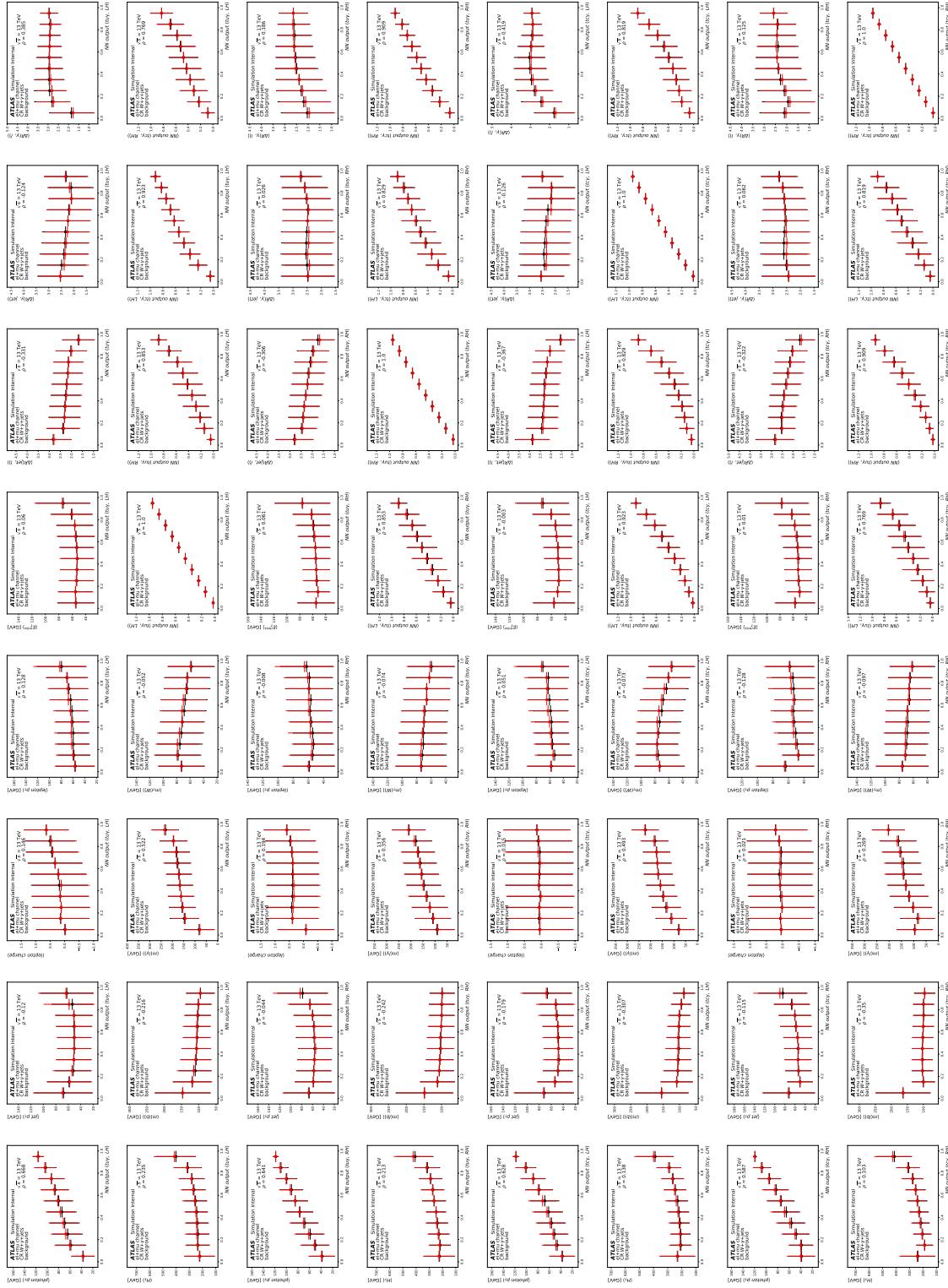


Figure 96: Distributions of the average of variable z_i against variable $\langle z_i \rangle$ in CR $W+\gamma+jets$ (part IV). Data is shown as black dots and simulation is shown as red dots.

1742 N Studies for neural network output

1743 N.1 Neural network output separated by lepton flavour

1744 In Figures 97 and 98, the NN output distributions are shown for the different couplings in the SR separately
 1745 for the electron and muon channel. It can be seen that the shapes of the NN are similar in both channels.

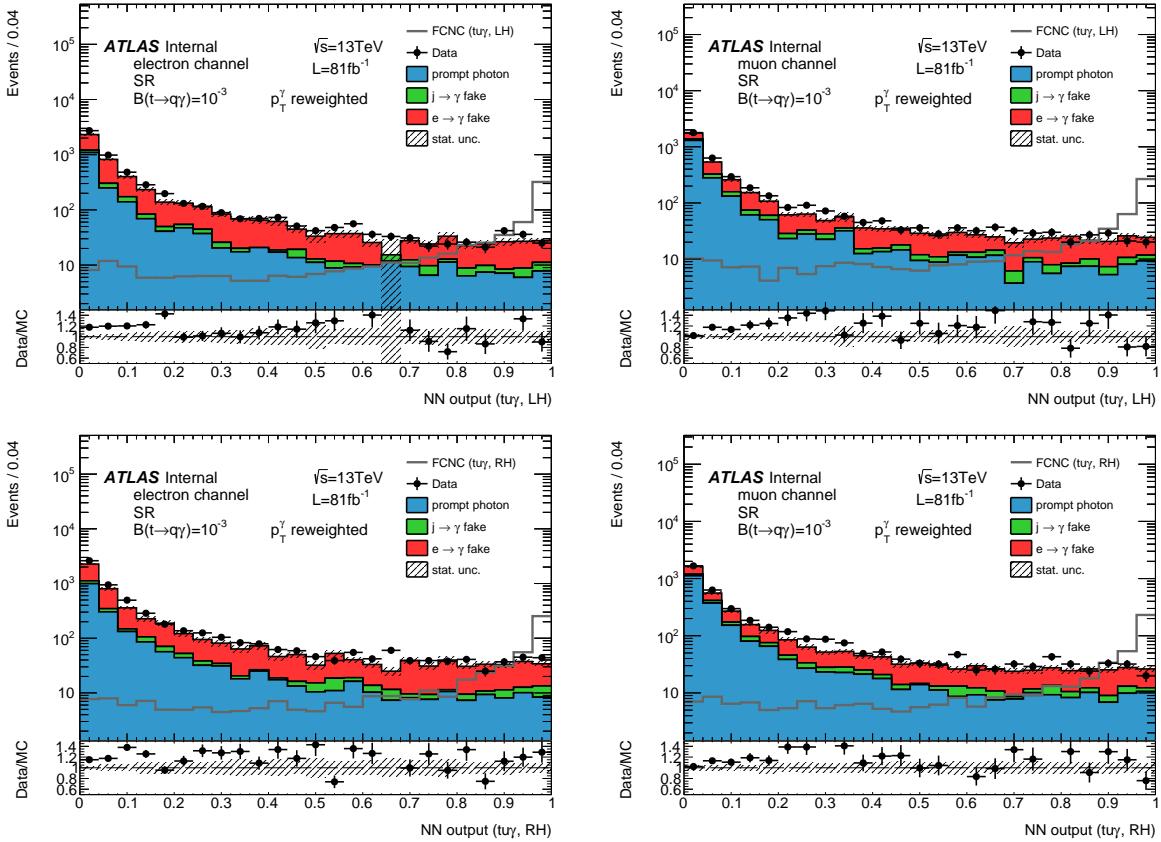


Figure 97: Output distributions of the neural network in the SR trained with the tuy coupling, left-handed (top) and right-handed (bottom), for the electron (left) and muon channel (right). Both signal modes are included. Only the statistical uncertainty is shown.

Not reviewed, for internal circulation only

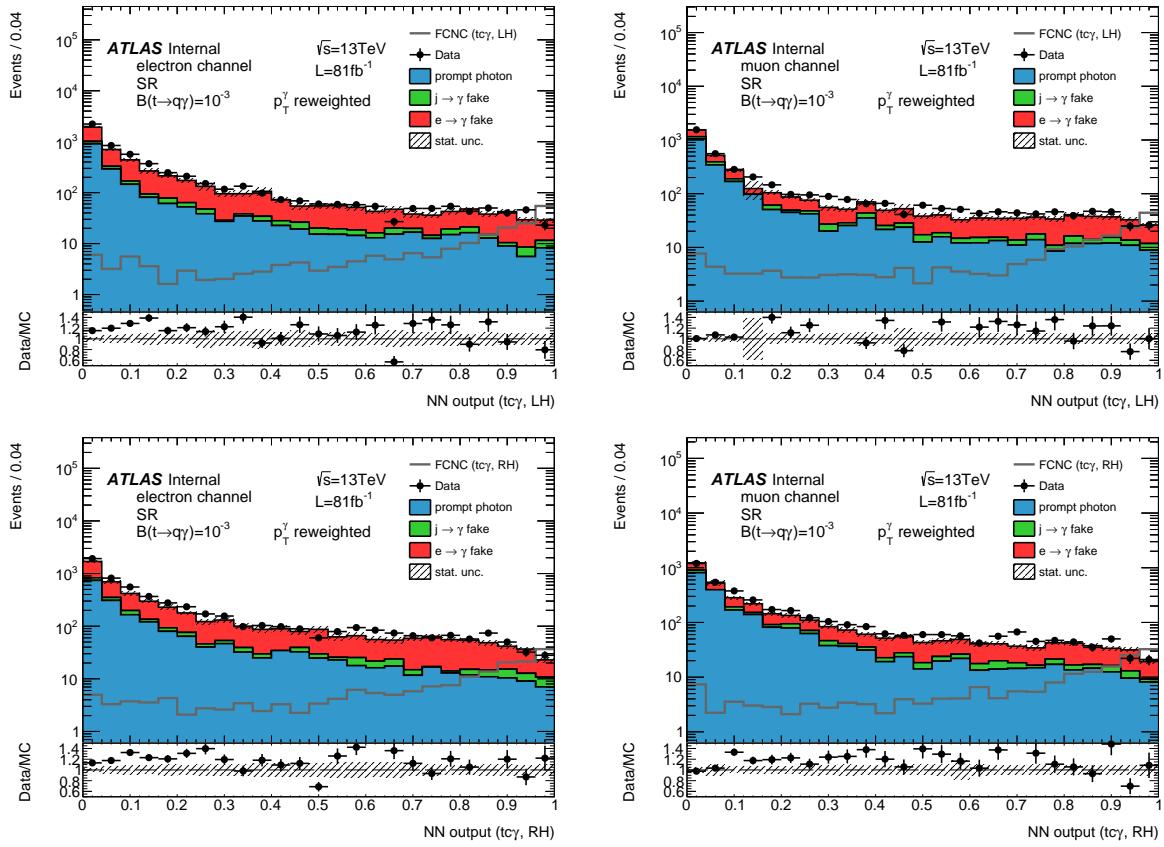


Figure 98: Output distributions of the neural network in the SR trained with the $tc\gamma$ coupling, left-handed (top) and right-handed (bottom), for the electron (left) and muon channel (right). Both signal modes are included. Only the statistical uncertainty is shown.

1746 N.2 Neural network output before and after the photon reweighting

1747 In Figures 99 and 100, the NN output distributions are shown for the different couplings in the CR
 1748 $W + \gamma + \text{jets}$ with and without applying the photon p_T reweighting. It can be seen that after reweighting, the
 1749 agreement between data and prediction improves.

Not reviewed, for internal circulation only

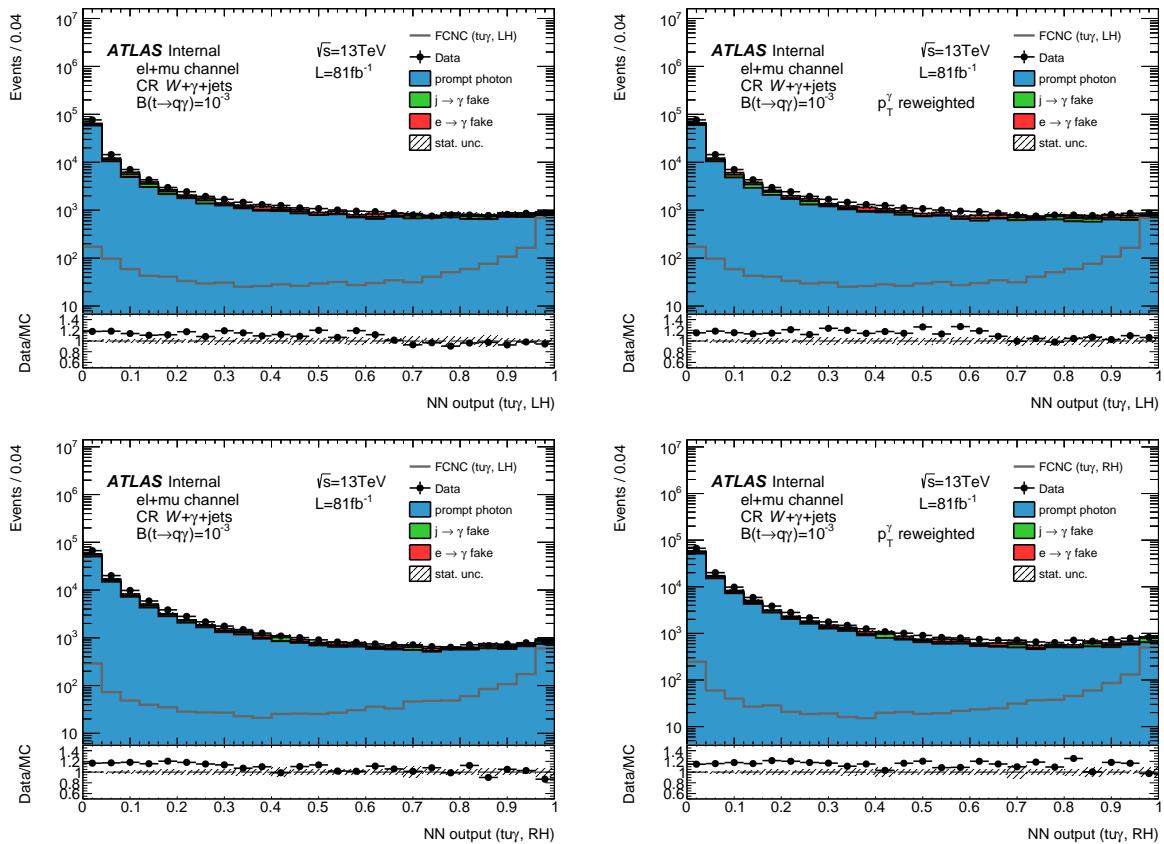


Figure 99: Output distributions of the neural network in the CR $W+\gamma+jets$ trained for the left-handed (top) and right-handed (bottom) $tuya$ coupling without (left) and with the photon p_T reweighting (right). Both signal modes are included. Only statistical uncertainties are shown.

Not reviewed, for internal circulation only

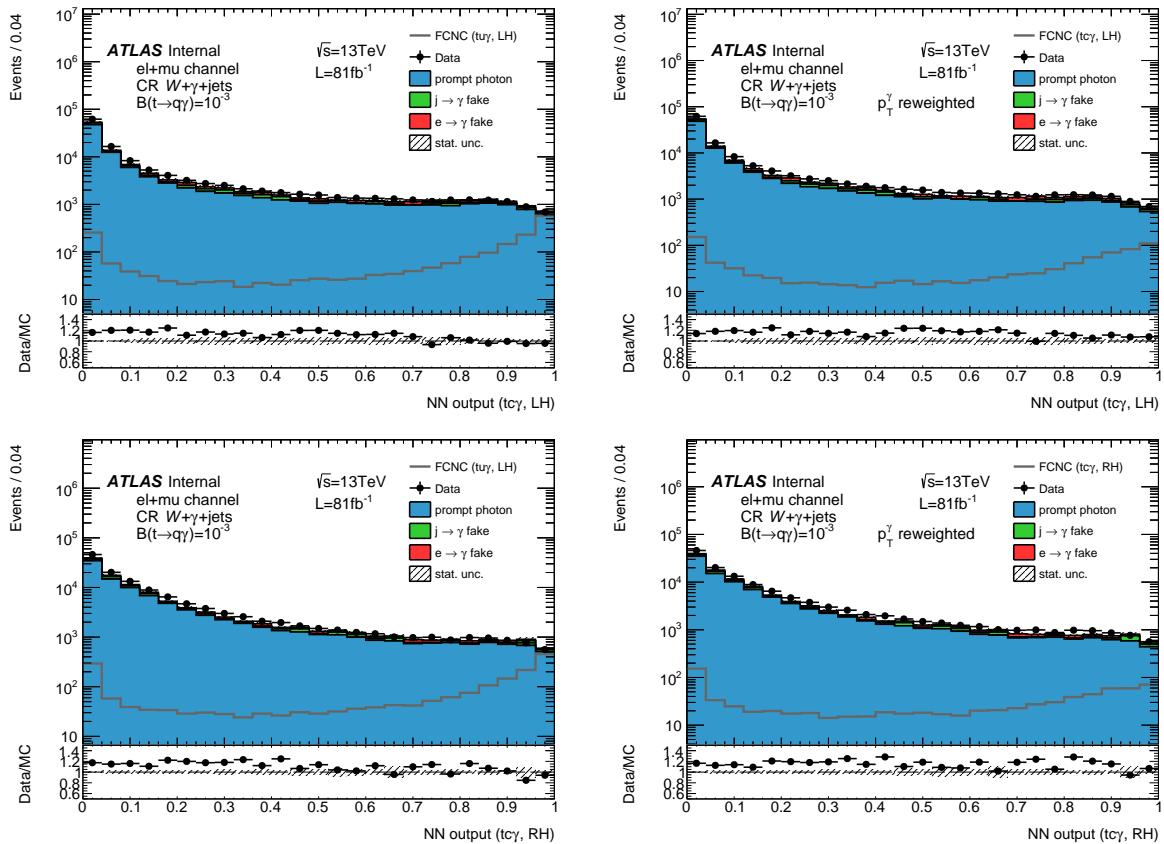


Figure 100: Output distributions of the neural network in the CR $W+\gamma+\text{jets}$ trained for the left-handed (top) and right-handed (bottom) $tc\gamma$ coupling without (left) and with the photon p_T reweighting (right). Both signal modes are included. Only statistical uncertainties are shown.

O Plots for systematic uncertainties

1750

Not reviewed, for internal circulation only

Signal coupling	Process	SR	Regions	
			CR $W+\gamma+\text{jets}$	CR $Z+\gamma$
left-handed $t\gamma\gamma$ coupling	Total background	O.1.1.1	O.1.2.1	O.1.3.1
	Signal	O.1.1.2	O.1.2.2	O.1.3.2
	$e \rightarrow \gamma$ fakes	O.1.1.3	O.1.2.3	O.1.3.3
	$j \rightarrow \gamma$ fakes	O.1.1.4	O.1.2.4	O.1.3.4
	$W+\gamma+\text{jets}$	O.1.1.5	O.1.2.5	O.1.3.5
	$Z+\gamma+\text{jets}$	O.1.1.6	O.1.2.6	O.1.3.6
	Other prompt photons	O.1.1.7	O.1.2.7	O.1.3.7
right-handed $t\gamma\gamma$ coupling	Total background	O.2.1.1	O.2.2.1	O.2.3.1
	Signal	O.2.1.2	O.2.2.2	O.2.3.2
	$e \rightarrow \gamma$ fakes	O.2.1.3	O.2.2.3	O.2.3.3
	$j \rightarrow \gamma$ fakes	O.2.1.4	O.2.2.4	O.2.3.4
	$W+\gamma+\text{jets}$	O.2.1.5	O.2.2.5	O.2.3.5
	$Z+\gamma+\text{jets}$	O.2.1.6	O.2.2.6	O.2.3.6
	Other prompt photons	O.2.1.7	O.2.2.7	O.2.3.7
left-handed $t\gamma\gamma$ coupling	Total background	O.3.1.1	O.3.2.1	O.3.3.1
	Signal	O.3.1.2	O.3.2.2	O.3.3.2
	$e \rightarrow \gamma$ fakes	O.3.1.3	O.3.2.3	O.3.3.3
	$j \rightarrow \gamma$ fakes	O.3.1.4	O.3.2.4	O.3.3.4
	$W+\gamma+\text{jets}$	O.3.1.5	O.3.2.5	O.3.3.5
	$Z+\gamma+\text{jets}$	O.3.1.6	O.3.2.6	O.3.3.6
	Other prompt photons	O.3.1.7	O.3.2.7	O.3.3.7
right-handed $t\gamma\gamma$ coupling	Total background	O.4.1.1	O.4.2.1	O.4.3.1
	Signal	O.4.1.2	O.4.2.2	O.4.3.2
	$e \rightarrow \gamma$ fakes	O.4.1.3	O.4.2.3	O.4.3.3
	$j \rightarrow \gamma$ fakes	O.4.1.4	O.4.2.4	O.4.3.4
	$W+\gamma+\text{jets}$	O.4.1.5	O.4.2.5	O.4.3.5
	$Z+\gamma+\text{jets}$	O.4.1.6	O.4.2.6	O.4.3.6
	Other prompt photons	O.4.1.7	O.4.2.7	O.4.3.7

1751 **O.1 Plots for the left-handed $t u \gamma$ coupling**

1752 **O.1.1 SR (left-handed $t u \gamma$ coupling)**

1753 **O.1.1.1 Total background (SR, left-handed $t u \gamma$ coupling)**

Not reviewed, for internal circulation only

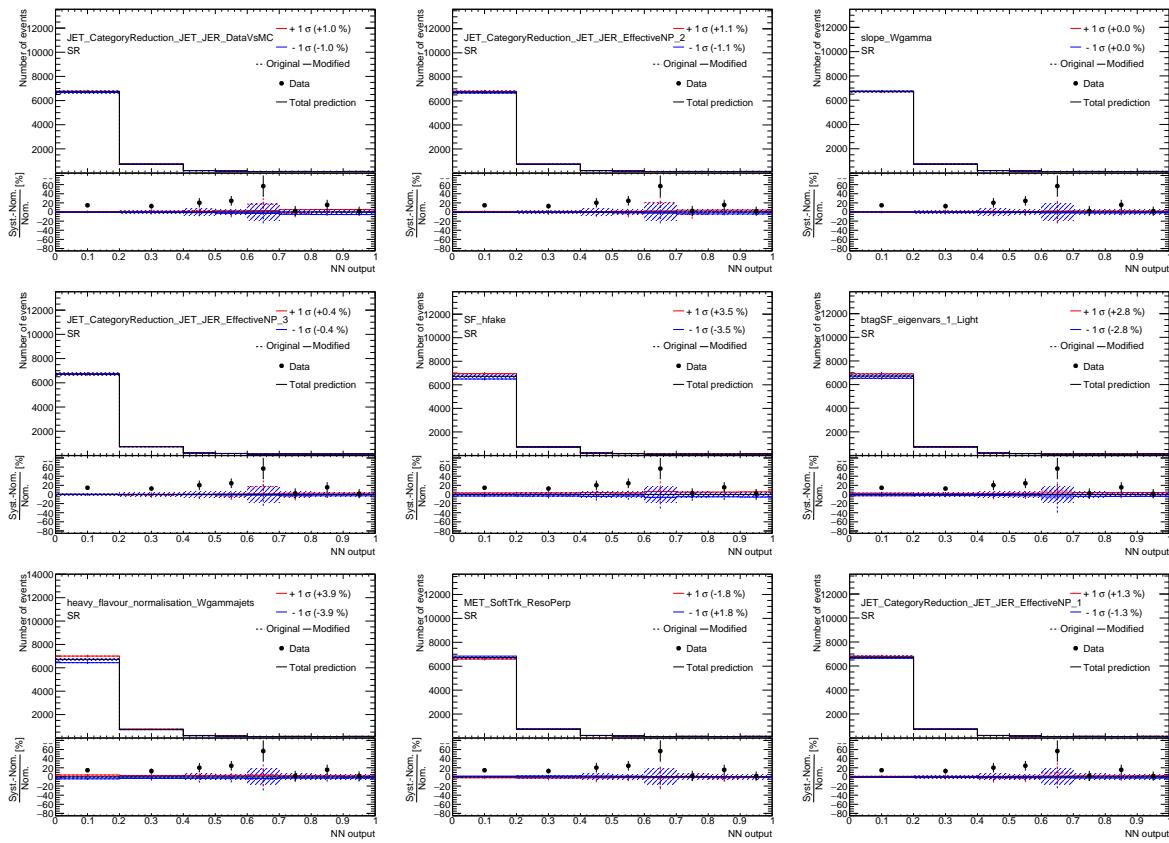


Figure 101: Plots showing the impact of 20 highest ranked systematic uncertainties on *Total background* for the left-handed $t u \gamma$ coupling coupling in the SR (1).

Not reviewed, for internal circulation only

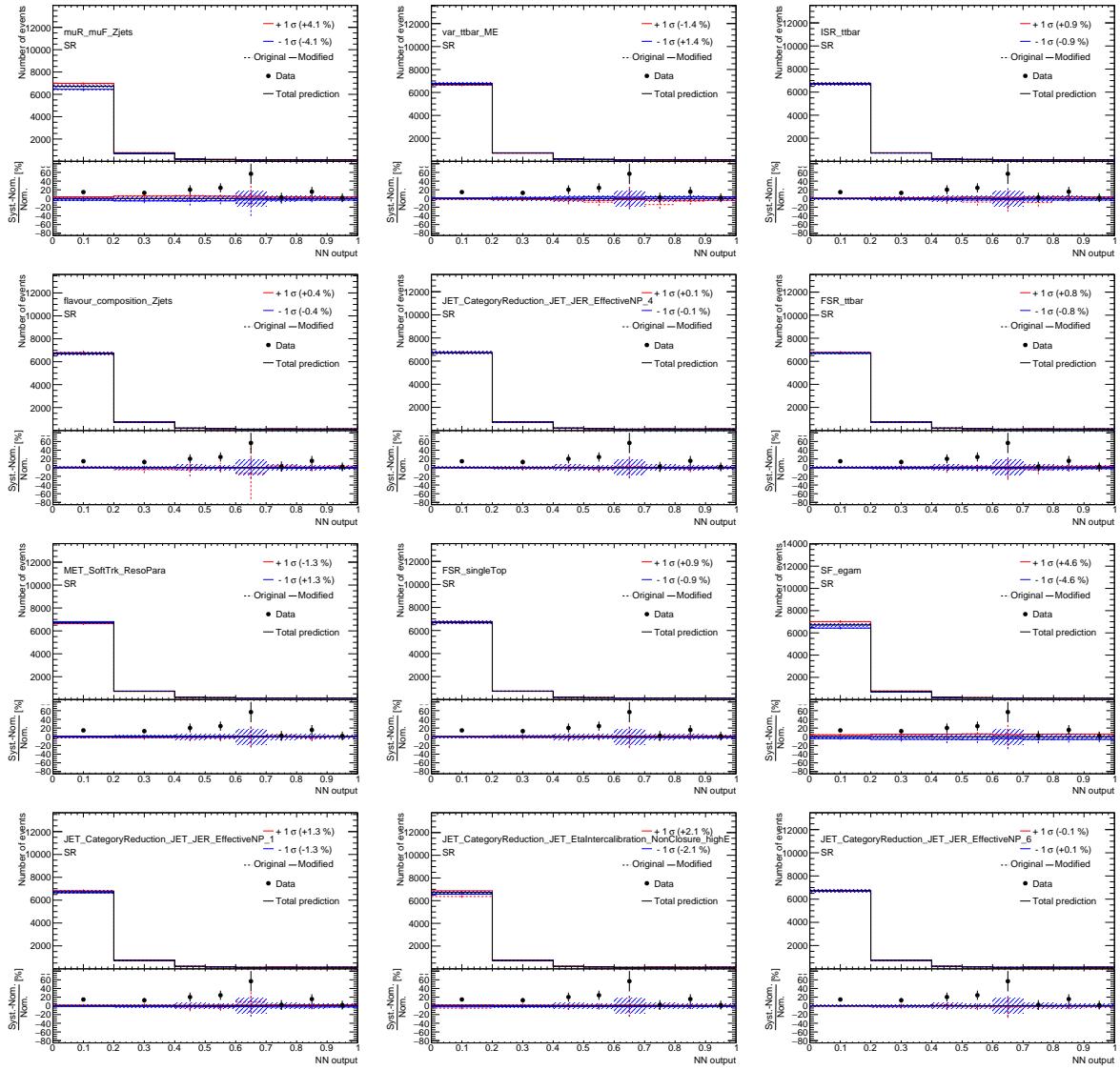


Figure 102: Plots showing the impact of 20 highest ranked systematic uncertainties on *Total background* for the left-handed $t\bar{u}\gamma$ coupling coupling in the SR (2).

1754 0.1.1.2 Signal (SR, left-handed $t u \gamma$ coupling)

Not reviewed, for internal circulation only

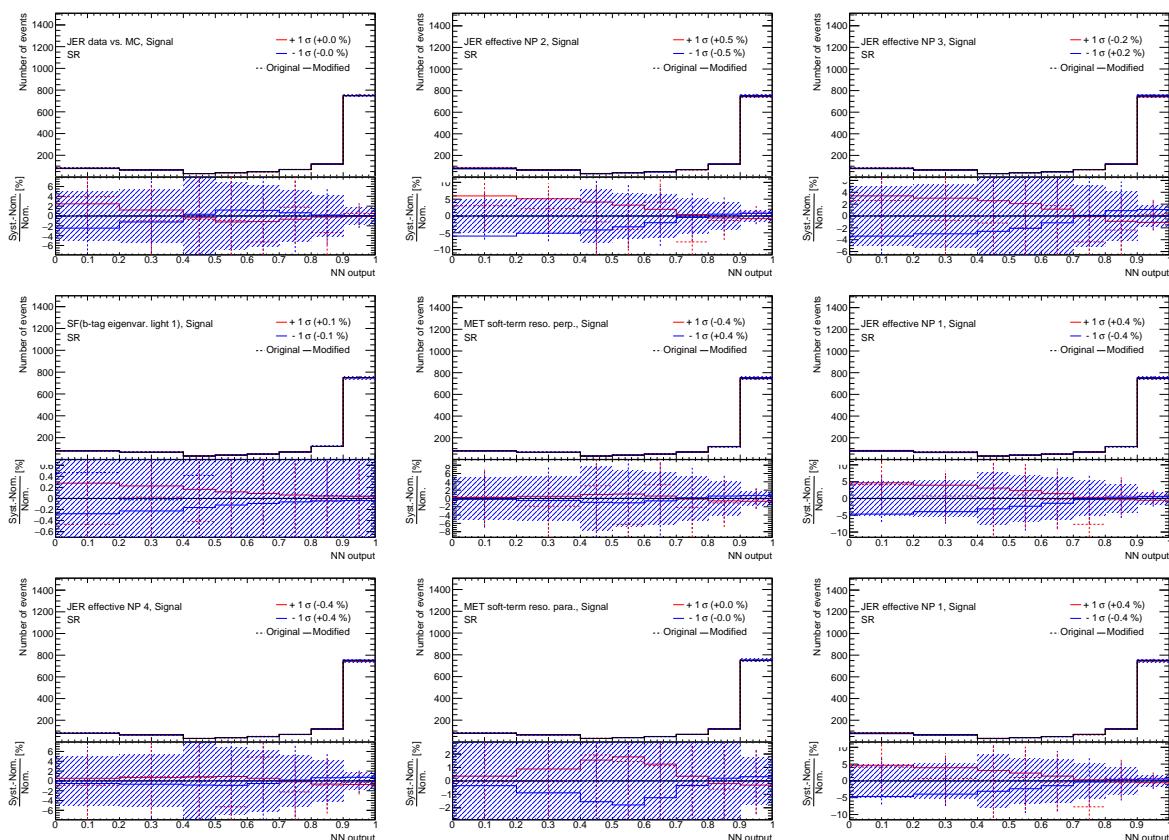


Figure 103: Plots showing the impact of 20 highest ranked systematic uncertainties on *Signal* for the left-handed $t u \gamma$ coupling coupling in the SR (1).

Not reviewed, for internal circulation only

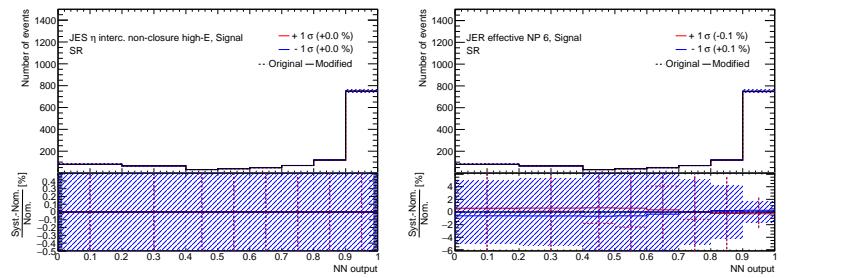


Figure 104: Plots showing the impact of 20 highest ranked systematic uncertainties on *Signal* for the left-handed $t\bar{u}\gamma$ coupling coupling in the SR (2).

1755 **O.1.1.3 $e \rightarrow \gamma$ fakes (SR, left-handed $t\bar{u}\gamma$ coupling)**

Not reviewed, for internal circulation only

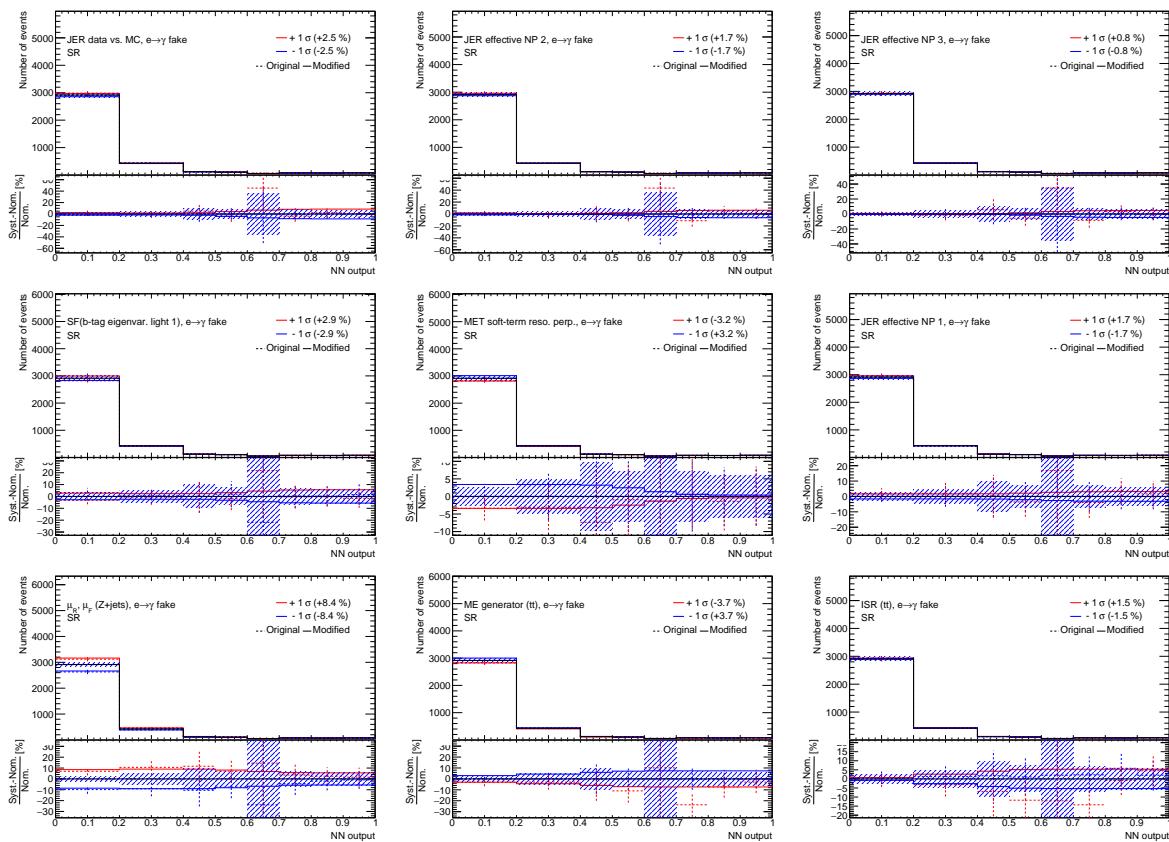


Figure 105: Plots showing the impact of 20 highest ranked systematic uncertainties on $e \rightarrow \gamma$ fakes for the left-handed $t\bar{u}\gamma$ coupling coupling in the SR (1).

Not reviewed, for internal circulation only

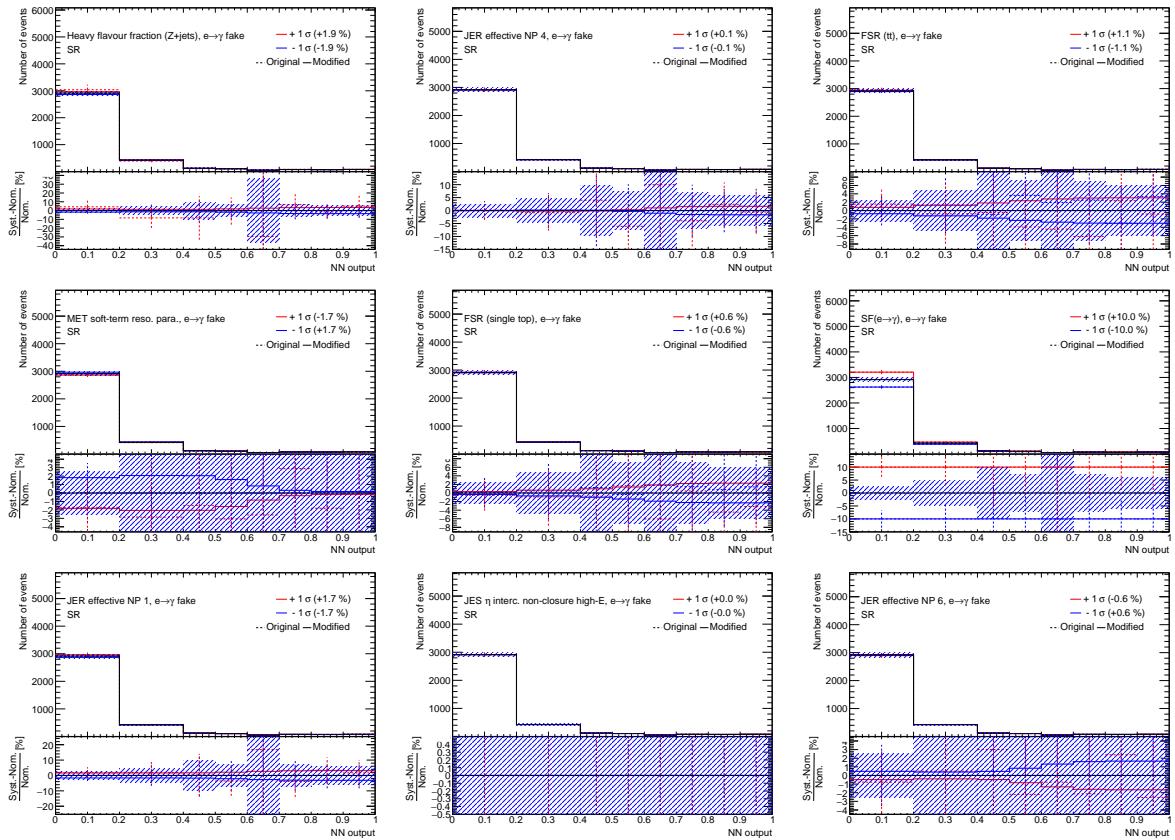


Figure 106: Plots showing the impact of 20 highest ranked systematic uncertainties on $e \rightarrow \gamma$ fakes for the left-handed $t u \gamma$ coupling coupling in the SR (2).

1756 **O.1.1.4 $j \rightarrow \gamma$ fakes (SR, left-handed $t u \gamma$ coupling)**

Not reviewed, for internal circulation only

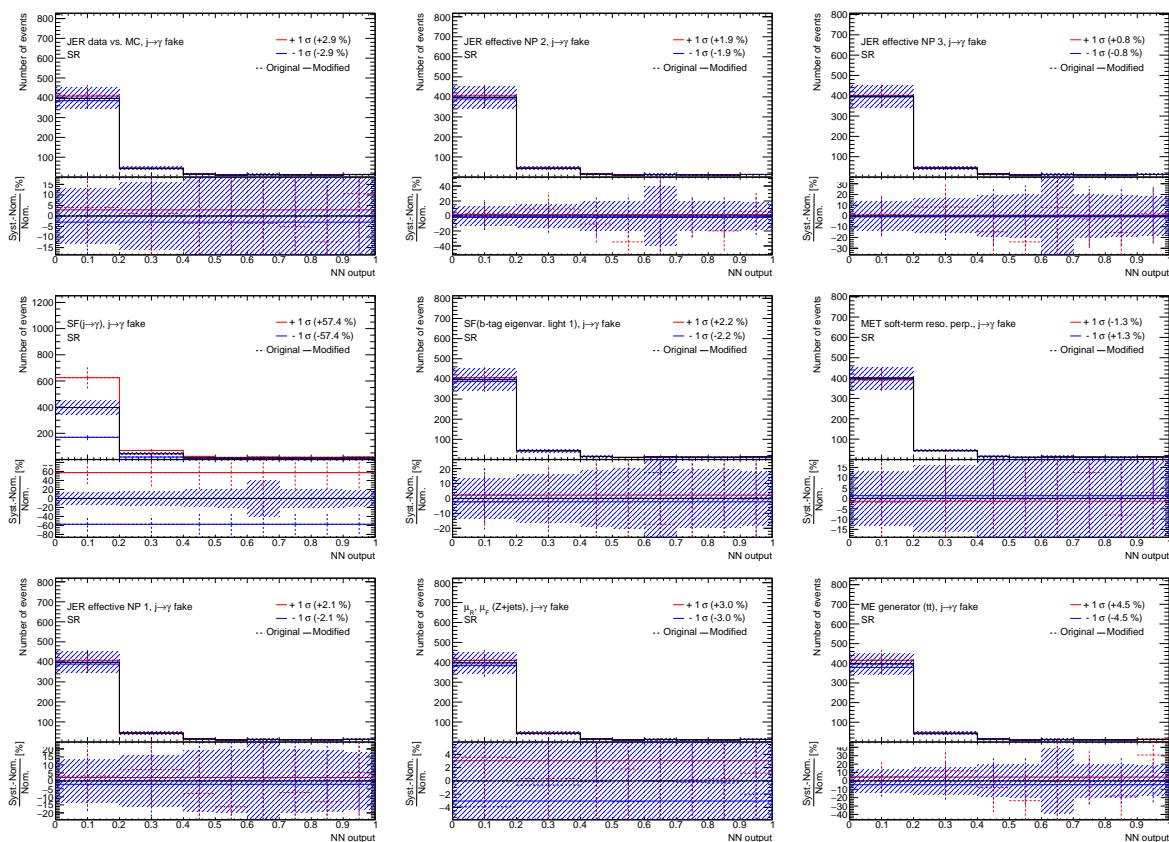


Figure 107: Plots showing the impact of 20 highest ranked systematic uncertainties on $j \rightarrow \gamma$ fakes for the left-handed $t u \gamma$ coupling coupling in the SR (1).

Not reviewed, for internal circulation only

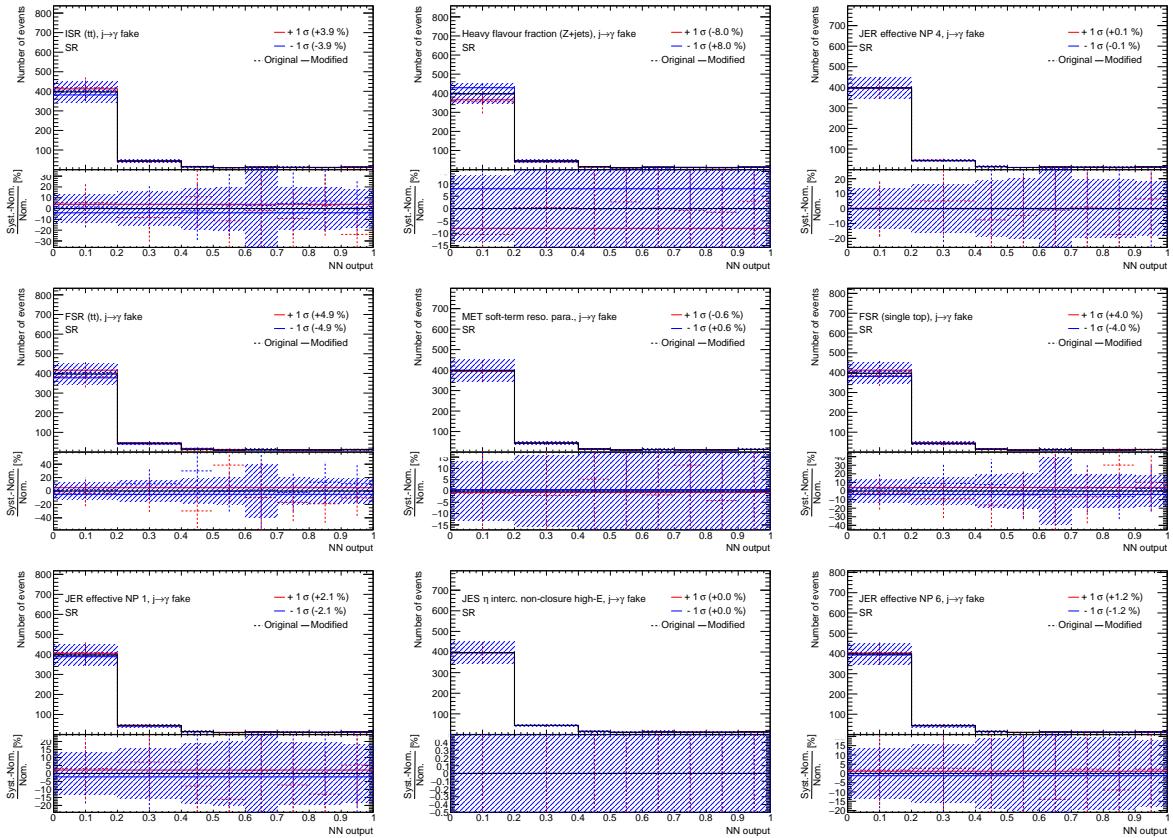


Figure 108: Plots showing the impact of 20 highest ranked systematic uncertainties on $j \rightarrow \gamma$ fakes for the left-handed $t u \gamma$ coupling coupling in the SR (2).

1757 O.1.1.5 $W+\gamma+jets$ (SR, left-handed $t\bar{u}\gamma$ coupling)

Not reviewed, for internal circulation only

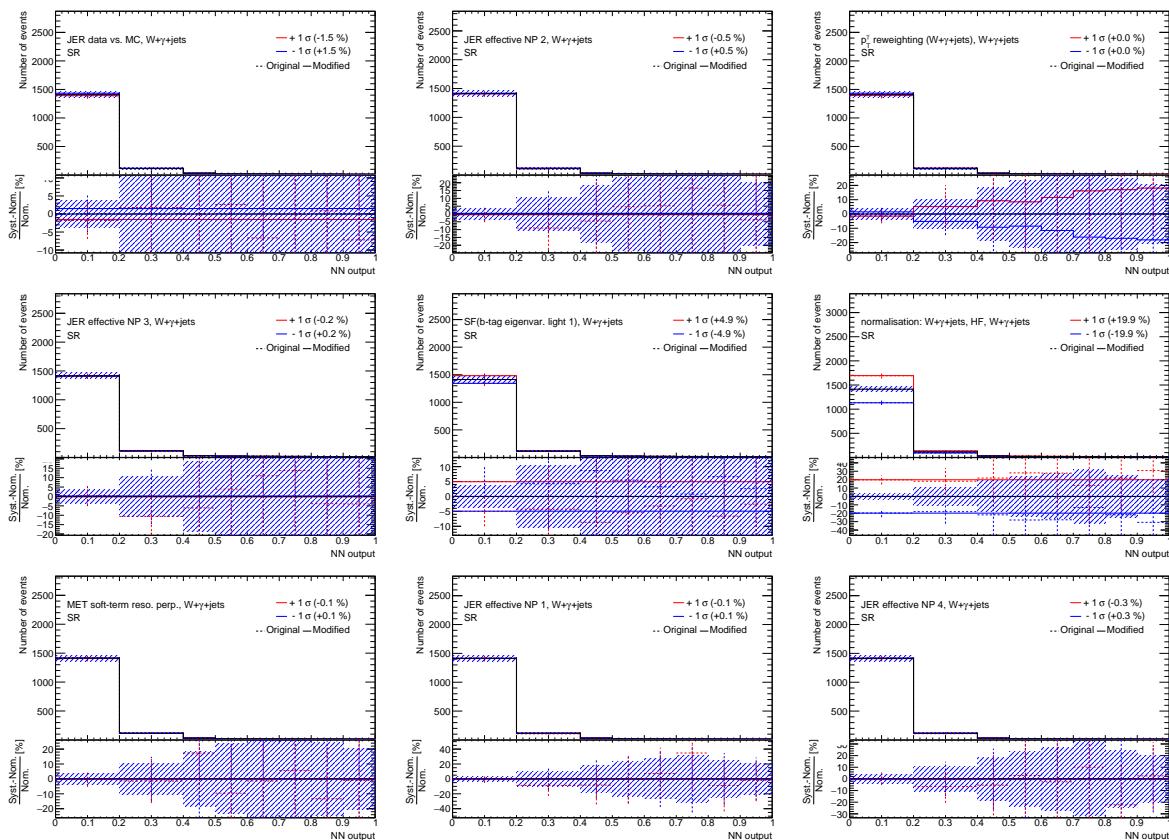


Figure 109: Plots showing the impact of 20 highest ranked systematic uncertainties on $W+\gamma+jets$ for the left-handed $t\bar{u}\gamma$ coupling coupling in the SR (1).

Not reviewed, for internal circulation only

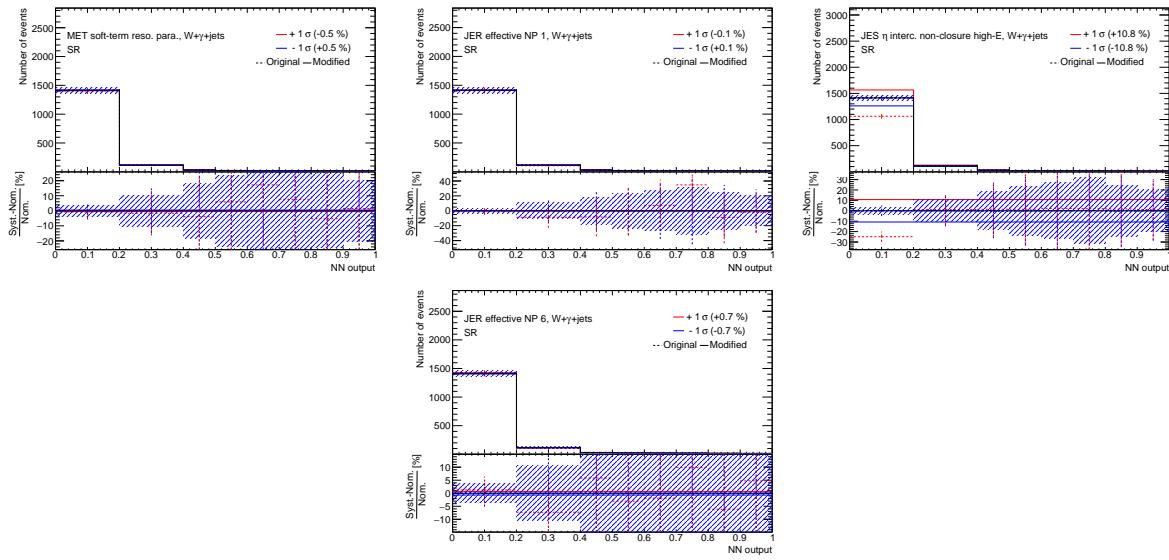


Figure 110: Plots showing the impact of 20 highest ranked systematic uncertainties on $W + \gamma + \text{jets}$ for the left-handed $t u \gamma$ coupling coupling in the SR (2).

1758 **O.1.1.6 $Z+\gamma+jets$ (SR, left-handed $t\bar{u}\gamma$ coupling)**

Not reviewed, for internal circulation only

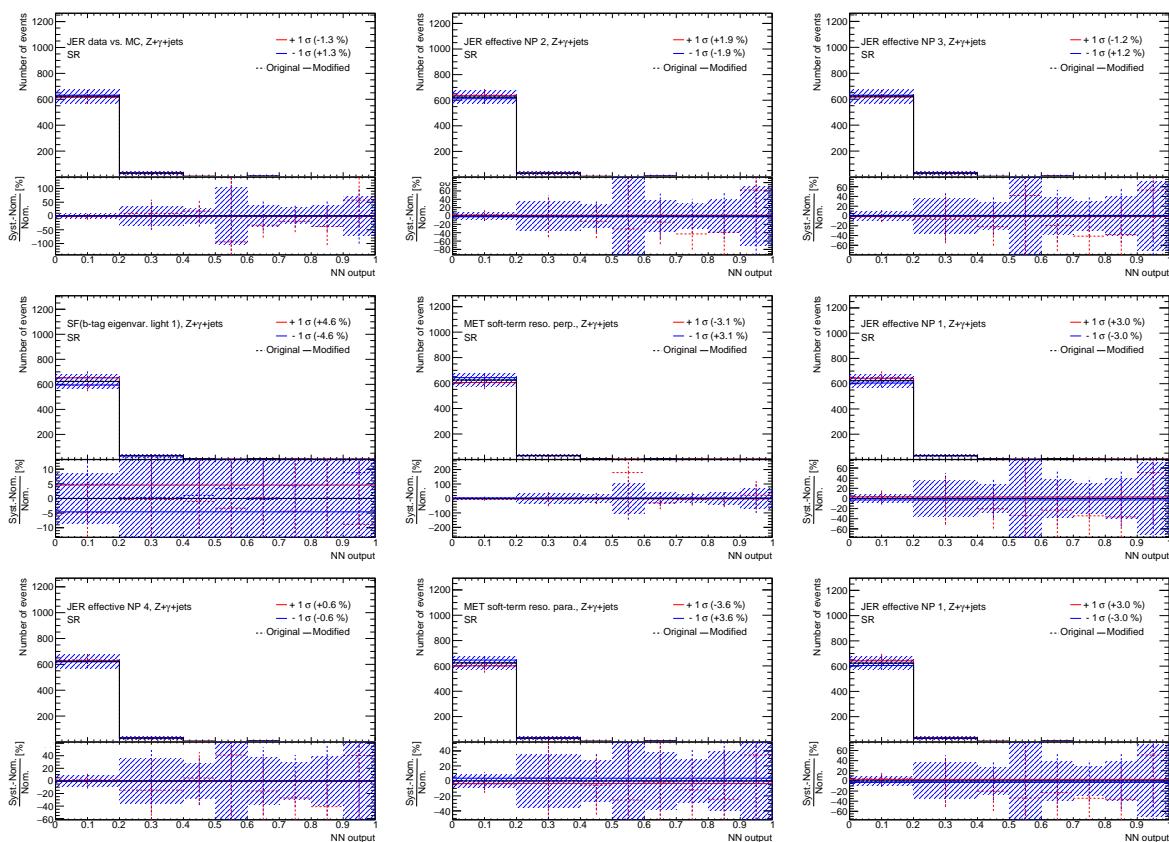


Figure 111: Plots showing the impact of 20 highest ranked systematic uncertainties on $Z+\gamma+jets$ for the left-handed $t\bar{u}\gamma$ coupling coupling in the SR (1).

Not reviewed, for internal circulation only

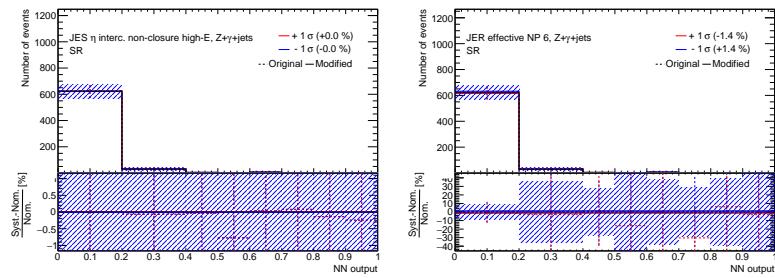


Figure 112: Plots showing the impact of 20 highest ranked systematic uncertainties on $Z + \gamma + \text{jets}$ for the left-handed $t u \gamma$ coupling coupling in the SR (2).

1759 **O.1.1.7 Other prompt photons (SR, left-handed $t u \gamma$ coupling)**

Not reviewed, for internal circulation only

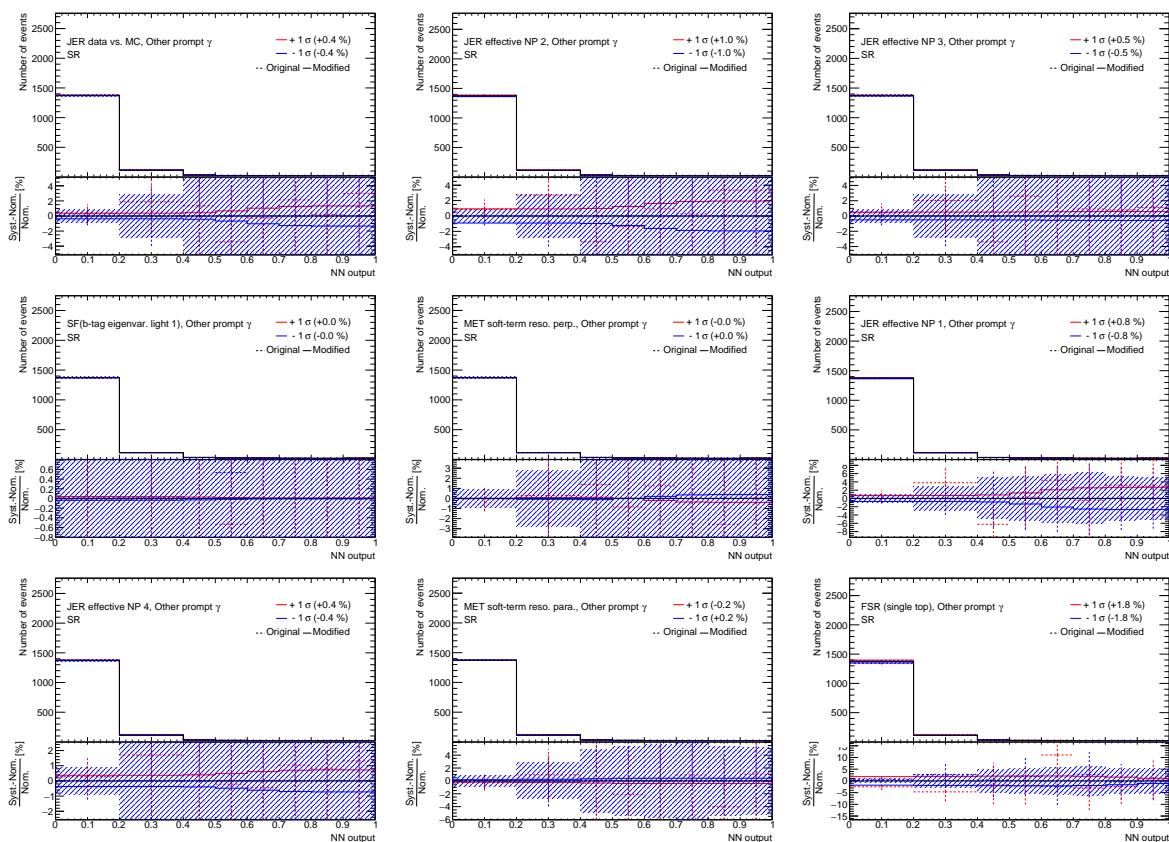


Figure 113: Plots showing the impact of 20 highest ranked systematic uncertainties on *Other prompt photons* for the left-handed $t u \gamma$ coupling coupling in the SR (1).

Not reviewed, for internal circulation only

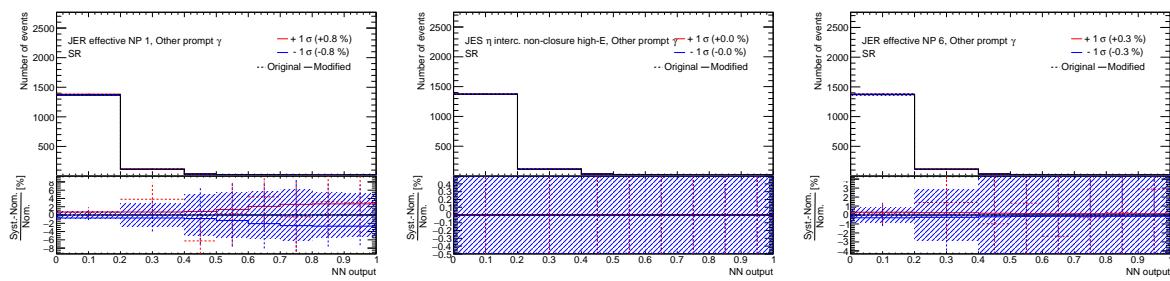


Figure 114: Plots showing the impact of 20 highest ranked systematic uncertainties on *Other prompt photons* for the left-handed *tuy* coupling coupling in the SR (2).

1760 **O.1.2 CR $W+\gamma+$ jets (left-handed $t u \gamma$ coupling)**1761 **O.1.2.1 Total background (CR $W+\gamma+$ jets, left-handed $t u \gamma$ coupling)**

Not reviewed, for internal circulation only

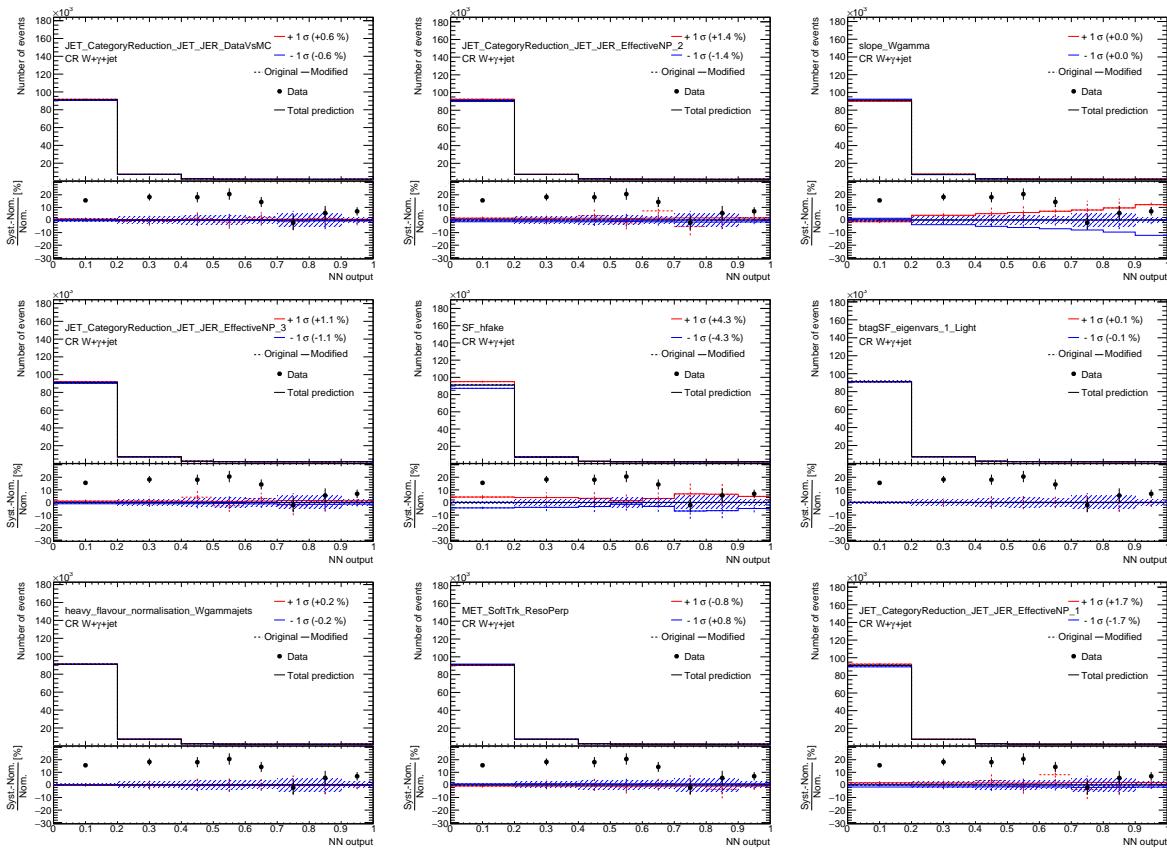


Figure 115: Plots showing the impact of 20 highest ranked systematic uncertainties on *Total background* for the left-handed $t u \gamma$ coupling coupling in the CR $W+\gamma+$ jets (1).

Not reviewed, for internal circulation only

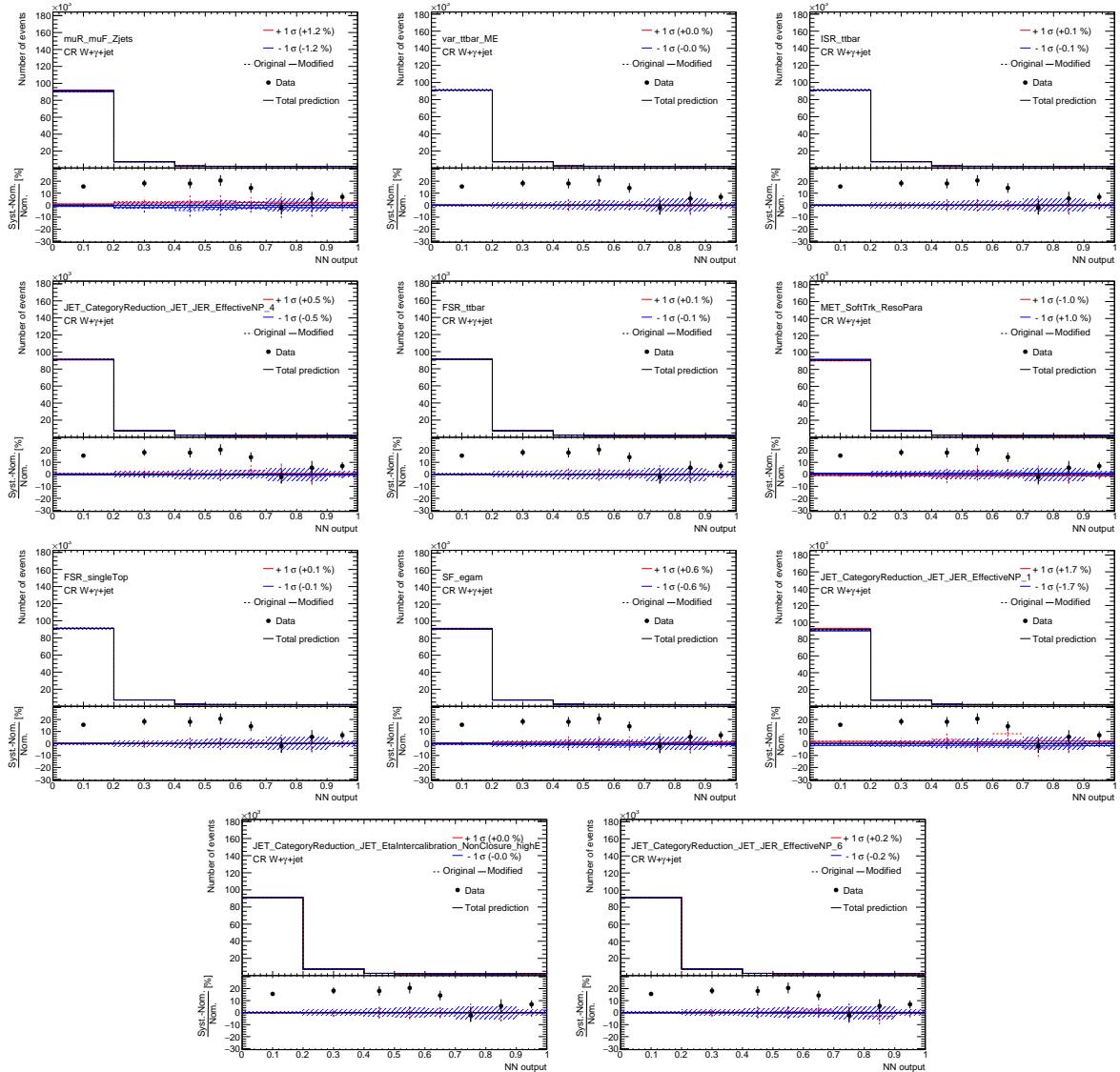


Figure 116: Plots showing the impact of 20 highest ranked systematic uncertainties on *Total background* for the left-handed $t\bar{u}\gamma$ coupling coupling in the CR $W+\gamma+jets$ (2).

1762 O.1.2.2 Signal (CR $W+\gamma+$ jets, left-handed $t\bar{u}\gamma$ coupling)

Not reviewed, for internal circulation only

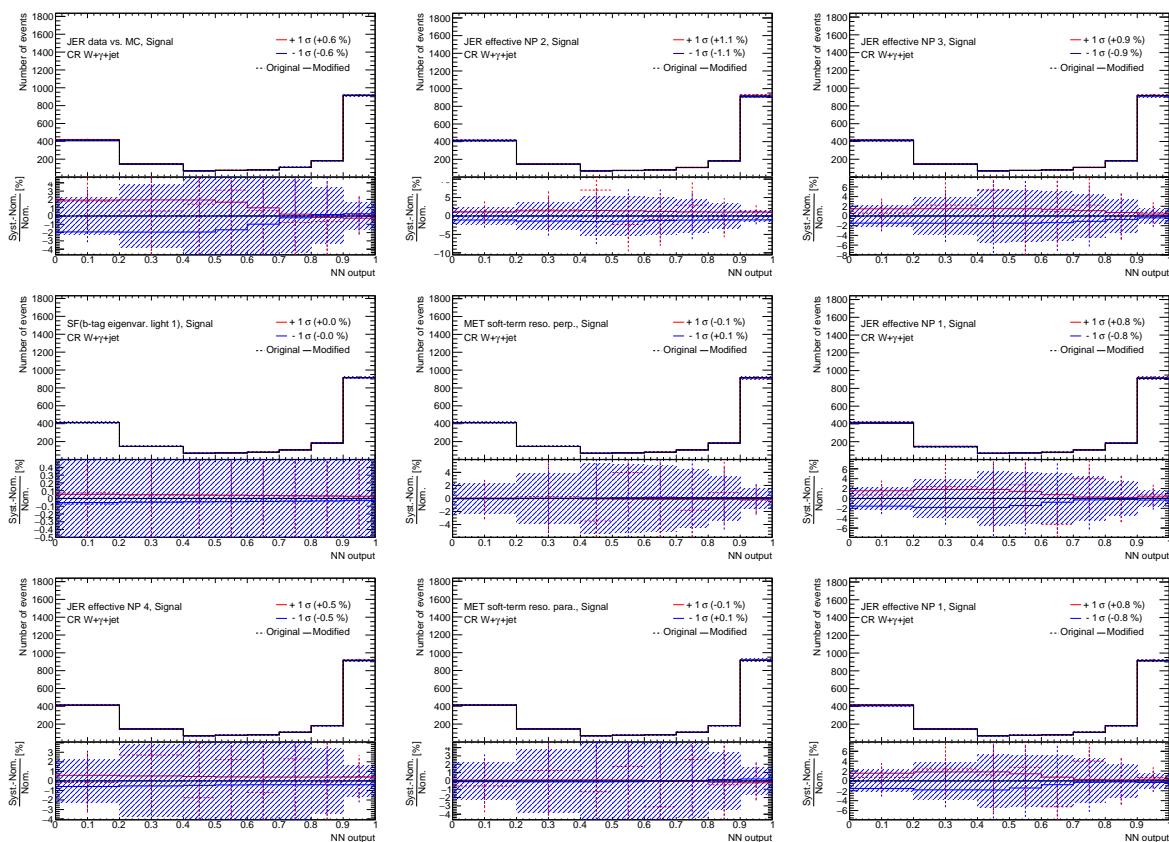


Figure 117: Plots showing the impact of 20 highest ranked systematic uncertainties on *Signal* for the left-handed $t\bar{u}\gamma$ coupling coupling in the CR $W+\gamma+$ jets (1).

Not reviewed, for internal circulation only

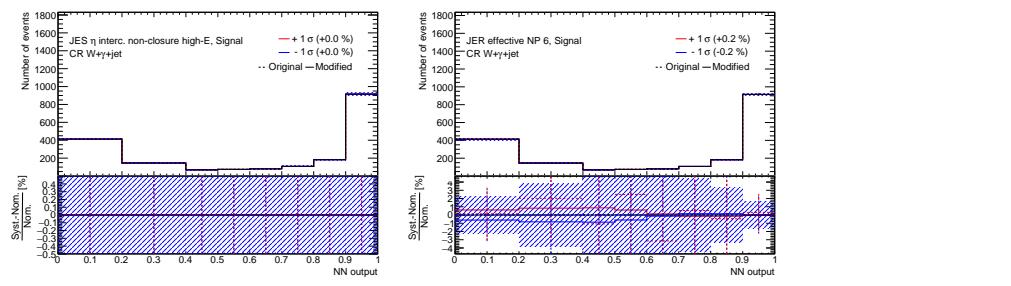


Figure 118: Plots showing the impact of 20 highest ranked systematic uncertainties on *Signal* for the left-handed $t\bar{u}\gamma$ coupling coupling in the CR $W+\gamma+jets$ (2).

1763 **O.1.2.3 $e \rightarrow \gamma$ fakes (CR $W+\gamma+\text{jets}$, left-handed $t\bar{u}\gamma$ coupling)**

Not reviewed, for internal circulation only

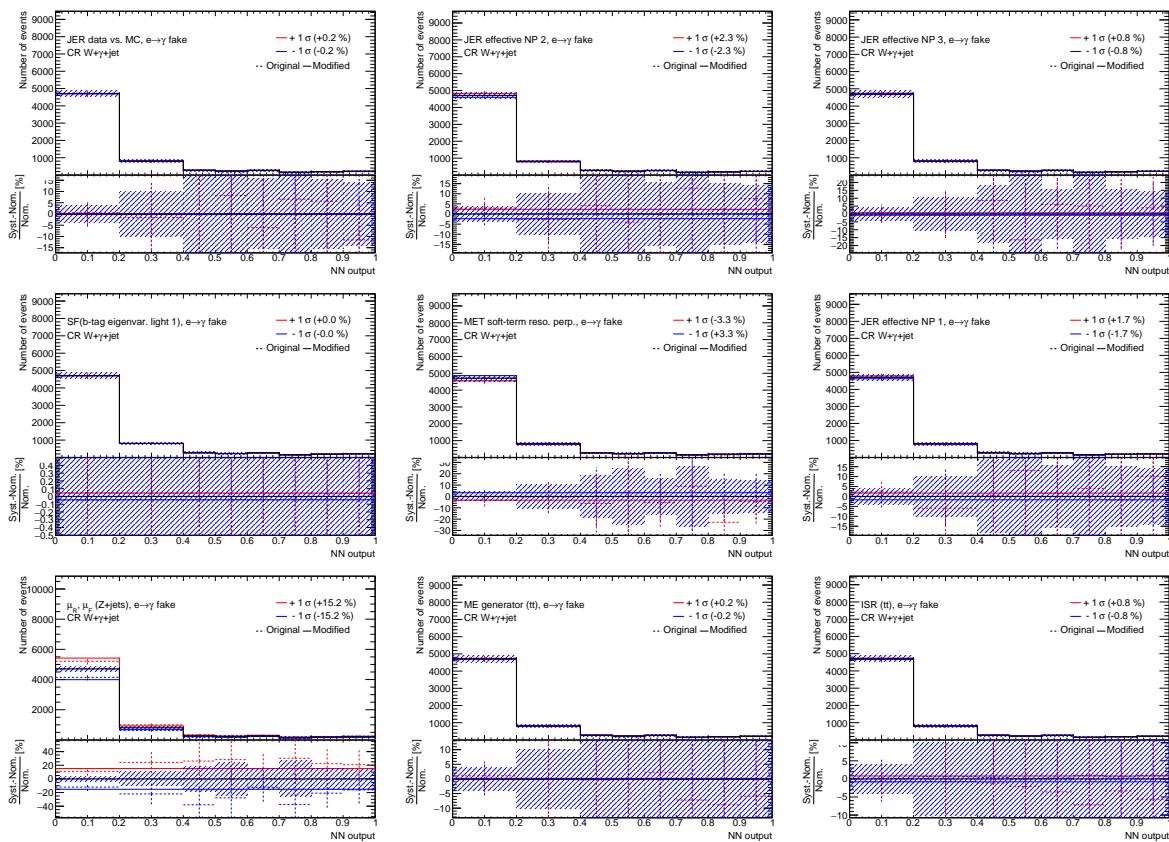


Figure 119: Plots showing the impact of 20 highest ranked systematic uncertainties on $e \rightarrow \gamma$ fakes for the left-handed $t\bar{u}\gamma$ coupling coupling in the CR $W+\gamma+\text{jets}$ (1).

Not reviewed, for internal circulation only

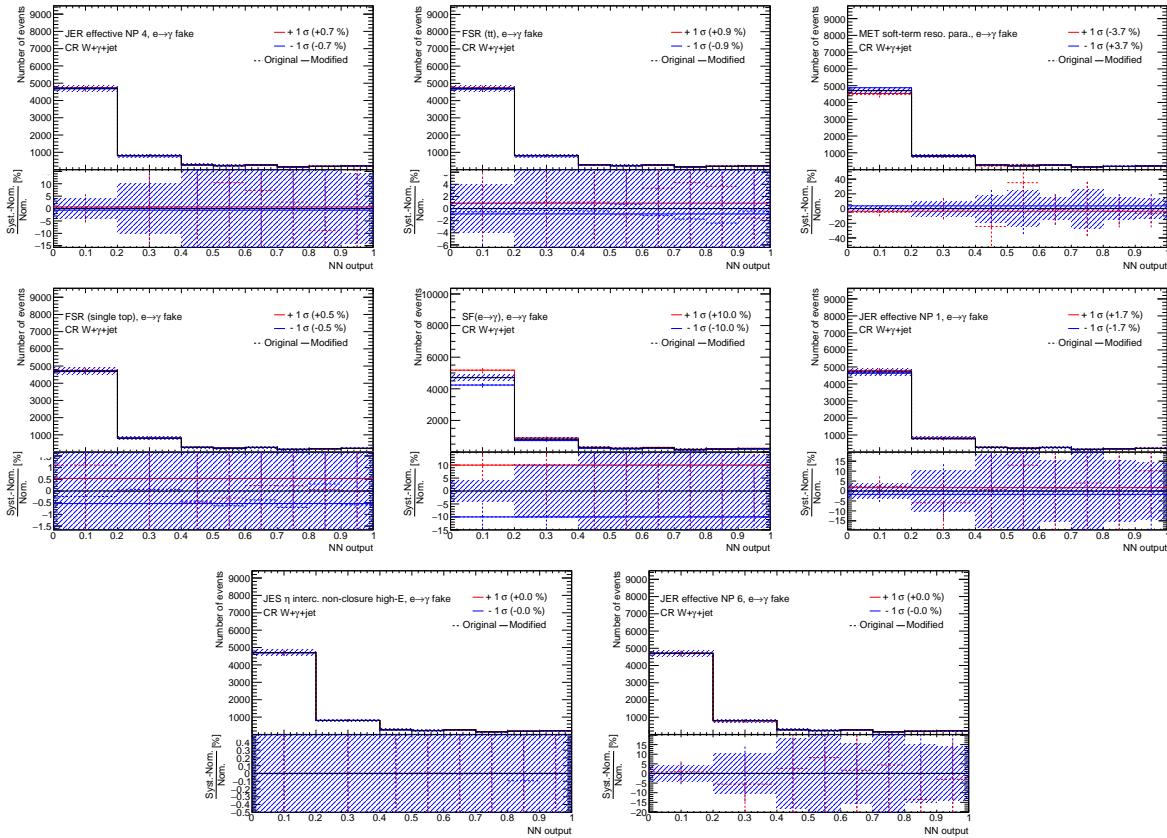


Figure 120: Plots showing the impact of 20 highest ranked systematic uncertainties on $e \rightarrow \gamma$ fakes for the left-handed $t u \gamma$ coupling coupling in the CR $W+\gamma+jets$ (2).

1764 **O.1.2.4 $j \rightarrow \gamma$ fakes (CR $W+\gamma+\text{jets}$, left-handed $t\bar{u}\gamma$ coupling)**

Not reviewed, for internal circulation only

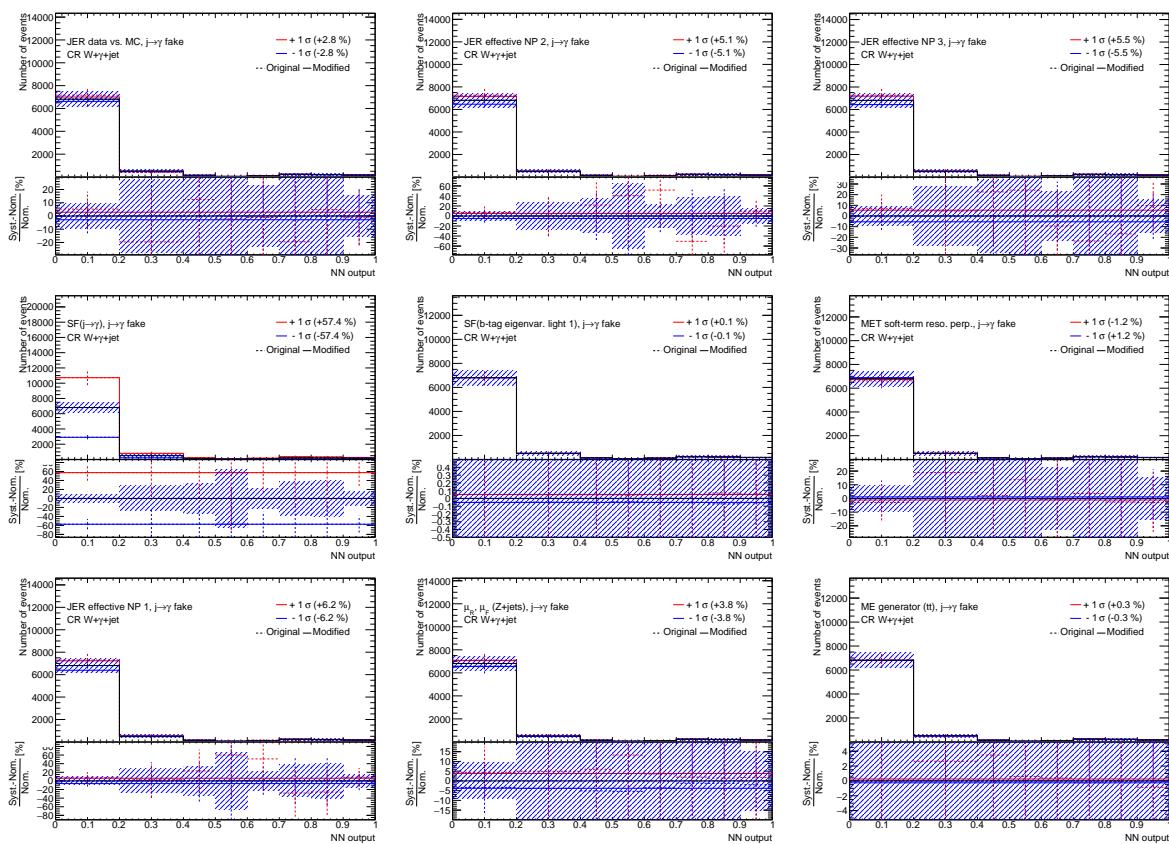


Figure 121: Plots showing the impact of 20 highest ranked systematic uncertainties on $j \rightarrow \gamma$ fakes for the left-handed $t\bar{u}\gamma$ coupling coupling in the CR $W+\gamma+\text{jets}$ (1).

Not reviewed, for internal circulation only

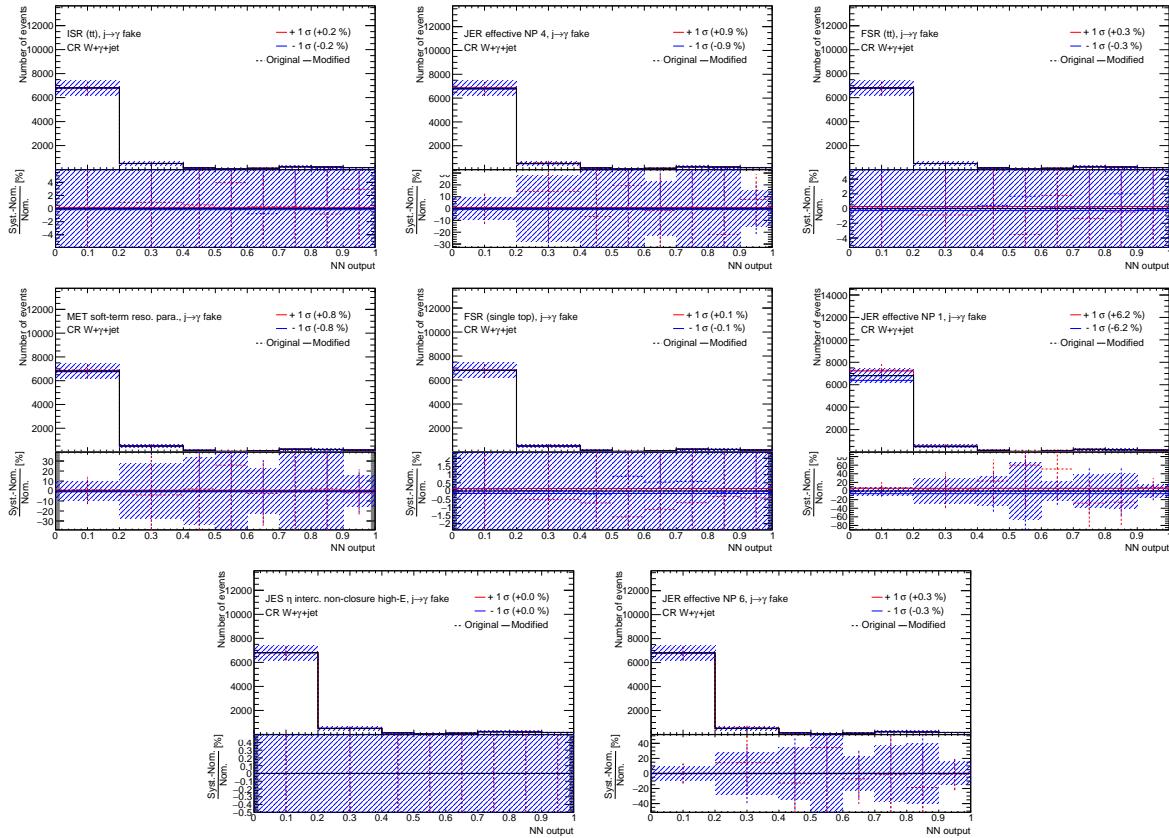


Figure 122: Plots showing the impact of 20 highest ranked systematic uncertainties on $j \rightarrow \gamma$ fakes for the left-handed $tW\gamma$ coupling coupling in the CR $W+\gamma+jets$ (2).

1765 **O.1.2.5 $W+\gamma+jets$ (CR $W+\gamma+jets$, left-handed $t\bar{u}\gamma$ coupling)**

Not reviewed, for internal circulation only

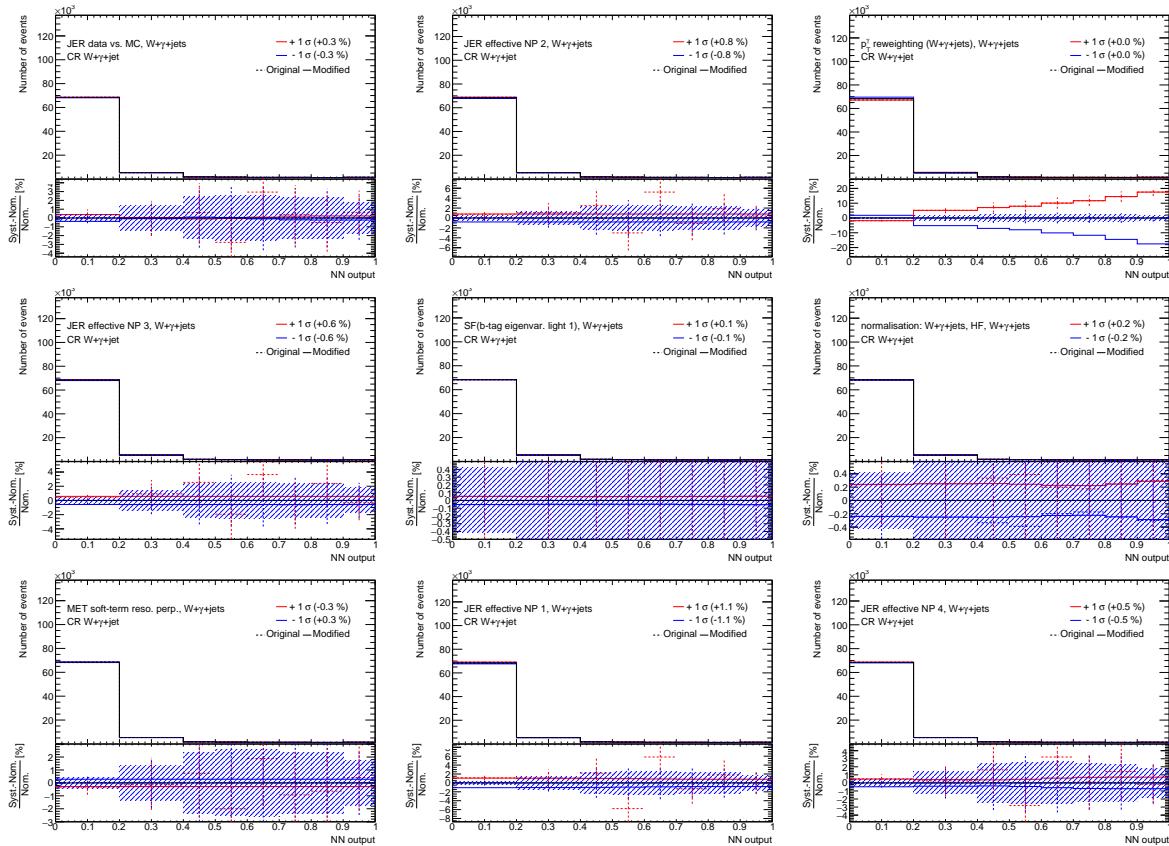


Figure 123: Plots showing the impact of 20 highest ranked systematic uncertainties on $W+\gamma+jets$ for the left-handed $t\bar{u}\gamma$ coupling coupling in the CR $W+\gamma+jets$ (1).

Not reviewed, for internal circulation only

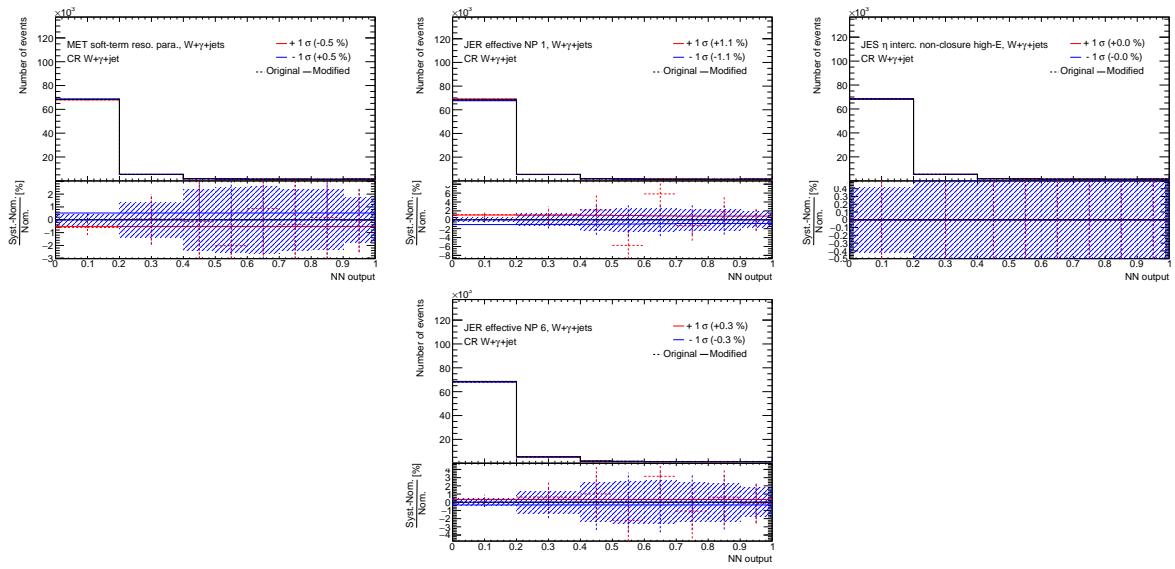


Figure 124: Plots showing the impact of 20 highest ranked systematic uncertainties on $W+\gamma+jets$ for the left-handed $t u \gamma$ coupling coupling in the CR $W+\gamma+jets$ (2).

1766 O.1.2.6 $Z+\gamma+jets$ (CR $W+\gamma+jets$, left-handed $t\bar{u}\gamma$ coupling)

Not reviewed, for internal circulation only

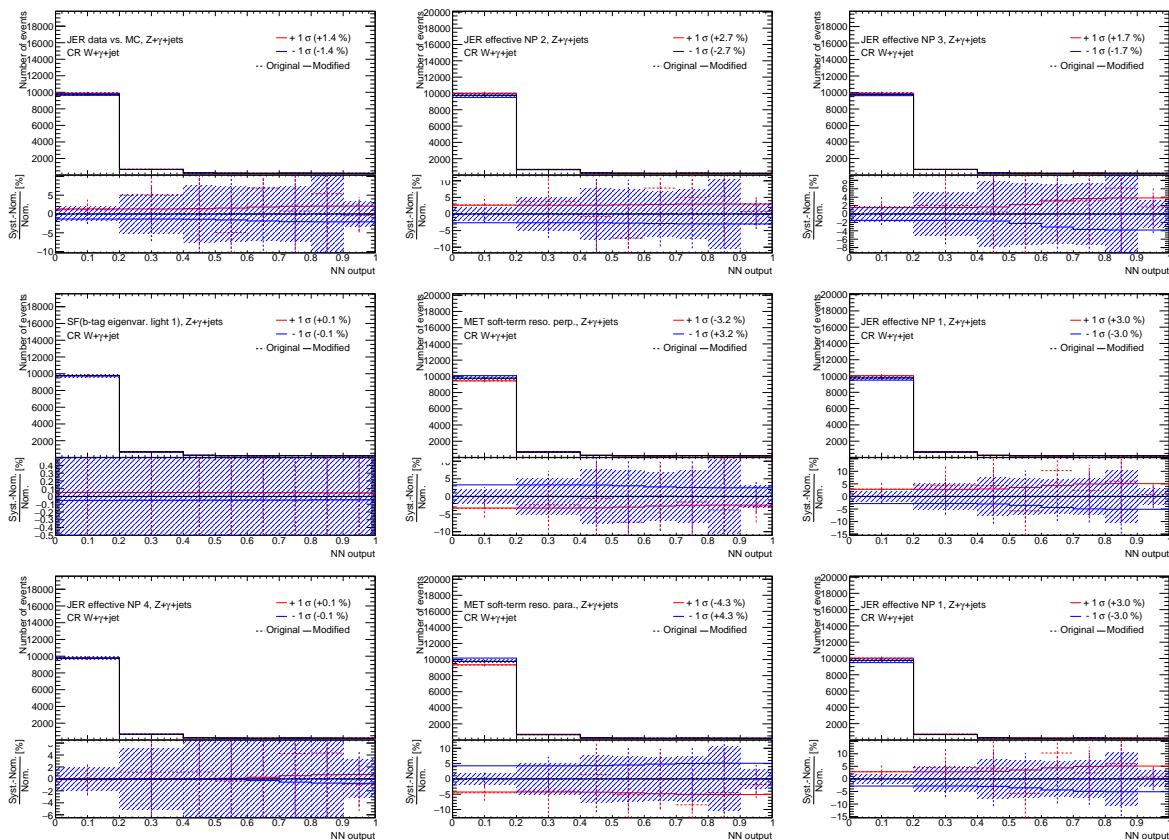


Figure 125: Plots showing the impact of 20 highest ranked systematic uncertainties on $Z+\gamma+jets$ for the left-handed $t\bar{u}\gamma$ coupling coupling in the CR $W+\gamma+jets$ (1).

Not reviewed, for internal circulation only

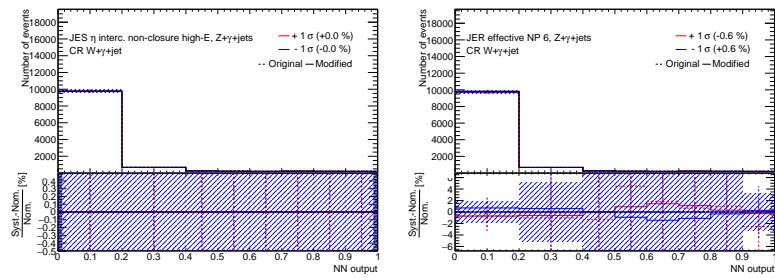


Figure 126: Plots showing the impact of 20 highest ranked systematic uncertainties on $Z+\gamma+jets$ for the left-handed $t u \gamma$ coupling coupling in the CR $W+\gamma+jets$ (2).

1767 **O.1.2.7 Other prompt photons (CR $W+\gamma+jets$, left-handed $t\gamma\gamma$ coupling)**

Not reviewed, for internal circulation only

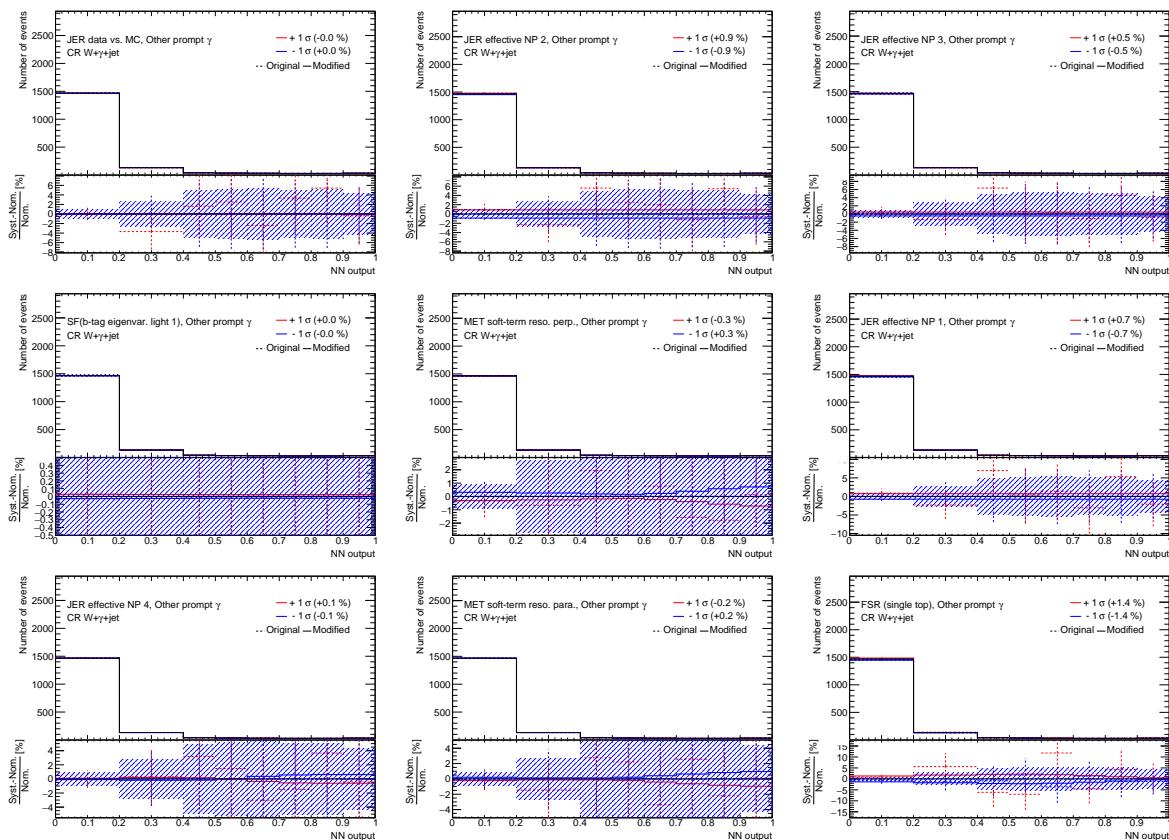


Figure 127: Plots showing the impact of 20 highest ranked systematic uncertainties on *Other prompt photons* for the left-handed tuy coupling coupling in the CR $W+\gamma+jets$ (1).

Not reviewed, for internal circulation only

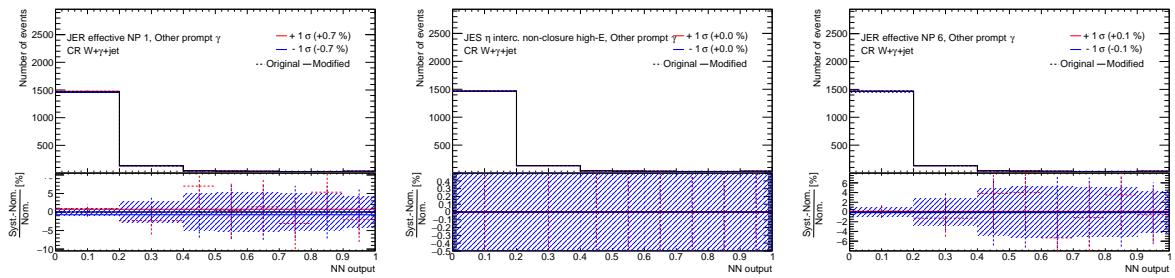


Figure 128: Plots showing the impact of 20 highest ranked systematic uncertainties on *Other prompt photons* for the left-handed *tuy* coupling coupling in the CR $W+\gamma+jets$ (2).

1768 **O.1.3 CR Z+ γ (left-handed $t u \gamma$ coupling)**1769 **O.1.3.1 Total background (CR Z+ γ , left-handed $t u \gamma$ coupling)**

Not reviewed, for internal circulation only

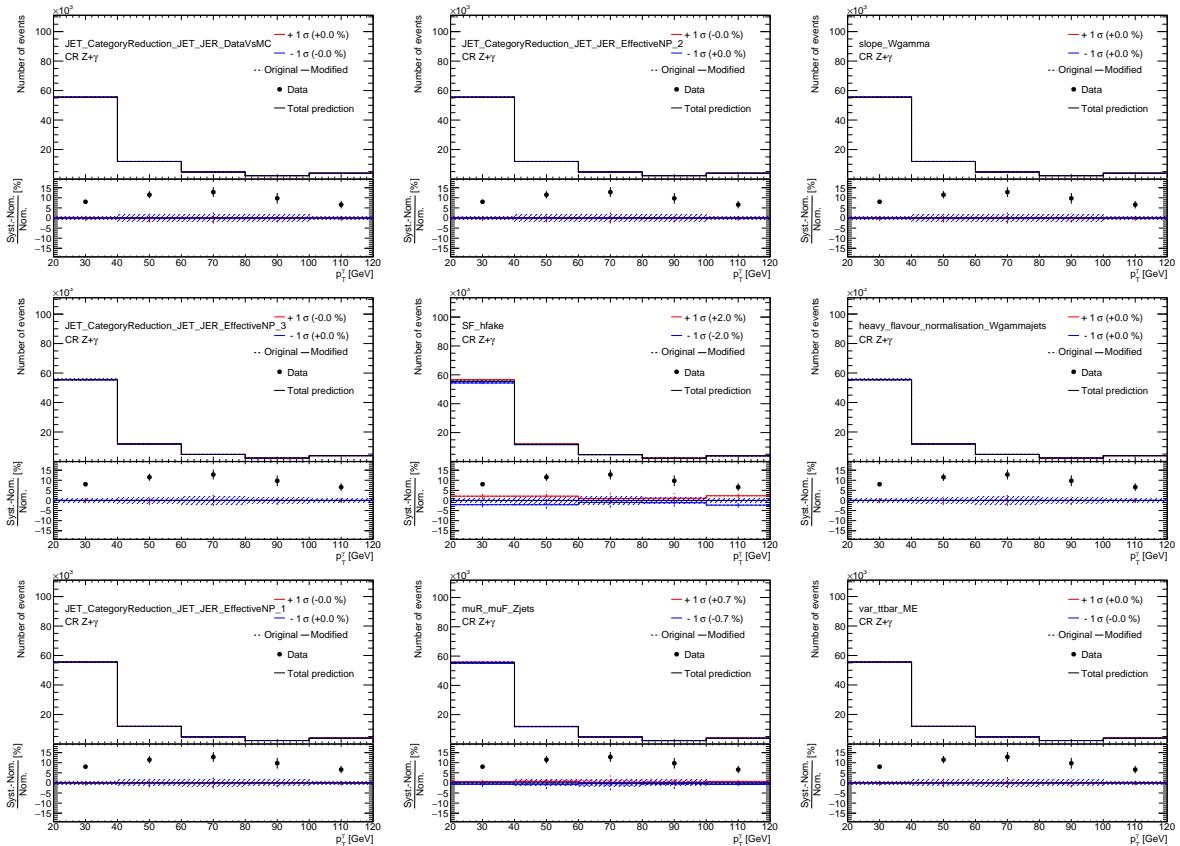


Figure 129: Plots showing the impact of 20 highest ranked systematic uncertainties on *Total background* for the left-handed $t u \gamma$ coupling coupling in the CR $Z+\gamma$ (1).

Not reviewed, for internal circulation only

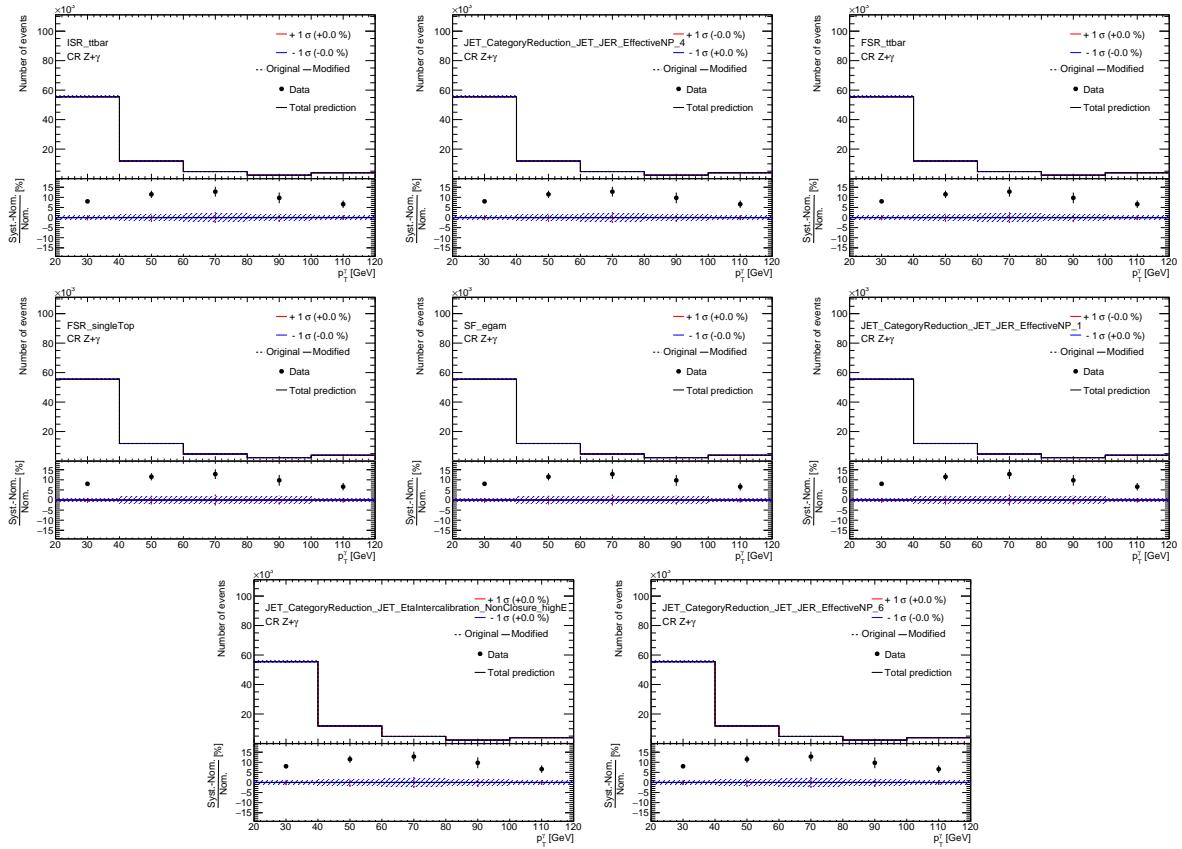


Figure 130: Plots showing the impact of 20 highest ranked systematic uncertainties on *Total background* for the left-handed $t\bar{u}\gamma$ coupling coupling in the CR $Z+\gamma$ (2).

1770 **O.1.3.2 Signal (CR $Z+\gamma$, left-handed $t\gamma\gamma$ coupling)**

Not reviewed, for internal circulation only

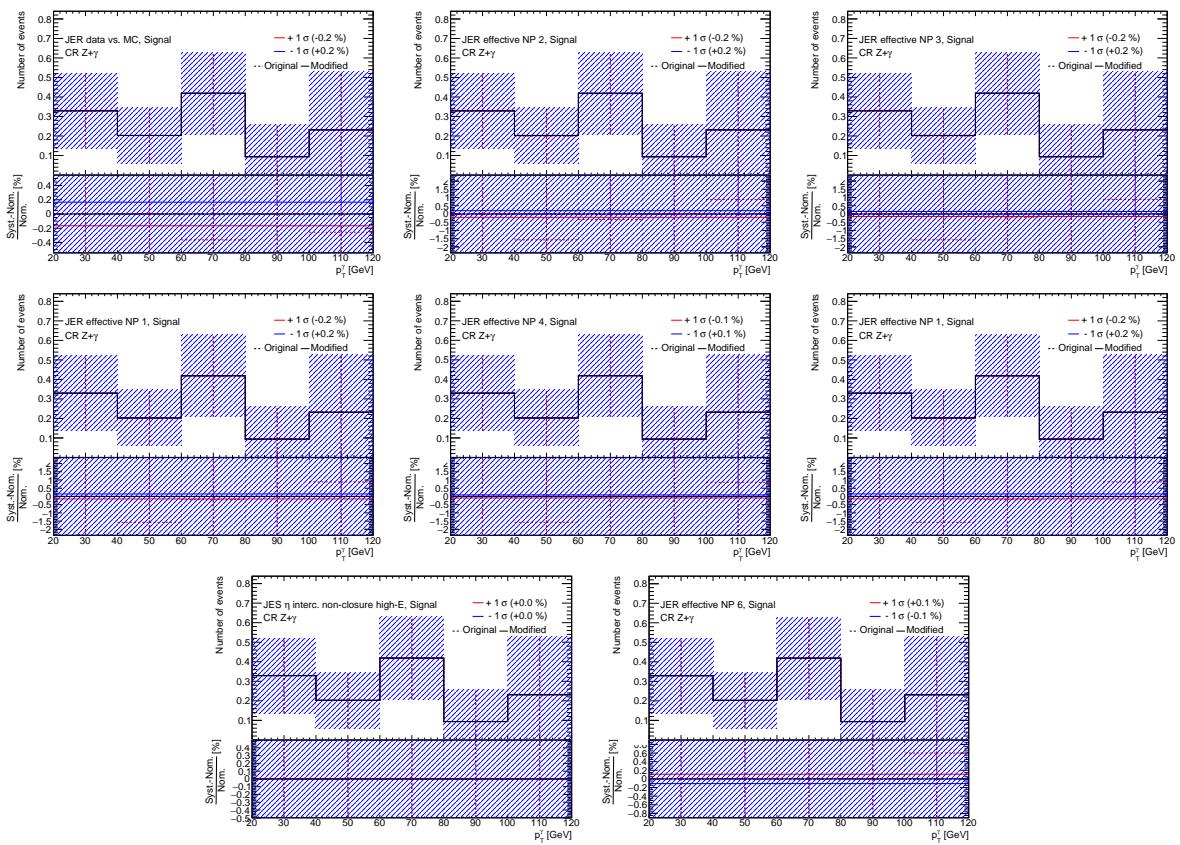


Figure 131: Plots showing the impact of 20 highest ranked systematic uncertainties on *Signal* for the left-handed $t\gamma\gamma$ coupling coupling in the CR $Z+\gamma$ (1).

1771 **O.1.3.3 $e \rightarrow \gamma$ fakes (CR Z+ γ , left-handed $t u \gamma$ coupling)**

Not reviewed, for internal circulation only

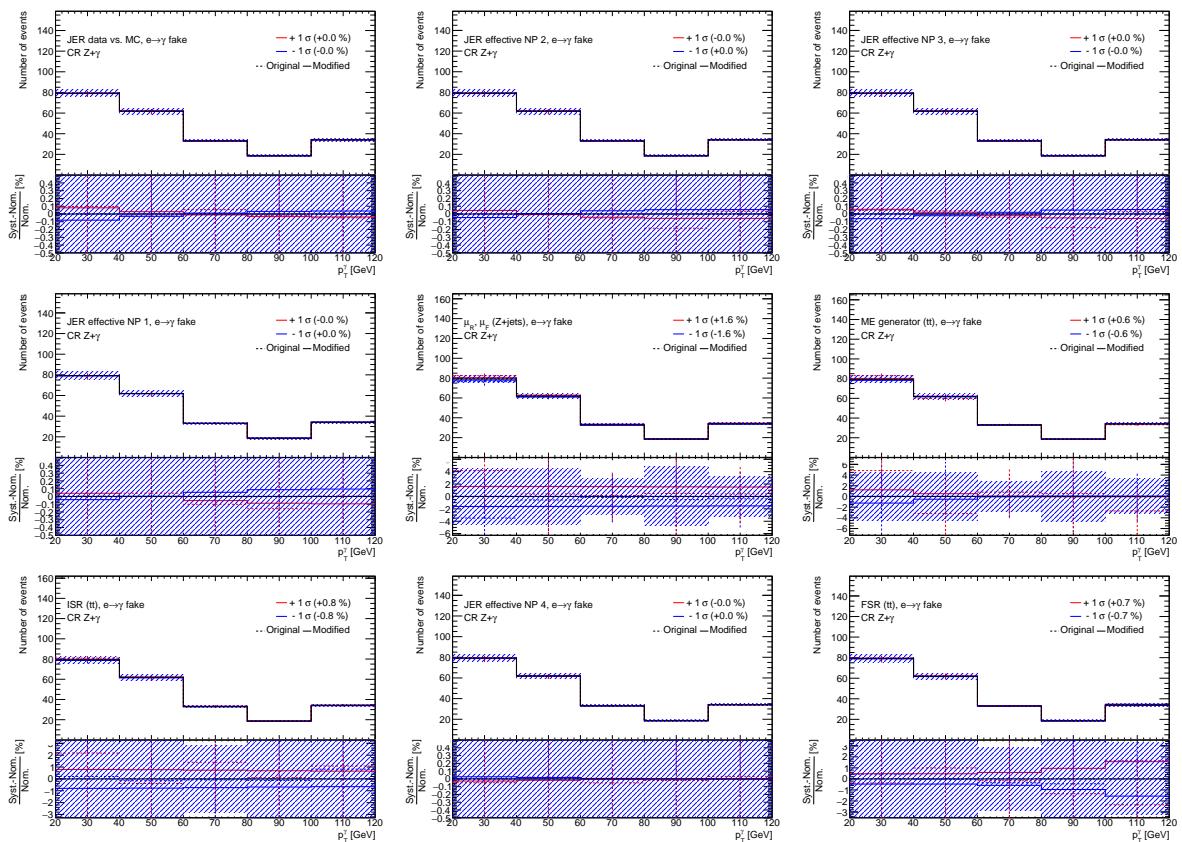


Figure 132: Plots showing the impact of 20 highest ranked systematic uncertainties on $e \rightarrow \gamma$ fakes for the left-handed $t u \gamma$ coupling coupling in the CR Z+ γ (1).

Not reviewed, for internal circulation only

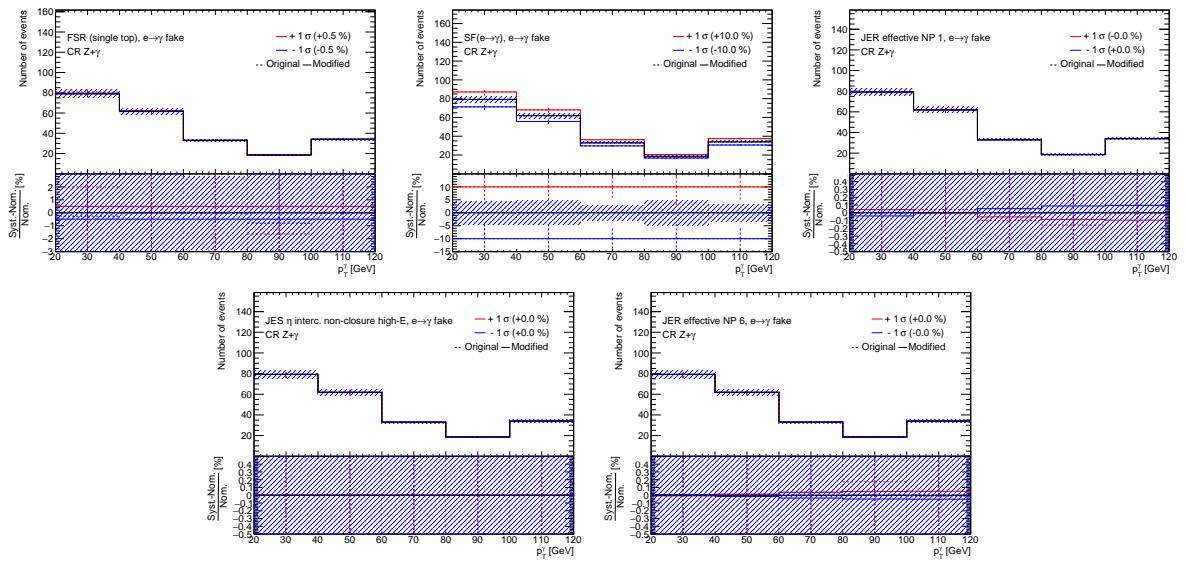


Figure 133: Plots showing the impact of 20 highest ranked systematic uncertainties on $e \rightarrow \gamma$ fakes for the left-handed $t u \gamma$ coupling coupling in the CR $Z + \gamma$ (2).

1772 **O.1.3.4 $j \rightarrow \gamma$ fakes (CR Z+ γ , left-handed $t u \gamma$ coupling)**

Not reviewed, for internal circulation only

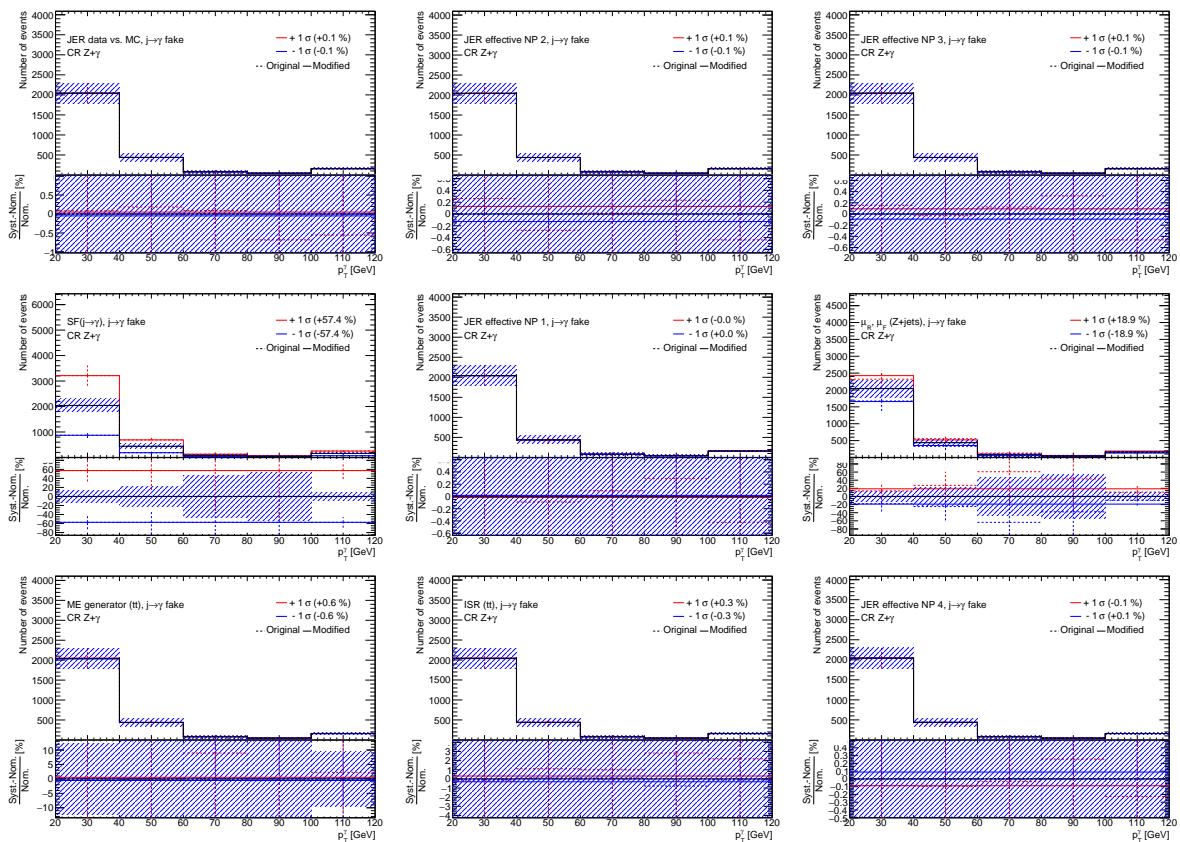


Figure 134: Plots showing the impact of 20 highest ranked systematic uncertainties on $j \rightarrow \gamma$ fakes for the left-handed $t u \gamma$ coupling coupling in the CR Z+ γ (1).

Not reviewed, for internal circulation only

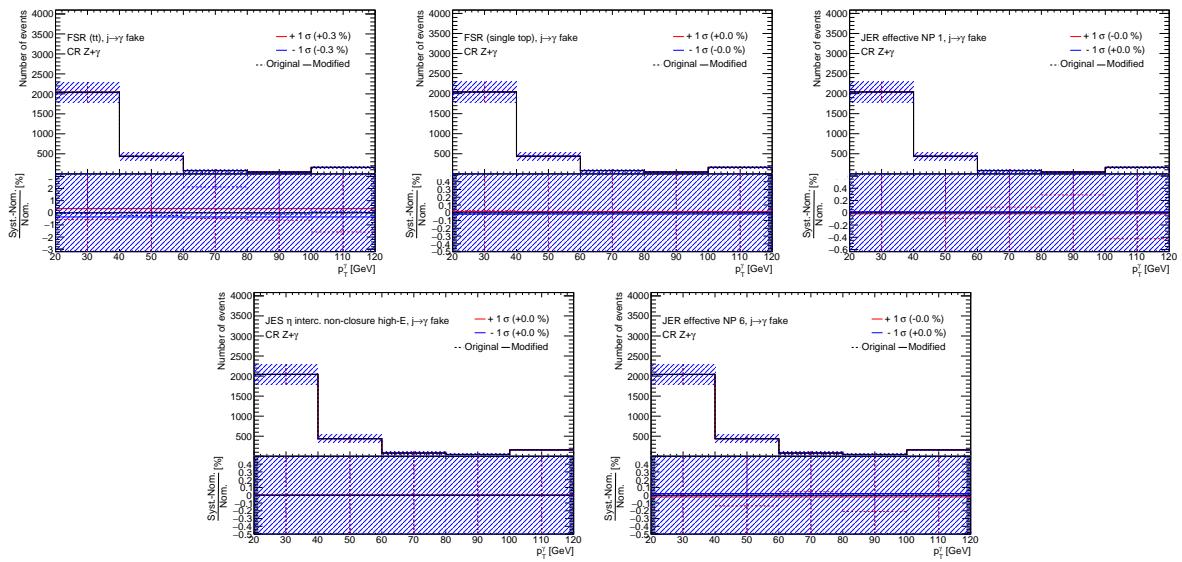


Figure 135: Plots showing the impact of 20 highest ranked systematic uncertainties on $j \rightarrow \gamma$ fakes for the left-handed $t\gamma$ coupling coupling in the CR $Z+\gamma$ (2).

1773 **O.1.3.5 $W+\gamma+jets$ (CR $Z+\gamma$, left-handed $t\bar{u}\gamma$ coupling)**

Not reviewed, for internal circulation only

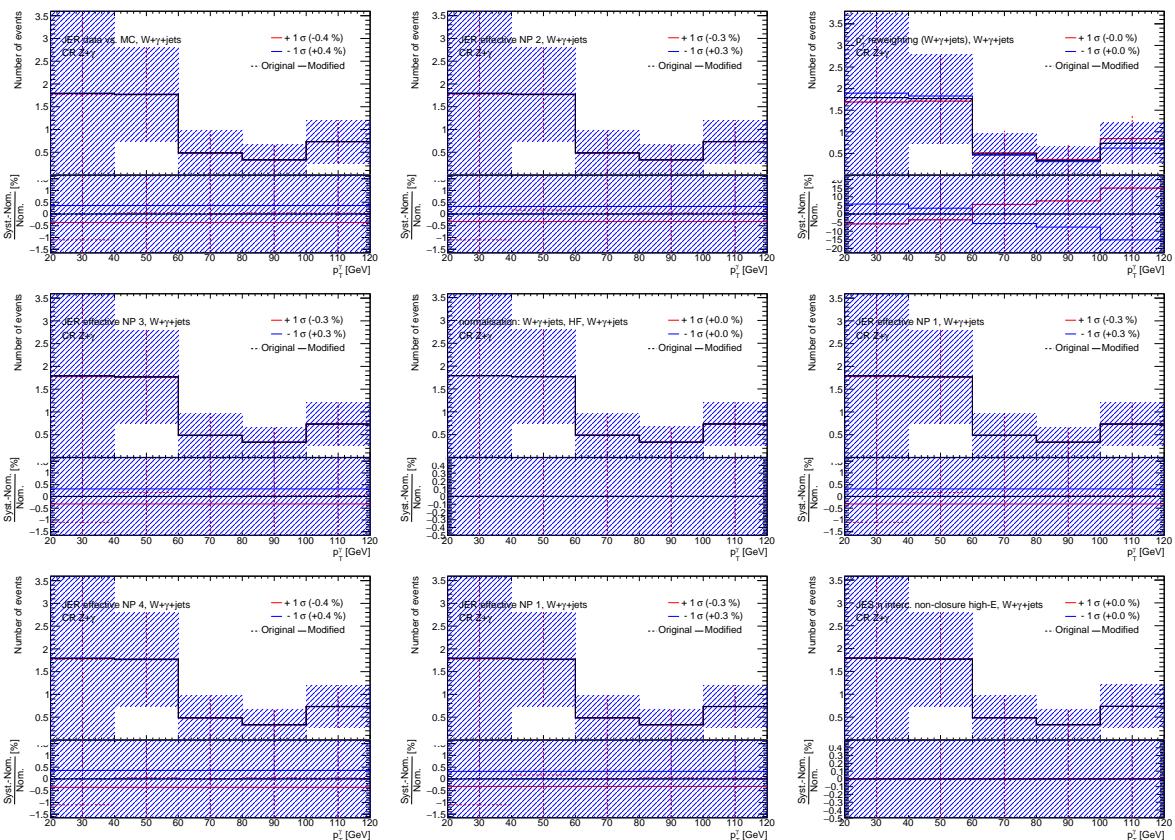


Figure 136: Plots showing the impact of 20 highest ranked systematic uncertainties on $W+\gamma+jets$ for the left-handed $t\bar{u}\gamma$ coupling coupling in the CR $Z+\gamma$ (1).

Not reviewed, for internal circulation only

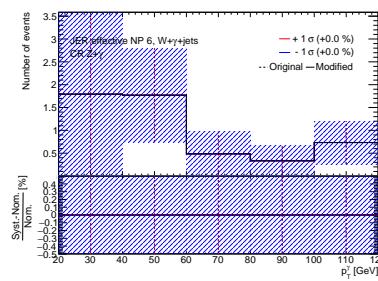


Figure 137: Plots showing the impact of 20 highest ranked systematic uncertainties on $W+\gamma+jets$ for the left-handed $t u \gamma$ coupling coupling in the CR $Z+\gamma$ (2).

1774 **O.1.3.6 $Z+\gamma+jets$ (CR $Z+\gamma$, left-handed $t u \gamma$ coupling)**

Not reviewed, for internal circulation only

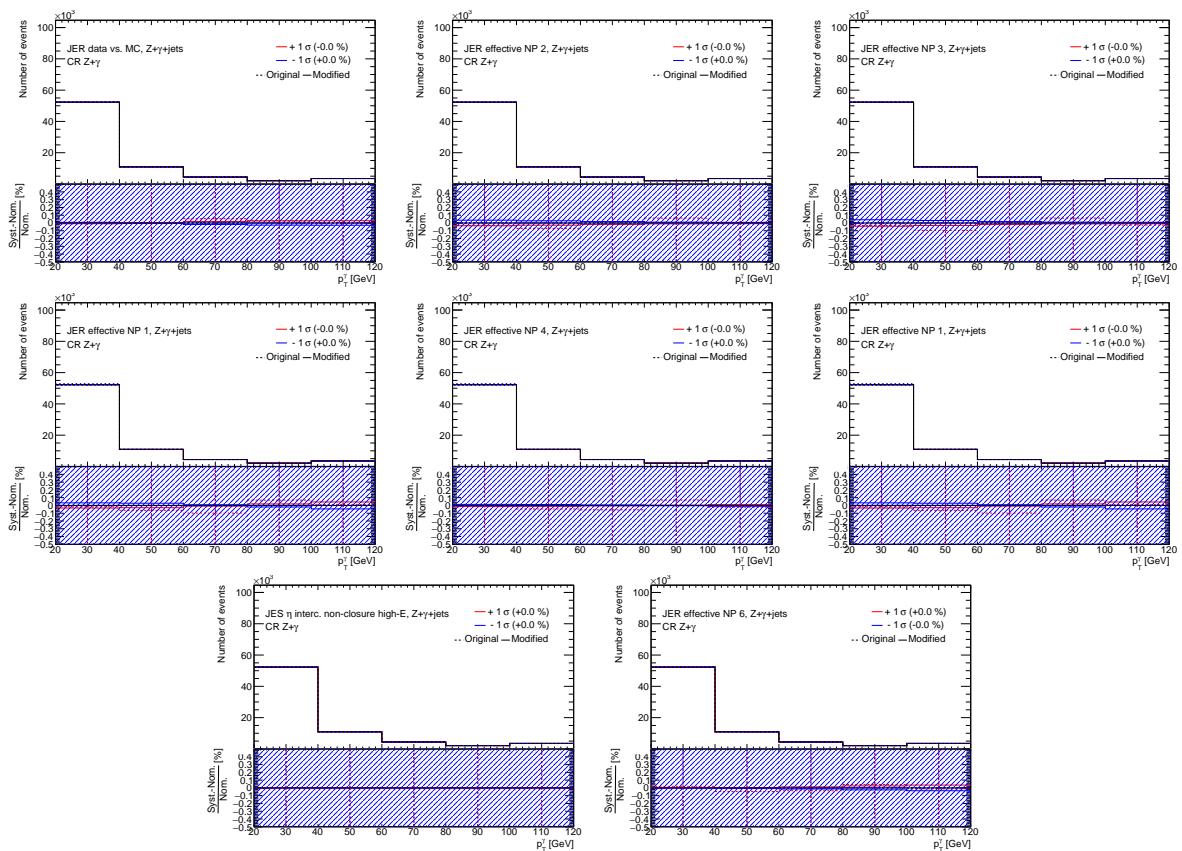


Figure 138: Plots showing the impact of 20 highest ranked systematic uncertainties on $Z+\gamma+jets$ for the left-handed $t u \gamma$ coupling coupling in the CR $Z+\gamma$ (1).

1775 **O.1.3.7 Other prompt photons (CR Z+ γ , left-handed $t u \gamma$ coupling)**

Not reviewed, for internal circulation only

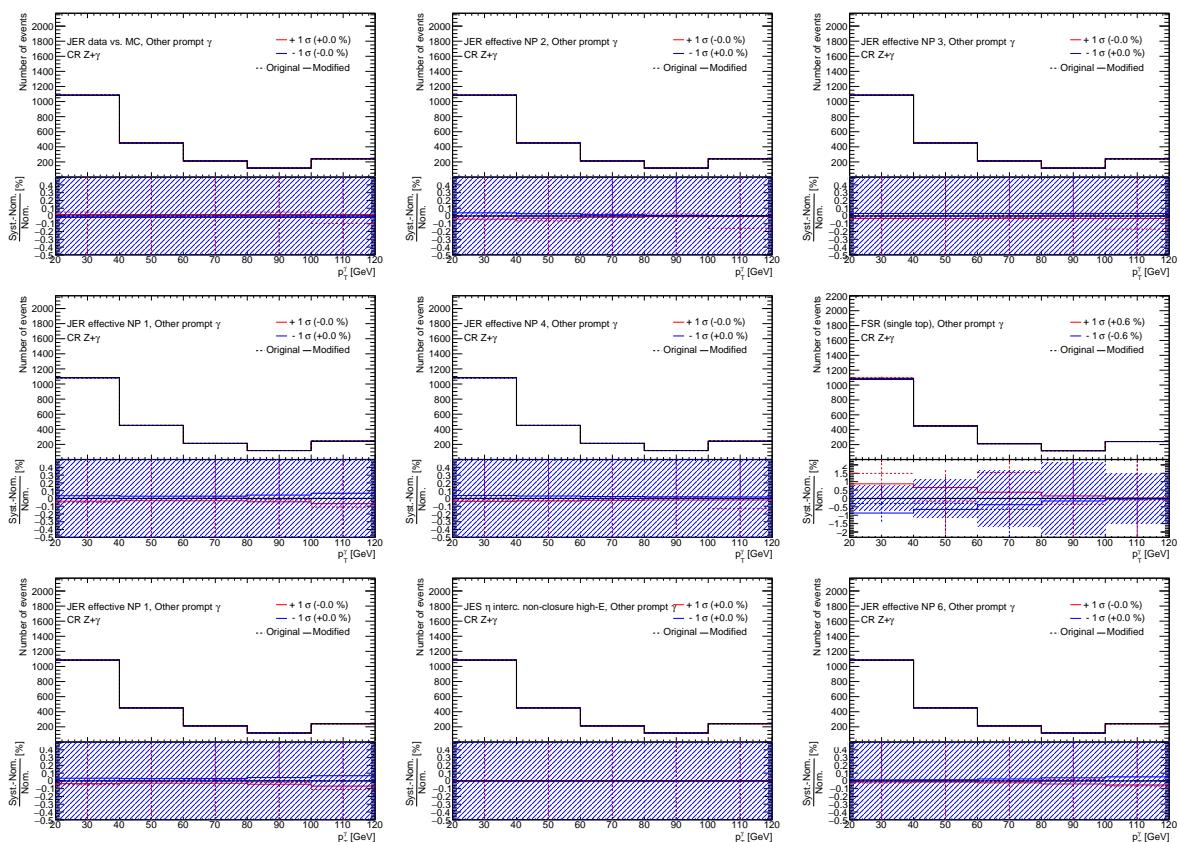


Figure 139: Plots showing the impact of 20 highest ranked systematic uncertainties on *Other prompt photons* for the left-handed $t u \gamma$ coupling coupling in the CR Z+ γ (1).

1776 **O.2 Plots for the right-handed $t u \gamma$ coupling**

1777 **O.2.1 SR (right-handed $t u \gamma$ coupling)**

1778 **O.2.1.1 Total background (SR, right-handed $t u \gamma$ coupling)**

Not reviewed, for internal circulation only

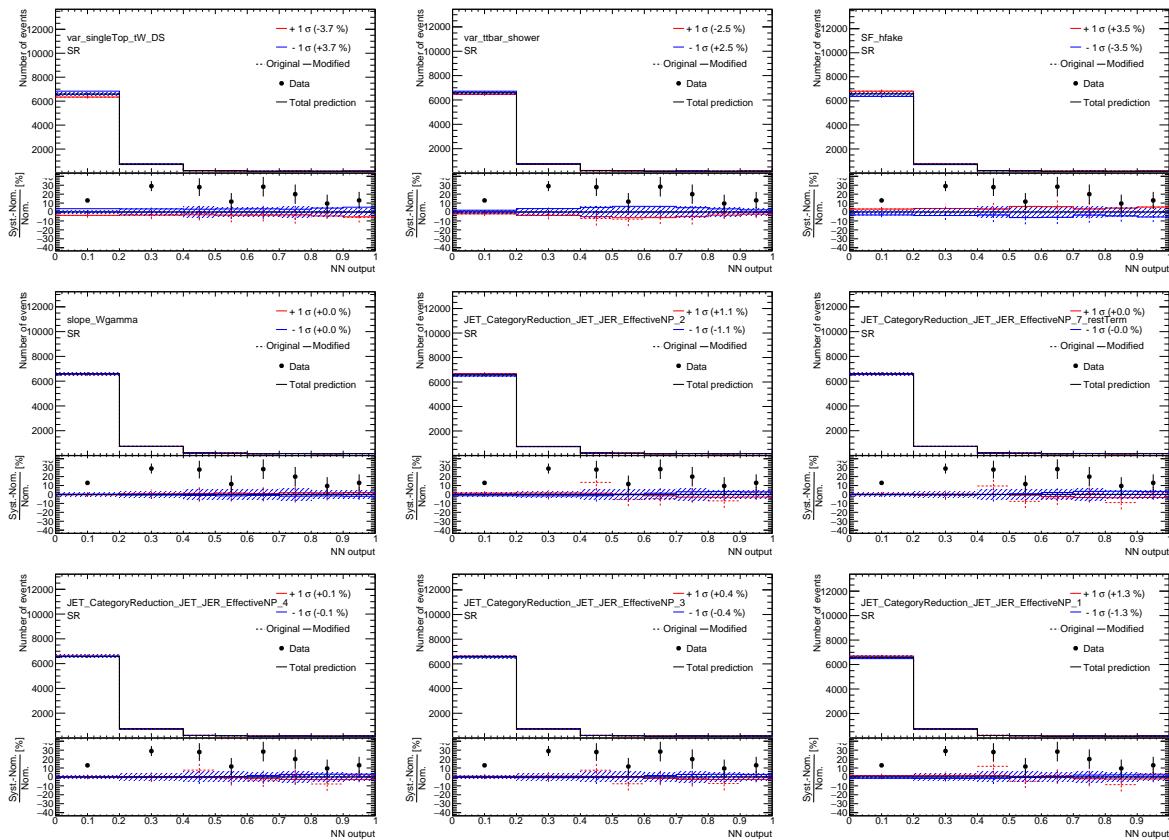


Figure 140: Plots showing the impact of 20 highest ranked systematic uncertainties on *Total background* for the right-handed $t u \gamma$ coupling coupling in the SR (1).

Not reviewed, for internal circulation only

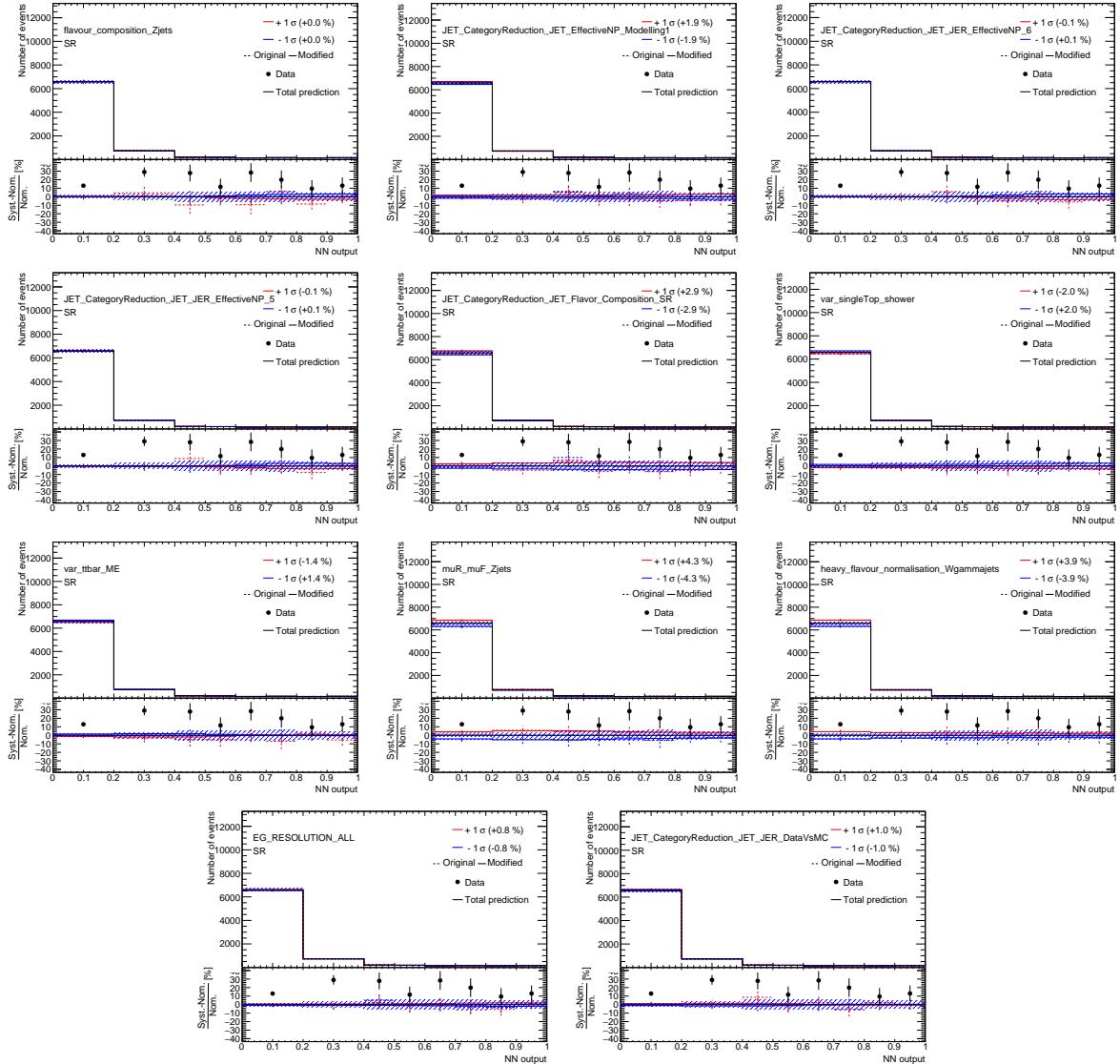


Figure 141: Plots showing the impact of 20 highest ranked systematic uncertainties on *Total background* for the right-handed *tuy* coupling coupling in the SR (2).

1779 **O.2.1.2 Signal (SR, right-handed $t\bar{u}\gamma$ coupling)**

Not reviewed, for internal circulation only

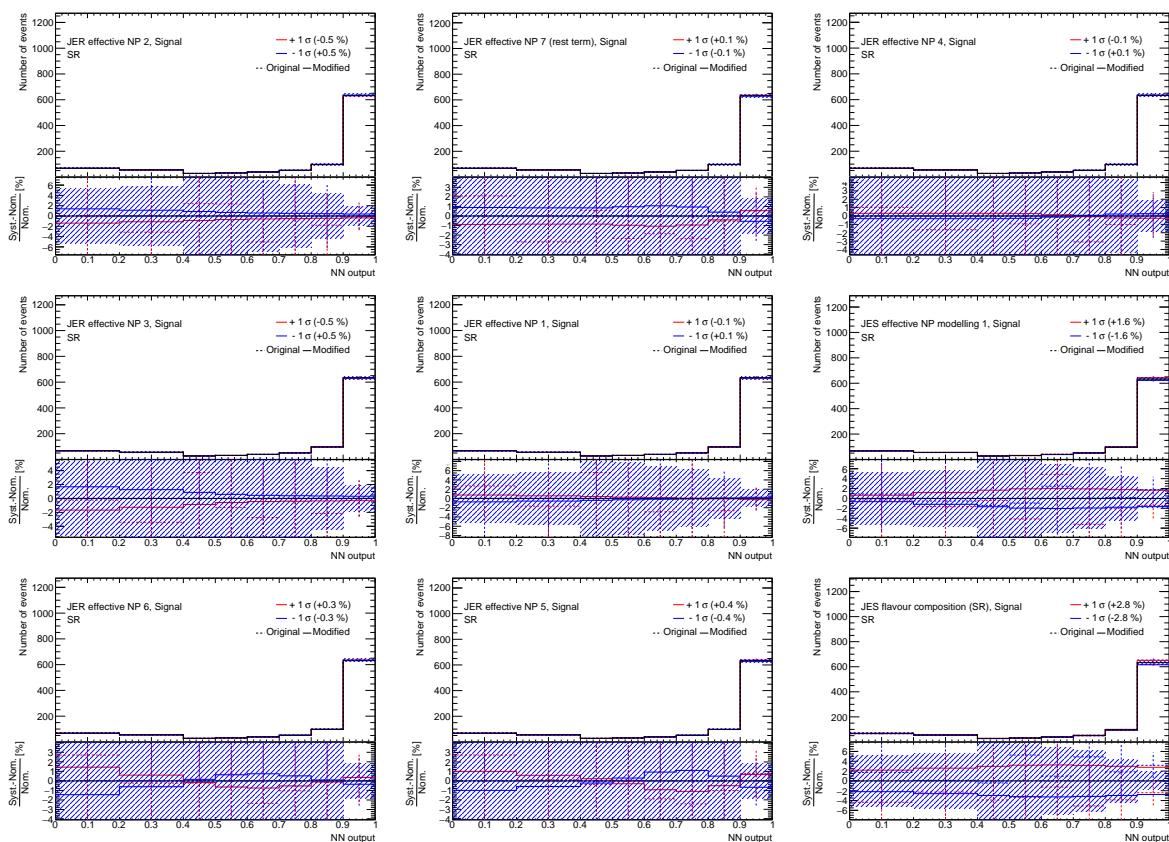


Figure 142: Plots showing the impact of 20 highest ranked systematic uncertainties on *Signal* for the right-handed $t\bar{u}\gamma$ coupling coupling in the SR (1).

Not reviewed, for internal circulation only

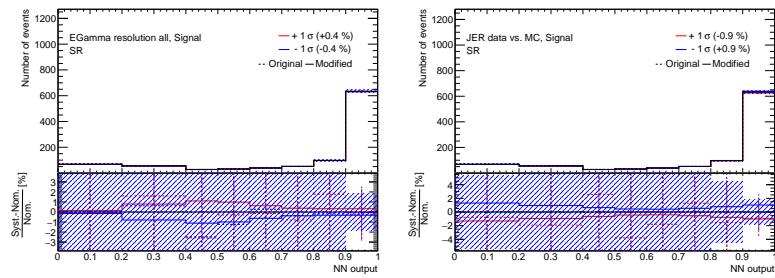


Figure 143: Plots showing the impact of 20 highest ranked systematic uncertainties on *Signal* for the right-handed $t u \gamma$ coupling coupling in the SR (2).

1780 O.2.1.3 $e \rightarrow \gamma$ fakes (SR, right-handed $t u \gamma$ coupling)

Not reviewed, for internal circulation only

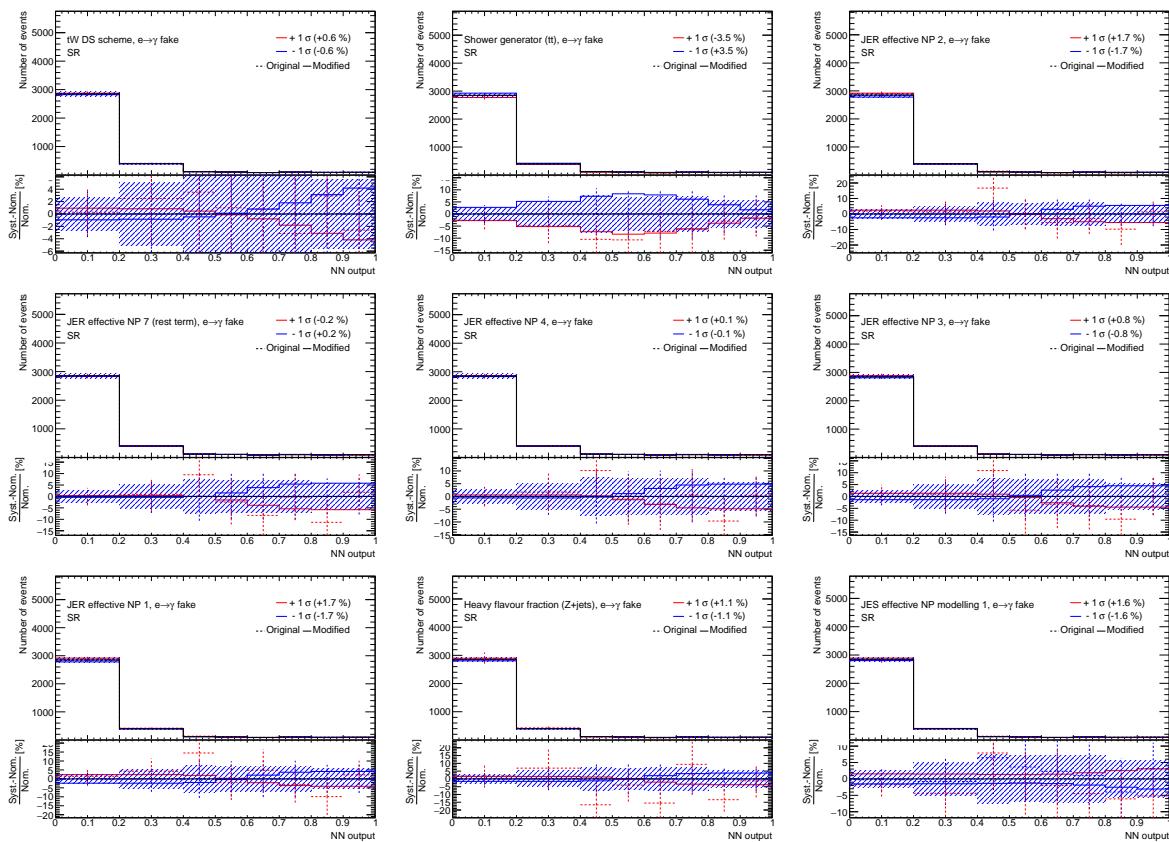


Figure 144: Plots showing the impact of 20 highest ranked systematic uncertainties on $e \rightarrow \gamma$ fakes for the right-handed $t u \gamma$ coupling coupling in the SR (1).

Not reviewed, for internal circulation only

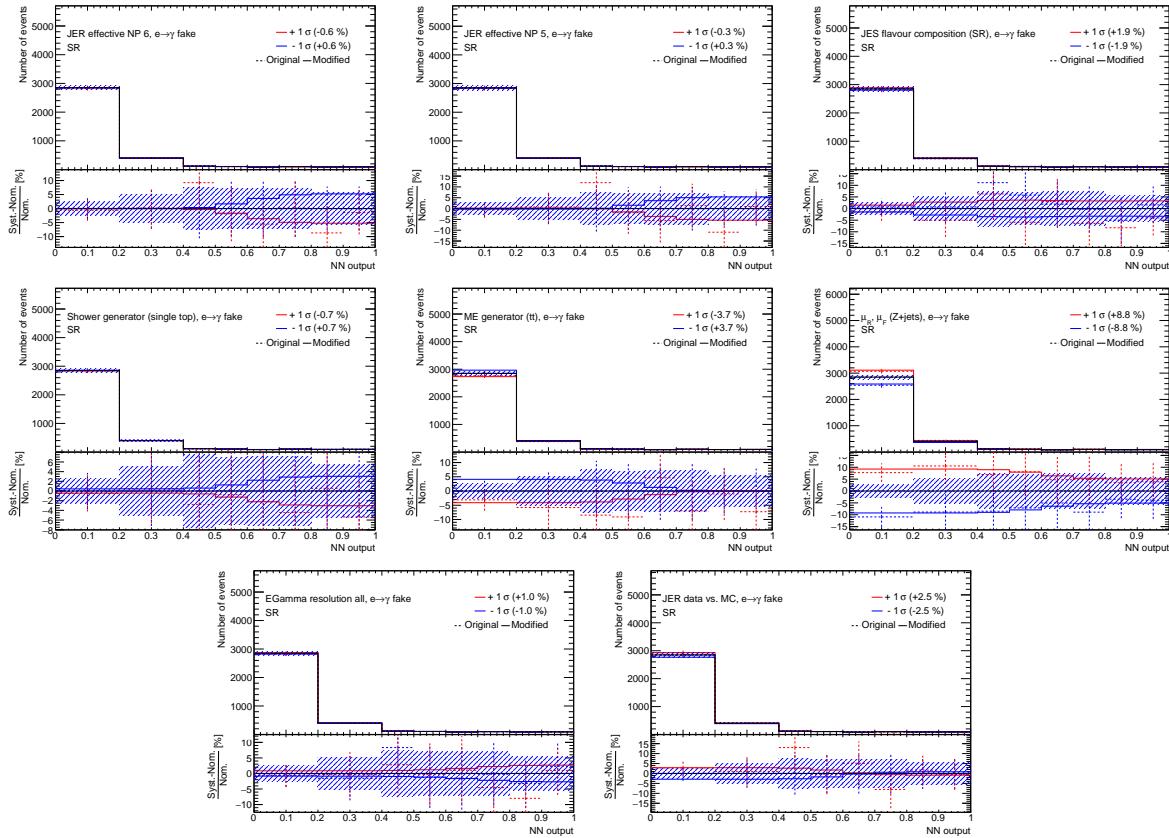


Figure 145: Plots showing the impact of 20 highest ranked systematic uncertainties on $e \rightarrow \gamma$ fakes for the right-handed $t\bar{u}\gamma$ coupling coupling in the SR (2).

1781 O.2.1.4 $j \rightarrow \gamma$ fakes (SR, right-handed $t u \gamma$ coupling)

Not reviewed, for internal circulation only

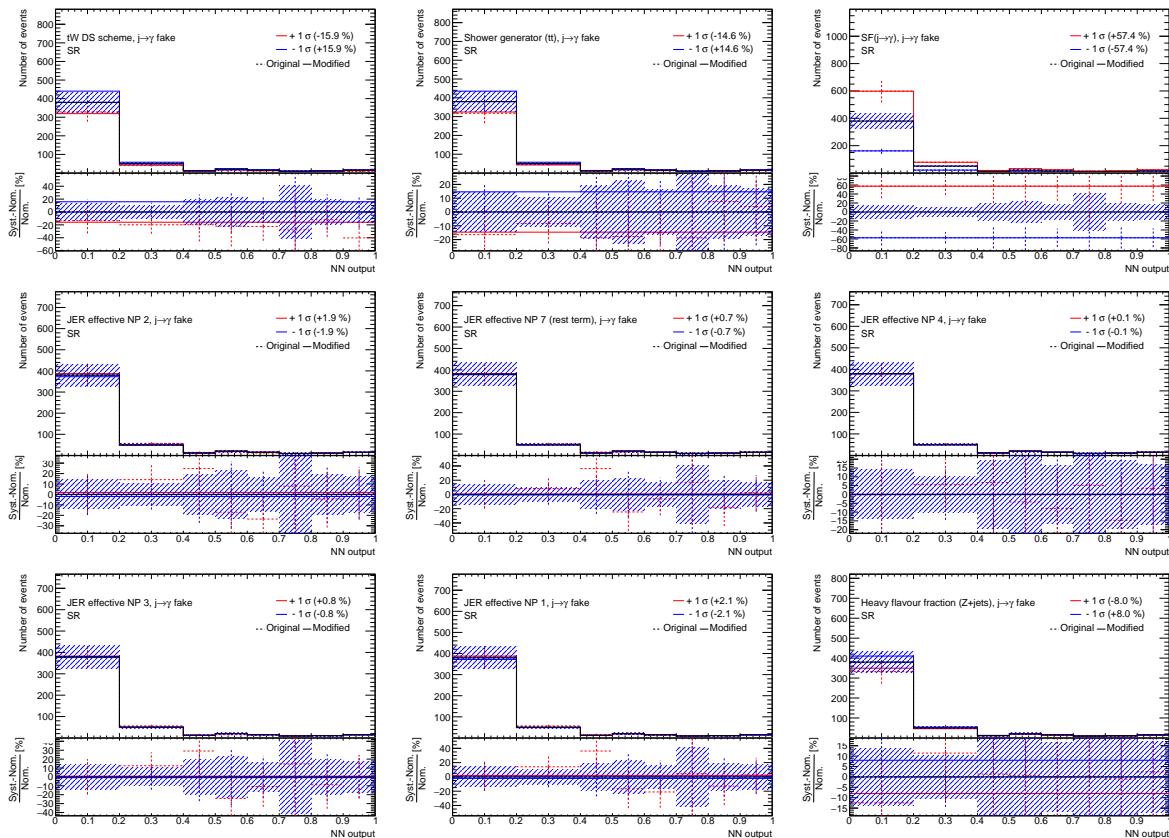


Figure 146: Plots showing the impact of 20 highest ranked systematic uncertainties on $j \rightarrow \gamma$ fakes for the right-handed $t u \gamma$ coupling coupling in the SR (1).

Not reviewed, for internal circulation only

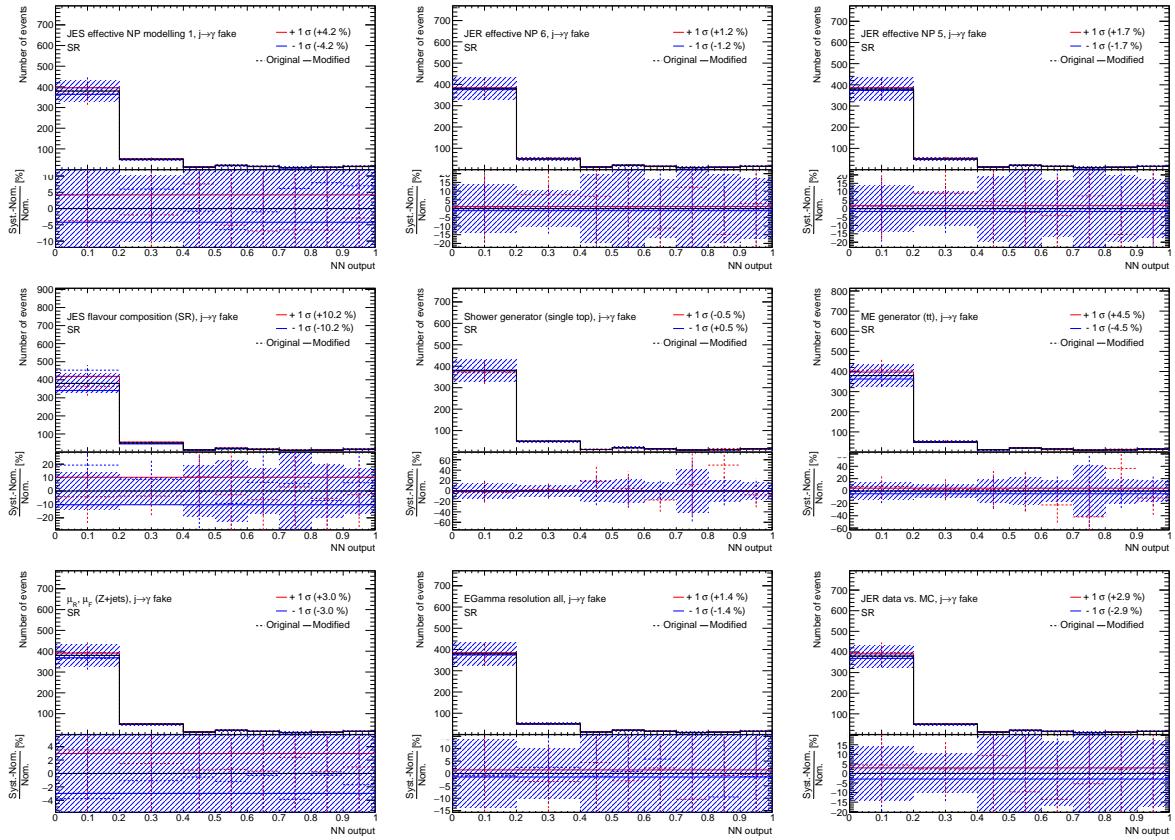


Figure 147: Plots showing the impact of 20 highest ranked systematic uncertainties on $j \rightarrow \gamma$ fakes for the right-handed tuy coupling coupling in the SR (2).

1782 O.2.1.5 $W+\gamma+jets$ (SR, right-handed $t\bar{u}\gamma$ coupling)

Not reviewed, for internal circulation only

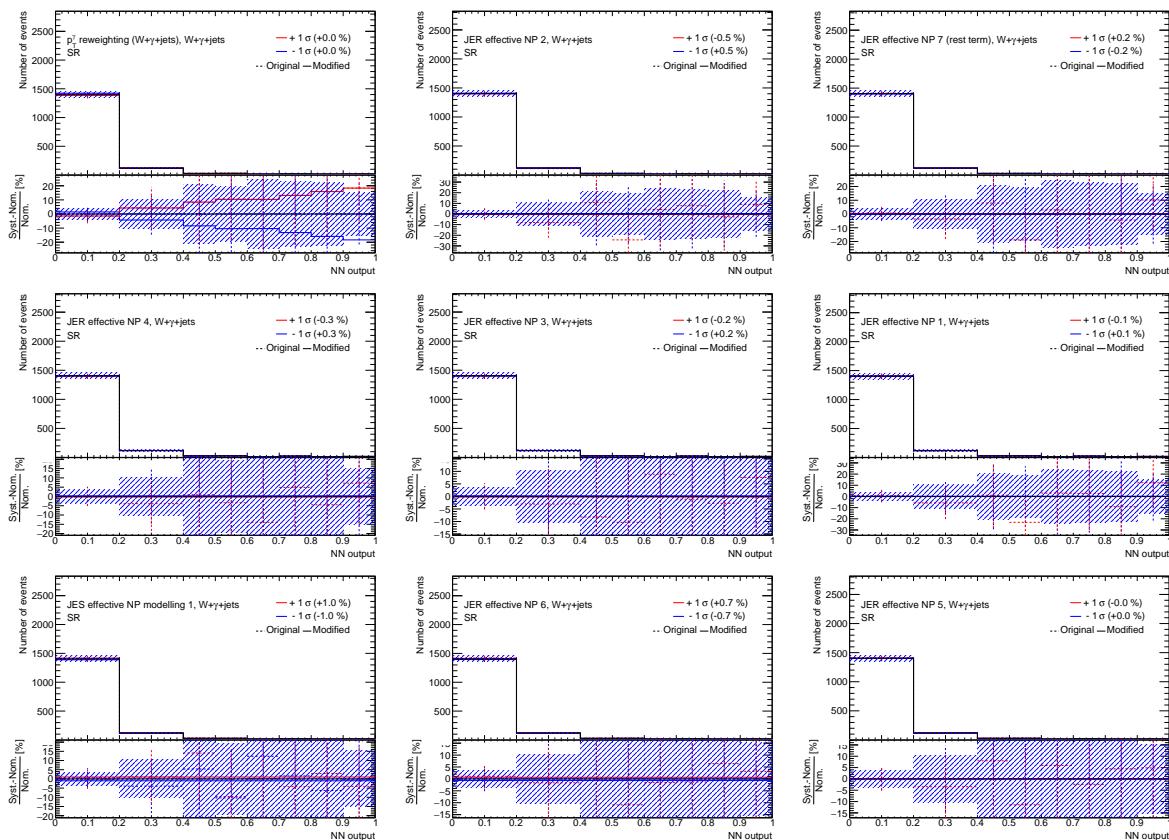


Figure 148: Plots showing the impact of 20 highest ranked systematic uncertainties on $W+\gamma+jets$ for the right-handed $t\bar{u}\gamma$ coupling coupling in the SR (1).

Not reviewed, for internal circulation only

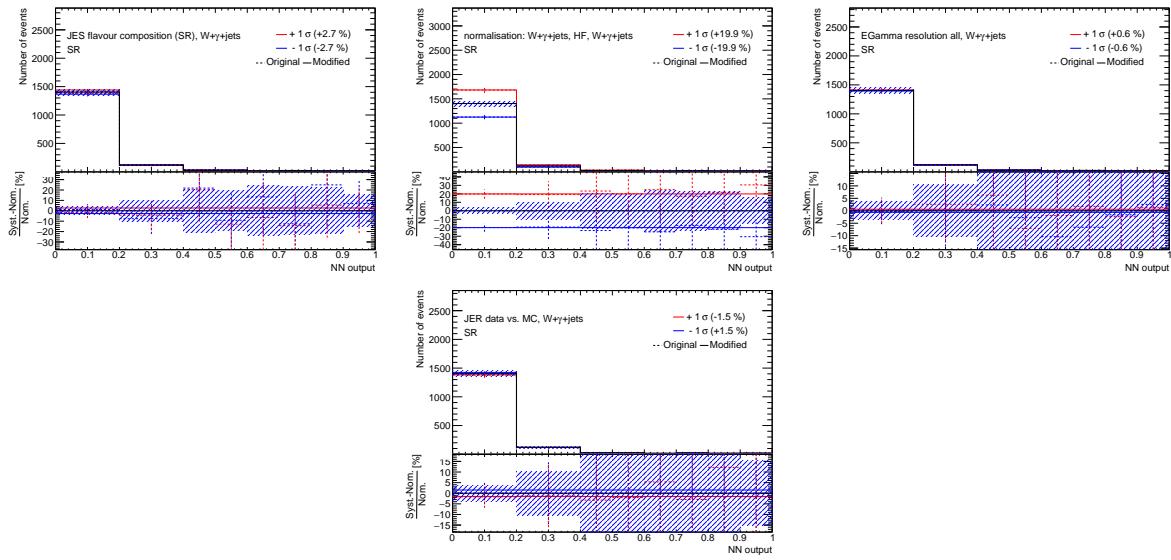


Figure 149: Plots showing the impact of 20 highest ranked systematic uncertainties on $W+\gamma+jets$ for the right-handed $t u \gamma$ coupling coupling in the SR (2).

1783 **O.2.1.6 $Z+\gamma+jets$ (SR, right-handed $t\bar{u}\gamma$ coupling)**

Not reviewed, for internal circulation only

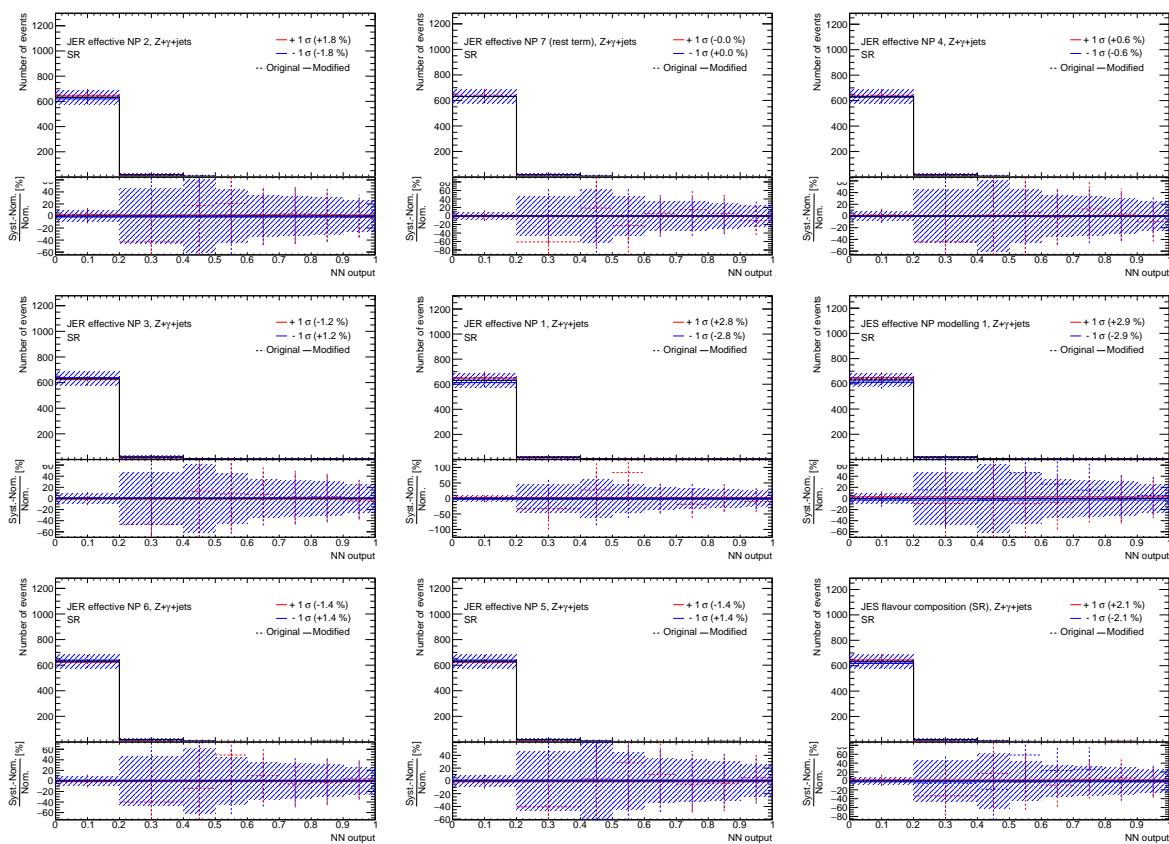


Figure 150: Plots showing the impact of 20 highest ranked systematic uncertainties on $Z+\gamma+jets$ for the right-handed $t\bar{u}\gamma$ coupling coupling in the SR (1).

Not reviewed, for internal circulation only

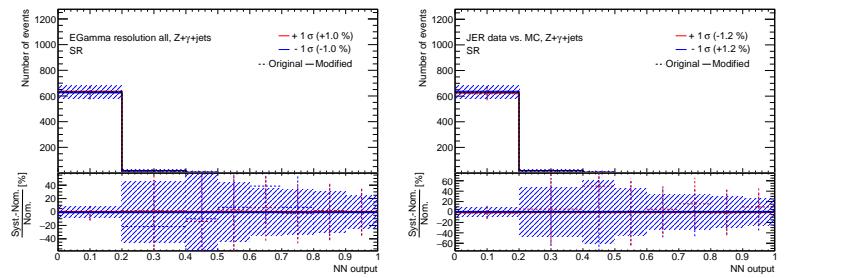


Figure 151: Plots showing the impact of 20 highest ranked systematic uncertainties on $Z+\gamma+jets$ for the right-handed $t\bar{u}\gamma$ coupling coupling in the SR (2).

1784 0.2.1.7 Other prompt photons (SR, right-handed $t\gamma\gamma$ coupling)

Not reviewed, for internal circulation only

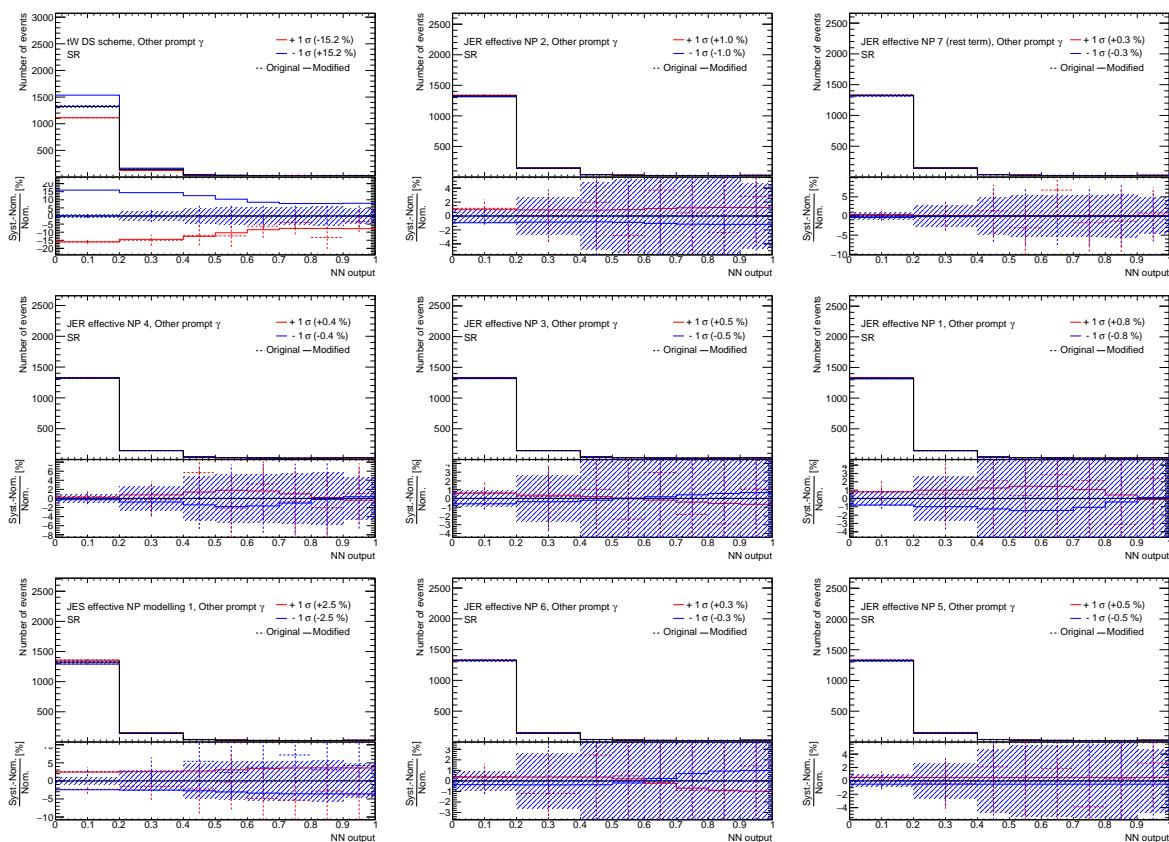


Figure 152: Plots showing the impact of 20 highest ranked systematic uncertainties on *Other prompt photons* for the right-handed $t\gamma\gamma$ coupling coupling in the SR (1).

Not reviewed, for internal circulation only

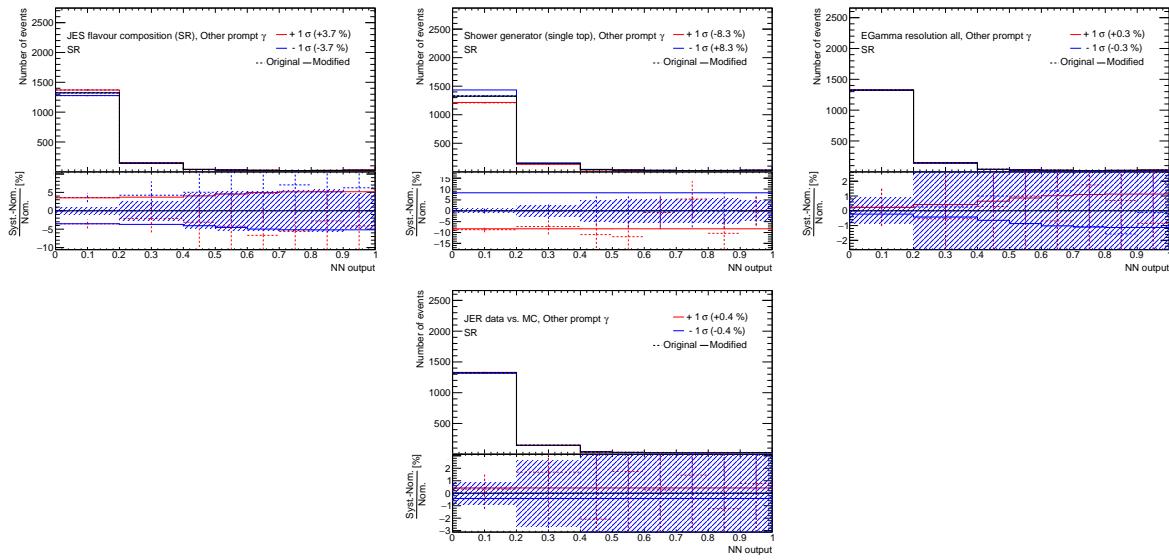


Figure 153: Plots showing the impact of 20 highest ranked systematic uncertainties on *Other prompt photons* for the right-handed $t\bar{u}\gamma$ coupling coupling in the SR (2).

1785 **O.2.2 CR $W+\gamma+jets$ (right-handed $t\bar{u}\gamma$ coupling)**

1786 **O.2.2.1 Total background (CR $W+\gamma+jets$, right-handed $t\bar{u}\gamma$ coupling)**

Not reviewed, for internal circulation only

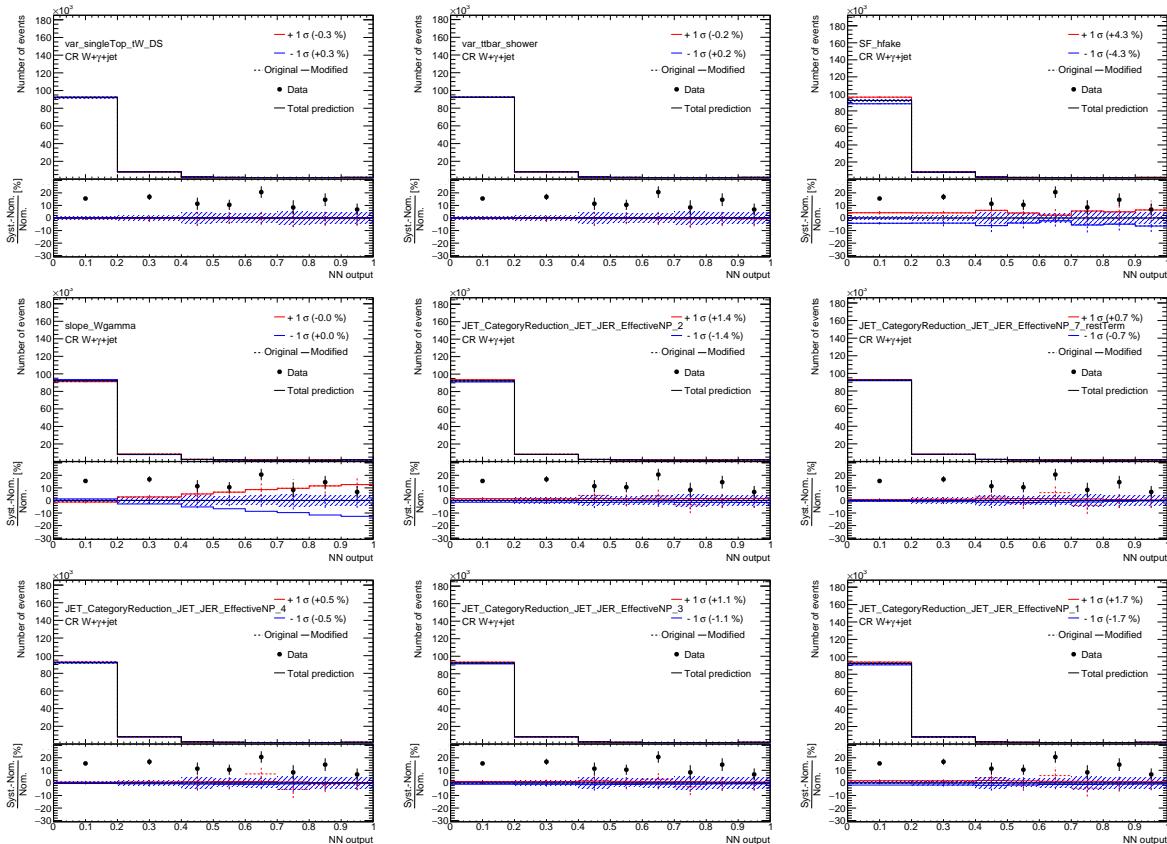


Figure 154: Plots showing the impact of 20 highest ranked systematic uncertainties on *Total background* for the right-handed $t\bar{u}\gamma$ coupling coupling in the CR $W+\gamma+jets$ (1).

Not reviewed, for internal circulation only

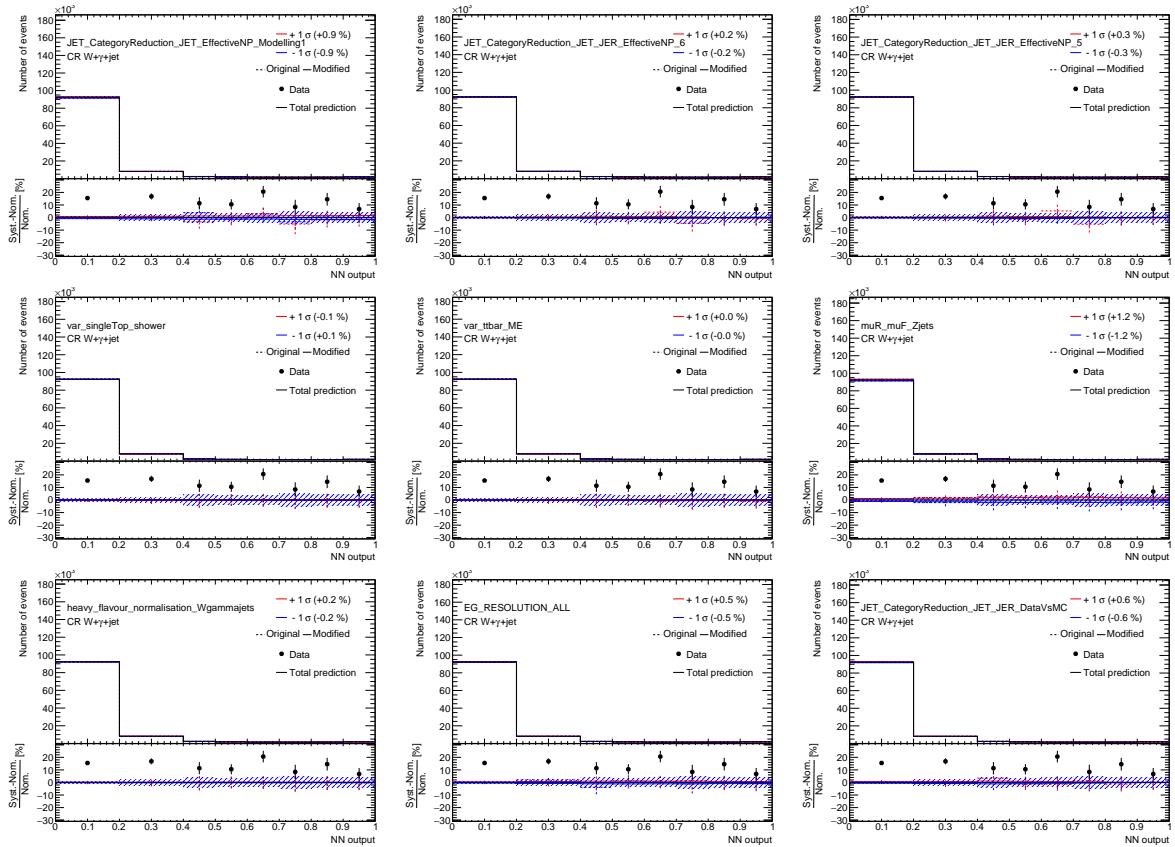


Figure 155: Plots showing the impact of 20 highest ranked systematic uncertainties on *Total background* for the right-handed $t\gamma\gamma$ coupling coupling in the CR $W+\gamma+jets$ (2).

1787 O.2.2.2 Signal (CR $W+\gamma+$ jets, right-handed $t\bar{u}\gamma$ coupling)

Not reviewed, for internal circulation only

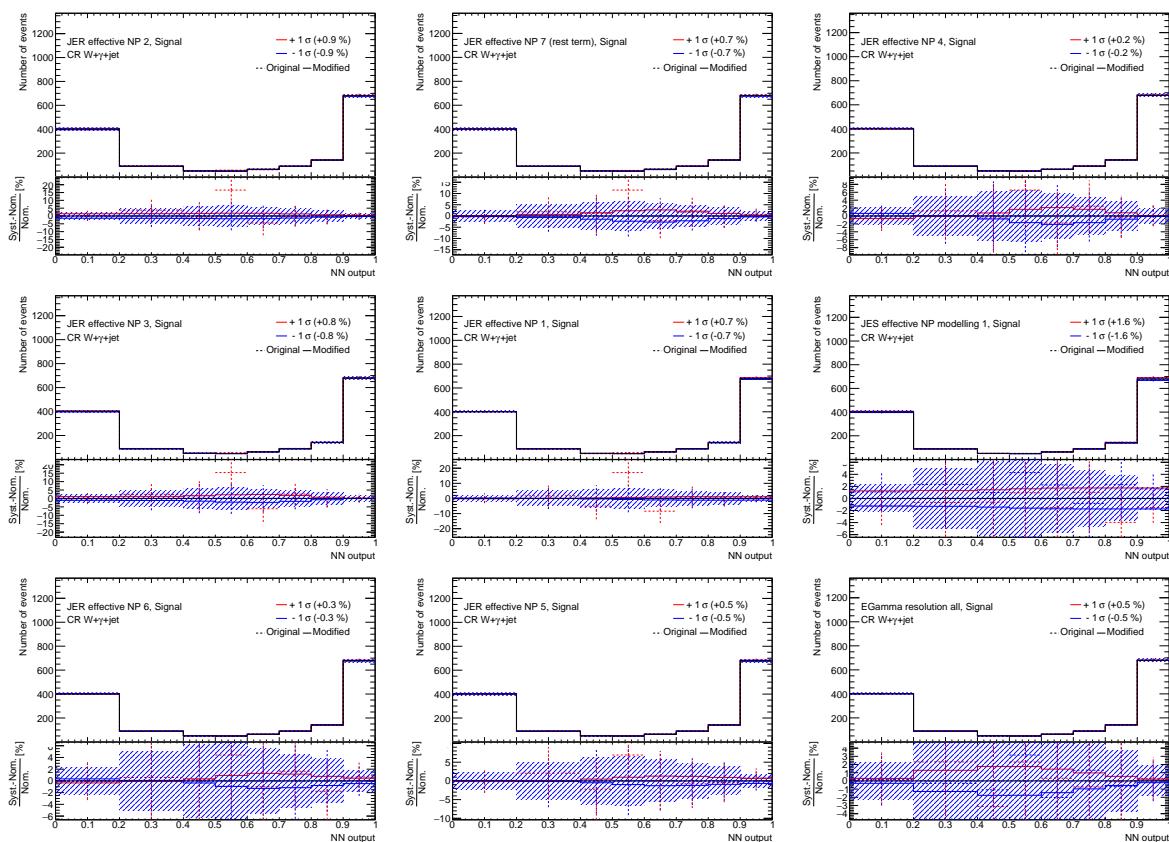


Figure 156: Plots showing the impact of 20 highest ranked systematic uncertainties on *Signal* for the right-handed $t\bar{u}\gamma$ coupling coupling in the CR $W+\gamma+$ jets (1).

[Not reviewed, for internal circulation only]

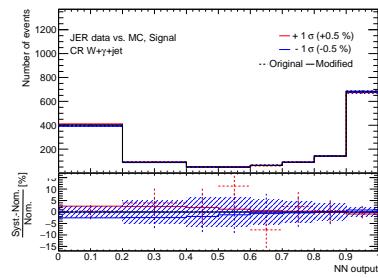


Figure 157: Plots showing the impact of 20 highest ranked systematic uncertainties on *Signal* for the right-handed $t\gamma\gamma$ coupling coupling in the CR $W+\gamma+\text{jets}$ (2).

1788 **O.2.2.3 $e \rightarrow \gamma$ fakes (CR $W+\gamma+\text{jets}$, right-handed $t u \gamma$ coupling)**

Not reviewed, for internal circulation only

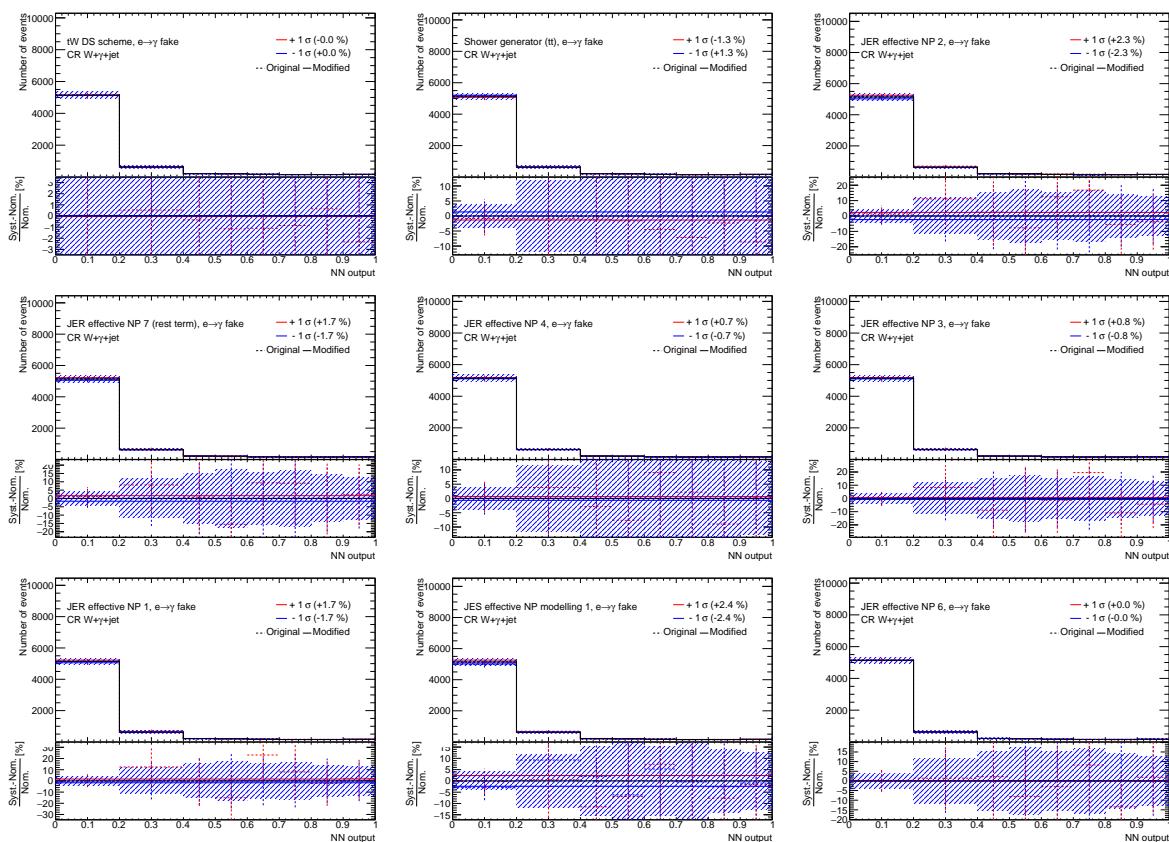


Figure 158: Plots showing the impact of 20 highest ranked systematic uncertainties on $e \rightarrow \gamma$ fakes for the right-handed $t u \gamma$ coupling coupling in the CR $W+\gamma+\text{jets}$ (1).

Not reviewed, for internal circulation only

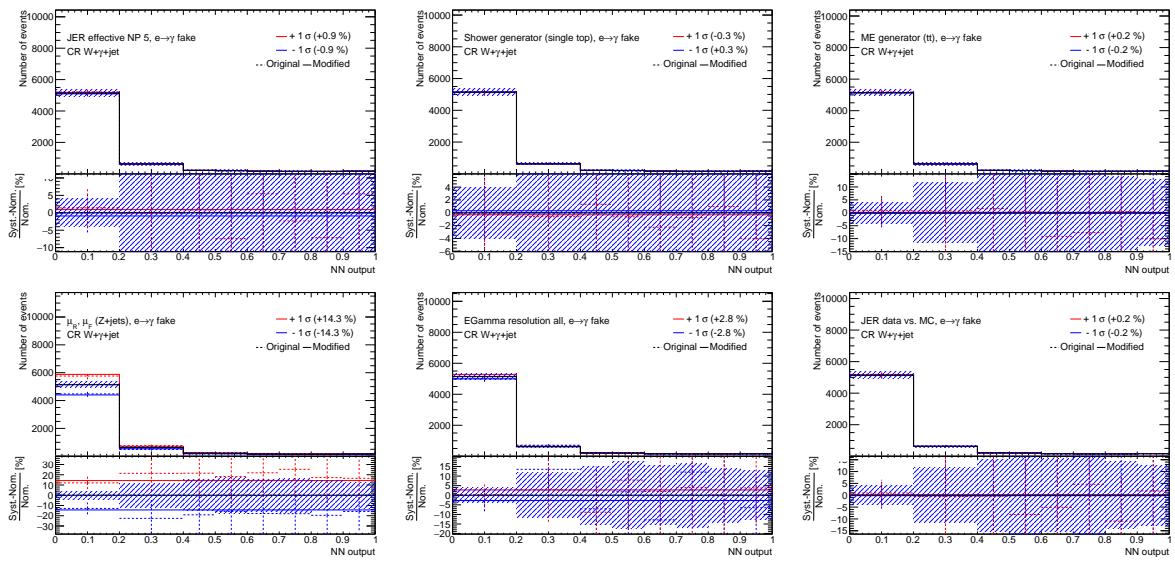


Figure 159: Plots showing the impact of 20 highest ranked systematic uncertainties on $e \rightarrow \gamma$ fakes for the right-handed tuy coupling coupling in the CR $W+\gamma+jets$ (2).

1789 **O.2.2.4 $j \rightarrow \gamma$ fakes (CR $W+\gamma+\text{jets}$, right-handed $t\gamma\gamma$ coupling)**

Not reviewed, for internal circulation only

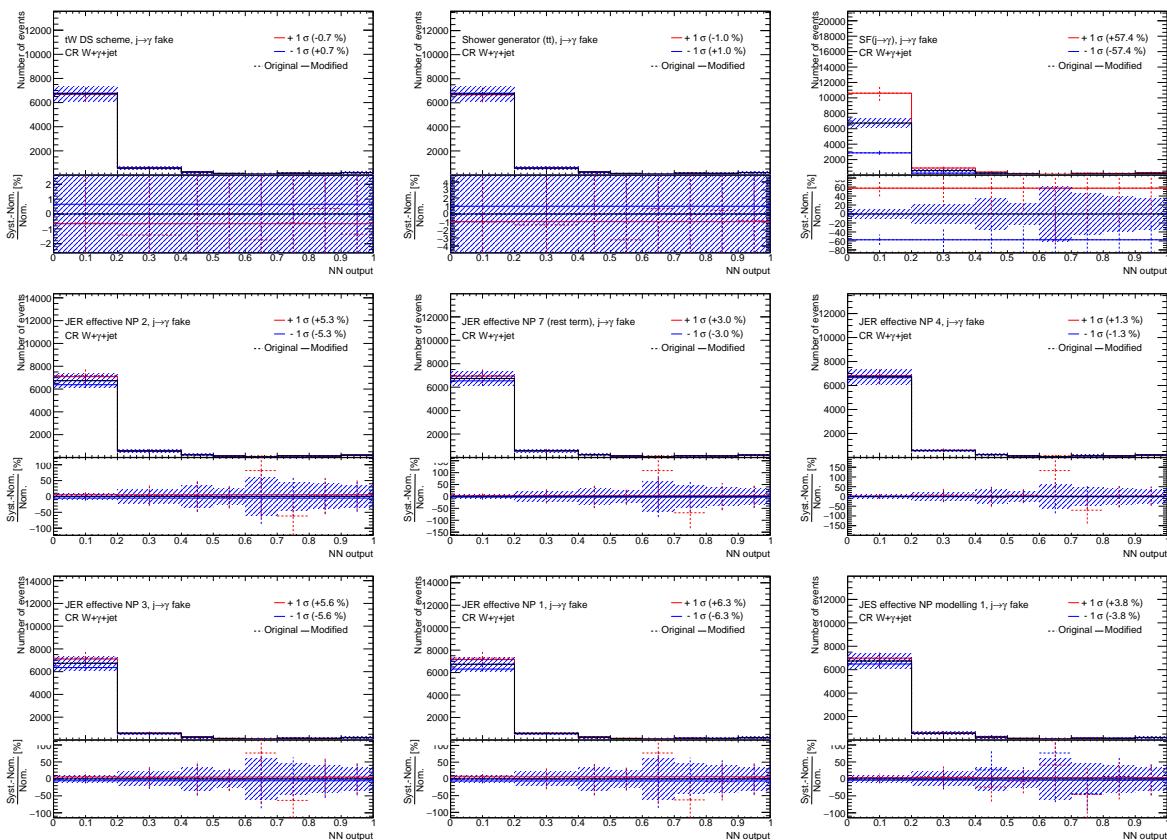


Figure 160: Plots showing the impact of 20 highest ranked systematic uncertainties on $j \rightarrow \gamma$ fakes for the right-handed $t\gamma\gamma$ coupling coupling in the CR $W+\gamma+\text{jets}$ (1).

Not reviewed, for internal circulation only

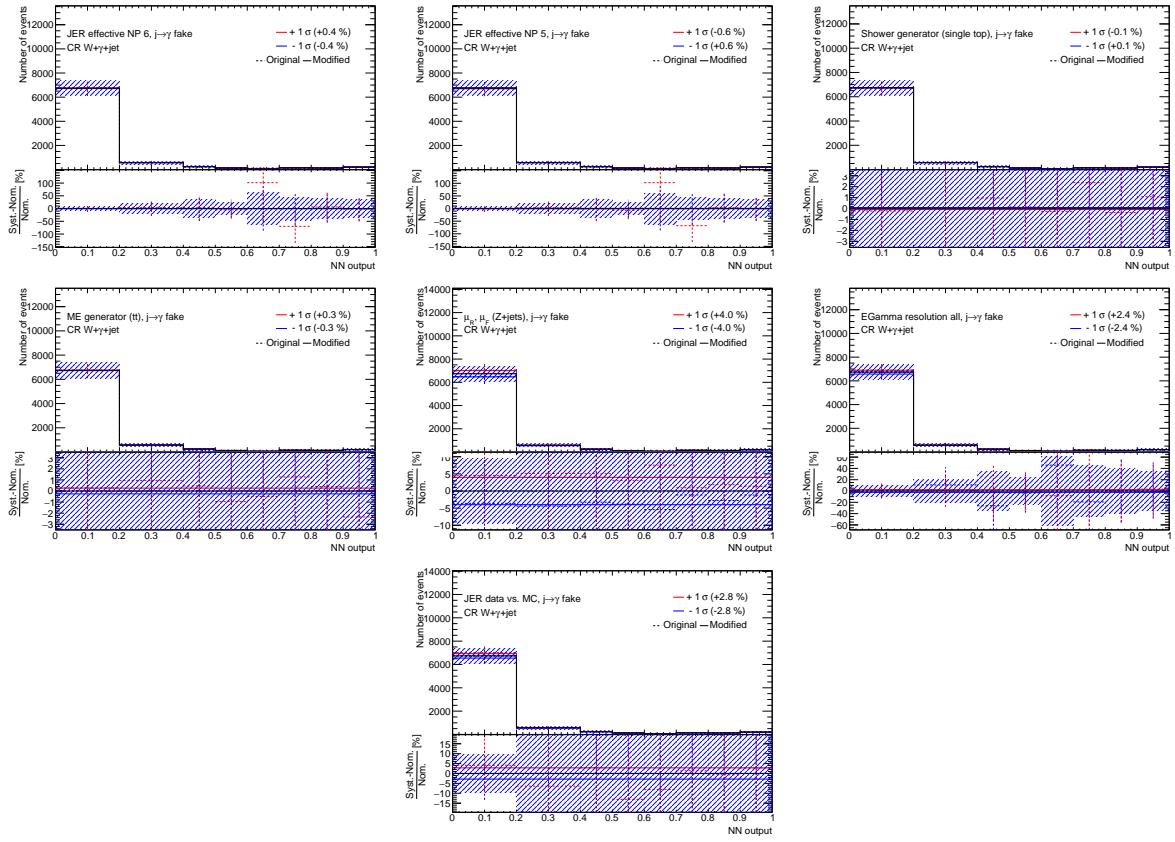


Figure 161: Plots showing the impact of 20 highest ranked systematic uncertainties on $j \rightarrow \gamma$ fakes for the right-handed tuy coupling coupling in the CR $W+\gamma+jets$ (2).

1790 **O.2.2.5 $W+\gamma+jets$ (CR $W+\gamma+jets$, right-handed $t u \gamma$ coupling)**

Not reviewed, for internal circulation only

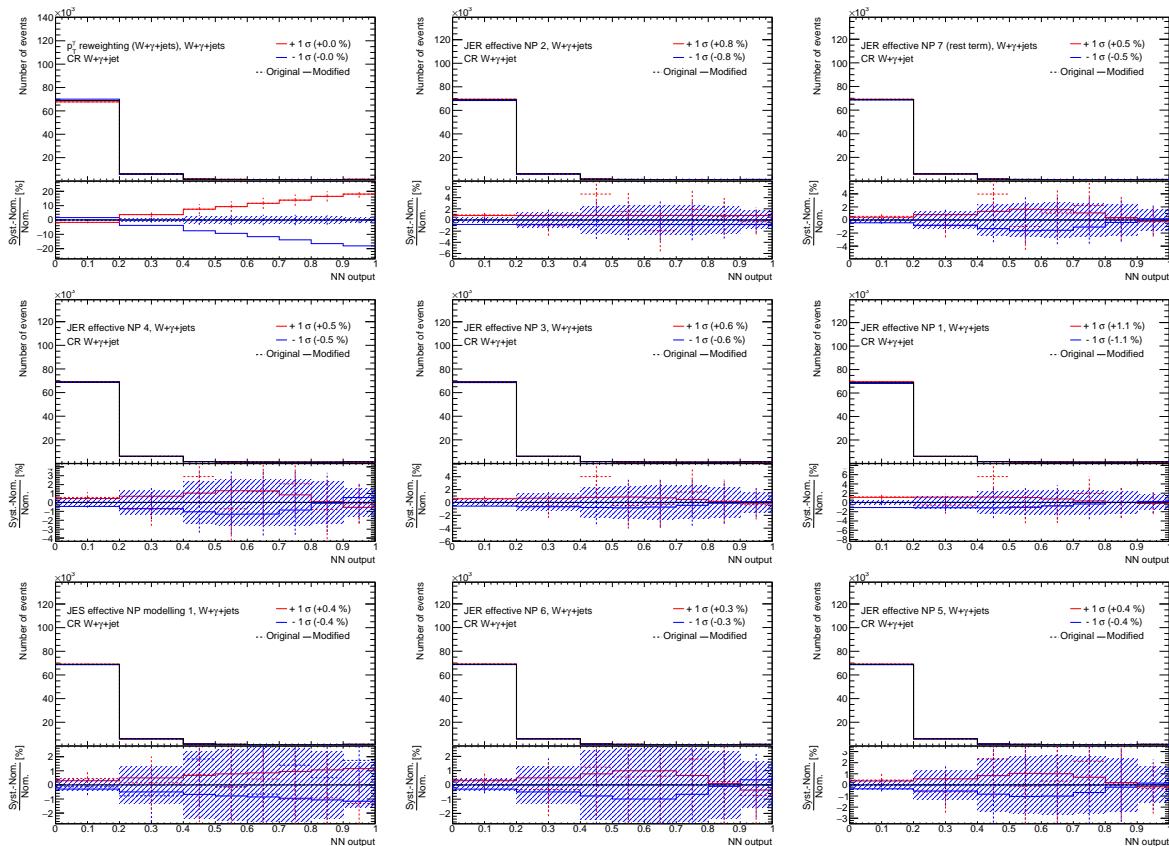


Figure 162: Plots showing the impact of 20 highest ranked systematic uncertainties on $W+\gamma+jets$ for the right-handed $t u \gamma$ coupling coupling in the CR $W+\gamma+jets$ (1).

Not reviewed, for internal circulation only

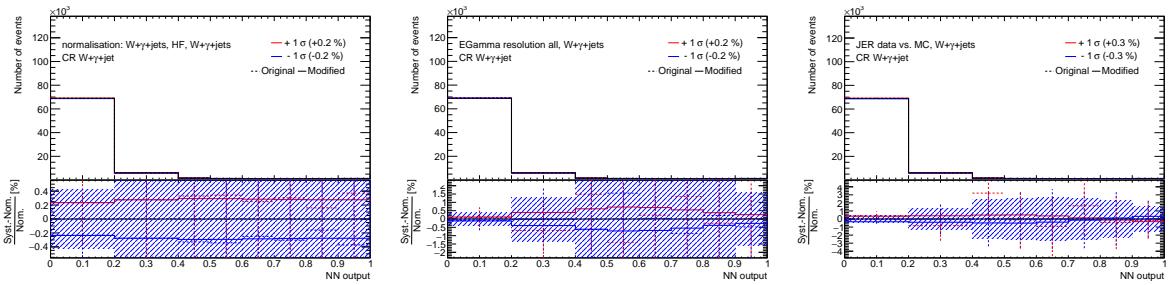


Figure 163: Plots showing the impact of 20 highest ranked systematic uncertainties on $W+\gamma+jets$ for the right-handed $tW\gamma$ coupling coupling in the CR $W+\gamma+jets$ (2).

1791 O.2.2.6 $Z+\gamma+jets$ (CR $W+\gamma+jets$, right-handed $t\bar{u}\gamma$ coupling)

Not reviewed, for internal circulation only

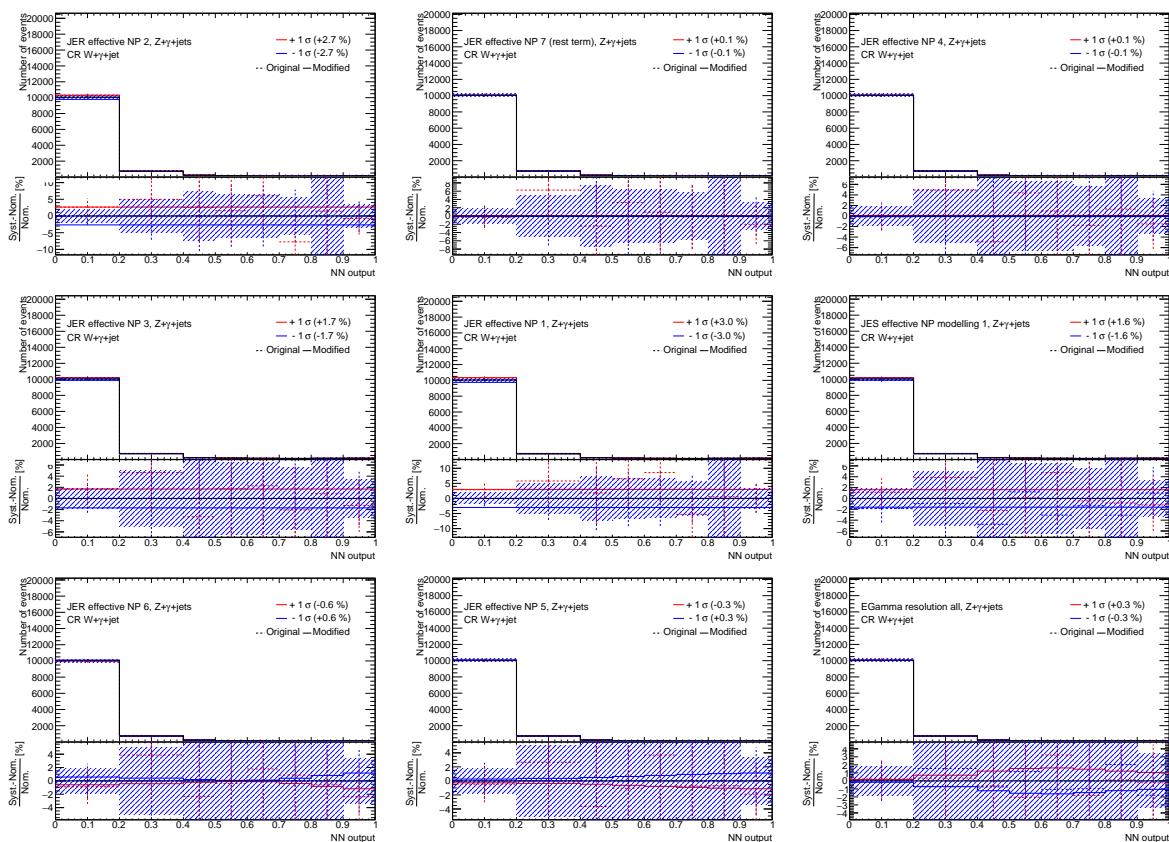


Figure 164: Plots showing the impact of 20 highest ranked systematic uncertainties on $Z+\gamma+jets$ for the right-handed $t\bar{u}\gamma$ coupling coupling in the CR $W+\gamma+jets$ (1).

Not reviewed, for internal circulation only

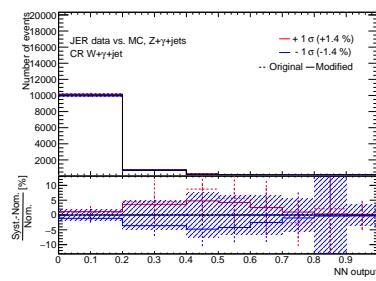


Figure 165: Plots showing the impact of 20 highest ranked systematic uncertainties on $Z+\gamma+jets$ for the right-handed $t\bar{u}\gamma$ coupling coupling in the CR $W+\gamma+jets$ (2).

1792 **O.2.2.7 Other prompt photons (CR $W+\gamma+jets$, right-handed $t\bar{u}\gamma$ coupling)**

Not reviewed, for internal circulation only

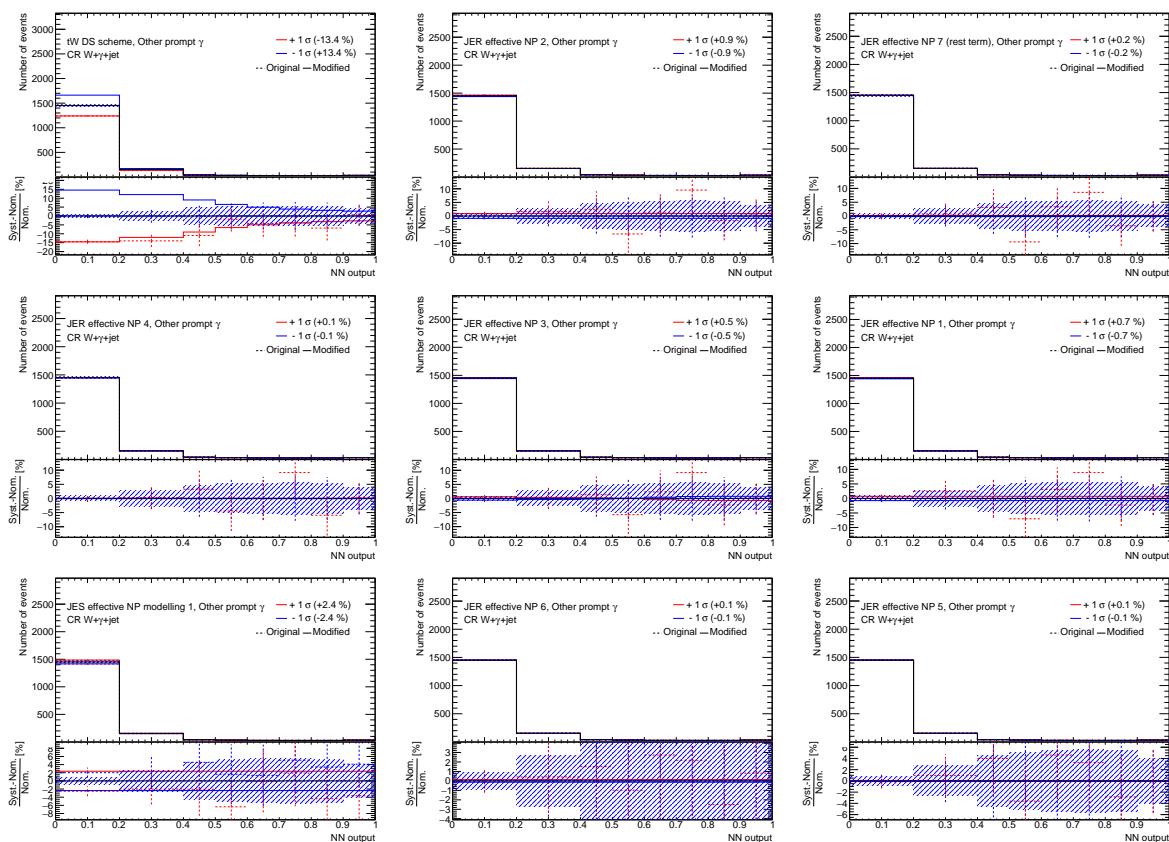


Figure 166: Plots showing the impact of 20 highest ranked systematic uncertainties on *Other prompt photons* for the right-handed $t\bar{u}\gamma$ coupling coupling in the CR $W+\gamma+jets$ (1).

Not reviewed, for internal circulation only

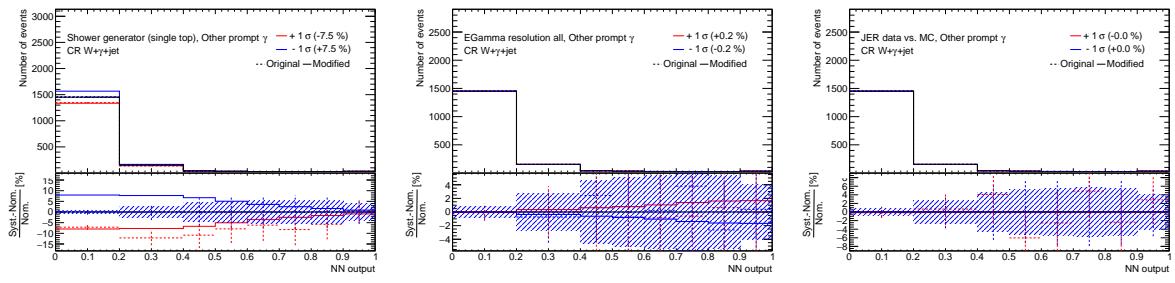


Figure 167: Plots showing the impact of 20 highest ranked systematic uncertainties on *Other prompt photons* for the right-handed $t\bar{u}\gamma$ coupling coupling in the CR $W+\gamma+jets$ (2).

1793 **O.2.3 CR Z+ γ (right-handed $t\bar{u}\gamma$ coupling)**

1794 **O.2.3.1 Total background (CR Z+ γ , right-handed $t\bar{u}\gamma$ coupling)**

Not reviewed, for internal circulation only

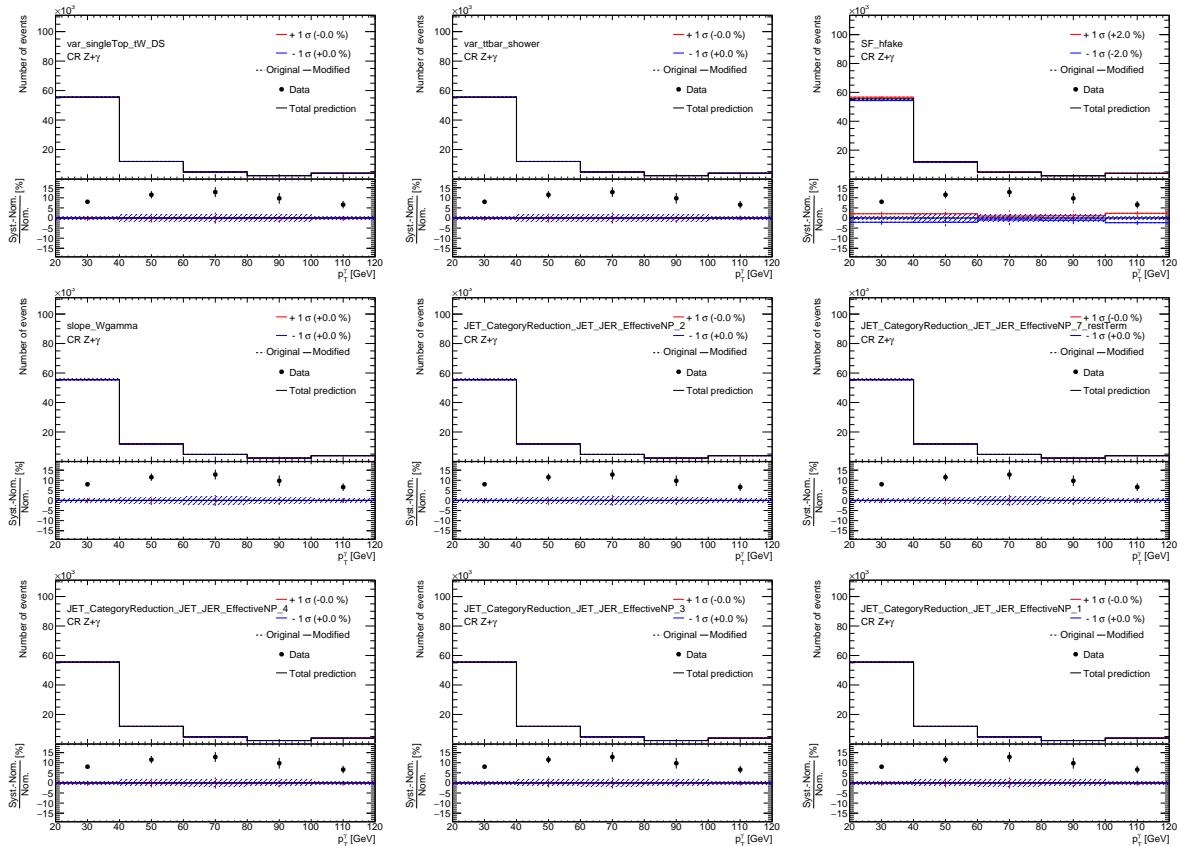


Figure 168: Plots showing the impact of 20 highest ranked systematic uncertainties on *Total background* for the right-handed $t\bar{u}\gamma$ coupling coupling in the CR $Z+\gamma$ (1).

Not reviewed, for internal circulation only

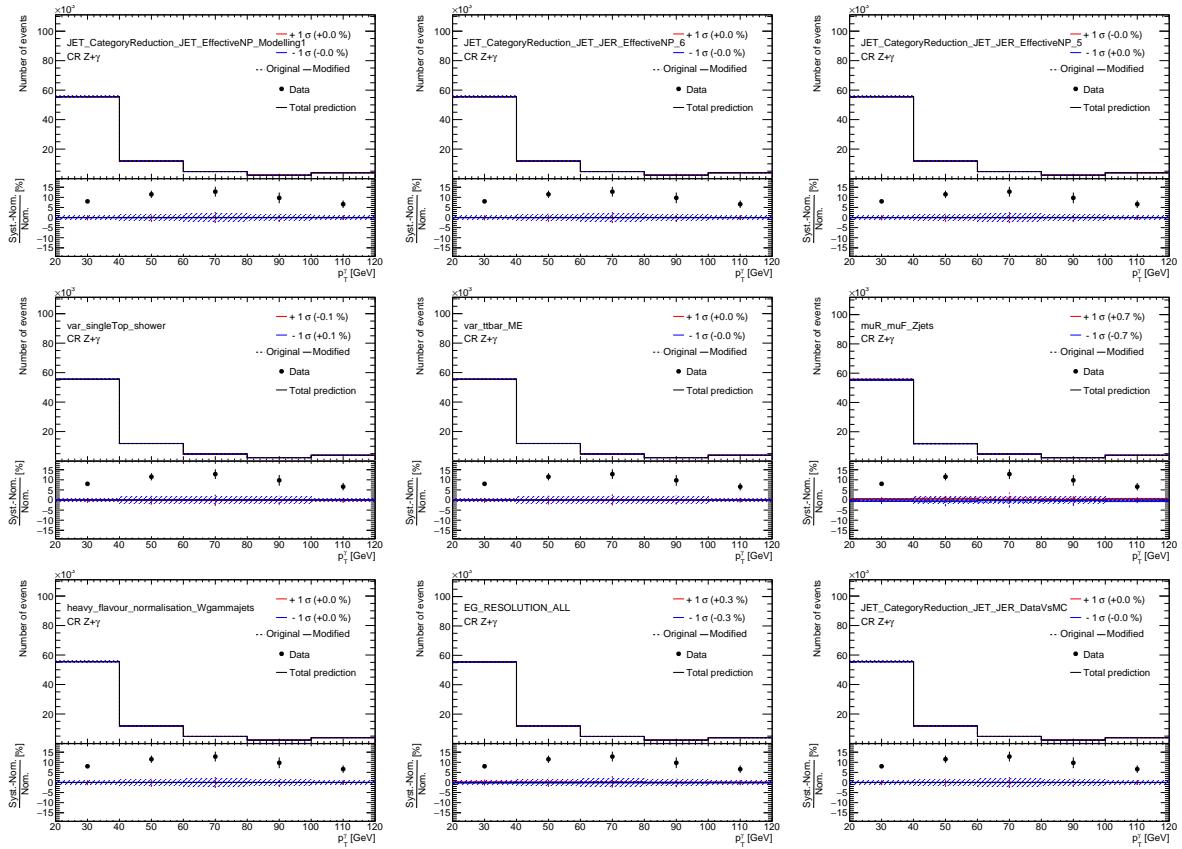


Figure 169: Plots showing the impact of 20 highest ranked systematic uncertainties on *Total background* for the right-handed $t\gamma\gamma$ coupling coupling in the CR $Z+\gamma$ (2).

1795 **O.2.3.2 Signal (CR $Z+\gamma$, right-handed $t u \gamma$ coupling)**

Not reviewed, for internal circulation only

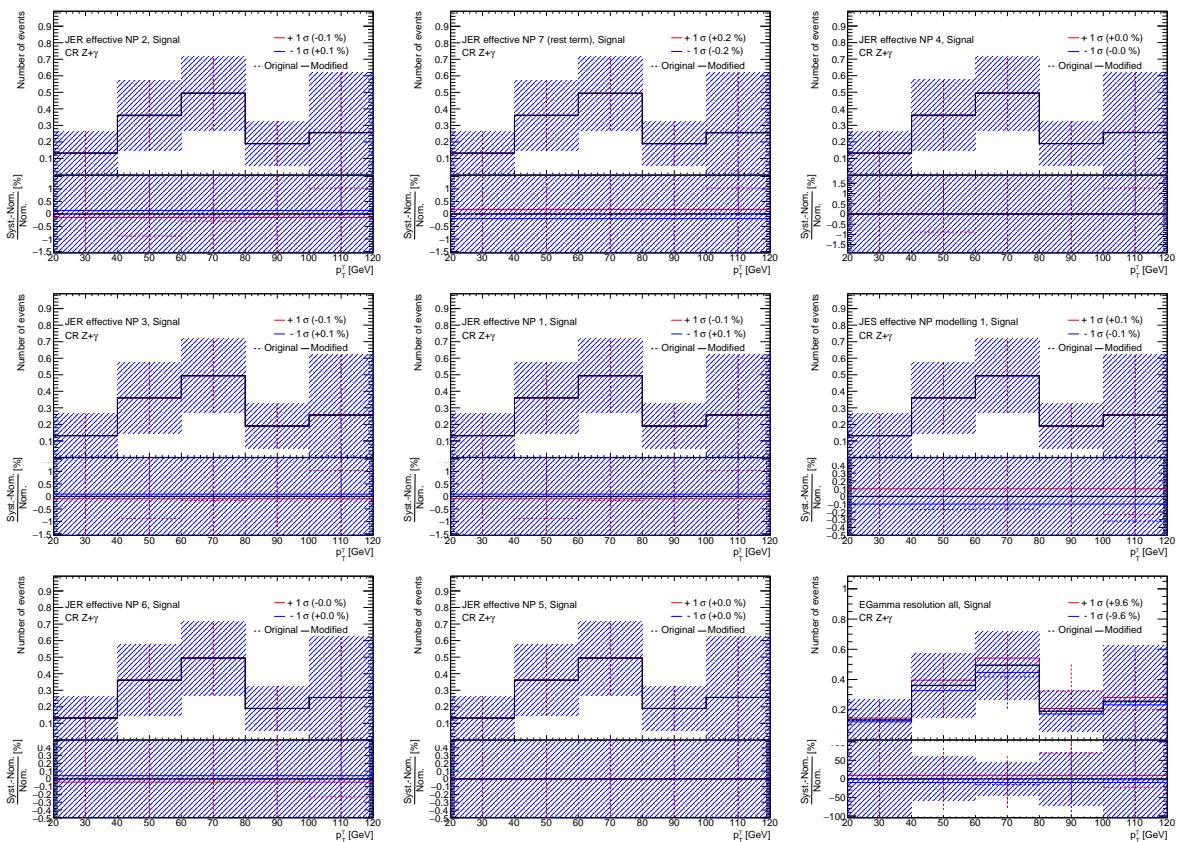


Figure 170: Plots showing the impact of 20 highest ranked systematic uncertainties on *Signal* for the right-handed $t u \gamma$ coupling coupling in the CR $Z+\gamma$ (1).

Not reviewed, for internal circulation only

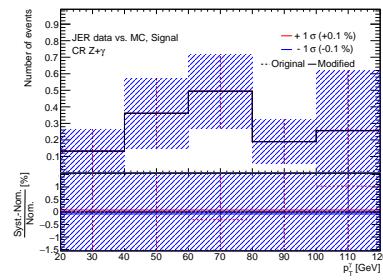


Figure 171: Plots showing the impact of 20 highest ranked systematic uncertainties on *Signal* for the right-handed $t u \gamma$ coupling coupling in the CR $Z + \gamma$ (2).

1796 **O.2.3.3 $e \rightarrow \gamma$ fakes (CR Z+ γ , right-handed $t u \gamma$ coupling)**

Not reviewed, for internal circulation only

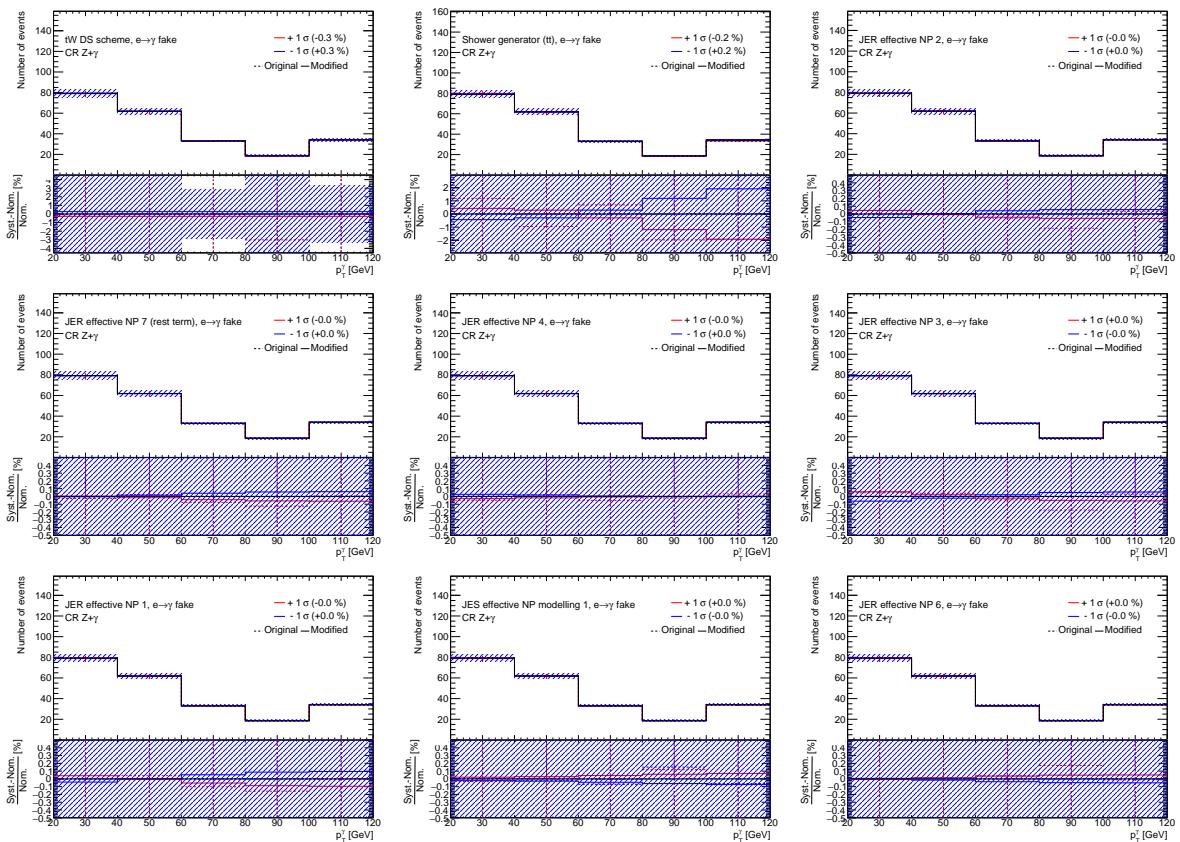


Figure 172: Plots showing the impact of 20 highest ranked systematic uncertainties on $e \rightarrow \gamma$ fakes for the right-handed $t u \gamma$ coupling coupling in the CR Z+ γ (1).

Not reviewed, for internal circulation only

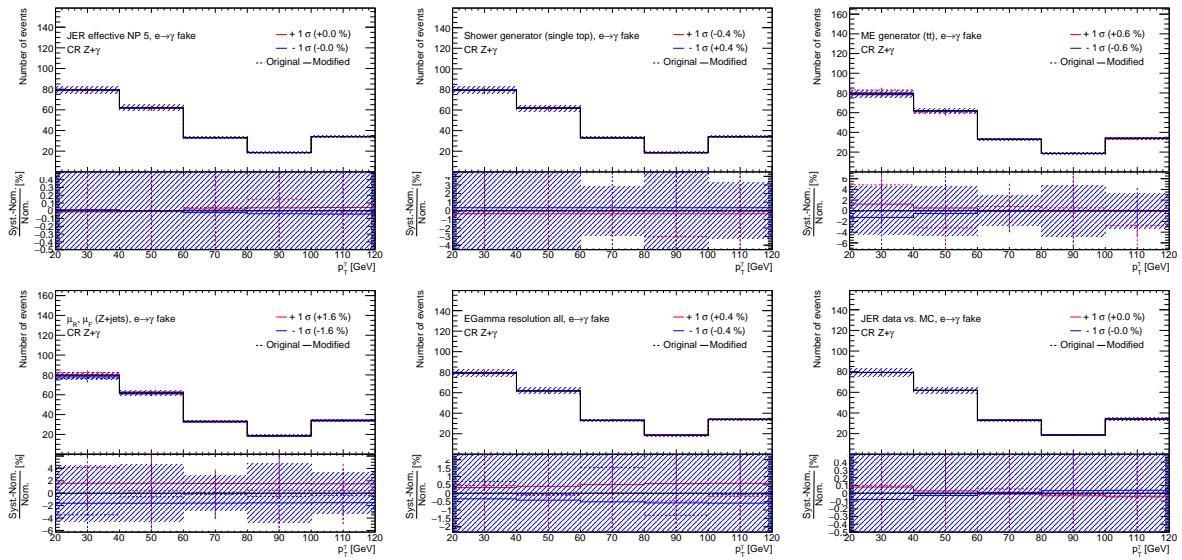


Figure 173: Plots showing the impact of 20 highest ranked systematic uncertainties on $e \rightarrow \gamma$ fakes for the right-handed tuy coupling coupling in the CR $Z + \gamma$ (2).

1797 **O.2.3.4 $j \rightarrow \gamma$ fakes (CR Z+ γ , right-handed $t u \gamma$ coupling)**

Not reviewed, for internal circulation only

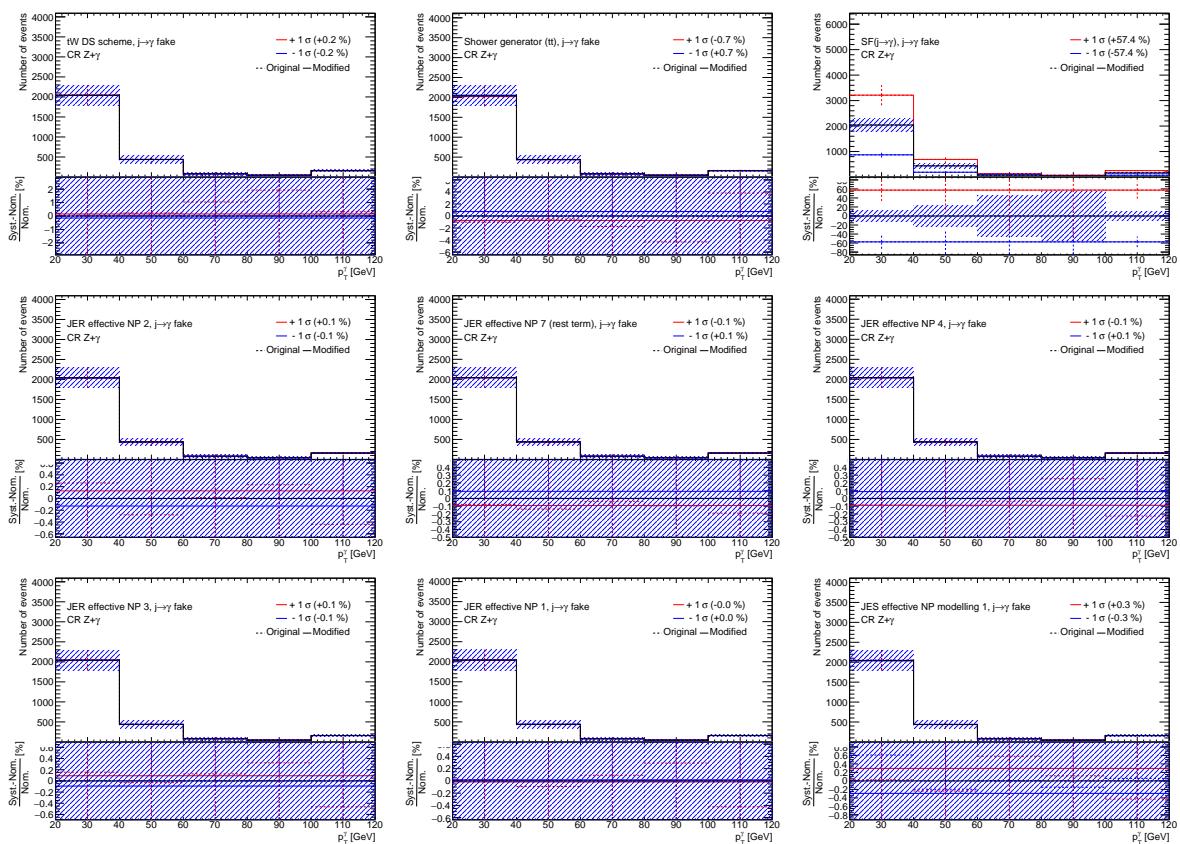


Figure 174: Plots showing the impact of 20 highest ranked systematic uncertainties on $j \rightarrow \gamma$ fakes for the right-handed $t u \gamma$ coupling coupling in the CR Z+ γ (1).

Not reviewed, for internal circulation only

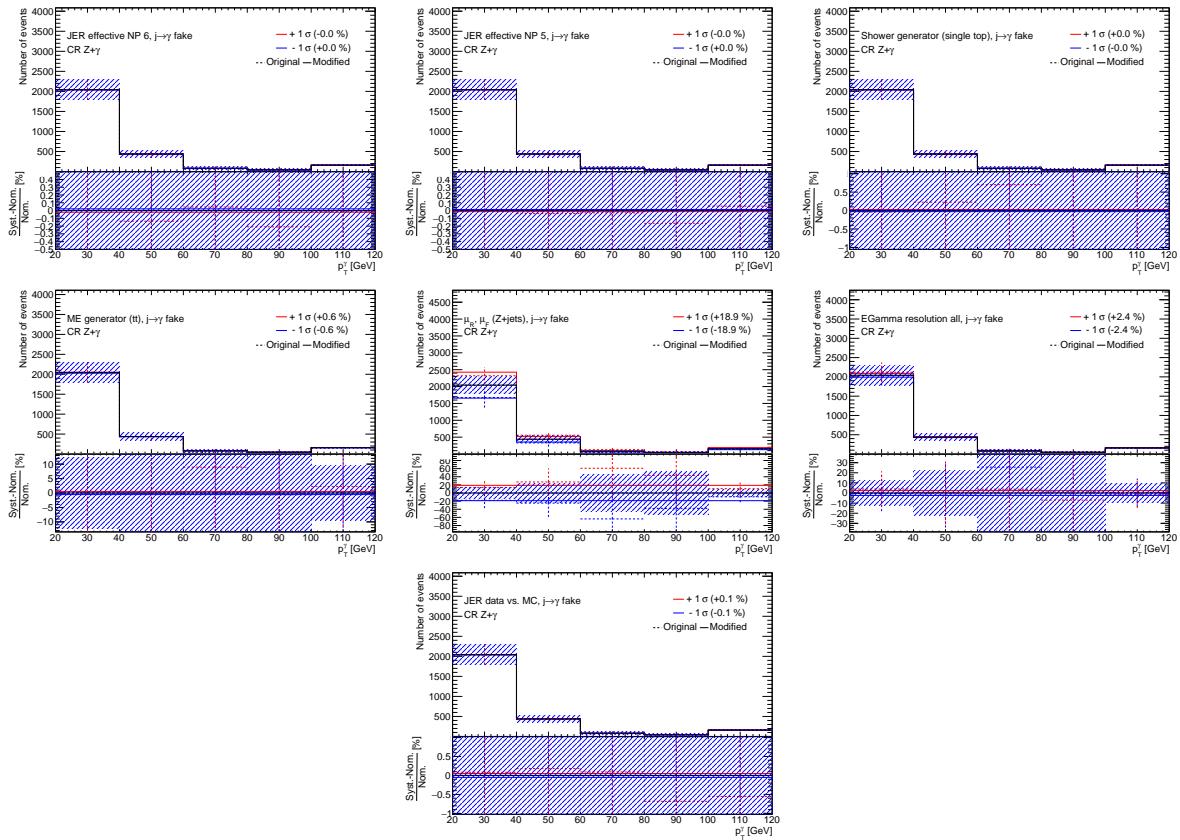


Figure 175: Plots showing the impact of 20 highest ranked systematic uncertainties on $j \rightarrow \gamma$ fakes for the right-handed tuy coupling coupling in the CR $Z+\gamma$ (2).

1798 O.2.3.5 $W+\gamma+jets$ (CR $Z+\gamma$, right-handed $t\bar{u}\gamma$ coupling)

Not reviewed, for internal circulation only

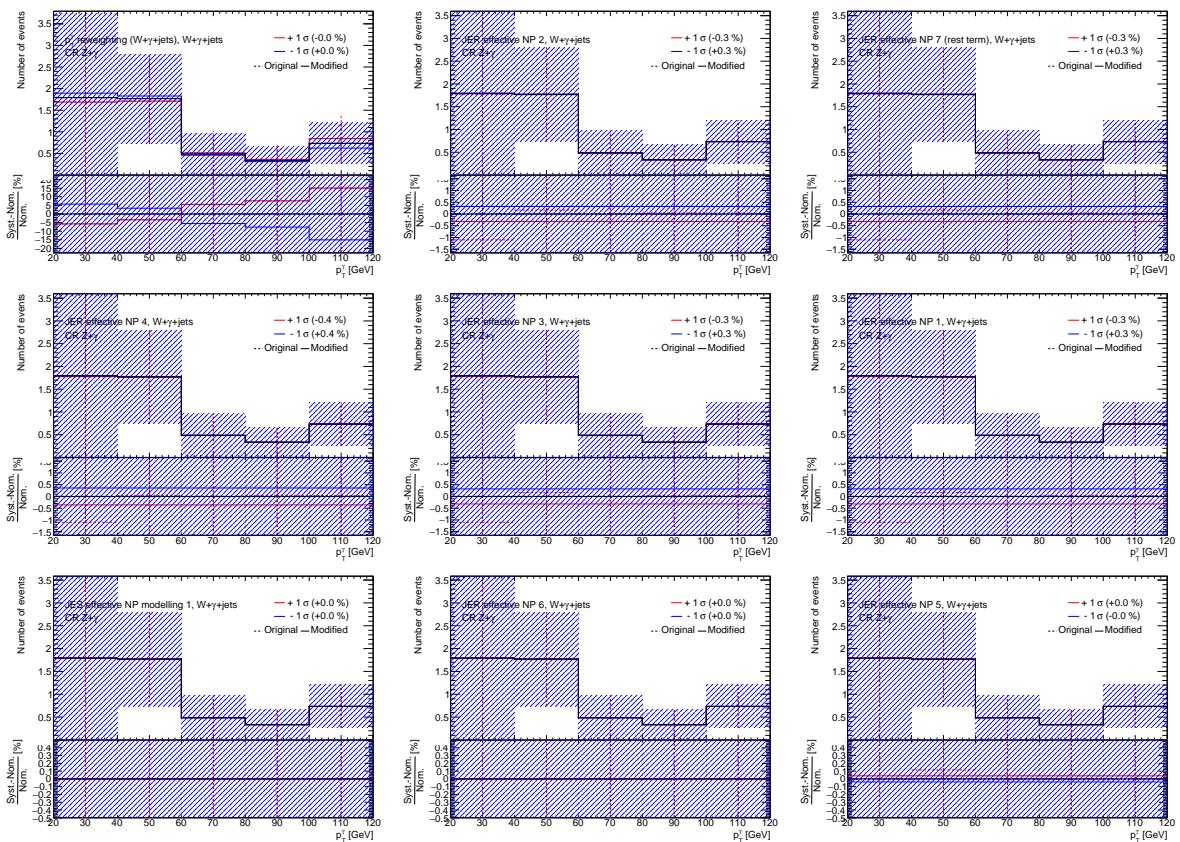


Figure 176: Plots showing the impact of 20 highest ranked systematic uncertainties on $W+\gamma+jets$ for the right-handed $t\bar{u}\gamma$ coupling coupling in the CR $Z+\gamma$ (1).

Not reviewed, for internal circulation only

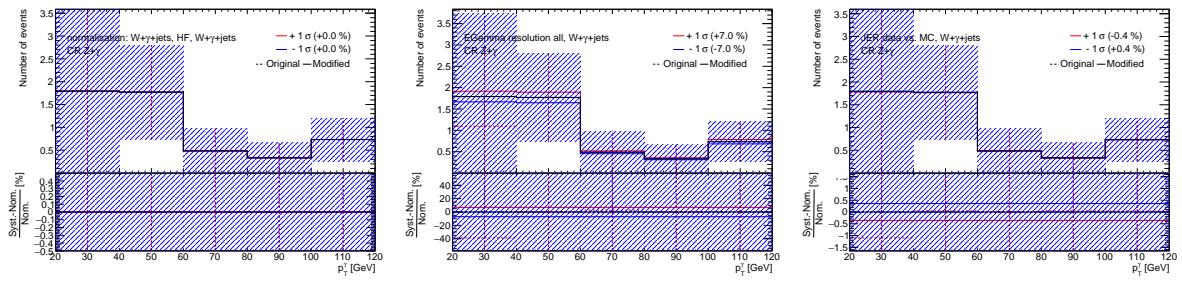


Figure 177: Plots showing the impact of 20 highest ranked systematic uncertainties on $W+\gamma+jets$ for the right-handed $t\bar{u}\gamma$ coupling coupling in the CR $Z+\gamma$ (2).

1799 **O.2.3.6 $Z+\gamma+jets$ (CR $Z+\gamma$, right-handed $t\gamma\gamma$ coupling)**

Not reviewed, for internal circulation only

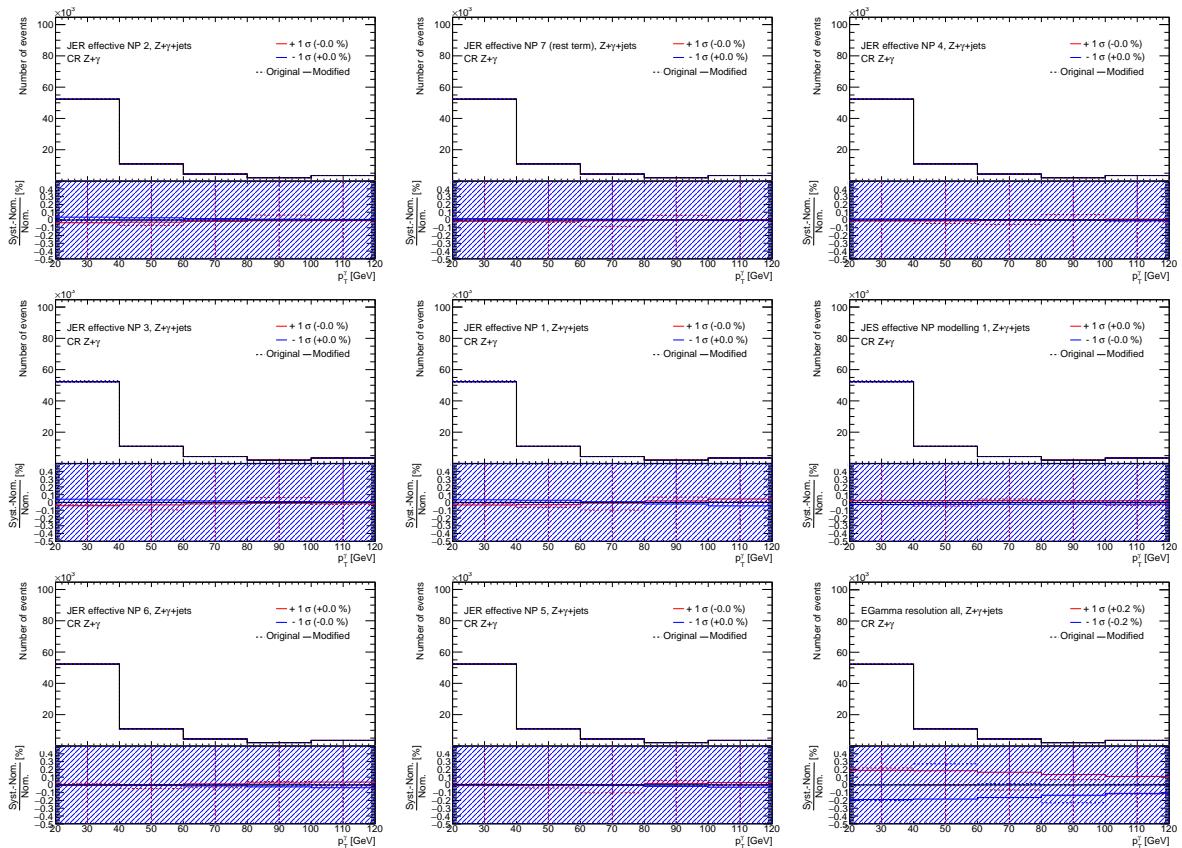


Figure 178: Plots showing the impact of 20 highest ranked systematic uncertainties on $Z+\gamma+jets$ for the right-handed $t\gamma\gamma$ coupling coupling in the CR $Z+\gamma$ (1).

Not reviewed, for internal circulation only

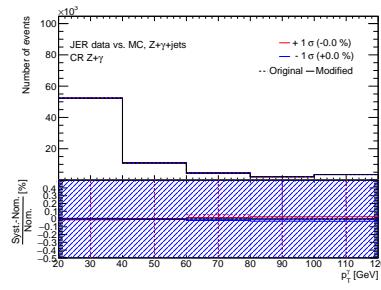


Figure 179: Plots showing the impact of 20 highest ranked systematic uncertainties on $Z+\gamma+jets$ for the right-handed $t\bar{u}\gamma$ coupling coupling in the CR $Z+\gamma$ (2).

1800 0.2.3.7 Other prompt photons (CR Z+ γ , right-handed $t\gamma\gamma$ coupling)

Not reviewed, for internal circulation only

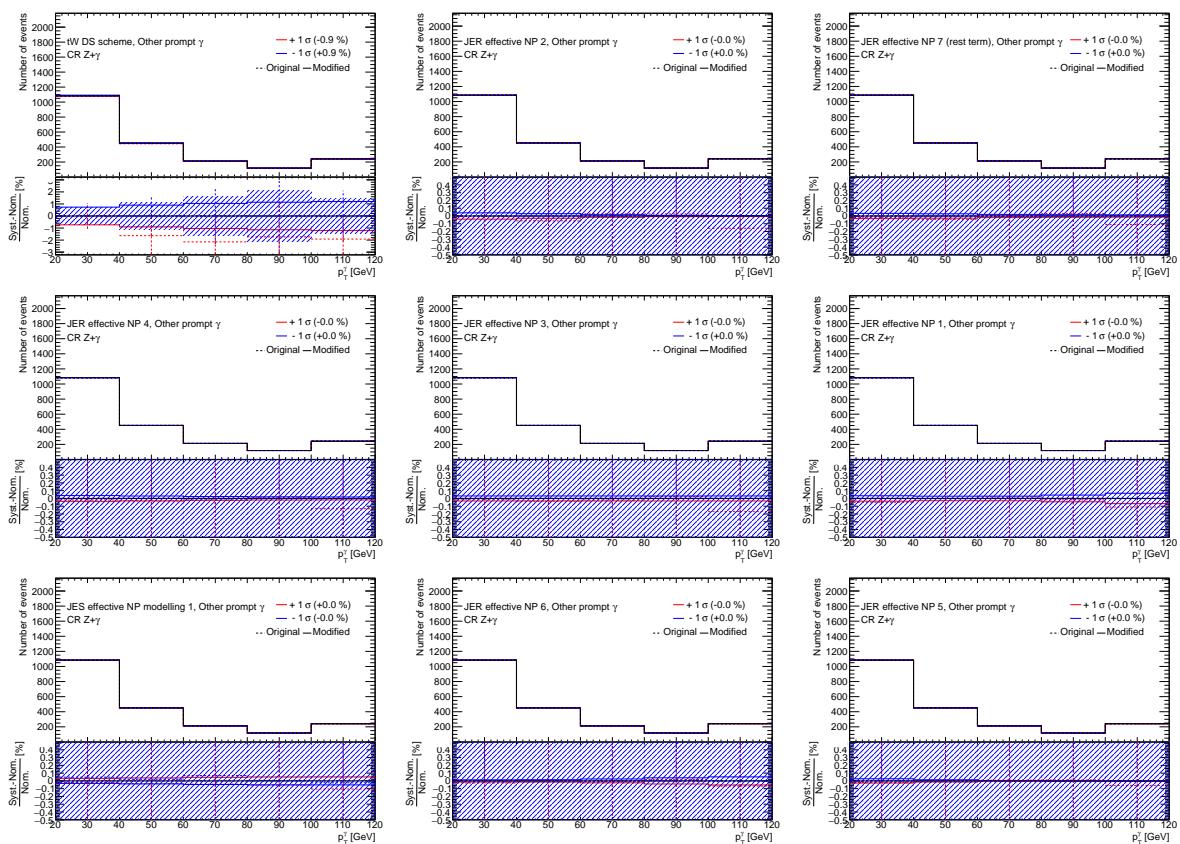


Figure 180: Plots showing the impact of 20 highest ranked systematic uncertainties on *Other prompt photons* for the right-handed $t\gamma\gamma$ coupling coupling in the CR $Z+\gamma$ (1).

Not reviewed, for internal circulation only

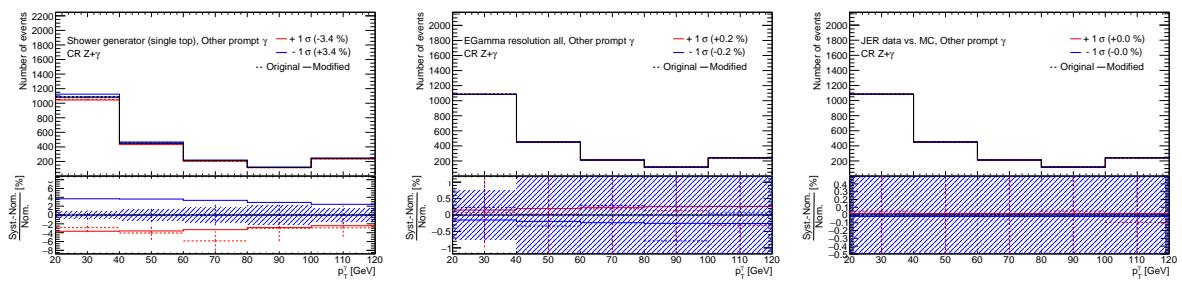


Figure 181: Plots showing the impact of 20 highest ranked systematic uncertainties on *Other prompt photons* for the right-handed $t\bar{u}\gamma$ coupling coupling in the CR $Z+\gamma$ (2).

1801 **O.3 Plots for the left-handed $t\gamma\gamma$ coupling**

1802 **O.3.1 SR (left-handed $t\gamma\gamma$ coupling)**

1803 **O.3.1.1 Total background (SR, left-handed $t\gamma\gamma$ coupling)**

Not reviewed, for internal circulation only

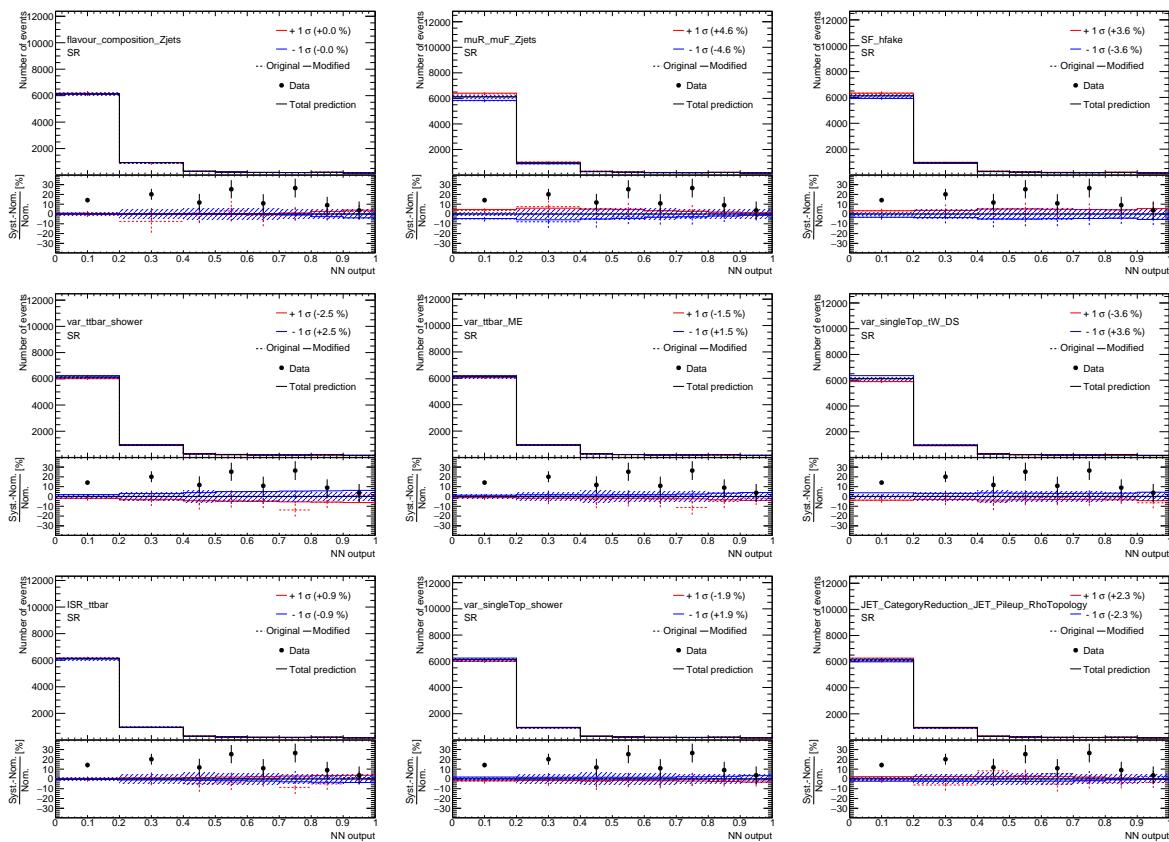


Figure 182: Plots showing the impact of 20 highest ranked systematic uncertainties on *Total background* for the left-handed $t\gamma\gamma$ coupling coupling in the SR (1).

Not reviewed, for internal circulation only

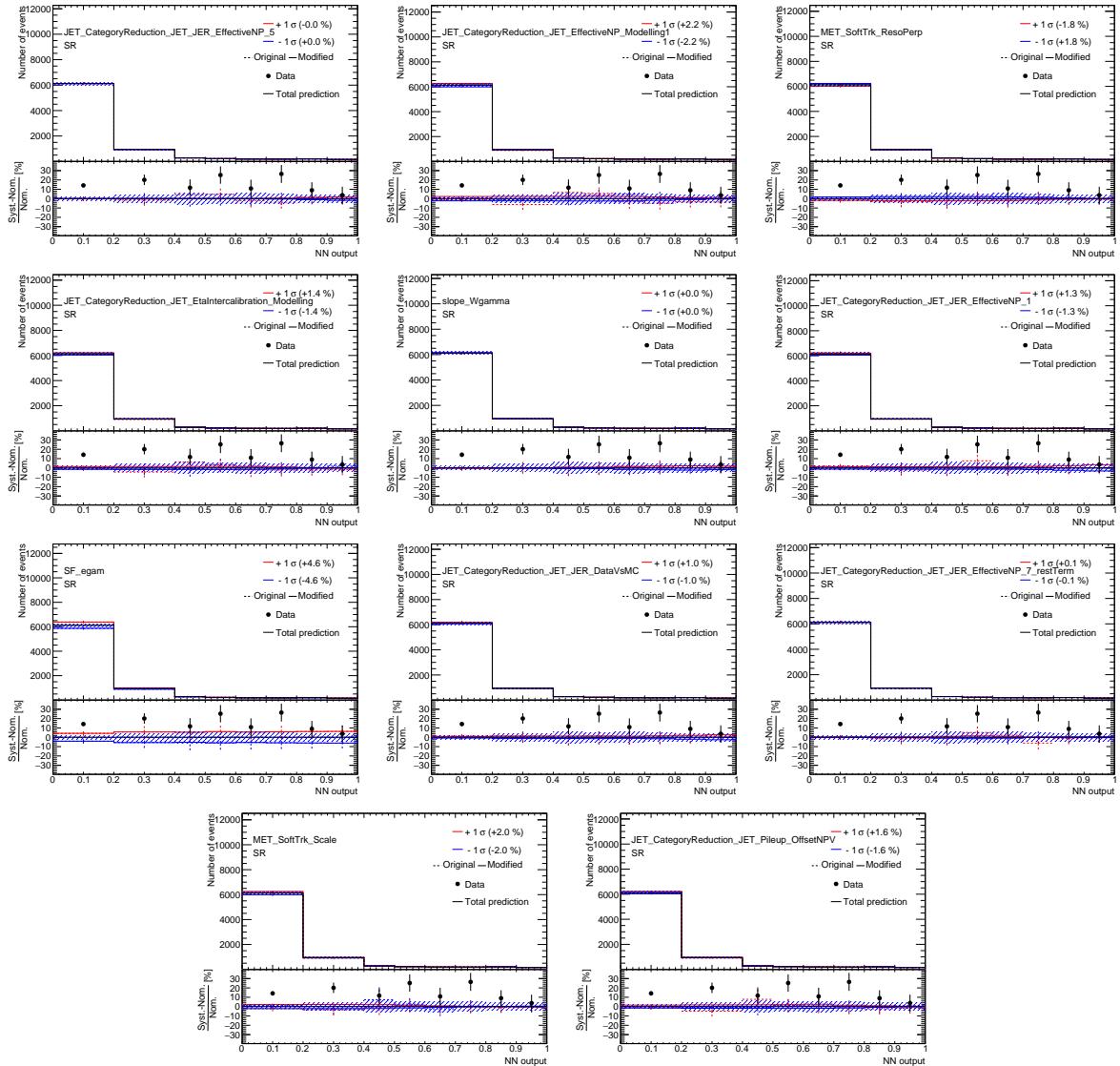


Figure 183: Plots showing the impact of 20 highest ranked systematic uncertainties on *Total background* for the left-handed $t\gamma\gamma$ coupling coupling in the SR (2).

1804 O.3.1.2 Signal (SR, left-handed $t\gamma\gamma$ coupling)

Not reviewed, for internal circulation only

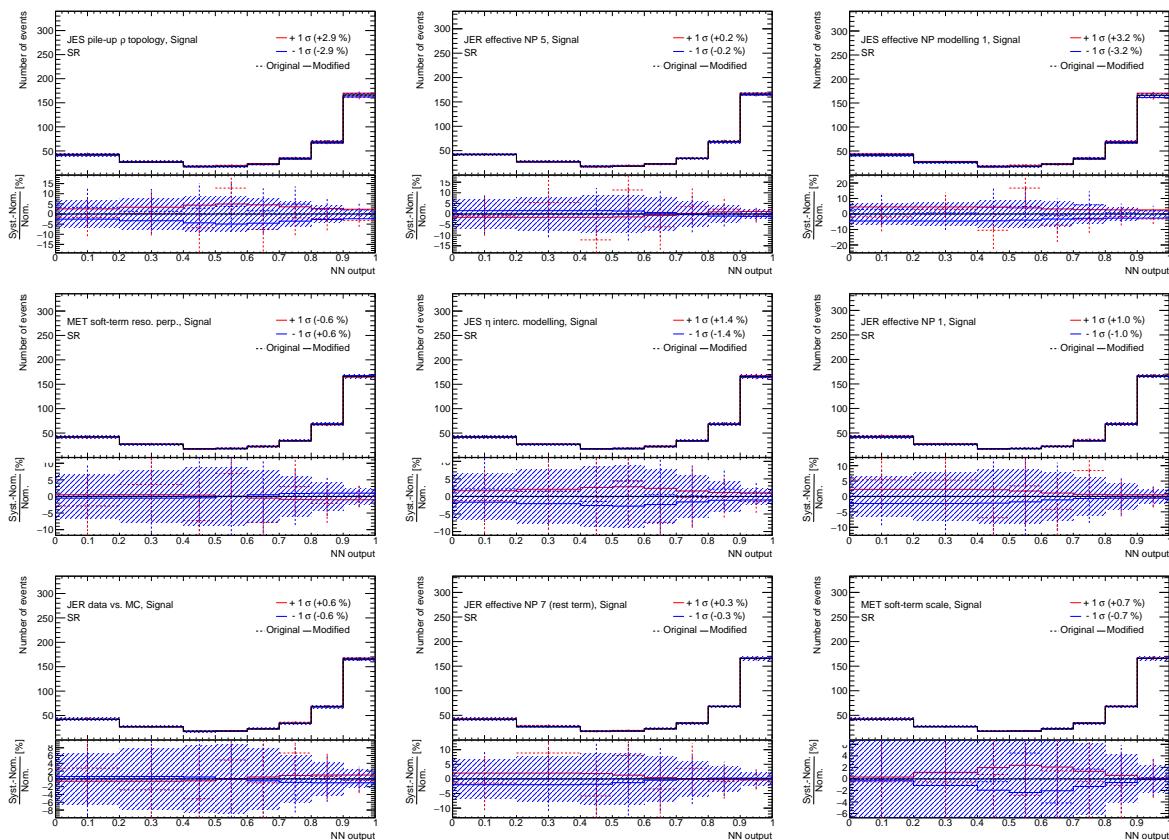


Figure 184: Plots showing the impact of 20 highest ranked systematic uncertainties on *Signal* for the left-handed $t\gamma\gamma$ coupling coupling in the SR (1).

[Not reviewed, for internal circulation only]

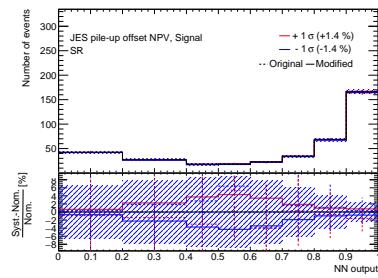


Figure 185: Plots showing the impact of 20 highest ranked systematic uncertainties on *Signal* for the left-handed $tc\gamma$ coupling coupling in the SR (2).

1805 O.3.1.3 $e \rightarrow \gamma$ fakes (SR, left-handed $t\gamma\gamma$ coupling)

Not reviewed, for internal circulation only

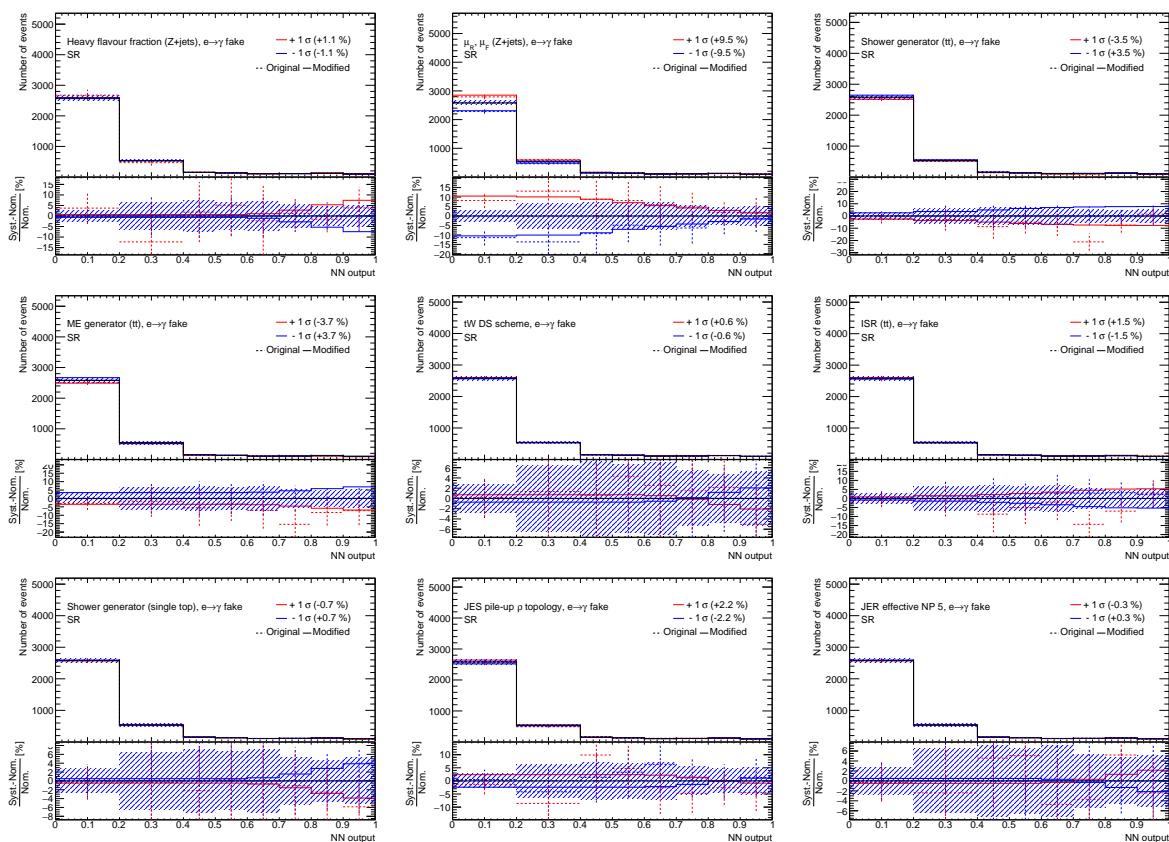


Figure 186: Plots showing the impact of 20 highest ranked systematic uncertainties on $e \rightarrow \gamma$ fakes for the left-handed $t\gamma\gamma$ coupling coupling in the SR (1).

Not reviewed, for internal circulation only

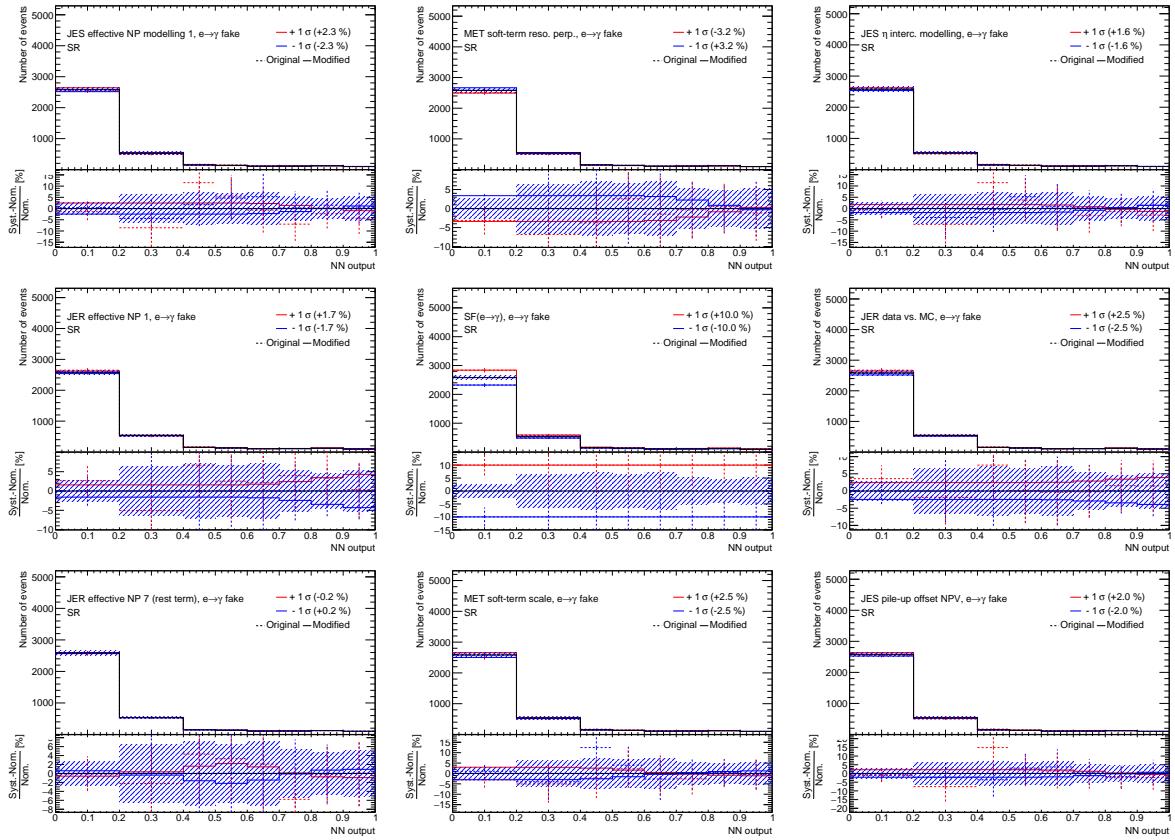


Figure 187: Plots showing the impact of 20 highest ranked systematic uncertainties on $e \rightarrow \gamma$ fakes for the left-handed $tc\gamma$ coupling coupling in the SR (2).

1806 O.3.1.4 $j \rightarrow \gamma$ fakes (SR, left-handed $t\gamma\gamma$ coupling)

Not reviewed, for internal circulation only

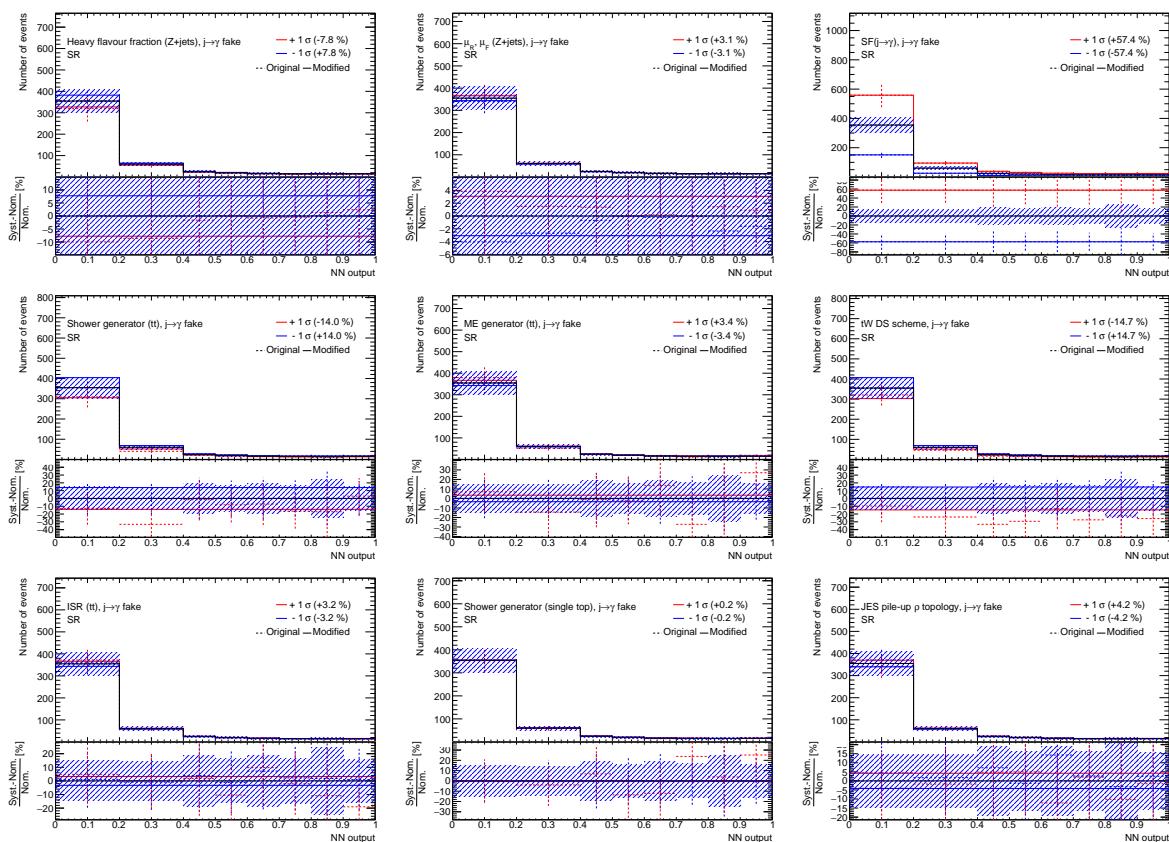


Figure 188: Plots showing the impact of 20 highest ranked systematic uncertainties on $j \rightarrow \gamma$ fakes for the left-handed $t\gamma\gamma$ coupling coupling in the SR (1).

Not reviewed, for internal circulation only

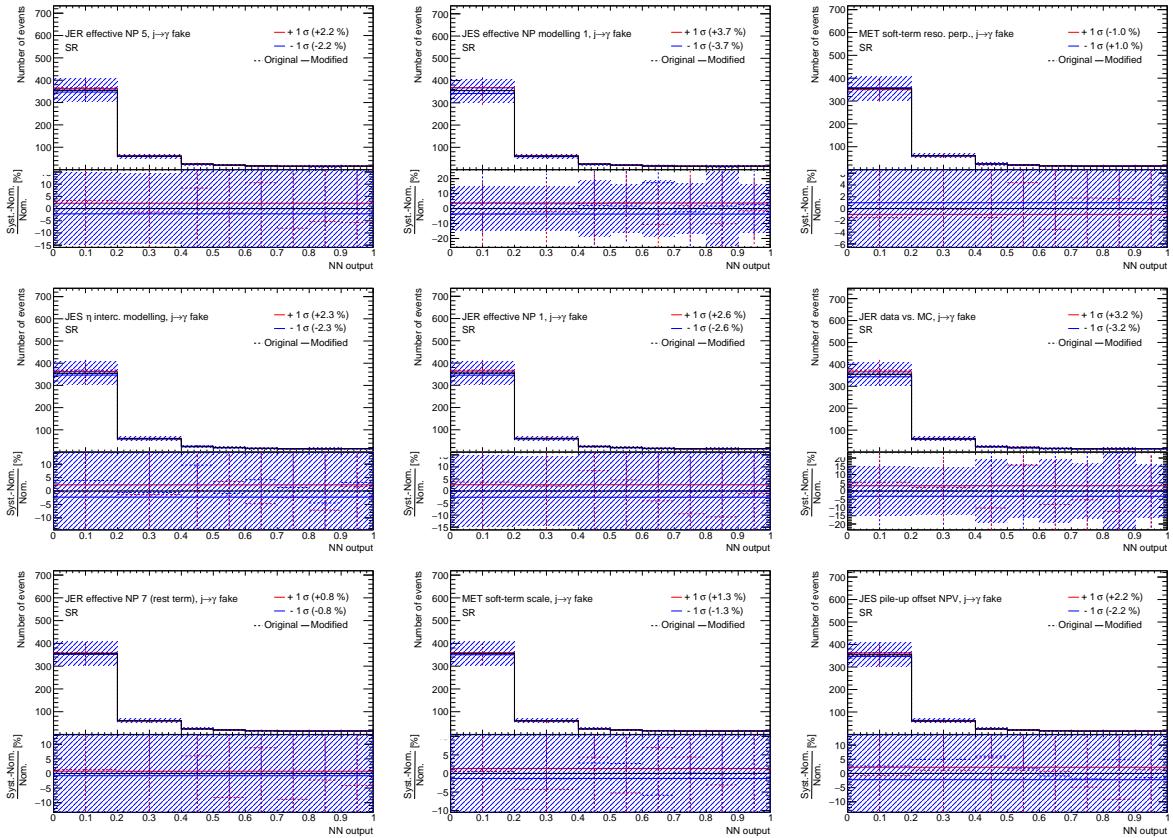


Figure 189: Plots showing the impact of 20 highest ranked systematic uncertainties on $j \rightarrow \gamma$ fakes for the left-handed $tc\gamma$ coupling coupling in the SR (2).

1807 **O.3.1.5 $W+\gamma+jets$ (SR, left-handed $t\bar{c}\gamma$ coupling)**

Not reviewed, for internal circulation only

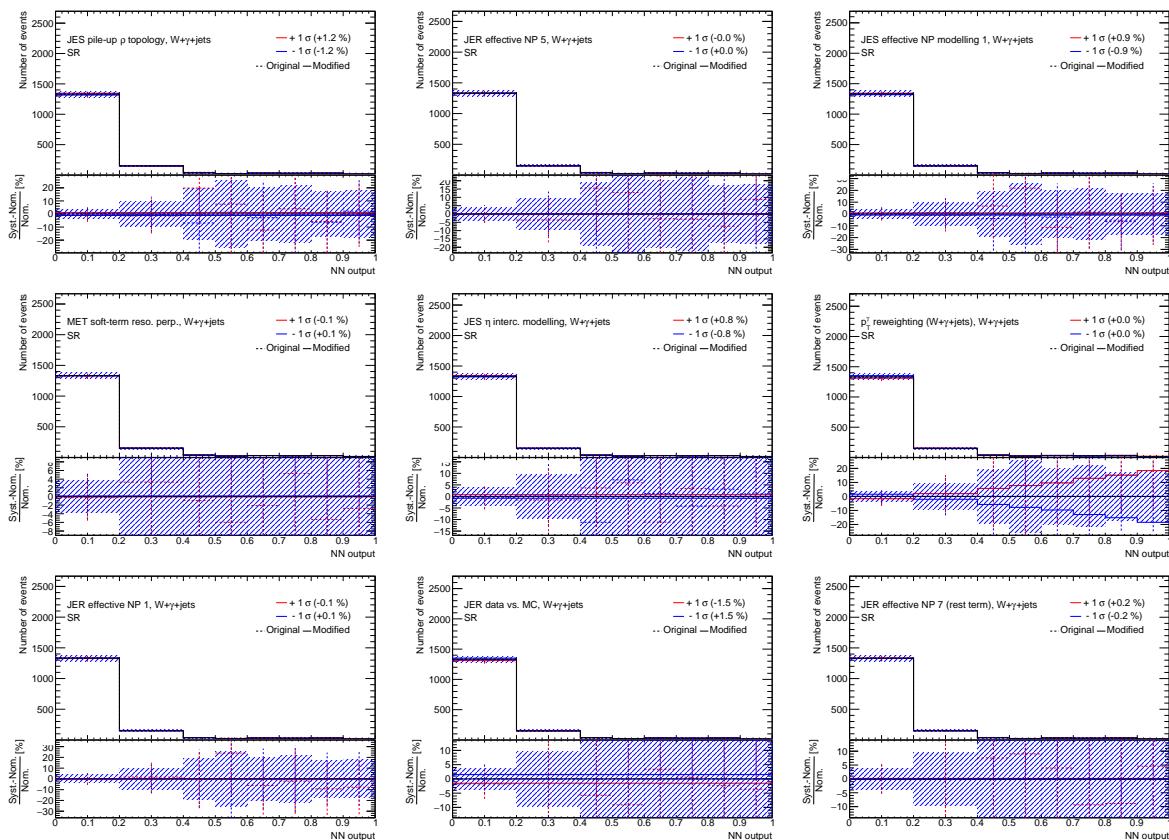


Figure 190: Plots showing the impact of 20 highest ranked systematic uncertainties on $W+\gamma+jets$ for the left-handed $t\bar{c}\gamma$ coupling coupling in the SR (1).

Not reviewed, for internal circulation only

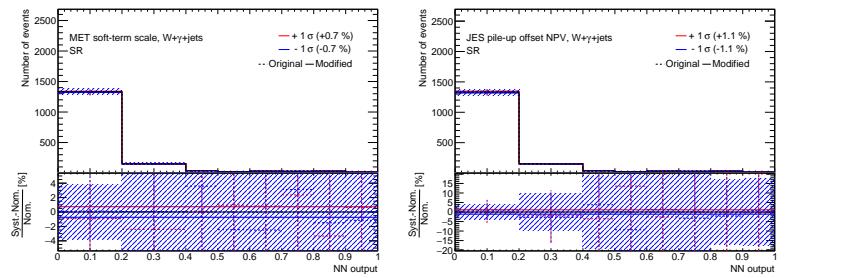


Figure 191: Plots showing the impact of 20 highest ranked systematic uncertainties on $W+\gamma+jets$ for the left-handed $t\gamma\gamma$ coupling coupling in the SR (2).

1808 **O.3.1.6 $Z+\gamma+jets$ (SR, left-handed $t\gamma\gamma$ coupling)**

Not reviewed, for internal circulation only

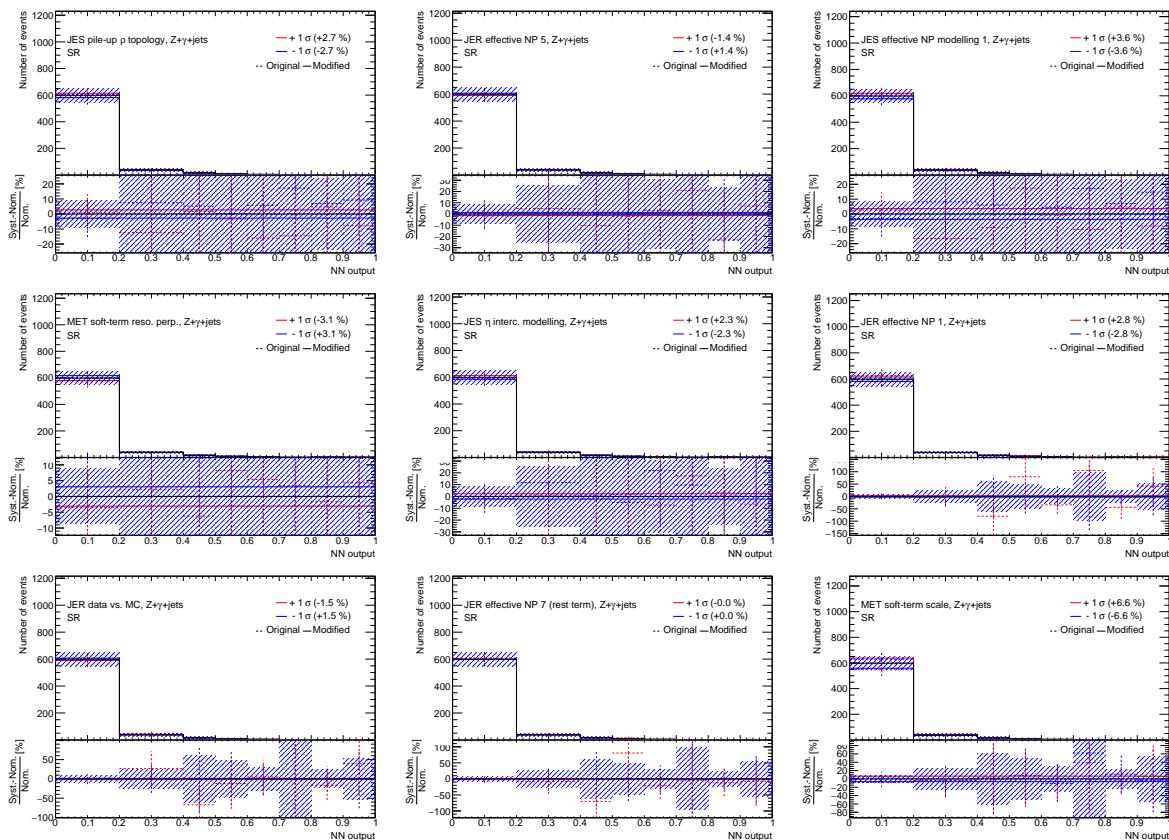


Figure 192: Plots showing the impact of 20 highest ranked systematic uncertainties on $Z+\gamma+jets$ for the left-handed $t\gamma\gamma$ coupling coupling in the SR (1).

Not reviewed, for internal circulation only

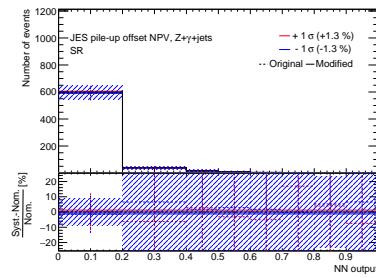


Figure 193: Plots showing the impact of 20 highest ranked systematic uncertainties on $Z+\gamma+jets$ for the left-handed $tc\gamma$ coupling coupling in the SR (2).

1809 0.3.1.7 Other prompt photons (SR, left-handed $t\gamma\gamma$ coupling)

Not reviewed, for internal circulation only

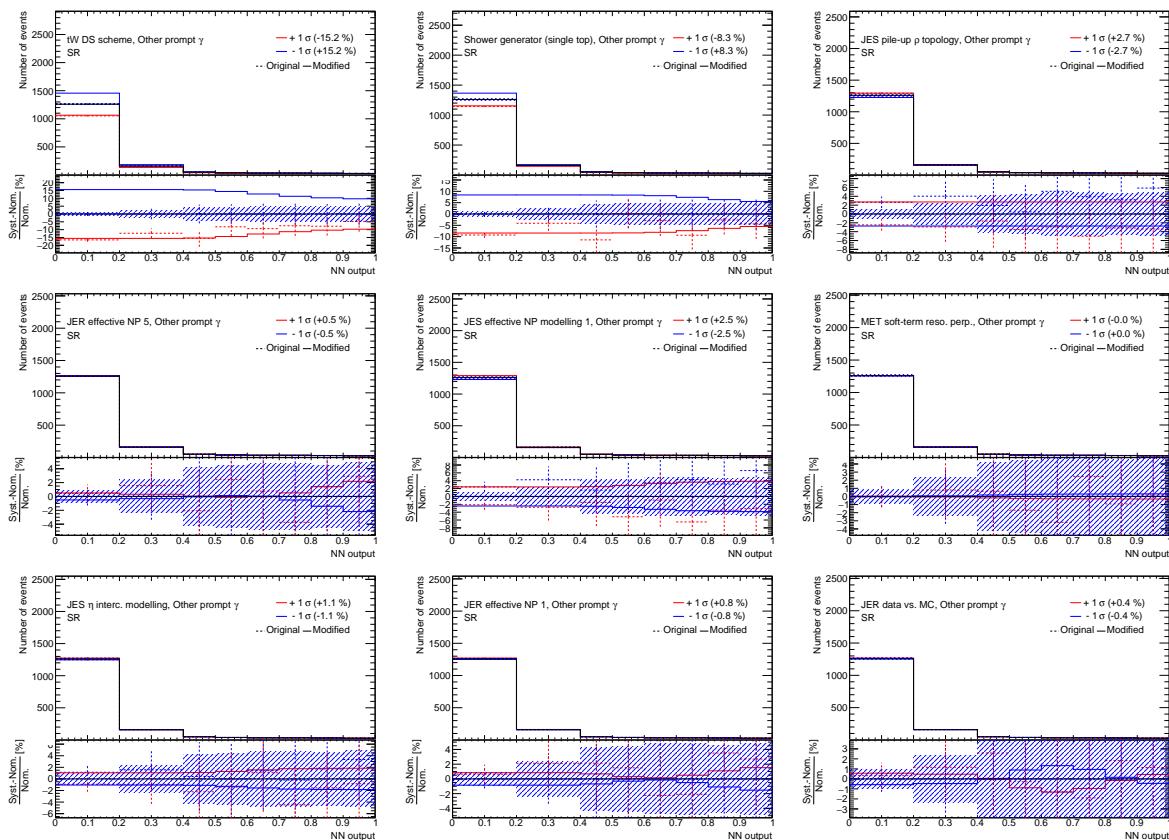


Figure 194: Plots showing the impact of 20 highest ranked systematic uncertainties on *Other prompt photons* for the left-handed $t\gamma\gamma$ coupling coupling in the SR (1).

Not reviewed, for internal circulation only

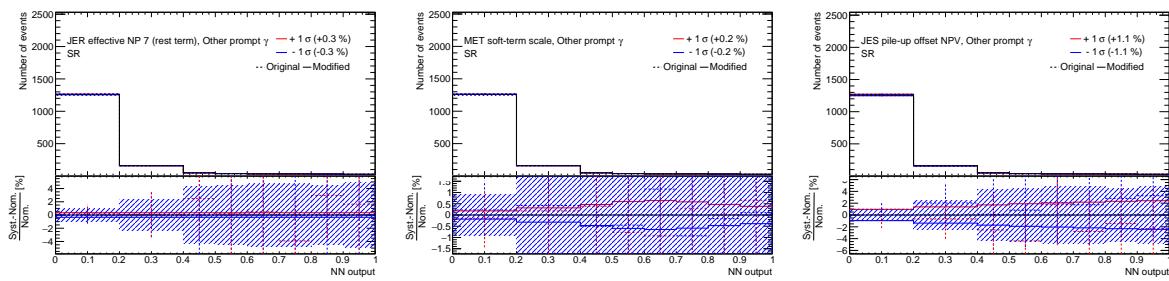


Figure 195: Plots showing the impact of 20 highest ranked systematic uncertainties on *Other prompt photons* for the left-handed $t\gamma$ coupling coupling in the SR (2).

1810 **O.3.2 CR $W+\gamma+$ jets (left-handed $t\gamma$ coupling)**

1811 **O.3.2.1 Total background (CR $W+\gamma+$ jets, left-handed $t\gamma$ coupling)**

Not reviewed, for internal circulation only

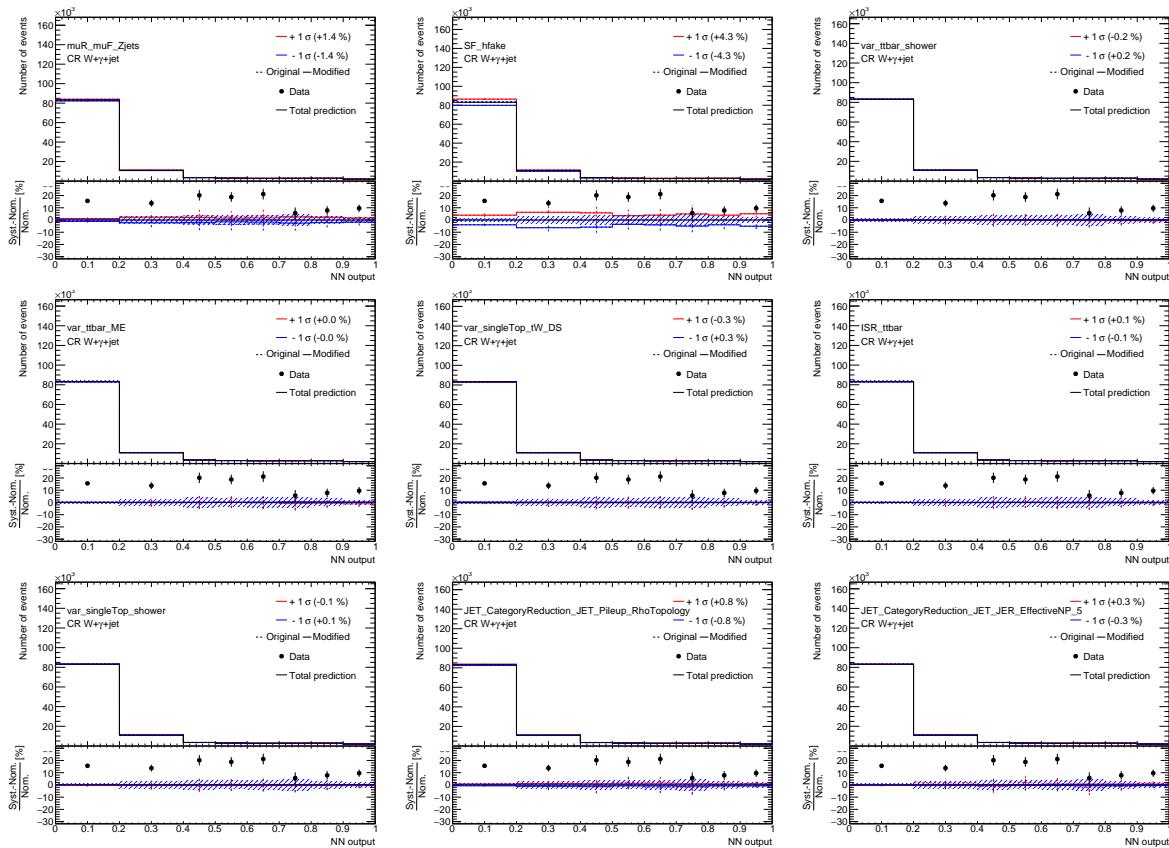


Figure 196: Plots showing the impact of 20 highest ranked systematic uncertainties on *Total background* for the left-handed $t\gamma$ coupling coupling in the CR $W+\gamma+$ jets (1).

Not reviewed, for internal circulation only

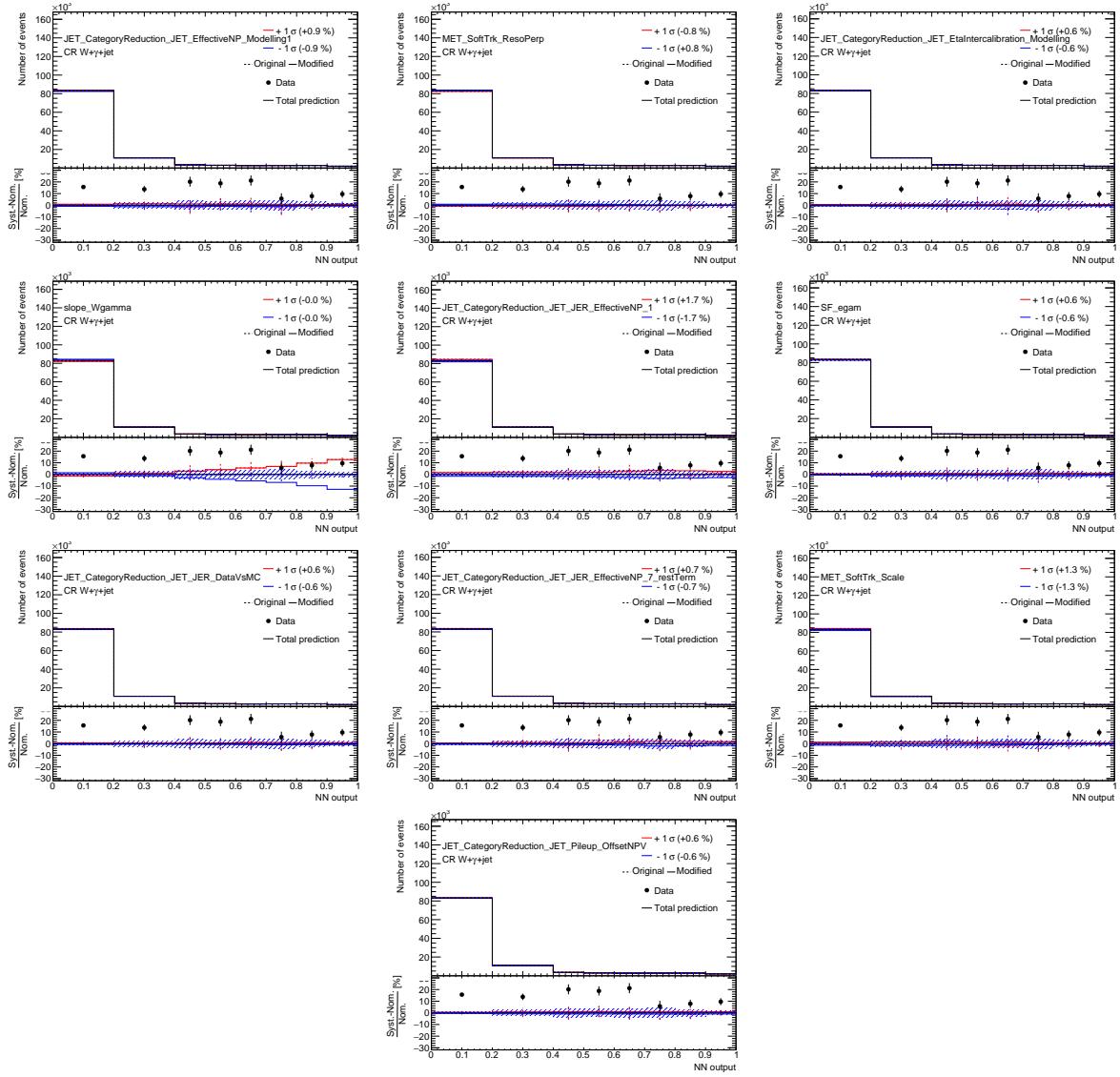


Figure 197: Plots showing the impact of 20 highest ranked systematic uncertainties on *Total background* for the left-handed $t\gamma\gamma$ coupling coupling in the CR $W+\gamma+jets$ (2).

1812 O.3.2.2 Signal (CR $W+\gamma+$ jets, left-handed $t\gamma\gamma$ coupling)

Not reviewed, for internal circulation only

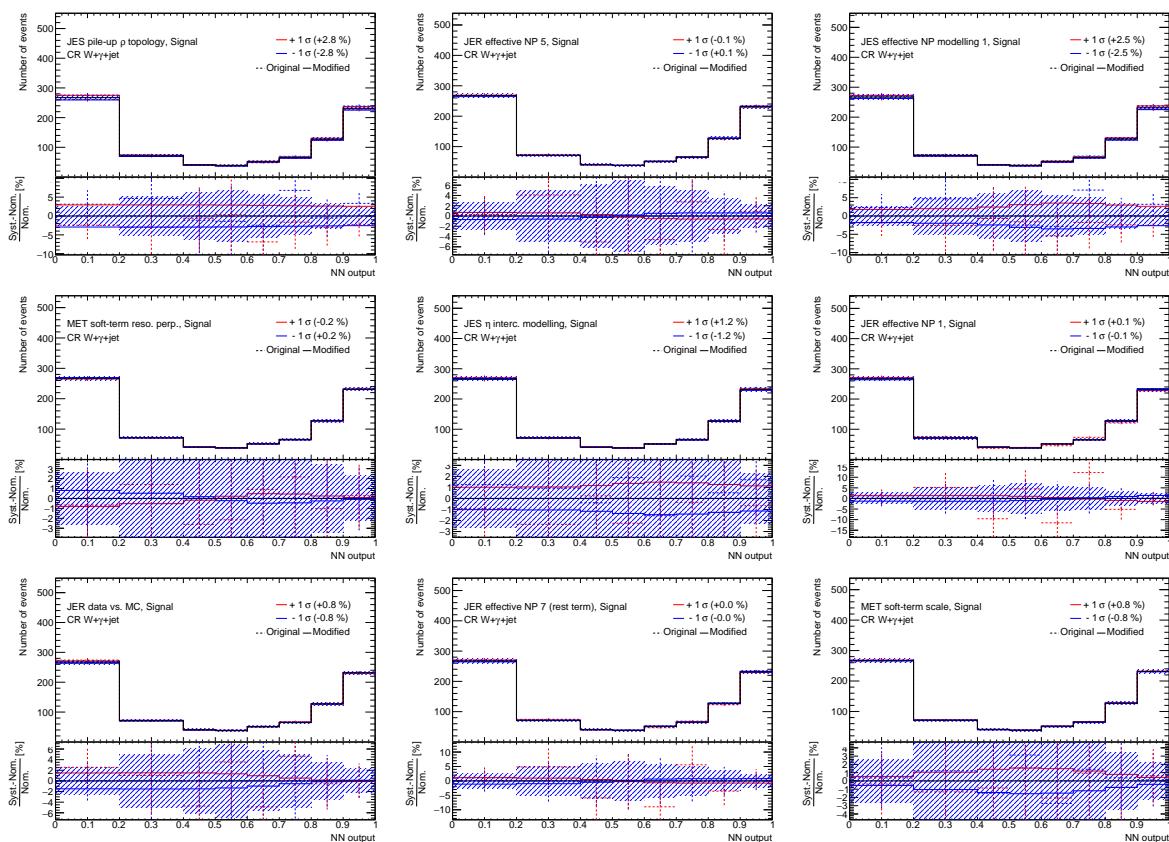


Figure 198: Plots showing the impact of 20 highest ranked systematic uncertainties on *Signal* for the left-handed $t\gamma\gamma$ coupling coupling in the CR $W+\gamma+$ jets (1).

Not reviewed, for internal circulation only

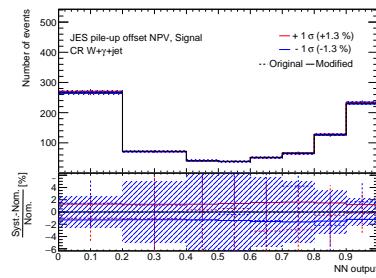


Figure 199: Plots showing the impact of 20 highest ranked systematic uncertainties on *Signal* for the left-handed $t\gamma\gamma$ coupling coupling in the CR $W+\gamma+\text{jets}$ (2).

1813 **O.3.2.3 $e \rightarrow \gamma$ fakes (CR $W+\gamma+\text{jets}$, left-handed $t\gamma\gamma$ coupling)**

Not reviewed, for internal circulation only

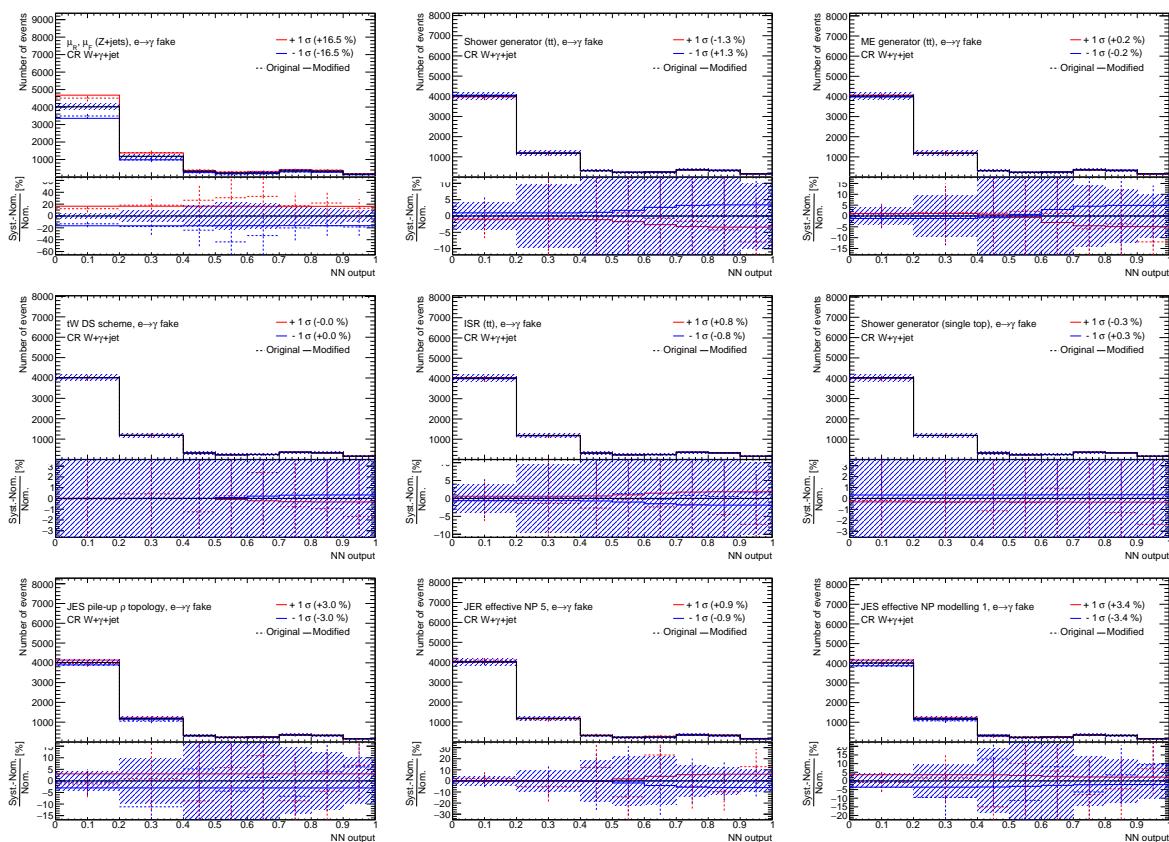


Figure 200: Plots showing the impact of 20 highest ranked systematic uncertainties on $e \rightarrow \gamma$ fakes for the left-handed $t\gamma\gamma$ coupling coupling in the CR $W+\gamma+\text{jets}$ (1).

Not reviewed, for internal circulation only

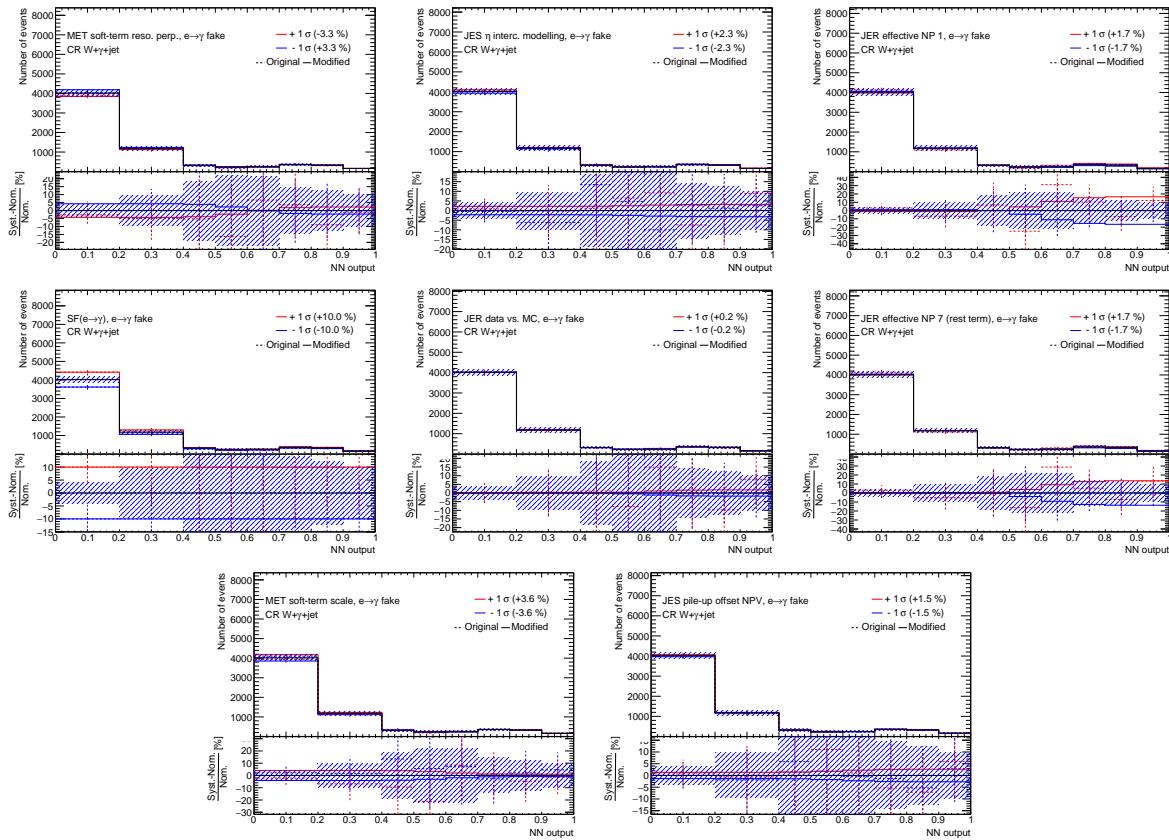


Figure 201: Plots showing the impact of 20 highest ranked systematic uncertainties on $e \rightarrow \gamma$ fakes for the left-handed $tc\gamma$ coupling coupling in the CR $W+\gamma+jets$ (2).

1814 O.3.2.4 $j \rightarrow \gamma$ fakes (CR $W+\gamma+\text{jets}$, left-handed $t\gamma\gamma$ coupling)

Not reviewed, for internal circulation only

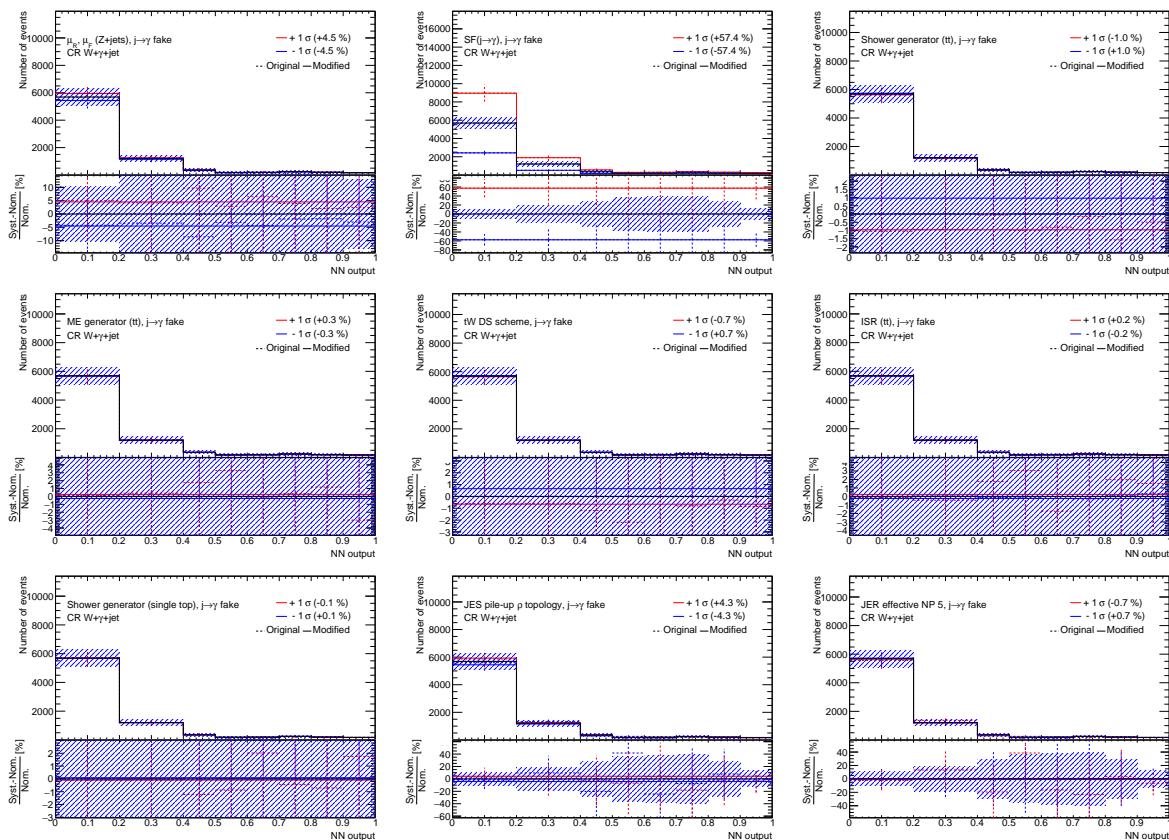


Figure 202: Plots showing the impact of 20 highest ranked systematic uncertainties on $j \rightarrow \gamma$ fakes for the left-handed $t\gamma\gamma$ coupling coupling in the CR $W+\gamma+\text{jets}$ (1).

Not reviewed, for internal circulation only

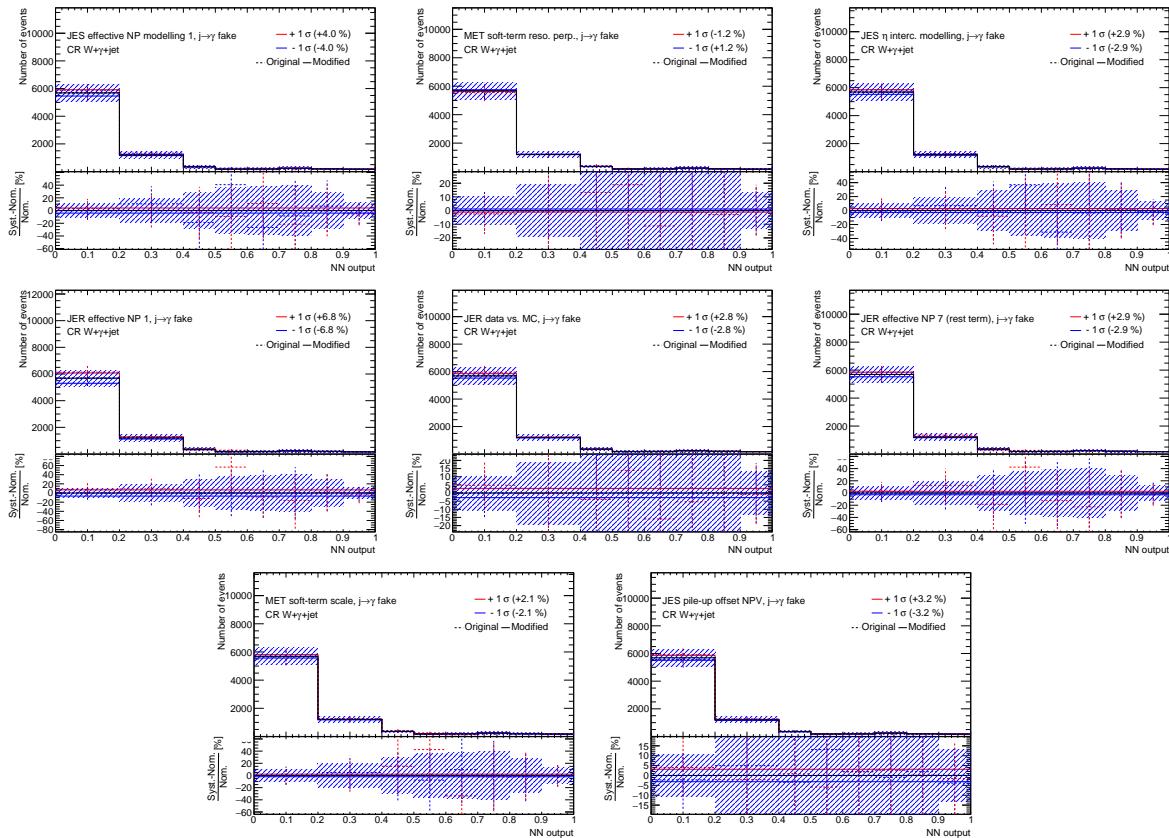


Figure 203: Plots showing the impact of 20 highest ranked systematic uncertainties on $j \rightarrow \gamma$ fakes for the left-handed $tc\gamma$ coupling coupling in the CR $W+\gamma+jets$ (2).

1815 **O.3.2.5 $W+\gamma+jets$ (CR $W+\gamma+jets$, left-handed $t\gamma\gamma$ coupling)**

Not reviewed, for internal circulation only

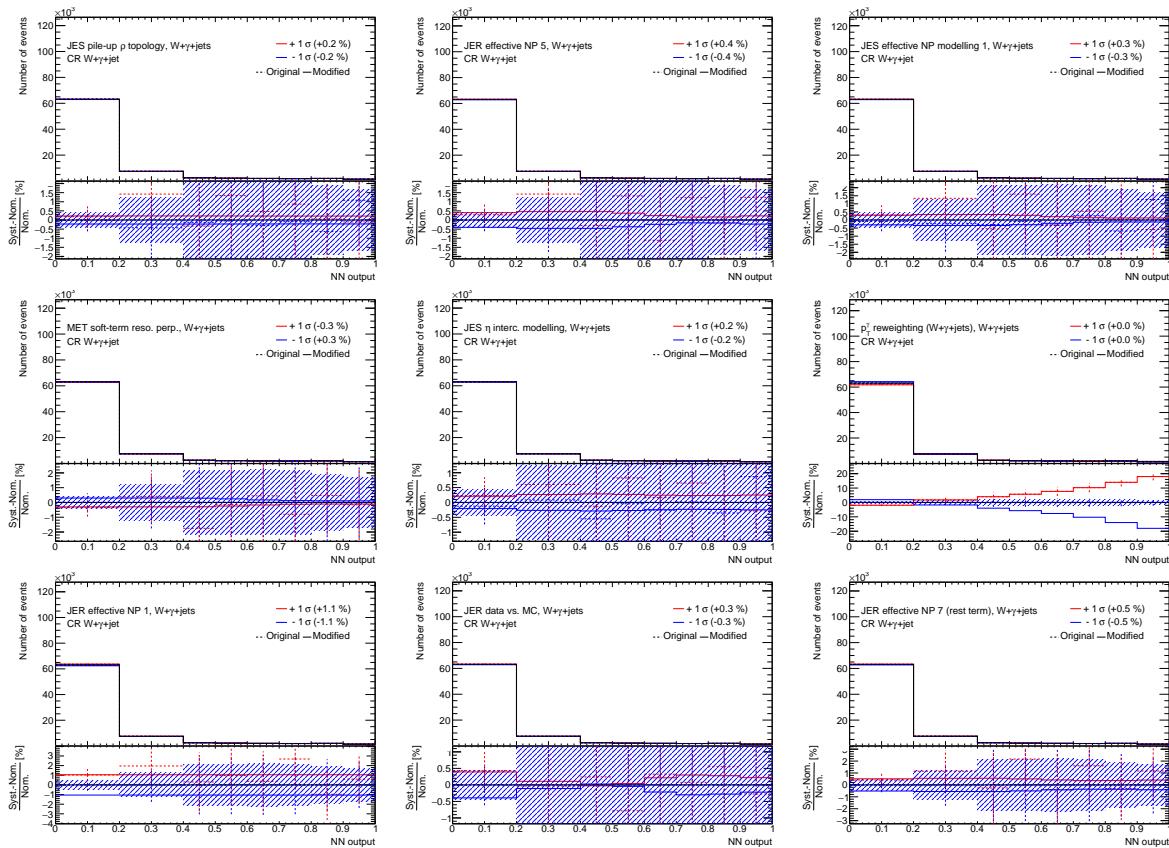


Figure 204: Plots showing the impact of 20 highest ranked systematic uncertainties on $W+\gamma+jets$ for the left-handed $t\gamma\gamma$ coupling coupling in the CR $W+\gamma+jets$ (1).

Not reviewed, for internal circulation only

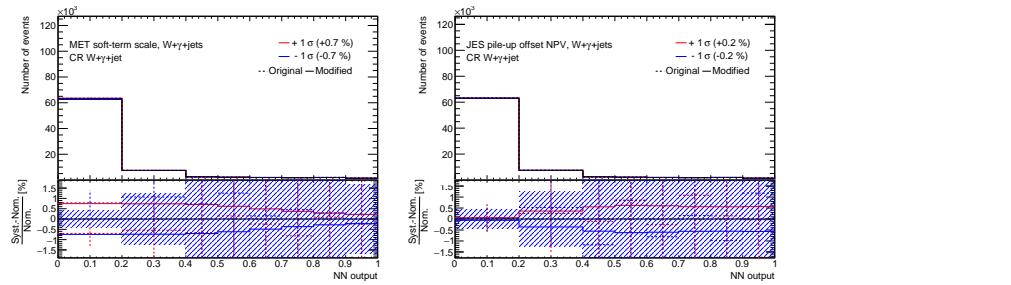


Figure 205: Plots showing the impact of 20 highest ranked systematic uncertainties on $W+\gamma+jets$ for the left-handed $tc\gamma$ coupling coupling in the CR $W+\gamma+jets$ (2).

1816 O.3.2.6 $Z+\gamma+jets$ (CR $W+\gamma+jets$, left-handed $t\gamma\gamma$ coupling)

Not reviewed, for internal circulation only

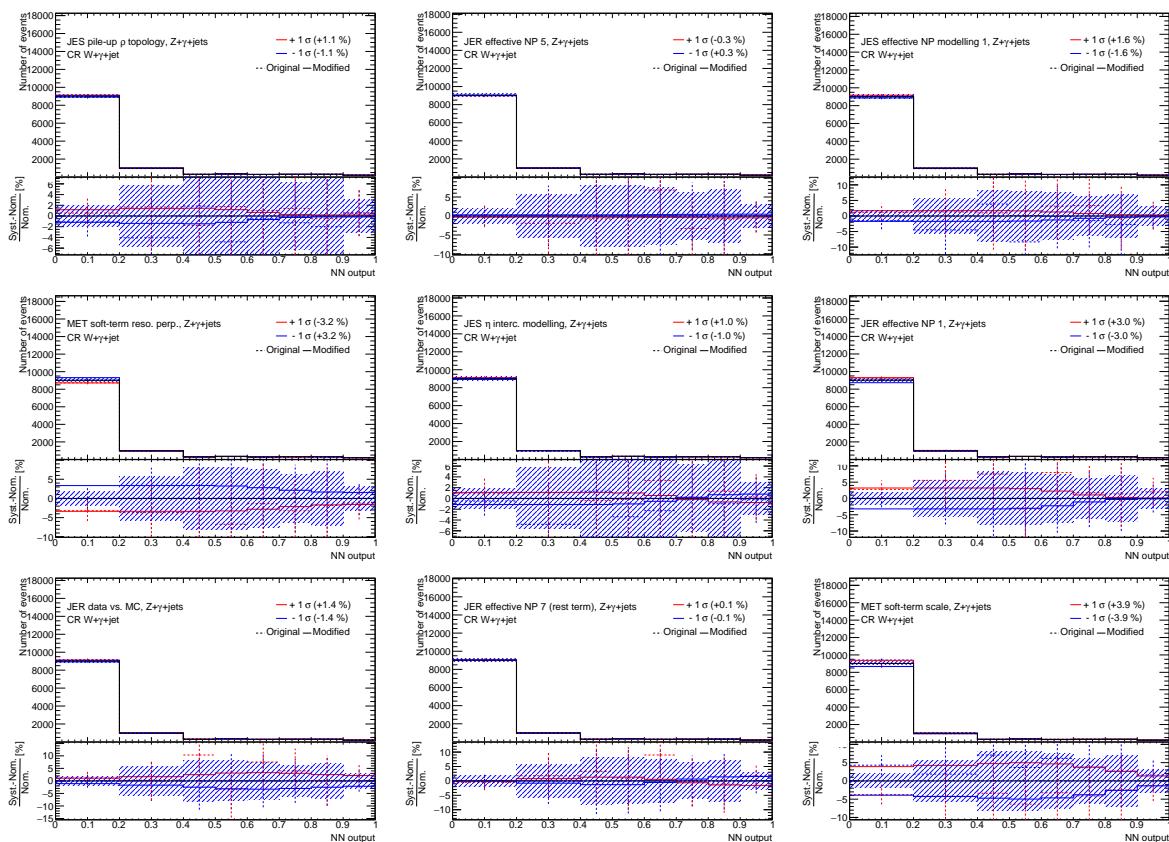


Figure 206: Plots showing the impact of 20 highest ranked systematic uncertainties on $Z+\gamma+jets$ for the left-handed $t\gamma\gamma$ coupling coupling in the CR $W+\gamma+jets$ (1).

Not reviewed, for internal circulation only

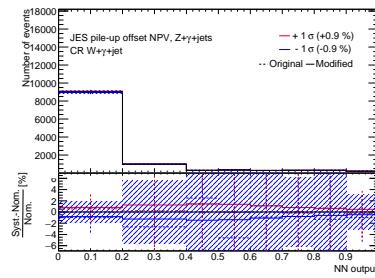


Figure 207: Plots showing the impact of 20 highest ranked systematic uncertainties on $Z+\gamma+jets$ for the left-handed $t\gamma\gamma$ coupling coupling in the CR $W+\gamma+jets$ (2).

1817 0.3.2.7 Other prompt photons (CR $W+\gamma+jets$, left-handed $t\gamma\gamma$ coupling)

Not reviewed, for internal circulation only

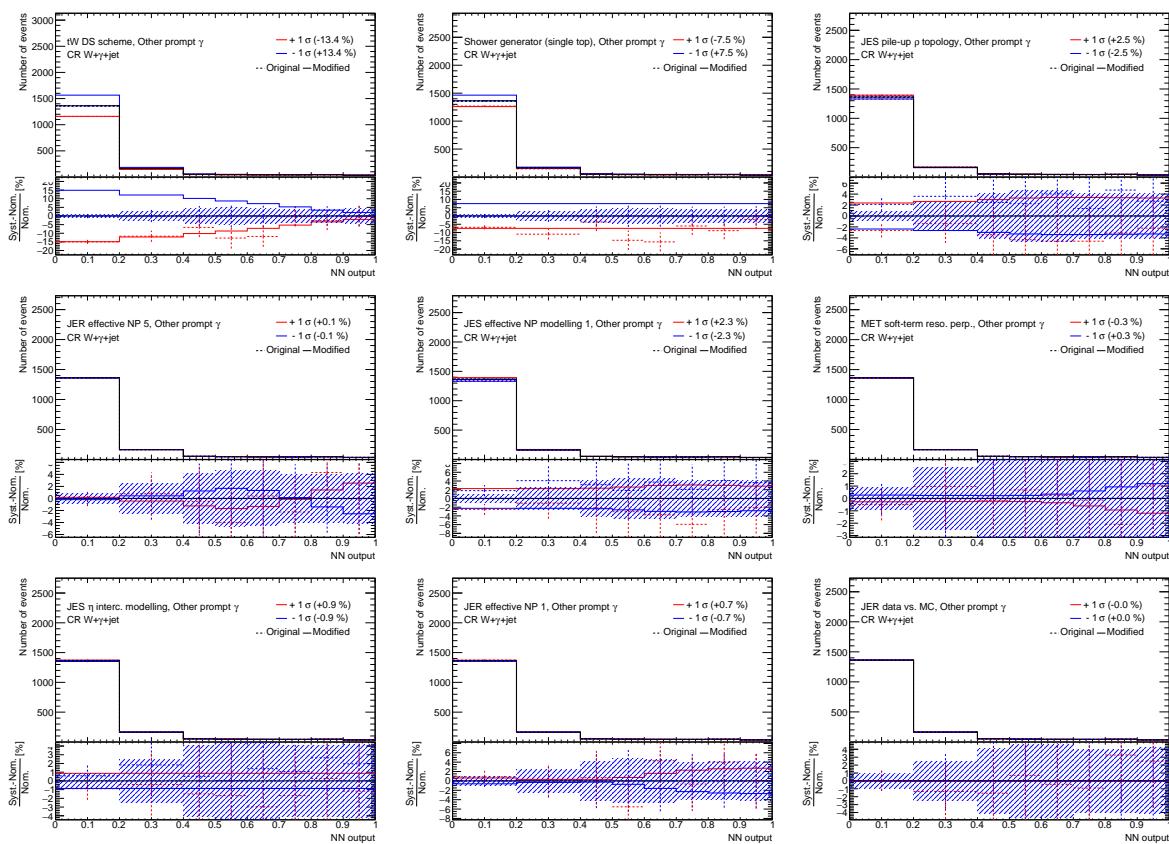


Figure 208: Plots showing the impact of 20 highest ranked systematic uncertainties on *Other prompt photons* for the left-handed $t\gamma\gamma$ coupling coupling in the CR $W+\gamma+jets$ (1).

Not reviewed, for internal circulation only

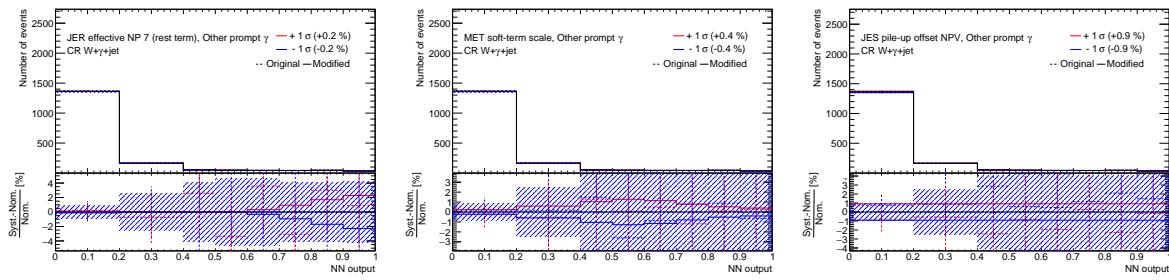


Figure 209: Plots showing the impact of 20 highest ranked systematic uncertainties on *Other prompt photons* for the left-handed $t\bar{c}\gamma$ coupling coupling in the CR $W+\gamma+jets(2)$.

1818 **O.3.3 CR Z+ γ (left-handed $t\gamma\gamma$ coupling)**1819 **O.3.3.1 Total background (CR Z+ γ , left-handed $t\gamma\gamma$ coupling)**

Not reviewed, for internal circulation only

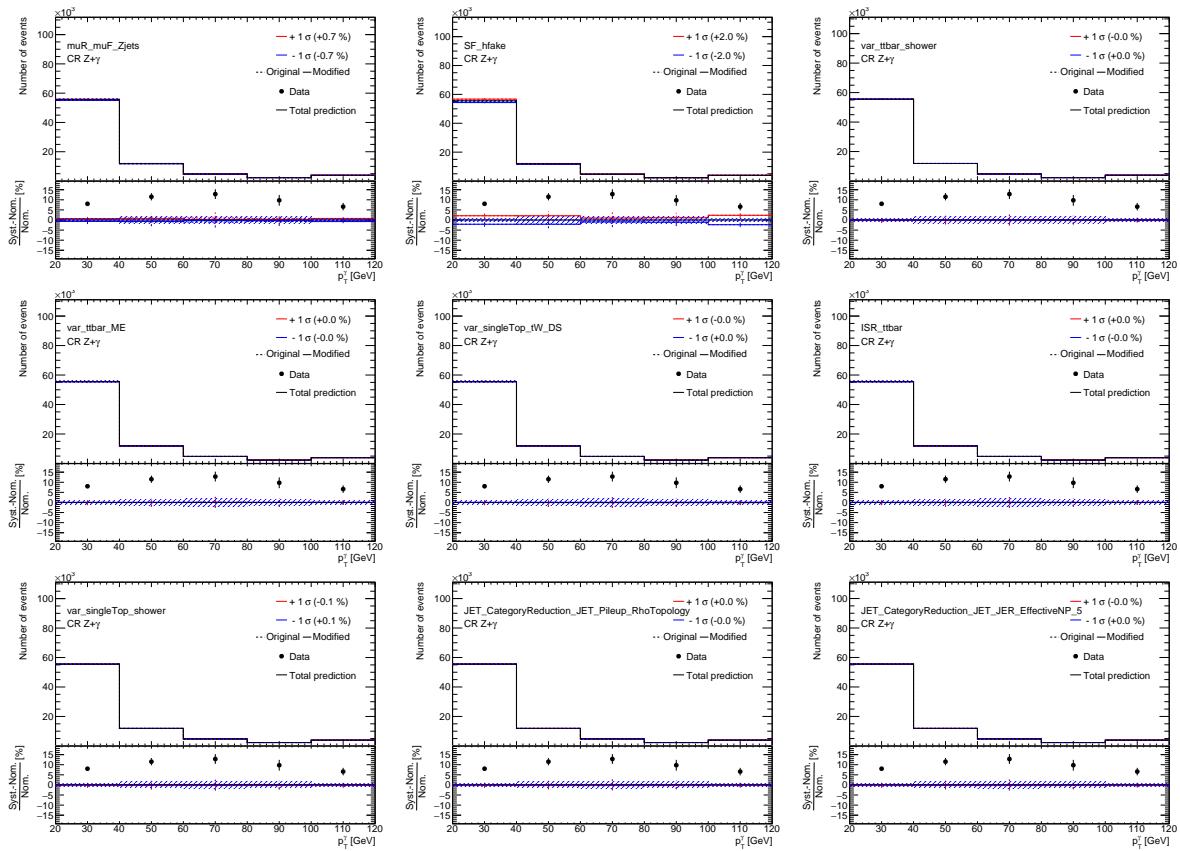


Figure 210: Plots showing the impact of 20 highest ranked systematic uncertainties on *Total background* for the left-handed $t\gamma\gamma$ coupling coupling in the CR $Z+\gamma$ (1).

Not reviewed, for internal circulation only

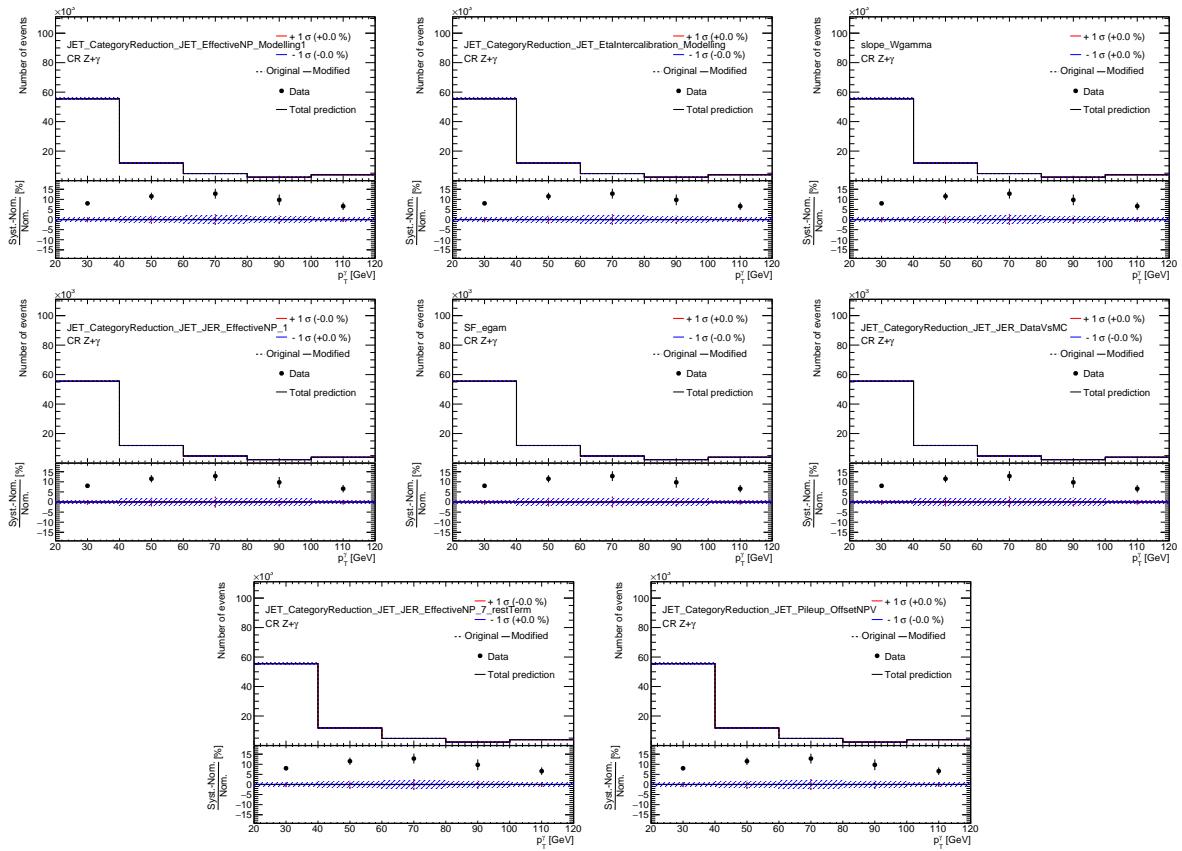


Figure 211: Plots showing the impact of 20 highest ranked systematic uncertainties on *Total background* for the left-handed $t\gamma\gamma$ coupling coupling in the CR $Z + \gamma$ (2).

1820 **O.3.3.2 Signal (CR Z+ γ , left-handed $t\gamma\gamma$ coupling)**

Not reviewed, for internal circulation only

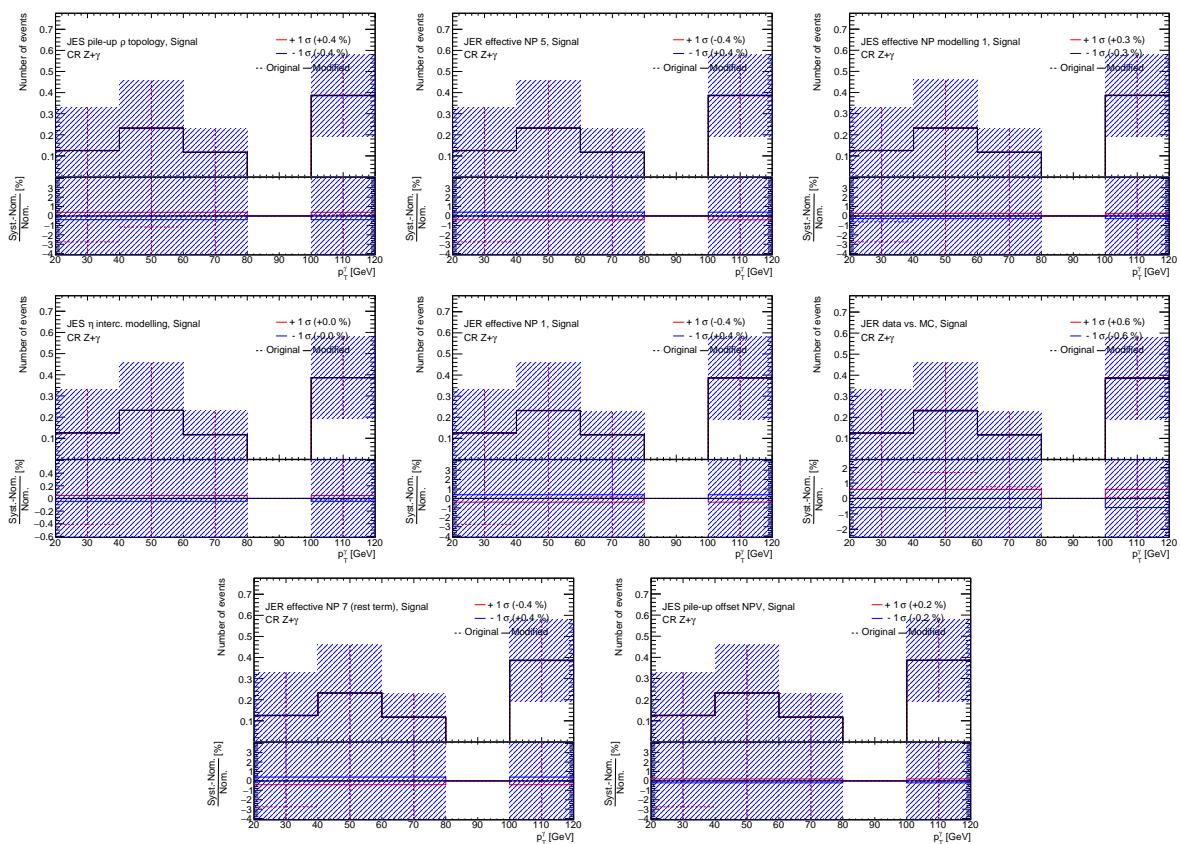


Figure 212: Plots showing the impact of 20 highest ranked systematic uncertainties on *Signal* for the left-handed $t\gamma\gamma$ coupling coupling in the CR $Z+\gamma$ (1).

1821 **O.3.3.3 $e \rightarrow \gamma$ fakes (CR Z+ γ , left-handed $t\gamma\gamma$ coupling)**

Not reviewed, for internal circulation only

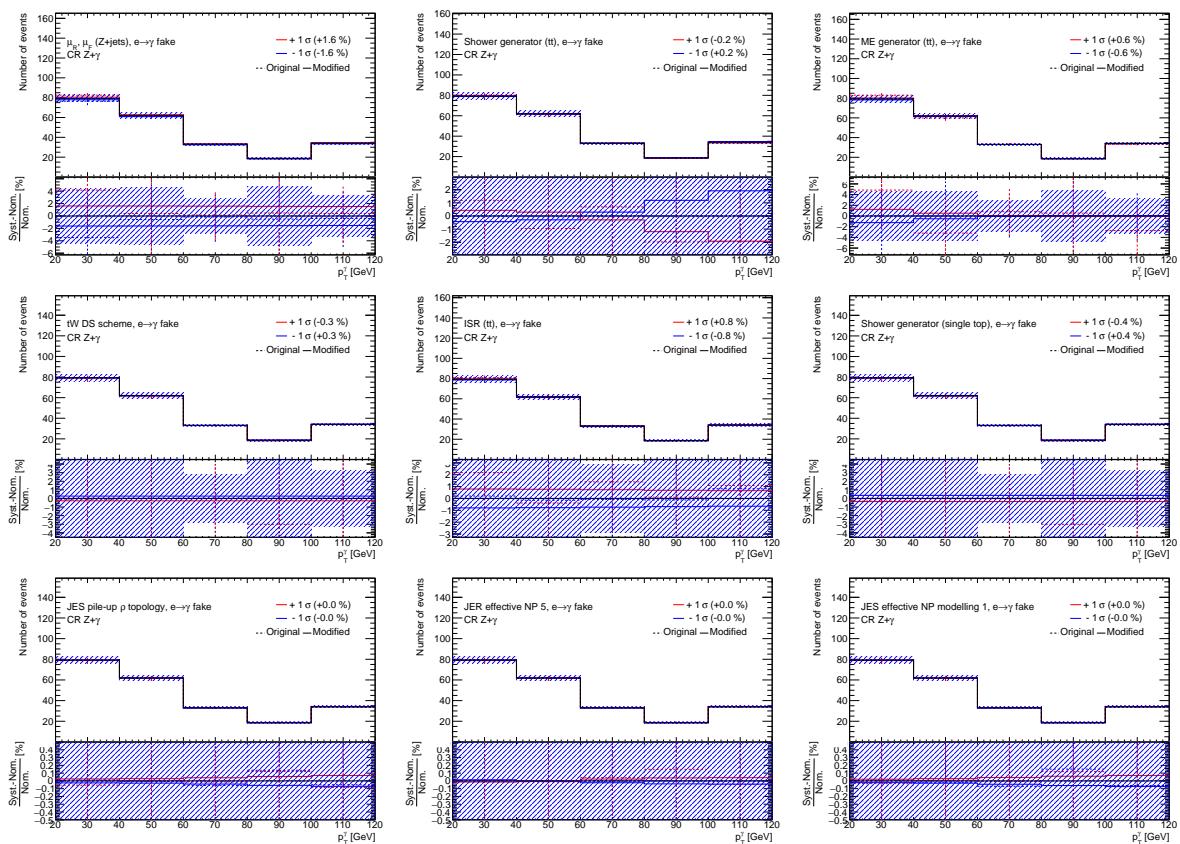


Figure 213: Plots showing the impact of 20 highest ranked systematic uncertainties on $e \rightarrow \gamma$ fakes for the left-handed $t\gamma\gamma$ coupling coupling in the CR Z+ γ (1).

Not reviewed, for internal circulation only

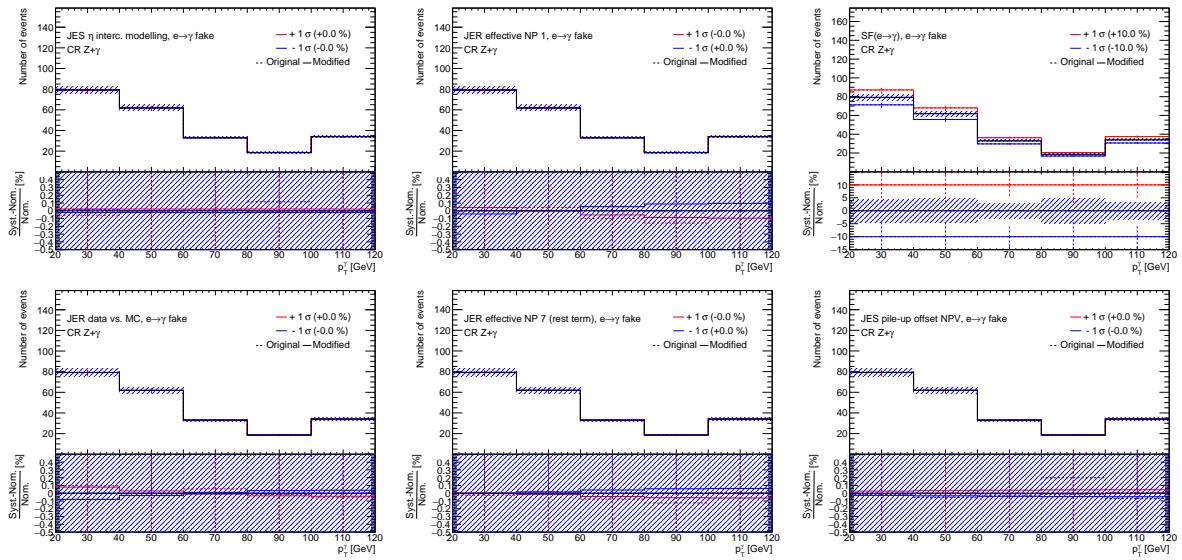


Figure 214: Plots showing the impact of 20 highest ranked systematic uncertainties on $e \rightarrow \gamma$ fakes for the left-handed $tc\gamma$ coupling coupling in the CR $Z+\gamma$ (2).

1822 **O.3.3.4 $j \rightarrow \gamma$ fakes (CR Z+ γ , left-handed $t\gamma\gamma$ coupling)**

Not reviewed, for internal circulation only

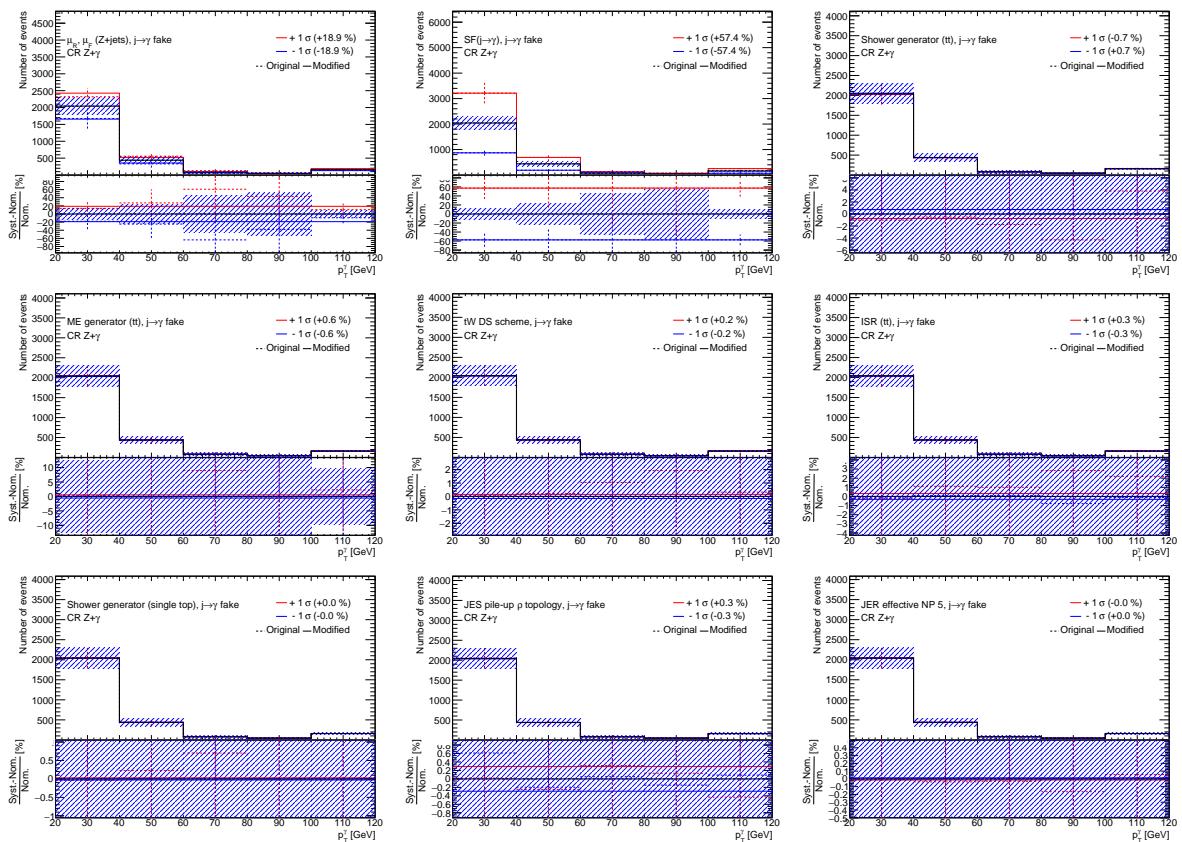


Figure 215: Plots showing the impact of 20 highest ranked systematic uncertainties on $j \rightarrow \gamma$ fakes for the left-handed $t\gamma\gamma$ coupling coupling in the CR Z+ γ (1).

Not reviewed, for internal circulation only

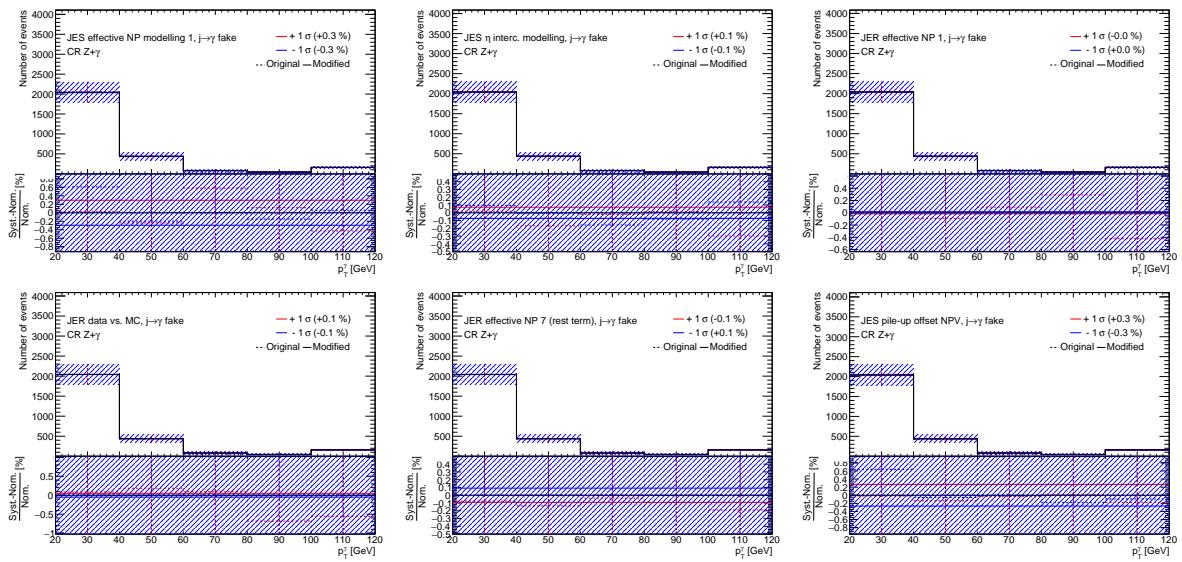


Figure 216: Plots showing the impact of 20 highest ranked systematic uncertainties on $j \rightarrow \gamma$ fakes for the left-handed $tc\gamma$ coupling coupling in the CR $Z+\gamma$ (2).

1823 **O.3.3.5 $W+\gamma+jets$ (CR $Z+\gamma$, left-handed $t\gamma\gamma$ coupling)**

Not reviewed, for internal circulation only

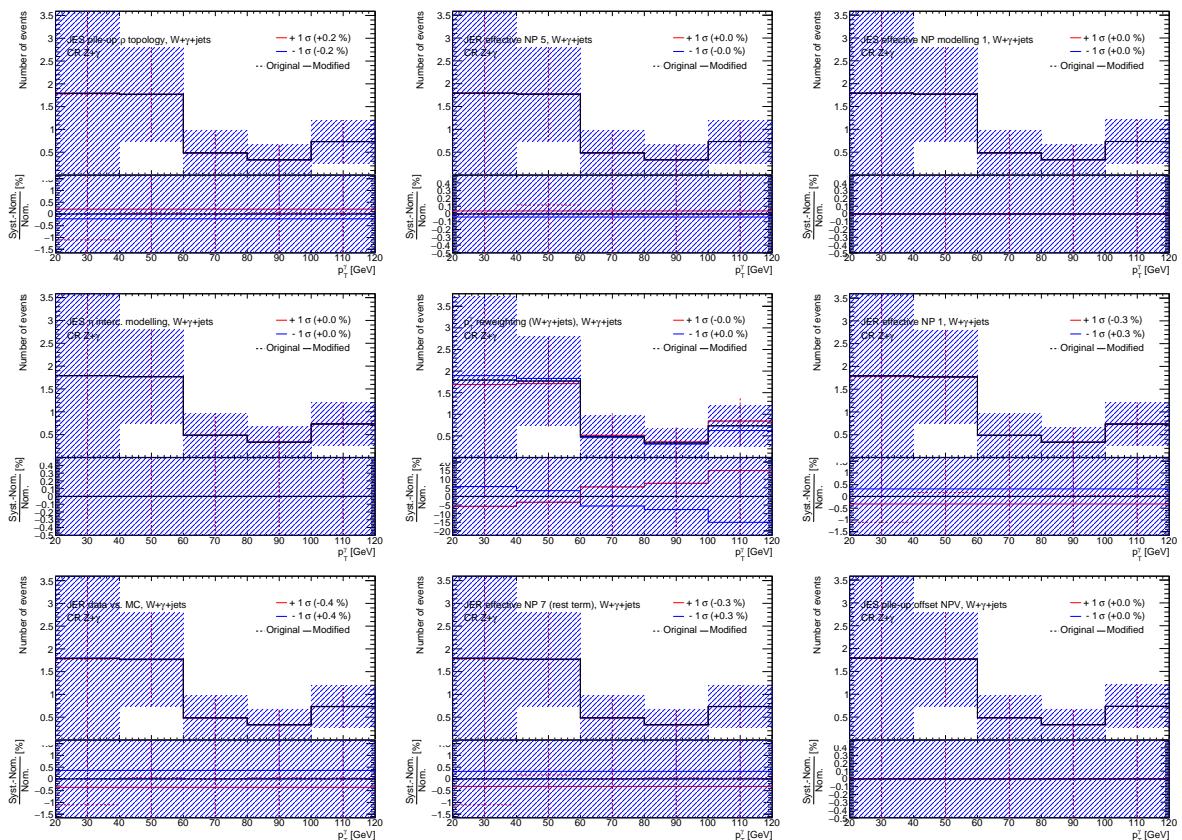


Figure 217: Plots showing the impact of 20 highest ranked systematic uncertainties on $W+\gamma+jets$ for the left-handed $t\gamma\gamma$ coupling coupling in the CR $Z+\gamma$ (1).

1824 O.3.3.6 $Z+\gamma+jets$ (CR $Z+\gamma$, left-handed $t\gamma\gamma$ coupling)

Not reviewed, for internal circulation only

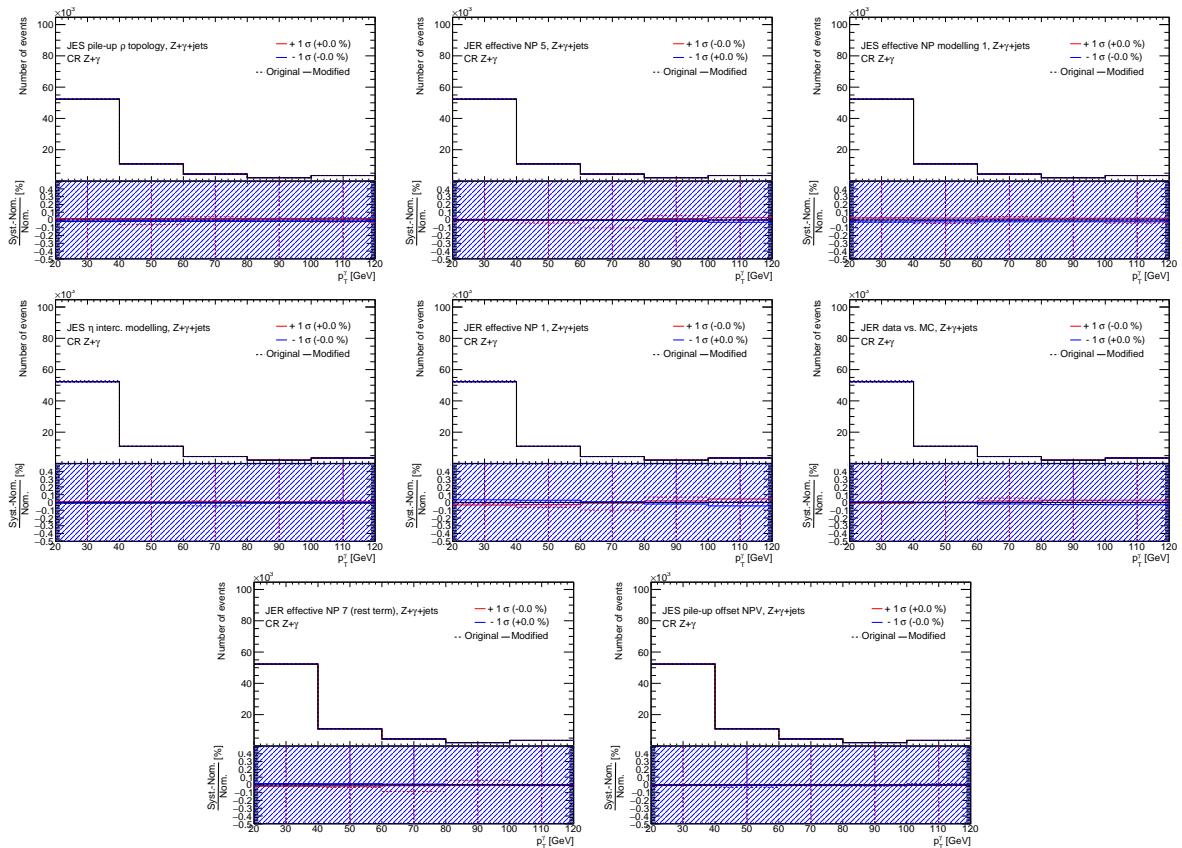


Figure 218: Plots showing the impact of 20 highest ranked systematic uncertainties on $Z+\gamma+jets$ for the left-handed $t\gamma\gamma$ coupling coupling in the CR $Z+\gamma$ (1).

1825 0.3.3.7 Other prompt photons (CR Z+ γ , left-handed $t\gamma\gamma$ coupling)

Not reviewed, for internal circulation only

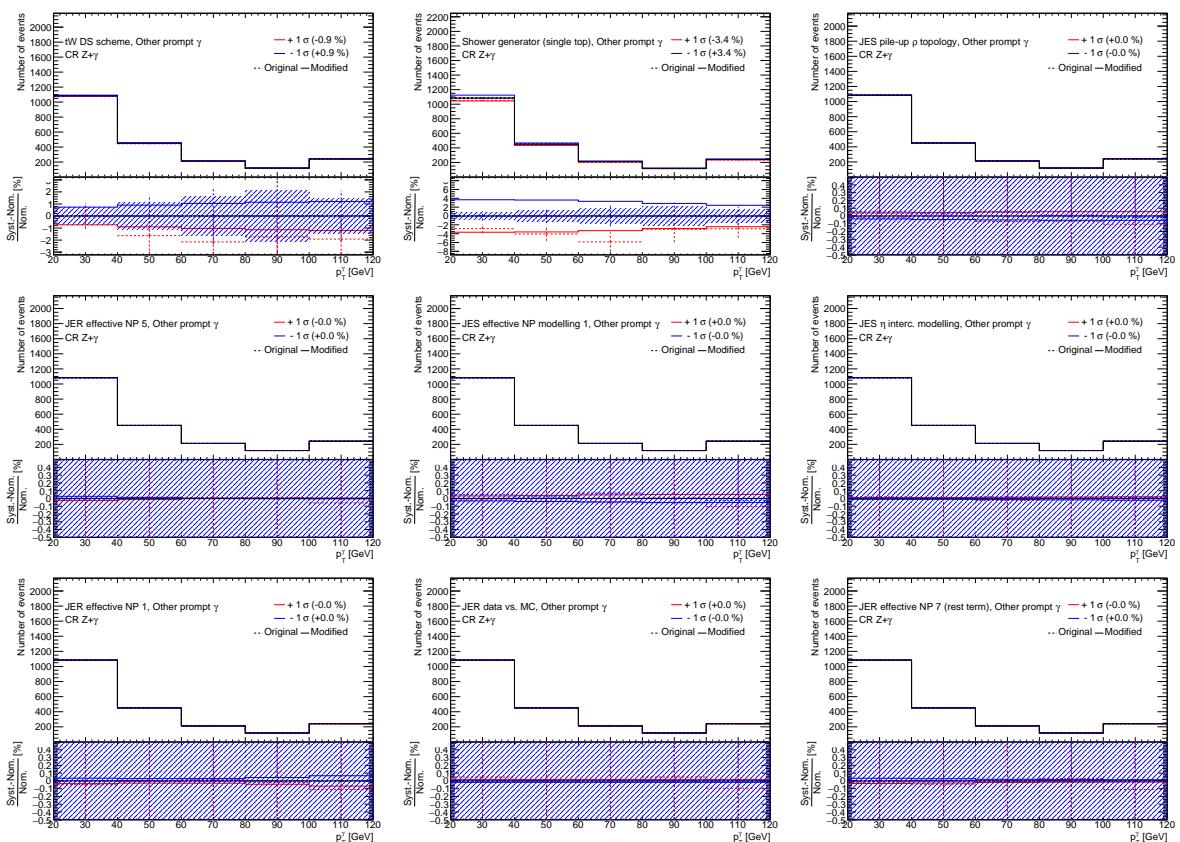


Figure 219: Plots showing the impact of 20 highest ranked systematic uncertainties on *Other prompt photons* for the left-handed $t\gamma\gamma$ coupling coupling in the CR Z+ γ (1).

Not reviewed, for internal circulation only

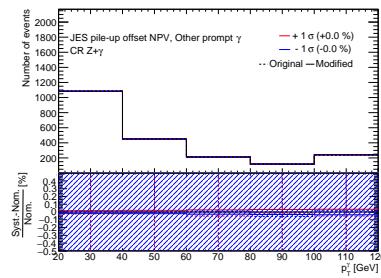


Figure 220: Plots showing the impact of 20 highest ranked systematic uncertainties on *Other prompt photons* for the left-handed $t\gamma\gamma$ coupling coupling in the CR $Z+\gamma$ (2).

1826 **O.4 Plots for the right-handed $t\gamma\gamma$ coupling**

1827 **O.4.1 SR (right-handed $t\gamma\gamma$ coupling)**

1828 **O.4.1.1 Total background (SR, right-handed $t\gamma\gamma$ coupling)**

Not reviewed, for internal circulation only

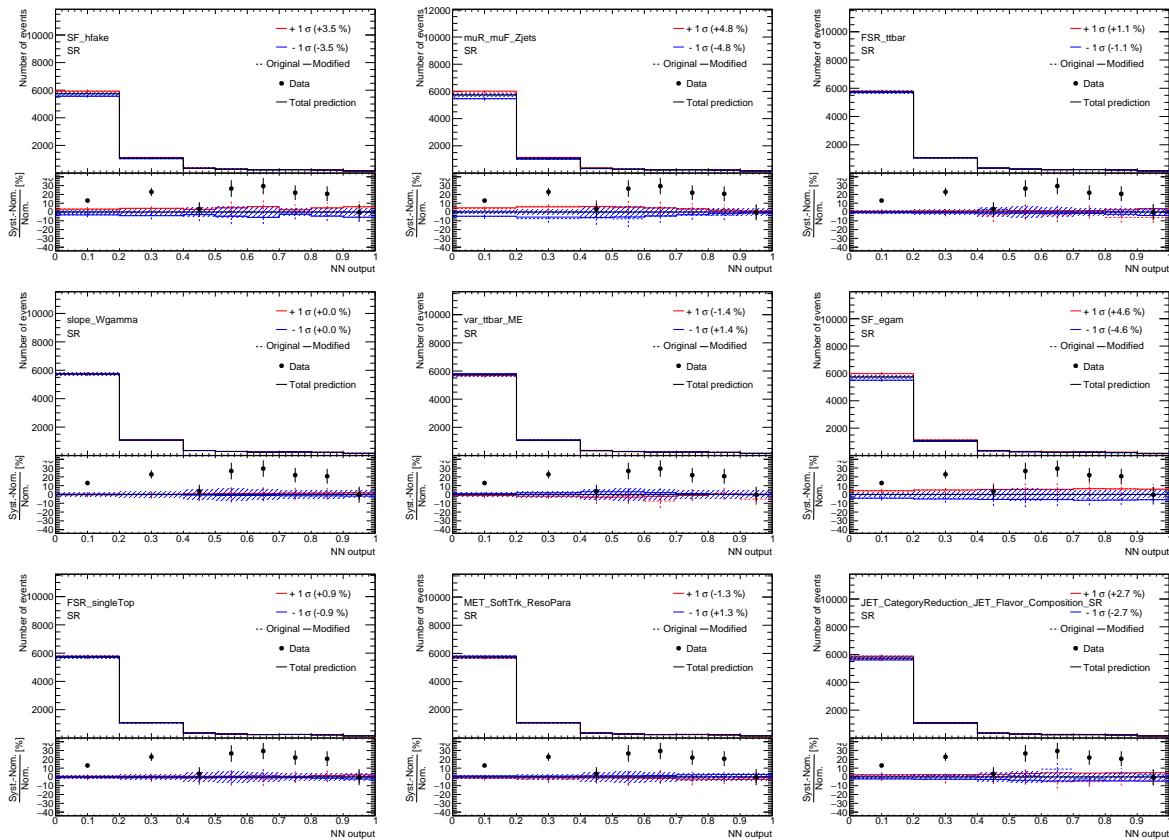


Figure 221: Plots showing the impact of 20 highest ranked systematic uncertainties on *Total background* for the right-handed $t\gamma\gamma$ coupling coupling in the SR (1).

Not reviewed, for internal circulation only

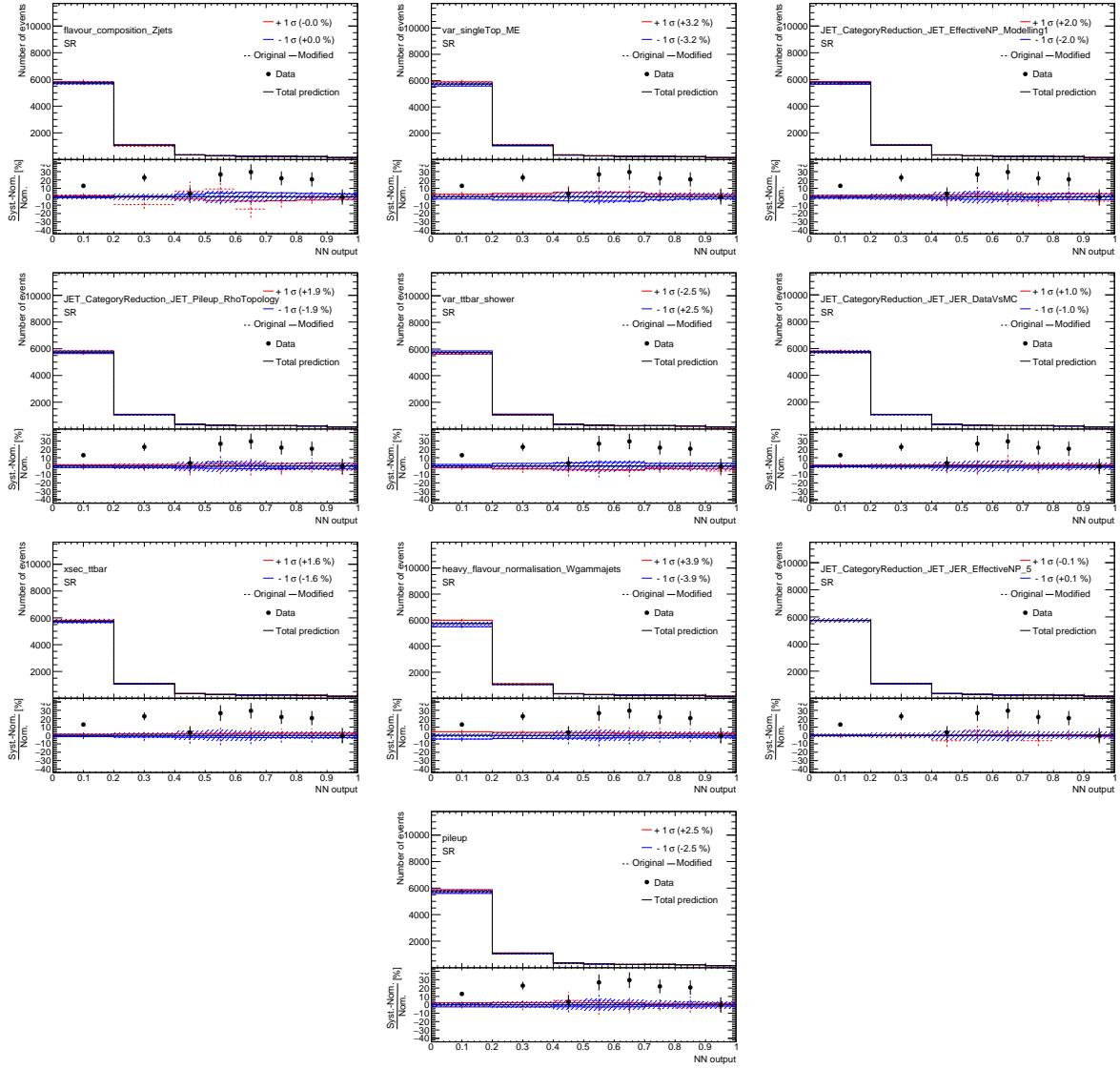


Figure 222: Plots showing the impact of 20 highest ranked systematic uncertainties on *Total background* for the right-handed $t\gamma$ coupling coupling in the SR (2).

1829 **O.4.1.2 Signal (SR, right-handed $t\gamma\gamma$ coupling)**

Not reviewed, for internal circulation only

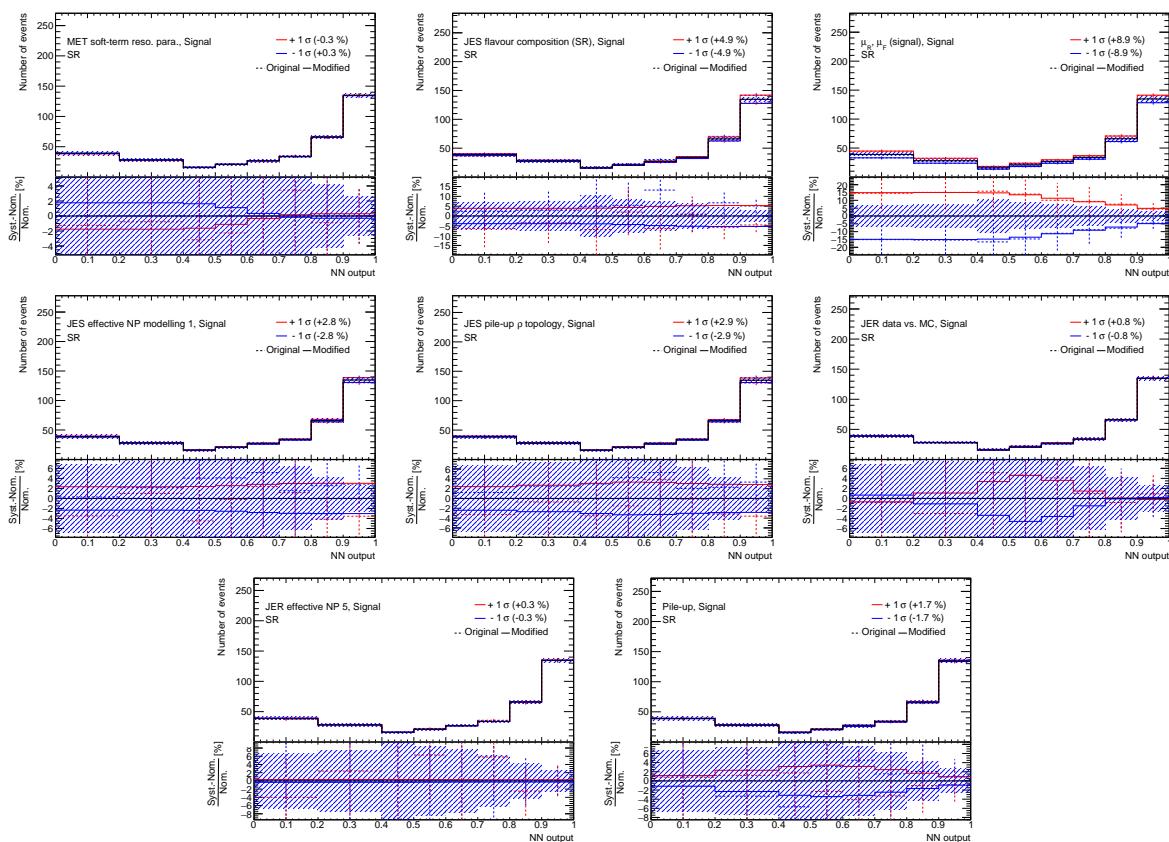


Figure 223: Plots showing the impact of 20 highest ranked systematic uncertainties on *Signal* for the right-handed $t\gamma\gamma$ coupling coupling in the SR (1).

1830 **O.4.1.3 $e \rightarrow \gamma$ fakes (SR, right-handed $t\bar{c}\gamma$ coupling)**

Not reviewed, for internal circulation only

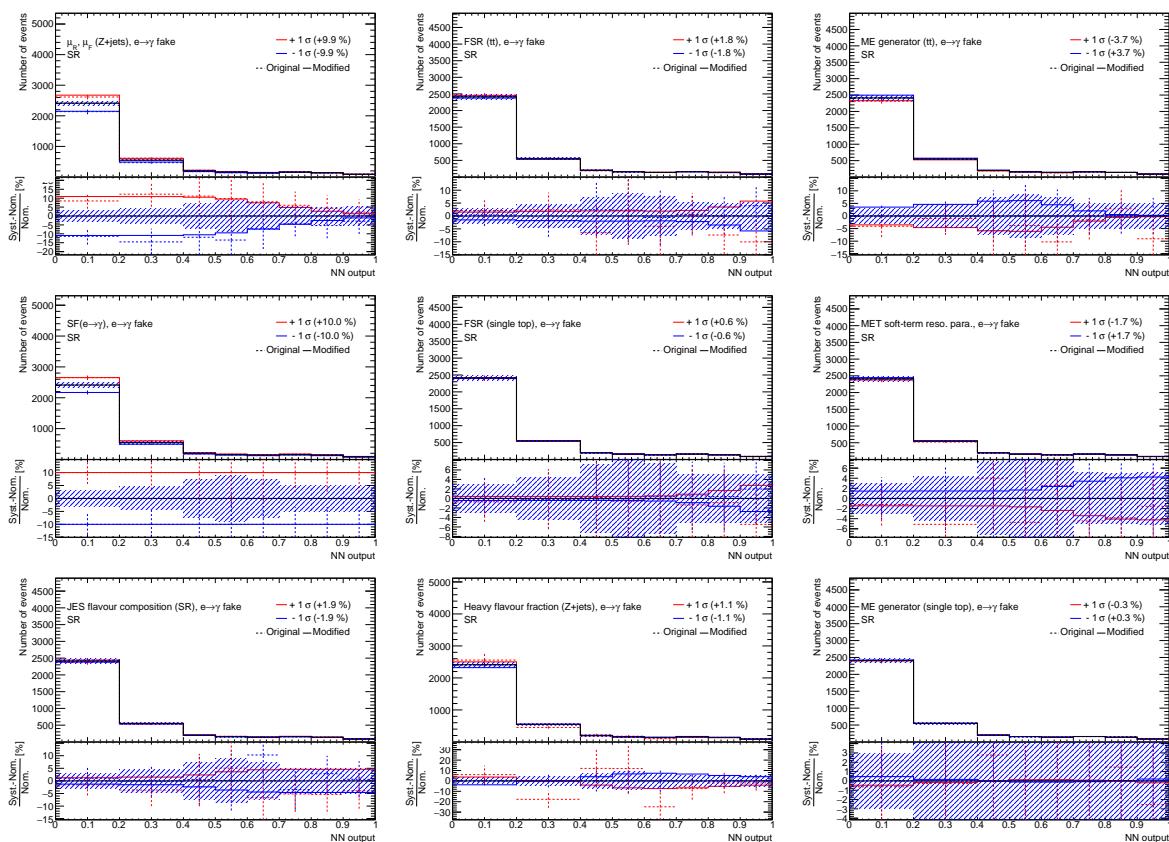


Figure 224: Plots showing the impact of 20 highest ranked systematic uncertainties on $e \rightarrow \gamma$ fakes for the right-handed $t\bar{c}\gamma$ coupling coupling in the SR (1).

Not reviewed, for internal circulation only

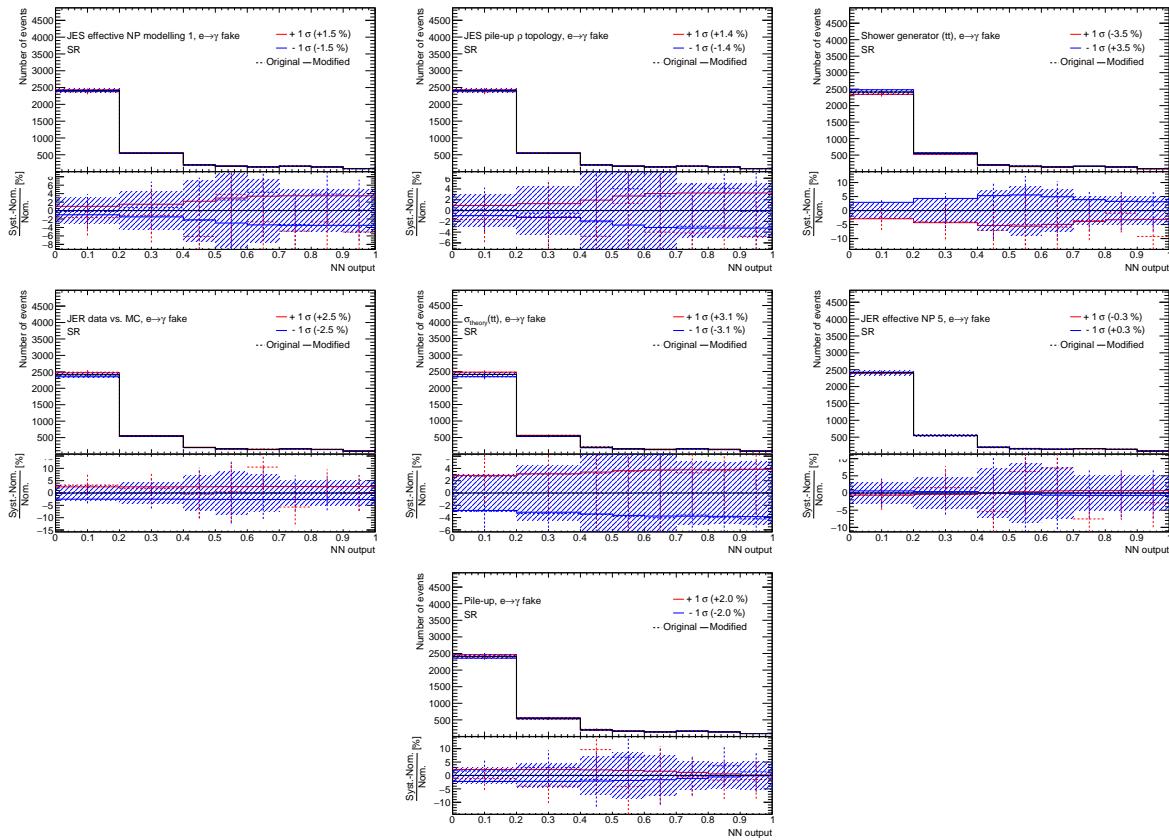


Figure 225: Plots showing the impact of 20 highest ranked systematic uncertainties on $e \rightarrow \gamma$ fakes for the right-handed $tc\gamma$ coupling coupling in the SR (2).

1831 **O.4.1.4 $j \rightarrow \gamma$ fakes (SR, right-handed $t\gamma\gamma$ coupling)**

Not reviewed, for internal circulation only

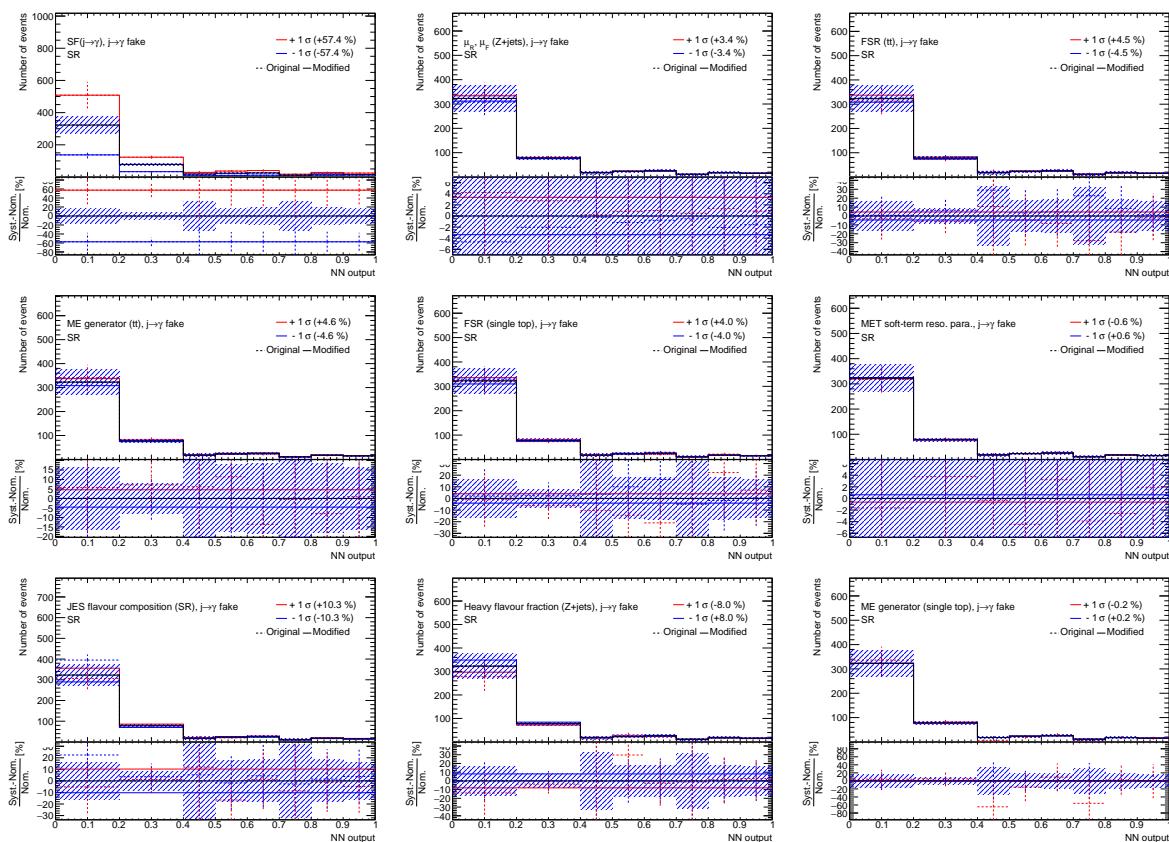


Figure 226: Plots showing the impact of 20 highest ranked systematic uncertainties on $j \rightarrow \gamma$ fakes for the right-handed $t\gamma\gamma$ coupling coupling in the SR (1).

Not reviewed, for internal circulation only

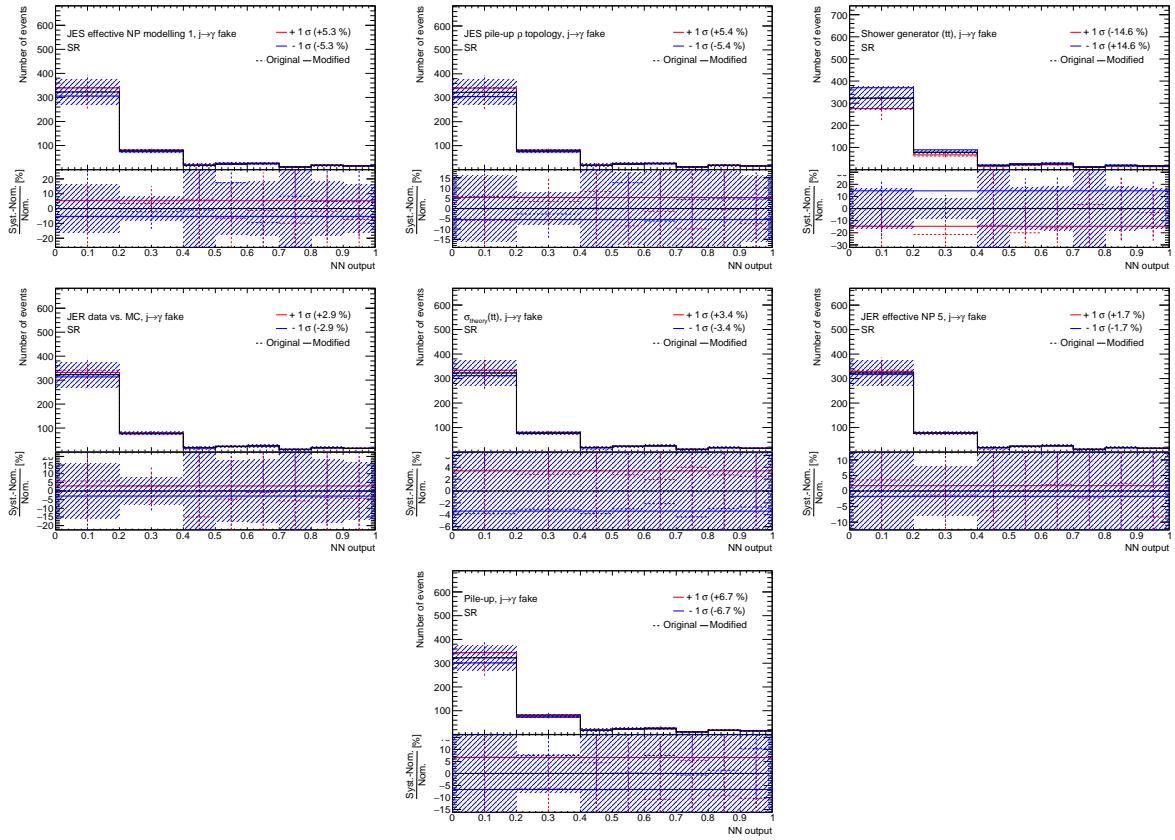


Figure 227: Plots showing the impact of 20 highest ranked systematic uncertainties on $j \rightarrow \gamma$ fakes for the right-handed $tc\gamma$ coupling coupling in the SR (2).

1832 **O.4.1.5 $W+\gamma+jets$ (SR, right-handed $t\bar{c}\gamma$ coupling)**

Not reviewed, for internal circulation only

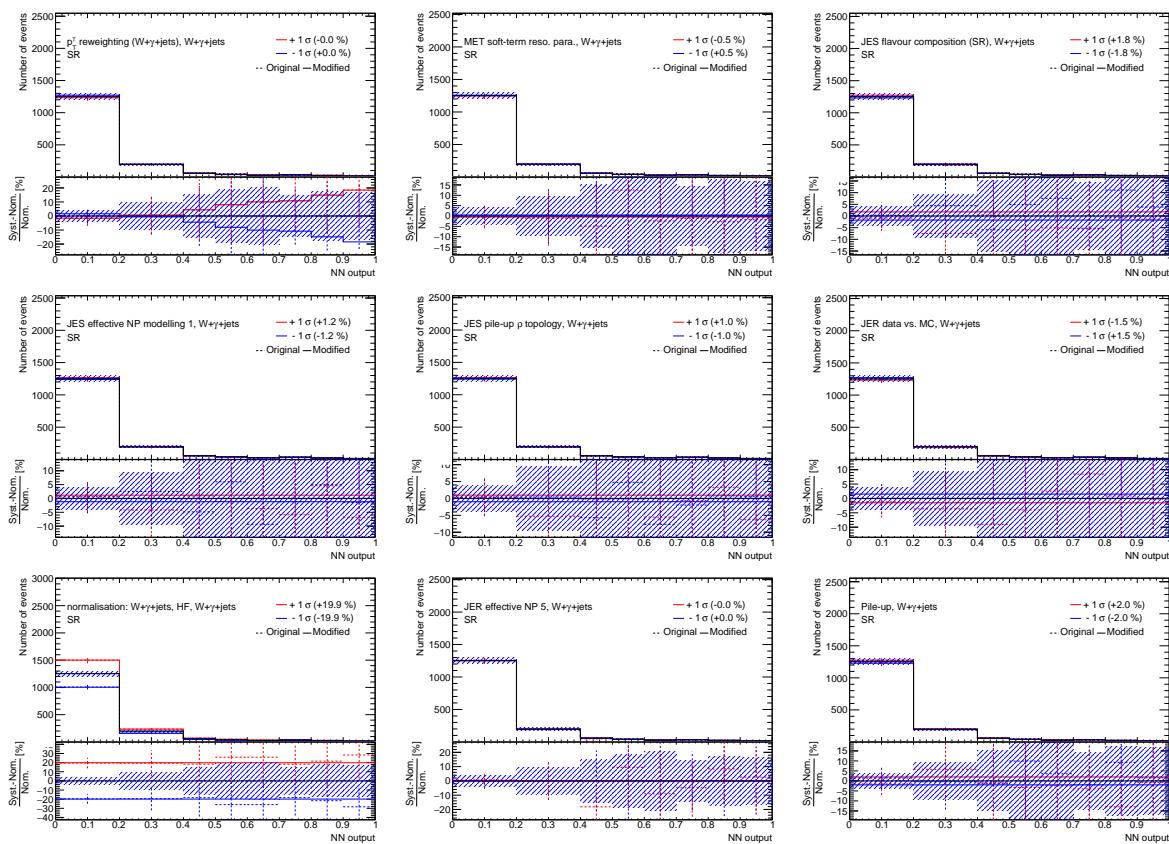


Figure 228: Plots showing the impact of 20 highest ranked systematic uncertainties on $W+\gamma+jets$ for the right-handed $t\bar{c}\gamma$ coupling coupling in the SR (1).

1833 O.4.1.6 $Z+\gamma+jets$ (SR, right-handed $t\bar{c}\gamma$ coupling)

Not reviewed, for internal circulation only

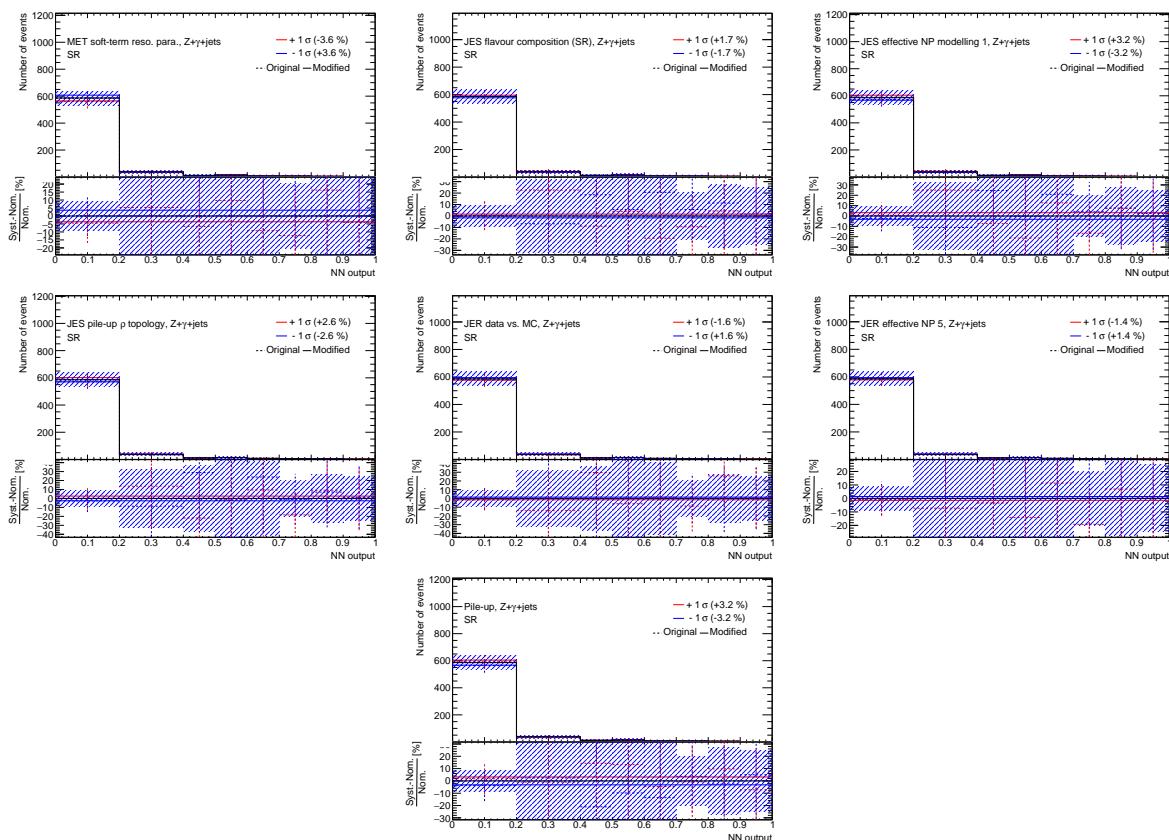


Figure 229: Plots showing the impact of 20 highest ranked systematic uncertainties on $Z+\gamma+jets$ for the right-handed $t\bar{c}\gamma$ coupling coupling in the SR (1).

1834 0.4.1.7 Other prompt photons (SR, right-handed $t\gamma\gamma$ coupling)

Not reviewed, for internal circulation only

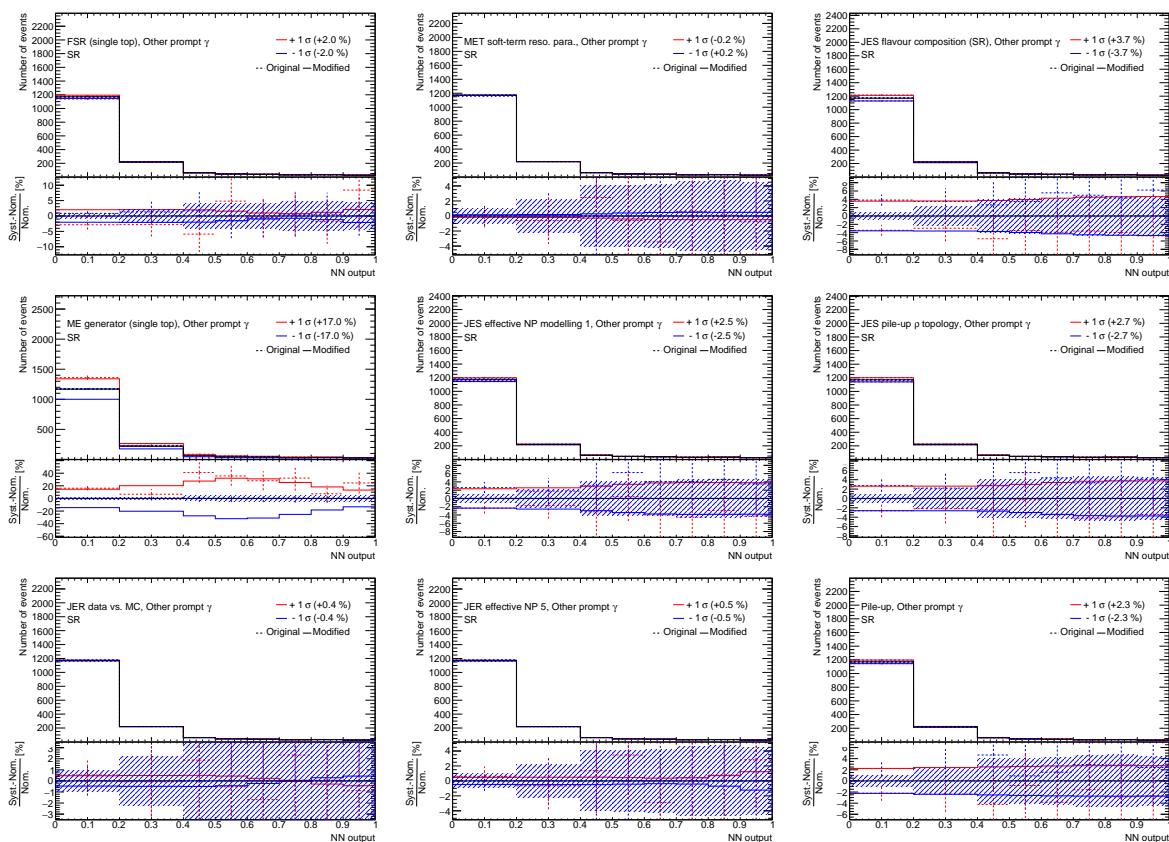


Figure 230: Plots showing the impact of 20 highest ranked systematic uncertainties on *Other prompt photons* for the right-handed $t\gamma\gamma$ coupling coupling in the SR (1).

1835 **O.4.2 CR $W+\gamma+jets$ (right-handed $t\gamma$ coupling)**

1836 **O.4.2.1 Total background (CR $W+\gamma+jets$, right-handed $t\gamma$ coupling)**

Not reviewed, for internal circulation only

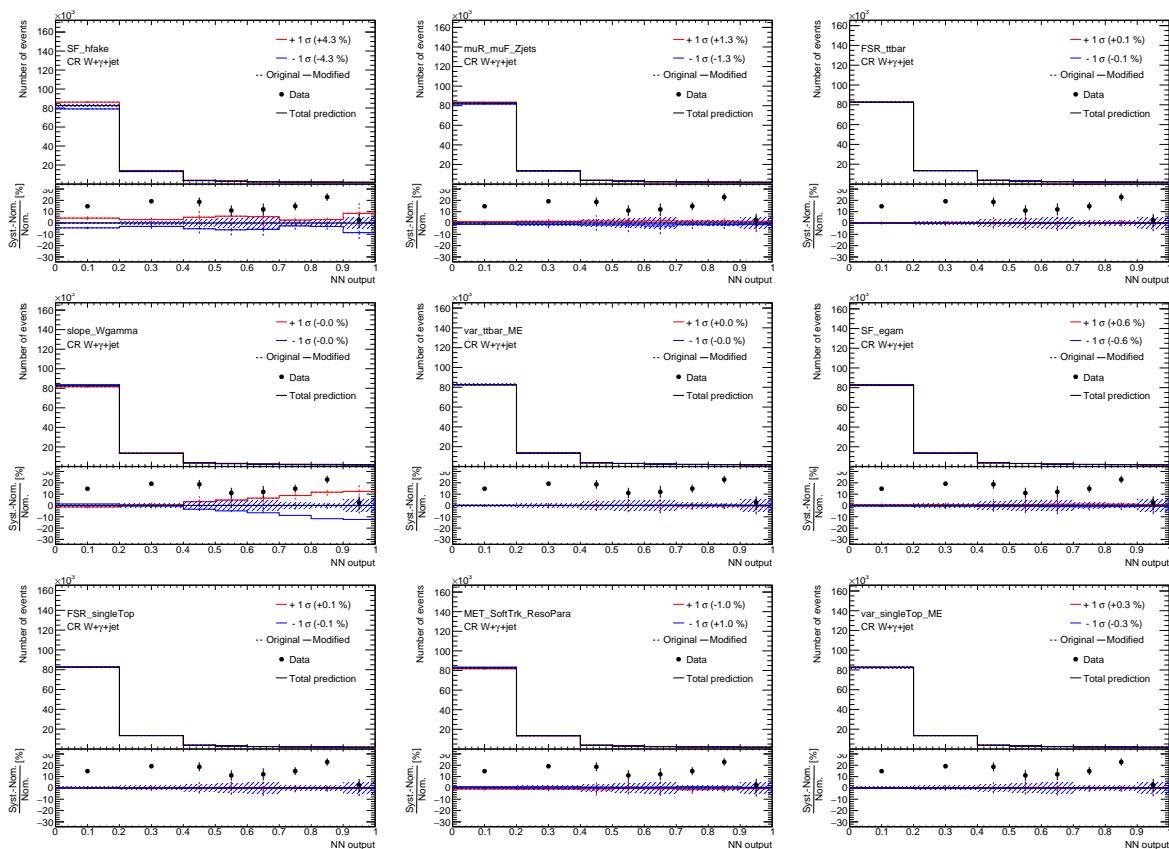


Figure 231: Plots showing the impact of 20 highest ranked systematic uncertainties on *Total background* for the right-handed $t\gamma$ coupling coupling in the CR $W+\gamma+jets$ (1).

Not reviewed, for internal circulation only

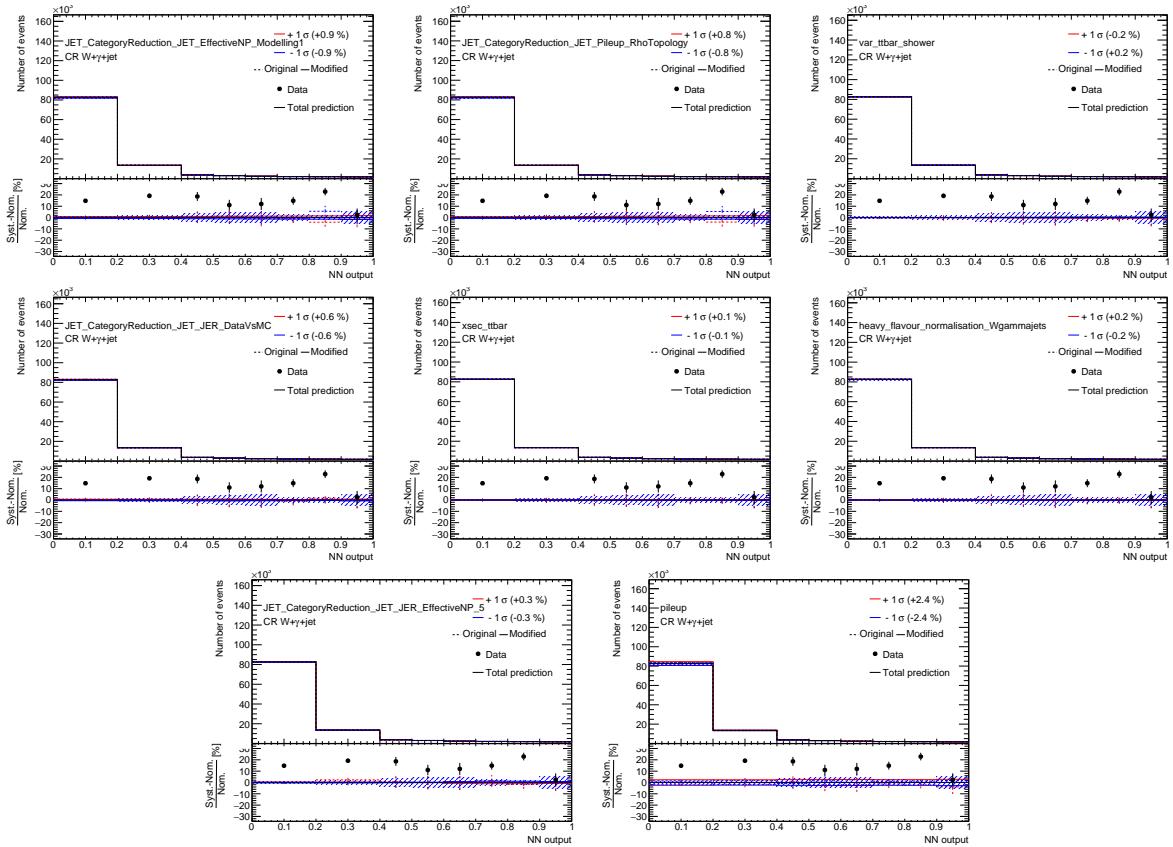


Figure 232: Plots showing the impact of 20 highest ranked systematic uncertainties on *Total background* for the right-handed $t\gamma$ coupling coupling in the CR $W+\gamma+jets$ (2).

1837 **O.4.2.2 Signal (CR $W+\gamma+$ jets, right-handed $t\gamma$ coupling)**

Not reviewed, for internal circulation only

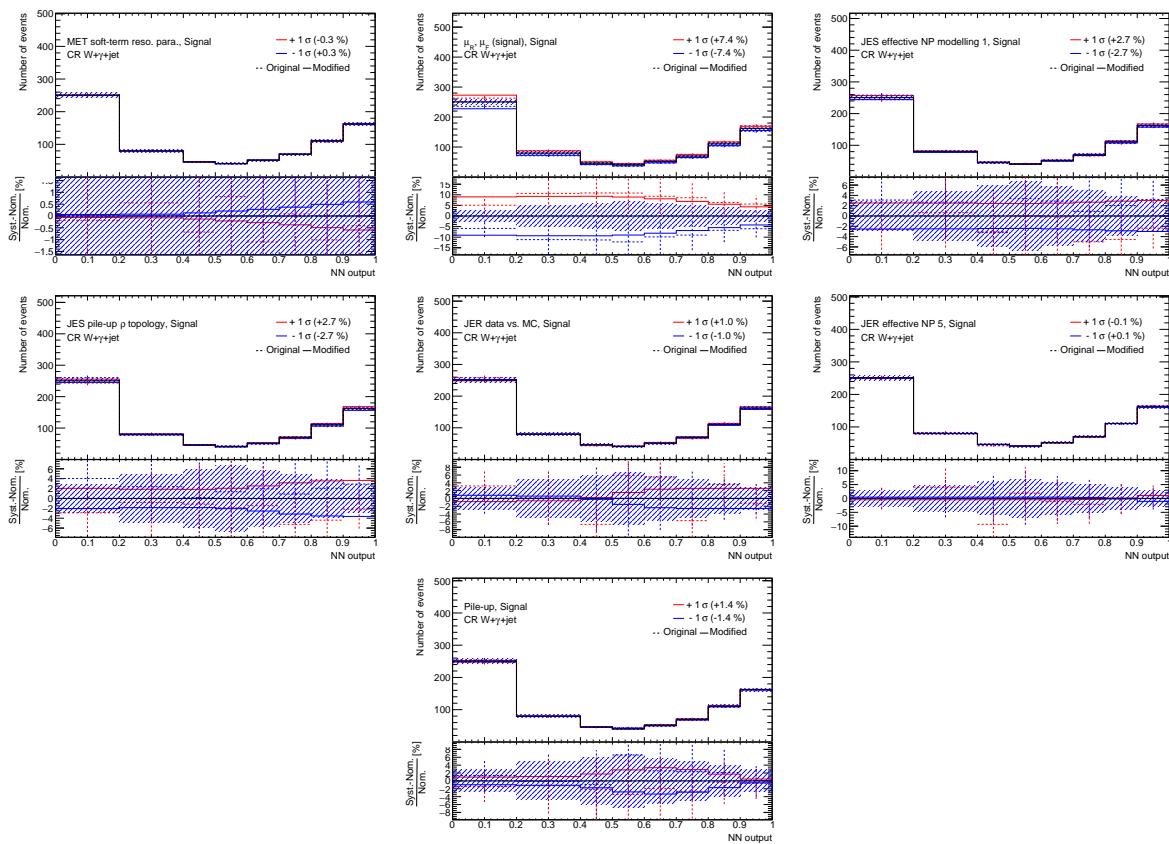


Figure 233: Plots showing the impact of 20 highest ranked systematic uncertainties on *Signal* for the right-handed $t\gamma$ coupling coupling in the CR $W+\gamma+$ jets (1).

1838 **O.4.2.3 $e \rightarrow \gamma$ fakes (CR $W+\gamma+\text{jets}$, right-handed $t\gamma\gamma$ coupling)**

Not reviewed, for internal circulation only

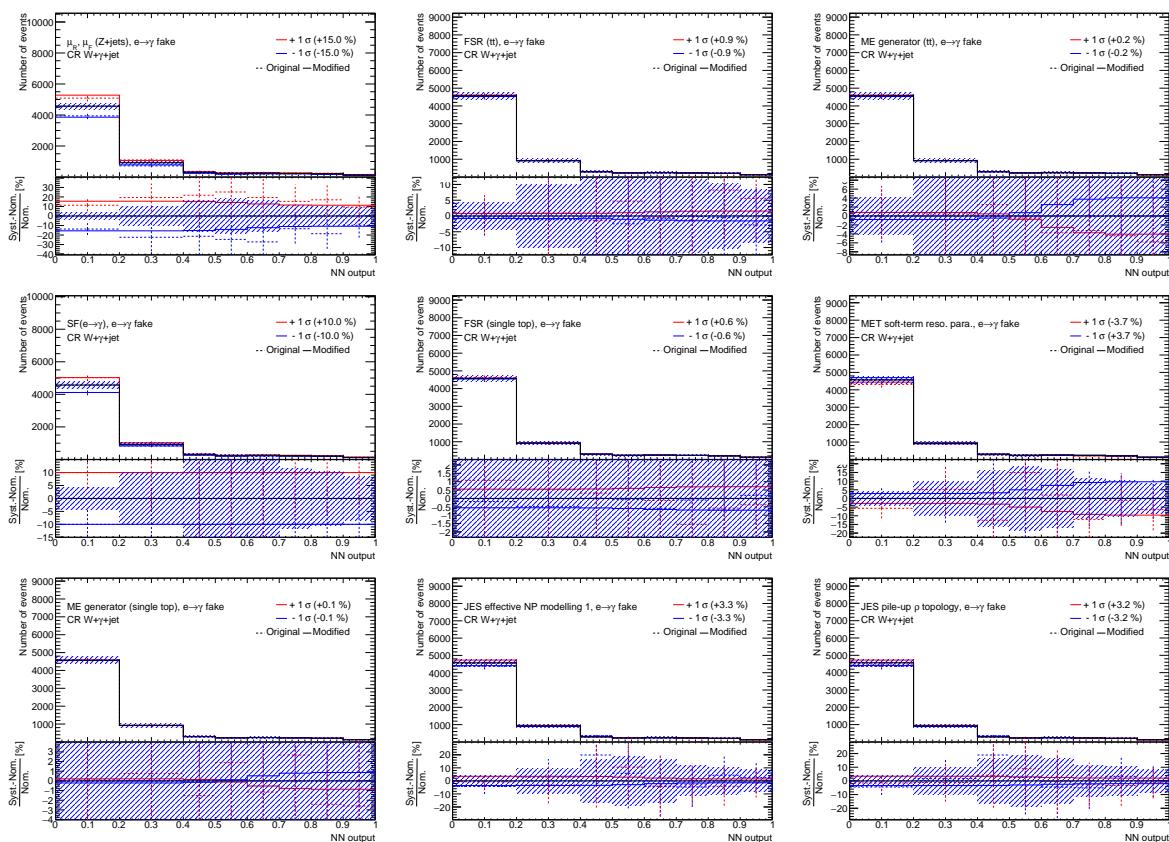


Figure 234: Plots showing the impact of 20 highest ranked systematic uncertainties on $e \rightarrow \gamma$ fakes for the right-handed $t\gamma\gamma$ coupling coupling in the CR $W+\gamma+\text{jets}$ (1).

Not reviewed, for internal circulation only

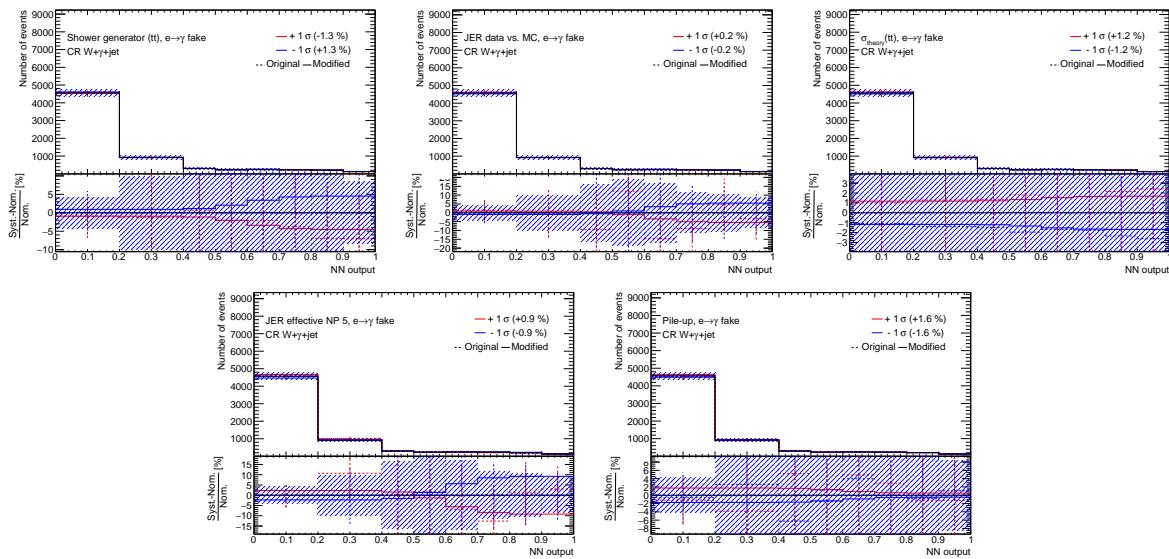


Figure 235: Plots showing the impact of 20 highest ranked systematic uncertainties on $e \rightarrow \gamma$ fakes for the right-handed $tc\gamma$ coupling coupling in the CR $W+\gamma+jets$ (2).

1839 **O.4.2.4 $j \rightarrow \gamma$ fakes (CR $W+\gamma+jets$, right-handed $t\gamma\gamma$ coupling)**

Not reviewed, for internal circulation only

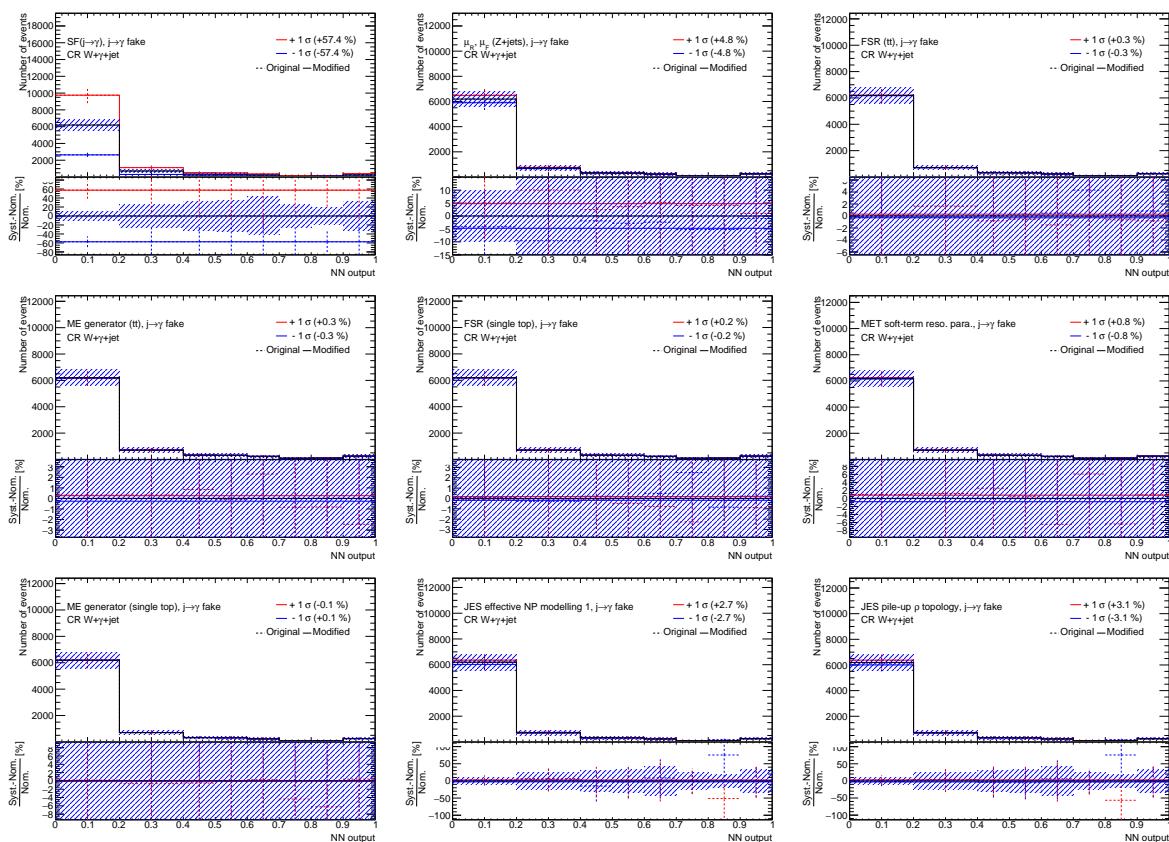


Figure 236: Plots showing the impact of 20 highest ranked systematic uncertainties on $j \rightarrow \gamma$ fakes for the right-handed $t\gamma\gamma$ coupling coupling in the CR $W+\gamma+jets$ (1).

Not reviewed, for internal circulation only

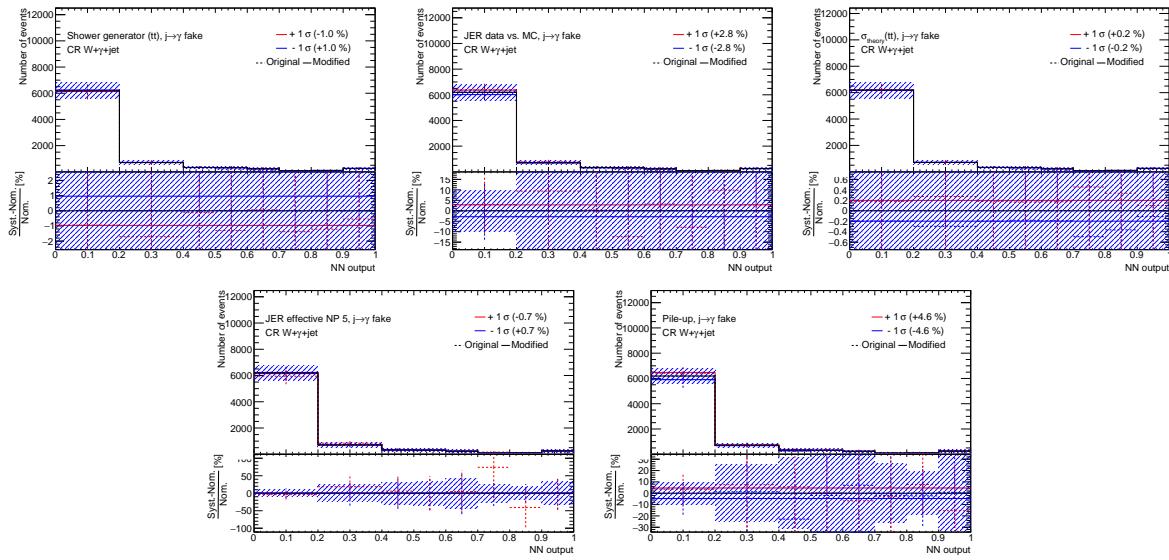


Figure 237: Plots showing the impact of 20 highest ranked systematic uncertainties on $j \rightarrow \gamma$ fakes for the right-handed $tc\gamma$ coupling coupling in the CR $W+\gamma+jets$ (2).

1840 **O.4.2.5 $W+\gamma+jets$ (CR $W+\gamma+jets$, right-handed $t\bar{c}\gamma$ coupling)**

Not reviewed, for internal circulation only

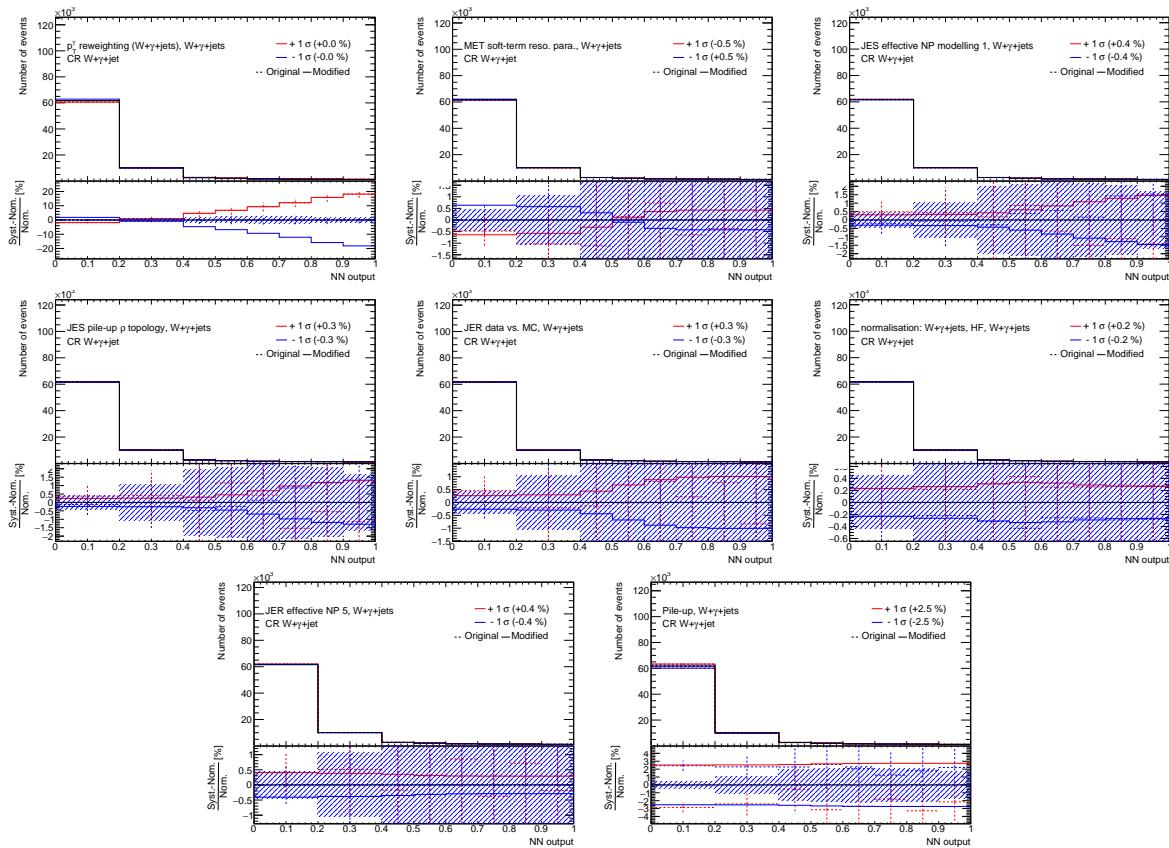


Figure 238: Plots showing the impact of 20 highest ranked systematic uncertainties on $W+\gamma+jets$ for the right-handed $t\bar{c}\gamma$ coupling coupling in the CR $W+\gamma+jets$ (1).

1841 **O.4.2.6 $Z+\gamma+jets$ (CR $W+\gamma+jets$, right-handed $t\bar{c}\gamma$ coupling)**

Not reviewed, for internal circulation only

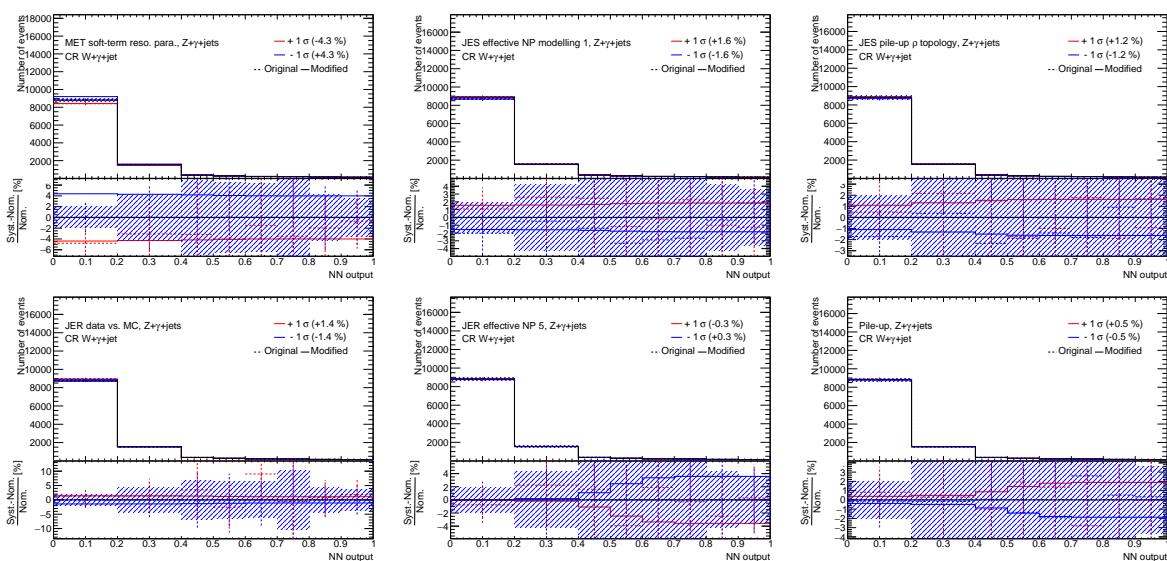


Figure 239: Plots showing the impact of 20 highest ranked systematic uncertainties on $Z+\gamma+jets$ for the right-handed $t\bar{c}\gamma$ coupling coupling in the CR $W+\gamma+jets$ (1).

1842 **O.4.2.7 Other prompt photons (CR $W+\gamma+jets$, right-handed $t\bar{c}\gamma$ coupling)**

Not reviewed, for internal circulation only

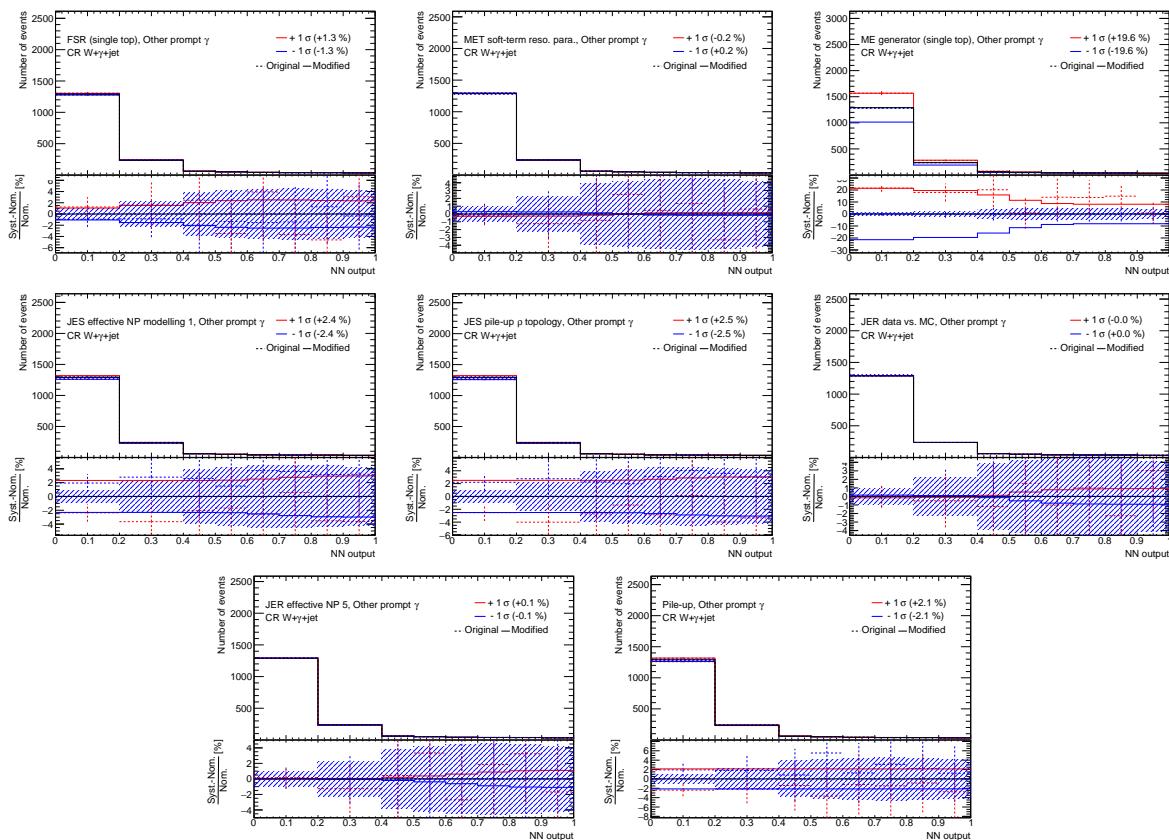


Figure 240: Plots showing the impact of 20 highest ranked systematic uncertainties on *Other prompt photons* for the right-handed $t\bar{c}\gamma$ coupling coupling in the CR $W+\gamma+jets$ (1).

1843 **O.4.3 CR Z+ γ (right-handed $t\gamma\gamma$ coupling)**1844 **O.4.3.1 Total background (CR Z+ γ , right-handed $t\gamma\gamma$ coupling)**

Not reviewed, for internal circulation only

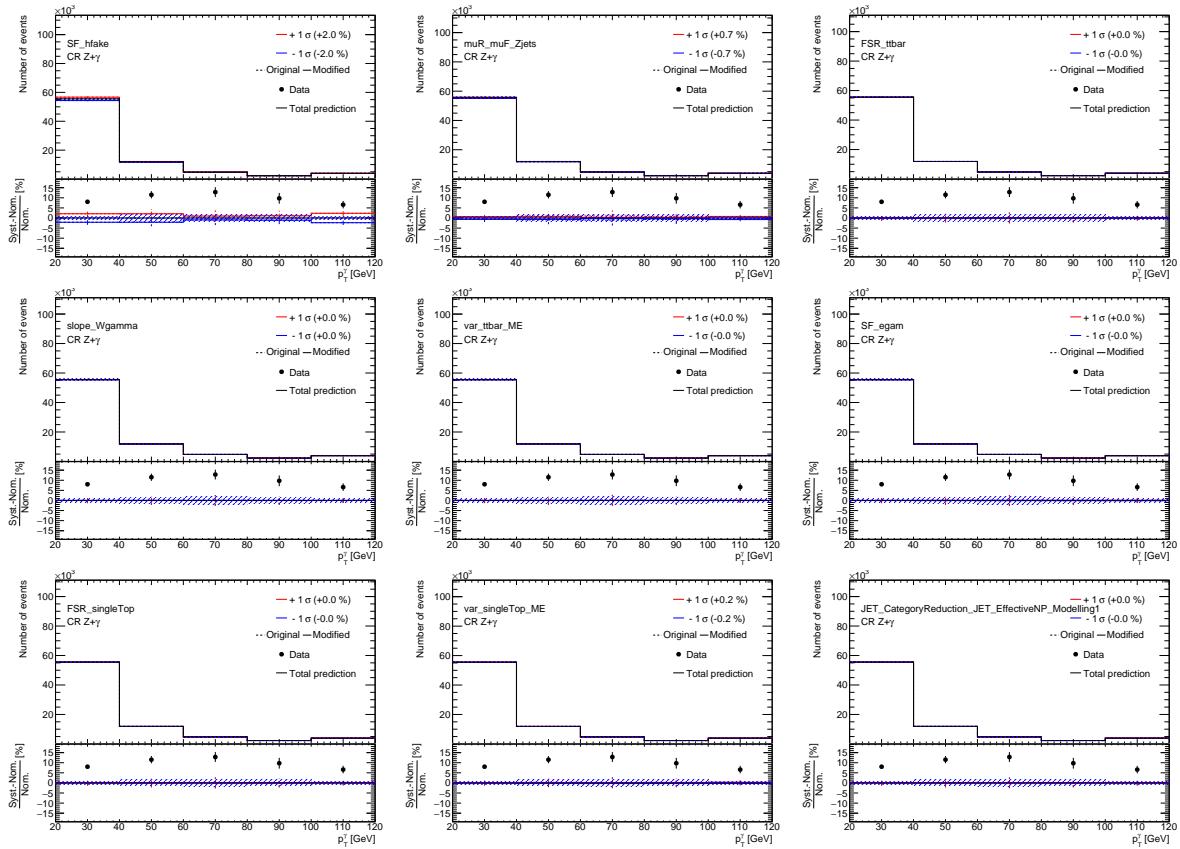


Figure 241: Plots showing the impact of 20 highest ranked systematic uncertainties on *Total background* for the right-handed $t\gamma\gamma$ coupling coupling in the CR $Z+\gamma$ (1).

Not reviewed, for internal circulation only

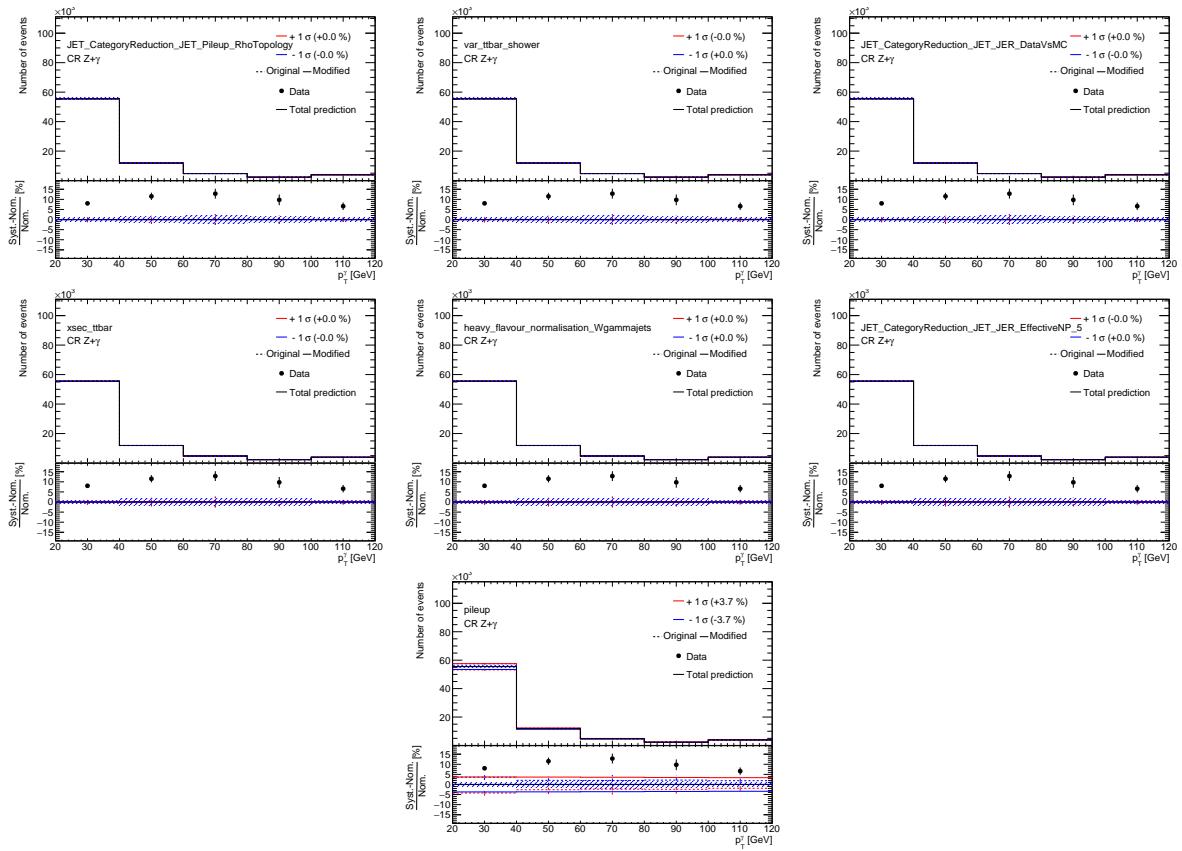


Figure 242: Plots showing the impact of 20 highest ranked systematic uncertainties on *Total background* for the right-handed $tc\gamma$ coupling coupling in the CR $Z+\gamma$ (2).

1845 **O.4.3.2 Signal (CR Z+ γ , right-handed $t\bar{c}\gamma$ coupling)**

Not reviewed, for internal circulation only

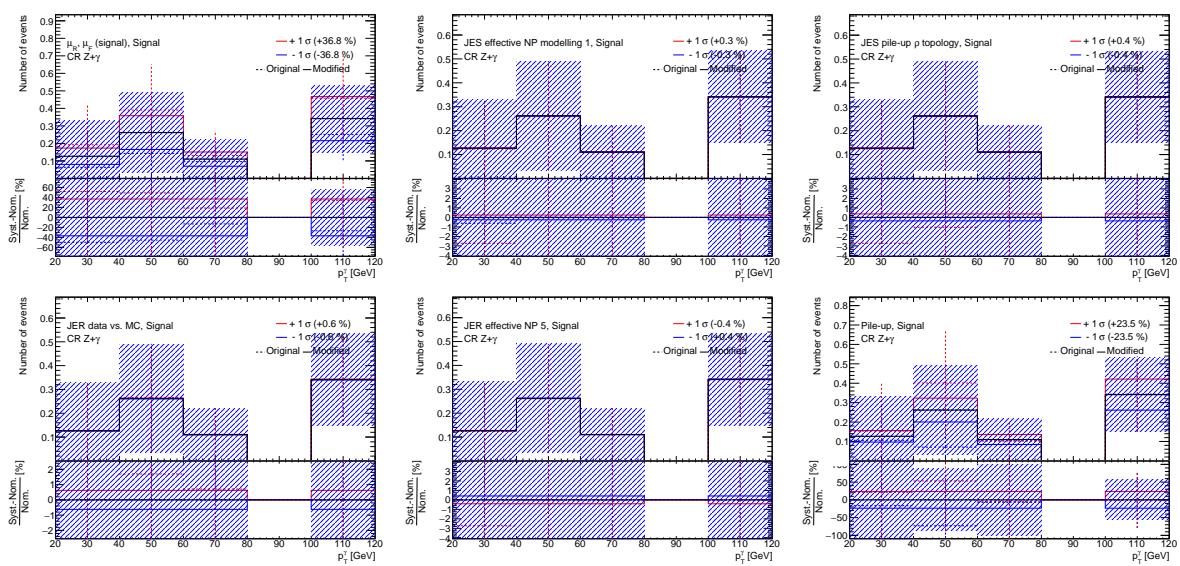


Figure 243: Plots showing the impact of 20 highest ranked systematic uncertainties on *Signal* for the right-handed $t\bar{c}\gamma$ coupling coupling in the CR $Z+\gamma$ (1).

1846 **O.4.3.3 $e \rightarrow \gamma$ fakes (CR Z+ γ , right-handed $t c \gamma$ coupling)**

Not reviewed, for internal circulation only

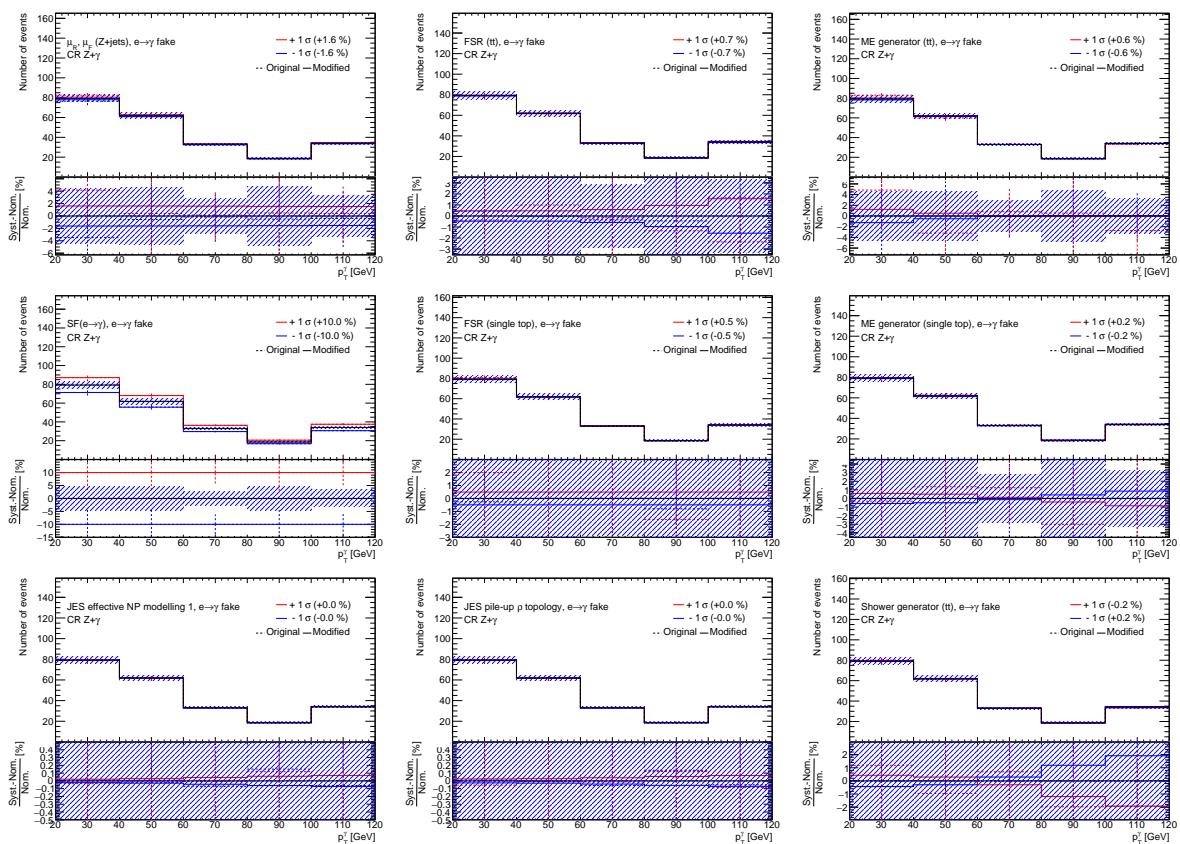


Figure 244: Plots showing the impact of 20 highest ranked systematic uncertainties on $e \rightarrow \gamma$ fakes for the right-handed $t c \gamma$ coupling coupling in the CR Z+ γ (1).

Not reviewed, for internal circulation only

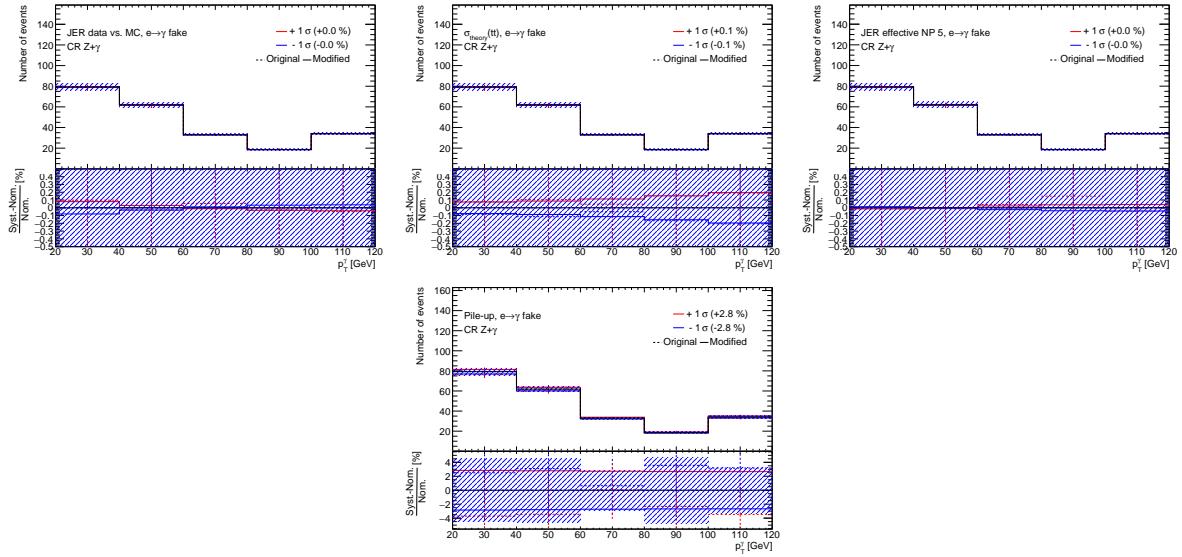


Figure 245: Plots showing the impact of 20 highest ranked systematic uncertainties on $e \rightarrow \gamma$ fakes for the right-handed $tc\gamma$ coupling coupling in the CR $Z+\gamma$ (2).

1847 **O.4.3.4 $j \rightarrow \gamma$ fakes (CR Z+ γ , right-handed $t c \gamma$ coupling)**

Not reviewed, for internal circulation only

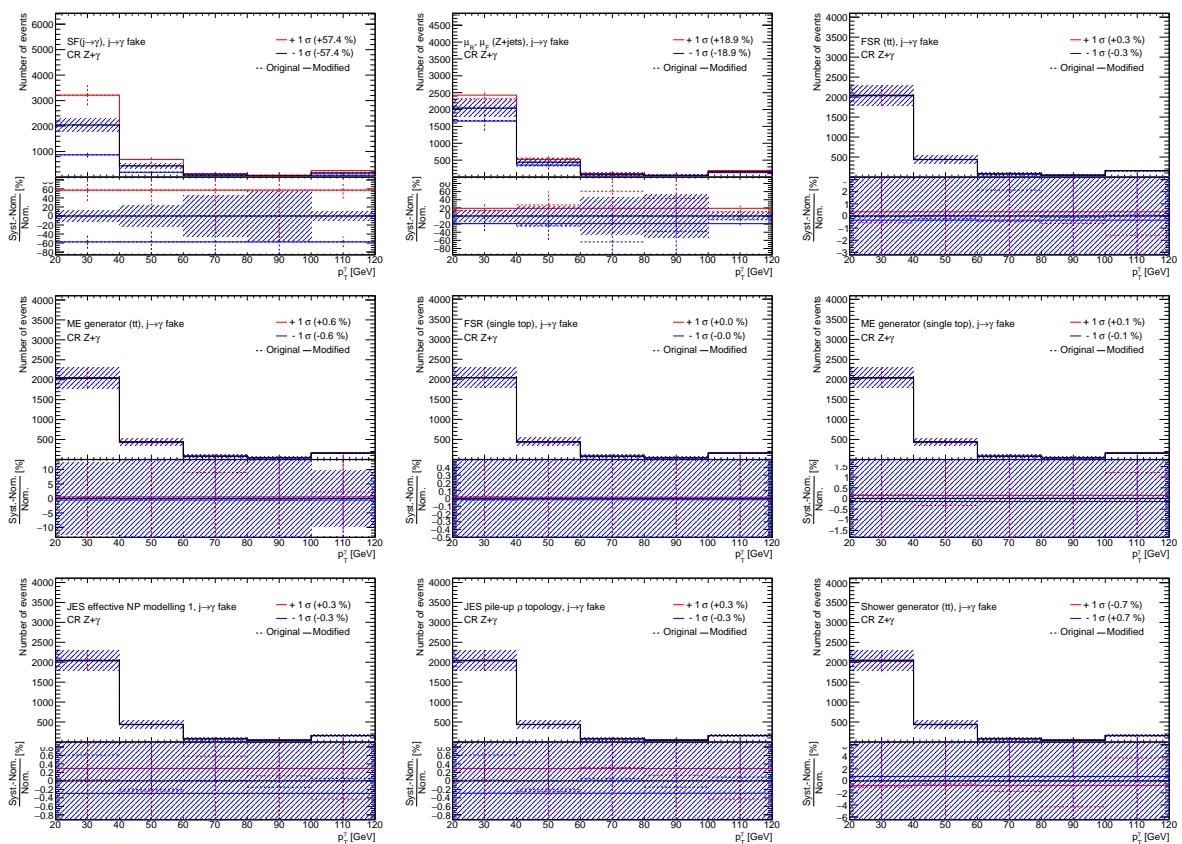


Figure 246: Plots showing the impact of 20 highest ranked systematic uncertainties on $j \rightarrow \gamma$ fakes for the right-handed $t c \gamma$ coupling coupling in the CR Z+ γ (1).

Not reviewed, for internal circulation only

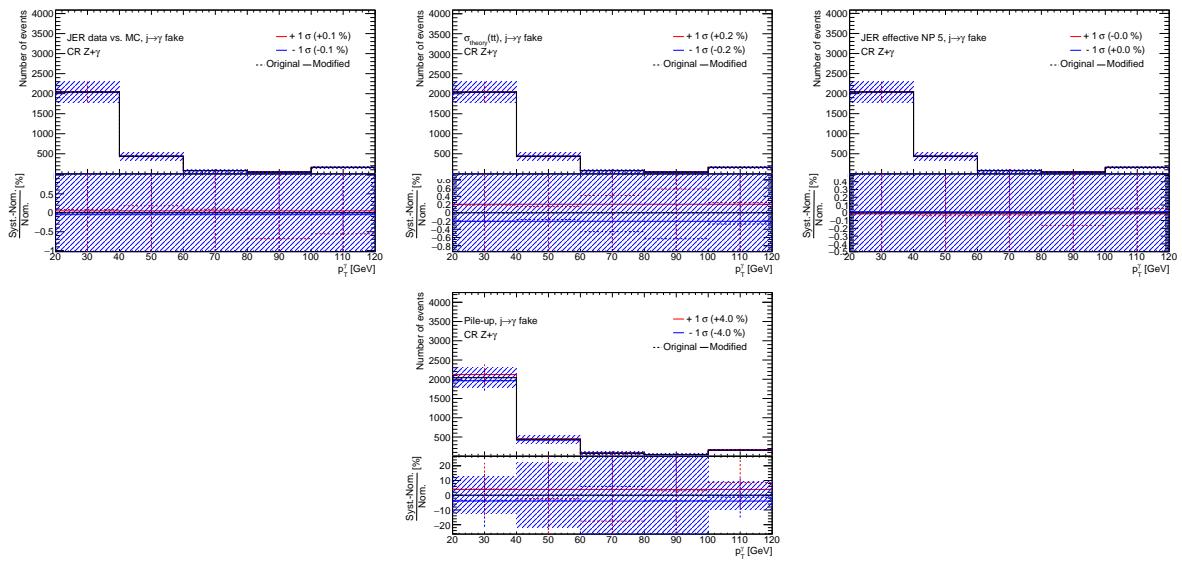


Figure 247: Plots showing the impact of 20 highest ranked systematic uncertainties on $j \rightarrow \gamma$ fakes for the right-handed $tc\gamma$ coupling coupling in the CR $Z + \gamma$ (2).

1848 **O.4.3.5 $W+\gamma+jets$ (CR $Z+\gamma$, right-handed $t\bar{c}\gamma$ coupling)**

Not reviewed, for internal circulation only

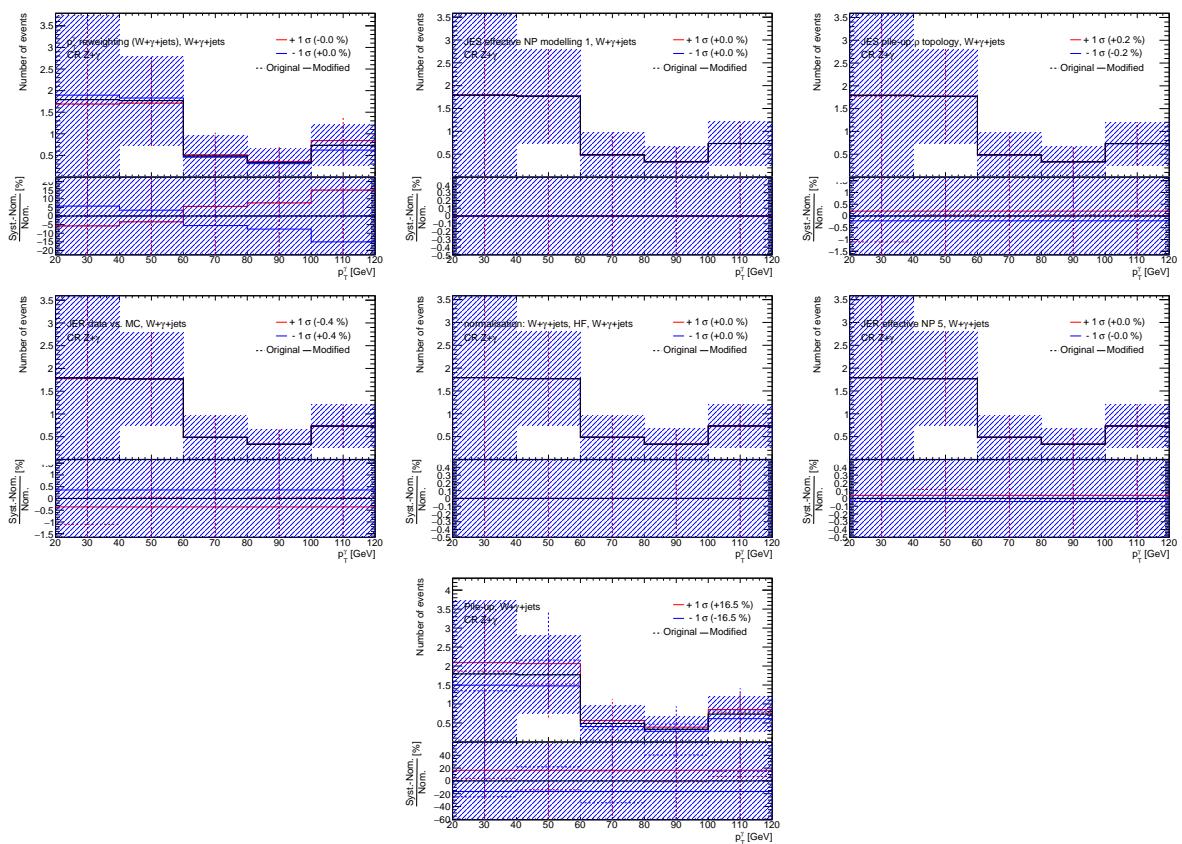


Figure 248: Plots showing the impact of 20 highest ranked systematic uncertainties on $W+\gamma+jets$ for the right-handed $t\bar{c}\gamma$ coupling coupling in the CR $Z+\gamma$ (1).

1849 **O.4.3.6 $Z+\gamma+jets$ (CR $Z+\gamma$, right-handed $t\gamma\gamma$ coupling)**

Not reviewed, for internal circulation only

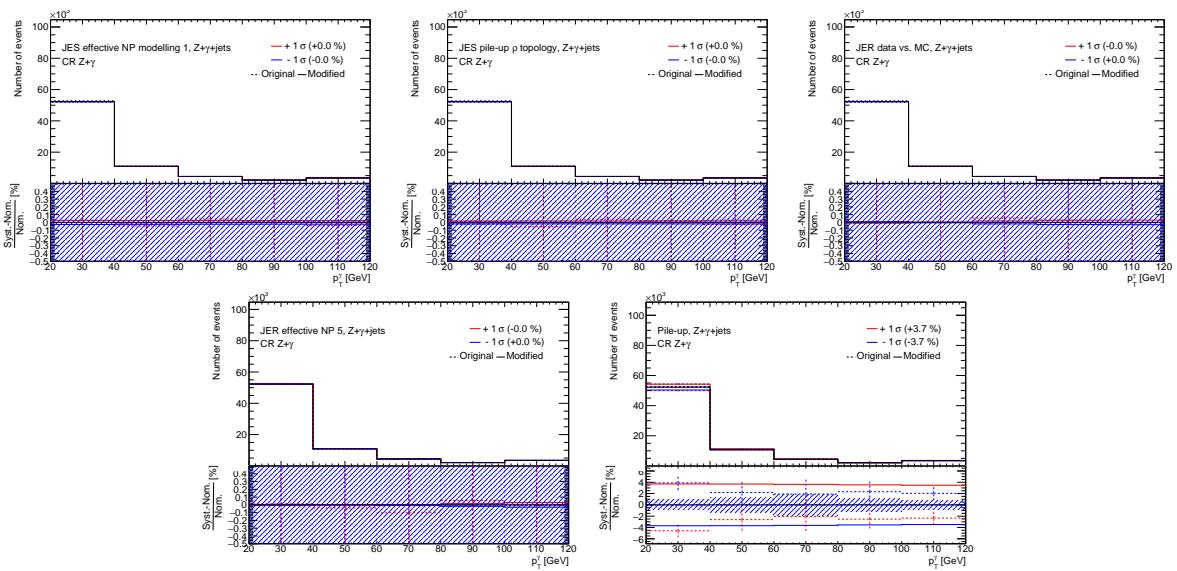


Figure 249: Plots showing the impact of 20 highest ranked systematic uncertainties on $Z+\gamma+jets$ for the right-handed $t\gamma\gamma$ coupling coupling in the CR $Z+\gamma$ (1).

1850 **O.4.3.7 Other prompt photons (CR Z+ γ , right-handed $t\gamma\gamma$ coupling)**

Not reviewed, for internal circulation only

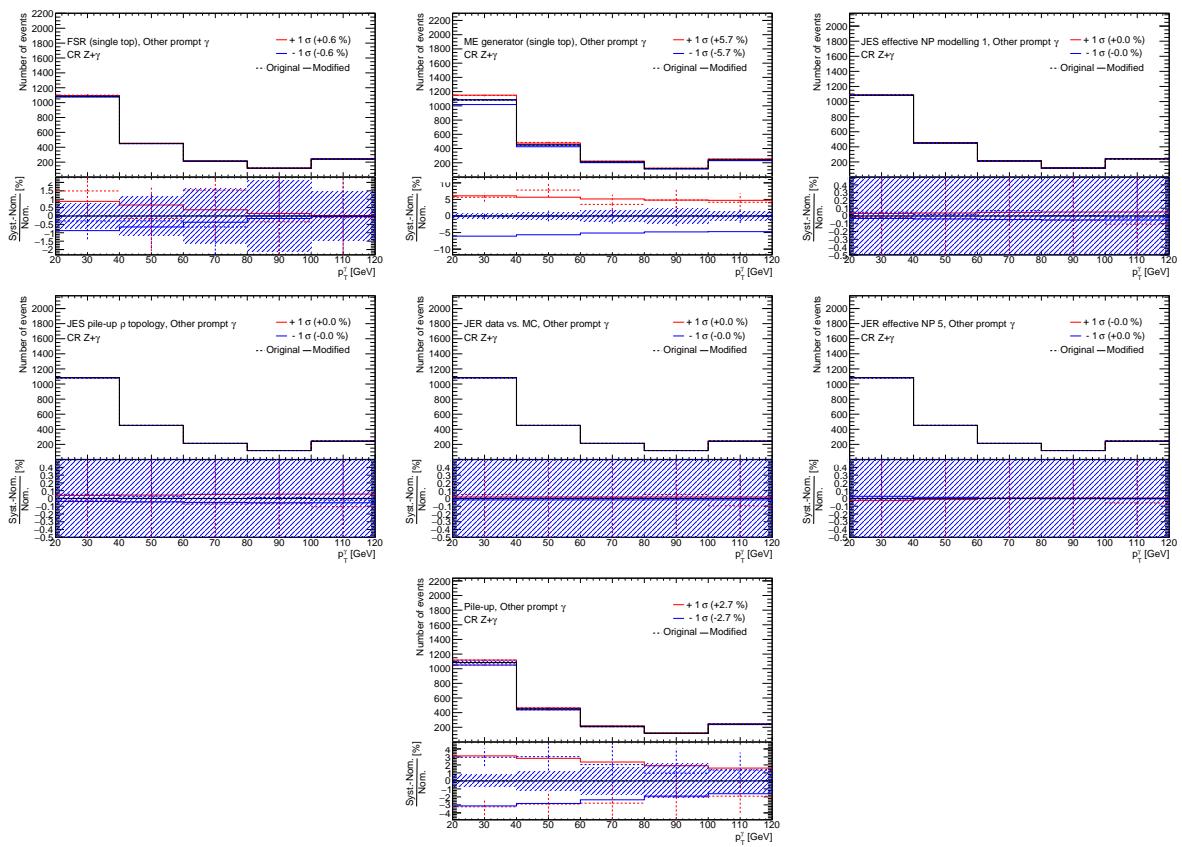


Figure 250: Plots showing the impact of 20 highest ranked systematic uncertainties on *Other prompt photons* for the right-handed $t\gamma\gamma$ coupling coupling in the CR $Z+\gamma$ (1).

1851 P Studies for an increased uncertainty of the cross section for the $t\bar{t} + \gamma$ 1852 process

1853 The uncertainty on the cross section of the $t\bar{t} + \gamma$ process of $^{+8.0\%}_{-7.8\%}$ is multiplied by a factor of 5 to check
1854 that using an inclusive k-factor for this process is valid. The fit is performed using data in all regions. The
1855 limits on the branching ratio is given in Table 46. The outcomes and in particular the limits for all four
1856 signal couplings give similar results as the default setup presented in Table 35. In Figures 251, 252, 253
1857 and 254, the pull plots for the left-handed $t\gamma$, right-handed $t\gamma$, left-handed $t\gamma$, and right-handed $t\gamma$
1858 coupling, respectively, are shown. Although the cross section uncertainty on the $t\bar{t} + \gamma$ process is slightly
1859 pulled, it is compatible with zero. Thus, it is conclude that the default uncertainty is sufficient.

Table 46: 95 % C.L. upper limits on the branching ratio $\mathcal{B}(t \rightarrow q\gamma)$ with $q = u, c$ for the different signal couplings when using an increased uncertainty on the cross section of the $t\bar{t} + \gamma$ process.

Signal coupling	$t\gamma$, left-handed	$t\gamma$, right-handed	$t\gamma$, left-handed	$t\gamma$, right-handed
$\mathcal{B}(t \rightarrow q\gamma) [10^{-5}]$	2.8	6.0	21.7	18.1

Not reviewed, for internal circulation only

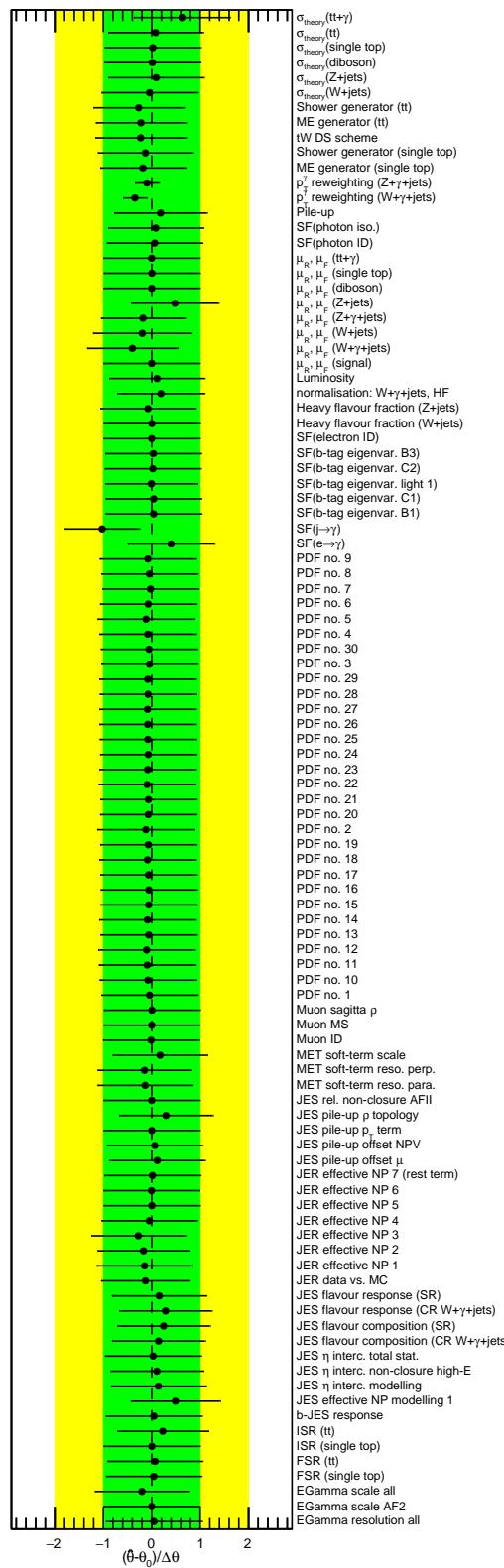


Figure 251: Pull values for the left-handed $t\bar{t}\gamma$ coupling for the different nuisance parameters considered in the fit using data in all regions with an increased uncertainty on the cross section of the $t\bar{t} + \gamma$ process.

Not reviewed, for internal circulation only

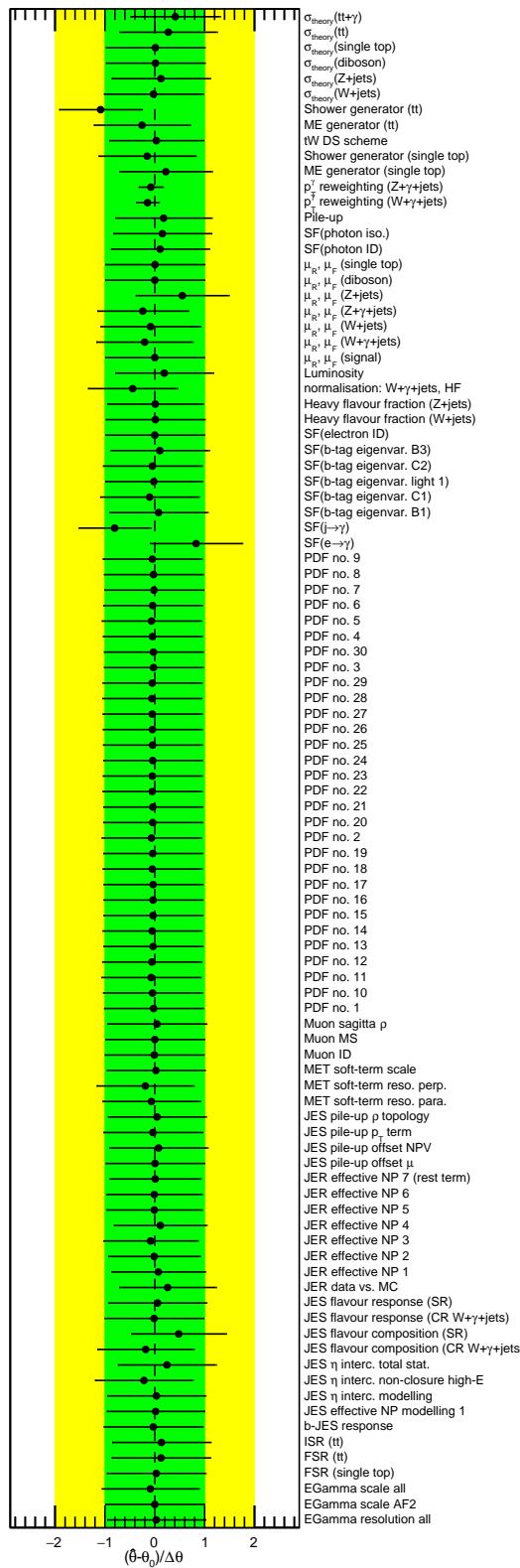


Figure 252: Pull values for the right-handed $t\bar{u}\gamma$ coupling for the different nuisance parameters considered in the fit using data in all regions with an increased uncertainty on the cross section of the $t\bar{t} + \gamma$ process.

Not reviewed, for internal circulation only

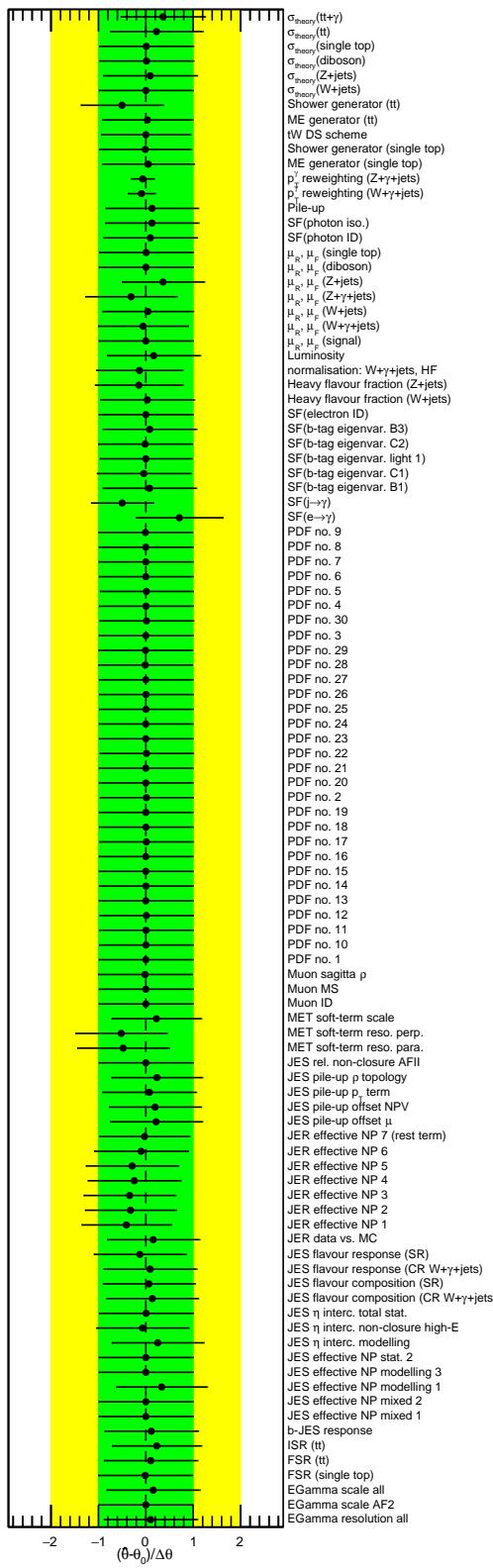


Figure 253: Pull values for the left-handed $tc\gamma$ coupling for the different nuisance parameters considered in the fit using data in all regions with an increased uncertainty on the cross section of the $t\bar{t} + \gamma$ process.

Not reviewed, for internal circulation only

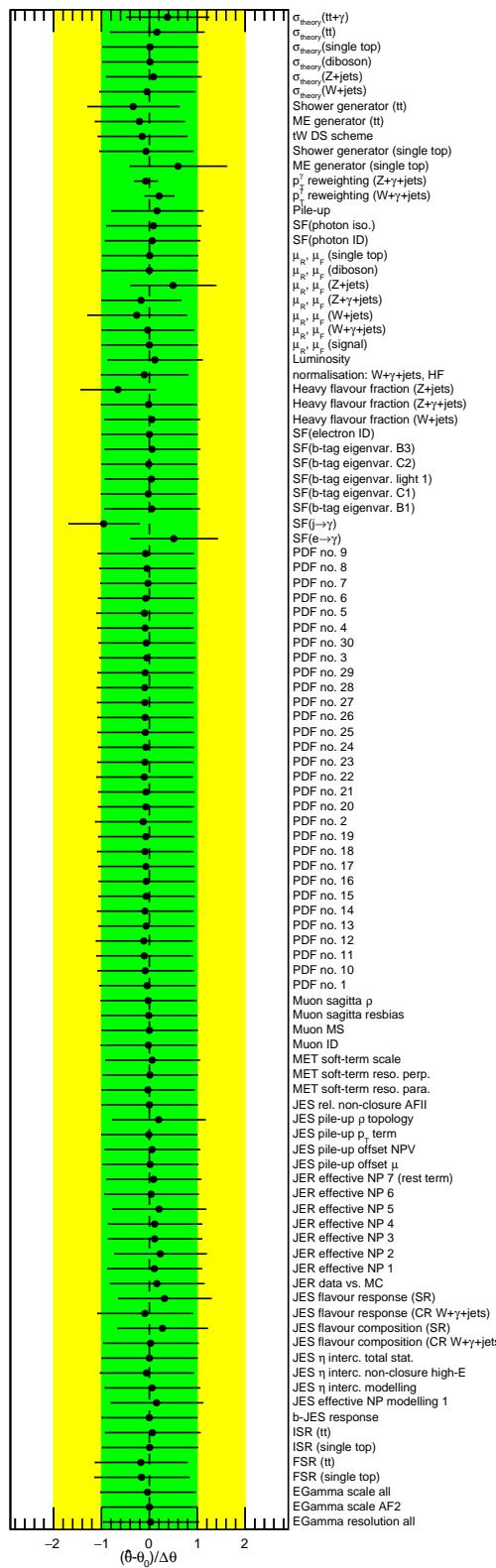


Figure 254: Pull values for the right-handed $tc\gamma$ coupling for the different nuisance parameters considered in the fit using data in all regions with an increased uncertainty on the cross section of the $t\bar{t} + \gamma$ process.

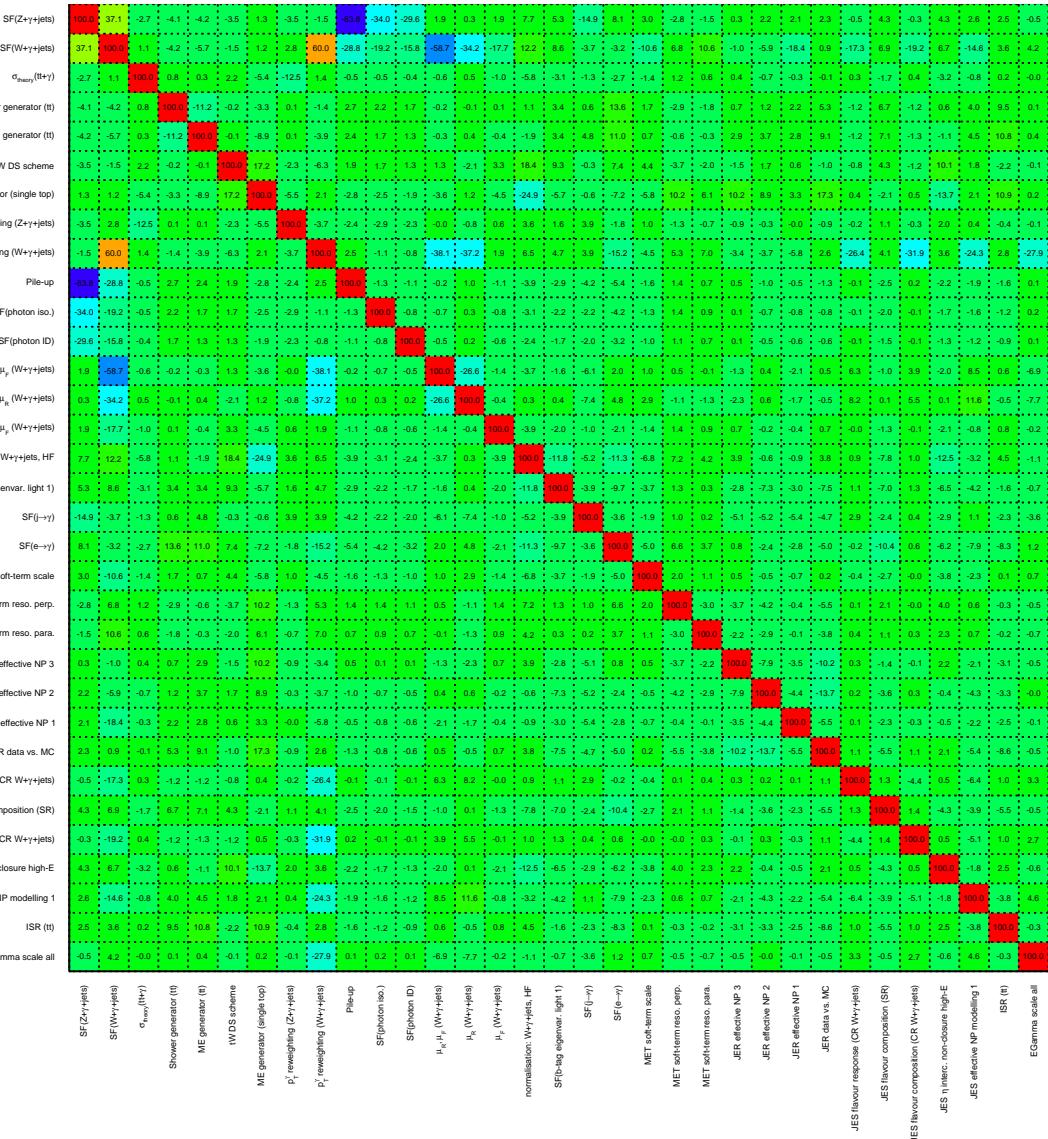
1860 Q Studies of a fit with a changed setup for the scale uncertainties

1861 The setup for the scale uncertainties is changed by introducing three variations only for the processes
 1862 $W+jets$, $W+\gamma+jets$, $Z+jets$, and $Z+\gamma+jets$ processes coming along with the largest scale uncertainties:
 1863 varying only the renormalisation scale μ_R , varying only the factorisation scale μ_F , and varying both
 1864 the factorisation μ_F and renormalisation scale μ_R . The fit is performed using data in all regions.
 1865 The observed limits on the branching ratio are given in Table 47. The outcomes and in particular the
 1866 limits for all four signal couplings give similar results as the default setup presented in Table 35. In
 1867 Figures 255, 257, 259, 261, the correlation matrices are show for the left-handed $t\gamma$, right-handed $t\gamma$,
 1868 left-handed $t\gamma\gamma$, and right-handed $t\gamma\gamma$ coupling, respectively. All the correlations are compatible with the
 1869 correlations seen using the default setup. The pull plots are presented in Figures 256, 258, 260 and 262
 1870 for the different signal couplings. As no unexpected behaviour compared to the default setup is observed,
 1871 it is conclude that the default setup for the scale uncertainties is sufficient.

Table 47: 95 % C.L. upper limits on the branching ratio $\mathcal{B}(t \rightarrow q\gamma)$ with $q = u, c$ for the different signal couplings with a varied setup for the scale uncertainties.

Signal coupling	$t\gamma$, left-handed	$t\gamma$, right-handed	$t\gamma\gamma$, left-handed	$t\gamma\gamma$, right-handed
$\mathcal{B}(t \rightarrow q\gamma) [10^{-5}]$	2.9	6.0	22.2	17.3

Not reviewed, for internal circulation only



9th July 2019 – 11:54

326

Not reviewed, for internal circulation only

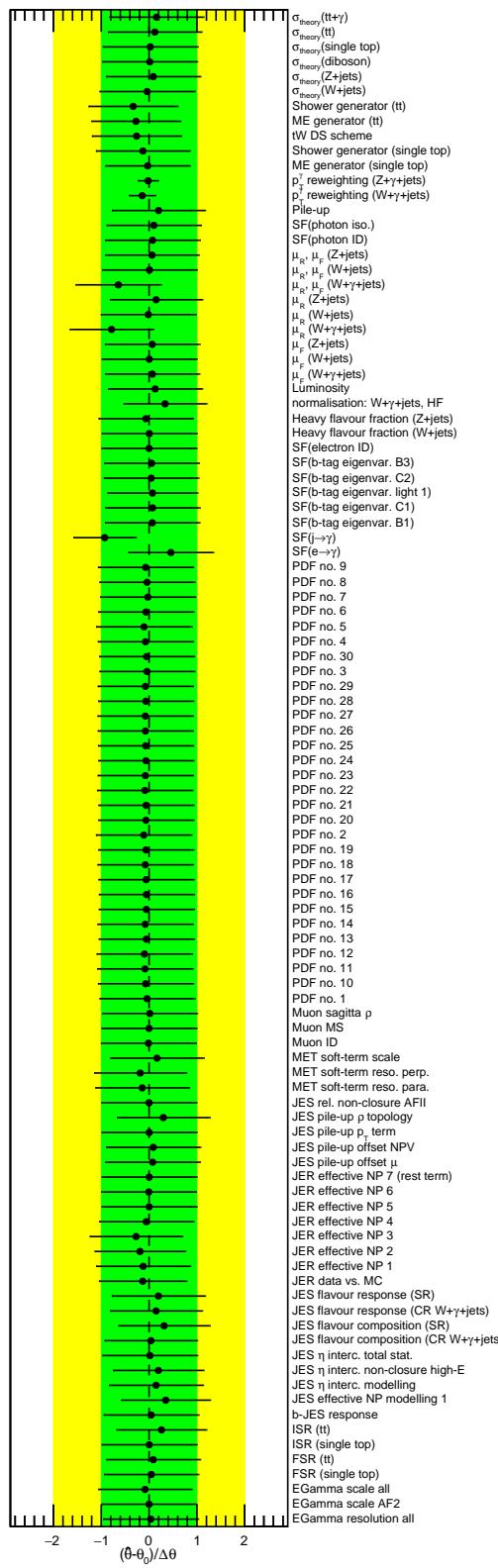
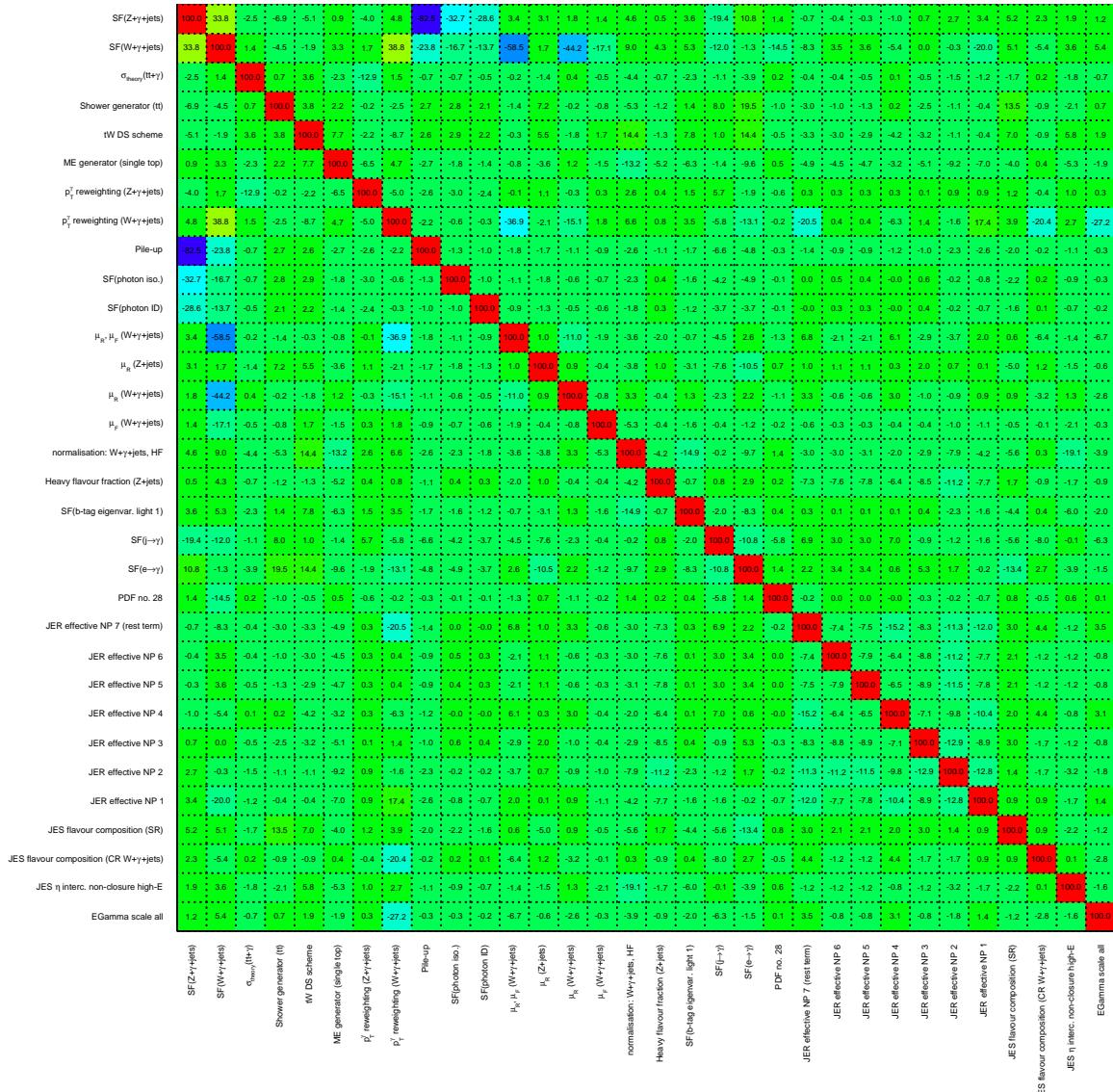


Figure 256: Pull values for the left-handed tuy coupling for the different nuisance parameters considered in the fit using data in all regions with a varied setup for the scale uncertainties.

Not reviewed, for internal circulation only



Not reviewed, for internal circulation only

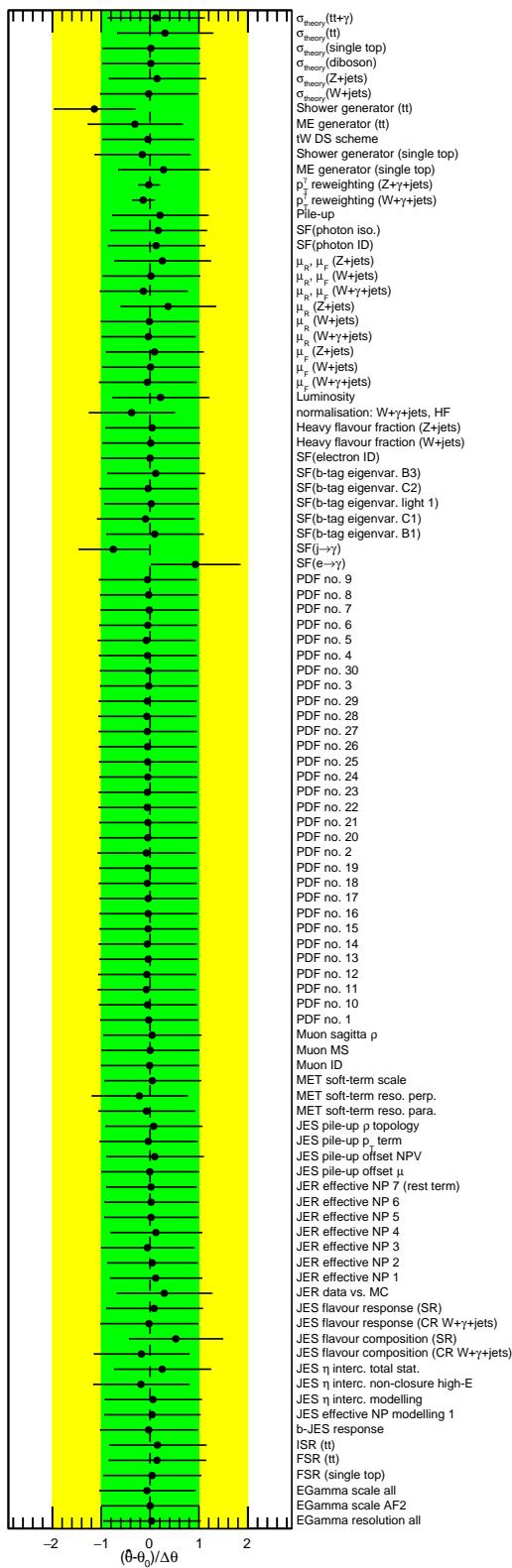


Figure 258: Pull values for the right-handed tuy coupling for the different nuisance parameters considered in the fit using data in all regions with a varied setup for the scale uncertainties.

Not reviewed, for internal circulation only

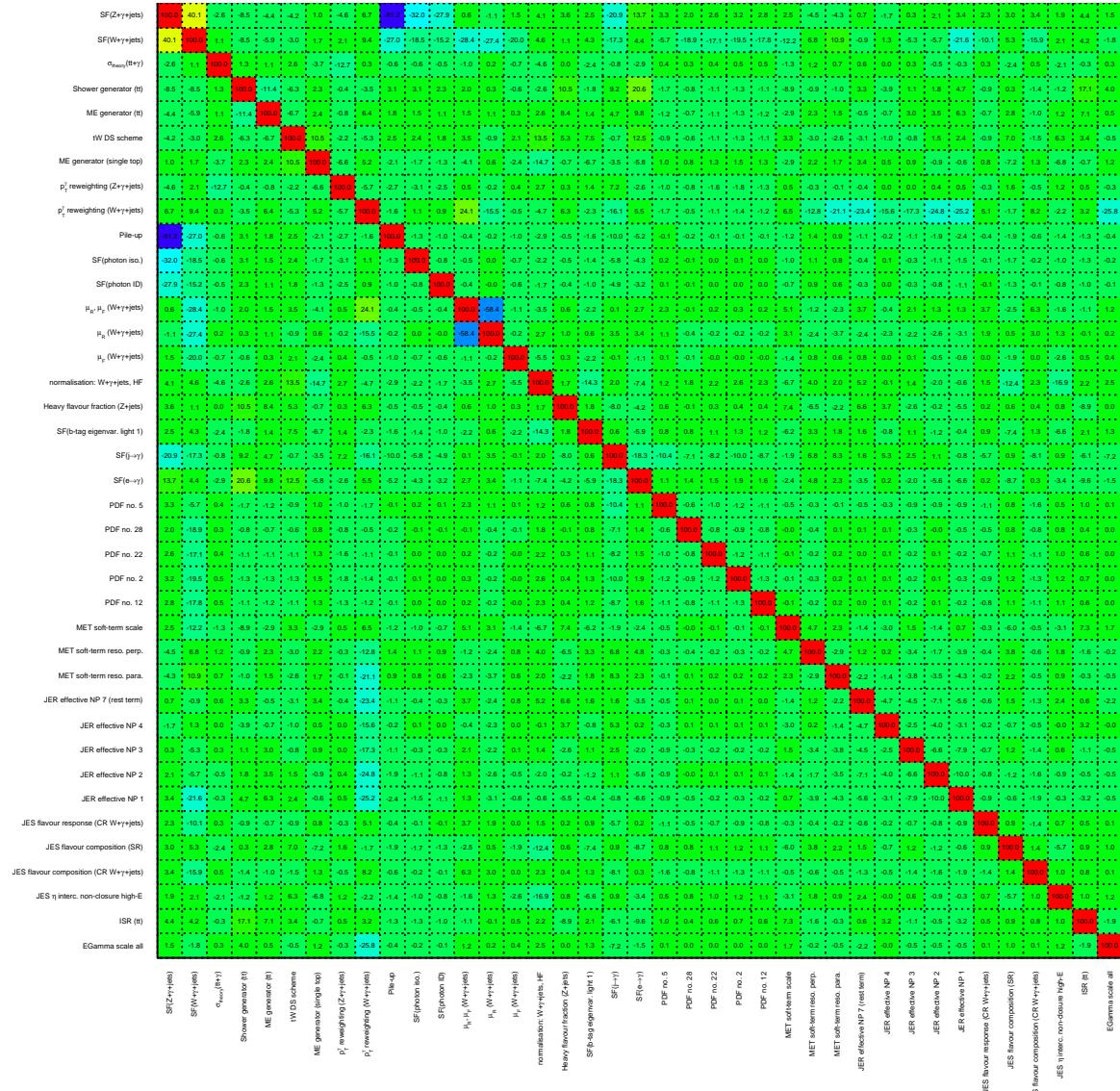


Figure 259: Correlation coefficients of all parameters with at least one coefficient above 10 % for the left-handed $tc\gamma$ coupling considered in the fit using data in all regions with a varied setup for the scale uncertainties.

Not reviewed, for internal circulation only

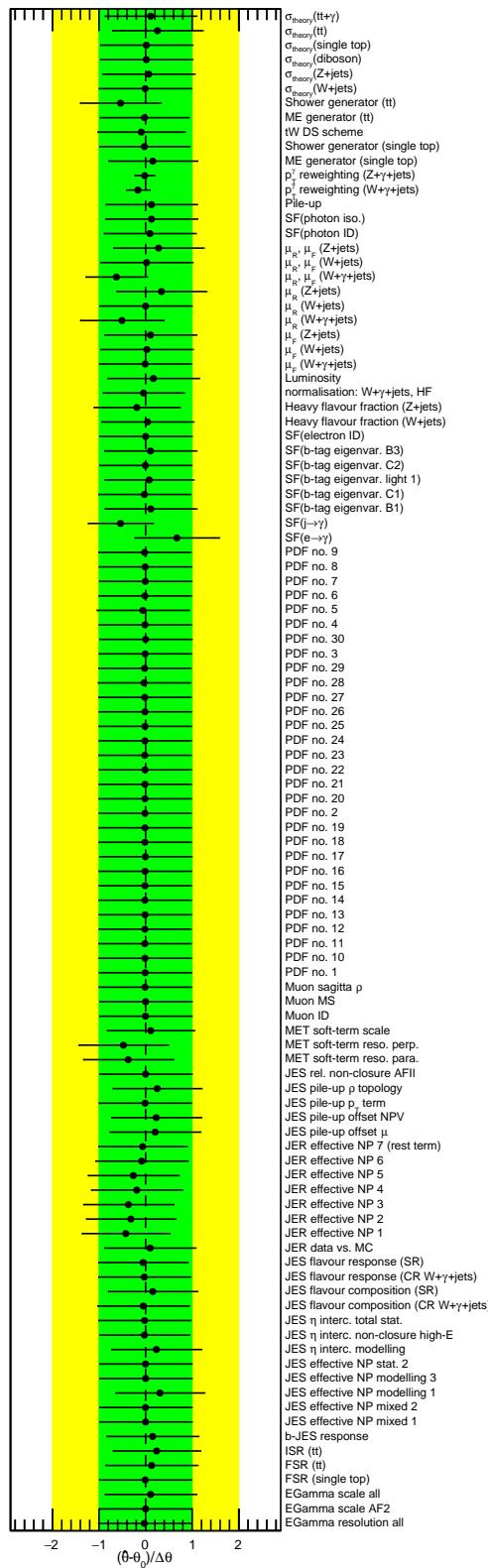


Figure 260: Pull values for the left-handed $tc\gamma$ coupling for the different nuisance parameters considered in the fit using data in all regions with a varied setup for the scale uncertainties.

Not reviewed, for internal circulation only

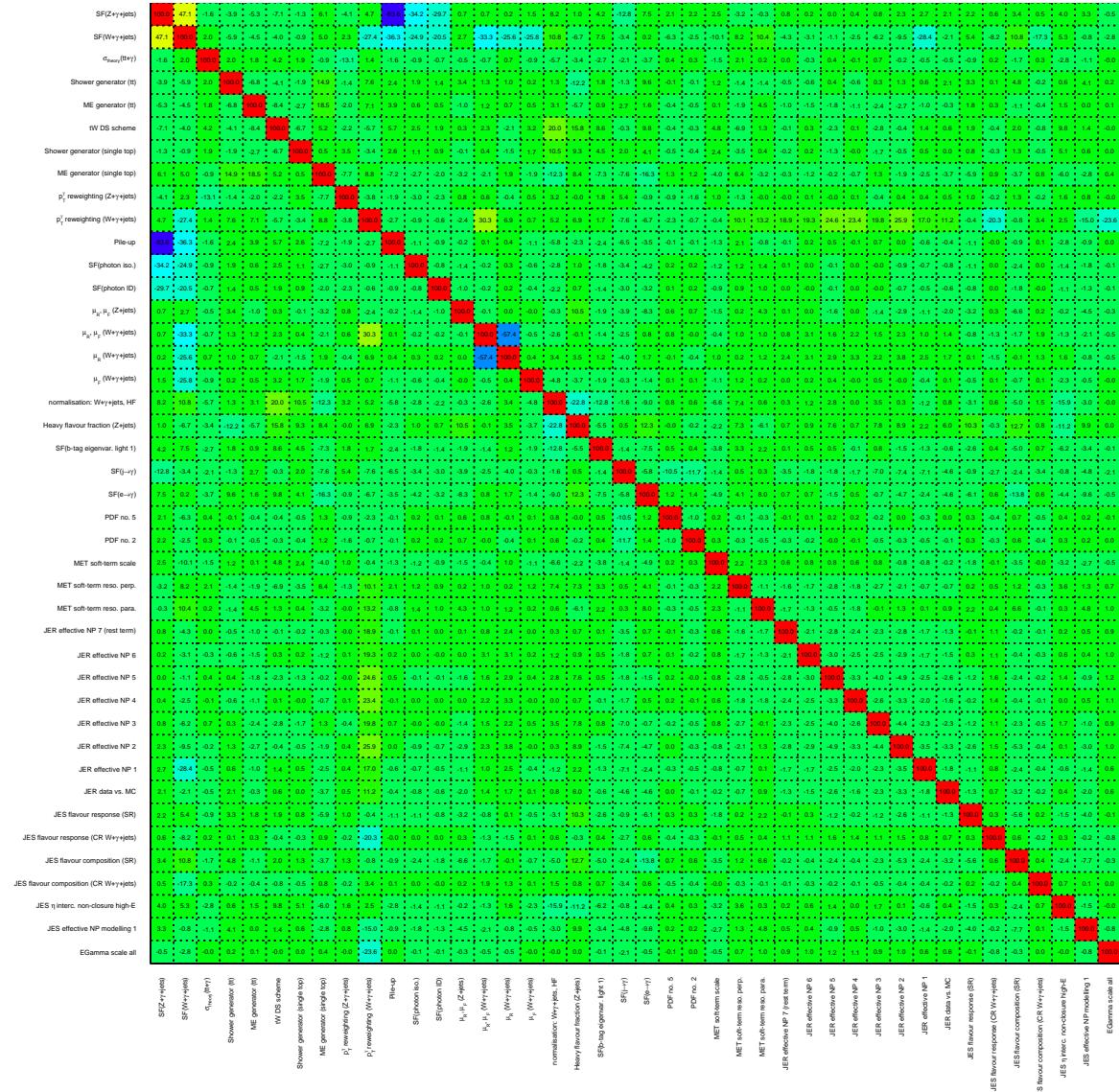


Figure 261: Correlation coefficients of all parameters with at least one coefficient above 10 % for the right-handed $tc\gamma$ coupling considered in the fit using data in all regions with a varied setup for the scale uncertainties.

Not reviewed, for internal circulation only

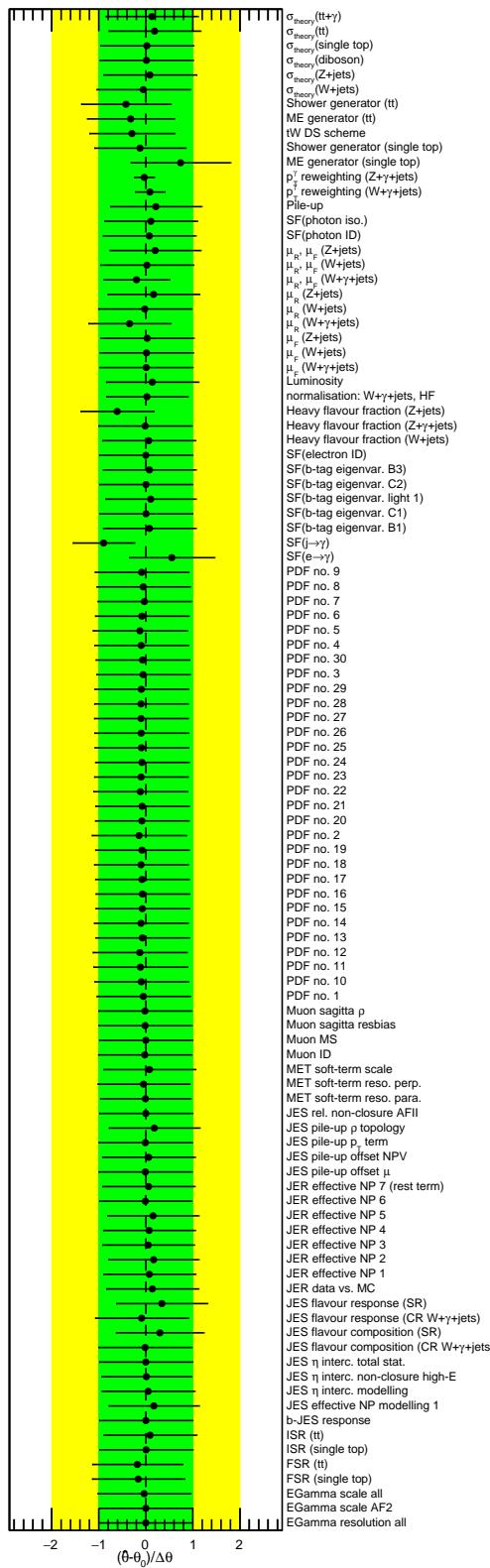


Figure 262: Pull values for the right-handed $tc\gamma$ coupling for the different nuisance parameters considered in the fit using data in all regions with a varied setup for the scale uncertainties.

R Studies for the default uncertainty on the SF($e \rightarrow \gamma$)

1872 The uncertainty on the electron-to-photon scale factor SF($e \rightarrow \gamma$) is 4 % as determined in the background
 1873 estimation presented in Section 7.1. In the nominal statistical fit, the uncertainty is multiplied by a factor
 1874 of 5 to reach the level of uncertainty as seen in other analyses. Now, the uncertainty as determined in
 1875 the background estimation is used in the fit being performed using data in all regions. The limits on
 1876 the branching ratio are given in Table 48. The outcomes and in particular the limits for all four signal
 1877 couplings give similar results as the setup presented in Table 35. In Figures 263, 264, 265 and 266,
 1878 the pull plots for the left-handed $t\gamma$, right-handed $t\gamma$, left-handed $t\gamma$, and right-handed $t\gamma$ coupling,
 1879 respectively, are shown. It can be seen that the uncertainty is less pulled compared to the default setup.
 1880

Table 48: 95 % C.L. upper limits on the branching ratio $\mathcal{B}(t \rightarrow q\gamma)$ with $q = u, c$ for the different signal couplings when using an increased uncertainty on electron-to-photon scale factor.

Signal coupling	$t\gamma$, left-handed	$t\gamma$, right-handed	$t\gamma$, left-handed	$t\gamma$, right-handed
$\mathcal{B}(t \rightarrow q\gamma) [10^{-5}]$	2.8	6.0	21.9	18.4

Not reviewed, for internal circulation only

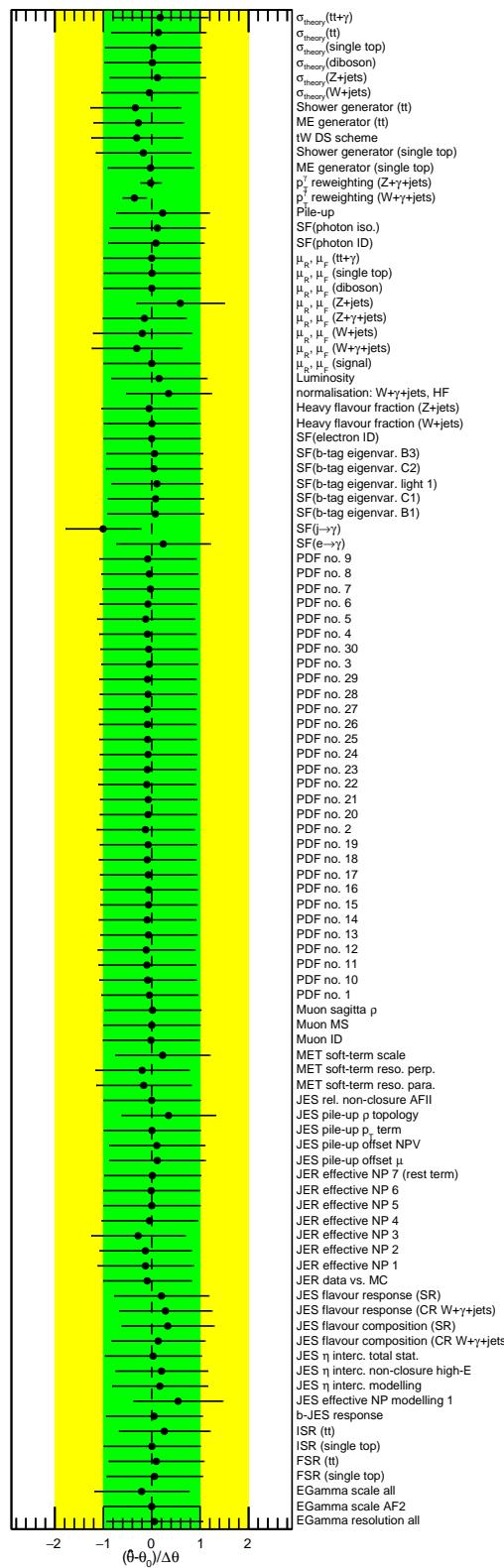


Figure 263: Pull values for the left-handed tuy coupling for the different nuisance parameters considered in the fit using data in all regions with an increased uncertainty on electron-to-photon scale factor.

Not reviewed, for internal circulation only

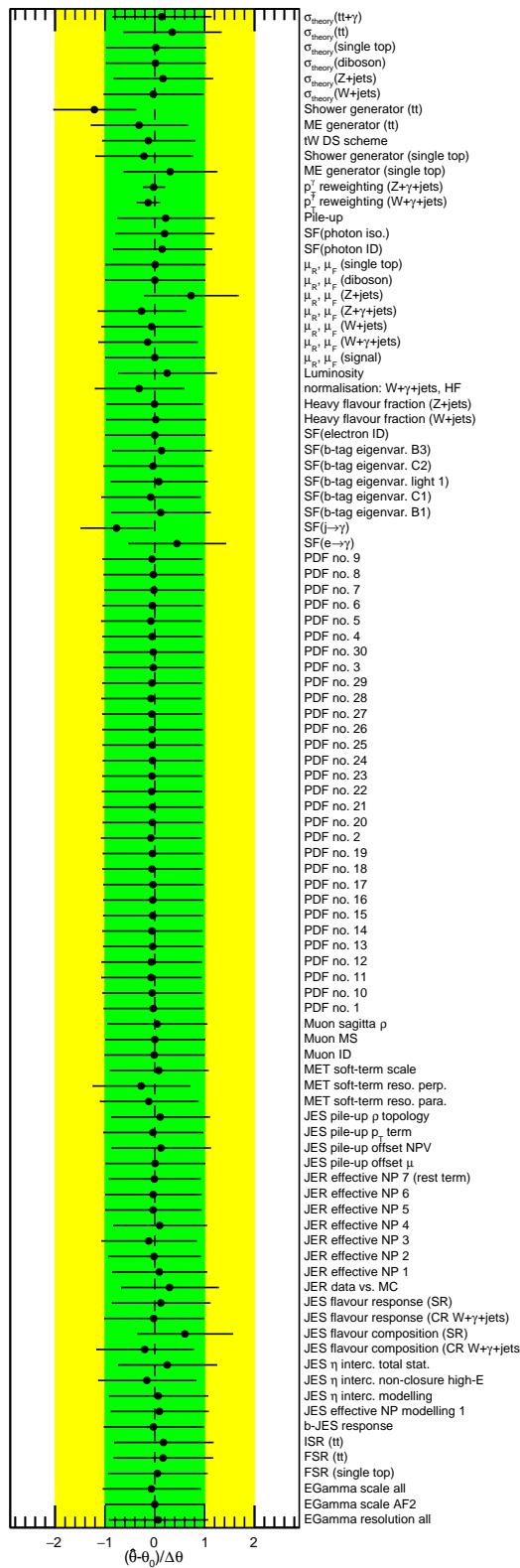


Figure 264: Pull values for the right-handed $t\gamma y$ coupling for the different nuisance parameters considered in the fit using data in all regions with an increased uncertainty on electron-to-photon scale factor.

Not reviewed, for internal circulation only

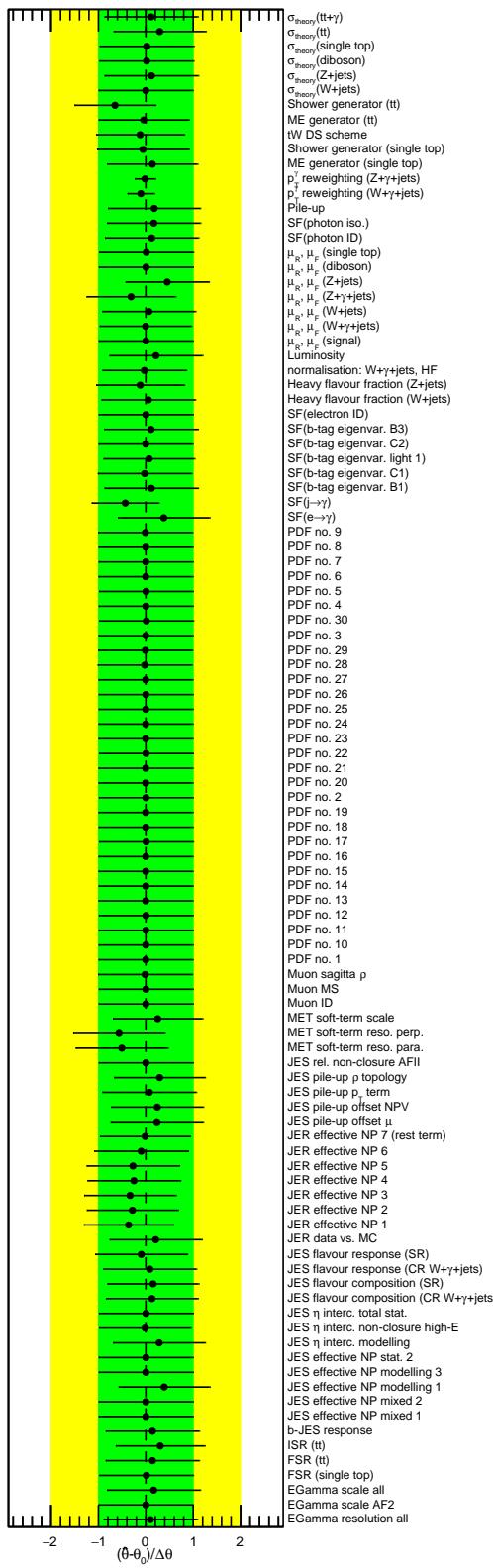


Figure 265: Pull values for the left-handed $tc\gamma$ coupling for the different nuisance parameters considered in the fit using data in all regions with an increased uncertainty on electron-to-photon scale factor.

Not reviewed, for internal circulation only

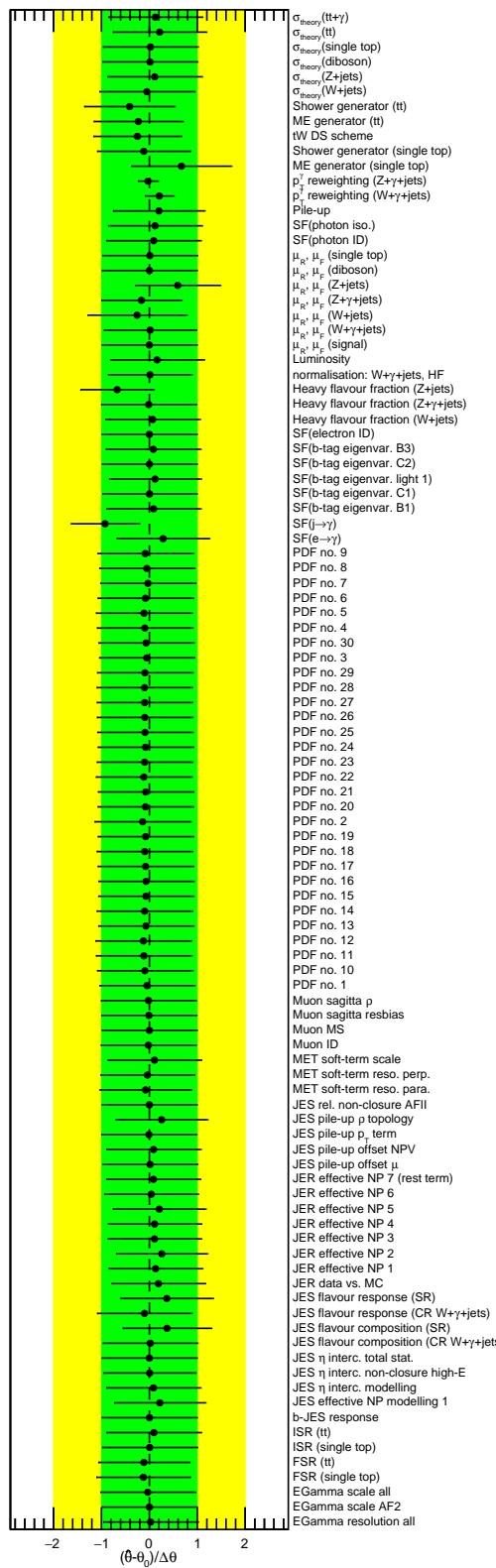


Figure 266: Pull values for the right-handed $tc\gamma$ coupling for the different nuisance parameters considered in the fit using data in all regions with an increased uncertainty on electron-to-photon scale factor.

1881 **S Studies with photon p_T as discriminating variable**

1882 Since the distribution of the photon p_T separates well between signal and background as can be seen in
 1883 Figures 29 and in Appendix L, the statistical fit is redone with this variable using Asimov data. The
 1884 expected limits on the branching ratio $\mathcal{B}(t \rightarrow q\gamma)$ are shown in Table 49. It can be seen that the limits
 1885 for the tuy couplings are close to the ones when using the NN output distribution as shown in Table 36,
 1886 while they become much weaker for the $tc\gamma$ couplings.

Table 49: 95 % C.L. expected upper limits on the branching ratio $\mathcal{B}(t \rightarrow q\gamma)$ with $q = u, c$ for the different signal
 couplings when using the photon p_T distribution as discriminating variable in the statistical fit.

Signal coupling	tuy , left-handed	tuy , right-handed	$tc\gamma$, left-handed	$tc\gamma$, right-handed
$\mathcal{B}(t \rightarrow q\gamma) [10^{-5}]$	4.4	5.3	31.5	36.7

1887 T Pruning of the nuisance parameters for the different signal couplings

Not reviewed, for internal circulation only

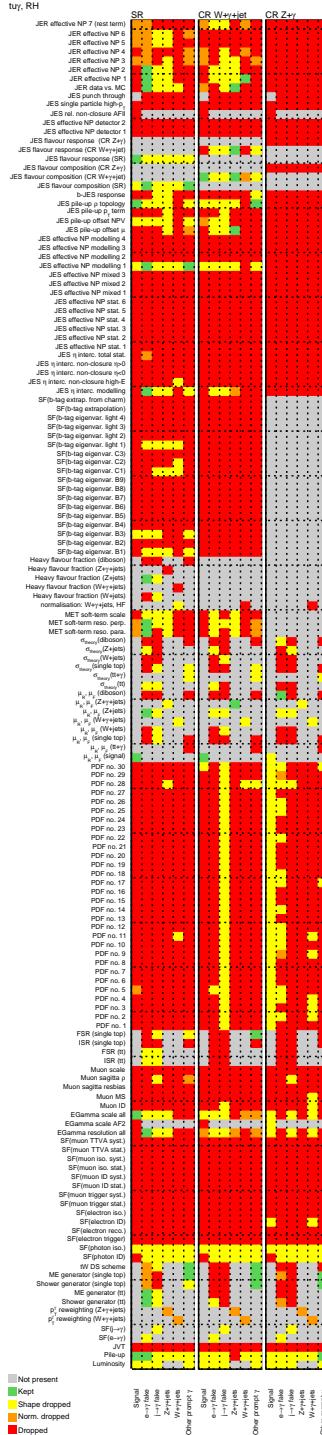


Figure 267: Overview of all nuisance parameters after pruning for the right-handed tuy coupling: if the shape and/or normalisation impacts are smaller than 1 %, the normalisation and/or shape of the parameter will be dropped, shown as orange, yellow or red square.

Not reviewed, for internal circulation only

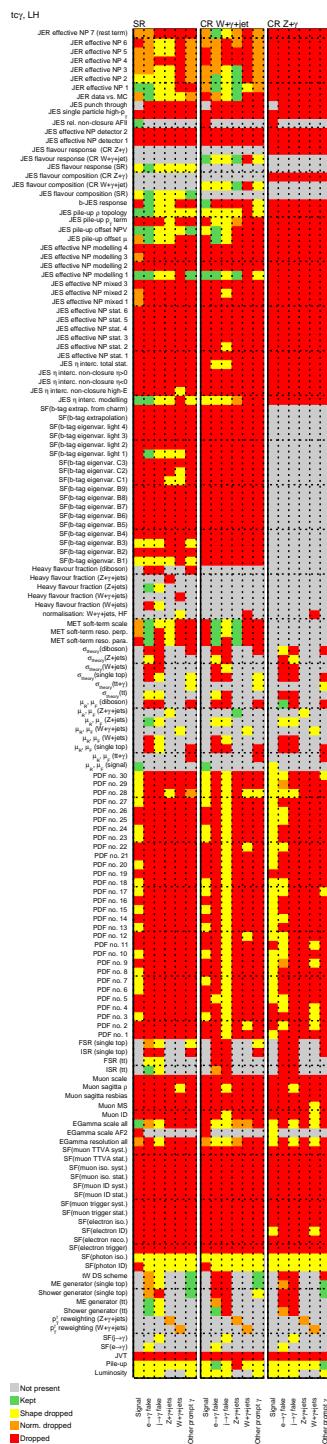


Figure 268: Overview of all nuisance parameters after pruning for the left-handed $t\gamma$ coupling: if the shape and/or normalisation impacts are smaller than 1 %, the normalisation and/or shape of the parameter will be dropped, shown as orange, yellow or red square.

Not reviewed, for internal circulation only

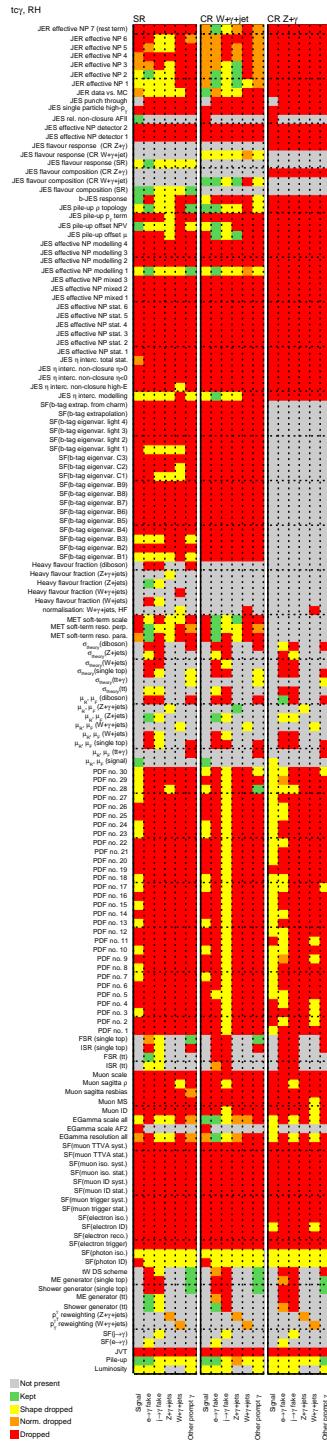


Figure 269: Overview of all nuisance parameters after pruning for the right-handed $t\gamma\gamma$ coupling: if the shape and/or normalisation impacts are smaller than 1 %, the normalisation and/or shape of the parameter will be dropped, shown as orange, yellow or red square.

1888 U Composition of physics processes of the photon fake categories

Not reviewed, for internal circulation only

Table 50: Expected number of events per physics process classified as $e \rightarrow \gamma$ fakes in the electron+muon channel in the SR, CR $W+\gamma+\text{jets}$, and CR $Z+\gamma$. The data-driven scale factors for the photon fake estimations are already considered. Only the statistical uncertainty is shown.

Process	SR	CR $W+\gamma+\text{jets}$	CR $Z+\gamma$
Single top	398 \pm 10	296.7 \pm 8.8	0.81 \pm 0.47
$t\bar{t}$	2 015 \pm 20	1 444 \pm 17	4.2 \pm 1.0
$W+\text{jets}$	3.5 \pm 3.1	10.4 \pm 3.6	<0.01 \pm < 0.01
$Z+\text{jets}$	1 408 \pm 76	4 530 \pm 230	4.1 \pm 3.1
Diboson	16.0 \pm 1.2	550.3 \pm 7.2	217.7 \pm 3.5
Total	3 840 \pm 79	6 840 \pm 230	226.9 \pm 4.8

Table 51: Expected number of events per physics process classified as $j \rightarrow \gamma$ fakes in the electron+muon channel in the SR, CR $W+\gamma+\text{jets}$, and CR $Z+\gamma$. The data-driven scale factors for the photon fake estimations are already considered. Only the statistical uncertainty is shown.

Process	SR	CR $W+\gamma+\text{jets}$	CR $Z+\gamma$
Single top	145.1 \pm 8.1	114.4 \pm 7.3	3.6 \pm 1.3
$t\bar{t}$	296 \pm 10	280 \pm 10	97.9 \pm 6.0
$W+\text{jets}$	53 \pm 51	6 990 \pm 650	<0.01 \pm < 0.01
$Z+\text{jets}$	16 \pm 12	780 \pm 120	2 630 \pm 280
Diboson	1.6 \pm 1.4	73.0 \pm 7.3	30.2 \pm 1.7
Total	511 \pm 54	8 230 \pm 660	2 760 \pm 280

Table 52: Expected number of events per physics process classified as *other prompt photons* in the electron+muon channel in the SR, CR $W+\gamma+\text{jets}$, and CR $Z+\gamma$. The data-driven scale factors for the photon fake estimations are already considered. Only the statistical uncertainty is shown.

Process	SR	CR $W+\gamma+\text{jets}$	CR $Z+\gamma$
Single top	427 \pm 11	456 \pm 11	154.5 \pm 6.4
$t\bar{t} + \gamma$	1 199.4 \pm 7.1	1 154.1 \pm 7.1	1 708.7 \pm 8.4
Diboson	4.66 \pm 0.68	179.5 \pm 3.9	244.2 \pm 3.5
Total	1 631 \pm 13	1 790 \pm 14	2 107 \pm 11

1889 V Statistical fit for different signal samples using Asimov data

1890 V.1 Statistical fit using Asimov data for the right-handed $t\bar{u}\gamma$ coupling

Not reviewed, for internal circulation only

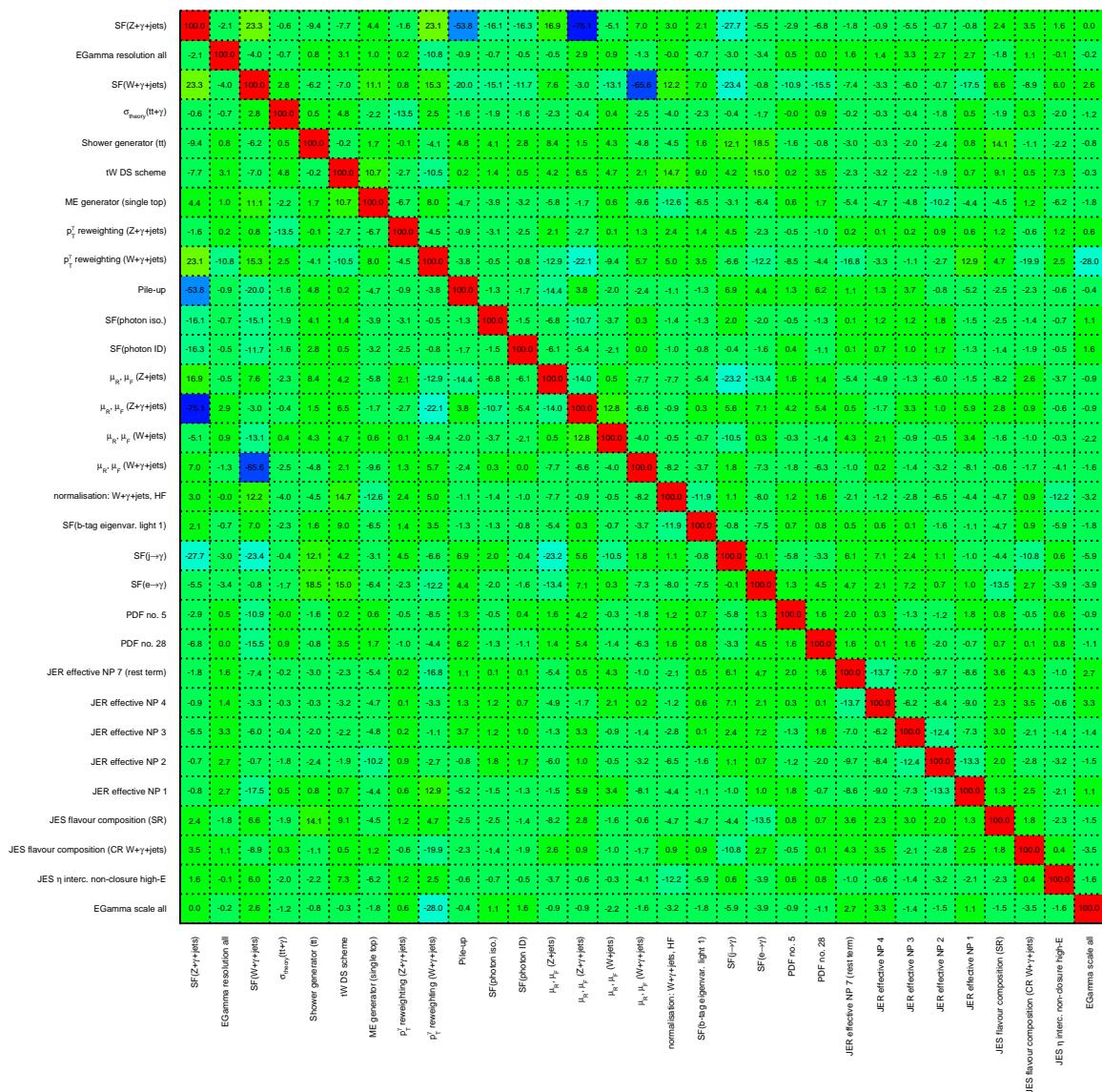


Figure 270: Correlation coefficients of all parameters with at least one coefficient above 10 % for the right-handed tuy coupling considered in the fit using Asimov data.

Not reviewed, for internal circulation only

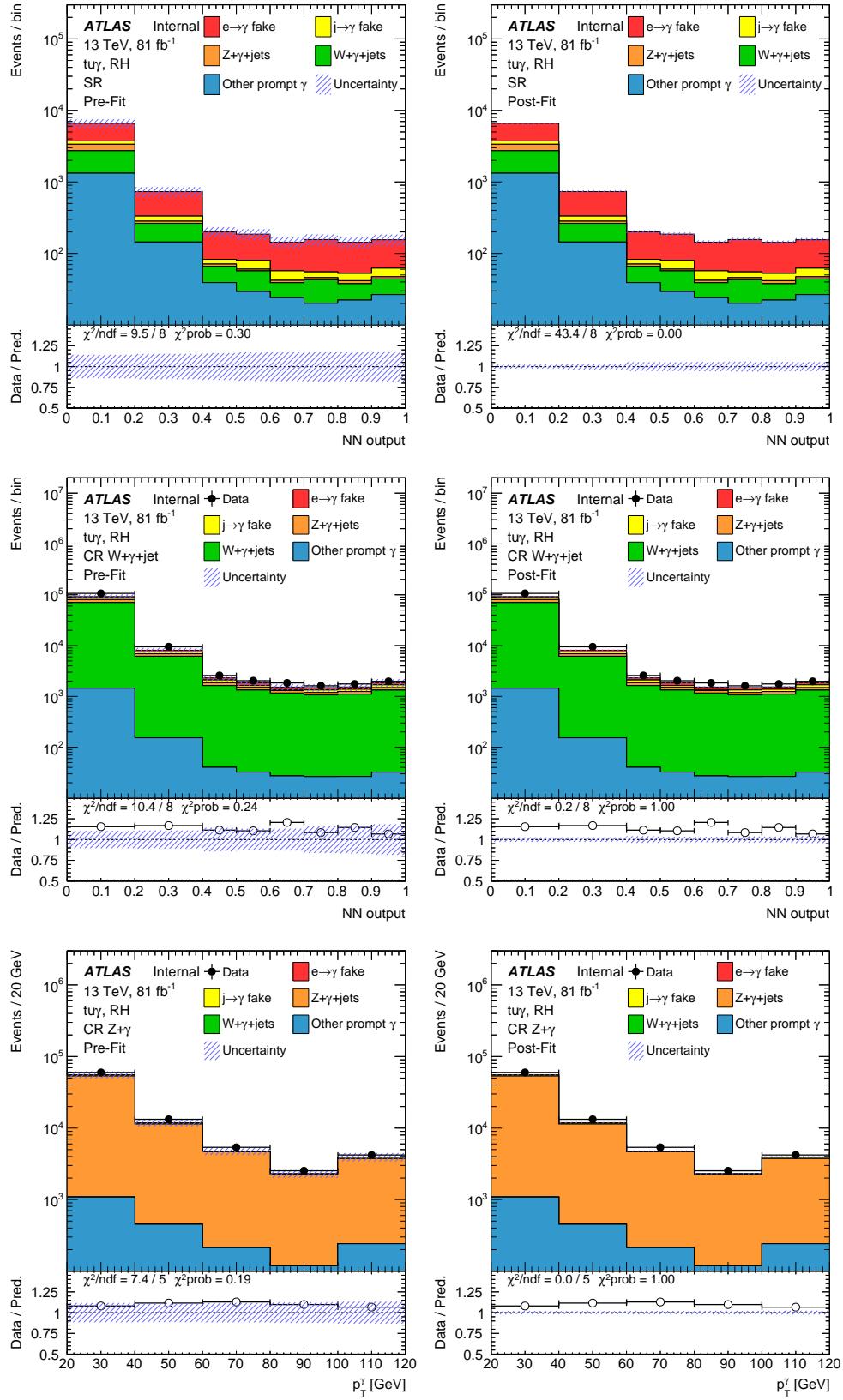


Figure 271: Pre- (left) and post-fit (right) distributions for the right-handed signal coupling tuy using Asimov data: NN output distribution in the SR (top) and in the CR $W + \gamma + \text{jets}$ (middle) and the photon p_T spectrum in the CR $Z + \gamma$ (bottom). Statistical and systematic uncertainties are included.

Not reviewed, for internal circulation only

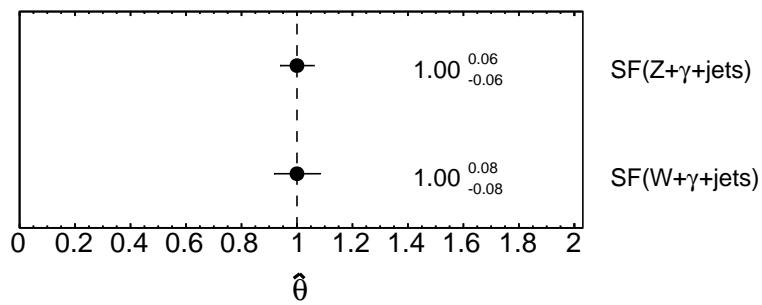


Figure 272: Normalisation factors for the $W+\gamma+jets$ and $Z+\gamma+jets$ process using Asimov data for the right-handed $t\gamma\gamma$ coupling.

Not reviewed, for internal circulation only

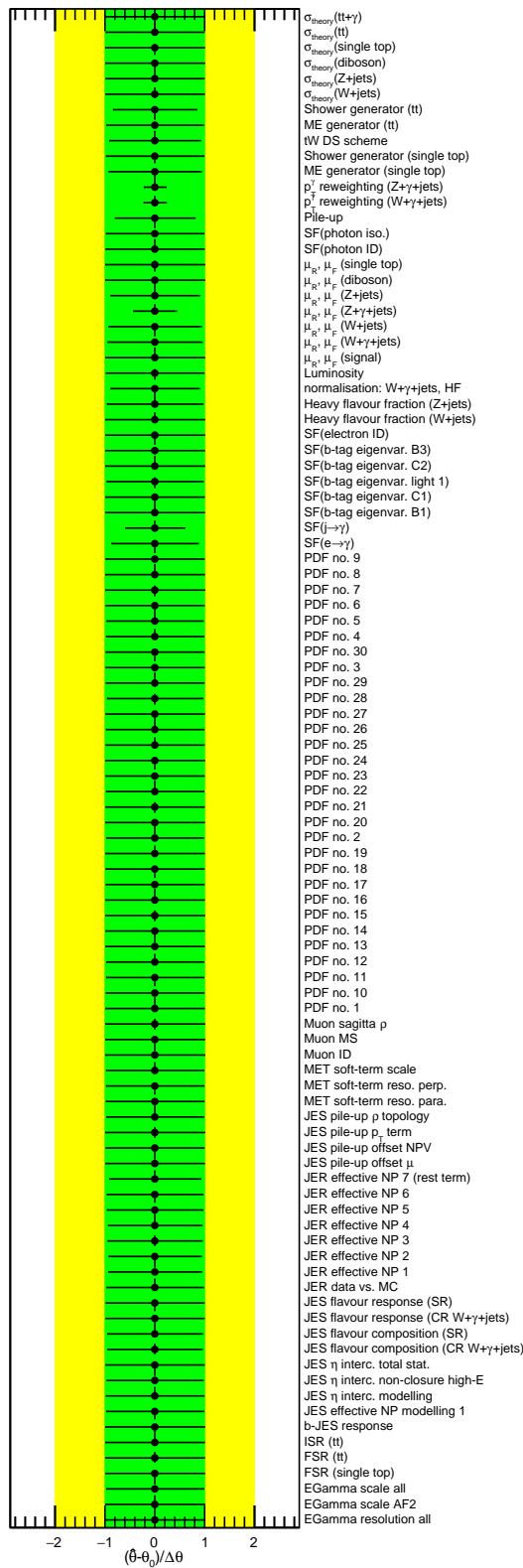


Figure 273: Pull values for the right-handed $t\bar{t}\gamma$ coupling for the different nuisance parameters considered in the fit using Asimov data.

Not reviewed, for internal circulation only

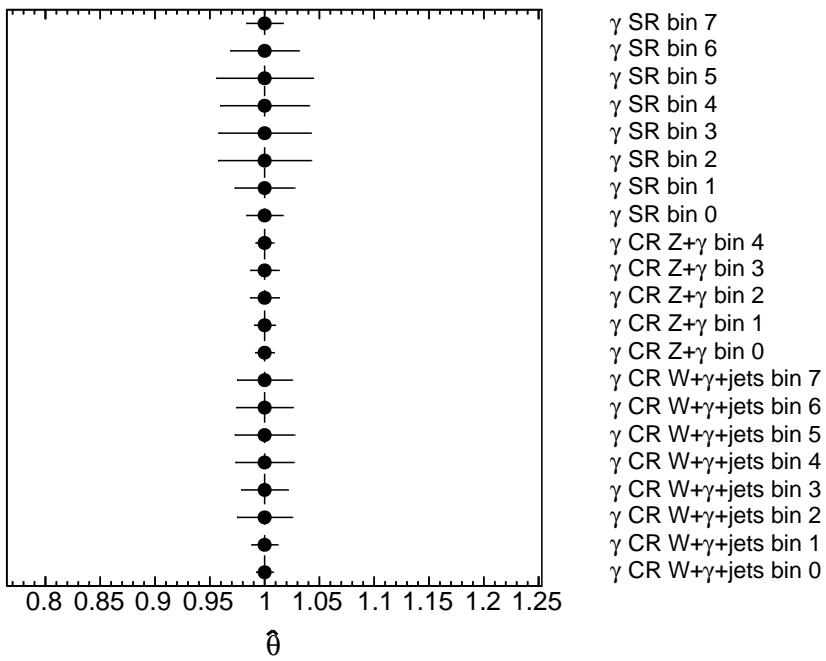


Figure 274: Normalisation factors γ for each bin in each region for the right-handed $t\bar{u}\gamma$ coupling using Asimov data.

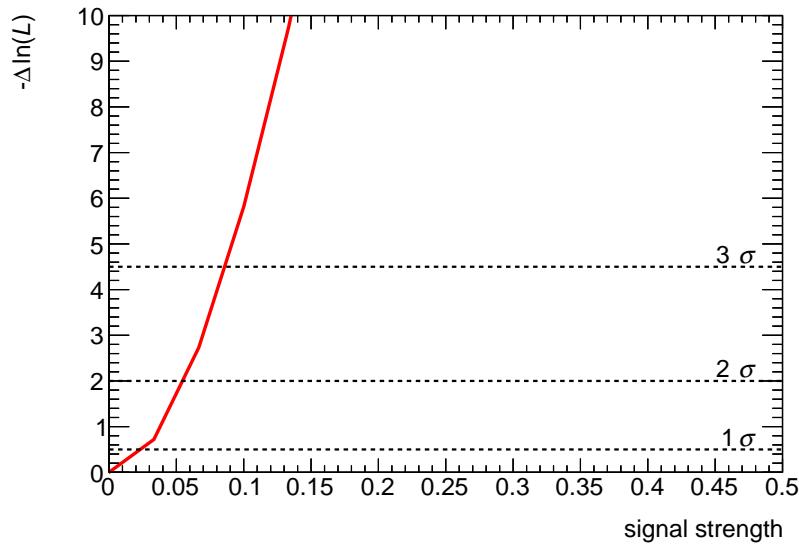


Figure 275: Distributions of the negative-log likelihood for the signal strength using Asimov data for the right-handed $t\bar{u}\gamma$ coupling. The one, two and three standard deviations are marked.

Not reviewed, for internal circulation only

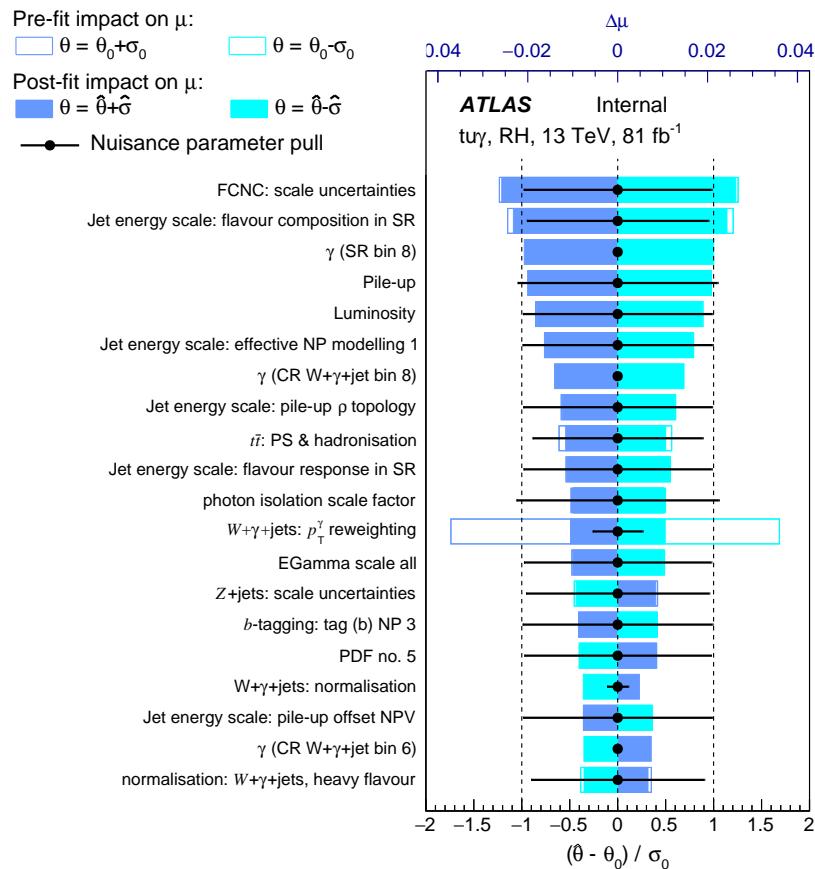


Figure 276: Ranking plot for the 20 nuisance parameters with the largest impact on the signal strength for the right-handed tuy coupling using Asimov data and $\mu = 1$.

1891 V.2 Statistical fit using Asimov data for the left-handed $t\gamma\gamma$ coupling

Not reviewed, for internal circulation only

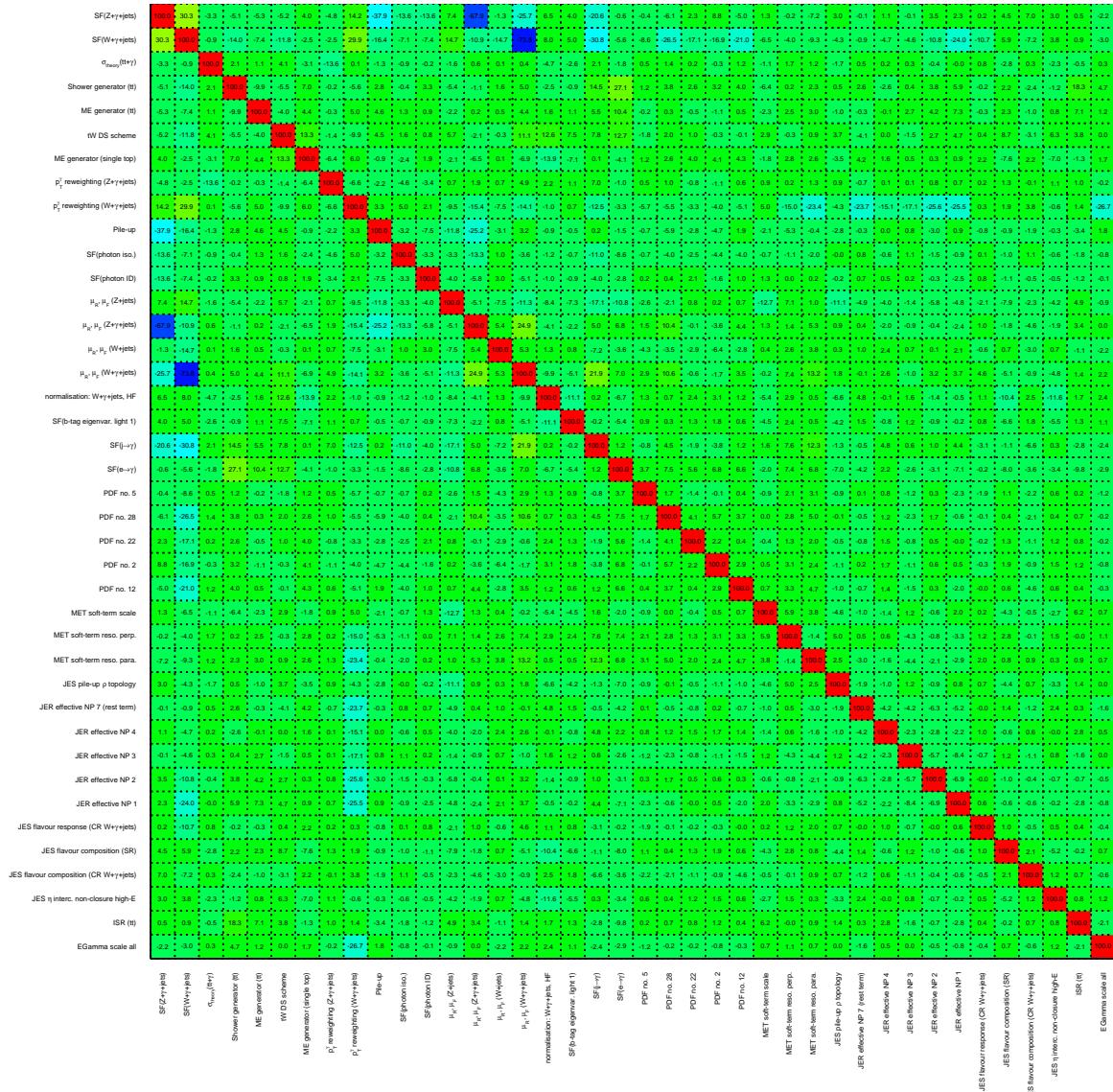


Figure 277: Correlation coefficients of all parameters with at least one coefficient above 10 % for the left-handed $t\gamma\gamma$ coupling considered in the fit using Asimov data.

Not reviewed, for internal circulation only

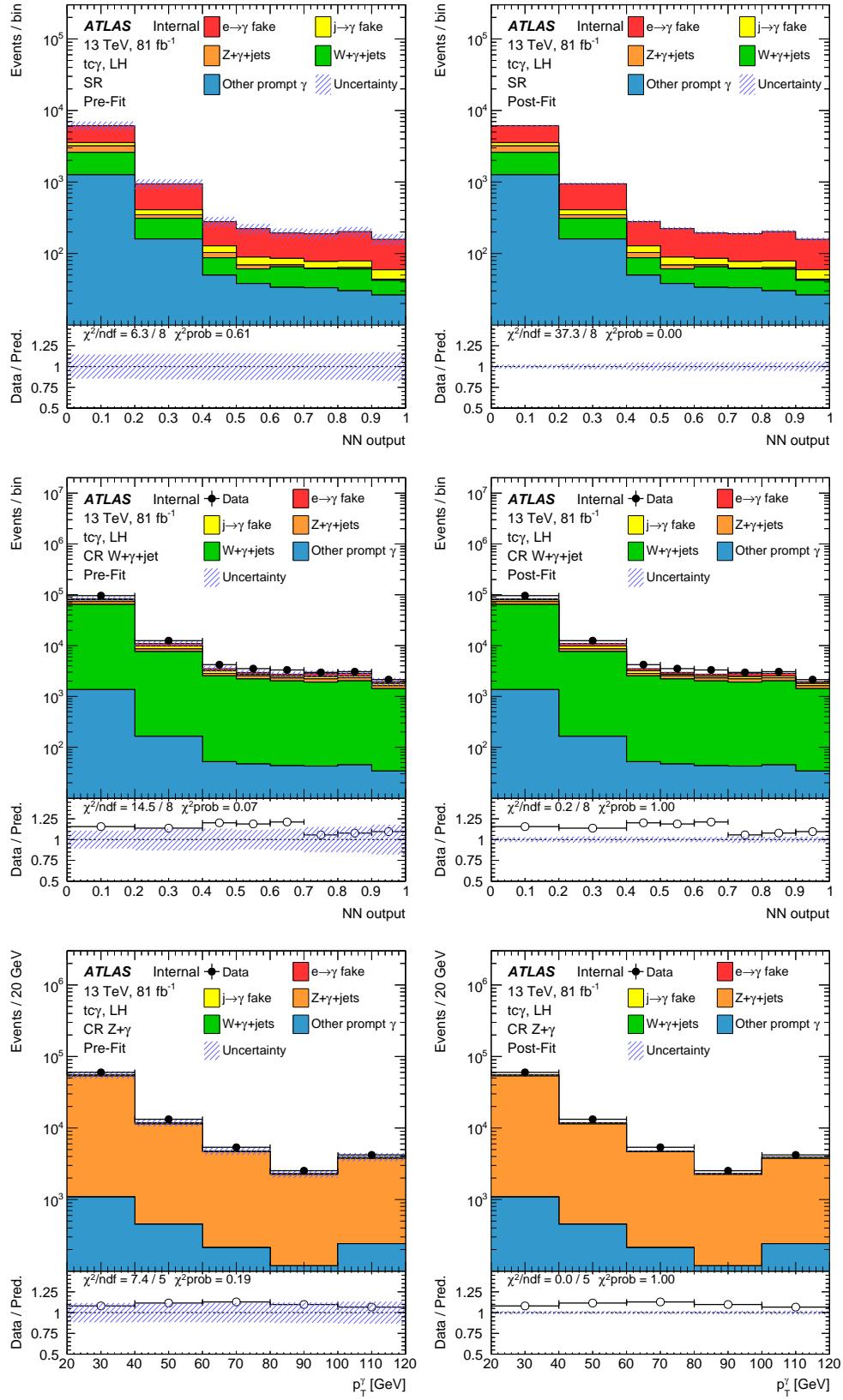


Figure 278: Pre- (left) and post-fit (right) distributions for the left-handed signal coupling $t\gamma\gamma$ using Asimov data: NN output distribution in the SR (top) and in the CR $W+\gamma+jets$ (middle) and the photon p_T spectrum in the CR $Z + \gamma$ (bottom). Statistical and systematic uncertainties are included.

Not reviewed, for internal circulation only

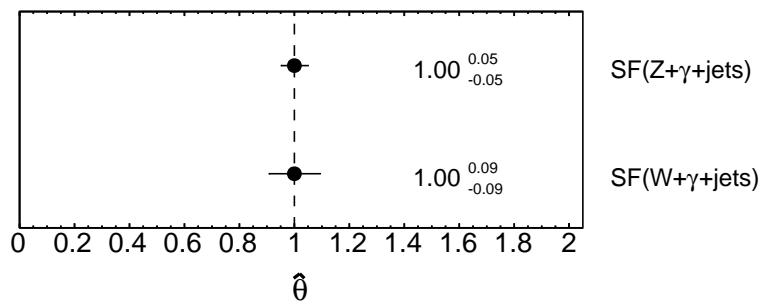


Figure 279: Normalisation factors for the $W+\gamma+\text{jets}$ and $Z+\gamma+\text{jets}$ process using Asimov data for the left-handed $t\gamma\gamma$ coupling.

Not reviewed, for internal circulation only

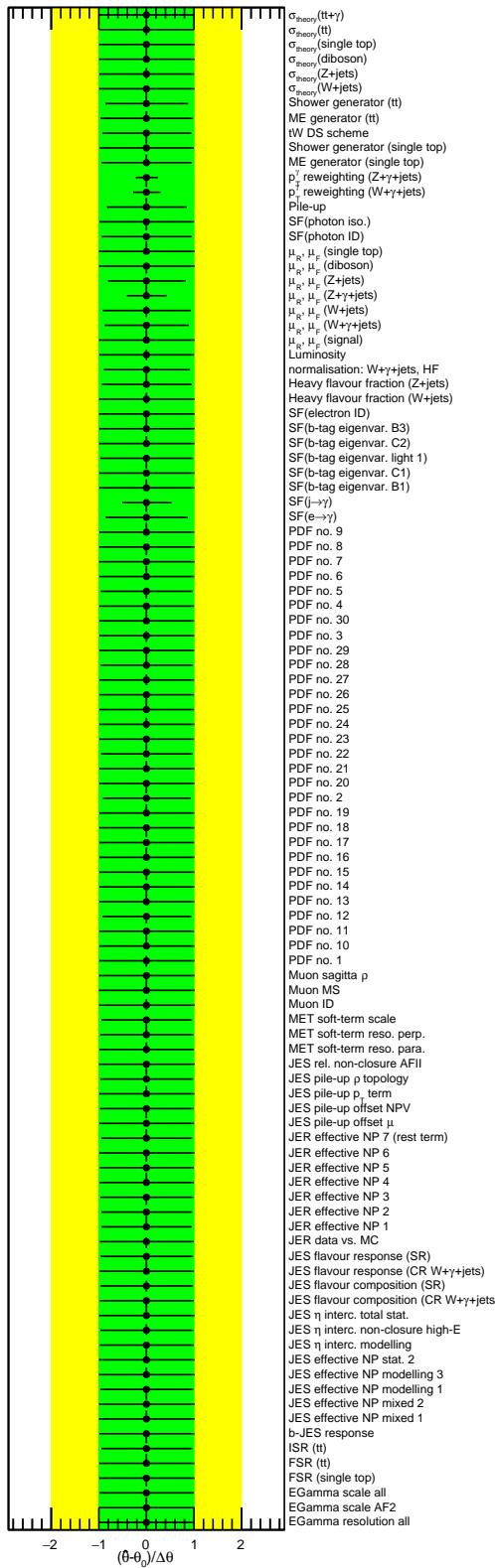


Figure 280: Pull values for the left-handed $tc\gamma$ coupling for the different nuisance parameters considered in the fit using Asimov data.

Not reviewed, for internal circulation only

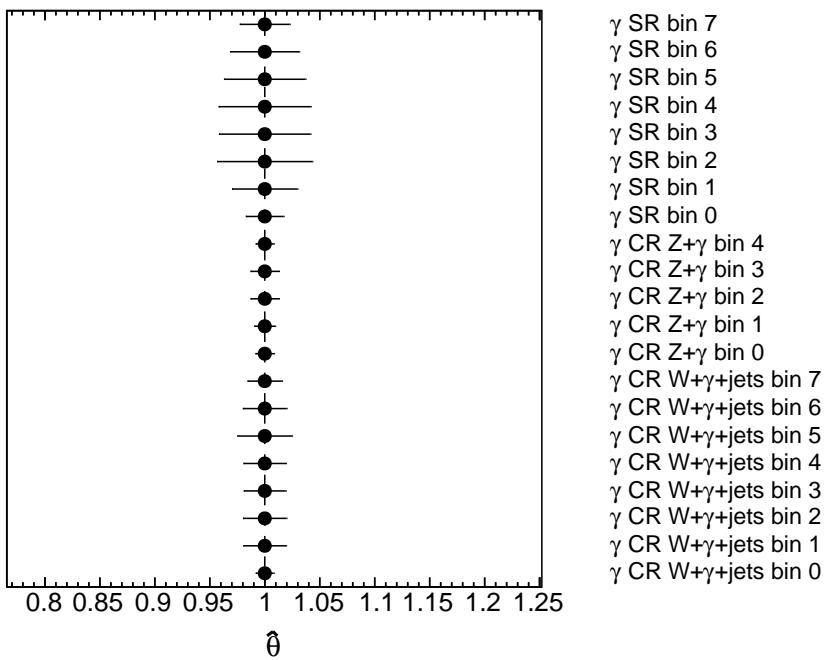


Figure 281: Normalisation factors γ for each bin in each region for the left-handed $t\gamma\gamma$ coupling using Asimov data.

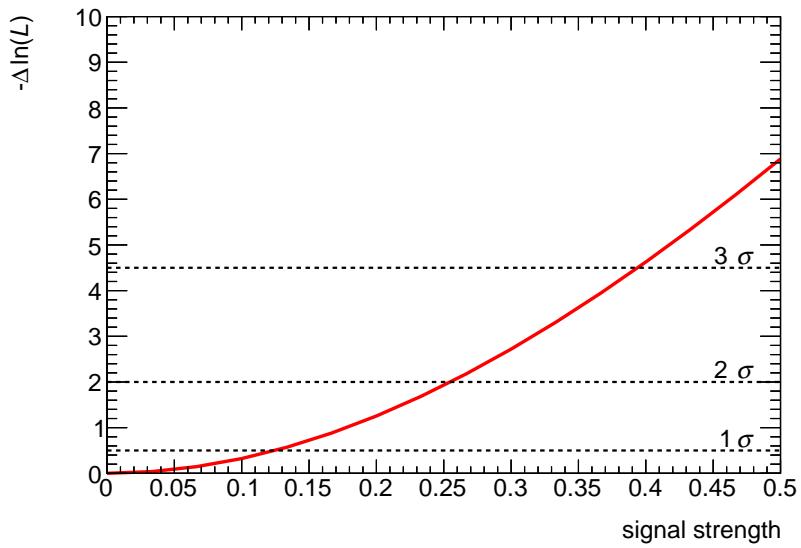


Figure 282: Distributions of the negative-log likelihood for the signal strength using Asimov data for the left-handed $t\gamma\gamma$ coupling. The one, two and three standard deviations are marked.

Not reviewed, for internal circulation only

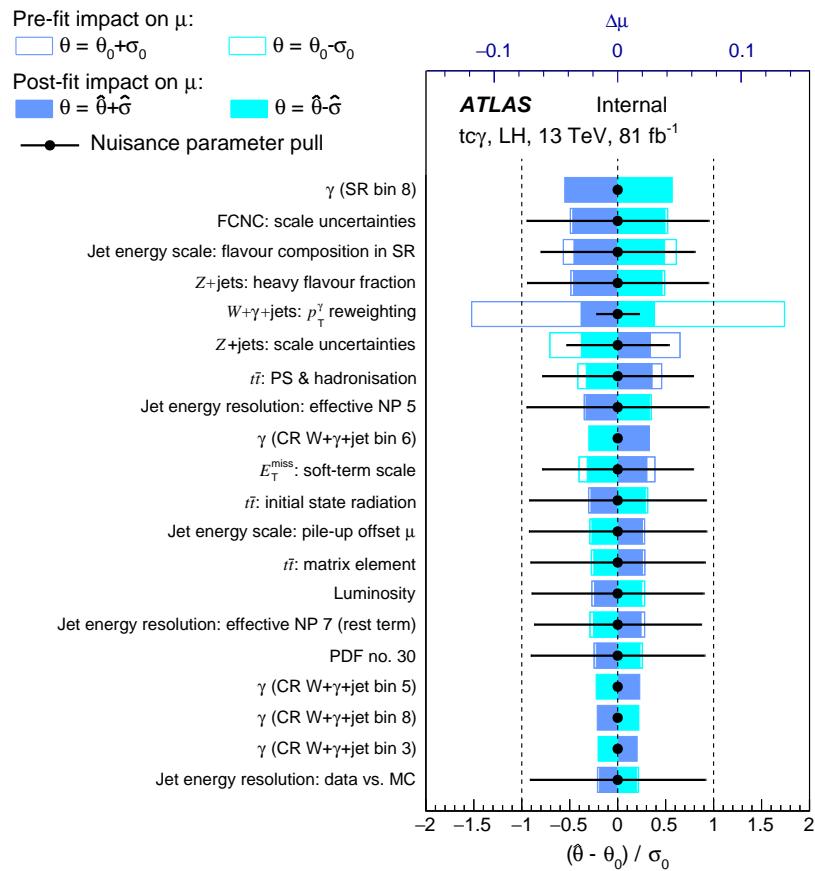


Figure 283: Ranking plot for the 20 nuisance parameters with the largest impact on the signal strength for the left-handed $tc\gamma$ coupling using Asimov data and $\mu = 1$.

1892 V.3 Statistical fit using Asimov data for the right-handed $t\gamma\gamma$ coupling

Not reviewed, for internal circulation only

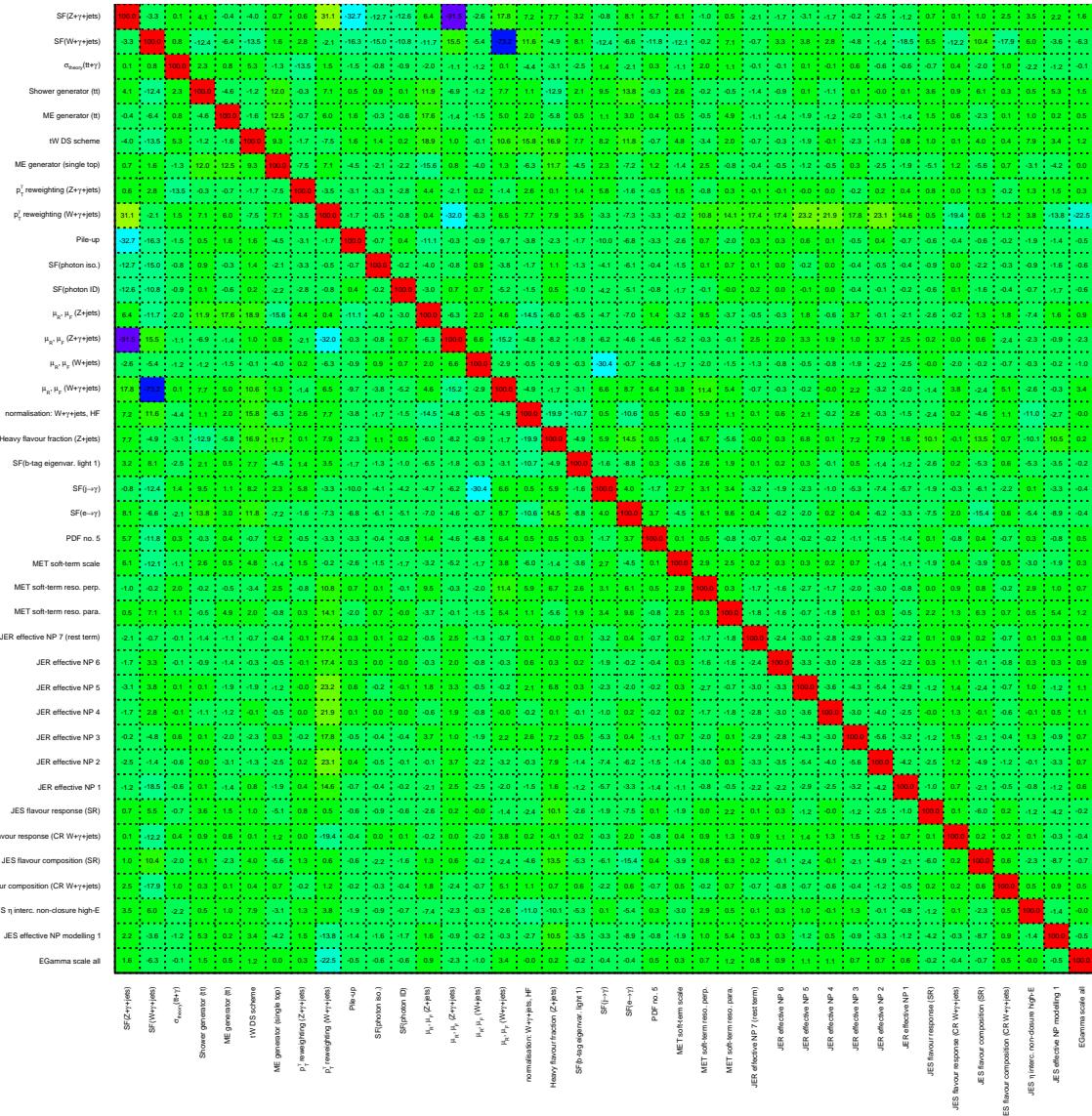


Figure 284: Correlation coefficients of all parameters with at least one coefficient above 10 % for the right-handed $t\gamma\gamma$ coupling considered in the fit using Asimov data.

Not reviewed, for internal circulation only

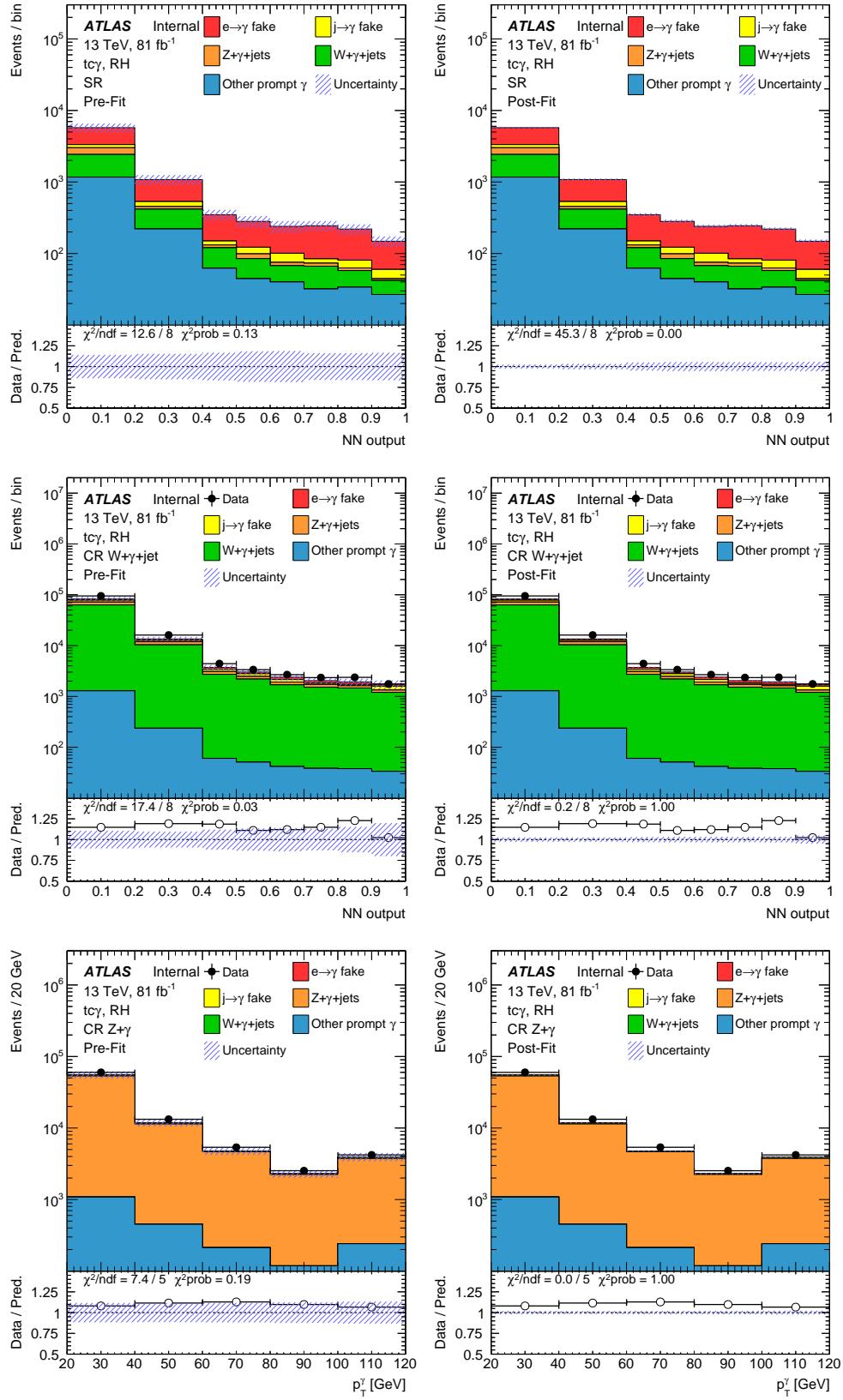


Figure 285: Pre- (left) and post-fit (right) distributions for the right-handed signal coupling $tc\gamma$ using Asimov data: NN output distribution in the SR (top) and in the CR $W+\gamma+jets$ (middle) and the photon p_T spectrum in the CR $Z + \gamma$ (bottom). Statistical and systematic uncertainties are included..

Not reviewed, for internal circulation only

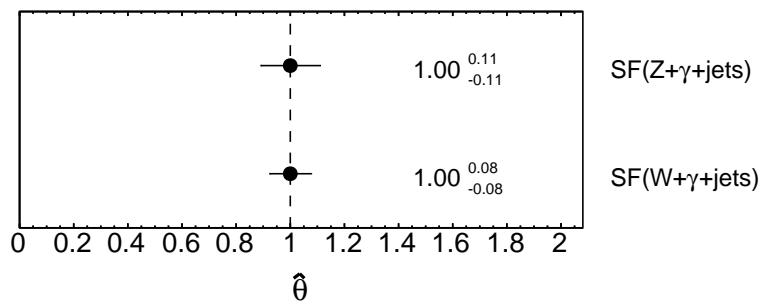


Figure 286: Normalisation factors for the $W+\gamma+jets$ and $Z+\gamma+jets$ process using Asimov data for the right-handed $t\gamma\gamma$ coupling.

Not reviewed, for internal circulation only

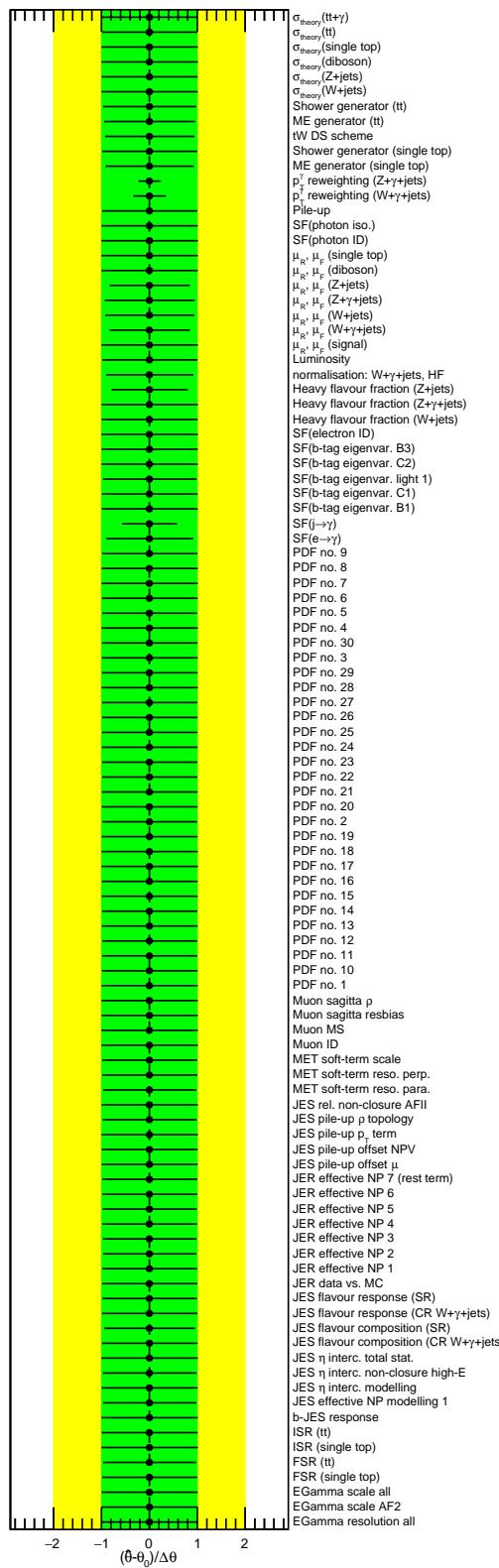


Figure 287: Pull values for the right-handed $tc\gamma$ coupling for the different nuisance parameters considered in the fit using Asimov data.

Not reviewed, for internal circulation only

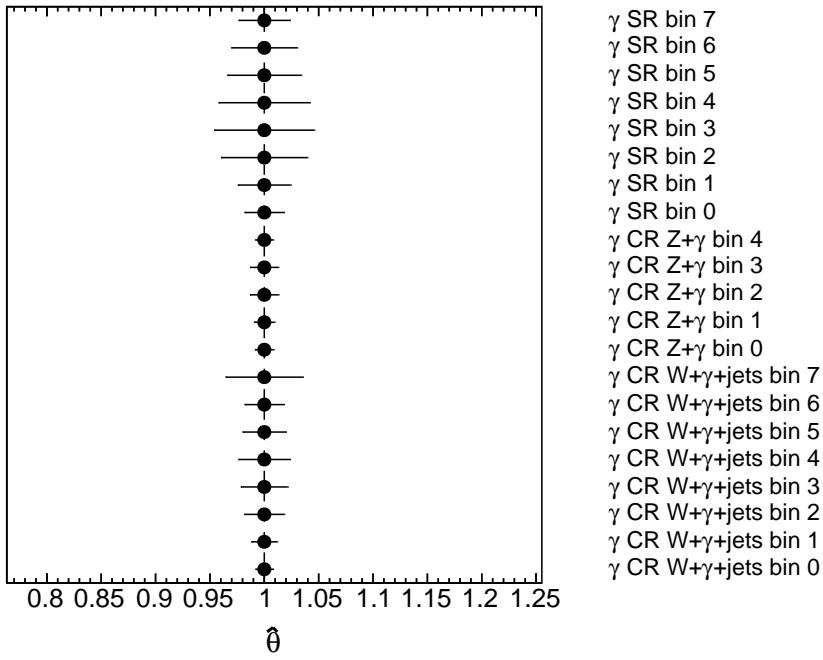


Figure 288: Normalisation factors γ for each bin in each region for the right-handed $t\gamma\gamma$ coupling using Asimov data.

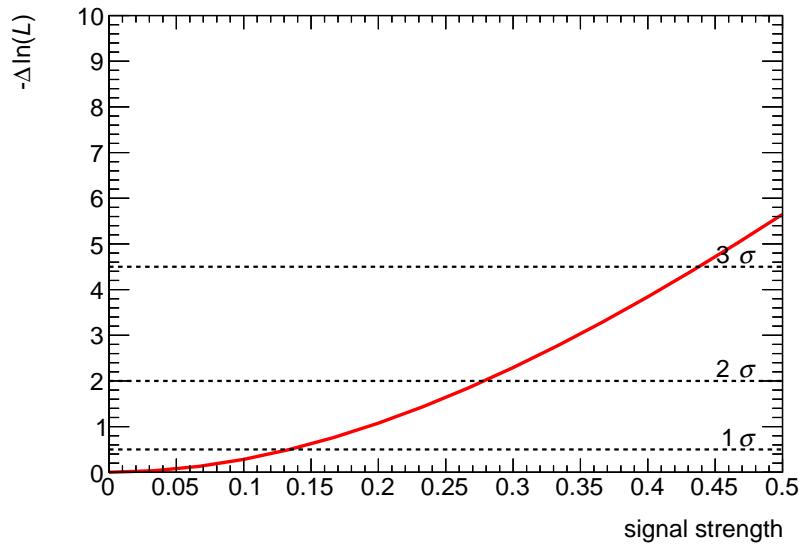


Figure 289: Distributions of the negative-log likelihood for the signal strength using Asimov data for the right-handed $t\gamma\gamma$ coupling. The one, two and three standard deviations are marked.

Not reviewed, for internal circulation only

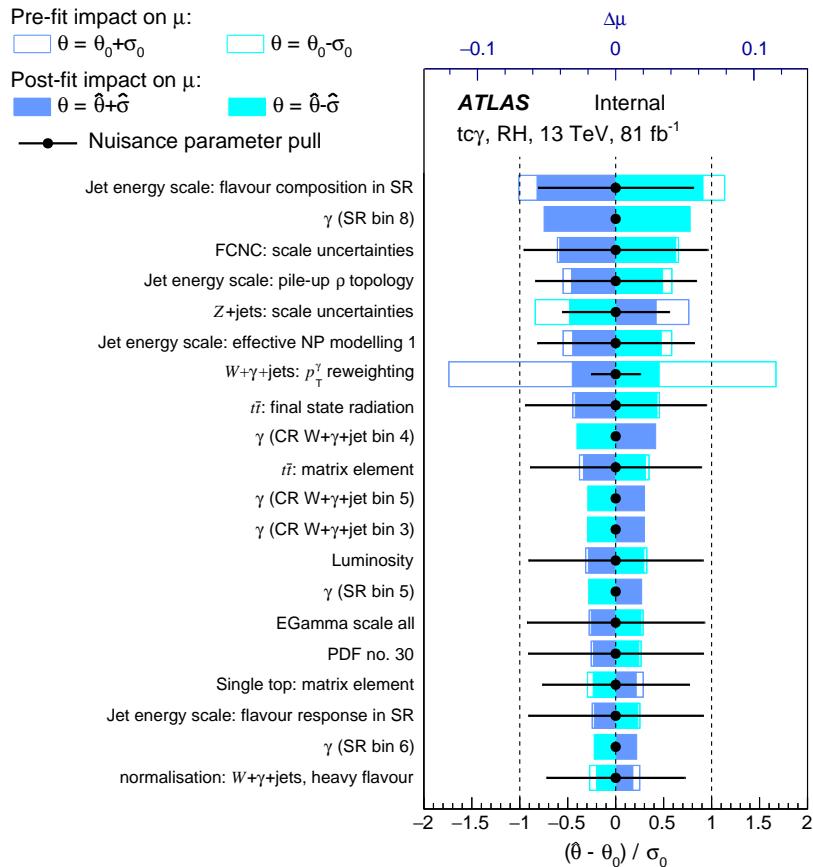


Figure 290: Ranking plot for the 20 nuisance parameters with the largest impact on the signal strength for the right-handed $tc\gamma$ coupling using Asimov data and $\mu = 1$.

1893 **W Statistical fit for different signal samples using data in control regions**

 1894 **W.1 Statistical fit using data in the control regions for the right-handed $t\gamma\gamma$ coupling**

Not reviewed, for internal circulation only

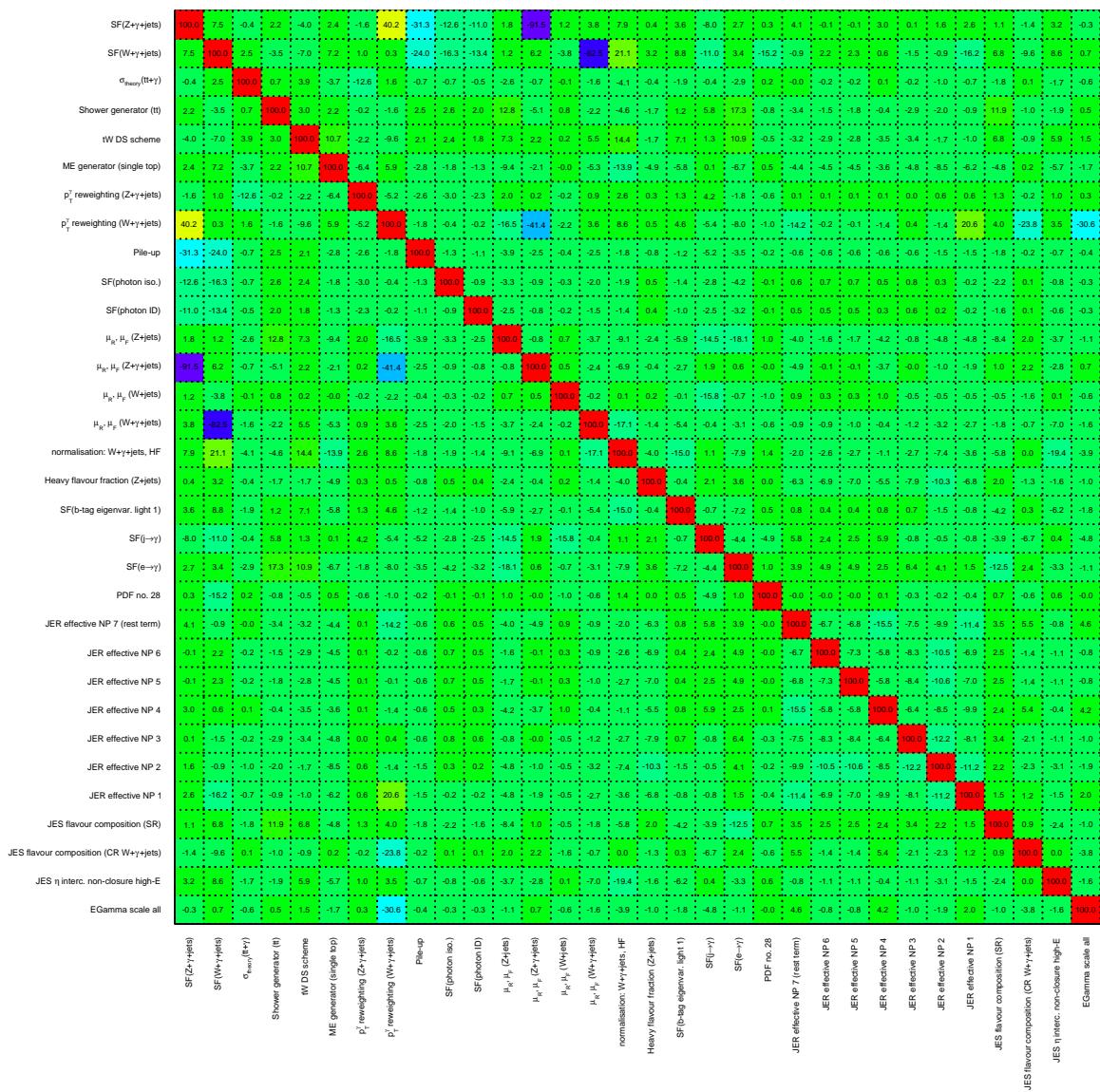


Figure 291: Correlation coefficients of all parameters with at least one coefficient above 10 % for the right-handed $t\gamma\gamma$ coupling considered in the fit using data in the CRs.

Not reviewed, for internal circulation only

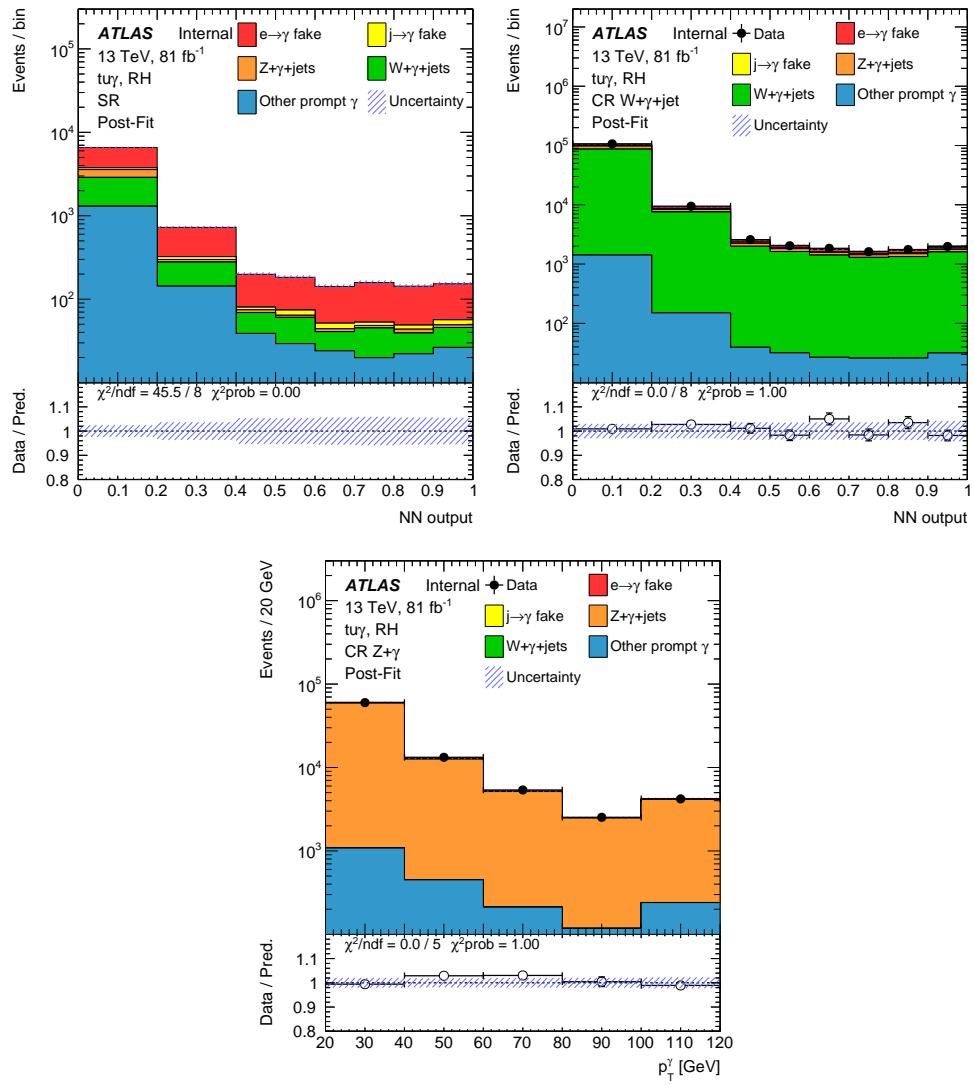


Figure 292: Post-fit distributions for the right-handed signal coupling $tuya$ using data in the CRs: NN output distribution in the SR (top left) and the CR $W+\gamma+\text{jets}$ (top right) and the photon p_T spectrum in the CR $Z+\gamma$ (bottom). Statistical and systematic uncertainties are included.

Table 53: Yields for the different contributions in the different regions after the fit using data in the CRs for the right-handed $t\gamma\gamma$ coupling. The statistical uncertainty and all systematic uncertainties are included.

Photon origin	SR		CR $W+\gamma+\text{jets}$			CR $Z+\gamma$	
$e \rightarrow \gamma$	3 830	\pm 410	6 700	\pm 1 100	226	\pm 30	
$j \rightarrow \gamma$	250	\pm 170	3 500	\pm 2 300	1 300	\pm 850	
$Z+\gamma+\text{jets}$	730	\pm 100	12 900	\pm 1 300	81 500	\pm 1 800	
$W+\gamma+\text{jets}$	1 860	\pm 360	101 900	\pm 3 300	6.1	\pm 1.9	
Other prompt photon	1 600	\pm 350	1 750	\pm 400	2 100	\pm 210	
Total SM	8 280	\pm 200	126 600	\pm 3 700	85 200	\pm 1 600	
Data	9 557		127 864		85 347		

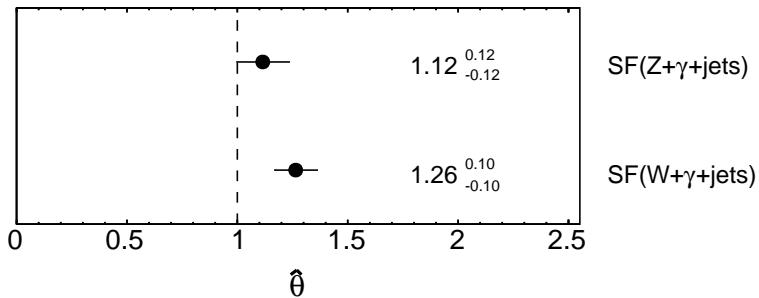


Figure 293: Normalisation factors for the $W+\gamma+\text{jets}$ and $Z+\gamma+\text{jets}$ process using the right-handed $t\gamma\gamma$ coupling using data in the CRs.

Not reviewed, for internal circulation only

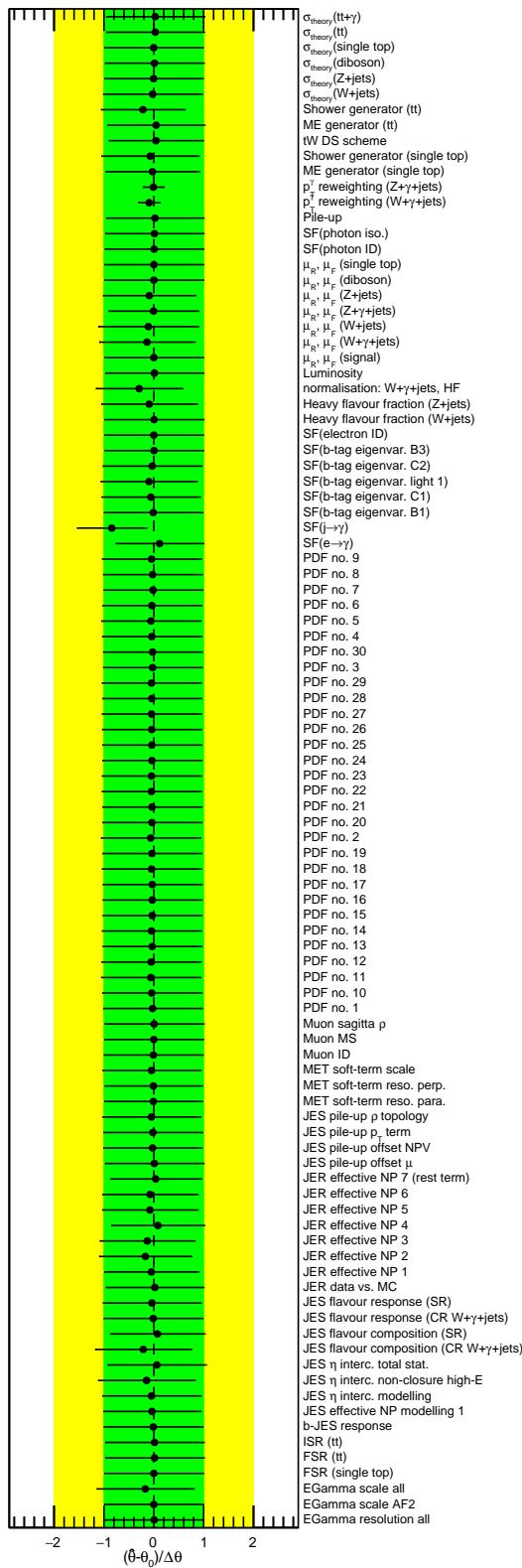


Figure 294: Pull values for the right-handed $t\gamma\gamma$ coupling for the different nuisance parameters considered in the fit using data in the CRs.

Not reviewed, for internal circulation only

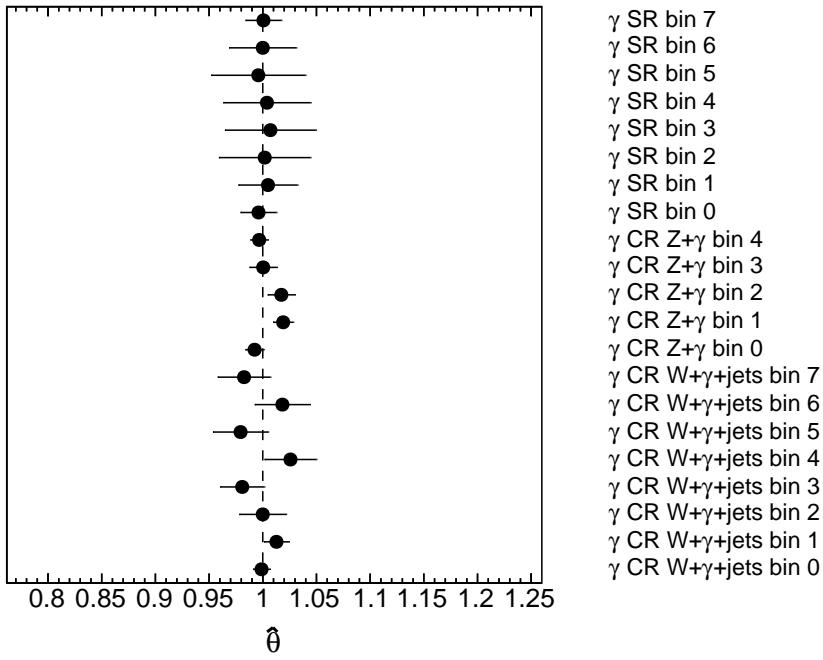


Figure 295: Normalisation factors γ for each bin in each region for the right-handed $t\bar{u}\gamma$ coupling using data in the CRs.

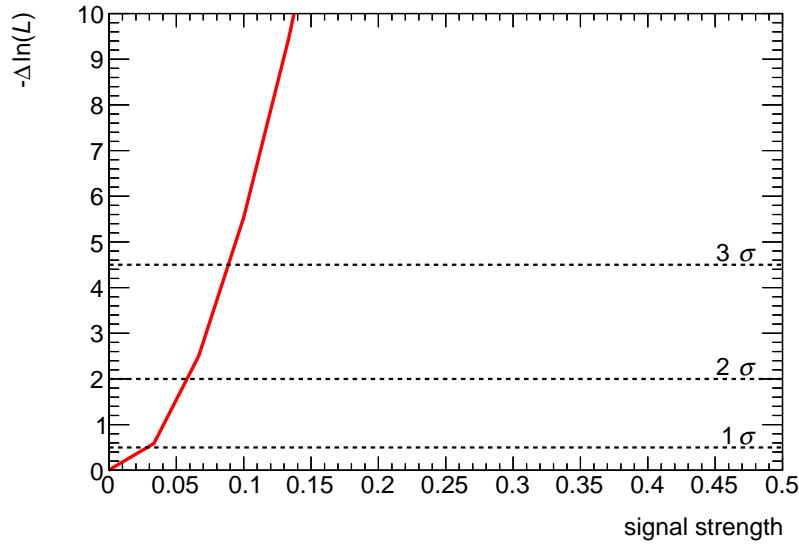


Figure 296: Distributions of the negative-log likelihood for the signal strength using data in the CRs for the right-handed $t\bar{u}\gamma$ coupling. The one, two and three standard deviations are marked.

1895 W.2 Statistical fit using data in the control regions for the left-handed $t\bar{c}\gamma$ coupling

Not reviewed, for internal circulation only

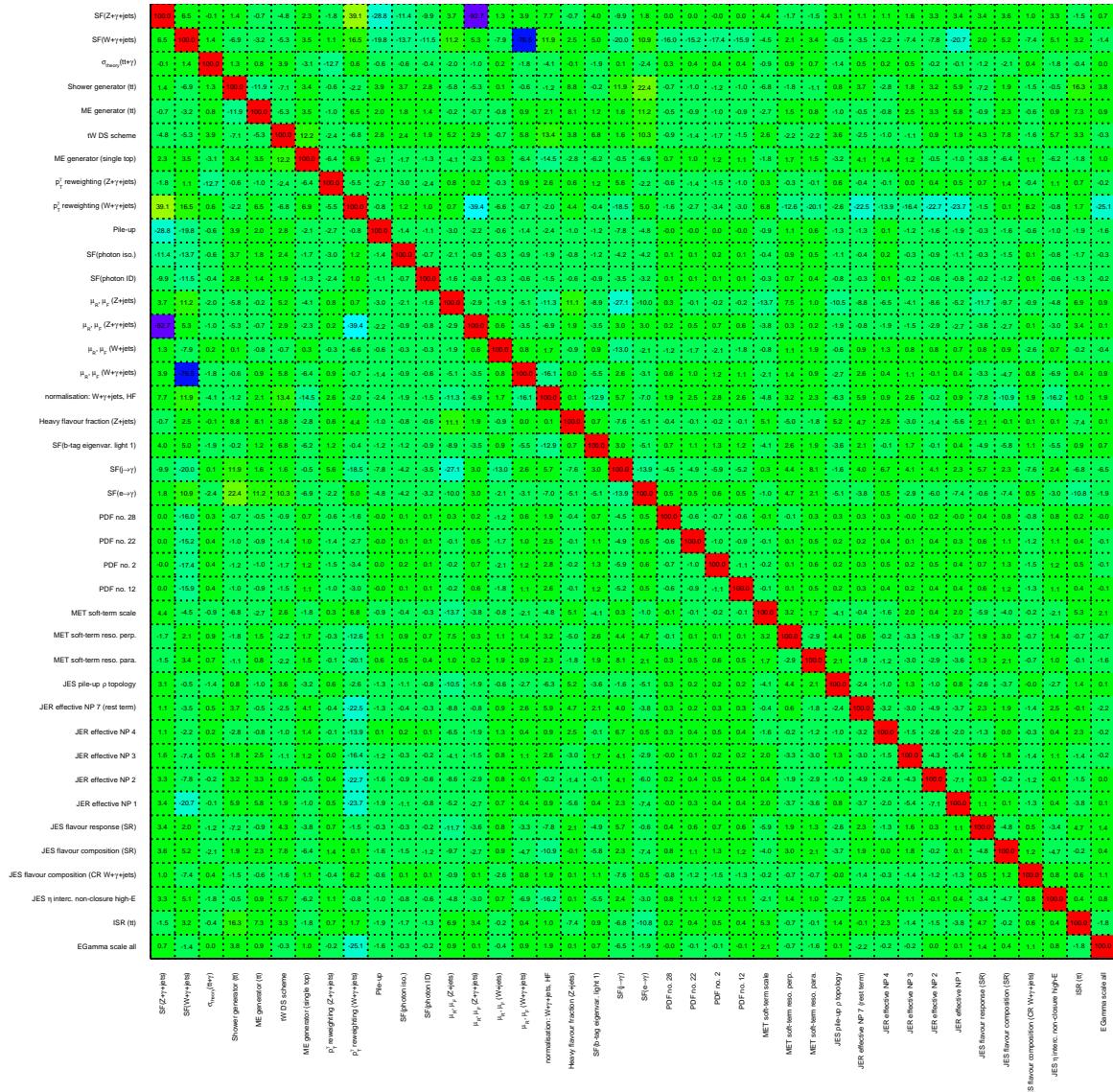


Figure 297: Correlation coefficients of all parameters with at least one coefficient above 10 % for the left-handed $t\bar{c}\gamma$ coupling considered in the fit using data in the CRs.

Not reviewed, for internal circulation only

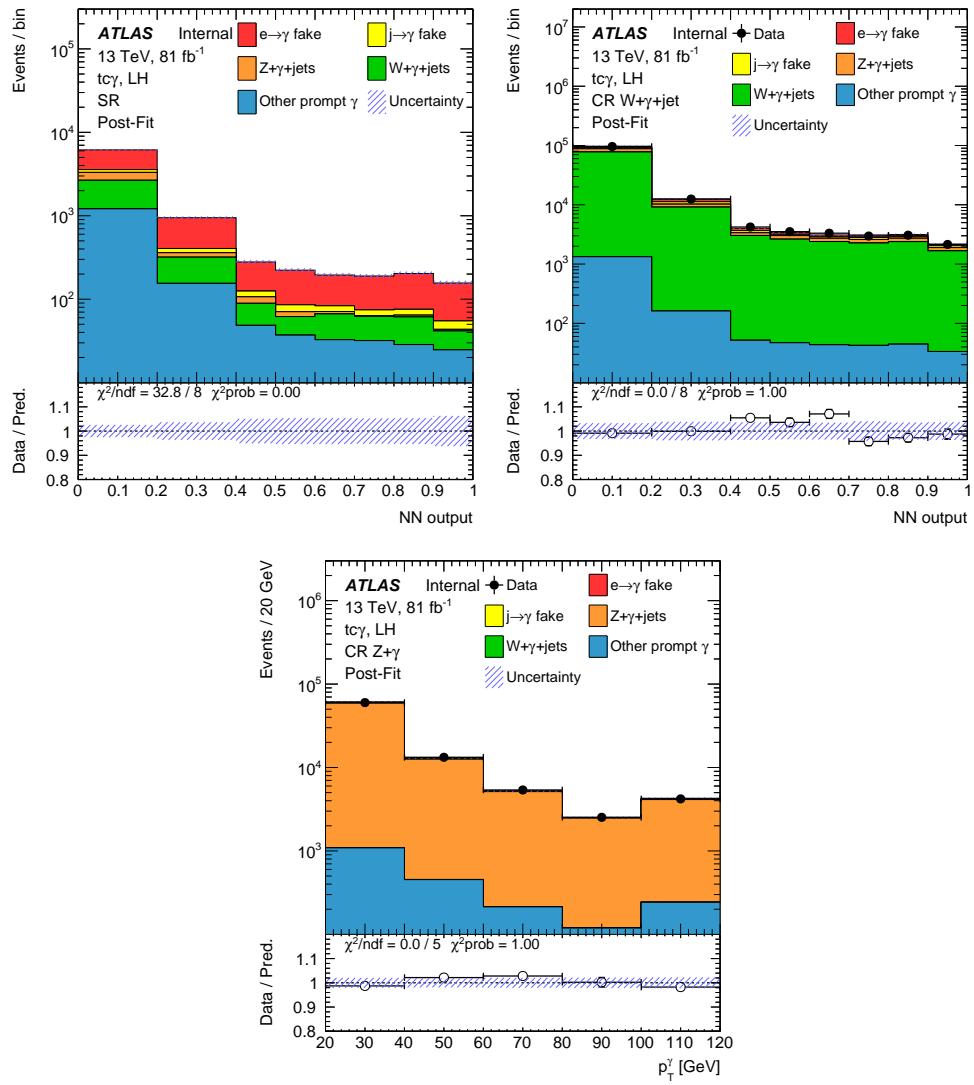


Figure 298: Post-fit distributions for the left-handed signal coupling $tc\gamma$ using data in the CRs: NN output distribution in the SR (top left) and the CR $W+\gamma+jets$ (top right) and the photon p_T spectrum in the CR $Z+\gamma$ (bottom). Statistical and systematic uncertainties are included.

Table 54: Yields for the different contributions in the different regions after the fit using data in the CRs for the left-handed $t\gamma\gamma$ coupling. The statistical uncertainty and all systematic uncertainties are included.

Photon origin	SR			CR $W+\gamma+\text{jets}$			CR $Z+\gamma$	
$e \rightarrow \gamma$	3 900	\pm	420	7 000	\pm	1 200	234	\pm 31
$j \rightarrow \gamma$	390	\pm	200	6 800	\pm	3 700	2 040	\pm 940
$Z+\gamma+\text{jets}$	730	\pm	100	13 300	\pm	1 300	81 400	\pm 2 000
$W+\gamma+\text{jets}$	1 790	\pm	360	99 600	\pm	4 200	6.1	\pm 2.0
Other prompt photon	1 570	\pm	340	1 750	\pm	400	2 120	\pm 210
Total SM	8 360	\pm	210	128 400	\pm	4 200	85 800	\pm 1 700
Data	9 557			127 864			85 347	

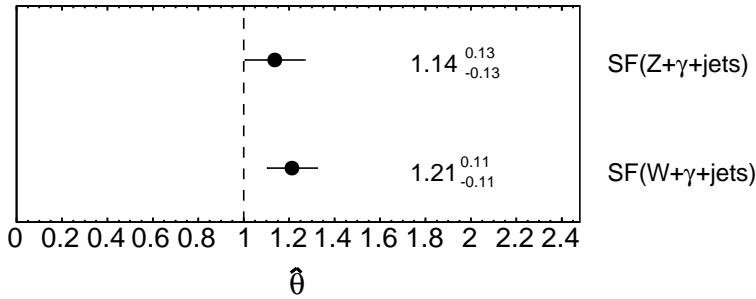


Figure 299: Normalisation factors for the $W+\gamma+\text{jets}$ and $Z+\gamma+\text{jets}$ process using the left-handed $t\gamma\gamma$ coupling using data in the CRs.

Not reviewed, for internal circulation only

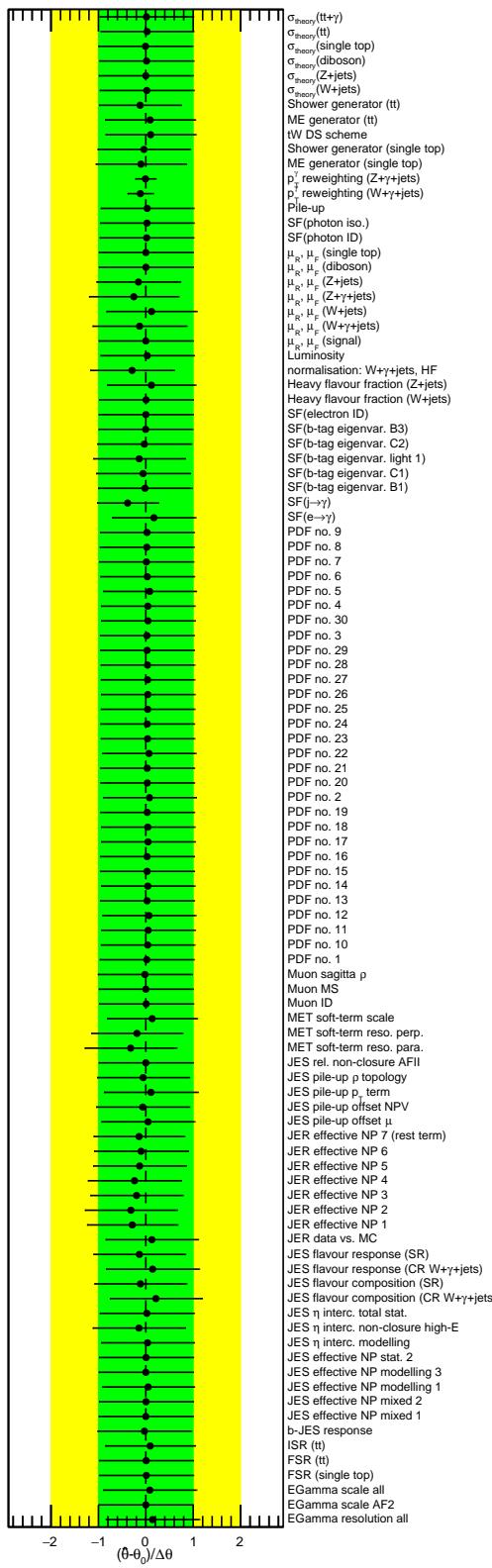


Figure 300: Pull values for the left-handed $t c \gamma$ coupling for the different nuisance parameters considered in the fit using data in the CRs.

Not reviewed, for internal circulation only

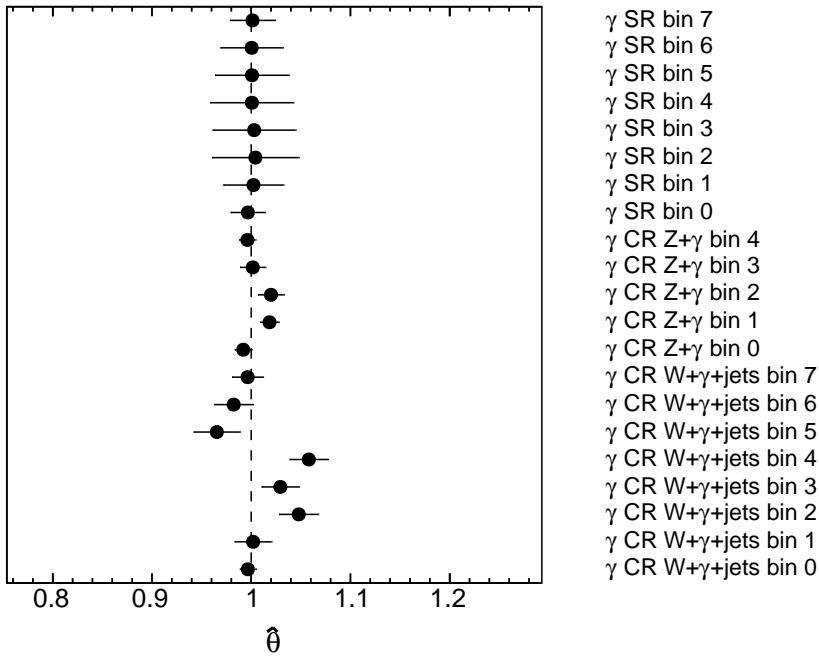


Figure 301: Normalisation factors γ for each bin in each region for the left-handed $t\gamma\gamma$ coupling using data in the CRs.

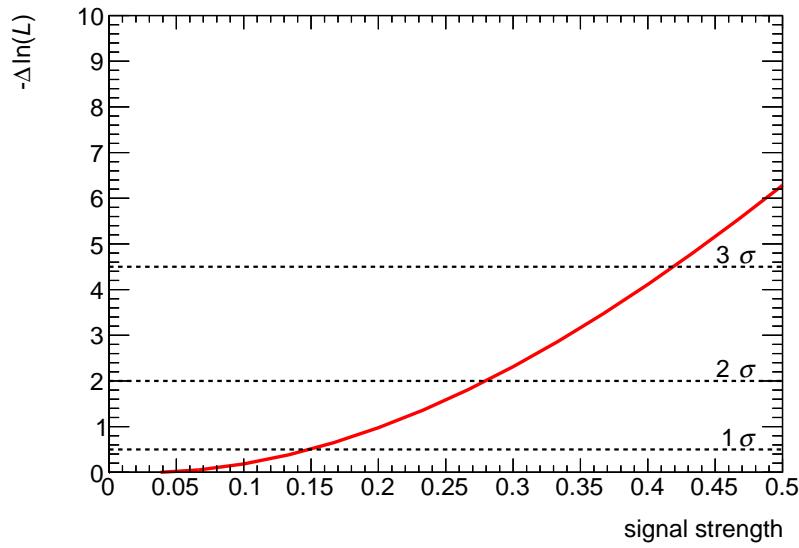


Figure 302: Distributions of the negative-log likelihood for the signal strength using data in the CRs for the left-handed $t\gamma\gamma$ coupling. The one, two and three standard deviations are marked.

1896 W.3 Statistical fit using data in the control regions for the right-handed $t\bar{c}\gamma$ coupling

Not reviewed, for internal circulation only

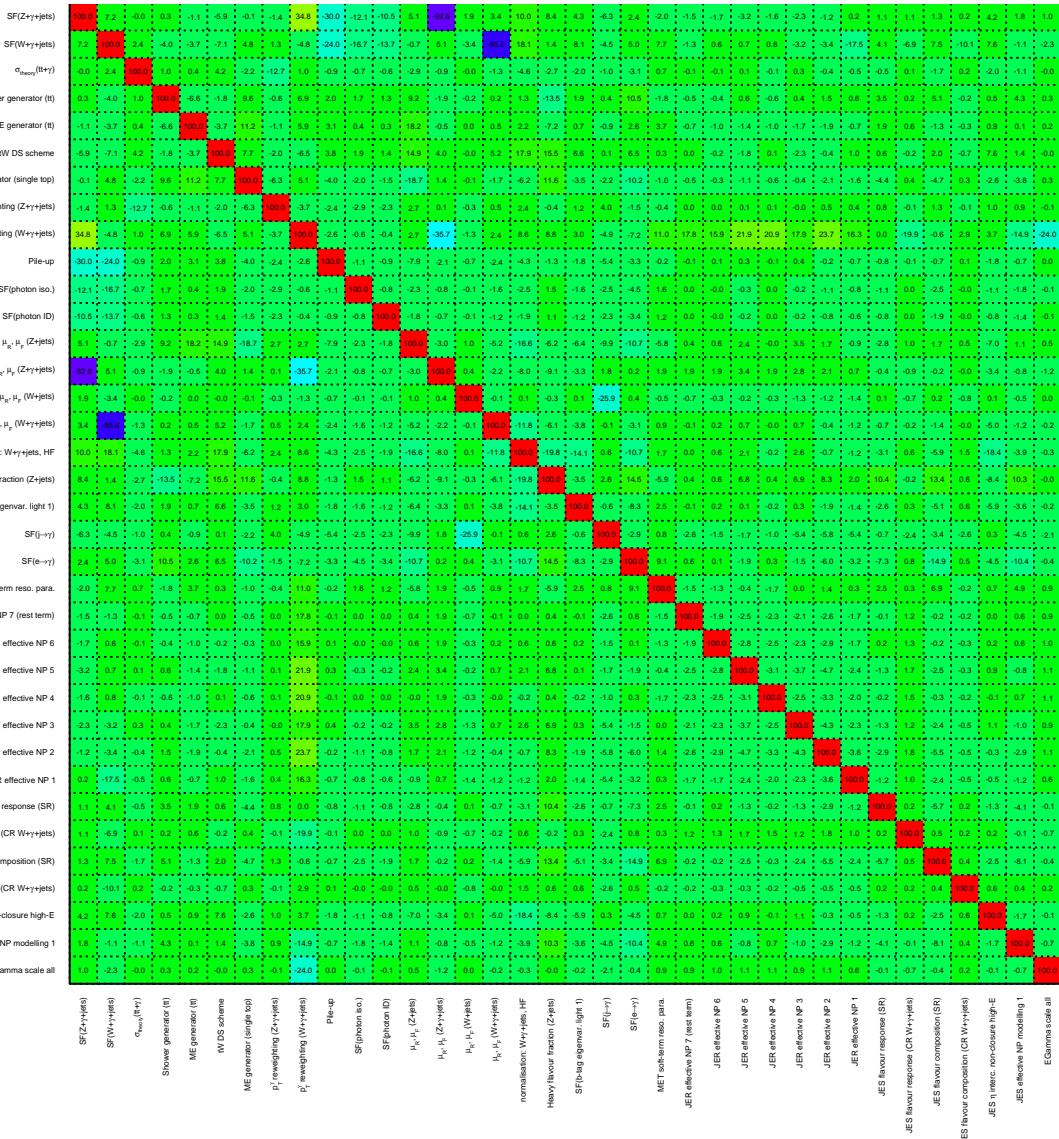


Figure 303: Correlation coefficients of all parameters with at least one coefficient above 10 % for the right-handed $t\bar{c}\gamma$ coupling considered in the fit using data in the CRs.

Not reviewed, for internal circulation only

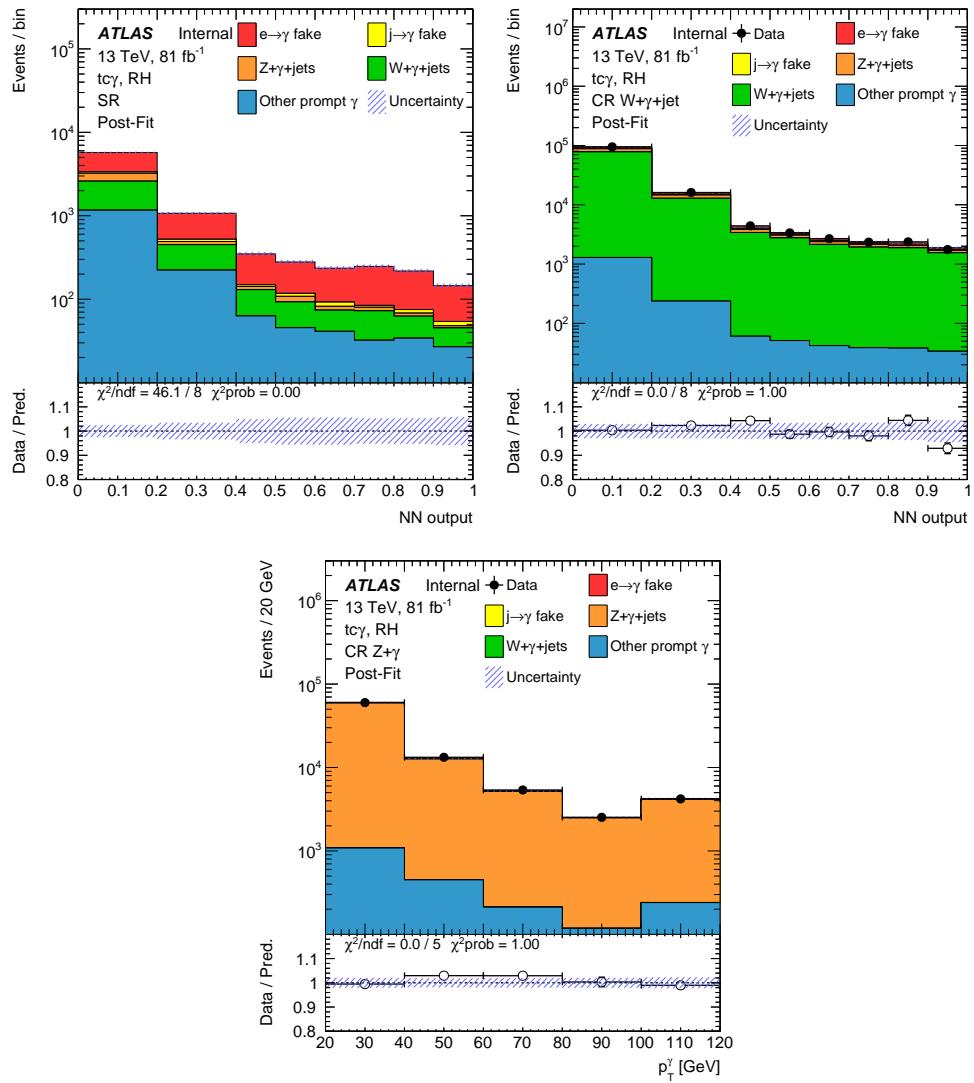


Figure 304: Post-fit distributions for the right-handed signal coupling $tc\gamma$ using data in the CRs: NN output distribution in the SR (top left) and the CR $W+\gamma+jets$ (top right) and the photon p_T spectrum in the CR $Z+\gamma$ (bottom). Statistical and systematic uncertainties are included.

Table 55: Yields for the different contributions in the different regions after the fit using data in the CRs for the right-handed $t\gamma\gamma$ coupling. The statistical uncertainty and all systematic uncertainties are included.

Photon origin	SR		CR $W+\gamma+\text{jets}$			CR $Z+\gamma$		
$e \rightarrow \gamma$	3 820	\pm 440	6 800	\pm 1 200	224	\pm 30		
$j \rightarrow \gamma$	200	\pm 140	2 700	\pm 1 800	1 110	\pm 790		
$Z+\gamma+\text{jets}$	720	\pm 110	13 100	\pm 1 300	81 700	\pm 1 800		
$W+\gamma+\text{jets}$	1 890	\pm 380	102 800	\pm 3 200	6.2	\pm 2.0		
Other prompt photon	1 630	\pm 360	1 790	\pm 410	2 100	\pm 210		
Total SM	8 270	\pm 210	127 100	\pm 3 700	85 200	\pm 1 600		
Data	9 557		127 864		85 347			

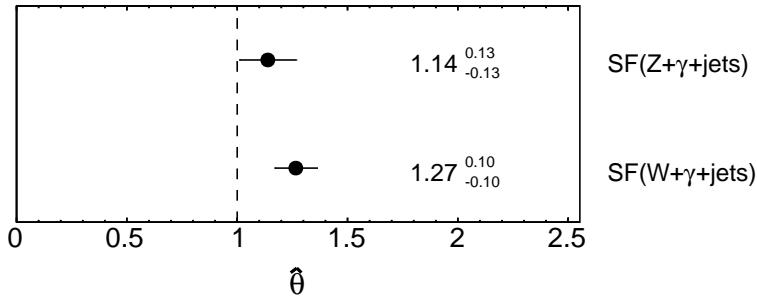


Figure 305: Normalisation factors for the $W+\gamma+\text{jets}$ and $Z+\gamma+\text{jets}$ process using the right-handed $t\gamma\gamma$ coupling using data in the CRs.

Not reviewed, for internal circulation only

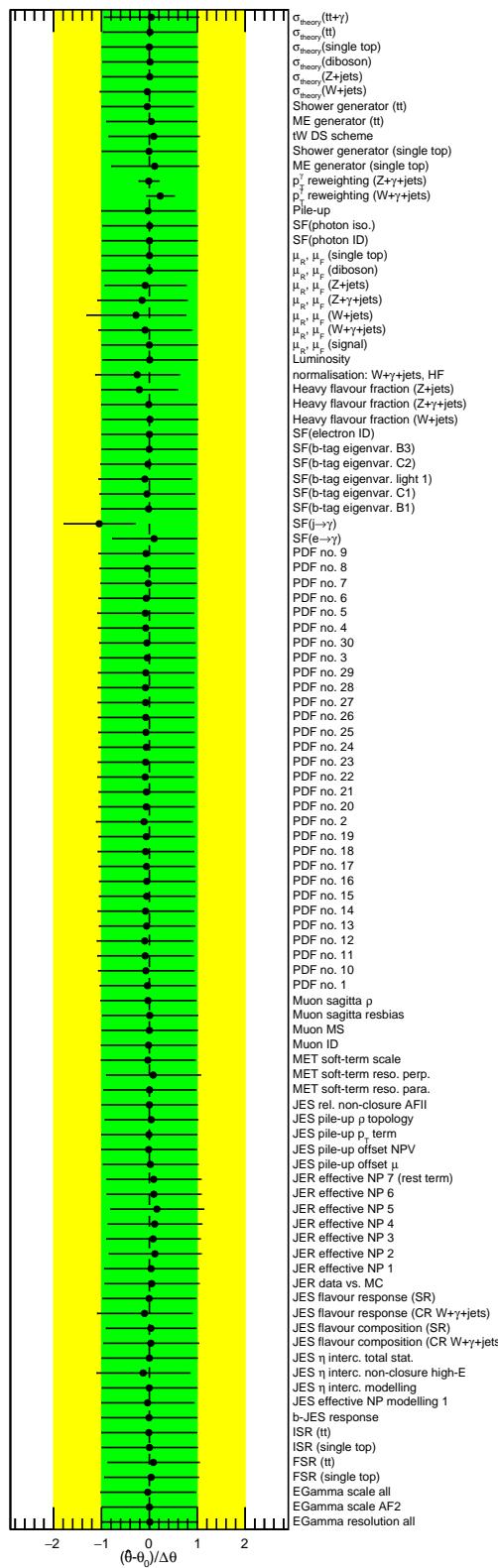


Figure 306: Pull values for the right-handed $tc\gamma$ coupling for the different nuisance parameters considered in the fit using data in the CRs.

Not reviewed, for internal circulation only

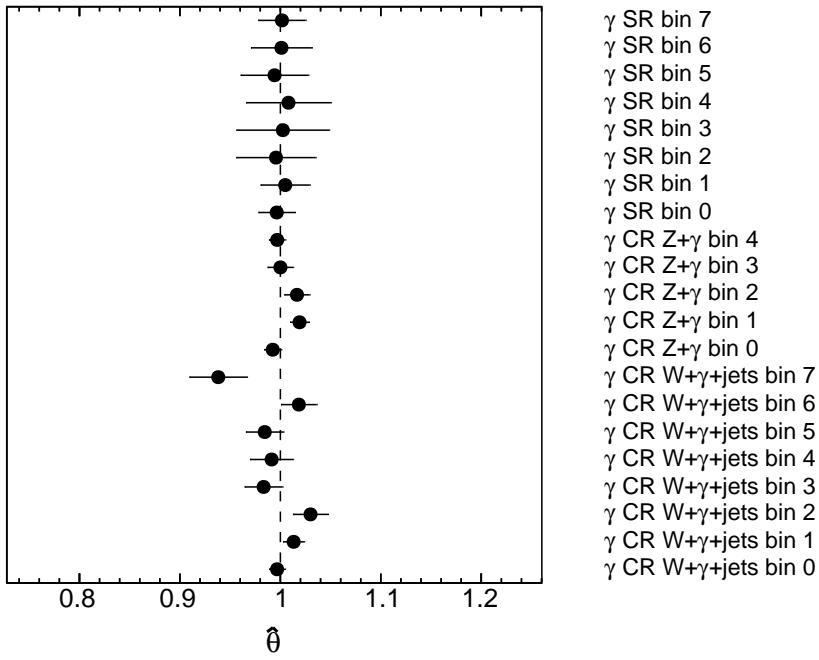


Figure 307: Normalisation factors γ for each bin in each region for the right-handed $t\gamma\gamma$ coupling using data in the CRs.

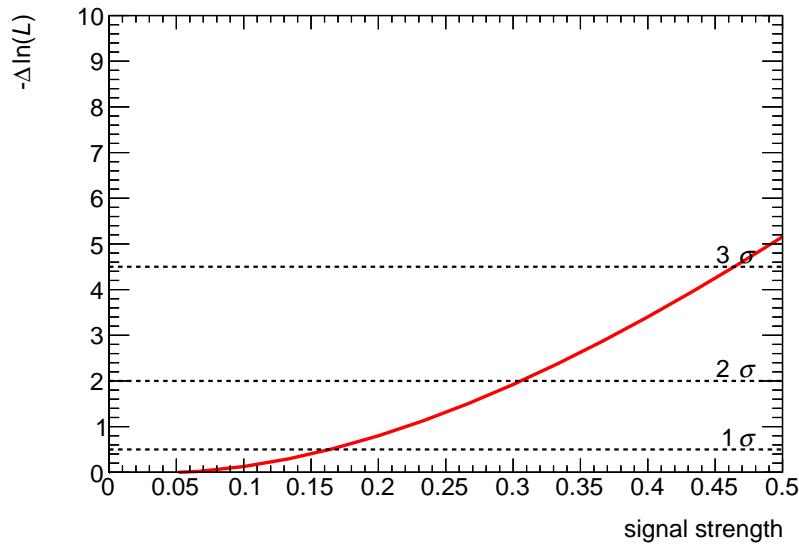


Figure 308: Distributions of the negative-log likelihood for the signal strength using data in the CRs for the right-handed $t\gamma\gamma$ coupling. The one, two and three standard deviations are marked.

1897 **X Tables with systematic uncertainties**

[Not reviewed, for internal circulation only]

Table 56: Relative effect of each systematic uncertainty (post-fit) on the yields in the SR for left-handed $\mu\bar{\nu}$ exchange using $\text{fitter}(\ell\bar{\nu})$ fit functions (I).

	Signal ($t\bar{t}\nu$, LH)	$e \rightarrow \gamma$ fake	$j \rightarrow \gamma$ fake	Z+jjets	W+jjets	other prompt
Luminosity	0.0197/-0.0197	0.0197/-0.0197	0.0197/-0.0197	0.0	0.0	0.0197/-0.0197
Pile-up	0.026/-0.026	0.0159/-0.0159	0.0625/-0.0623	0.0297/-0.0297	0.0199/-0.0199	0.0222/-0.0222
JVT	0.000757/-0.000757	0.000503/-0.000503	0.0018/-0.0018	0.00112/-0.00112	0.000808/-0.000808	0.00215/-0.00215
$Sf(e \rightarrow \gamma)$	0.0	0.0884/-0.0855	-0.0325/-0.0326	-0.133/-0.134	0.0	0.0
Shower generator ($t\bar{t}$)	0.0	0.0	-0.0343/-0.0343	0.024/-0.0423	0.0	0.0
ME generator (single top)	0.0	0.0	-0.00692/-0.00692	-0.0047/-0.0047	0.0	0.0
TW DS scheme	0.0	0.0	0.00519/-0.00518	-0.0195/-0.00195	0.0	0.0
$Sf(\text{photon ID})$	0.00585/-0.00585	0.0117/-0.0117	-0.145/-0.147	0.0	0.0	-0.138/-0.14
$Sf(\text{photon iso})$	0.0109/-0.0109	0.0154/-0.0154	0.0121/-0.0121	0.0131/-0.0131	0.0116/-0.0116	0.0115/-0.0115
$Sf(\text{electron trigger})$	0.00107/-0.00107	0.00158/-0.00158	0.00149/-0.0149	0.0152/-0.0152	0.0143/-0.0143	0.0142/-0.0142
$Sf(\text{electron reco.})$	0.000678/-0.000678	0.000738/-0.000738	0.000635/-0.000635	0.000825/-0.000825	0.00107/-0.00107	0.00111/-0.00111
$Sf(\text{electron ID})$	0.00462/-0.00462	0.00527/-0.00527	0.00484/-0.00484	0.00256/-0.00256	0.00344/-0.00344	0.000543/-0.000543
$Sf(\text{electron iso.})$	0.000836/-0.000836	0.000648/-0.000648	0.000491/-0.000491	0.000349/-0.000349	0.00044/-0.00044	0.000475/-0.000475
$Sf(\text{muon trigger stat.})$	0.000879/-0.000879	0.000521/-0.000521	0.00134/-0.00134	0.00123/-0.00123	0.00084/-0.00084	0.000857/-0.000857
$Sf(\text{muon ID stat.})$	0.000315/-0.000315	0.00199/-0.00199	0.00357/-0.00357	0.00373/-0.00373	0.00301/-0.00301	0.00327/-0.00327
$Sf(\text{muon ID syst.})$	0.000258/-0.000258	0.000163/-0.00163	0.00027/-0.00027	0.000331/-0.000331	0.000269/-0.000269	0.000266/-0.000266
$Sf(\text{muon iso. stat.})$	0.0017/-0.0017	0.000927/-0.000927	0.000172/-0.000172	0.000175/-0.000175	0.00153/-0.00153	0.00146/-0.00146
$Sf(\text{muon iso. syst.})$	0.000154/-0.000154	8.87e-05/-8.87e-05	0.000127/-0.000127	0.000436/-0.000436	0.000527/-0.000527	0.00039/-0.00039
$Sf(\text{muon TTVA stat.})$	0.00109/-0.00109	0.000708/-0.000708	0.000108/-0.000108	0.000153/-0.00153	0.00021/-0.00021	0.000115/-0.000115
$Sf(\text{muon TTVA syst.})$	0.000108/-0.000108	6.67e-05/-6.67e-05	0.000113/-0.000113	0.000246/-0.000246	0.000446/-0.000446	0.000436/-0.000436
$E\gamma$ gamma resolution all	0.00503/-0.00503	0.00691/-0.00691	0.0113/-0.0113	0.0113/-0.0113	0.0114/-0.0114	0.00147/-0.00147
$E\gamma$ gamma scale all	0.0127/-0.0127	0.0073/-0.00729	0.0144/-0.0144	0.00893/-0.00893	0.00627/-0.00627	0.000534/-0.000534
Muon ID	0.000169/-0.000169	0.000634/-0.000634	0.00621/-0.00621	0.00436/-0.00436	0.000527/-0.000527	0.000346/-0.000346
Muon MS	0.00111/-0.00111	0.00111/-0.00111	0.00222/-0.00222	0.00637/-0.00637	0.00246/-0.00246	0.000436/-0.000436
Muon sagitta biasias	0.00213/-0.00213	0.00201/-0.00201	0.004201/-0.004201	0.004046/-0.004046	0.000416/-0.000416	0.000416/-0.000416
Muon scale ρ	0.00356/-0.00356	0.00142/-0.00142	0.000365/-0.000365	0.0019/-0.0019	0.00532/-0.00532	0.000514/-0.000514
ISR ($t\bar{t}$)	0.0	0.0104/-0.0104	0.0368/-0.0367	0.0	0.0	0.0
FSR ($t\bar{t}$)	0.0	0.0104/-0.0104	0.0481/-0.0481	0.0	0.0	0.0
ISR (single top)	0.0	0.0187/-0.0187	0.0103/-0.0103	0.0	0.0	0.0
FSR (single top)	0.0	0.00556/-0.00556	0.0389/-0.0389	0.0	0.0	0.0
PDF no. 1	0.00192/-0.00192	0.00109/-0.00109	0.001124/-0.001124	0.0013/-0.0013	0.000975/-0.000975	0.000406/-0.000406
PDF no. 2	0.0024/-0.0024	0.00143/-0.00143	0.00245/-0.00245	0.00401/-0.00401	0.00146/-0.00146	0.00268/-0.00268
PDF no. 3	0.00511/-0.00511	0.00101/-0.00101	0.001/-0.001	0.00333/-0.00333	0.00378/-0.00378	0.00362/-0.00362
PDF no. 4	0.00683/-0.00683	0.00341/-0.00341	0.00293/-0.00293	0.00235/-0.00235	0.00154/-0.00154	0.00334/-0.00334
PDF no. 5	0.00186/-0.00186	0.00114/-0.00114	0.000773/-0.000773	0.000908/-0.000908	0.000691/-0.000691	0.00427/-0.00427
PDF no. 6	0.00235/-0.00235	0.00145/-0.00145	0.00182/-0.00182	0.000169/-0.000169	0.000602/-0.000602	0.00693/-0.00693
PDF no. 7	0.00372/-0.00372	0.00236/-0.00236	0.00223/-0.00223	0.00835/-0.00835	0.00602/-0.00602	0.00378/-0.00378
PDF no. 8	0.00344/-0.00344	0.00966/-0.00966	0.00642/-0.00642	0.00277/-0.00277	0.00589/-0.00589	0.00131/-0.00131
PDF no. 9	0.00089/-0.00089	0.00596/-0.00596	0.0033/-0.0033	0.00137/-0.00137	0.000272/-0.000272	0.00497/-0.00497
PDF no. 10	0.00389/-0.00389	0.00177/-0.00177	0.00194/-0.00194	0.00128/-0.00128	0.00121/-0.00121	0.00121/-0.00121
PDF no. 11	0.00138/-0.00138	0.000973/-0.000973	0.000997/-0.000997	0.00313/-0.00313	0.00892/-0.00892	0.000232/-0.000232
PDF no. 12	0.00449/-0.00449	0.00154/-0.00154	0.00102/-0.00102	0.000937/-0.000937	0.00289/-0.00289	0.000438/-0.000438
PDF no. 13	0.00294/-0.00293	0.00219/-0.00219	0.00151/-0.00151	0.00239/-0.00239	0.000905/-0.000905	0.00522/-0.00522
PDF no. 14	0.00102/-0.00102	0.000929/-0.000929	0.000915/-0.000915	0.00114/-0.00114	0.000197/-0.000197	0.00288/-0.00288
PDF no. 15	0.00273/-0.00273	0.00056/-0.00056	0.00052/-0.00052	0.00169/-0.00169	0.00444/-0.00444	0.00448/-0.00448
PDF no. 16	0.000866/-0.000866	0.00133/-0.00133	0.000805/-0.000805	0.00134/-0.00134	0.00813/-0.00813	0.00774/-0.00774
PDF no. 17	0.00525/-0.00525	0.00307/-0.00307	0.00197/-0.00197	0.000555/-0.000555	0.00232/-0.00232	0.00863/-0.00863
PDF no. 18	0.00307/-0.00307	0.00862/-0.00862	0.0016/-0.0016	0.000287/-0.000287	0.000917/-0.000917	0.00617/-0.00617
PDF no. 19	0.000568/-0.000568	0.00159/-0.00159	0.00136/-0.00136	0.000804/-0.000804	0.000397/-0.000397	0.00131/-0.00131
PDF no. 20	0.00246/-0.00246	0.00145/-0.00145	0.00105/-0.00105	0.000598/-0.000598	0.00193/-0.00193	0.00384/-0.00384
PDF no. 21	0.00225/-0.00225	0.000235/-0.000235	0.000185/-0.000185	0.000651/-0.000651	0.000234/-0.000234	0.00448/-0.00448
PDF no. 22	0.000832/-0.000832	0.00139/-0.00139	0.000899/-0.000899	0.00135/-0.00135	0.000298/-0.000298	0.00355/-0.00355
PDF no. 23	0.00191/-0.00191	0.00175/-0.00175	0.00174/-0.00174	0.000524/-0.000524	0.000585/-0.000585	0.00438/-0.00438
PDF no. 24	0.00303/-0.00303	0.0016/-0.0016	0.000674/-0.000674	0.00176/-0.00176	0.000156/-0.000156	0.00617/-0.00617
PDF no. 25	0.000774/-0.000774	0.00176/-0.00176	0.0011/-0.0011	0.00358/-0.00358	0.000438/-0.000438	0.00338/-0.00338
PDF no. 26	0.00411/-0.00411	0.00173/-0.00173	0.00132/-0.00132	0.00523/-0.00523	0.000855/-0.000855	0.00449/-0.00449
PDF no. 27	0.00289/-0.00289	0.00175/-0.00175	0.00115/-0.00115	0.000298/-0.000298	0.00115/-0.00115	0.00471/-0.00471
PDF no. 28	0.0034/-0.0034	0.00457/-0.00457	0.00312/-0.00312	0.00116/-0.00116	0.000208/-0.000208	0.0084/-0.0084
PDF no. 29	0.00266/-0.00266	0.000515/-0.000515	0.00032/-0.00032	0.000581/-0.000581	0.00214/-0.00214	0.00472/-0.00472
PDF no. 30	0.00704/-0.00704	0.00179/-0.00179	0.000829/-0.000829	0.00168/-0.00168	0.000372/-0.000372	0.00991/-0.00991
σ_{R, H_F} (single top)	0.0	0.00334/-0.00334	0.0137/-0.0138	0.0	0.0	0.0
σ_{R, H_F} (W+jets)	0.0	0.000123/-0.000123	0.15/-0.148	0.0	0.0	0.0
σ_{R, H_F} (Z +jets)	0.0	0.0756/-0.0753	0.0275/-0.0271	0.0	0.0	0.0
σ_{R, H_F} (diboson)	0.0	0.00621/-0.00621	0.00247/-0.00247	0.0	0.0	0.000603/-0.000603
$\sigma^{\text{theory}}(t\bar{t})$	0.0	0.0301/-0.0301	0.0331/-0.0331	0.0	0.0	0.0
$\sigma^{\text{theory}}(\text{single top})$	0.0	0.00545/-0.00545	0.0129/-0.0129	0.0	0.0	0.0118/-0.0118
$\sigma^{\text{theory}}(W)$	0.0	4.47e-05/-4.48e-05	0.00518/-0.00518	0.0	0.0	0.00752/-0.00752
$\sigma^{\text{theory}}(Z+\text{jets})$	0.0	0.0184/-0.0184	0.00168/-0.00168	0.0	0.0	0.0
$\sigma^{\text{theory}}(\text{diboson})$	0.0	0.00248/-0.00248	0.00195/-0.00195	0.0	0.0	0.00017/-0.00017
E_T^{miss} soft-term reso. para.	0.00043/-0.00043	-0.0171/-0.017	-0.00617/-0.00617	-0.0351/-0.0352	-0.00468/-0.00468	-0.00208/-0.00208
E_T^{miss} soft-term reso. perp.	-0.0305/-0.0305	-0.0128/-0.0128	-0.00829/-0.00829	-0.0295/-0.0295	-0.00105/-0.00105	-0.000171/-0.000171
E_T^{miss} soft-term scale	0.00417/-0.00417	0.0205/-0.0205	0.00697/-0.00697	0.00626/-0.00626	0.0109/-0.0109	0.00244/-0.00244

Table 57: Relative effect of each systematic uncertainty (post-fit) on the yields in the SR for the left-handed $t\bar{t}$ -coupling using data in all regions (II).

	Signal ($t\bar{t}\gamma$, LH)	$e \rightarrow \gamma$ fake	$j \rightarrow \gamma$ fake	$Z_{\gamma\gamma} + \text{jets}$	$\text{Not reviewed, } W_{\gamma\gamma} + \text{jets}$	$\text{Interrat circulation only}$
Heavy flavour fraction ($W+\text{jets}$)	0/0	-0.00105 / 0.00105	0.013 / -0.013	0/0	0/0	0/0
Heavy flavour fraction ($Z+\text{jets}$)	0/0	0.0184 / -0.0184	-0.0787 / 0.0787	0/0	0/0	0/0
Heavy flavour fraction (diboson)	0/0	-0.000139 / 0.000139	0.00455 / 0.00455	0/0	0/0	0.000185 / 0.000185
SF(b -tag eigenvar. B1)	0.0119 / -0.0119	0.0129 / -0.0129	0.0147 / -0.0147	0.0174 / -0.0174	0.00811 / -0.00811	0.012 / -0.012
SF(b -tag eigenvar. B2)	(0.0195 / 0.0095)	0.0049 / 0.0049	0.00156 / 0.00156	0.00129 / 0.00129	0.00859 / 0.00859	0.00167 / 0.00167
SF(b -tag eigenvar. B3)	0.0108 / -0.0108	0.00971 / 0.00971	0.00941 / 0.00941	0.00227 / 0.00227	0.00823 / 0.00823	0.000583 / 0.000583
SF(b -tag eigenvar. B4)	0.00108 / 0.00108	0.000918 / 0.000918	0.00108 / 0.00108	0.00292 / 0.00292	4.32e-05 / 4.32e-05	0.00112 / 0.00112
SF(b -tag eigenvar. B5)	0.0008331 / 0.0008331	0.000815 / 0.000815	9.79e-05 / 9.79e-05	0.000102 / 0.00102	6.42e-05 / 6.42e-05	0.00125 / 0.00125
SF(b -tag eigenvar. B6)	0.0012 / 0.0012	8.92e-05 / 8.92e-05	1.91e-05 / 1.91e-05	2.6e-05 / 2.6e-05	1.32e-05 / 1.32e-05	1.68e-05 / 1.68e-05
SF(b -tag eigenvar. B7)	1.17e-05 / 1.17e-05	4.9e-05 / 4.9e-05	8.95e-06 / 8.95e-06	8.98e-06 / 8.98e-06	2.84e-06 / 2.84e-06	1.74e-06 / 1.74e-06
SF(b -tag eigenvar. B8)	3.15e-06 / 3.15e-06	4.21e-06 / 4.21e-06	6.89e-07 / 6.89e-07	2.88e-06 / 2.88e-06	5.90e-07 / 5.90e-07	2.32e-07 / 2.32e-07
SF(b -tag eigenvar. B9)	3.27e-07 / 3.27e-07	8.35e-07 / 8.35e-07	0.022 / -0.022	0.0176 / -0.0176	0.0321 / -0.0321	0.00244 / -0.00244
SF(b -tag eigenvar. C1)	0.000105 / -0.000105	0.00515 / -0.00515	0.00195 / -0.00195	0.00626 / -0.00626	0.0238 / -0.0238	0.000289 / -0.00029
SF(b -tag eigenvar. C2)	0.00011 / -0.00011	0.00016 / -0.00016	0.000691 / -0.000691	0.00196 / -0.00196	0.00655 / -0.00655	9.1e-05 / 9.1e-05
SF(b -tag eigenvar. C3)	4e-05 / -4e-05	0.000618 / 0.000618	0.00076 / 0.00076	0.0429 / -0.043	0.0463 / -0.0464	0.00034 / -0.00034
SF(b -tag eigenvar. light 1)	0.00701 / -0.00701	0.0275 / -0.0275	0.0211 / -0.0211	0.0167 / -0.0167	0.00673 / -0.00673	0.0114 / -0.0114
SF(b -tag eigenvar. light 2)	8.19e-05 / 8.19e-05	0.0357 / 0.0357	0.00293 / 0.00293	0.00346 / 0.00346	0.00236 / 0.00236	1.43e-05 / 1.43e-05
SF(b -tag eigenvar. light 3)	5.05e-05 / 5.05e-05	0.0015 / 0.0015	0.00091 / 0.00091	0.00146 / 0.00146	3.13e-05 / 3.13e-05	0.000304 / 0.000304
SF(b -tag eigenvar. light 4)	3.17e-05 / 3.17e-05	0.000363 / 0.000363	0.000686 / 0.000686	0.0012 / 0.0012	3.31e-06 / 3.31e-06	1.17e-05 / 1.17e-05
SF(b -tag extrapolation)	4.12e-06 / 4.12e-06	1.94e-05 / 1.94e-05	1.41e-05 / 1.41e-05	0.00011 / 0.00011	1.26e-05 / 1.26e-05	0.000163 / 0.000163
SF($t\bar{t}$ -tag extrap., from charm)	-1.22e-08 / -1.22e-08	1.45e-05 / 1.45e-05	0.00106 / 0.00106	0.016 / 0.016	0.00116 / 0.00116	0.00034 / -0.00034
JES η interc. modelling	0.00527 / -0.00527	0.0267 / -0.0267	0.0211 / -0.0211	0.0167 / -0.0167	0.00673 / -0.00673	0.0114 / -0.0114
JES η interc. non-closure high- E_T	1.28e-07 / -1.28e-07	2.25e-07 / -2.25e-07	0 / 0	0.00101 / -0.00101	0.101 / -0.101	9.47e-08 / -7.87e-08
JES η interc. non-closure $\eta < 0$	0.000501 / 0.000501	0.000978 / 0.000978	0.00393 / 0.00393	0.00108 / 0.00108	0.000802 / 0.000802	0.000304 / 0.000304
JES η interc. non-closure $\eta > 0$	0.000546 / 0.000546	0.000351 / 0.000351	0.00432 / 0.00432	0.000107 / 0.00107	0.000256 / 0.000256	9.11e-05 / 9.11e-05
JES η interc. total stat.	0.00242 / -0.00242	0.00342 / -0.00342	0.00776 / -0.00776	0.00589 / -0.00589	0.00752 / -0.00752	0.00328 / -0.00328
JES effective NP stat. 1	0.00125 / 0.00125	0.00188 / 0.00188	0.00161 / 0.00161	0.00161 / 0.00161	0.00118 / 0.00118	0.000118 / 0.000118
JES effective NP stat. 2	0.00214 / 0.00214	0.00335 / 0.00335	0.0064 / 0.0064	0.00674 / 0.00674	0.00616 / 0.00616	0.00247 / 0.00247
JES effective NP stat. 3	0.000674 / 0.000674	0.000443 / 0.000443	0.00527 / 0.00527	0.00013 / 0.00013	0.000798 / 0.000798	0.000267 / 0.000267
JES effective NP stat. 4	0.000768 / 0.000768	0.000907 / 0.000907	0.00238 / 0.00238	0.000939 / 0.000939	0.000118 / 0.000118	0.000681 / 0.000681
JES effective NP stat. 5	0.000923 / 0.000923	0.000414 / 0.000414	0.00135 / 0.00135	0.000156 / 0.000156	0.000645 / 0.000645	0.000225 / 0.000225
JES effective NP stat. 6	0.000678 / 0.000678	0.000776 / 0.000776	0.00162 / 0.00162	0.000154 / 0.000154	0.000986 / 0.000986	0.000271 / 0.000271
JES effective NP mixed 1	0.00125 / 0.00125	0.00127 / 0.00127	0.0023 / 0.0023	0.00754 / 0.00754	0.00263 / 0.00263	0.000416 / 0.000416
JES effective NP mixed 2	0.00215 / 0.00215	0.00198 / 0.00198	0.0002 / 0.0002	0.00347 / 0.00347	0.00561 / 0.00561	0.00135 / 0.00135
JES effective NP mixed 3	0.000421 / 0.000421	0.00705 / 0.00705	0.00141 / 0.00141	8.72e-05 / 8.72e-05	0.00122 / 0.00122	0.000301 / 0.000301
JES pile-up p_T term	0.0123 / -0.0122	0.0125 / -0.0125	0.0379 / -0.0379	0.0105 / -0.0105	0.0108 / -0.0108	0.0234 / -0.0231
JES pile-up ρ topology	0.00228 / 0.00228	0.00338 / 0.00338	0.00516 / 0.00516	0.00242 / 0.00242	0.00516 / 0.00516	0.00261 / 0.00261
<i>b</i> -JES response	0.00124 / 0.00124	0.0016 / 0.0016	0.00852 / 0.00852	0.00298 / 0.00298	0.00223 / 0.00223	0.00122 / 0.00122
JES flavour composition (SR)	0.000442 / 0.000442	0.00369 / 0.00369	0.0011 / 0.0011	8.64e-05 / 8.64e-05	0.000757 / 0.000757	0.000133 / 0.000133
JES effective NP modelling 4	0.00449 / -0.00449	0.00709 / -0.00709	0.00726 / -0.00726	0.0122 / -0.0122	0.00506 / -0.00506	0.00376 / -0.00376
JES pile-up offset H	0.00172 / 0.00172	0.00172 / 0.00172	0.0271 / -0.0271	0.01 / -0.01	0.016 / -0.0116	0.0108 / -0.0109
JES pile-up offset NP	0.00617 / -0.00617	0.0133 / -0.0133	0.00414 / -0.00414	0.0105 / -0.0105	0.00445 / -0.00445	0.00101 / -0.0101
JES effective NP modelling 1	0.00269 / -0.00269	0.00532 / 0.00532	0.0146 / -0.0146	0.0415 / -0.0414	0.0164 / -0.0164	0.0263 / -0.0262
JES effective NP modelling 2	0.0137 / -0.0136	0.0146 / -0.0146	0.0163 / -0.0163	0.0163 / -0.0163	0.00593 / -0.00593	0.00832 / -0.00832
JES effective NP modelling 3	0.0083 / -0.0083	0.00851 / -0.00851	0.0178 / -0.0178	0.0157 / -0.0157	0.00931 / -0.00931	0.0349 / -0.0349
JES effective NP modelling 4	0.00268 / -0.00268	0.0135 / -0.0135	0.0391 / -0.0391	0.0211 / -0.0209	0.00835 / -0.00835	0.0123 / -0.0123
JES effective NP detector 1	0.00119 / -0.0119	0.0119 / -0.0119	0.0309 / -0.0309	0.0183 / -0.0183	0.018 / -0.018	0.016 / -0.016
JES effective NP detector 2	0.00146 / 0.00146	0.00206 / 0.00206	0.00544 / 0.00544	0.00248 / 0.00248	0.00285 / 0.00285	0.00115 / 0.00115
JES effective NP detector 3	0.00029 / 0.00029	0.00662 / 0.00662	0.00191 / 0.00191	8.64e-05 / 8.64e-05	0.00407 / 0.00407	6.16e-05 / 6.16e-05
JES single particle high- p_T	3.57e-07 / 3.57e-07	9.87e-06 / 9.87e-06	0 / 0	0.00106 / 0.00106	0.000256 / 0.000256	9.36e-08 / 9.36e-08
JES panch through	0 / 0	0.0232 / -0.0232	0.0266 / -0.0267	0.0102 / -0.0101	0.00257 / 0.00257	8.84e-05 / 8.84e-05
JER data vs. MC	0.000398 / -0.000398	0.0173 / -0.0173	0.021 / -0.0209	0.0298 / -0.0298	0.00094 / 0.00094	0.0082 / -0.0082
JER effective NP 1	0.00447 / -0.00447	0.016 / -0.016	0.0183 / -0.0183	0.018 / -0.018	0.0044 / 0.0044	0.00922 / -0.00922
JER effective NP 2	0.000711 / 0.000711	0.00753 / -0.00753	0.00793 / -0.00792	-0.0108 / 0.0108	0.00229 / 0.00229	0.0493 / -0.0493
JER effective NP 3	-0.00366 / 0.00366	0.000534 / -0.000533	0.000976 / -0.000976	0.00607 / -0.00607	-0.00318 / 0.00318	0.0387 / -0.0387
JER effective NP 4	-0.00233 / 0.00233	-0.00335 / 0.00335	0.017 / -0.017	-0.0141 / 0.0141	-0.00174 / 0.00174	0.0487 / -0.0487
JER effective NP 5	-0.000555 / 0.000555	-0.00121 / 0.00121	-0.0143 / 0.0143	-0.00494 / 0.00494	-0.00289 / 0.00289	0.00289 / -0.00289
JER effective NP 6	-0.000219 / 0.000219	-0.00213 / 0.00213	-0.0066 / -0.0066	-0.000142 / 0.000142	0.00187 / -0.00187	0.00344 / -0.00344
SF($j \rightarrow \gamma$)	0 / 0	0 / 0	1.01 / -0.484	0 / 0	0 / 0	0 / 0
p_T^γ reweighting ($Z + \gamma + \text{jets}$)	0 / 0	0 / 0	0 / 0	1.68e-05 / -1.68e-05	0 / 0	0 / 0
μ_R - μ_F ($t\bar{t} + \gamma$)	0 / 0	0 / 0	0 / 0	0.169 / -0.171	0 / 0	0 / 0
Heavy flavour fraction ($Z + \gamma + \text{jets}$)	0 / 0	0 / 0	0 / 0	-0.000727 / -0.000727	0 / 0	0 / 0
p_T^γ reweighting ($W + \gamma + \text{jets}$)	0 / 0	0 / 0	0 / 0	8.79e-05 / -8.79e-05	0 / 0	0 / 0
μ_R - μ_F ($W + \gamma + \text{jets}$)	0 / 0	0 / 0	0 / 0	0.155 / -0.155	0 / 0	0 / 0
normalisation: $W + \gamma + \text{jets}$, HF	0 / 0	0 / 0	0 / 0	0 / 0	0.17 / -0.167	0 / 0
Heavy flavour fraction ($W + \gamma + \text{jets}$)	0 / 0	0 / 0	0 / 0	0.00113 / 0.00113	0 / 0	0 / 0
$\sigma_{\text{theory}}(t\bar{t} + \gamma)$	0 / 0	0 / 0	0 / 0	0.00373 / -0.00373	0 / 0	0 / 0
γ SR bin 0	0.00102 / -0.00102	0.0123 / -0.0123	0.0126 / -0.0126	0.0152 / -0.0152	0.00576 / -0.00576	0.00667 / -0.00667
γ SR bin 1	0.00142 / -0.00142	0.0024 / -0.0024	0.0035 / -0.0035	0.00032 / -0.00032	0.00838 / -0.00838	0.00956 / -0.00956
γ SR bin 2	0.00121 / -0.00121	0.0054 / -0.0054	0.0026 / -0.0026	0.000231 / -0.000231	0.00141 / -0.00141	0.0138 / -0.0138
γ SR bin 3	0.0045 / -0.0045	0.0048 / -0.0048	0.0023 / -0.0023	0.000263 / -0.000263	0.0019 / -0.0019	0.0047 / -0.0047
γ SR bin 4	0.00148 / -0.00148	0.00802 / -0.00802	0.000854 / -0.000854	0.000142 / -0.000142	0.00402 / -0.00402	0.000474 / -0.000474
γ SR bin 5	0.00229 / -0.00229	0.000607 / -0.000607	0.000654 / -0.000654	0.000364 / -0.000364	0.000282 / -0.000282	0.000344 / -0.000344
γ SR bin 6	0.00315 / -0.00315	0.000607 / -0.000607	0.000329 / -0.000329	0.000126 / -0.000126	0.000207 / -0.000207	0.000207 / -0.000207
γ SR bin 7	0.00991 / -0.00991	0 / 0	0 / 0	0.103 / -0.103	0 / 0	0 / 0
SF($Z + \gamma + \text{jets}$)	0 / 0	0 / 0	0 / 0	0 / 0	0.0752 / -0.0752	0 / 0
SF($W + \gamma + \text{jets}$)	0 / 0	0 / 0	0 / 0	0 / 0	0 / 0	0 / 0

Table 58: Relative effect of each systematic uncertainty (post-fit) on the yields in the CR $W + \gamma + \text{jets}$ coupling using data in all regions (I).

	Signal ($t\bar{t}$, LH)	$e \rightarrow \gamma + \text{jets}$	$j \rightarrow \gamma + \text{jets}$	$Z \rightarrow \gamma + \text{jets}$	$W \rightarrow \gamma + \text{jets}$	other prompt γ
Luminosity	0.0197/-0.0197	0.0197/-0.0197	0.0197/-0.0197	0/0	0/0	0.0197/-0.0197
Pile-up	0.0124/-0.0125	0.0125/-0.0125	0.0125/-0.0125	0.00481/-0.0048	0.00492/-0.00492	0.0245/-0.0245
JVT	0.000881/0.000881	0.000889/0.000889	0.000106/0.00106	0.000378/0.000378	0.000957/0.000957	0.00184/0.00184
SF($e \rightarrow \gamma$)	0/0	0.0884/-0.0885	0/0	0/0	0/0	0/0
Shower generator ($t\bar{t}$)	0/0	-0.0125/0.0126	-0.00896/0.00897	0/0	0/0	0/0
ME generator ($t\bar{t}$)	0/0	0.00187/-0.00187	0.00242/-0.00242	0/0	0/0	0/0
Showr. generator (single top)	0/0	-0.00311/0.00311	-0.00091/-0.00091	0/0	0/0	-0.0729/0.0731
ME generator (single top)	0/0	0.000774/-0.000774	-0.000453/-0.000453	0/0	0/0	0.172/-0.176
tW DS scheme	0/0	-0.000379/0.000379	-0.000615/0.000615	0/0	0/0	-0.122/0.124
SF(photon ID)	0.00594/-0.00594	0.0113/-0.0113	0.014/-0.014	0.0125/-0.0125	0.0117/-0.0117	0.0113/-0.0113
SF(photon iso.)	0.0108/-0.0108	0.0152/-0.0152	0.00152/-0.00152	0.0142/-0.0142	0.014/-0.014	0.014/-0.014
SF(electron trigger)	0/0	0.00204/-0.00204	0.000119/0.000119	0.000139/0.000139	0.000124/-0.000124	0.00121/0.00121
SF(electron reco.)	0/0	0.000912/0.000912	0.00046/0.00046	0.000576/0.000576	0.000558/0.000558	0.000583/0.000583
SF(electron ID)	0/0	0.00533/-0.00633	0.00379/-0.00379	0.00444/-0.00444	0.00412/-0.00412	0.00412/-0.00412
SF(electron iso.)	0/0	0.0051/-0.0051	0.0014/-0.0014	0.000492/0.000492	0.000483/0.000483	0.000518/0.000518
SF(muon trigger stat.)	0/0	0.000304/0.000304	0.0007/0.0007	0.000787/0.000787	0.000851/0.000851	0.000854/0.000854
SF(muon trigger syst.)	0/0	0.000313/0.000313	0.00314/0.00314	0.000289/0.000289	0.000306/0.000306	0.000306/0.000306
SF(muon ID stat.)	0/0	0.000249/0.000249	9.63e-05/9.63e-05	0.000245/0.000245	0.000252/0.000252	0.000257/0.000257
SF(muon ID syst.)	0/0	0.00168/0.00168	0.000553/0.000553	0.00139/0.00139	0.00141/0.00141	0.00147/0.00147
SF(muon iso. stat.)	0/0	0.00156/0.00156	5.42e-05/5.42e-05	0.000148/0.000148	0.000146/0.000146	0.000146/0.000146
SF(muon iso. syst.)	0/0	0.00106/0.00106	0.000412/0.000412	0.000119/0.000119	0.000115/0.000115	0.000114/0.000114
SF(muon TTVA stat.)	0/0	0.000104/0.000104	3.92e-05/3.92e-05	0.000111/0.000111	0.000104/0.000104	0.000107/0.000107
SF(muon TTVA syst.)	4.07e-05/4.07e-05	1.66e-05/1.66e-05	5.69e-05/5.69e-05	5.69e-05/5.69e-05	5.21e-05/5.21e-05	4.61e-05/4.61e-05
EGamma resolution all	0.00383/-0.00383	0.0209/-0.0209	0.0179/-0.0179	0.00338/-0.00338	0.00151/-0.00151	0.00154/-0.00154
EGamma scale all	0.00961/-0.0096	0.0357/-0.0356	0.0194/-0.0193	0.0077/-0.0077	0.008/-0.008	0.00758/-0.00757
Muon ID	0/0	0.00146/-0.00146	0.000599/-0.000599	0.0145/-0.0145	0.00189/-0.00189	0.000781/-0.000781
Muon MS	0/0	0.00192/-0.00192	0.000542/-0.000541	0.000644/-0.000644	0.00226/-0.00226	0.000514/-0.000514
Muon sagitta bias	0/0	0.00207/0.00207	0.000615/0.000615	0.000399/0.000399	0.00107/0.00107	0.00068/0.00068
Muon scale	0.00322/-0.00322	0.00314/-0.00314	0.000719/-0.000719	0.00134/-0.00134	0.000251/-0.000251	0.00121/-0.00121
ISR ($t\bar{t}$)	0/0	0.00061/0.00061	0.00076/-0.00759	0.00164/-0.00164	0/0	0/0
FSR ($t\bar{t}$)	0/0	0.00869/-0.00869	0.00273/-0.00273	0/0	0/0	0/0
ISR (single top)	0/0	0.00085/-0.00085	0.000329/-0.000329	0/0	0/0	0.00166/-0.00166
FSR (single top)	0/0	0.00531/-0.00531	0.00148/-0.00148	0/0	0/0	0.0138/-0.0138
PDF no. 1	0.00328/-0.00328	0.00429/-0.00429	0.00429/-0.00429	0.00117/-0.00117	0.000897/0.000898	0.004383/-0.004383
PDF no. 2	0.00148/-0.00148	0.00291/-0.00291	0.0123/-0.0123	0.00169/-0.00169	0.000344/-0.000344	0.000707/-0.000707
PDF no. 3	0.00539/-0.00539	0.00415/-0.00415	0.00453/-0.00453	0.00578/-0.00578	0.00426/-0.00426	0.00282/-0.00282
PDF no. 4	0.00559/-0.00559	0.00523/-0.00523	0.00823/-0.00822	0.00154/-0.00154	0.00545/-0.00545	0.00194/-0.00194
PDF no. 5	0.00312/-0.00312	0.00331/-0.00331	0.014/-0.014	0.000762/-0.000761	0.00227/-0.00226	0.00441/-0.00441
PDF no. 6	0.00371/-0.00371	0.000954/-0.000954	0.0689/-0.0689	0.000208/-0.000208	0.00203/-0.00203	0.00514/-0.00514
PDF no. 7	0.00512/-0.00512	0.00151/-0.00151	0.0265/-0.0265	0.00116/-0.00116	0.000991/-0.000991	0.00615/-0.00615
PDF no. 8	0.00458/-0.00458	0.000972/-0.000972	0.0445/-0.0445	0.00657/-0.00657	0.000883/-0.000883	0.00441/-0.00441
PDF no. 9	0.000587/-0.000587	0.0026/-0.00261	0.0697/-0.0696	0.00272/-0.00272	0.0012/-0.0012	0.00178/-0.00178
PDF no. 10	0.00538/-0.00538	0.00022/-0.00022	0.0793/-0.0792	0.00243/-0.00243	0.00404/-0.00404	0.00569/-0.00569
PDF no. 11	0.000849/-0.000849	0.00141/-0.00141	0.0945/-0.0943	0.00224/-0.00224	0.000107/-0.00107	0.000308/-0.000308
PDF no. 12	0.00567/-0.00567	0.00211/-0.00211	0.106/-0.106	0.000205/-0.000205	0.00384/-0.00384	0.00411/-0.00411
PDF no. 13	0.00453/-0.00453	0.00259/-0.00259	0.06072/-0.06072	0.00177/-0.00177	0.00038/-0.00038	0.00619/-0.00619
PDF no. 14	0.00235/-0.00235	0.00107/-0.00107	0.0876/-0.0874	0.00121/-0.00121	0.000424/-0.000424	0.00398/-0.00398
PDF no. 15	0.0042/-0.0042	0.00352/-0.00352	0.000431/-0.000434	0.00652/-0.00651	0.000628/-0.000628	0.0055/-0.0055
PDF no. 16	0.000925/-0.000925	0.00021/-0.00021	0.0577/-0.0576	0.000463/-0.000463	0.000523/-0.000523	0.003736/-0.003736
PDF no. 17	0.00767/-0.00766	0.00243/-0.00243	0.0754/-0.0753	0.00208/-0.00208	0.000502/-0.000502	0.00921/-0.00921
PDF no. 18	0.00493/-0.00493	0.00112/-0.00112	0.0858/-0.0856	7.29e-05/-7.29e-05	0.00254/-0.00254	0.0007/-0.0007
PDF no. 19	0.000762/-0.000762	0.000913/-0.000913	0.0671/-0.0671	0.000128/-0.000128	0.00179/-0.00179	0.000322/-0.000322
PDF no. 20	0.00365/-0.00365	0.00153/-0.00153	0.0683/-0.0683	0.000399/-0.000399	0.00021/-0.00021	0.00494/-0.00494
PDF no. 21	0.00425/-0.00425	0.00118/-0.00118	0.0831/-0.0829	0.00131/-0.00131	0.00117/-0.00117	0.00465/-0.00465
PDF no. 22	0.0019/-0.00185	0.0092/-0.0092	0.0992/-0.0989	0.00123/-0.00123	0.000523/-0.000523	0.00372/-0.00372
PDF no. 23	0.00377/-0.00377	0.00108/-0.00108	0.0811/-0.0811	0.000382/-0.000382	0.00103/-0.00103	0.00548/-0.00548
PDF no. 24	0.00479/-0.00479	0.000493/-0.000493	0.068/-0.068	0.000236/-0.000236	0.00195/-0.00195	0.00632/-0.00632
PDF no. 25	0.00221/-0.00221	0.000827/-0.000827	0.0781/-0.0781	0.000409/-0.000409	0.000233/-0.000233	0.00409/-0.00409
PDF no. 26	0.00476/-0.00476	0.0008/-0.0008	0.0833/-0.0832	0.00128/-0.00128	0.000225/-0.000225	0.00564/-0.00563
PDF no. 27	0.00425/-0.00425	0.00118/-0.00118	0.0831/-0.0829	0.000314/-0.000314	0.00026/-0.00026	0.00572/-0.00572
PDF no. 28	0.00567/-0.00567	0.00366/-0.00366	0.0698/-0.0698	0.00694/-0.00694	0.000829/-0.000829	0.0107/-0.0107
PDF no. 29	0.00449/-0.00449	0.000946/-0.000946	0.0746/-0.0745	0.00214/-0.00214	0.00184/-0.00184	0.00534/-0.00534
PDF no. 30	0.00942/-0.00942	0.000752/-0.000752	0.0682/-0.0682	0.00053/-0.00053	0.000107/-0.000107	0.00987/-0.00987
μ_R - μ_F (single top)	0/0	0.000841/-0.000844	0.00628/-0.00628	0/0	0/0	0.00583/-0.00583
μ_R - μ_F ($Z + \text{jets}$)	0/0	0.136/-0.128	0.0342/-0.0337	0/0	0/0	0/0
μ_R - μ_F (diboson)	0/0	0.00511/-0.00511	0.0198/-0.0198	0/0	0/0	0.00571/-0.00571
$\sigma_{\text{theory}}(t\bar{t})$	0/0	0.00228/-0.00228	0.000664/-0.000664	0/0	0/0	0.0118/-0.0118
$\sigma_{\text{theory}}(W + \text{jets})$	0/0	7.92e-05/-7.89e-05	0.0423/-0.0423	0/0	0/0	0/0
$\sigma_{\text{theory}}(Z + \text{jets})$	0/0	0.0327/-0.0327	0.00465/-0.00465	0/0	0/0	0/0
$\sigma_{\text{theory}}(\text{diboson})$	0/0	0.00448/-0.00448	0.000528/-0.000528	0/0	0/0	0.00598/-0.00598

Table 59: Relative effect of each systematic uncertainty (post-fit) on the yields in the CR $W + \gamma + \text{jet}$ regions (II).

	Signal (try, LH)	$e \rightarrow \gamma$ fake	$j \rightarrow \gamma$ fake	$Z\gamma$ -jets	$W\gamma$ -jets	other prompt γ
E_T^{miss} soft-term reso. para.	-0.00851 / 0.00851	-0.0357 / 0.0358	0.00796 / -0.00796	-0.0424 / 0.0424	-0.00517 / 0.00518	-0.00235 / 0.00235
E_T^{miss} soft-term reso. perp.	-0.008877 / 0.00877	-0.0315 / 0.0315	-0.0112 / 0.0112	-0.0311 / 0.0311	-0.00273 / 0.00273	-0.00298 / 0.00298
$SR(b\text{-tag eigenvar. B1})$	0.0035 / -0.0035	0.0397 / -0.0396	0.017 / -0.017	0.0382 / -0.0381	0.00694 / -0.00694	0.003 / -0.003
$SR(b\text{-tag eigenvar. B2})$	0.00746 / -0.00746	0.00368 / -0.00368	0.000749 / -0.000749	0.000556 / -0.000555	0.000133 / -0.000133	0.00841 / -0.00841
$SR(b\text{-tag eigenvar. B3})$	0.00133 / 0.00133	0.004667 / 0.004667	7.5e-05 / 7.5e-05	0.000176 / 0.000176	1.62e-05 / 1.62e-05	0.00119 / 0.00119
$SR(b\text{-tag eigenvar. B4})$	0.00679 / 0.00679	0.00332 / 0.00332	0.000534 / 0.000534	0.000251 / -0.000251	6.93e-05 / 6.91e-05	0.00748 / -0.00748
$SR(b\text{-tag eigenvar. B5})$	0.000147 / 0.000147	0.000147 / 0.000147	5.6e-05 / 5.6e-05	5.19e-05 / 5.19e-05	9.8e-06 / 9.8e-06	0.000349 / 0.000349
$SR(b\text{-tag eigenvar. B6})$	0.000501 / 0.000501	0.000339 / 0.000339	3.64e-05 / 3.64e-05	1.48e-05 / 1.48e-05	0.000691 / 0.000691	0.000227 / -0.000227
$SR(b\text{-tag eigenvar. B7})$	0.000155 / 0.000155	5.36e-05 / 5.36e-05	8.98e-06 / 8.98e-06	7.83e-06 / 7.83e-06	8.3e-07 / 8.3e-07	7.85e-05 / 7.85e-05
$SR(b\text{-tag eigenvar. B8})$	9.38e-06 / 9.38e-06	1.34e-05 / 1.34e-05	1.32e-06 / 1.32e-06	2.27e-06 / 2.27e-06	2.73e-07 / 2.73e-07	1.67e-05 / 1.67e-05
$SR(b\text{-tag eigenvar. B9})$	2.61e-06 / 2.61e-06	1.02e-06 / 1.02e-06	0.5e-07 / 0.5e-07	5.83e-08 / 5.83e-08	1.44e-06 / 1.44e-06	4.57e-07 / 4.57e-07
$SR(b\text{-tag eigenvar. C1})$	5.26e-07 / 5.26e-07	9.82e-08 / 9.82e-08	9.86e-08 / 9.86e-08	9.35e-08 / 9.35e-08	2.29e-08 / 2.29e-08	0.00163 / -0.000163
$SR(b\text{-tag eigenvar. C2})$	7.8e-05 / -7.79e-05	0.000239 / -0.000239	0.000143 / -0.000143	0.000251 / -0.000251	0.000406 / -0.000406	0.000163 / -0.000163
$SR(b\text{-tag eigenvar. C3})$	1.32e-05 / 1.32e-05	4.96e-05 / 4.96e-05	1.87e-05 / 1.87e-05	5.96e-05 / 5.96e-05	0.000102 / 0.000102	5.84e-05 / 5.84e-05
$SR(b\text{-tag eigenvar. light 1})$	0.000351 / -0.000351	0.000411 / -0.000411	0.000479 / -0.000479	0.000475 / -0.000475	0.000449 / -0.000449	0.000257 / -0.000257
$SR(b\text{-tag eigenvar. light 2})$	2.75e-05 / 2.75e-05	2.9e-05 / 2.9e-05	4.72e-05 / 4.72e-05	3.72e-05 / 3.72e-05	1.06e-05 / 1.06e-05	4.98e-06 / 4.98e-06
$SR(b\text{-tag eigenvar. light 3})$	5.63e-06 / 5.63e-06	6.17e-06 / 6.17e-06	1e-05 / 1e-05	2.58e-06 / 2.58e-06	2.22e-06 / 2.22e-06	2.89e-06 / 2.89e-06
$SR(b\text{-tag eigenvar. light 4})$	4.06e-06 / 4.06e-06	4.05e-06 / 4.05e-06	6.81e-06 / 6.81e-06	6.53e-06 / 6.53e-06	5.24e-06 / 5.24e-06	4.72e-05 / 4.72e-05
$SR(b\text{-tag extrapolation})$	5.32e-05 / 5.32e-05	5.75e-05 / 5.75e-05	5.47e-06 / 5.47e-06	5.73e-06 / 5.73e-06	4.31e-05 / 4.31e-05	7.51e-05 / 7.51e-05
JES η interc. from charm	5.49e-07 / 5.49e-07	2.19e-06 / 2.19e-06	2.74e-06 / 2.74e-06	0.0192 / -0.0192	0.0101 / -0.0101	0.000213 / -0.000213
JES η interc. non-closest high- E_T	0.00771 / -0.00771	0.0215 / -0.0215	0.0215 / -0.0215	0.0213 / -0.0213	0.00982 / -0.00982	0.000257 / -0.000257
JES η interc. non-closest $\eta < 0$	0.000447 / 0.000447	1.31e-05 / -1.31e-05	0 / 0	6.66e-06 / -6.79e-06	0 / 0	0 / 0
JES η interc. non-closest $\eta > 0$	0.000641 / 0.000641	0.000732 / 0.000732	0.00161 / 0.00161	0.00082 / 0.00082	0.000368 / 0.000368	0.000347 / 0.000347
JES η interc. total stat.	0.00282 / -0.00282	0.01 / -0.01	0.000763 / 0.000763	0.000358 / 0.000358	0.000104 / 0.000104	0.000104 / 0.000104
JES effective NP stat. 1	0.000135 / 0.000135	0.00356 / 0.00356	0.00415 / -0.00415	0.000338 / -0.000338	0.000384 / -0.000384	0.000384 / -0.000384
JES effective NP stat. 2	0.000196 / 0.000196	0.000873 / 0.000873	0.00235 / 0.00235	0.00222 / 0.00222	0.000322 / 0.000322	0.00126 / 0.00126
JES effective NP stat. 3	0.00014 / 0.00014	0.000869 / 0.000869	0.00271 / 0.00271	0.000328 / 0.000328	0.000492 / 0.000492	0.00315 / 0.00315
JES effective NP stat. 4	0.000929 / 0.000929	0.000292 / 0.000292	0.00177 / 0.00177	0.000645 / 0.000645	0.000249 / 0.000249	0.000422 / 0.000422
JES effective NP stat. 5	0.000641 / 0.000641	0.000845 / 0.000845	0.00189 / 0.00189	0.00189 / 0.00189	0.000429 / 0.000429	0.000318 / 0.000318
JES effective NP stat. 6	0.000763 / 0.000763	0.00162 / 0.00162	0.00183 / 0.00183	0.00172 / 0.00172	0.000255 / 0.000255	0.000255 / 0.000255
JES effective NP mixed 1	0.000114 / 0.000114	0.00247 / 0.00247	0.000728 / 0.000728	0.00187 / 0.00187	0.000658 / 0.000658	0.00054 / 0.00054
JES effective NP mixed 2	0.00014 / 0.00014	0.000436 / 0.000436	0.00738 / 0.00738	0.00191 / 0.00191	0.000502 / 0.000502	0.00126 / 0.00126
JES effective NP mixed 3	0.000539 / 0.000539	0.00117 / 0.00117	0.000177 / 0.000177	0.000645 / 0.000645	0.000191 / 0.000191	0.000197 / 0.000197
JES effective NP modeling 1	0.0156 / -0.0156	0.0247 / -0.0244	0.0265 / -0.0261	0.0145 / -0.0144	0.0219 / -0.0217	0.0252 / 0.0252
JES effective NP modeling 2	0.00226 / 0.00226	0.00788 / 0.00788	0.00838 / 0.00838	0.00124 / 0.00124	0.00298 / 0.00298	0.00177 / 0.00177
JES effective NP modeling 3	0.000965 / 0.000965	0.00281 / 0.00281	0.00179 / 0.00179	0.00172 / 0.00172	0.00168 / 0.00168	0.00112 / 0.00112
JES effective NP modeling 4	0.000355 / 0.000355	0.000362 / 0.000362	0.0017 / 0.0017	0.000566 / 0.000566	0.000175 / 0.000175	0.00148 / 0.00148
JES pile-up offset μ	0.00673 / -0.00673	0.0213 / -0.0212	0.0274 / -0.0274	0.00997 / -0.00997	0.00191 / -0.00191	0.00353 / -0.00353
JES pile-up offset NP	0.0068 / -0.0068	0.0161 / -0.0161	0.0337 / -0.0337	0.00839 / -0.00839	0.00131 / -0.00131	0.0095 / -0.0095
JES pile-up p_T term	0.00204 / -0.00204	0.009 / -0.009	0.00849 / -0.00849	0.00341 / -0.00341	0.000609 / -0.000609	0.00139 / -0.00139
JES pile-up ρ topology	0.0157 / -0.0157	0.0276 / -0.0275	0.0317 / -0.0315	0.0108 / -0.0108	0.0248 / -0.0247	0.0126 / -0.0126
b -JES response	0.00679 / -0.00679	0.00423 / -0.00423	0.00164 / -0.00164	0.00371 / -0.00371	0.00168 / -0.00168	0.0269 / -0.0269
JES flavour composition (CR $W + \gamma + \text{jet}$)	0.0194 / -0.0194	0.0519 / -0.052	0.0488 / -0.0488	0.0293 / -0.0293	0.00608 / -0.00608	0.0111 / -0.0111
JES flavour response (CR $W + \gamma + \text{jet}$)	0.0105 / -0.0105	0.0314 / -0.0313	0.0282 / -0.0282	0.0187 / -0.0187	0.00391 / -0.00391	0.00111 / -0.00111
JES data vs. MC	0.00128 / 0.00128	0.00406 / 0.00406	0.00411 / 0.00411	0.00259 / 0.00259	0.00026 / 0.00026	0.00111 / 0.00111
JER effective NP detector 1	0.00026 / 0.00026	0.00529 / 0.00529	0.00147 / 0.00147	0.000345 / 0.000345	6.16e-05 / 6.16e-05	0.000112 / 0.000112
JER effective NP detector 2	0 / 0	2.85e-05 / 2.85e-05	0 / 0	0 / 0	-3.62e-09 / -3.62e-09	0 / 0
JES single particle high- p_T	0 / 0	4.78e-05 / 4.78e-05	7.01e-07 / 7.01e-07	1.21e-05 / 1.21e-05	2.27e-05 / 2.27e-05	9.46e-06 / 9.46e-06
JES punch through	0 / 0	0.0164 / -0.0164	0.0259 / -0.0259	0.0127 / -0.0127	0.00304 / -0.00304	-0.000324 / 0.000324
JER effective NP 1	0.000531 / -0.000531	0.0166 / -0.0166	0.0614 / -0.0612	0.0296 / -0.0296	0.0104 / -0.0104	0.00732 / -0.00731
JER effective NP 2	0.0107 / -0.0107	0.022 / -0.022	0.0484 / -0.0485	0.0253 / -0.0253	0.00757 / -0.00757	0.00832 / -0.00832
JER effective NP 3	0.00856 / -0.00856	0.0075 / -0.00749	0.0535 / -0.0531	0.0164 / -0.0164	0.00554 / -0.00554	0.00466 / -0.00466
JER effective NP 4	0.00448 / -0.00448	0.00635 / -0.00635	0.00879 / -0.00879	0.0013 / -0.0013	0.00481 / -0.00481	0.00639 / -0.00639
JER effective NP 5	0.0032 / -0.0032	0.00907 / -0.00907	-0.0077 / 0.0077	-0.00316 / 0.00316	0.00388 / -0.00388	0.000329 / -0.000329
JER effective NP 6	0.00239 / -0.00239	8.77e-05 / -8.77e-05	0.00259 / -0.00259	-0.00554 / 0.00554	0.00136 / -0.00136	0.00212 / -0.00212
JER effective NP 7 (rest term)	0.00498 / -0.00498	0.0166 / -0.0166	0.0285 / -0.0285	0.00108 / -0.00108	0.00504 / -0.00504	0.00214 / -0.00214
$\mu_R \mu_F (t\bar{t} \rightarrow \gamma)$	0 / 0	0 / 0	1.01 / -0.483	0 / 0	0 / 0	0 / 0
P_T^γ reweighting ($Z\gamma$ -jets)	0 / 0	0 / 0	0 / 0	4.9e-08 / 2.39e-08	0 / 0	0 / 0
$\mu_R \mu_F (Z\gamma\text{-jets})$	0.205 / 0.205	0.689 / 0.689	0.828 / 0.828	0.837 / 0.837	0.835 / 0.835	0.0505 / -0.0504
γ CR $W + \gamma + \text{jet}$ bin 0	0.0728 / 0.0728	0.118 / 0.118	0.0616 / 0.0616	0.0573 / 0.0573	0.0642 / 0.0642	0.0742 / 0.0742
γ CR $W + \gamma + \text{jet}$ bin 1	0.035 / 0.035	0.0399 / 0.0399	0.0169 / 0.0169	0.0215 / 0.0215	0.0212 / 0.0212	0.0225 / 0.0225
γ CR $W + \gamma + \text{jet}$ bin 2	0.0377 / 0.0377	0.0329 / 0.0329	0.0129 / 0.0129	0.0185 / 0.0185	0.0185 / 0.0185	0.0189 / 0.0189
γ CR $W + \gamma + \text{jet}$ bin 3	0.0409 / 0.0409	0.039 / 0.039	0.0129 / 0.0129	0.0161 / 0.0161	0.0158 / 0.0158	0.0171 / 0.0171
γ CR $W + \gamma + \text{jet}$ bin 4	0.0547 / 0.0547	0.025 / 0.0225	0.0284 / 0.0284	0.0178 / 0.0178	0.0157 / 0.0157	0.0149 / 0.0149
γ CR $W + \gamma + \text{jet}$ bin 5	0.0928 / 0.0928	0.0278 / 0.0277	0.0164 / 0.0164	0.0164 / 0.0164	0.0143 / 0.0143	0.0147 / 0.0147
γ CR $W + \gamma + \text{jet}$ bin 6	0.161 / 0.161	0.0311 / 0.0311	0.0203 / 0.0203	0.016 / 0.016	0.0157 / 0.0157	0.0168 / 0.0168
γ CR $W + \gamma + \text{jet}$ bin 7	0 / 0	0 / 0	0.103 / 0.103	0 / 0	0 / 0	0 / 0
SFW $\gamma\gamma$ -jets	0 / 0	0 / 0	0 / 0	0 / 0	0 / 0	0 / 0
SFW $\gamma\gamma\text{-jets}$	0 / 0	0 / 0	0 / 0	0 / 0	0 / 0	0 / 0

Not reviewed, for internal circulation only

Table 60: Relative effect of each systematic uncertainty (post-fit) on the yields in the CR $Z + \gamma$ for the left-handed $t\bar{u}y$ coupling using data in all regions (I).

	Signal ($t\bar{u}y$, LH)	$e \rightarrow \gamma$ fake	$j \rightarrow \gamma$ fake	$Z \rightarrow \gamma$ fake	$Z \gamma + \text{jets}$	$W \gamma + \text{jets}$	other prompt γ
Luminosity	0.0197/-0.0197	0.0197/-0.0197	0.0197/-0.0197	0.0197/-0.0197	0.0351/-0.035	0.156/-0.155	0.0197/-0.0197
Pile-up	0.0986/-0.0982	0.0263/-0.0264	0.00954/0.00954	0.000841/0.000841	0.000585/0.000585	0.00173/0.00173	0.0262/-0.0262
IVT	0.00741/0.00741	0.00954/0.00954	0.0884/-0.0855	0.0/0	0/0	0/0	0.0037/0.0037
SF($e \rightarrow \gamma$)	0/0	-0.00185/0.00185	-0.0069/-0.0069	-0.0069/-0.0069	0/0	0/0	0/0
Shower generator ($t\bar{t}$)	0/0	0.00531/-0.00531	0.00515/-0.00515	0/0	0/0	0/0	0/0
ME generator (single top)	0/0	-0.00348/0.00348	0.00285/-0.00285	0/0	0/0	0/0	-0.0335/0.0336
ME generator (single top)	0/0	0.00175/-0.00175	0.00126/-0.00126	0/0	0/0	0/0	-0.0499/-0.0502
TW DS scheme	0/0	-0.00257/0.00257	0.00144/-0.00144	0/0	0/0	0/0	-0.00823/0.00824
SF(photon ID)	0.00759/-0.00759	0.012/-0.012	0.0152/-0.0152	0.0128/-0.0128	0.0117/-0.0117	0.0109/-0.0109	0/0
SF(photon iso.)	0.0143/-0.0143	0.0153/-0.0153	0.0153/-0.0153	0.0153/-0.0153	0.0138/-0.0138	0.0138/-0.0138	0/0
SF(electron trigger)	0.006543/0.000543	0.00023/0.00023	0.00241/0.000241	0.000234/0.000234	0.000234/0.000234	0.000152/0.000152	0.000152/0.000152
SF(electron reco.)	0.00213/0.00213	0.0013/0.0013	0.000872/0.000872	0.000936/0.000936	0.000936/0.000936	0.00145/0.00145	0.00103/0.00103
SF(electron ID)	0.0234/-0.0234	0.00983/-0.00983	0.00749/-0.00749	0.00749/-0.00749	0.00736/-0.00736	0.00736/-0.00736	0/0
SF(electron iso.)	0.00301/0.00301	0.0012/0.0012	0.00836/0.00836	0.00836/0.00836	0.00836/0.00836	0.00205/0.00205	0.000904/0.000904
SF(muon trigger stat.)	5.19e-05/5.19e-05	0.000396/0.000396	0.000444/0.000444	0.000444/0.000444	0.000528/0.000528	0.000447/0.000447	0.000519/0.000519
SF(muon trigger syst.)	0.000372/0.000372	0.000871/0.000871	0.000273/0.000273	0.000273/0.000273	0.000273/0.000273	0.000119/0.00119	0.000119/0.00119
SF(muon ID stat.)	0.00035/0.00035	0.000453/0.000453	0.000633/0.000633	0.000633/0.000633	0.000633/0.000633	0.000626/0.000626	0.000626/0.000626
SF(muon ID syst.)	0.000884/0.000884	0.0027/0.0027	0.00471/0.00471	0.00372/0.00372	0.00372/0.00372	0.00371/0.00371	0/0
SF(muon iso. syst.)	9.94e-05/9.94e-05	0.0002397/0.0002397	0.000236/0.000236	0.000236/0.000236	0.000336/0.000336	0.000333/0.000333	0.000333/0.000333
SF(muon iso. syst.)	0.000617/0.000617	0.00187/0.00187	0.00254/0.00254	0.00254/0.00254	0.00273/0.00273	0.00254/0.00254	0.00254/0.00254
SF(muon TTV stat.)	5.56e-05/5.56e-05	0.000178/0.000178	0.000229/0.000229	0.000261/0.000261	0.000128/0.000128	0.000251/0.000251	0/0
SF(muon TTV syst.)	4.58e-05/4.58e-06	7.59e-05/7.59e-05	0.000101/0.00101	0.000129/0.000129	6.25e-05/6.25e-05	0.000105/0.000105	0.000105/0.000105
EGamma resolution all	0.106/-0.106	0.00436/-0.00436	0.0236/-0.0236	0.00178/-0.00178	0.00178/-0.00178	0.00186/-0.00186	0/0
EGamma scale all	0.139/-0.138	0.00798/-0.00797	0.0275/-0.0274	0.00943/-0.00943	0.00943/-0.00943	0.0044/-0.0044	0/0
Muon ID	0/0	0.00819/-0.00819	0.00457/-0.00457	0.00693/-0.00693	0.00693/-0.00693	0.00456/-0.00456	0.000627/-0.000627
Muon MS	0/0	0.000766/-0.000766	0.00921/-0.00921	0.00746/-0.00746	0.0561/-0.0561	0.000627/-0.000627	0/0
Muon sagitta residuals	0/0	0.000521/0.000521	0.00465/0.00465	0.000146/0.000146	0.000144/-0.000144	0.000199/-0.000199	0.000489/-0.000488
Muon scale	0/0	0.00119/-0.00119	0.0121/-0.0121	0.000111/0.00111	0/0	0/0	0.00063/0.00063
ISR ($t\bar{t}$)	0/0	0.000885/0.000885	0.00182/0.00182	0/0	0/0	0/0	0/0
FSR ($t\bar{t}$)	0/0	0.000707/-0.000707	0.00297/-0.00297	0/0	0/0	0/0	0/0
ISR (single top)	0/0	0.000152/-0.000152	0.00114/-0.000114	0/0	0/0	0/0	0/0
FSR (single top)	0/0	0.000489/-0.000489	0.000166/-0.000166	0/0	0/0	0/0	0/0
PDF no. 1	0.0349/-0.0349	0.00329/-0.00329	0.00164/-0.00164	0.00123/-0.00123	0.00192/-0.00192	0.00433/-0.00433	0.00433/-0.00433
PDF no. 2	0.0743/-0.0743	0.0296/-0.0296	0.00156/-0.00156	0.00173/-0.00173	0.0128/-0.0128	0.00418/-0.00418	0.00418/-0.00418
PDF no. 3	0.0422/-0.0422	0.00208/-0.00208	0.0072/-0.0072	0.00634/-0.00634	0.0241/-0.0241	0.00345/-0.00345	0.00345/-0.00345
PDF no. 4	0.0144/-0.0144	0.01447/-0.01447	0.00475/-0.00475	0.00361/-0.00361	0.0143/-0.0143	0.00338/-0.00338	0.00338/-0.00338
PDF no. 5	0.158/-0.0141	0.0118/-0.0118	0.00871/-0.00871	0.000868/-0.000868	0.00112/-0.00112	0.00392/-0.00392	0.00392/-0.00392
PDF no. 6	0.0576/-0.0575	0.00799/-0.00799	0.00039/-0.00039	0.000253/-0.000253	0.00155/-0.00155	0.00471/-0.00471	0.00471/-0.00471
PDF no. 7	0.0628/-0.0629	0.00411/-0.00411	0.00064/-0.00064	0.00283/-0.00283	0.00756/-0.00756	0.00428/-0.00428	0.00428/-0.00428
PDF no. 8	0.0957/-0.0849	0.00339/-0.00339	0.000542/-0.000542	0.000706/-0.000706	0.00141/-0.00141	0.00518/-0.00518	0.00518/-0.00518
PDF no. 9	0.0364/-0.0364	0.00652/-0.00652	0.00478/-0.00478	0.00275/-0.00275	0.0127/-0.0127	0.005381/-0.005381	0.005381/-0.005381
PDF no. 10	0.106/-0.0859	0.0116/-0.0116	0.00161/-0.00161	0.00184/-0.00184	0.0043/-0.0043	0.00556/-0.00556	0.00556/-0.00556
PDF no. 11	0.0582/-0.0581	0.0184/-0.0184	0.001/-0.001	0.00257/-0.00257	0.0162/-0.0162	0.00115/-0.00115	0.00115/-0.00115
PDF no. 12	0.0923/-0.0862	0.0185/-0.0185	0.00324/-0.00324	0.00245/-0.00245	0.004/-0.004	0.00362/-0.00362	0.00362/-0.00362
PDF no. 13	0.0833/-0.0833	0.00962/-0.00962	0.00232/-0.00232	0.00172/-0.00172	0.00428/-0.00428	0.00589/-0.00589	0.00589/-0.00589
PDF no. 14	0.0347/-0.034	0.00851/-0.00851	0.000465/-0.000464	0.000166/-0.000166	0.00431/-0.00431	0.00513/-0.00513	0.00513/-0.00513
PDF no. 15	0.0602/-0.0602	0.00648/-0.00648	0.006551/-0.006551	0.00103/-0.00103	0.0046/-0.0046	0.0049/-0.0049	0.0049/-0.0049
PDF no. 16	0.0281/-0.0281	0.00259/-0.00259	0.000555/-0.000555	0.000537/-0.000537	0.00165/-0.00165	0.00243/-0.00243	0.00243/-0.00243
PDF no. 17	0.0825/-0.0824	0.01/-0.01	0.00326/-0.00326	0.00301/-0.00301	0.00416/-0.00416	0.0106/-0.0106	0.0106/-0.0106
PDF no. 18	0.0926/-0.0888	0.0101/-0.0101	0.000448/-0.000448	0.00023/-0.00023	0.00162/-0.00162	0.00647/-0.00647	0.00647/-0.00647
PDF no. 19	0.0591/-0.059	0.0366/-0.0366	0.000799/-0.000799	0.000376/-0.000376	0.00269/-0.00269	0.00314/-0.00314	0.00314/-0.00314
PDF no. 20	0.034/-0.034	0.00851/-0.00851	0.000465/-0.000464	0.000166/-0.000166	0.00431/-0.00431	0.0045/-0.0045	0.0045/-0.0045
PDF no. 21	0.041/-0.041	0.00536/-0.00536	0.00103/-0.00103	0.00126/-0.00126	0.00421/-0.00421	0.00392/-0.00392	0.00392/-0.00392
PDF no. 22	0.076/-0.0798	0.0283/-0.0283	0.00191/-0.00191	0.00127/-0.00127	0.00473/-0.00473	0.00404/-0.00404	0.00404/-0.00404
PDF no. 23	0.076/-0.0759	0.00845/-0.00845	0.000808/-0.000808	0.000391/-0.000391	0.00572/-0.00572	0.00494/-0.00494	0.00494/-0.00494
PDF no. 24	0.0681/-0.0688	0.00871/-0.00871	0.00023/-0.00023	0.000505/-0.000505	0.00251/-0.00251	0.00695/-0.00695	0.00695/-0.00695
PDF no. 25	0.0591/-0.059	0.0366/-0.0366	0.000799/-0.000799	0.000376/-0.000376	0.00199/-0.00199	0.00368/-0.00368	0.00368/-0.00368
PDF no. 26	0.0586/-0.0586	0.0142/-0.0142	0.00234/-0.00234	0.00141/-0.00141	0.00434/-0.00434	0.00384/-0.00384	0.00384/-0.00384
PDF no. 27	0.107/-0.0847	0.00979/-0.00979	0.000566/-0.000566	0.000301/-0.000301	0.00242/-0.00242	0.00356/-0.00356	0.00356/-0.00356
PDF no. 28	0.0765/-0.0764	0.0161/-0.0116	0.00101/-0.00101	0.00822/-0.00822	0.00783/-0.00783	0.00783/-0.00783	0.00783/-0.00783
PDF no. 29	0.0767/-0.0766	0.00703/-0.00703	0.000536/-0.000536	0.00198/-0.00198	0.00533/-0.00533	0.00503/-0.00503	0.00503/-0.00503
PDF no. 30	0.0746/-0.0746	0.0105/-0.0105	0.000138/-0.000138	0.000636/-0.000636	0.00419/-0.00419	0.00404/-0.00404	0.00404/-0.00404

Table 61: Relative effect of each systematic uncertainty (post-fit) on the yields in the CR $Z + \gamma$ for the left-handed $t\bar{u}y$ coupling using data in all regions (II).

	Signal ($t\bar{u}y$, LH)	$e \rightarrow y$ fake	$j \rightarrow y$ fake	$Z \gamma + \text{jets}$	$W \gamma + \text{jets}$	other prompt γ
μ_R, μ_F (single top)	0/0	0.000119/-0.000119	0.000102/-0.000102	0/0	0/0	0.00273/-0.00273
μ_R, μ_F (W+jets)	0/0	0/0	0/0	0/0	0/0	0/0
μ_R, μ_F (Z+jets)	0/0	0.0144/-0.0143	0.168/-0.156	0/0	0/0	0/0
μ_R, μ_F (diboson)	0/0	0.0473/-0.0473	0.0019/-0.0019	0/0	0/0	0.00449/-0.0045
$\sigma_{\text{theory}}(t\bar{t})$	0/0	0.00106/-0.00106	0.00203/-0.00203	0/0	0/0	0/0
σ_{theory} (single top)	0/0	0.000187/-0.000187	6.84e-05/-6.83e-05	0/0	0/0	0.00386/-0.00386
$\sigma_{\text{theory}}(W+\text{jets})$	0/0	0/0	0/0	0/0	0/0	0/0
$\sigma_{\text{theory}}(Z+\text{jets})$	0/0	0.000902/-0.000902	0.0469/-0.0469	0/0	0/0	0/0
σ_{theory} (diboson)	0/0	0.0571/-0.0572	0.000652/-0.000652	0/0	0/0	0.0069/-0.0069
JES η interc. modeling	0.000286/-0.000286	0.000226/-0.000226	0.000709/-0.000709	9.73e-05/-9.71e-05	0/0	0.000132/-0.000132
JES η interc. non-closure high- E_T	0/0	0/0	0/0	0/0	0/0	0/0
JES η interc. non-closure $\eta < 0$	0/0	3.69e-06/3.69e-06	1.13e-05/1.13e-05	8.74e-06/8.74e-06	0/0	7.99e-06/7.99e-06
JES η interc. non-closure $\eta > 0$	0/0	1.05e-07/1.05e-07	0/0	9.18e-07/9.18e-07	0/0	5.46e-07/5.46e-07
JES η interc. total stat.	0/0	0.000147/-0.000147	2.53e-05/-2.55e-05	5.58e-05/-5.59e-05	0/0	5.18e-05/-5.19e-05
JES effective NP stat. 1	0/0	3.16e-05/3.16e-05	2.98e-05/2.98e-05	2.01e-05/2.01e-05	0/0	2.32e-05/2.32e-05
JES effective NP stat. 2	0/0	0.000132/0.000132	3.46e-05/3.46e-05	4.04e-05/4.04e-05	0/0	7.07e-05/7.07e-05
JES effective NP stat. 3	0/0	7.13e-06/7.13e-06	4.88e-07/4.88e-07	7.14e-06/7.14e-06	0/0	8.9e-06/8.9e-06
JES effective NP stat. 4	0/0	9.37e-06/9.37e-06	8.22e-07/8.22e-07	6.91e-06/6.91e-06	0/0	1.05e-05/1.05e-05
JES effective NP stat. 5	0/0	1.06e-05/1.06e-05	5.72e-07/5.72e-07	7.88e-06/7.88e-06	0/0	6.27e-06/6.27e-06
JES effective NP stat. 6	0/0	1.18e-06/1.18e-05	9.16e-06/9.16e-06	1.05e-05/1.05e-05	0/0	1.05e-05/1.05e-05
JES effective NP mixed 1	0/0	1.37e-05/1.37e-05	2.15e-06/2.15e-06	1.11e-05/1.11e-05	0/0	1.77e-05/1.77e-05
JES effective NP mixed 2	0/0	3.81e-05/3.81e-05	6.13e-05/6.13e-05	2.18e-05/2.18e-05	0/0	2.64e-05/2.64e-05
JES effective NP mixed 3	0/0	1e-05/1e-05	4.88e-07/4.88e-07	1.03e-05/1.03e-05	0/0	7.57e-06/7.57e-06
JES effective NP modelling 1	0.00107/-0.00107	0.000347/-0.000347	0.00272/-0.00272	0.00024/-0.00024	0/0	0.000353/-0.000353
JES effective NP modelling 2	0/0	9.8e-05/9.8e-05	6.7e-05/6.7e-05	6.99e-05/6.99e-05	0/0	7.15e-05/7.15e-05
JES effective NP modelling 3	0/0	3.22e-05/3.22e-05	4.32e-06/4.32e-06	1.87e-05/1.87e-05	0/0	2.88e-05/2.88e-05
JES effective NP modelling 4	0/0	5.6e-06/5.6e-06	3.81e-07/3.81e-07	2.99e-06/2.99e-06	0/0	4.8e-06/4.8e-06
JES pile-up offset μ	0.000516/-0.000516	0.000291/-0.000291	0.000249/-0.000249	0.000121/-0.00012	0/0	0.00017/-0.00017
JES pile-up offse NPV	0.000517/-0.000516	0.000341/-0.000341	0.00264/-0.00264	5.22e-05/-5.23e-05	0/0	0.000219/-0.000218
JES pile-up p_T term	0/0	4.53e-05/-4.53e-05	9.4e-05/-9.4e-05	1.67e-05/-1.68e-05	0/0	1.84e-05/-1.85e-05
JES pile-up ρ topology	0.000587/-0.000587	0.000368/-0.000369	0.00282/-0.00282	0.000186/-0.000186	0.002/-0.002	0.000425/-0.000425
b-JES response	0/0	3.08e-05/-3.08e-05	7.18e-05/-7.38e-05	8.51e-05/-8.51e-05	0/0	0/0
JES flavour composition (CR $Z + \gamma$)	0.000887/0.000887	0.000417/0.000417	0.00281/0.00281	0.000396/0.000396	0.0023/0.0023	0.000646/0.000646
JES flavour response (CR $Z + \gamma$)	0.00011/0.00011	0.00038/0.00038	0.00307/0.00307	0.000238/0.000228	0/0	0.000221/0.000221
JES effective NP detector 1	0/0	3.23e-05/3.23e-05	1.9e-05/1.9e-05	3.05e-05/3.05e-05	0/0	2.39e-05/2.39e-05
JES effective NP detector 2	0/0	1.66e-06/1.66e-06	4.37e-05/4.37e-05	2.76e-06/2.76e-06	0/0	2.91e-06/2.91e-06
JES single particle high- p_T	0/0	0/0	0/0	0/0	0/0	0/0
JES punch through	0/0	1.05e-07/1.05e-07	0/0	1.23e-07/1.23e-07	0/0	2.35e-07/2.35e-07
JER data vs. MC	-0.000151/0.000151	0.000235/-0.000235	0.000465/-0.000465	-1.93e-05/1.94e-05	-0.00328/0.00328	0.000172/-0.000172
JER effective NP 1	-0.00015/0.00015	-0.000151/0.000151	-0.000172/0.000172	-0.000256/0.000256	-0.00316/0.00316	-0.000367/0.000367
JER effective NP 2	-0.00119/0.00119	-0.00119/-0.00119	-0.00121/-0.00121	-0.000301/0.000301	-0.000303/0.000303	-0.000283/0.000283
JER effective NP 3	-0.00148/0.00148	0.000108/-0.000109	0.000892/-0.000892	-0.000354/0.000354	-0.000313/0.000313	-0.000313/0.000313
JER effective NP 4	-0.000932/0.000932	-0.000149/0.000149	-0.000873/0.000873	-0.000112/0.000112	-0.000355/0.000355	-0.000313/0.000313
JER effective NP 5	-0.00155/0.00155	8.7e-05/-8.72e-05	-0.000139/-0.000139	-2.19e-05/-2.19e-05	0.000393/-0.000393	-0.000166/0.000167
JER effective NP 6	0.00108/-0.00108	0.000182/-0.000183	-0.000218/0.000218	6.04e-05/-6.04e-05	0/0	-0.000209/0.000209
JER effective NP 7 (rest term)	0.00159/-0.00159	-0.000228/0.000228	-0.000091/0.000091	-0.000152/0.000152	-0.00318/0.00318	-0.000279/0.000279
p_T^γ reweighting ($Z + \gamma + \text{jets}$)	0/0	0/0	1.01/-0.483	0/0	0/0	0/0
p_T^γ reweighting ($Z + \gamma + \text{jets}$)	0/0	0/0	0/0	-2.7e-08/-6.6e-08	0/0	0/0
p_T^γ reweighting ($W + \text{jets}$)	0/0	0/0	0/0	0.0947/-0.0954	0/0	0/0
normalisation: $W + \gamma + \text{jets}$, HF	0/0	0/0	0/0	4.65e-08/8.78e-08	0/0	0/0
μ_R, μ_F ($W + \gamma + \text{jets}$)	0/0	0/0	0/0	0.335/-0.311	0/0	0/0
μ_R, μ_F ($t\bar{t} + \gamma$)	0/0	0/0	0/0	1.19e-07/4.65e-08	0/0	0/0
$\sigma_{\text{theory}}(t\bar{t} + \gamma)$	0/0	0/0	0/0	0/0	0.00451/-0.00451	0/0
γ CR $Z + \gamma$ bin 0	0.258/0.258	0.347/0.347	0.738/0.738	0.714/0.714	0.358/0.358	0.515/0.515
γ CR $Z + \gamma$ bin 1	0.159/0.159	0.272/0.272	0.158/0.158	0.149/0.149	0.35/0.35	0.214/0.214
γ CR $Z + \gamma$ bin 2	0.328/0.328	0.446/0.446	0.0293/0.0293	0.0605/0.0605	0.031/0.031	0.101/0.101
γ CR $Z + \gamma$ bin 3	0.0737/0.0737	0.0829/0.0829	0.0161/0.0161	0.0289/0.0289	0.0635/0.0635	0.114/0.114
γ CR $Z + \gamma$ bin 4	0.181/0.181	0.152/0.152	0.0578/0.0578	0.0477/0.0477	0/0	0/0
SF($Z + \gamma + \text{jets}$)	0/0	0/0	0/0	0.103/-0.103	0/0	0/0
SF($W + \gamma + \text{jets}$)	0/0	0/0	0/0	0.0752/-0.0752	0/0	0/0

Table 62: Relative effect of each systematic uncertainty (post-fit) on the yields in the SR for $\text{N} \neq \text{T}$ right-handed $t\bar{t}$ sampling distributions in regions (1).

	Signal ($t\bar{t}$, RH)	$e \rightarrow \gamma$ fake	$j \rightarrow \gamma$ fake	$Z\gamma\gamma$ jets	$W\gamma\gamma$ jets	other prompt
Luminosity	0.0196/-0.0196	0.0196/-0.0196	0.0196/-0.0196	0.0/-0.0	0.0/-0.0	0.0196/-0.0196
Pile-up	0.0251/-0.0251	0.014/-0.014	0.0607/-0.0606	0.037/-0.037	0.0119/-0.0119	0.0226/-0.0225
JVT	0.000502/0.000502	0.000498/0.000498	0.00172/0.00172	0.000652/0.000652	0.000862/0.000862	0.00215/0.00215
$Sf(e \rightarrow \gamma)$	0.0/-0.0	-0.0281/0.029	-0.106/-0.12	0.0/-0.0	0.0/-0.0	0.0/-0.0
Shower generator ($t\bar{t}$)	0.0/-0.0	-0.0533/0.0535	0.0441/-0.0438	0.0/-0.0	0.0/-0.0	0.0/-0.0
ME generator (single top)	0.0/-0.0	-0.00683/0.00683	-0.00468/-0.00468	0.0/-0.0	0.0/-0.0	-0.0802/0.0803
TW DS scheme	0.0/-0.0	-0.00282/0.00282	-0.00195/0.00195	0.0/-0.0	0.0/-0.0	0.155/-0.154
$Sf(\text{photon ID})$	0.00589/-0.00589	0.00516/-0.00516	-0.149/0.148	0.0/-0.0	0.0/-0.0	-0.142/-0.141
$Sf(\text{photon iso})$	0.011/-0.011	0.0116/-0.0116	0.0121/-0.0121	0.013/-0.013	0.0116/-0.0116	0.0114/-0.0114
$Sf(\text{electron trigger})$	0.00107/0.00107	0.00158/0.00158	0.00149/-0.0149	0.0152/-0.0151	0.0143/-0.0143	0.0141/-0.0141
$Sf(\text{electron reco.})$	0.000607/0.000607	0.000635/0.000635	0.000126/0.00126	0.000825/0.000825	0.00107/0.00107	0.00111/0.00111
$Sf(\text{electron ID})$	0.00393/-0.00393	0.00527/-0.00527	0.00484/-0.00484	0.00256/-0.00256	0.00344/-0.00344	0.000543/0.000543
$Sf(\text{electron iso.})$	0.000678/0.000678	0.000647/0.000647	0.000491/0.000491	0.000348/0.000348	0.00044/-0.00044	0.000475/0.000475
$Sf(\text{muon trigger stat.})$	0.000843/0.000843	0.00052/0.00052	0.00134/0.00134	0.00124/-0.00124	0.000844/-0.000844	0.000857/0.000857
$Sf(\text{muon trigger syst.})$	0.000331/0.000331	0.00199/0.00199	0.00357/0.00357	0.00373/0.00373	0.00301/0.00301	0.00327/0.00327
$Sf(\text{muon ID stat.})$	0.000265/0.000265	0.000163/0.000163	0.00027/0.00027	0.000331/0.000331	0.000269/0.000269	0.000266/0.000266
$Sf(\text{muon ID syst.})$	0.000153/0.000153	0.00026/0.00026	0.000172/0.000172	0.000175/0.000175	0.000147/0.000147	0.00146/0.00146
$Sf(\text{muon iso. stat.})$	0.000147/0.000147	8.8e-05/-8.8e-05	0.000127/0.000127	0.000153/0.000153	0.000142/0.000142	0.00039/-0.0039
$Sf(\text{muon iso. syst.})$	0.0014/-0.0014	0.000707/0.000707	0.000108/0.000108	0.00021/0.00021	0.000115/0.000115	0.000475/0.000475
$Sf(\text{muon TTVA stat.})$	0.000111/0.000111	6.67e-05/6.67e-05	0.00013/0.00013	0.000108/0.000108	0.000109/0.000109	0.000109/0.000109
$Sf(\text{muon TTVA syst.})$	4.64e-05/4.64e-05	2.71e-05/2.71e-05	5.4e-05/5.4e-05	4.55e-05/4.55e-05	5.31e-05/5.31e-05	4.85e-05/4.85e-05
EGamma resolution all	0.00389/-0.00389	0.00992/-0.00992	0.0141/-0.0141	0.01/-0.01	0.00623/-0.00623	0.00311/-0.00311
EGamma scale all	0.00153/0.00153	0.0122/-0.0122	0.0183/-0.0183	0.0177/-0.0177	0.00653/0.00653	0.00628/-0.00628
Muon ID	0.000147/0.000147	0.000748/-0.000749	0.00452/-0.00452	0.00671/-0.00671	0.000524/-0.00524	0.00104/-0.00104
$Sf(\text{muon iso.})$	0.00073/-0.00073	0.000973/-0.000973	0.00231/-0.00231	0.00682/-0.00682	0.00444/-0.00444	0.000989/-0.000989
$Sf(\text{muon TTVVA})$	0.000111/0.000111	0.000111/0.000111	0.00106/-0.00106	0.00762/-0.00762	0.00042/-0.00042	0.00042/-0.00042
$Sf(\text{muon TTVVA syst.})$	4.64e-05/4.64e-05	2.71e-05/2.71e-05	5.4e-05/5.4e-05	4.55e-05/4.55e-05	5.31e-05/5.31e-05	4.85e-05/4.85e-05
Muon scale	0.000818/0.000818	0.000439/0.000439	0.00147/0.00147	0.00378/0.00378	0.00227/0.00227	0.000509/0.000509
ISR ($t\bar{t}$)	0.0/-0.0	0.0128/-0.0128	0.0328/-0.0327	0.0/-0.0	0.0/-0.0	0.0/-0.0
FSR ($t\bar{t}$)	0.0/-0.0	0.00199/0.00199	0.0406/-0.0405	0.0/-0.0	0.0/-0.0	0.00141/0.00141
ISR (single top)	0.0/-0.0	0.0024/-0.0024	0.00276/0.00276	0.00276/0.00276	0.00276/0.00276	0.00276/0.00276
FSR (single top)	0.00245/-0.00245	0.00108/-0.00108	0.00105/-0.00105	0.000204/-0.000204	0.000778/-0.000778	0.00405/-0.00405
PDF no. 1	0.00226/-0.00226	0.00138/-0.00138	0.00293/-0.00293	0.00531/-0.00531	0.0012/-0.0012	0.00266/-0.00266
PDF no. 2	0.003581/-0.003581	0.00149/-0.00149	0.00127/-0.00127	0.00795/-0.00795	0.00382/-0.00382	0.00362/-0.00362
PDF no. 3	0.00654/-0.00654	0.00321/-0.00321	0.00326/-0.00326	0.00392/-0.00392	0.00623/-0.00623	0.00331/-0.00331
PDF no. 4	0.006819/-0.006819	0.0011/-0.0011	0.00055/-0.00055	0.000377/-0.000377	0.000592/-0.000591	0.00117/-0.00117
PDF no. 5	0.00262/-0.00262	0.00137/-0.00137	0.00161/-0.00161	0.00135/-0.00135	0.000869/-0.000869	0.00287/-0.00287
PDF no. 6	0.00365/-0.00365	0.00209/-0.00209	0.00195/-0.00195	0.00671/-0.00671	0.00658/-0.00658	0.00602/-0.00602
PDF no. 7	0.003751/-0.003751	0.000761/-0.000761	0.000673/-0.000674	0.00169/-0.00169	0.00046/-0.00046	0.00376/-0.00376
PDF no. 8	0.00851/-0.00851	0.003067/-0.003066	0.00395/-0.00395	0.000688/-0.000688	0.00473/-0.00473	0.0013/-0.0013
PDF no. 9	0.0049/-0.0049	0.00182/-0.00182	0.00194/-0.00195	0.00234/-0.00234	0.00343/-0.00343	0.00495/-0.00495
PDF no. 10	0.00126/-0.00126	0.000723/-0.000723	0.000966/-0.000966	0.00176/-0.00176	0.01/-0.01	0.00117/-0.00117
PDF no. 11	0.005711/-0.005711	0.003151/-0.003151	0.00207/-0.00207	0.00697/-0.00697	0.00257/-0.00257	0.0086/-0.0086
PDF no. 12	0.00346/-0.00346	0.00213/-0.00213	0.00125/-0.00125	0.00375/-0.00375	0.000741/-0.000741	0.0052/-0.0052
PDF no. 13	0.000527/-0.000527	0.00158/-0.00158	0.00124/-0.00124	0.00051/-0.00051	0.000236/-0.000235	0.00286/-0.00286
PDF no. 14	0.00123/-0.00123	0.000863/-0.000863	0.00104/-0.00104	9.57e-05/9.58e-05	0.000575/-0.000575	0.00376/-0.00376
PDF no. 15	0.003067/-0.003066	0.00445/-0.00446	0.00506/-0.00505	0.000683/-0.000683	0.00446/-0.00446	0.00446/-0.00446
PDF no. 16	0.00111/-0.00111	0.00127/-0.00127	0.000643/-0.000643	0.000208/-0.000207	0.000907/-0.000907	0.00273/-0.00273
PDF no. 17	0.005711/-0.005711	0.00171/-0.00171	0.00124/-0.00124	0.00113/-0.00113	0.00257/-0.00257	0.0086/-0.0086
PDF no. 18	0.003451/-0.003454	0.000831/-0.000831	0.00018/-0.00018	0.000969/-0.000969	0.000223/-0.000223	0.00287/-0.00287
PDF no. 19	0.000527/-0.000527	0.00158/-0.00158	0.00138/-0.00138	0.00051/-0.00051	0.000236/-0.000235	0.00286/-0.00286
PDF no. 20	0.00272/-0.00272	0.00146/-0.00146	0.000825/-0.000825	0.00189/-0.00189	0.000205/-0.000205	0.00382/-0.00382
PDF no. 21	0.002531/-0.002531	0.000431/-0.000431	0.0016/-0.0016	0.00214/-0.00214	0.00346/-0.00346	0.00385/-0.00385
PDF no. 22	0.001131/-0.001131	0.001431/-0.001431	0.000999/-0.000999	0.00264/-0.00264	0.000233/-0.000233	0.00353/-0.00353
PDF no. 23	0.00226/-0.00226	0.001711/-0.001711	0.00124/-0.00124	0.00113/-0.00113	0.000628/-0.000628	0.00436/-0.00436
PDF no. 24	0.00338/-0.00338	0.00159/-0.00159	0.00105/-0.00105	0.00289/-0.00289	0.000199/-0.000199	0.00337/-0.00337
PDF no. 25	0.00105/-0.00105	0.00182/-0.00182	0.00138/-0.00138	0.00487/-0.00487	0.000369/-0.000369	0.00286/-0.00286
PDF no. 26	0.00424/-0.00424	0.001631/-0.001631	0.00104/-0.00104	0.00434/-0.00434	0.00049/-0.00049	0.00448/-0.00448
PDF no. 27	0.003951/-0.003959	0.001731/-0.001731	0.000944/-0.000944	0.00142/-0.00142	0.00123/-0.00123	0.00468/-0.00468
PDF no. 28	0.00381/-0.00381	0.004631/-0.004631	0.00263/-0.00263	0.00136/-0.00136	0.00148/-0.00148	0.00337/-0.00337
PDF no. 29	0.003031/-0.003033	0.000761/-0.000761	0.00113/-0.00113	0.00106/-0.00105	0.000225/-0.000225	0.00047/-0.00047
PDF no. 30	0.000751/-0.000755	0.001771/-0.00177	0.000738/-0.000738	0.00295/-0.00295	0.000394/-0.000394	0.00988/-0.00988
μ_R , μ_F (single top)	0.0/-0.0	0.00321/-0.00322	0.0135/-0.0135	0.0/-0.0	0.0/-0.0	0.00761/-0.00761
μ_R , μ_F (W+jets)	0.0/-0.0	0.00122/-0.00122	0.0158/-0.0158	0.0/-0.0	0.0/-0.0	0.0/-0.0
μ_R , μ_F (Z +jets)	0.0/-0.0	0.00189/-0.00187	0.0277/-0.0273	0.0/-0.0	0.0/-0.0	0.00175/-0.00175
μ_R , μ_F (diboson)	0.0/-0.0	0.006671/-0.006671	0.00233/-0.00233	0.0/-0.0	0.0/-0.0	0.000512/-0.000512
σ^{theory} ($t\bar{t}$)	0.0/-0.0	0.0299/-0.0298	0.0329/-0.0328	0.0/-0.0	0.0/-0.0	0.0/-0.0
σ^{theory} (single top)	0.0/-0.0	0.00544/-0.00544	0.0129/-0.0129	0.0/-0.0	0.0/-0.0	0.0118/-0.0118
σ^{theory} (W+jets)	0.0/-0.0	4.47e-05/-4.48e-05	0.00315/-0.00315	0.0/-0.0	0.0/-0.0	0.0/-0.0
σ^{theory} (Z +jets)	0.0/-0.0	0.00181/-0.00181	0.00166/-0.00166	0.0/-0.0	0.0/-0.0	0.000175/-0.000175
E_T^{miss} soft-term reso. para.	0.00293/-0.00293	-0.0171/-0.0171	-0.00617/-0.00617	-0.0345/-0.0344	-0.00468/-0.00468	-0.00209/-0.00208
E_T^{miss} soft-term reso. perp.	-0.00438/-0.00439	-0.0307/-0.0308	-0.0129/-0.0129	-0.0296/-0.0297	-0.00105/-0.00105	-0.00168/-0.00168
E_T^{miss} soft-term scale	0.03222/-0.03222	0.00366/-0.00366	0.00995/-0.00995	0.00615/-0.00615	0.00264/-0.00264	0.00065/-0.00065

Table 63: Relative effect of each systematic uncertainty (post-fit) on the yields in the SR for the right-handed $t\bar{t}\gamma$ -coupling using data in all regions (II).

	Signal ($t\bar{t}\gamma$, RH)	$e \rightarrow \gamma$ fake	$j \rightarrow \gamma$ fake	$\text{SF}(j \rightarrow \gamma)$, $W\gamma\gamma\text{jets}$ other prompt
Heavy flavour fraction ($W\gamma\gamma\text{jets}$)	0/0	-0.00105 / 0.00105	0.0347 / -0.0348	0/0
Heavy flavour fraction ($Z\gamma\gamma\text{jets}$)	0/0	0.0102 / -0.0102	-0.0768 / 0.0765	0/0
Heavy flavour fraction (diboson)	0/0	-0.000138 / -0.000138	0.000456 / 0.000456	0/0
SF(b -tag eigenvar. B1)	0.00954 / -0.00954	0.0129 / -0.0129	0.0147 / -0.0147	0.0174 / -0.0174
SF(b -tag eigenvar. B2)	0.00272 / 0.00272	0.00149 / 0.00149	0.00156 / 0.00156	0.00129 / 0.00129
SF(b -tag eigenvar. B3)	0.0103 / -0.0103	0.0116 / -0.0116	0.00827 / 0.00826	0.00419 / -0.00419
SF(b -tag eigenvar. B4)	0.00192 / 0.00192	0.00101 / 0.00101	0.00101 / 0.00101	0.00228 / 0.00228
SF(b -tag eigenvar. B5)	0.00082 / 0.00082	0.000816 / 0.000816	0.00106 / 0.00106	0.000259 / 0.000259
SF(b -tag eigenvar. B6)	0.00028 / 0.00028	8.04e-05 / 8.04e-05	0.000201 / 0.000208	6.88e-05 / 6.88e-05
SF(b -tag eigenvar. B7)	1.62e-05 / 1.62e-05	1.32e-05 / 1.32e-05	4.97e-05 / 4.97e-05	2.3e-05 / 2.3e-05
SF(b -tag eigenvar. B8)	3.44e-06 / 3.44e-06	9.89e-06 / 9.89e-06	6.4e-06 / 6.4e-06	1.33e-06 / 1.33e-06
SF(b -tag eigenvar. B9)	8.79e-07 / 8.79e-07	8.52e-07 / 8.52e-07	1.04e-06 / 1.04e-06	2.1e-06 / 2.1e-06
SF(b -tag eigenvar. C1)	0.000126 / -0.000126	0.00522 / 0.00522	0.0221 / -0.0221	0.0176 / -0.0176
SF(b -tag eigenvar. C2)	8.11e-05 / -8.11e-05	0.00196 / -0.00196	0.00994 / -0.00994	0.00628 / -0.00628
SF(b -tag eigenvar. C3)	2.62e-05 / 2.62e-05	0.00062 / 0.00062	0.00887 / 0.00887	0.0196 / 0.0196
SF(b -tag eigenvar. light 1)	0.000435 / -0.000435	0.0244 / -0.0244	0.0217 / -0.0217	0.0502 / -0.0503
SF(b -tag eigenvar. light 2)	7.16e-05 / 7.16e-05	0.00264 / 0.00264	0.00293 / 0.00293	0.0364 / 0.0364
SF(b -tag eigenvar. light 3)	8.06e-06 / 8.06e-06	0.000409 / 0.000409	0.000686 / 0.000686	0.00147 / 0.00147
SF(b -tag extrapolation)	3.02e-05 / 3.02e-05	1.96e-05 / 1.96e-05	1.41e-05 / 1.41e-05	3.32e-06 / 3.32e-06
SF(b -tag extrap. from charm)	0/0	1.59e-05 / 1.59e-05	0.00107 / 0.00107	0/0
JES η interc. modelling	0.007 / -0.007	2.86e-07 / -2.27e-07	0.0267 / -0.0267	0.0197 / -0.0197
JES η interc. non-closure high- E_T	0/0	-9.95e-09 / 0	6.63e-05 / -6.63e-05	0.0108 / -0.0108
JES η interc. non-closure $\eta < 0$	0.000509 / 0.000509	0.00111 / 0.00111	0.00393 / 0.00393	0/0
JES η interc. non-closure $\eta > 0$	0.000151 / 0.000151	0.00414 / 0.00414	0.00432 / 0.00432	6.68e-05 / 6.68e-05
JES η interc. total stat.	0.0234 / -0.0234	0.00389 / -0.00389	0.00772 / -0.00771	0.00635 / -0.00634
JES effective NP stat. 1	0/0	0.00164 / 0.00164	0.00977 / 0.00977	0.0018 / 0.0018
JES effective NP stat. 2	0.0017 / 0.0017	0.00275 / 0.00275	0.00553 / 0.00553	0.00721 / 0.00721
JES effective NP stat. 3	0.000789 / 0.000789	0.00076 / 0.00076	0.000708 / 0.000708	0.00047 / 0.00047
JES effective NP stat. 4	0.00112 / 0.00112	0.000662 / 0.000662	0.0026 / 0.0026	0.000886 / 0.000886
JES effective NP stat. 5	0.000901 / 0.000901	0.000663 / 0.000663	0.00375 / 0.00375	0.000427 / 0.000427
JES effective NP stat. 6	0.000956 / 0.000956	0.000834 / 0.000834	0.00129 / 0.00129	0.00492 / 0.00492
JES effective NP stat. 1	0.000162 / 0.000162	0.00164 / 0.00164	0.00361 / 0.00361	0.00168 / 0.00168
JES effective NP stat. 2	0.00017 / 0.00017	0.00275 / 0.00275	0.00305 / 0.00305	0.00299 / 0.00299
JES effective NP stat. 3	0.000297 / 0.000297	0.000976 / 0.000976	0.0035 / 0.0035	0.00351 / 0.00351
JES effective NP stat. 4	0.000949 / 0.000949	0.000712 / 0.000712	0.00435 / 0.00435	0.00037 / 0.00037
JES effective NP modelling 1	0.0157 / -0.0157	0.0154 / -0.0154	0.0147 / -0.0147	0.0166 / -0.0166
JES effective NP modelling 2	0.002117 / 0.002117	0.00331 / 0.00331	0.00492 / 0.00492	0.00154 / 0.00154
JES effective NP modelling 3	0.00128 / 0.00128	0.00156 / 0.00156	0.00173 / 0.00173	0.00635 / 0.00634
JES effective NP modelling 4	0.000726 / 0.000726	0.00353 / 0.00353	0.00028 / 0.00028	0.000371 / 0.000371
JES pile-up offset μ	0.00539 / -0.00539	0.00904 / -0.00904	0.00903 / -0.00903	0.0114 / -0.0114
JES pile-up offset NPV	0.0102 / -0.0102	0.0145 / -0.0145	0.0244 / -0.0244	0.0145 / -0.0145
JES pile-up NP term	0.00221 / -0.00221	0.00476 / -0.00476	0.00699 / -0.00699	0.0107 / -0.0107
JES pile-up ρ topology	0.002117 / 0.002117	0.00331 / 0.00331	0.00492 / 0.00492	0.00252 / 0.00252
JES effective NP modelling 1	0.00062 / 0.00062	0.000353 / 0.000353	0.000318 / 0.000318	0.00329 / 0.00329
JES effective NP modelling 2	0.000192 / 0.000192	0.000169 / 0.000169	0.000977 / 0.000977	0.0018 / 0.0018
JES effective NP modelling 3	0.000141 / 0.000141	0.00094 / 0.00094	0.00297 / 0.00297	0.00361 / 0.00361
JES effective NP modelling 4	0.000297 / 0.000297	0.000949 / 0.000949	0.00435 / 0.00435	0.000371 / 0.000371
JES effective NP modelling 1	0.000949 / 0.000949	0.000712 / 0.000712	0.00435 / 0.00435	0.000785 / 0.000785
JES effective NP modelling 2	0.000221 / -0.00221	0.00417 / -0.00417	0.00899 / -0.00899	0.00282 / -0.00282
JES effective NP modelling 3	0.000153 / -0.00153	0.0147 / -0.0147	0.0242 / -0.0242	0.00312 / -0.0312
JES effective NP modelling 4	0.000362 / -0.00362	0.00838 / -0.00838	0.0113 / -0.0113	0.013 / -0.013
JES flavour composition (SR)	0.000537 / 0.000537	0.0181 / -0.0181	0.0967 / -0.0967	0.02 / -0.02
JES effective NP detector 1	0.00132 / -0.00132	0.0146 / -0.0146	0.0327 / -0.0327	0.0215 / -0.0215
JES effective NP detector 2	0.000157 / 0.000157	0.00226 / 0.00226	0.00549 / 0.00549	0.00273 / 0.00273
JES single particle high- p_T	0.000364 / 0.000364	3.17e-07 / 3.17e-07	0.000937 / 0.000937	0.000152 / 0.000152
JES pile-through	0/0	1.73e-05 / 1.73e-05	-1.42e-09 / -1.42e-09	6.77e-05 / 6.77e-05
JER data vs. MC	-0.00013 / 0.00014	0.000442 / 0.000442	-1.42e-09 / -1.42e-09	0.00154 / 0.00154
JER effective NP 1	-0.000557 / 0.000557	0.0164 / -0.0164	0.0199 / -0.0199	0.0255 / -0.0255
JER effective NP 2	-0.00491 / 0.00491	0.0153 / -0.0153	0.0177 / -0.0177	0.0215 / -0.0215
JER effective NP 3	-0.00472 / 0.00472	0.00726 / -0.00726	0.00775 / -0.00775	0.0165 / -0.0166
JER effective NP 4	-0.00126 / 0.00126	0.000442 / 0.000442	0.00092 / -0.00092	0.00559 / -0.00559
JER effective NP 5	0.00363 / -0.00363	-0.00325 / 0.00325	0.0164 / -0.0164	-0.0136 / 0.0136
JER effective NP 6	0.0025 / -0.0025	-0.00358 / 0.00358	-0.0117 / -0.0117	-0.0132 / 0.0132
JER effective NP 7 (rest term)	0.000539 / -0.000539	-0.00202 / 0.00202	0.00608 / -0.00608	-0.000321 / 0.000321
SF($j \rightarrow \gamma$)	0/0	0/0	0.904 / -0.474	0/0
p_T^γ reweighting ($Z\gamma\gamma\text{jets}$)	0/0	0/0	0/0	2.01e-05 / -2.01e-05
μ_R , μ_F ($t\bar{t}\gamma\gamma$)	0/0	0/0	0/0	0/0
$\sigma_{t\bar{t}}^{\text{theory}}$ ($t\bar{t}\gamma\gamma$)	0/0	0/0	0/0	0/0
Heavy flavour fraction ($Z\gamma\gamma\text{jets}$)	0.0011 / -0.0011	0.0121 / -0.0121	0.0122 / -0.0122	0.0155 / -0.0155
γ SR bin 0	0.00158 / -0.00158	0.00116 / -0.00116	0.00158 / -0.00158	0.00194 / -0.00194
γ SR bin 1	0.00118 / -0.00118	0.00138 / -0.00138	0.00087 / -0.00087	0.000321 / -0.000321
γ SR bin 2	0.00125 / -0.00125	0.000966 / -0.000966	0.00188 / -0.00188	0.000666 / -0.000666
γ SR bin 3	0.00163 / -0.00163	0.00123 / -0.00123	0.00188 / -0.00188	0.000371 / -0.000371
γ SR bin 4	0.00224 / -0.00224	0.00116 / -0.00116	0.00098 / -0.00098	0.000397 / -0.000397
γ SR bin 5	0.00116 / -0.00116	0.00076 / -0.00076	0.000656 / -0.000656	0.00018 / -0.00018
γ SR bin 6	0.00298 / -0.00298	0.00076 / -0.00076	0.000491 / -0.000491	7.78e-05 / -7.78e-05
γ SR bin 7	0.0105 / -0.0105	0.00385 / -0.00385	0/0	0.104 / -0.104
SF($Z\gamma\gamma\text{jets}$)	0/0	0/0	0/0	0.0774 / -0.0774
SF($W\gamma\gamma\text{jets}$)	0/0	0/0	0/0	0/0

Table 64: Relative effect of each systematic uncertainty (post-fit) on the yields in the CR $W+\gamma+jets$ coupling using data in all regions (I).

	Signal ($t\bar{t}\nu$, RH)	$e \rightarrow \gamma + jets$	$j \rightarrow \gamma + jets$	$Z \rightarrow \gamma + jets$	$W \rightarrow \gamma + jets$	other prompt γ
Luminosity	0.0196/-0.0196	0.0196/-0.0196	0.0196/-0.0196	0.0196/-0.0196	0/0	0/0
Pile-up	0.0156/-0.0189	0.0156/-0.0189	0.0156/-0.0189	0.0156/-0.0189	0.0243/-0.0243	0.0196/-0.0196
JVT	0.00829/-0.000829	0.00715/-0.000715	0.00964/-0.00964	0.000294/-0.000294	0.000956/-0.000956	0.00184/-0.00184
SF($e \rightarrow \gamma$)	0/0	0.0911/-0.0836	0/0	0/0	0/0	0/0
Shower generator ($t\bar{t}$)	0/0	0.0111/-0.0111	-0.00789/-0.00795	0/0	0/0	0/0
ME generator ($t\bar{t}f$)	0/0	0.00194/-0.00194	0.00251/-0.00251	0/0	0/0	0/0
Shower generator (single top)	0/0	-0.00309/-0.00309	-0.000905/-0.000905	0/0	0/0	-0.0725/-0.0727
ME generator (single top)	0/0	0.000818/-0.000818	-0.000479/-0.000479	0/0	0/0	0.178/-0.177
tW DS scheme	0/0	-0.000377/-0.000377	-0.00613/-0.00613	0/0	0/0	-0.125/-0.124
SF(photon ID)	0.00607/-0.00607	0.0113/-0.0113	0.014/-0.014	0.0125/-0.0125	0.0117/-0.0117	0.0113/-0.0113
SF(photon iso.)	0.0108/-0.0108	0.0152/-0.0152	0.0151/-0.0151	0.0145/-0.0145	0.0141/-0.0141	0.0139/-0.0139
SF(electron trigger)	0.00108/-0.00108	0.00204/-0.00204	0.00119/-0.00119	0.00139/-0.00139	0.00124/-0.00124	0.00121/-0.00121
SF(electron reco.)	0.000643/-0.000643	0.000912/-0.000912	0.000459/-0.000459	0.000576/-0.000576	0.000558/-0.000558	0.000584/-0.000584
SF(electron ID)	0.00408/-0.00408	0.00633/-0.00633	0.00412/-0.00412	0.00444/-0.00444	0.00412/-0.00412	0.00412/-0.00412
SF(electron iso.)	0.000739/-0.000739	0.000861/-0.000861	0.00043/-0.00043	0.000492/-0.000492	0.000483/-0.000483	0.000518/-0.000518
SF(muon trigger stat.)	0.000825/-0.000825	0.000304/-0.000304	0.0007/-0.0007	0.000787/-0.000787	0.000851/-0.000851	0.000854/-0.000854
SF(muon trigger syst.)	0.000308/-0.000308	0.00115/-0.00115	0.000246/-0.000246	0.000252/-0.000252	0.000268/-0.000268	0.000257/-0.000257
SF(muon ID stat.)	0.000261/-0.000261	9.64e-05/-9.64e-05	0.000261/-0.000261	0.000261/-0.000261	0.000261/-0.000261	0.000261/-0.000261
SF(muon ID syst.)	0.00151/-0.00151	0.000553/-0.000553	0.00139/-0.00139	0.00141/-0.00141	0.00148/-0.00148	0.00147/-0.00147
SF(muon iso. stat.)	0.000145/-0.000145	5.43e-05/-5.43e-05	0.000148/-0.000148	0.000146/-0.000146	0.000146/-0.000146	0.000146/-0.000146
SF(muon iso. syst.)	0.000112/-0.000112	0.000412/-0.000412	0.000119/-0.000119	0.000115/-0.000115	0.000117/-0.000117	0.000114/-0.000114
SF(muon TTVA stat.)	0.000106/-0.000106	3.93e-05/-3.93e-05	0.000111/-0.000111	0.000104/-0.000104	0.000109/-0.000109	0.000107/-0.000107
SF(muon TTVA syst.)	4.36e-05/-4.36e-05	1.66e-05/-1.66e-05	5.60e-05/-5.60e-05	5.21e-05/-5.21e-05	4.6e-05/-4.6e-05	4.6e-05/-4.6e-05
EGamma resolution all	0.00512/-0.00513	0.0272/-0.0272	0.024/-0.024	0.0297/-0.0297	0.00173/-0.00173	0.00156/-0.00156
EGamma scale all	0.00991/-0.00992	0.0237/-0.0237	0.0237/-0.0237	0.00747/-0.00747	0.00798/-0.00799	0.00816/-0.00816
Muon ID	0.00193/-0.00193	0.000614/-0.000614	0.0153/-0.0153	0.0145/-0.0145	0.00015/-0.00015	0.000189/-0.000189
Muon MS	0.00207/-0.00207	0.000476/-0.000476	0.00961/-0.00961	0.00239/-0.00239	0.000459/-0.000459	0.000101/-0.000101
Muon sagitta resbias	0.00294/-0.00294	0.000427/-0.000427	0.00414/-0.00414	0.000933/-0.000933	0.000607/-0.000607	0.000686/-0.000686
Muon scale	0.00954/-0.00954	0.00578/-0.00578	0.00819/-0.00819	0.00205/-0.00205	0.000992/-0.000992	0.000992/-0.000992
ISR ($t\bar{t}$)	0/0	0.000397/-0.000397	0.00467/-0.00467	0.000459/-0.000459	0.000889/-0.000889	0.000524/-0.000524
FSR ($t\bar{t}$)	0/0	0.00827/-0.00827	0.00156/-0.00156	0/0	0/0	0/0
ISR (single top)	0/0	0.00976/-0.00976	0.00246/-0.00246	0/0	0/0	0/0
FSR (single top)	0/0	0.00904/-0.00904	0.000306/-0.000306	0/0	0/0	0.000719/-0.000719
PDF no. 1	0/0	0.00553/-0.00553	0.00151/-0.00151	0/0	0/0	0.0112/-0.0112
PDF no. 2	0.00382/-0.00382	0.000581/-0.000581	0.00411/-0.00411	0.00122/-0.00122	0.00297/-0.00297	0.004384/-0.004384
PDF no. 3	0.00145/-0.00145	0.00337/-0.00337	0.018/-0.018	0.00119/-0.00119	0.008899/-0.008899	0.000523/-0.000523
PDF no. 4	0.0058/-0.0058	0.00447/-0.00447	0.0425/-0.0425	0.00611/-0.00611	0.00228/-0.00228	0.00286/-0.00286
PDF no. 5	0.00512/-0.00512	0.00367/-0.00367	0.0194/-0.0194	0.0108/-0.0108	0.000746/-0.000746	0.000448/-0.000448
PDF no. 6	0.00425/-0.00425	0.00121/-0.00121	0.0658/-0.0658	0.000157/-0.000157	0.00463/-0.00463	0.00519/-0.00519
PDF no. 7	0.00583/-0.00583	0.000888/-0.000888	0.0258/-0.0258	0.00019/-0.00019	0.00232/-0.00232	0.00616/-0.00616
PDF no. 8	0.00303/-0.00303	0.000364/-0.000364	0.0424/-0.0424	0.000491/-0.000491	0.00189/-0.00189	0.00442/-0.00442
PDF no. 9	0.00826/-0.00826	0.0013/-0.0013	0.0662/-0.0662	0.00301/-0.00301	0.00381/-0.00381	0.00173/-0.00173
PDF no. 10	0.00601/-0.00601	0.0023/-0.0023	0.0242/-0.0242	0.00242/-0.00242	0.00576/-0.00576	0.00064/-0.00064
PDF no. 11	0.00695/-0.00695	0.00111/-0.00111	0.0903/-0.0902	0.00192/-0.00192	0.00459/-0.00459	0.00024/-0.00024
PDF no. 12	0.00571/-0.00571	0.00316/-0.00316	0.101/-0.101	8.94e-05/-8.93e-05	0.00801/-0.00801	0.00704/-0.00704
PDF no. 13	0.00516/-0.00516	0.00246/-0.00246	0.0574/-0.0574	0.00186/-0.00186	0.00622/-0.00622	0.00408/-0.00408
PDF no. 14	0.00288/-0.00288	0.00129/-0.00129	0.0833/-0.0833	0.00104/-0.00104	0.00598/-0.00597	0.00408/-0.00408
PDF no. 15	0.00474/-0.00474	0.00123/-0.00123	0.0653/-0.0653	0.000494/-0.000494	0.00458/-0.00458	0.00558/-0.00558
PDF no. 16	0.00224/-0.00224	0.00077/-0.00077	0.0551/-0.0551	0.00475/-0.00475	0.00358/-0.00358	0.0038/-0.0038
PDF no. 17	0.00863/-0.00863	0.00287/-0.00287	0.0719/-0.0719	0.00192/-0.00192	0.00808/-0.00808	0.0024/-0.0024
PDF no. 18	0.0057/-0.0057	0.00173/-0.00173	0.0816/-0.0816	0.000122/-0.000122	0.00538/-0.00538	0.00704/-0.00704
PDF no. 19	0.00882/-0.00882	0.00079/-0.00079	0.0643/-0.0643	0.00122/-0.00122	0.00419/-0.00419	0.00622/-0.00622
PDF no. 20	0.00412/-0.00412	0.00187/-0.00187	0.0793/-0.0793	0.000422/-0.000422	0.00477/-0.00477	0.00501/-0.00501
PDF no. 21	0.00398/-0.00398	0.00044/-0.00044	0.0623/-0.0623	0.00124/-0.00124	0.00358/-0.00358	0.00447/-0.00447
PDF no. 22	0.00271/-0.00271	0.00064/-0.00064	0.0942/-0.0942	0.000903/-0.000903	0.00749/-0.00749	0.0107/-0.0107
PDF no. 23	0.00449/-0.00449	0.00111/-0.00111	0.0771/-0.0771	0.000544/-0.000544	0.00374/-0.00374	0.00555/-0.00555
PDF no. 24	0.00559/-0.00559	0.00151/-0.00151	0.0648/-0.0648	0.000332/-0.000332	0.00449/-0.00449	0.00635/-0.00635
PDF no. 25	0.00279/-0.00279	0.00125/-0.00125	0.074/-0.074	0.000862/-0.000862	0.00489/-0.00489	0.00412/-0.00412
PDF no. 26	0.005/-0.005	0.00106/-0.00106	0.0653/-0.0653	0.00134/-0.00134	0.00542/-0.00542	0.00569/-0.00569
PDF no. 27	0.00479/-0.00479	0.0002/-0.0002	0.0791/-0.0791	0.000278/-0.000278	0.00483/-0.00483	0.00576/-0.00576
PDF no. 28	0.00664/-0.00664	0.00118/-0.00118	0.0712/-0.0712	0.00179/-0.00179	0.00442/-0.00442	0.00542/-0.00542
PDF no. 29	0.00468/-0.00468	0.00135/-0.00135	0.0652/-0.0652	0.000498/-0.000498	0.00342/-0.00342	0.00992/-0.00992
PDF no. 30	0.0105/-0.0105	0.00132/-0.00132	0.06023/-0.06023	0/0	0/0	0.0067/-0.0067
$\mu_R \cdot \mu_F$ (singl top)	0/0	0.000781/-0.000781	0.0224/-0.0223	0/0	0/0	0/0
$\mu_R \cdot \mu_F$ ($Z + jets$)	0/0	0.1331/-0.123	0.0372/-0.0363	0/0	0/0	0/0
$\mu_R \cdot \mu_F$ (diboson)	0/0	0.0508/-0.0508	0.0192/-0.0192	0/0	0/0	0/0
$\sigma_{theory}(t\bar{t})$	0/0	0.0121/-0.012	0.00194/-0.00194	0/0	0/0	0/0
$\sigma_{theory}(W + jets)$	0/0	0.00228/-0.00228	0.000664/-0.000664	0/0	0/0	0.0118/-0.0118
$\sigma_{theory}(W + jets)$	0/0	7.57e-05/-7.57e-05	0.0422/-0.0422	0/0	0/0	0/0
$\sigma_{theory}(Z + jets)$	0/0	0.0327/-0.0327	0.00466/-0.00466	0/0	0/0	0/0
$\sigma_{theory}(diboson)$	0/0	0.00448/-0.00448	0.000528/-0.000528	0/0	0/0	0.00598/-0.00598

Table 65: Relative effect of each systematic uncertainty (post-fit) on the yields in the CR $W+\gamma+jets$ coupling using data in all regions (II). Not reviewed, for internal circulation only

Signal ($t\bar{t}\nu$, RH)	$e \rightarrow \gamma$ fake	$j \rightarrow \gamma$ fake	$Z+\gamma+jets$	$W+\gamma+jets$	other prompt γ
E_{miss}^T soft-term reso. para.	-0.000524 / 0.000539	-0.0358 / 0.0358	0.00795 / -0.00795	-0.0425 / 0.0424	-0.00517 / 0.00517
E_{miss}^T soft-term reso. perp.	-0.000802 / 0.000802	-0.0317 / 0.0317	-0.0112 / 0.0113	-0.0313 / 0.0313	-0.00275 / 0.00275
E_{miss}^T soft-term scale	0.00361 / -0.00361	0.0363 / -0.0363	0.00822 / -0.00822	0.0386 / -0.0387	0.00697 / -0.00697
SF(b -tag eigenvar. B1)	0.000226 / 0.000226	0.000467 / 0.000467	0.00749 / -0.00749	0.000535 / -0.000535	0.000132 / -0.000132
SF(b -tag eigenvar. B2)	0.000683 / -0.00683	0.00332 / -0.00332	0.00554 / -0.00534	0.000176 / -0.000176	1.61e-06 / 1.61e-05
SF(b -tag eigenvar. B3)	0.00132 / 0.00132	0.00143 / 0.00143	0.56e-05 / 5.56e-05	5.26e-05 / 5.26e-05	6.9e-05 / -6.89e-05
SF(b -tag eigenvar. B4)	0.000517 / 0.000517	0.000339 / 0.000339	3.31e-05 / 3.31e-05	1.59e-05 / 1.59e-05	0.000176 / 0.000176
SF(b -tag eigenvar. B5)	0.000194 / 0.00194	4.47e-05 / 4.47e-05	7.89e-06 / 7.89e-06	8.81e-06 / 8.81e-06	1.05e-06 / 1.05e-06
SF(b -tag eigenvar. B6)	1.36e-05 / 1.36e-05	1.15e-05 / 1.15e-05	1.67e-06 / 1.67e-06	2.57e-06 / 2.57e-06	7.31e-07 / 7.31e-07
SF(b -tag eigenvar. B7)	4.17e-06 / 4.17e-06	6.67e-07 / 6.67e-07	6.78e-07 / 6.78e-07	6.93e-07 / 6.93e-07	1.08e-07 / 1.08e-07
SF(b -tag eigenvar. B8)	4.55e-07 / 4.55e-07	3.42e-07 / 3.42e-07	1.47e-07 / 1.47e-07	9.15e-08 / 9.15e-08	4.89e-09 / -4.89e-09
SF(b -tag eigenvar. B9)	9.56e-05 / -4.93e-05	0.000245 / -0.000241	8.98e-05 / -9e-05	0.000161 / -0.000161	0.000163 / -0.000163
SF(b -tag eigenvar. C1)	4.5e-05 / -4.5e-05	0.000149 / -0.000149	4.96e-05 / 4.96e-05	1.87e-05 / 1.87e-05	0.000336 / -0.000336
SF(b -tag eigenvar. C2)	9.68e-06 / 9.68e-06	2.89e-05 / -0.000423	0.000442 / -0.000492	0.000449 / -0.000489	0.000102 / 0.000102
SF(b -tag eigenvar. C3)	2.00e-06 / -0.000346	7.53e-06 / 7.53e-06	9.02e-06 / 9.02e-06	1.65e-06 / 1.65e-06	0.000264 / -0.000264
SF(b -tag eigenvar. light 1)	2.18e-05 / 2.18e-05	4.71e-05 / 4.71e-05	9.02e-06 / 9.02e-06	2.02e-06 / 2.02e-06	1.07e-05 / 1.07e-05
SF(b -tag eigenvar. light 2)	9.26e-06 / 9.26e-06	7.01e-06 / 7.01e-06	6.41e-06 / 6.41e-06	5.14e-06 / 5.14e-06	4.85e-06 / 4.85e-06
SF(b -tag eigenvar. light 3)	4.71e-06 / 4.71e-06	4.34e-06 / 4.34e-06	5.59e-06 / 5.59e-06	2.72e-06 / 2.72e-06	2.8e-06 / 2.8e-06
SF(b -tag eigenvar. light 4)	0.000162 / 0.00162	6.11e-06 / 6.11e-06	2.96e-06 / 2.96e-06	4.32e-05 / 4.32e-05	4.71e-05 / 4.71e-05
SF(b -tag extrapolation)	3.15e-07 / 3.15e-07	2.14e-06 / 2.14e-06	0.0199 / -0.0199	5.97e-05 / 5.97e-05	7.53e-05 / 7.53e-05
SF(b -tag extrap. from charm)	0.00822 / -0.00822	0.0207 / -0.0207	0.000429 / -0.000429	0.000449 / -0.000489	0.000261 / 0.000261
JES D interc. modelling	0 / 0	1.28e-05 / -1.26e-05	0 / 0	6.77e-06 / -6.85e-06	0 / 0
JES n interc. non-closure $\eta < 0$	0.000778 / 0.000778	0.000626 / 0.000626	0.00175 / 0.00175	0.000665 / 0.000665	0.000111 / 0.000111
JES D interc. non-closure $\eta > 0$	0.000383 / -0.000383	0.000932 / -0.000931	0.000832 / -0.000832	0.000238 / -0.000238	0.000927 / 0.000927
JES effective NP stat. 1	0.001553 / 0.00153	0.00339 / 0.00339	0.00156 / 0.00156	0.00085 / 0.00085	0.000354 / 0.000354
JES effective NP stat. 2	0.00244 / 0.00244	0.00897 / 0.00897	0.00249 / 0.00249	0.00235 / 0.00235	0.000591 / 0.000591
JES effective NP stat. 3	0.000526 / 0.000526	0.000932 / 0.000932	0.00192 / 0.00192	0.000708 / 0.000708	0.000175 / 0.000175
JES effective NP stat. 4	0.000954 / 0.000954	0.00303 / 0.00303	0.00258 / 0.00258	0.000411 / 0.000411	0.000304 / 0.000304
JES effective NP stat. 5	0.000645 / 0.000645	0.00832 / 0.00832	0.00221 / 0.00221	0.000259 / 0.000259	0.000407 / 0.000407
JES effective NP stat. 6	0.000556 / 0.000556	0.00149 / 0.00149	0.0023 / 0.0023	0.000791 / 0.000791	0.000197 / 0.000197
JES effective NP mixed 1	0.00146 / 0.00146	0.00299 / 0.00299	0.00201 / 0.00201	0.00123 / 0.00123	0.000705 / 0.000705
JES effective NP mixed 2	0.00188 / 0.00188	0.00491 / 0.00491	0.00467 / 0.00467	0.00122 / 0.00122	0.000159 / 0.000159
JES effective NP mixed 3	0.000372 / 0.000372	0.00124 / 0.00124	0.00209 / 0.00209	0.000359 / 0.000359	0.000159 / 0.000159
JES effective NP modelling 1	0.0154 / -0.0154	0.0233 / -0.0233	0.0367 / -0.0368	0.0157 / -0.0157	0.003557 / -0.003557
JES effective NP modelling 2	0.000222 / 0.000222	0.00832 / 0.00832	0.00201 / 0.00201	0.000787 / 0.000787	0.000248 / 0.000248
JES effective NP modelling 3	0.000556 / 0.000556	0.00141 / 0.00141	0.00156 / 0.00156	0.000368 / 0.000368	0.000491 / 0.000491
JES effective NP modelling 4	0.000348 / 0.000348	0.0044 / -0.00493	0.00212 / 0.00212	0.000277 / 0.000277	0.000155 / 0.000155
JES pile-up offset μ	0.00385 / -0.00385	0.0266 / -0.0266	0.0192 / -0.0192	0.000122 / 0.000122	0.000277 / -0.00277
JES pile-up offset NPV	0.00746 / 0.00746	0.0162 / 0.0162	0.0365 / -0.0365	0.00919 / -0.00919	0.00192 / 0.00192
JES pile-up PT term	0.00295 / -0.00295	0.00919 / -0.00919	0.0123 / -0.0123	0.00253 / -0.00253	0.0231 / -0.0231
JES pile-up ρ topology	0.0148 / -0.0148	0.028 / -0.028	0.036 / -0.036	0.0114 / -0.0114	0.00248 / 0.00248
b -JES response	0.00691 / 0.00691	0.0041 / 0.0041	0.00156 / 0.00156	0.000102 / -0.000102	0.0122 / -0.0122
JES flavour composition (CR $W+\gamma+jet$)	0.0219 / -0.0219	0.044 / -0.0493	0.0462 / -0.0461	0.031 / -0.031	0.00653 / -0.00653
JES flavour response (CR $W+\gamma+jet$)	0.00962 / -0.00962	0.0385 / -0.0385	0.026 / -0.026	0.0194 / -0.0194	0.0116 / -0.0116
JES effective NP detector 1	0.00119 / 0.00119	0.00412 / 0.00412	0.00353 / 0.00353	0.00133 / 0.00133	0.000468 / 0.000468
JES effective NP detector 2	0.00026 / 0.00026	2.86e-05 / 2.86e-05	0.00192 / 0.00192	0.000321 / 0.000321	0.000104 / 0.000104
JES single particle high- p_T	0 / 0	6.63e-05 / 6.63e-05	2.41e-07 / 2.41e-07	1.03e-05 / 1.03e-05	1.87e-05 / 1.87e-05
JES punch through	0 / 0	0.00175 / -0.00175	0.0275 / -0.0274	0.0135 / -0.0135	0.00324 / -0.00324
JER data vs. MC	0.00533 / -0.00532	0.0391 / -0.0391	0.0155 / -0.0155	0.00445 / -0.00445	0.00045 / 0.00045
JER effective NP 1	0.0637 / -0.0637	0.0158 / -0.0158	0.0482 / -0.0484	0.0244 / -0.0245	0.00898 / -0.00898
JER effective NP 2	0.00861 / 0.00862	0.0213 / -0.0213	0.0529 / -0.0533	0.0161 / -0.0161	0.00542 / -0.00542
JER effective NP 3	0.00725 / -0.00725	0.00734 / -0.00734	0.0121 / -0.0121	0.00107 / -0.00107	0.00453 / -0.00453
JER effective NP 4	0.00196 / -0.00196	0.00874 / -0.00874	-0.00616 / 0.00616	-0.00304 / 0.00304	0.00374 / -0.00374
JER effective NP 5	0.00496 / -0.00497	0.00824 / -0.00824	0.00342 / -0.00342	-0.00536 / 0.00536	0.00318 / -0.00318
JER effective NP 6	0.00321 / -0.00321	8.48e-05 / -8.49e-05	0.0272 / -0.0273	0.00992 / -0.00992	0.00465 / -0.00465
JER effective NP 7 (rest term)	0.00662 / -0.00662	0.0153 / -0.0153	0.904 / -0.474	0 / 0	0 / 0
SF($j \rightarrow \gamma$)	0 / 0	0 / 0	0 / 0	4.52e-08 / 3.71e-08	0 / 0
P_T^γ reweighting ($Z+\gamma+jets$)	0 / 0	0 / 0	0 / 0	0.079 / -0.0789	0 / 0
μ_R , μ_F ($Z+\gamma+jets$)	0 / 0	0 / 0	0 / 0	-1.08e-07 / -5.38e-08	0 / 0
normalisation: $W+\gamma+jets$, HF	0 / 0	0 / 0	0 / 0	0 / 0	0 / 0
σ theory ($t\bar{t} + \gamma$)	0 / 0	0 / 0	0 / 0	0 / 0	0.0042 / 0.0042
y CR $W+\gamma+jet$ bin 0	0.256 / 0.256	0.752 / 0.752	0.819 / 0.819	0.858 / 0.858	0.839 / 0.839
y CR $W+\gamma+jet$ bin 1	0.0573 / 0.0573	0.099 / 0.099	0.07 / 0.07	0.0618 / 0.0618	0.0727 / 0.0727
y CR $W+\gamma+jet$ bin 2	0.0317 / 0.0317	0.0316 / 0.0316	0.0298 / 0.0298	0.0191 / 0.0191	0.0224 / 0.0224
y CR $W+\gamma+jet$ bin 3	0.0408 / 0.0408	0.0244 / 0.0244	0.0157 / 0.0157	0.0143 / 0.0143	0.0156 / 0.0156
y CR $W+\gamma+jet$ bin 4	0.0577 / 0.0577	0.0255 / 0.0255	0.0176 / 0.0176	0.0103 / 0.0103	0.0136 / 0.0136
y CR $W+\gamma+jet$ bin 5	0.0908 / 0.0908	0.0227 / 0.0227	0.016 / 0.016	0.0118 / 0.0118	0.0124 / 0.0124
y CR $W+\gamma+jet$ bin 6	0.433 / 0.433	0.0242 / 0.0242	0.025 / 0.025	0.0127 / 0.0127	0.0152 / 0.0152
y CR $W+\gamma+jet$ bin 7	0 / 0	0 / 0	0 / 0	0.104 / -0.104	0 / 0
SF($Z+\gamma+jets$)	0 / 0	0 / 0	0 / 0	0.0774 / -0.0774	0 / 0
SF($W+\gamma+jets$)	0 / 0	0 / 0	0 / 0	0 / 0	0 / 0

Not reviewed, for internal circulation only

Table 66: Relative effect of each systematic uncertainty (post-fit) on the yields in the CR $Z + \gamma$ for the right-handed tuy coupling using data in all regions (I).

	Signal (tuy , RH)	$e \rightarrow \gamma$ take	$j \rightarrow \gamma$ take	$Z \gamma + \text{jets}$	$W \gamma + \text{jets}$	other prompt γ
Luminosity	0.0196/-0.0196	0.0196/-0.0196	0.0196/-0.0196	0.0351/-0.0351	0.156/-0.156	0.0196/-0.0196
Pile-up	0.111/-0.111	0.0265/-0.0265	0.000954/0.000954	0.000841/0.000841	0.000585/0.000585	0.0262/-0.0262
JVT	0.00783/-0.00783	0.000954/0.000954	0.000911/-0.00836	0.000608/-0.00612	0.000173/-0.00173	0.0037/-0.0037
$SF(e \rightarrow \gamma)$	0/0	-0.00164/-0.00164	-0.00535/-0.00535	0/0	0/0	0/0
Shower generator ($t\bar{t}$)	0/0	0.00552/-0.00551	0.000283/-0.000283	0/0	0/0	0/0
ME generator (single top)	0/0	-0.00346/-0.00346	0.00133/-0.00133	0/0	0/0	-0.0334/-0.0334
ME generator (single top)	0/0	0.00184/-0.00184	0.00143/-0.00143	0/0	0/0	0.0524/-0.0523
tW DS scheme	0/0	-0.00256/-0.00256	0.00152/-0.00152	0/0	0/0	-0.00821/-0.00821
SF(photon ID)	0.00773/-0.00773	0.0119/-0.0119	0.0152/-0.0152	0.0128/-0.0128	0.0116/-0.0116	0.0109/-0.0109
SF(photon iso.)	0.0121/-0.0121	0.0153/-0.0153	0.0153/-0.0152	0.0147/-0.0147	0.0138/-0.0138	0.0138/-0.0138
SF(electron trigger syst.)	0.006327/0.000523	0.000234/0.000242	0.000242/0.000242	0.000234/0.000234	0.000234/0.000234	0.000152/-0.000152
SF(electron reco.)	0.00201/0.00201	0.0013/0.0013	0.000872/0.000872	0.000936/0.000936	0.001451/0.00145	0.00103/0.00103
SF(electron ID)	0.0262/-0.0262	0.00983/-0.00983	0.00749/-0.00749	0.00749/-0.00749	0.0151/-0.0151	0.00736/-0.00736
SF(electron iso.)	0.00514/0.00514	0.0012/0.0012	0.000836/0.000836	0.00077/-0.00077	0.00205/-0.00205	0.000904/0.000904
SF(muon trigger stat.)	2.53e-05/2.53e-05	0.000396/0.000396	0.000444/0.000444	0.000528/0.000528	0.000447/0.000447	0.000519/0.000519
SF(muon trigger syst.)	0.000201/0.000201	0.000871/0.000871	0.00101/0.00101	0.0026/0.0026	0.00119/-0.00119	0.000119/-0.00119
SF(muon ID stat.)	0.000137/0.000137	0.000453/0.000453	0.000653/0.000653	0.000663/0.000663	0.000358/0.000358	0.000626/0.000626
SF(muon ID syst.)	0.000813/0.000813	0.0027/0.0027	0.00471/0.00471	0.00372/0.00372	0.00182/0.00182	0.00371/0.00371
SF(muon iso. stat.)	9.0e-05/1.907e-05	0.00236/0.00236	0.000297/0.000297	0.000336/0.000336	0.000205/0.000205	0.00033/-0.00033
SF(muon iso. syst.)	0.000637/0.000637	0.00187/0.00187	0.00254/0.00254	0.00273/0.00273	0.00162/0.00162	0.00254/-0.00254
SF(muon TIVV stat.)	6.55e-05/6.55e-05	0.000178/0.000178	0.000229/0.000229	0.000261/0.000261	0.000128/0.000128	0.000251/0.000251
SF(muon TIVV syst.)	1.15e-05/1.15e-05	7.59e-05/7.59e-05	0.000101/0.000101	0.000273/0.000273	0.000126/0.000126	0.000105/0.000105
E γ Gamma resolution all	0.0943/-0.0945	0.00433/-0.00433	0.0235/-0.0235	0.00177/-0.00177	0.0687/-0.0688	0.00185/-0.00185
E γ Gamma scale all	0.164/-0.164	0.00798/-0.00798	0.0274/-0.0275	0.00944/-0.00944	0.0683/-0.0683	0.0044/-0.0044
Muon ID	-2.23e-08/-2.23e-08	0.000819/-0.000819	0.00457/-0.00457	0.000693/-0.000693	0.0561/-0.0561	0.000456/-0.000456
Muon MS	-2.23e-08/-2.23e-08	0.000766/-0.000766	0.000921/-0.000921	0.000746/-0.000746	0.0561/-0.0561	0.000627/-0.000627
Muon sagitta biasas	-2.23e-08/-2.23e-08	0.000521/0.000521	0.000465/0.000465	0.000146/-0.000146	0/0	0.000293/0.000293
Muon scale σ	0/0	0.00119/-0.00119	0.00121/-0.00121	0.000144/-0.000144	0.000199/-0.000199	0.000489/-0.000489
ISR ($t\bar{t}$)	0/0	0.00743/-0.00743	0.00512/-0.00512	0.0011/0.0011	0/0	0.00063/-0.00063
FSR ($t\bar{t}$)	0/0	0.00681/0.00681	0.0034/-0.0034	0/0	0/0	0/0
ISR (single top)	0/0	0.00053/-0.00053	0.000115/0.000115	0/0	0/0	0.00323/-0.00323
FSR (single top)	0/0	0.00491/-0.00491	0.00167/-0.00167	0/0	0/0	0.00632/-0.00632
PDF no. 1	0.0322/-0.0322	0.00329/-0.00329	0.00164/-0.00164	0.00123/-0.00123	0.00192/-0.00192	0.00432/-0.00432
PDF no. 2	0.0658/-0.0657	0.0294/-0.0294	0.00155/-0.00155	0.00172/-0.00172	0.0127/-0.0127	0.00415/-0.00415
PDF no. 3	0.0347/-0.0347	0.00208/-0.00208	0.00072/-0.00072	0.00634/-0.00634	0.024/-0.024	0.00345/-0.00345
PDF no. 4	0.012/-0.012	0.0144/-0.0144	0.00474/-0.00474	0.00136/-0.00136	0.0342/-0.0342	0.00379/-0.00379
PDF no. 5	0.146/-0.14	0.0118/-0.0118	0.000866/-0.000866	0.000802/-0.000802	0.00112/-0.00112	0.00339/-0.00339
PDF no. 6	0.0525/-0.0525	0.00797/-0.00797	0.000389/-0.000389	0.000252/-0.000253	0.00155/-0.00155	0.00469/-0.00469
PDF no. 7	0.0567/-0.0567	0.00411/-0.00411	0.00064/-0.00064	0.00283/-0.00283	0.00752/-0.00752	0.000432/-0.000432
PDF no. 8	0.0354/-0.0354	0.00339/-0.00339	0.000541/-0.000541	0.000705/-0.000705	0.00427/-0.00427	0.00518/-0.00518
PDF no. 9	0.0645/-0.0645	0.00651/-0.00651	0.00476/-0.00476	0.00275/-0.00275	0.0126/-0.0126	0.000582/-0.000582
PDF no. 10	0.103/-0.103	0.0116/-0.0116	0.00184/-0.00184	0.00184/-0.00184	0.00558/-0.00558	0.00598/-0.00598
PDF no. 11	0.0536/-0.0536	0.0183/-0.0183	0.000966/-0.000966	0.000256/-0.000256	0.0162/-0.0162	0.00115/-0.00115
PDF no. 12	0.0855/-0.0854	0.0184/-0.0184	0.00523/-0.00523	0.000244/-0.000244	0.0036/-0.0036	0.00645/-0.00645
PDF no. 13	0.0691/-0.0691	0.0697/-0.0697	0.00232/-0.00232	0.00167/-0.00167	0.00346/-0.00346	0.00588/-0.00588
PDF no. 14	0.0854/-0.0854	0.0106/-0.0106	0.00306/-0.00306	0.00167/-0.00167	0.00141/-0.00141	0.00312/-0.00312
PDF no. 15	0.0545/-0.0545	0.0647/-0.0647	0.000654/-0.000654	0.00103/-0.00103	0.00459/-0.00459	0.00489/-0.00489
PDF no. 16	0.023/-0.023	0.0259/-0.0259	0.000549/-0.000549	0.000536/-0.000536	0.00165/-0.00165	0.00242/-0.00242
PDF no. 17	0.0737/-0.0737	0.01/-0.01	0.00325/-0.00325	0.00034/-0.00034	0.00162/-0.00162	0.00106/-0.00106
PDF no. 18	0.0851/-0.0851	0.00447/-0.00447	3.39e-05/-3.38e-05	0.000548/-0.000548	0.00398/-0.00398	0.00036/-0.00036
PDF no. 19	0.0905/-0.0905	0.0365/-0.0365	0.000447/-0.000447	3.39e-05/-3.38e-05	0.00162/-0.00162	0.00645/-0.00645
PDF no. 20	0.0317/-0.0317	0.0849/-0.0849	0.000464/-0.000464	0.000751/-0.000751	0.00268/-0.00268	0.00198/-0.00198
PDF no. 21	0.0415/-0.0415	0.00535/-0.00535	0.00103/-0.00103	0.00166/-0.00166	0.00581/-0.00581	0.00431/-0.00431
PDF no. 22	0.0545/-0.0545	0.00976/-0.00976	0.000565/-0.000565	0.000303/-0.000303	0.00241/-0.00241	0.00391/-0.00391
PDF no. 23	0.0679/-0.0679	0.00843/-0.00843	0.000806/-0.000806	0.00039/-0.00039	0.00471/-0.00471	0.00403/-0.00403
PDF no. 24	0.0608/-0.0608	0.00869/-0.00869	0.000229/-0.000229	0.000504/-0.000504	0.00162/-0.00162	0.00694/-0.00694
PDF no. 25	0.0533/-0.0533	0.0106/-0.0106	0.000797/-0.000797	0.000376/-0.000376	0.00268/-0.00268	0.00367/-0.00367
PDF no. 26	0.0279/-0.0279	0.0141/-0.0141	0.00233/-0.00233	0.00141/-0.00141	0.00382/-0.00382	0.00449/-0.00449
PDF no. 27	0.0966/-0.0965	0.00976/-0.00976	0.000565/-0.000565	0.000303/-0.000303	0.00241/-0.00241	0.00534/-0.00534
PDF no. 28	0.0719/-0.0719	0.0282/-0.0282	0.0019/-0.0019	0.00126/-0.00126	0.00459/-0.00459	0.00078/-0.00078
PDF no. 29	0.0693/-0.0693	0.00701/-0.00701	0.000535/-0.000535	0.00197/-0.00197	0.00532/-0.00532	0.00501/-0.00501
PDF no. 30	0.0653/-0.0653	0.0105/-0.0105	0.00138/-0.00138	0.000634/-0.000634	0.00448/-0.00448	0.0128/-0.0128

Not reviewed, for internal circulation only

Table 67: Relative effect of each systematic uncertainty (post-fit) on the yields in the CR $Z + \gamma$ for the right-handed tuy coupling using data in all regions (II).

	Signal (tuy , RH)	$e \rightarrow \gamma$ fake	$j \rightarrow \gamma$ fake	$Z \gamma + \text{jets}$	$W \gamma + \text{jets}$	other prompt γ
μ_R, μ_F (single top)	0/0	0.000119/-0.000119	0.000102/-0.000102	0/0	0/0	0.00273/-0.00273
μ_R, μ_F (W+jets)	0/0	0/0	0/0	0/0	0/0	0/0
μ_R, μ_F ($Z+\text{jets}$)	0/0	0.0149/-0.0147	0.174/-0.157	0/0	0/0	0/0
μ_R, μ_F (diboson)	0/0	0.0473/-0.00473	0.019/-0.019	0/0	0/0	0.00449/-0.00445
$\sigma^{\text{theory}}(t\bar{t})$	0/0	0.00105/-0.00105	0.00202/-0.00202	0/0	0/0	0/0
σ^{theory} (single top)	0/0	0.000187/-0.000187	6.85e-05/-6.85e-05	0/0	0/0	0.00386/-0.00386
σ^{theory} (W+jets)	0/0	0/0	0/0	0/0	0/0	0/0
σ^{theory} ($Z+\text{jets}$)	0/0	0/0	0/0	0/0	0/0	0/0
σ^{theory} (diboson)	0/0	0.0571/-0.0572	0.000652/-0.000652	0/0	0/0	0.0069/-0.0069
JES η interc. modelling	0.000204/-0.000204	0.000227/-0.000227	0.000711/-0.000711	9.75e-05/-9.74e-05	0/0	0.000132/-0.000132
JES η interc. non-closure high- E	-2.23e-08/-2.23e-08	0/0	0/0	0/0	0/0	0/0
JES η interc. non-closure $\eta < 0$	-2.23e-08/-2.23e-08	3.71e-06/3.71e-06	1.13e-05/1.13e-05	8.76e-06/8.76e-06	0/0	8.02e-06/8.02e-06
JES η interc. total $\eta > 0$	-2.23e-08/-2.23e-08	9.92e-08/9.92e-08	2.5e-05/2.53e-05	9.14e-07/9.14e-07	0/0	5.46e-07/5.46e-07
JES η interc. total stat.	-2.23e-08/-2.23e-08	0.000146/-0.000146	2.99e-05/2.99e-05	2.02e-05/2.02e-05	0/0	5.14e-05/5.14e-05
JES effective NP stat. 1	-2.23e-08/-2.23e-08	3.17e-05/3.17e-05	3.46e-05/3.46e-05	4.04e-05/4.04e-05	0/0	2.32e-05/2.32e-05
JES effective NP stat. 2	-2.23e-08/-2.23e-08	0.000132/0.000132	7.12e-06/7.12e-06	7.16e-06/7.16e-06	0/0	7.07e-05/7.07e-05
JES effective NP stat. 3	-2.23e-08/-2.23e-08	9.32e-06/9.32e-06	8.28e-07/8.28e-07	6.92e-06/6.92e-06	0/0	8.92e-06/8.92e-06
JES effective NP stat. 4	-2.23e-08/-2.23e-08	1.05e-05/1.05e-05	6.06e-07/6.06e-07	7.89e-06/7.89e-06	0/0	1.05e-05/1.05e-05
JES effective NP stat. 5	-2.23e-08/-2.23e-08	1.34e-06/1.34e-06	1.16e-06/1.16e-06	0/0	0/0	6.32e-06/6.32e-06
JES effective NP stat. 6	-2.23e-08/-2.23e-08	1.37e-05/1.37e-05	2.16e-06/2.16e-06	1.11e-05/1.11e-05	0/0	1.04e-05/1.04e-05
JES effective NP mixed 1	-2.23e-08/-2.23e-08	3.81e-05/3.81e-05	6.13e-05/6.13e-05	2.18e-05/2.18e-05	0/0	2.65e-05/2.65e-05
JES effective NP mixed 2	-2.23e-08/-2.23e-08	1e-05/1e-05	4.93e-07/4.93e-07	1.03e-05/1.03e-05	0/0	7.56e-06/7.56e-06
JES effective NP mixed 3	-2.23e-08/-2.23e-08	0.000368/-0.000368	0.00287/-0.00287	0.00254/-0.00254	0/0	0.00373/-0.00373
JES effective NP modelling 1	0.000957/-0.000957	0.000368/-0.000368	0.00286/-0.00286	0.00189/-0.00189	0/0	7.15e-05/7.15e-05
JES effective NP modelling 2	-2.23e-08/-2.23e-08	9.8e-05/9.8e-05	6.7e-05/6.7e-05	7e-05/7e-05	0/0	2.89e-05/2.89e-05
JES effective NP modelling 3	-2.23e-08/-2.23e-08	3.22e-05/3.22e-05	4.33e-06/4.33e-06	1.87e-05/1.87e-05	0/0	4.79e-05/4.79e-05
JES effective NP modelling 4	-2.23e-08/-2.23e-08	5.61e-06/5.61e-06	3.2e-07/3.2e-07	2.99e-06/2.99e-06	0/0	0.0017/-0.00171
JES pile-up offset μ	-2.23e-08/-2.23e-08	0.000291/-0.000291	0.00025/-0.00025	0.00012/-0.00012	0/0	0.000219/-0.000219
JES pile-up offset NPV	-2.23e-08/-2.23e-08	0.000341/-0.000341	0.00264/-0.00264	5.23e-05/5.24e-05	0/0	1.84e-05/1.85e-05
JES pile-up p_T term	-2.23e-08/-2.23e-08	4.53e-05/-4.52e-05	9.4e-05/-9.41e-05	1.67e-05/1.68e-05	0/0	0.000431/-0.000431
JES pile-up ρ topology	0.000479/-0.000479	0.000374/-0.000374	4.57e-05/4.57e-05	2.76e-06/2.76e-06	0/0	8.52e-05/-8.52e-05
b -JES response	-2.23e-08/-2.23e-08	0/0	0/0	0/0	0/0	0/0
JES flavour composition (CR $Z + \gamma$)	0.00098/0.00098	0.000417/0.000417	7.38e-05/-7.38e-05	1.03e-05/1.03e-05	0/0	0.000646/0.000646
JES flavour response (CR $Z + \gamma$)	0.00098/0.00098	0.00038/0.00038	0.000307/0.000307	0.000228/0.000228	0/0	0.000222/0.000222
JES effective NP detector 1	-2.23e-08/-2.23e-08	3.23e-05/3.23e-05	3.05e-05/3.05e-05	1.9e-05/1.9e-05	0/0	2.39e-05/2.39e-05
JES effective NP detector 2	-2.23e-08/-2.23e-08	1.63e-06/1.63e-06	4.37e-05/4.37e-05	2.76e-06/2.76e-06	0/0	2.96e-06/2.96e-06
JES single particle high- p_T	-2.23e-08/-2.23e-08	0/0	0/0	0/0	0/0	0/0
JES punch through	0/0	9.92e-08/9.92e-08	0/0	1.23e-07/1.23e-07	0/0	2.31e-07/2.31e-07
JER data vs. MC	0.000764/-0.000764	0.000251/-0.000251	0.000496/-0.000496	-2.06e-05/2.06e-05	-0.0035/0.0035	0.00184/-0.00184
JER effective NP 1	-0.000878/0.000878	-0.000144/0.000144	-0.000163/0.000163	-0.000244/0.000244	-0.00301/0.00301	-0.00349/0.00349
JER effective NP 2	-0.00125/0.00125	-4.24e-05/4.24e-05	-0.00118/-0.00118	-0.00275/0.00275	-0.00294/0.00294	-0.00275/0.00275
JER effective NP 3	-0.000886/0.000886	0.000107/-0.000107	0.000874/-0.000874	-0.000347/0.000347	-0.00304/0.00304	-0.00307/0.00307
JER effective NP 4	3.74e-05/-3.73e-05	-0.00014/-0.00014	-0.000823/0.000824	-0.000105/0.000105	-0.00296/0.00296	-0.00335/0.00335
JER effective NP 5	-2.23e-08/-2.23e-08	8.39e-05/-8.39e-05	-0.000134/0.000134	-1.11e-05/1.11e-05	-0.000376/0.000376	-0.0016/0.0016
JER effective NP 6	-0.000397/0.000397	0.000177/-0.000177	-0.000211/0.000211	5.84e-05/5.85e-05	0/0	-0.000202/0.000202
JER effective NP 7 (rest term)	0.00169/-0.00169	-0.00021/0.00021	-0.000839/0.000838	-0.00014/-0.00014	-0.00293/0.00293	-0.000257/0.000257
$SF(j \rightarrow \gamma)$	0/0	0/0	0.902/-0.473	0/0	0/0	0/0
P_T^γ reweighting ($Z\gamma$ -jets)	0/0	0/0	0/0	-5.11e-08/-1.2e-07	0/0	0/0
μ_R, μ_F ($Z\gamma$ -jets)	0/0	0/0	0/0	0.0954/-0.0952	0/0	0/0
P_T^γ reweighting (W γ -jets)	0/0	0/0	0/0	0/0	-1.48e-08/2.47e-08	0/0
normalisation: W γ -jets, HF	0/0	0/0	0/0	0/0	0/0	0/0
μ_R, μ_F ($t\bar{t} \gamma$)	0/0	0/0	0/0	0/0	3.96e-08/3.96e-08	0/0
$\sigma^{\text{theory}}(t\bar{t} \gamma)$	0/0	0/0	0/0	0/0	0.00454/0.00454	0/0
y CR $Z\gamma$ bin 0	0.0922/0.0922	0.346/0.346	0.738/0.738	0.714/0.714	0.353/0.353	0.516/0.516
y CR $Z\gamma$ bin 1	0.252/0.252	0.272/0.272	0.158/0.158	0.149/0.149	0.348/0.348	0.214/0.214
y CR $Z\gamma$ bin 2	0.345/0.345	0.146/0.146	0.0293/0.0293	0.0605/0.0605	0.0942/0.0942	0.0559/0.0559
y CR $Z\gamma$ bin 3	0.133/0.133	0.0832/0.0832	0.0161/0.0161	0.0289/0.0289	0.0477/0.0477	0.14/0.14
y CR $Z\gamma$ bin 4	0.179/0.179	0.153/0.153	0.0578/0.0578	0.104/0.104	0/0	0.14/0.14
$SF(Z\gamma$ -jets)	0/0	0/0	0/0	0/0	0.0774/0.0774	0/0
$SF(W\gamma$ -jets)	0/0	0/0	0/0	0/0	0.0774/0.0774	0/0

Table 68: Relative effect of each systematic uncertainty (post-fit) on the yields in the SR for NB lepton flavour using data or MC simulations (I).

	Signal ($t\bar{t}$, LH)	$e \rightarrow \gamma$ fake	$j \rightarrow \gamma$ fake	Z+j+res	W+j+res	other prompt γ
Luminosity	0.0196/-0.0196	0.0196/-0.0196	0.0196/-0.0196	0.0/0	0/0	0.0196/-0.0196
Pile-up	0.0172/-0.0172	0.015/-0.015	0.049/-0.0489	0.031/-0.031	0.0228/-0.0228	0.0228/-0.0228
JVT	0.00187/0.00187	0.000449/0.000449	0.00179/0.00179	0.00117/0.00117	0.000912/0.000912	0.00215/0.00215
$SF(e \rightarrow \gamma)$	0/0	-0.0297/0.0302	-0.113/0.119	0/0	0/0	0/0
Shower generator ($t\bar{t}$)	0/0	-0.0352/0.0351	0.0324/-0.0325	0/0	0/0	0/0
ME generator (single top)	0/0	-0.00679/-0.00679	-0.0215/-0.0215	0/0	0/0	-0.0804/-0.0802
TW DS scheme	0/0	-0.0029/-0.0029	-0.0204/-0.0204	0/0	0/0	0.161/-0.162
ME generator (single top)	0/0	0.00519/-0.00519	-0.138/-0.136	0/0	0/0	-0.143/-0.141
$SF(\text{photon ID})$	0.00622/-0.00622	0.0171/-0.0117	-0.0121/-0.0121	0.0131/-0.0131	0.016/-0.0116	0.0115/-0.0115
$SF(\text{photon iso})$	0.0107/-0.0107	0.0154/-0.0154	0.0148/-0.0148	0.0152/-0.0152	0.0143/-0.0143	0.0142/-0.0142
$SF(\text{electron trigger})$	0.00102/0.00102	0.00158/0.00158	0.00116/0.00116	0.000825/0.000825	0.00107/0.00107	0.00111/0.00111
$SF(\text{electron rec.})$	0.000605/0.000596	0.000759/0.000759	0.000398/0.000398	0.000476/0.000476	0.000543/0.000543	
$SF(\text{electron ID})$	0.00379/-0.00379	0.00527/-0.00527	0.0454/-0.00454	0.00267/-0.0026	0.00344/-0.00344	0.0039/-0.0039
$SF(\text{electron iso.})$	0.000695/0.000695	0.000648/0.000648	0.000451/0.000451	0.000349/0.000349	0.00044/0.00044	0.000475/0.000475
$SF(\text{muon trigger stat.})$	0.000879/0.000879	0.000521/0.000521	0.00127/0.00127	0.00124/0.00124	0.000857/0.000857	
$SF(\text{muon trigger syst.})$	0.000324/0.000324	0.00198/0.00198	0.00357/0.00357	0.00375/0.00375	0.003/0.003	0.00327/0.00327
$SF(\text{muon ID stat.})$	0.000249/0.000249	0.000163/0.000163	0.000291/0.000291	0.000331/0.000331	0.000269/0.000269	0.000267/0.000267
$SF(\text{muon ID syst.})$	0.00146/0.00146	0.000926/0.000926	0.00185/0.00185	0.00172/0.00172	0.00153/0.00153	0.00146/0.00146
$SF(\text{muon iso. stat.})$	0.00014/0.00014	0.000144/0.000144	0.000144/0.000144	0.000175/0.000175	0.000147/0.000147	0.000142/0.000142
$SF(\text{muon iso. syst.})$	0.00012/0.00112	0.000708/0.000708	0.00117/0.00117	0.00153/0.00153	0.00121/0.00121	0.00115/0.00115
$SF(\text{muon trigger stat.})$	0.000109/0.000109	0.00013/0.000115	0.00013/0.000115	0.000108/0.000108	0.000109/0.000109	
$SF(\text{muon TTVA syst.})$	4.6e-05/-4.6e-05	2.71e-05/2.71e-05	4.9e-05/4.9e-05	4.48e-05/4.48e-05	5.28e-05/5.28e-05	4.87e-05/4.87e-05
$E\Gamma\text{gamma resolution all EGamma scale all}$	0.00761/-0.00761	0.00889/-0.00889	0.0148/-0.0148	0.00939/-0.00939	0.00928/-0.00927	0.00243/-0.00243
Muon ID	0.00309/-0.00309	0.00139/-0.00139	0.02/-0.02	0.00707/-0.00707	0.00892/-0.00892	0.00694/-0.00694
Muon MS	0.00205/-0.00205	0.000986/-0.000986	0.00782/-0.00782	0.00485/-0.00485	0.00322/-0.00322	0.00114/-0.00114
Muon sagitta residuals	0.00209/0.00209	0.00117/0.00117	0.00238/0.00238	0.00716/-0.00716	0.00403/-0.00403	0.00117/-0.00117
Muon sagitta p_T	0.00433/-0.00433	0.00139/-0.00139	0.0367/-0.0367	0.00762/-0.00762	0.00568/0.00568	0.000567/0.000567
Muon scale	0.000289/0.000289	0.000918/0.000918	0.00259/0.00259	0.00365/0.00365	0.0018/0.0018	0.000486/0.000486
ISR ($t\bar{t}$)	0/0	0.0124/-0.0124	0.0432/-0.0432	0/0	0/0	0/0
FSR ($t\bar{t}$)	0/0	0.00228/0.00228	0.00971/0.00971	0/0	0/0	0/0
ISR (single top)	0/0	0.00547/-0.00547	0.0343/-0.0343	0/0	0/0	0/0
FSR (single top)	0/0	0.00108/-0.00108	0.00651/-0.00651	0.00141/-0.00141	0.000977/-0.000978	0.00405/-0.00405
PDF no. 1	0.00985/-0.00985	0.00141/-0.0141	0.00166/-0.00166	0.00531/-0.00531	0.0024/-0.0024	0.00263/-0.00263
PDF no. 2	0.00477/-0.00477	0.00139/-0.0139	0.00784/-0.00784	0.00844/-0.00844	0.00377/-0.00377	
PDF no. 3	0.0121/-0.0121	0.00329/-0.00329	0.02026/-0.00206	0.00282/-0.00282	0.0036/-0.0036	
PDF no. 4	0.00333/-0.00333	0.00108/-0.0108	0.000774/-0.000774	0.000951/-0.000951	0.003227/-0.00327	
PDF no. 5	0.06871/-0.00871	0.00142/-0.00142	0.00145/-0.00145	0.000145/-0.00145	0.00424/-0.00424	
PDF no. 6	0.0101/-0.0101	0.00251/-0.00251	0.00113/-0.00113	0.00881/-0.00881	0.00691/-0.00691	0.00602/-0.00602
PDF no. 7	0.0106/-0.0106	0.000771/-0.000771	0.000934/-0.000934	0.00266/-0.00266	0.000738/-0.000738	0.00376/-0.00376
PDF no. 8	0.0107/-0.0107	0.000866/-0.000866	0.00134/-0.00134	0.001671/-0.001671	0.0061/-0.0061	0.00131/-0.00131
PDF no. 9	0.00473/-0.00473	0.000728/-0.000728	0.00126/-0.00126	0.00289/-0.00289	0.003/-0.003	0.00493/-0.00493
PDF no. 10	0.0117/-0.0117	0.00159/-0.00159	0.00562/-0.000562	0.00306/-0.00306	0.00931/-0.00931	0.00123/-0.00123
PDF no. 11	0.00233/-0.00233	0.000773/-0.000773	0.00816/-0.000816	0.002851/-0.002851	0.002851/-0.002851	0.00856/-0.00856
PDF no. 12	0.00825/-0.00825	0.00148/-0.00148	0.008041/-0.000941	0.000941/-0.000941	0.002367/-0.002367	0.00159/-0.00159
PDF no. 13	0.0117/-0.0117	0.0021/-0.0021	0.00128/-0.00128	0.00121/-0.00121	0.000232/-0.000232	0.002851/-0.002851
PDF no. 14	0.00823/-0.00823	0.00084/-0.00084	0.00101/-0.00101	0.00121/-0.00121	0.000232/-0.000232	0.002851/-0.002851
PDF no. 15	0.0115/-0.0115	0.000428/-0.000428	0.00134/-0.00134	0.00151/-0.00151	0.000206/-0.000206	0.00445/-0.00445
PDF no. 16	0.00728/-0.00728	0.00126/-0.00126	0.00668/-0.00068	0.0013/-0.0013	0.00072/-0.00072	0.00273/-0.00273
PDF no. 17	0.0173/-0.0173	0.00317/-0.00317	0.00164/-0.00164	0.00583/-0.00583	0.00209/-0.00209	0.00856/-0.00856
PDF no. 18	0.0133/-0.0133	0.00835/-0.00835	0.000941/-0.000941	0.000958/-0.000958	0.00213/-0.00213	0.0061/-0.0061
PDF no. 19	0.0015/-0.0015	0.00155/-0.00155	0.000908/-0.000908	0.000874/-0.000874	0.000316/-0.000316	0.00135/-0.00135
PDF no. 20	0.00997/-0.00997	0.00143/-0.00143	0.00082/-0.00082	0.000354/-0.000354	0.00227/-0.00227	0.00381/-0.00381
PDF no. 21	0.009551/-0.009551	0.000149/-0.000149	0.00107/-0.00107	0.00159/-0.00159	0.00066/-0.00066	0.00445/-0.00445
PDF no. 22	0.00785/-0.00785	0.00135/-0.00135	0.0008/-0.0008	0.00152/-0.00152	0.000555/-0.000555	0.00349/-0.00349
PDF no. 23	0.0121/-0.0121	0.00171/-0.00171	0.00135/-0.00135	0.000771/-0.000771	0.00619/-0.00619	0.00434/-0.00434
PDF no. 24	0.0129/-0.0129	0.00159/-0.00159	0.000653/-0.000653	0.00136/-0.00136	0.00585/-0.00585	
PDF no. 25	0.00847/-0.00847	0.00182/-0.00182	0.00129/-0.00129	0.00324/-0.00324	0.00127/-0.00127	0.00336/-0.00336
PDF no. 26	0.00953/-0.00953	0.00117/-0.00117	0.00155/-0.00155	0.00333/-0.00333	0.00128/-0.00128	0.00485/-0.00485
PDF no. 27	0.00109/-0.0109	0.00173/-0.00173	0.00117/-0.00117	0.000942/-0.000942	0.00123/-0.00123	0.00466/-0.00466
PDF no. 28	0.0139/-0.0139	0.00465/-0.00465	0.00252/-0.00252	0.00123/-0.00123	0.00176/-0.00176	0.00832/-0.00833
PDF no. 29	0.0111/-0.0111	0.00075/-0.00075	0.000981/-0.000981	0.000265/-0.000265	0.00216/-0.00216	0.00468/-0.00468
PDF no. 30	0.0203/-0.0203	0.00178/-0.00178	0.000855/-0.000855	0.00173/-0.00173	0.00399/-0.00399	0.00984/-0.00984
μ_R, μ_F (single top)	0/0	0.00366/-0.00366	0.0133/-0.0133	0/0	0/0	0.00855/-0.00855
μ_R, μ_F ($W+j\text{jets}$)	0/0	0.00116/-0.00117	0.113/-0.114	0/0	0/0	0/0
μ_R, μ_F ($Z+j\text{jets}$)	0/0	0.0812/-0.0796	0.0266/-0.0265	0/0	0/0	0/0
μ_R, μ_F (diboson)	0/0	0.000646/-0.000646	0.00117/-0.00117	0/0	0/0	0.000505/-0.000505
$\sigma^{\text{theory}}(t\bar{t})$	0/0	0.0299/-0.0298	0.0299/-0.0298	0/0	0/0	0/0
$\sigma_{\text{theory}}(\text{single top})$	0/0	0.00544/-0.00544	0.0119/-0.0119	0/0	0/0	0.0118/-0.0118
$\sigma_{\text{theory}}(W+j\text{jets})$	0/0	4.46e-05/-4.47e-05	0.0092/-0.0092	0/0	0/0	0/0
$\sigma_{\text{theory}}(Z+j\text{jets})$	0/0	0.000248/-0.000248	0.0208/-0.0208	0/0	0/0	0/0
$E_{\text{T}}^{\text{miss}}$ soft-term res. para.	-0.02266/-0.02266	-0.0167/-0.0169	7.56e-05/-7.57e-05	0/0	0/0	0.00017/-0.00017
$E_{\text{T}}^{\text{miss}}$ soft-term res. perp.	-0.00552/-0.00554	-0.03/0.0305	-0.00948/-0.00952	-0.029/0.0294	-0.00462/-0.00463	-0.000205/-0.000205
$E_{\text{T}}^{\text{miss}}$ soft-term scale	0.00659/-0.00658	0.0239/-0.0238	0.0127/-0.0126	0.0019/-0.0117	0.00093/-0.00092	-0.000169/-0.000169

Table 69: Relative effect of each systematic uncertainty (post-fit) on the yields in the SR for the left-handed $t\bar{t}\gamma$ -coupling using data in all regions (II).

	Signal ($t\bar{t}\gamma$, LH)	$e \rightarrow \gamma$ fake	$j \rightarrow \gamma$ fake	$\text{Not reviewed, } W_{\gamma\gamma+\text{jets}}$	$\text{Not reviewed, } W_{\gamma\gamma+\text{jets}}$ other prompt γ
Heavy flavour fraction (W +jets)	0/0	-0.00105 / 0.00105	0/0	0/0	0/0
Heavy flavour fraction (Z +jets)	0/0	-0.00989 / -0.0099	-0.0716 / 0.0715	0/0	0/0
SF(b -tag eigenvar. B1)	0.0119 / -0.0119	-0.000139 / -0.000139	-0.00128 / -0.0028	0/0	0/0
SF(b -tag eigenvar. B2)	0.00153 / 0.00153	0.00149 / 0.00149	0.00133 / -0.00133	0.0174 / -0.0174	0.0081 / -0.0081
SF(b -tag eigenvar. B3)	0.0107 / -0.0107	0.00103 / -0.00103	0.00106 / -0.00106	0.00227 / 0.000227	0.00419 / -0.00419
SF(b -tag eigenvar. B4)	0.000901 / 0.000901	0.000972 / 0.000972	0.000804 / 0.000804	0.000823 / 0.000823	0.000581 / 0.000581
SF(b -tag eigenvar. B5)	0.000967 / 0.000967	0.000817 / 0.000817	0.000979 / 0.000979	0.00149 / 0.000419	4.8e-05 / 4.8e-05
SF(b -tag eigenvar. B6)	0.000189 / 0.000189	0.000207 / 0.000207	0.000207 / 0.000207	0.000158 / 0.000158	5.14e-05 / 5.14e-05
SF(b -tag eigenvar. B7)	1.9e-05 / 1.9e-05	3e-05 / 3e-05	5.02e-05 / 5.02e-05	3.13e-05 / 3.13e-05	2.12e-05 / 2.12e-05
SF(b -tag eigenvar. B8)	5.2e-06 / 5.2e-06	4.19e-06 / 4.19e-06	6.05e-06 / 6.05e-06	1.29e-05 / 1.29e-05	4.4e-06 / 4.4e-06
SF(b -tag eigenvar. B9)	7.92e-07 / 7.92e-07	1.25e-06 / 1.25e-06	8.38e-07 / 8.38e-07	3.56e-06 / 3.56e-06	7.02e-06 / 7.02e-06
SF(b -tag eigenvar. C1)	0.00225 / -0.00225	0.00516 / -0.00516	0.00294 / -0.00294	0.0176 / -0.0176	0.00323 / -0.00323
SF(b -tag eigenvar. C2)	0.00336 / -0.00336	0.00196 / -0.00196	0.00113 / -0.00113	0.00627 / -0.00627	0.00238 / -0.00239
SF(b -tag eigenvar. C3)	0.00106 / 0.00106	0.00019 / 0.00019	0.00101 / 0.00101	0.0016 / 0.0016	9.09e-05 / 9.09e-05
SF(b -tag eigenvar. light 1)	5.91e-05 / 5.91e-05	0.0226 / -0.0226	0.0211 / -0.0211	0.0444 / -0.0444	0.00484 / -0.00485
SF(b -tag eigenvar. light 2)	4.2e-06 / 4.2e-06	0.0273 / 0.0273	0.00287 / 0.00287	0.0035 / 0.0035	0.00254 / 0.00254
SF(b -tag eigenvar. light 3)	4.05e-06 / 4.05e-06	0.00142 / 0.00142	0.00024 / 0.00024	0.00179 / 0.00179	0.0141 / 0.0141
SF(b -tag eigenvar. light 4)	2.57e-06 / 2.57e-06	0.00351 / 0.00351	0.00067 / 0.00067	0.00121 / 0.00121	0.00038 / 0.00038
SF(b -tag extrapolation)	2.55e-05 / 2.55e-05	1.95e-05 / 1.95e-05	1.38e-05 / 1.38e-05	3.19e-06 / 3.19e-06	1.18e-05 / 1.18e-05
SF(b -tag extrap. from charm)	0.0139 / 0.0139	0.0153 / 0.0153	0.00105 / 0.00105	0/0	0.000162 / 0.000162
JES η interc. modelling	0/0	3.39e-07 / 3.32e-07	0/0	0.00222 / -0.00222	0.0108 / -0.0108
JES η interc. non-closure high- E_T	0/0	0.00024 / 0.00024	0/0	0.00185 / -0.00085	0/0
JES η interc. non-closure $\eta > 0$	0.00108 / 0.00108	0.00033 / 0.00033	0.00024 / 0.00024	0.00161 / 0.00161	0.000266 / 0.000266
JES η interc. total stat.	0.0684 / -0.0684	0.00384 / -0.00384	0.00662 / -0.00662	0.00555 / -0.00555	0.00312 / -0.00312
JES effective NP stat. 1	0.00217 / 0.00217	0.00151 / 0.00151	0.000876 / 0.000876	0.00162 / 0.00162	0.00113 / 0.00113
JES effective NP stat. 2	0.00373 / -0.00373	0.00311 / -0.00311	0.00557 / -0.00557	0.00611 / -0.00611	0.00255 / -0.00255
JES effective NP stat. 3	0.0013 / 0.0013	0.00425 / 0.00425	0.00124 / 0.00124	0.00208 / 0.00209	0.00427 / 0.00427
JES effective NP stat. 4	0.00245 / 0.00245	0.00076 / 0.00076	0.00323 / 0.00323	0.00481 / 0.00481	0.00075 / 0.00075
JES effective NP stat. 5	0.00159 / 0.00159	0.000406 / 0.000406	0.00114 / 0.00114	0.00161 / 0.00161	0.000237 / 0.000237
JES effective NP stat. 6	0.00175 / 0.00175	0.00101 / 0.00101	0.000204 / 0.000204	0.00151 / 0.00151	0.000345 / -0.00345
JES effective NP stat. 7	0.00156 / -0.00156	0.00135 / -0.00135	0.000507 / -0.000507	0.000796 / -0.000796	0.000671 / -0.000671
JES effective NP stat. 8	0.000718 / 0.000718	0.000623 / 0.000623	0.000428 / 0.000428	0.000165 / 0.000165	0.00164 / -0.00164
JES pile-up NP modelling 1	0.0304 / -0.0302	0.00216 / -0.00215	0.03553 / -0.03553	0.00481 / 0.00481	0.000743 / 0.000743
JES pile-up NP modelling 2	0.00424 / 0.00424	0.00299 / 0.00299	0.00488 / 0.00488	0.00359 / 0.00359	0.000235 / 0.000235
JES pile-up NP modelling 3	0.00312 / -0.00312	0.00199 / 0.00199	0.00313 / -0.00313	0.00291 / -0.00291	0.000322 / 0.000322
JES pile-up NP modelling 4	0.000762 / 0.000762	0.000325 / 0.000325	0.000486 / 0.000486	0.00165 / 0.00165	0.000206 / 0.000206
JES pile-up offset NPV	0.014 / -0.014	0.0193 / -0.0192	0.0135 / -0.0135	0.0111 / -0.0111	0.00364 / -0.00364
JES pile-up p_T term	0.00657 / -0.00657	0.0054 / -0.0054	0.00664 / -0.00664	0.0122 / -0.0122	0.0111 / -0.0111
JES pile-up p_T topology	0.0281 / -0.028	0.0211 / -0.021	0.0403 / -0.0401	0.0125 / -0.0125	0.00483 / -0.00483
JES pile-up p_T response	0.09332 / -0.09331	0.0121 / -0.0121	0.018 / -0.018	0.0111 / -0.0111	0.026 / -0.0259
JES flavour composition (SR)	0.0483 / -0.0483	0.025 / -0.025	0.0783 / -0.0784	0.0111 / -0.0111	0.00736 / -0.00736
JES pile-up response (SR)	0.0224 / -0.0224	0.0163 / -0.0163	0.0244 / -0.0244	0.0208 / -0.0208	0.0354 / -0.0354
JES effective NP detector 1	0.00266 / 0.00266	0.00205 / 0.00205	0.00695 / 0.00695	0.00292 / 0.00292	0.0158 / -0.0158
JES effective NP detector 2	0.000234 / 0.000234	0.00073 / 0.00073	0.000922 / 0.000922	0.000165 / 0.000165	0.00271 / 0.00271
JES single particle high- p_T	0/0	3.46e-07 / 3.46e-07	0/0	0.00191 / 0.00191	0.000241 / 0.000241
JES punch through	0/0	9.79e-06 / 9.79e-06	0/0	0.00191 / 0.00191	0.000281 / 0.000281
JER data vs. MC	0.00541 / -0.00541	0.0246 / -0.0246	0.0311 / -0.0311	0.00204 / -0.00204	0.0013 / -0.0013
JER effective NP 1	0.00983 / -0.00988	0.0166 / -0.0165	0.0247 / -0.0245	0.0269 / -0.0266	0.00026 / 0.00026
JER effective NP 2	0.0106 / -0.0106	0.0162 / -0.0161	0.0214 / -0.0214	0.017 / -0.017	0.00446 / 0.00447
JER effective NP 3	0.0286 / -0.0286	0.00746 / -0.00744	0.0111 / -0.0111	0.0119 / 0.0119	0.00493 / -0.00493
JER effective NP 4	0.000224 / -0.000224	0.000497 / -0.000497	0.00788 / -0.00788	0.00588 / -0.00588	0.00315 / -0.00315
JER effective NP 5	0.00215 / -0.00215	-0.00328 / 0.00328	0.0213 / -0.0213	-0.0138 / 0.0138	0.00487 / -0.00487
JER effective NP 6	9.45e-05 / -9.46e-05	-0.00584 / 0.00584	-0.0143 / 0.0143	-0.00695 / 0.00695	0.00289 / -0.00289
JER effective NP 7 (rest term)	0.00331 / -0.00331	-0.00202 / 0.00202	0.00733 / -0.00733	-0.000333 / 0.000333	0.00329 / -0.00329
SF($j \rightarrow \gamma$)	0/0	0/0	0.619 / -0.448	0/0	0/0
p_T^γ reweighting (Z + γ +jets)	0/0	0/0	0/0	1.06e-05 / -1.06e-05	0/0
μ_R , μ_F ($t\bar{t}\gamma$)	0/0	9.79e-06 / 9.79e-06	0/0	0.23e-05 / -0.214	0/0
Heavy flavour fraction (Z + γ +jets)	0/0	0/0	0/0	0.00145 / 0.00145	0/0
p_T^γ reweighting (W + γ +jets)	0/0	0/0	0/0	4.31e-05 / -4.3e-05	0/0
μ_R , μ_F (W + γ +jets)	0/0	0/0	0/0	0.161 / -0.163	0/0
normalisation: W + γ +jets, HF	0/0	0/0	0/0	0.178 / -0.181	0/0
Heavy flavour fraction (W + γ +jets)	0/0	0/0	0/0	0.00113 / 0.00113	0/0
$\sigma_{\text{theory}}(t\bar{t}\gamma)$	0/0	0/0	0/0	0.00443 / 0.00443	0/0
γ SR bin 0	0.00179 / -0.00179	0.0115 / -0.0115	0.0117 / -0.0117	0.0153 / -0.0153	0.0079 / -0.0079
γ SR bin 1	0.00186 / -0.00186	0.00152 / -0.00152	0.00165 / -0.00165	0.00093 / -0.00093	0.00594 / -0.00594
γ SR bin 2	0.00201 / -0.00201	0.00114 / -0.00114	0.00126 / -0.00126	0.000763 / -0.000763	0.00132 / -0.00132
γ SR bin 3	0.00236 / -0.00236	0.00144 / -0.00144	0.00162 / -0.00162	0.000725 / -0.000725	0.000843 / -0.000843
γ SR bin 4	0.00334 / -0.00334	0.00109 / -0.00109	0.00111 / -0.00111	5.48e-05 / -5.48e-05	0.000648 / -0.000648
γ SR bin 5	0.00334 / -0.00334	0.000944 / -0.000944	0.000986 / -0.000986	0.00132 / -0.00132	0.000567 / -0.000567
γ SR bin 6	0.00943 / -0.00943	0.000527 / -0.000527	0.000664 / -0.000664	0.00127 / -0.00127	0.000365 / -0.000365
$\text{SF}(Z$ + γ +jets)	0/0	0/0	0/0	0.127 / -0.127	0/0
$\text{SF}(W$ + γ +jets)	0/0	0/0	0/0	0.0839 / -0.0839	0/0

Table 70: Relative effect of each systematic uncertainty (post-fit) on the yields in the CR $W+\gamma+jets$ coupling using data in all regions (I).

	Signal (rcy , LH)	$e \rightarrow \gamma$ fake	$j \rightarrow \gamma$ fake	$Z \gamma + jets$	$W \gamma + jets$	other prompt γ
Luminosity	0.0196/-0.0196	0.0196/-0.0196	0.0196/-0.0196	0/0	0/0	0.0196/-0.0196
Pile-up	0.0177/-0.0177	0.0186/-0.0185	0.0461/-0.046	0.00546/-0.00546	0.025/-0.025	0.021/-0.021
JVT	0.00103/-0.00103	0.000846/-0.000846	0.0014/-0.0014	0.000525/-0.000525	0.000956/-0.000956	0.00184/-0.00184
SF($e \rightarrow \gamma$)	0/0	0.0908/-0.0844	0/0	0/0	0/0	0/0
Shower generator ($t\bar{t}$)	0/0	-0.0116/-0.0116	-0.00827/-0.00831	0/0	0/0	0/0
ME generator (single top)	0/0	0.00191/-0.00191	0.00248/-0.00248	0/0	0/0	0/0
ME generator (single top)	0/0	-0.00308/-0.00308	-0.0009/-0.0009	0/0	0/0	-0.0727/-0.0725
tW DS scheme	0/0	0.00844/-0.00844	-0.000494/-0.000494	0/0	0/0	0.186/-0.187
SF(photon ID)	0.00651/-0.00651	0.01141/-0.0114	0.0141/-0.0141	0.0125/-0.0125	0.0118/-0.0117	0.0113/-0.0113
SF(photon iso.)	0.0108/-0.0108	0.0153/-0.0153	0.0152/-0.0152	0.0142/-0.0142	0.014/-0.014	0.014/-0.014
SF(electron trigger)	0.00113/-0.00113	0.00204/-0.00204	0.00119/-0.00119	0.00139/-0.00139	0.00124/-0.00124	0.00121/-0.00121
SF(electron reco.)	0.000665/-0.000665	0.000912/-0.000912	0.000459/-0.000459	0.000576/-0.000576	0.000558/-0.000558	0.000584/-0.000584
SF(electron ID)	0.00409/-0.00409	0.00633/-0.00633	0.00142/-0.00142	0.0044/-0.0044	0.00412/-0.00412	0.00412/-0.00412
SF(electron iso.)	0.000766/-0.000766	0.000861/-0.000861	0.00043/-0.00043	0.000492/-0.000492	0.000483/-0.000483	0.000518/-0.000518
SF(muon trigger stat.)	0.000769/-0.000769	0.000303/-0.000303	0.0007/-0.0007	0.000787/-0.000787	0.000851/-0.000851	0.000854/-0.000854
SF(muon trigger syst.)	0.000293/-0.000293	0.000151/-0.00015	0.000134/-0.000134	0.000289/-0.000289	0.000316/-0.000316	0.000306/-0.000306
SF(muon ID stat.)	0.000249/-0.000249	9.63e-05/-9.63e-05	0.000246/-0.000246	0.000252/-0.000252	0.000268/-0.000268	0.000257/-0.000257
SF(muon ID syst.)	0.00142/-0.00142	0.000553/-0.000553	0.00139/-0.00139	0.00141/-0.00141	0.00148/-0.00148	0.00147/-0.00147
SF(muon iso. stat.)	0.00014/-0.00014	5.43e-05/-5.43e-05	0.00148/-0.00148	0.00146/-0.00146	0.00146/-0.00146	0.00146/-0.00146
SF(muon iso. syst.)	0.000107/-0.000107	0.000411/-0.000411	0.00119/-0.00119	0.00115/-0.00115	0.00117/-0.00117	0.00114/-0.00114
SF(muon TTVA stat.)	0.000101/-0.000101	3.93e-05/-3.93e-05	5.69e-05/-5.69e-05	5.68e-05/-5.68e-05	5.68e-05/-5.68e-05	4.61e-05/-4.61e-05
SF(muon TTVA syst.)	3.82e-05/-3.82e-05	1.67e-05/-1.67e-05	0.0186/-0.0186	0.0305/-0.0305	0.00494/-0.00494	0.0014/-0.0014
EGamma resolution all	0.00471/-0.00471	0.0251/-0.0251	0.0222/-0.0222	0.00953/-0.00953	0.00804/-0.00803	0.00767/-0.00767
EGamma scale all	0.0092/-0.0092	0.00682/-0.00682	0.016/-0.016	0.00675/-0.00675	0.00119/-0.00119	0.00119/-0.00119
Muon ID	0/0	0.00766/-0.00766	0.00808/-0.00808	0.00724/-0.00724	0.000489/-0.000489	0.0006/-0.0006
Muon MS	0.00142/-0.00142	0.00678/-0.00678	0.000644/-0.000644	0.000329/-0.000329	0.00119/-0.00119	0.00063/-0.00063
Muon sagitta bias	0.00246/-0.00246	0.000415/-0.000415	0.000415/-0.000415	0.00224/-0.00224	0.00063/-0.00063	0.000791/-0.000791
Muon scale	0.00149/-0.00149	0.000475/-0.000475	0.000456/-0.000456	0.0023/-0.0023	0.000901/-0.000901	0.000641/-0.000641
ISR ($t\bar{t}$)	0/0	0.00766/-0.00766	0.00227/-0.00227	0/0	0/0	0/0
FSR ($t\bar{t}$)	0/0	0.00923/-0.00923	0.00291/-0.00291	0/0	0/0	0/0
FSR (single top)	0/0	0.000888/-0.000888	0.000416/-0.000416	0/0	0/0	0.00165/-0.00165
PDF no. 1	0/0	0.00604/-0.00604	0.00149/-0.00149	0/0	0/0	0.0112/-0.0112
PDF no. 2	0.00446/-0.00446	0.000786/-0.000786	0.00145/-0.00145	0.00122/-0.00122	0.00432/-0.00432	0.004385/-0.004385
PDF no. 3	0.0101/-0.0101	0.00366/-0.00366	0.114/-0.114	0.00152/-0.00152	0.0114/-0.0114	0.00055/-0.00055
PDF no. 4	0.02651/-0.0265	0.00489/-0.00489	0.0474/-0.0474	0.00638/-0.00638	0.0026/-0.0026	0.00294/-0.00294
PDF no. 5	0.0088/-0.0088	0.00228/-0.00228	0.107/-0.107	0.00142/-0.00142	0.00142/-0.00142	0.00182/-0.00182
PDF no. 6	0.00923/-0.00923	0.001/-0.001	0.0656/-0.0656	0.00017/-0.00017	0.00617/-0.00617	0.00515/-0.00515
PDF no. 7	0.0105/-0.0105	0.00874/-0.00874	0.0427/-0.0427	0.000382/-0.000382	0.00249/-0.00249	0.00615/-0.00615
PDF no. 8	0.00938/-0.00938	0.000594/-0.000594	0.0487/-0.0487	0.00301/-0.00301	0.00536/-0.00536	0.00438/-0.00438
PDF no. 9	0.00392/-0.00392	0.00152/-0.00152	0.0659/-0.066	0.00208/-0.00208	0.00872/-0.00872	0.0018/-0.0018
PDF no. 10	0.0107/-0.0107	0.0192/-0.0192	0.0751/-0.0751	0.000758/-0.000758	0.00748/-0.00748	0.0057/-0.0057
PDF no. 11	0.00145/-0.00145	0.0018/-0.0018	0.0904/-0.0905	0.00185/-0.00185	0.00723/-0.00723	0.000534/-0.000534
PDF no. 12	0.00704/-0.00704	0.00308/-0.00308	0.0991/-0.0992	5.51e-05/-5.52e-05	0.0106/-0.0106	0.00416/-0.00417
PDF no. 13	0.0108/-0.0108	0.00234/-0.00234	0.0572/-0.0573	0.00179/-0.00179	0.00734/-0.00734	0.00619/-0.00619
PDF no. 14	0.00759/-0.00759	0.00129/-0.00129	0.0827/-0.0827	0.00109/-0.00109	0.00808/-0.00808	0.00401/-0.00401
PDF no. 15	0.0103/-0.0103	0.00146/-0.00146	0.0565/-0.0565	0.000486/-0.000486	0.0006/-0.0006	0.00555/-0.00555
PDF no. 16	0.00671/-0.00671	0.00236/-0.00236	0.0566/-0.0566	0.00383/-0.00383	0.00381/-0.00381	0.0021/-0.0021
PDF no. 17	0.0166/-0.0166	0.00249/-0.00249	0.0718/-0.0718	0.00181/-0.00181	0.00978/-0.00978	0.00921/-0.00921
PDF no. 18	0.0123/-0.0123	0.00154/-0.00154	0.0811/-0.0811	0.000111/-0.000111	0.0007/-0.0007	0.00698/-0.00698
PDF no. 19	0.00894/-0.00894	0.00092/-0.00092	0.0641/-0.0641	0.000498/-0.000498	0.00547/-0.00547	0.00027/-0.00027
PDF no. 20	0.0089/-0.0089	0.0017/-0.0017	0.0651/-0.0651	0.000527/-0.000527	0.0065/-0.0065	0.00497/-0.00497
PDF no. 21	0.00856/-0.00856	0.000505/-0.000505	0.0662/-0.0662	0.00115/-0.00115	0.0052/-0.0052	0.00467/-0.00467
PDF no. 22	0.00755/-0.00755	0.00236/-0.00236	0.0932/-0.0934	0.000836/-0.000836	0.0065/-0.0065	0.00573/-0.00573
PDF no. 23	0.0109/-0.0109	0.00115/-0.00115	0.0782/-0.0782	0.000519/-0.000519	0.00458/-0.00458	0.00537/-0.00537
PDF no. 24	0.012/-0.012	0.00141/-0.00141	0.0645/-0.0645	0.000468/-0.000469	0.00660/-0.00660	0.00631/-0.00631
PDF no. 25	0.00778/-0.00778	0.00127/-0.00127	0.0745/-0.0745	0.000627/-0.000626	0.00665/-0.00665	0.00401/-0.00401
PDF no. 26	0.00843/-0.00843	0.00172/-0.00172	0.0789/-0.0789	0.00155/-0.00155	0.00713/-0.00713	0.00566/-0.00566
PDF no. 27	0.01/-0.01	0.00193/-0.00193	0.0789/-0.0789	0.000298/-0.000298	0.0065/-0.0065	0.00573/-0.00573
PDF no. 28	0.0137/-0.0137	0.00576/-0.00576	0.0664/-0.0665	0.00715/-0.00715	0.0122/-0.0122	0.0107/-0.0107
PDF no. 29	0.0166/-0.0166	0.00169/-0.00169	0.069/-0.0691	0.00152/-0.00152	0.00690/-0.00690	0.00537/-0.00537
PDF no. 30	0.0192/-0.0192	0.00147/-0.00147	0.0654/-0.0655	0.000468/-0.000469	0.00526/-0.00526	0.00698/-0.00698
μ_R - μ_F (single top)	0/0	0.00135/-0.00135	0.00685/-0.00685	0/0	0/0	0.0069/-0.0069
μ_R - μ_F ($W+jets$)	0/0	0.000789/-0.000789	0.239/-0.242	0/0	0/0	0/0
μ_R - μ_F ($Z+jets$)	0/0	0.14/-0.136	0.0391/-0.0388	0/0	0/0	0/0
μ_R - μ_F (diboson)	0/0	0.00527/-0.00527	0.0211/-0.0221	0/0	0/0	0/0
σ_{theory} ($t\bar{t}$)	0/0	0.012/-0.012	0.00194/-0.00194	0/0	0/0	0/0
σ_{theory} ($W+jets$)	0/0	0.00228/-0.00228	0.000664/-0.000664	0/0	0/0	0.0118/-0.0118
σ_{theory} ($W+jets$)	0/0	8.16e-05/-8.17e-05	0.0421/-0.0421	0/0	0/0	0/0
σ_{theory} ($Z+jets$)	0/0	0.0328/-0.0328	0.00466/-0.00466	0/0	0/0	0/0
σ_{theory} (diboson)	0/0	0.00048/-0.00048	0.000528/-0.000528	0/0	0/0	0.00598/-0.00598

Table 71: Relative effect of each systematic uncertainty (post-fit) on the yields in the CR $W + \gamma + \text{jet}$ regions (II).

Signal ($\tau\tau$, LH)	$e \rightarrow \gamma$ fake	$j \rightarrow \gamma$ fake	$Z\gamma$ -jets	W -jets	other prompt γ
E_T^{miss} soft-term reso. para.	-0.00229 / 0.00229	-0.0349 / 0.0354	0.0079 / -0.00787	-0.0412 / 0.042	-0.00233 / 0.00233
E_T^{miss} soft-term reso. perp.	-0.00156 / 0.00156	-0.031 / 0.0315	-0.0111 / 0.0112	-0.0306 / 0.0311	-0.00298 / 0.00298
E_T^{miss} soft-term scale	0.000727 / -0.00726	0.0339 / -0.0338	0.00202 / -0.00202	0.0371 / -0.0369	0.00335 / -0.00335
SF(b -tag eigenvar. B1)	0.00546 / -0.00546	0.00367 / -0.00367	0.000749 / -0.000749	0.000555 / -0.000555	0.000132 / -0.000132
SF(b -tag eigenvar. B2)	0.00694 / 0.00694	0.00467 / -0.00467	7.5e-05 / 7.5e-05	1.61e-05 / 1.61e-05	0.00119 / 0.00119
SF(b -tag eigenvar. B3)	0.00468 / -0.00468	0.00332 / -0.00332	0.000534 / 0.000534	0.000176 / 0.000176	6.91e-05 / 6.92e-05
SF(b -tag eigenvar. B4)	0.000402 / 0.000402	0.00029 / 0.00029	5.49e-05 / 5.49e-05	5.2e-05 / 5.2e-05	9.68e-06 / 9.68e-06
SF(b -tag eigenvar. B5)	0.000406 / 0.000406	0.000339 / 0.000339	3.46e-05 / 3.46e-05	3.16e-05 / 3.16e-05	0.000349 / 0.000349
SF(b -tag eigenvar. B6)	9.25e-05 / 9.25e-05	6.78e-05 / 6.78e-05	1.08e-05 / 1.08e-05	9.34e-06 / 9.34e-06	0.000692 / 0.000692
SF(b -tag eigenvar. B7)	9.78e-06 / 9.78e-06	1.13e-05 / 1.13e-05	1.55e-06 / 1.55e-06	2.38e-06 / 2.38e-06	8.24e-06 / 8.24e-06
SF(b -tag eigenvar. B8)	2.15e-06 / 2.15e-06	9.22e-07 / 9.22e-07	6.32e-07 / 6.32e-07	2.12e-07 / 2.12e-07	1.67e-05 / 1.67e-05
SF(b -tag eigenvar. B9)	1.88e-07 / 1.88e-07	2.66e-07 / 2.66e-07	2.24e-07 / 2.24e-07	1.04e-07 / 1.04e-07	3.22e-06 / 3.22e-06
SF(b -tag eigenvar. C1)	0.00116 / -0.00116	0.00024 / -0.00024	0.000144 / -0.000144	0.000252 / -0.000252	7.06e-07 / 7.06e-07
SF(b -tag eigenvar. C2)	0.00151 / -0.00151	0.00049 / -0.00049	9.15e-05 / -9.13e-05	0.000161 / -0.000161	0.000163 / -0.000163
SF(b -tag eigenvar. C3)	0.000466 / 0.000466	5.04e-05 / 5.04e-05	1.98e-05 / 1.98e-05	6e-05 / 6e-05	0.000102 / 0.000102
SF(b -tag eigenvar. light 1)	0.000131 / -0.000131	0.00042 / -0.00042	0.00049 / -0.00049	0.000486 / -0.000487	5.84e-05 / 5.84e-05
SF(b -tag eigenvar. light 2)	8.81e-06 / 8.81e-06	2.9e-05 / 2.9e-05	2.94e-05 / 2.94e-05	0.000501 / -0.000501	0.000263 / -0.000263
SF(b -tag eigenvar. light 3)	1.17e-06 / 1.17e-06	6.32e-06 / 6.32e-06	8.85e-06 / 8.85e-06	3.06e-06 / 3.06e-06	4.87e-06 / 4.87e-06
SF(b -tag eigenvar. light 4)	1.7e-06 / 1.7e-06	4.28e-06 / 4.28e-06	6.48e-06 / 6.48e-06	6.55e-06 / 6.55e-06	2.88e-06 / 2.88e-06
SF(b -tag extrapolation)	5.14e-05 / 5.14e-05	5.95e-06 / 5.95e-06	5.48e-06 / 5.48e-06	4.32e-05 / 4.32e-05	4.71e-05 / 4.71e-05
SF(b -tag extrap. from charm)	2.32e-07 / 2.32e-07	2.12e-06 / 2.12e-06	2.86e-06 / 2.86e-06	-1.24e-09 / -1.24e-09	7.52e-05 / 7.52e-05
JES η interc. modelling	0.0113 / -0.0113	0.0226 / -0.0226	0.028 / -0.0279	0.00966 / -0.00965	0.00213 / -0.00213
JES η interc. non-closure high- E_T	0 / 0	1.27e-07 / 1.26e-05	5.67e-07 / 5.32e-07	6.64e-07 / 6.64e-06	7.49e-07 / 7.35e-07
JES η interc. non-closure $\eta < 0$	0.00117 / 0.00117	0.000262 / 0.00262	0.00128 / 0.00128	1.7e-05 / 1.7e-05	1.07e-05 / 1.07e-05
JES η interc. non-closure $\eta > 0$	0.000759 / 0.000759	0.000182 / 0.000182	0.000655 / 0.000655	2.29e-06 / 2.29e-06	4.87e-06 / 4.87e-06
JES η interc. total stat.	0.000612 / -0.000612	0.0132 / -0.0132	0.0112 / -0.0112	5.2e-06 / 5.2e-06	2.88e-06 / 2.88e-06
JES effective NP stat. 1	0.000195 / 0.000195	0.000476 / 0.000476	0.00573 / 0.00573	0.00119 / 0.00119	0.00311 / -0.00311
JES effective NP stat. 2	0.000463 / -0.000463	0.00784 / -0.00784	0.0113 / -0.0113	0.00204 / -0.00204	0.00089 / 0.00089
JES effective NP stat. 3	0.000112 / 0.000112	0.000688 / 0.000668	0.00153 / 0.00153	0.000252 / 0.000252	0.000525 / -0.000525
JES effective NP stat. 4	0.000196 / 0.000196	0.000213 / 0.000213	0.00183 / 0.00183	0.00108 / 0.00108	0.000445 / 0.000445
JES effective NP stat. 5	0.000587 / 0.000587	0.000524 / 0.000524	0.000182 / 0.000182	0.00104 / 0.00104	0.000245 / 0.000245
JES effective NP stat. 6	0.000132 / 0.000132	0.000161 / 0.000161	0.00168 / 0.00168	0.00121 / 0.00121	0.000246 / 0.000246
JES effective NP mixed 1	0.000198 / -0.000198	0.000218 / -0.000218	0.00393 / 0.00393	0.00208 / -0.00208	0.000466 / 0.000466
JES effective NP mixed 2	0.000203 / -0.000203	0.0042 / -0.0042	0.0104 / -0.0104	0.000183 / -0.00183	0.000525 / -0.000525
JES effective NP mixed 3	0.000694 / 0.000694	0.00148 / 0.00148	0.00157 / 0.00157	0.000939 / 0.000939	0.000167 / 0.000167
JES effective NP mixed 4	0.00239 / -0.0238	0.0323 / -0.0321	0.0384 / -0.0381	0.0155 / -0.0155	0.000279 / -0.0279
JES pile-up offset μ	0.03346 / 0.03346	0.00794 / 0.00794	0.00599 / 0.00599	0.00151 / 0.00151	0.000516 / 0.000516
JES pile-up offset NP	0.0186 / -0.0086	0.00316 / -0.00316	0.00398 / -0.00398	0.00171 / 0.00171	0.00399 / 0.00399
JES pile-up offset μ	0.00696 / -0.00696	0.0202 / -0.0202	0.0258 / -0.0257	0.00879 / -0.00879	0.000718 / -0.000718
JES pile-up offset NP mixed 3	0.013 / -0.013	0.0149 / -0.0149	0.0306 / -0.0305	0.00838 / -0.00837	0.000157 / -0.00157
JES pile-up ρ modelling 1	0.0264 / -0.0263	0.029 / -0.0289	0.0409 / -0.0408	0.0107 / -0.0107	0.00211 / -0.00211
JES pile-up ρ modelling 2	0.035 / -0.0135	0.00414 / -0.00414	0.00239 / -0.00239	0.000417 / -0.000417	0.000351 / 0.000351
JES pile-up ρ modelling 3	0.0307 / -0.0307	0.0502 / -0.0502	0.0591 / -0.0591	0.0308 / -0.0308	0.00466 / 0.00466
JES pile-up ρ modelling 4	0.0146 / -0.0146	0.0325 / -0.0325	0.0445 / -0.0445	0.0208 / -0.0208	0.000629 / -0.000629
JES flavour composition (CR $W + \gamma + \text{jet}$)	0 / 0	8.75e-05 / 8.75e-05	3.75e-07 / 3.75e-07	2.64e-05 / 2.64e-05	0.00368 / 0.00368
JES flavour response (CR $W + \gamma + \text{jet}$)	0.00171 / 0.00171	0.00472 / 0.00472	0.00945 / 0.00945	0.00212 / 0.00212	0.00025 / -0.00025
JES effective NP detector 1	0.000417 / 0.000417	0.000509 / 0.000509	0.00149 / 0.00149	0.000711 / 0.000711	0.000121 / 0.000121
JES effective NP detector 2	0 / 0	2.85e-05 / 2.85e-05	0 / 0	8.99e-09 / 8.99e-09	0 / 0
JES single particle high- p_T	0 / 0	8.75e-05 / 8.75e-05	3.75e-07 / 3.75e-07	1.4e-05 / 1.4e-05	9.29e-06 / 9.29e-06
JER data vs. MC	0.000758 / -0.00758	0.00176 / -0.00176	0.0276 / -0.0275	0.0136 / -0.0136	0.00661 / 0.00661
JER effective NP 1	0.000944 / -0.000944	0.016 / -0.0159	0.0653 / -0.0654	0.0285 / -0.0283	0.00996 / -0.00993
JER effective NP 2	0.00365 / -0.00365	0.0224 / -0.0224	0.0566 / -0.0556	0.0285 / -0.0257	0.00769 / -0.00768
JER effective NP 3	0.00163 / -0.00163	0.0075 / -0.00749	0.0553 / -0.0546	0.0165 / -0.0164	0.00554 / -0.00554
JER effective NP 4	-0.00227 / 0.00227	0.0065 / -0.00649	0.00873 / -0.00872	0.00112 / 0.00112	0.00477 / -0.00476
JER effective NP 5	0.000521 / 0.000521	0.00894 / -0.00893	-0.00664 / 0.00665	0.00571 / 0.00571	0.00322 / 0.00322
JER effective NP 6	0.000344 / -0.000344	8.77e-05 / -8.8e-05	0.00259 / -0.00259	-0.00555 / 0.00555	0.00329 / -0.00329
JER effective NP 7 (rest term)	0.000269 / -0.000269	0.0158 / -0.0158	0.0272 / -0.0272	0.00103 / 0.00103	0.00482 / -0.00482
SF($\ell \rightarrow \gamma$)	0 / 0	0 / 0	0.619 / -0.448	0 / 0	0 / 0
P_1^γ reweighting ($Z + \gamma + \text{jets}$)	0 / 0	0 / 0	-1.35e-08 / -4.95e-08	0 / 0	0 / 0
P_1^γ reweighting ($W + \gamma + \text{jets}$)	0 / 0	0 / 0	0.104 / -0.102	0 / 0	0 / 0
μ_R , μ_F ($W + \gamma + \text{jets}$)	0 / 0	0 / 0	0 / 0	9.91e-09 / 3.72e-09	0 / 0
normalisation: $W + \gamma + \text{jets}$, HF	0 / 0	0 / 0	0 / 0	0.0648 / -0.065	0 / 0
μ_R , μ_F ($t\bar{t} + \gamma$)	0 / 0	0 / 0	0 / 0	0.00217 / -0.00217	0.00421 / 0.00421
$\sigma_{\text{theory}}(t\bar{t} + \gamma)$	0.294 / 0.294	0.616 / 0.616	0.691 / 0.691	0.771 / 0.771	0.057 / -0.057
γ CR $W + \gamma + \text{jet}$ bin 0	0.0785 / 0.0785	0.181 / 0.181	0.146 / 0.146	0.0838 / 0.0838	0.768 / 0.768
γ CR $W + \gamma + \text{jet}$ bin 1	0.0453 / 0.0453	0.0478 / 0.0478	0.0432 / 0.0432	0.0252 / 0.0252	0.0901 / 0.0901
γ CR $W + \gamma + \text{jet}$ bin 2	0.0453 / 0.0453	0.0322 / 0.0322	0.022 / 0.022	0.0241 / 0.0241	0.0237 / 0.0237
γ CR $W + \gamma + \text{jet}$ bin 3	0.0583 / 0.0583	0.0298 / 0.0298	0.023 / 0.023	0.0241 / 0.0241	0.024 / 0.024
γ CR $W + \gamma + \text{jet}$ bin 4	0.0742 / 0.0742	0.0398 / 0.0398	0.025 / 0.025	0.0236 / 0.0236	0.0233 / 0.0233
γ CR $W + \gamma + \text{jet}$ bin 5	0.145 / 0.145	0.0355 / 0.0355	0.026 / 0.026	0.0164 / 0.0164	0.0243 / 0.0243
γ CR $W + \gamma + \text{jet}$ bin 6	0.262 / 0.262	0.0173 / 0.0173	0.021 / 0.021	0.0165 / 0.0165	0.0181 / 0.0181
γ CR $W + \gamma + \text{jet}$ bin 7	0 / 0	0 / 0	0 / 0	0.127 / -0.127	0 / 0
SF($W + \gamma + \text{jets}$)	0 / 0	0 / 0	0 / 0	0.0839 / -0.0839	0 / 0

Not reviewed, for internal circulation only

Table 72: Relative effect of each systematic uncertainty (post-fit) on the yields in the CR $Z + \gamma$ for the left-handed $t\gamma\gamma$ coupling using data in all regions (I).

	Signal ($t\gamma\gamma$, LH)	$e \rightarrow \gamma$ fake	$j \rightarrow \gamma$ fake	$Z \rightarrow \gamma$ fake	$Z\gamma$ +jets	$W\gamma$ +jets	other prompt γ
Luminosity	0.0196/-0.0196	0.0196/-0.0196	0.0196/-0.0196	0.0196/-0.0196	0.0196/-0.0196	0.161/-0.161	0.0196/-0.0196
Pile-up	0.2351/-0.233	0.0272/-0.0272	0.009554/0.000954	0.000841/0.000841	0.000585/0.000585	0.00173/0.00173	0.0271/-0.0269
IVT	0.00257/0.00257						0.0037/0.0037
SF($e \rightarrow \gamma$)	0/0	0/0	0/0	0/0	0/0	0/0	0/0
Shower generator ($t\bar{t}$)	0/0	0/0	0.00543/-0.00543	0.00527/-0.00527	0/0	0/0	0/0
ME generator (single top)	0/0	0/0	-0.00345/0.00345	0.000282/-0.000282	0/0	0/0	-0.0333/0.0333
ME generator (single top)	0/0	0/0	-0.0019/-0.0019	0.00138/-0.00138	0/0	0/0	-0.0543/-0.0543
TW DS scheme	0/0	0/0	-0.00257/0.00257	0.00143/-0.00143	0/0	0/0	-0.00822/0.00821
SF(photon ID)	0/0	0/0	0.0152/-0.0152	0.0152/-0.0152	0.0129/-0.0129	0.0117/-0.0117	0.011/-0.011
SF(photon iso.)	0.0152/-0.0152	0.0153/-0.0153	0.0148/-0.0148	0.0153/-0.0153	0.0139/-0.0139	0.0111/-0.0111	0.0113/-0.0139
SF(electron trigger)	0.00045/-0.00045	0.00023/0.00023	0.000242/0.000242	0.000234/0.000234	0.000234/0.000234	0.000152/0.000152	0.000152/0.000152
SF(electron reco.)	0.00235/0.00235	0.0013/0.0013	0.000872/0.000872	0.000936/0.000936	0.00145/0.00145	0.00103/0.00103	0.00103/0.00103
SF(electron ID)	0.0173/-0.0173	0.00983/-0.00983	0.00749/-0.00749	0.00749/-0.00749	0.0151/-0.0151	0.00736/-0.00736	0.00736/-0.00736
SF(electron iso.)	0.00289/0.00289	0.0012/0.0012	0.000836/0.000836	0.000836/0.000836	0.00205/0.00205	0.000904/0.000904	0.000904/0.000904
SF(fusion trigger stat.)	0.000104/0.000104	0.000396/0.000396	0.000444/0.000444	0.000444/0.000444	0.000528/0.000528	0.000447/0.000447	0.000519/0.000519
SF(fusion trigger syst.)	0.000358/0.000358	0.000871/0.000871	0.00126/0.00126	0.00126/0.00126	0.00126/0.00126	0.00119/0.00119	0.00119/0.00119
SF(fusion ID stat.)	0.000227/0.000227	0.000453/0.000453	0.000633/0.000633	0.000633/0.000633	0.000663/0.000663	0.000626/0.000626	0.000626/0.000626
SF(fusion ID syst.)	0.00126/0.00126	0.0027/0.0027	0.00471/0.00471	0.00471/0.00471	0.00372/0.00372	0.00182/0.00182	0.00371/0.00371
SF(muon iso. stat.)	0.000151/0.000151	0.000236/0.000236	0.000297/0.000297	0.000297/0.000297	0.000336/0.000336	0.00026/0.00026	0.00033/0.00033
SF(muon iso. syst.)	0.00128/0.00128	0.00187/0.00187	0.00254/0.00254	0.00254/0.00254	0.00273/0.00273	0.00162/0.00162	0.00254/0.00254
SF(muon TTV stat.)	0.000113/0.000113	0.000178/0.000178	0.000229/0.000229	0.000261/0.000261	0.000261/0.000261	0.00128/0.00128	0.000251/0.000251
SF(muon TTV syst.)	6.91e-05/6.91e-05	7.59e-05/7.59e-05	0.000101/0.000101	0.000101/0.000101	0.000129/0.000129	6.25e-05/6.25e-05	0.000105/0.000105
EGamma resolution all	0.209/-0.209	0.00434/-0.00434	0.0235/-0.0235	0.0235/-0.0235	0.0178/-0.0178	0.0687/-0.0687	0.0185/-0.0185
EGamma scale all	0.0611/-0.0611	0.00803/-0.00803	0.0276/-0.0275	0.0276/-0.0275	0.00951/-0.00951	0.0683/-0.0682	0.00403/-0.00403
Muon ID	0/0	0.00818/-0.00818	0.00457/-0.00457	0.00457/-0.00457	0.00693/-0.00693	0.0561/-0.0561	0.00456/-0.00456
Muon MS	0/0	0.00766/-0.00766	0.00921/-0.00921	0.00746/-0.00746	0.00561/-0.00561	0.00627/-0.00627	0.00627/-0.00627
Muon sagitta residuals	0/0	0.000521/0.000521	0.00465/0.00465	0.000465/0.000465	0.000146/0.000146	0/0	0.000293/0.000293
Muon sagitta ρ	0/0	0.00119/-0.00119	0.0121/-0.0121	0.000144/-0.000144	0.000199/-0.000199	0.000489/-0.000489	0.00063/0.00063
Muon scale	0/0	0.000885/0.000885	0.00182/0.00182	0.0011/0.0011	0/0	0/0	0/0
ISR ($t\bar{t}$)	0/0	0.00707/-0.00707	0.00297/-0.00297	0/0	0/0	0/0	0/0
FSR ($t\bar{t}$)	0/0	0.00681/-0.00681	0.00339/-0.00339	0/0	0/0	0/0	0/0
ISR (single top)	0/0	0.000153/0.000153	0.000115/0.000115	0/0	0/0	0/0	0/0
FSR (single top)	0/0	0.00449/-0.00449	0.000167/-0.000167	0/0	0/0	0/0	0/0
PDF no. 1	0.0175/-0.0175	0.00328/-0.00328	0.00164/-0.00164	0.00123/-0.00123	0.00192/-0.00192	0.00432/-0.00432	0.00432/-0.00432
PDF no. 2	0.00456/-0.00456	0.0289/-0.0289	0.00153/-0.00153	0.00169/-0.00169	0.0125/-0.0125	0.00409/-0.00409	0.00409/-0.00409
PDF no. 3	0.0916/-0.0916	0.00207/-0.00207	0.00077/-0.00077	0.00633/-0.00633	0.024/-0.024	0.00344/-0.00344	0.00344/-0.00344
PDF no. 4	0.00302/-0.00302	0.0143/-0.0143	0.00471/-0.00471	0.00135/-0.00135	0.03771/-0.03771	0.003771/-0.03771	0.003771/-0.03771
PDF no. 5	0.0149/-0.0149	0.0116/-0.0116	0.00853/-0.00853	0.00079/-0.00079	0.0011/-0.0011	0.00384/-0.00384	0.00384/-0.00384
PDF no. 6	0.018/-0.018	0.00794/-0.00794	0.000388/-0.000387	0.000252/-0.000252	0.00154/-0.00154	0.00467/-0.00467	0.00467/-0.00467
PDF no. 7	0.0135/-0.0135	0.00389/-0.00389	0.00054/-0.00054	0.000283/-0.000283	0.00192/-0.00192	0.00751/-0.00751	0.00751/-0.00751
PDF no. 8	0.0133/-0.0133	0.00389/-0.00389	0.00054/-0.00054	0.000704/-0.000704	0.00427/-0.00427	0.00409/-0.00409	0.00409/-0.00409
PDF no. 9	0.0105/-0.0105	0.00648/-0.00648	0.00475/-0.00475	0.00274/-0.00274	0.0126/-0.0126	0.00058/-0.00058	0.00058/-0.00058
PDF no. 10	0.0162/-0.0163	0.0115/-0.0115	0.01159/-0.01159	0.00183/-0.00183	0.042/-0.042	0.00424/-0.00424	0.00424/-0.00424
PDF no. 11	0.0171/-0.0171	0.0182/-0.0182	0.009989/-0.009989	0.00254/-0.00254	0.0161/-0.0161	0.00114/-0.00114	0.00114/-0.00114
PDF no. 12	0.0137/-0.0137	0.0182/-0.0182	0.00319/-0.00319	0.000241/-0.000241	0.00356/-0.00356	0.00161/-0.00161	0.00161/-0.00161
PDF no. 13	0.0211/-0.0211	0.00695/-0.00695	0.00231/-0.00231	0.00171/-0.00171	0.00454/-0.00454	0.00586/-0.00586	0.00586/-0.00586
PDF no. 14	0.0179/-0.0179	0.0105/-0.0105	0.00205/-0.00205	0.00159/-0.00159	0.0031/-0.0031	0.00311/-0.00311	0.00311/-0.00311
PDF no. 15	0.02/-0.02	0.00645/-0.00645	0.00652/-0.00652	0.00103/-0.00103	0.00458/-0.00458	0.00488/-0.00488	0.00488/-0.00488
PDF no. 16	0.0162/-0.0163	0.00258/-0.00258	0.00548/-0.00548	0.00353/-0.00353	0.0064/-0.0064	0.00558/-0.00558	0.00558/-0.00558
PDF no. 17	0.0273/-0.0273	0.00996/-0.00996	0.00324/-0.00324	0.00299/-0.00299	0.00413/-0.00413	0.0105/-0.0105	0.0105/-0.0105
PDF no. 18	0.024/-0.024	0.00996/-0.00997	0.00044/-0.00044	3.37/-0.51/-3.36/-0.05	0.00161/-0.00161	0.00641/-0.00641	0.00641/-0.00641
PDF no. 19	0.00546/-0.00546	0.00364/-0.00364	0.00795/-0.00795	0.000375/-0.000374	0.00267/-0.00267	0.00586/-0.00586	0.00586/-0.00586
PDF no. 20	0.0172/-0.0172	0.00533/-0.00533	0.00102/-0.00102	0.00159/-0.00159	0.00311/-0.00311	0.00312/-0.00312	0.00312/-0.00312
PDF no. 21	0.0164/-0.0164	0.0279/-0.0279	0.00188/-0.00188	0.00125/-0.00125	0.00419/-0.00419	0.0039/-0.0039	0.0039/-0.0039
PDF no. 22	0.0191/-0.0192	0.00838/-0.00838	0.000802/-0.000802	0.000388/-0.000388	0.00466/-0.00466	0.00877/-0.00877	0.00877/-0.00877
PDF no. 23	0.0186/-0.0186	0.00866/-0.00866	0.00228/-0.00228	0.000502/-0.000502	0.00249/-0.00249	0.00499/-0.00499	0.00499/-0.00499
PDF no. 24	0.0154/-0.0154	0.0105/-0.0105	0.000748/-0.000748	0.000774/-0.000774	0.00267/-0.00267	0.00198/-0.00198	0.00198/-0.00198
PDF no. 25	0.0169/-0.0169	0.014/-0.014	0.00462/-0.00462	0.00165/-0.00165	0.00579/-0.00579	0.00429/-0.00429	0.00429/-0.00429
PDF no. 26	0.0185/-0.0185	0.00971/-0.00971	0.000562/-0.000562	0.000299/-0.000299	0.00242/-0.00242	0.00351/-0.00351	0.00351/-0.00351
PDF no. 27	0.0164/-0.0164	0.0015/-0.0115	0.00997/-0.00997	0.00816/-0.00816	0.00466/-0.00466	0.00399/-0.00399	0.00399/-0.00399
PDF no. 28	0.0407/-0.0407	0.0191/-0.0191	0.00698/-0.00698	0.000532/-0.000532	0.00196/-0.00196	0.0053/-0.0053	0.0053/-0.0053
PDF no. 29	0.0191/-0.0191	0.00104/-0.0104	0.00138/-0.00138	0.000632/-0.000632	0.00417/-0.00417	0.0127/-0.0127	0.0127/-0.0127

Table 73: Relative effect of each systematic uncertainty (post-fit) on the yields in the CR $Z + \gamma$ for the left-handed $t\gamma$ coupling using data in all regions (II).

Signal ($t\gamma$, LH)	$e \rightarrow \gamma$ fake	$j \rightarrow \gamma$ fake	$Z \gamma + \text{jets}$	$W \gamma + \text{jets}$	other prompt γ
μ_R, μ_F (single top)	0/0	0.000119/-0.000119	0.000102/-0.000102	0/0	0/0
μ_R, μ_F ($W + \text{jets}$)	0/0	0/0	0/0	0/0	0/0
μ_R, μ_F ($Z + \text{jets}$)	0/0	0.0138/-0.0138	0.16/-0.154	0/0	0/0
μ_R, μ_F (diboson)	0/0	0.0473/-0.00473	0.019/-0.0019	0/0	0/0
$\sigma^{\text{theory}}(t\bar{t})$	0/0	0.00105/-0.00105	0.00202/-0.00202	0/0	0/0
$\sigma^{\text{theory}}(\text{single top})$	0/0	0.000187/-0.000187	6.85e-05/-6.83e-05	0/0	0/0
$\sigma^{\text{theory}}(\text{W} + \text{jets})$	0/0	0/0	0/0	0/0	0/0
$\sigma^{\text{theory}}(\text{Z} + \text{jets})$	0/0	0.000905/-0.000905	0.047/-0.047	0/0	0/0
$\sigma^{\text{theory}}(\text{diboson})$	0/0	0.0571/-0.0572	0.000652/-0.000652	0/0	0/0
JES η interc. modelling	0/0	0.000223/-0.000223	0.000659/-0.000699	9.58e-05/-9.57e-05	0/0
JES η interc. non-closure high- E_T	0/0	0/0	0/0	0/0	0/0
JES η interc. non-closure $\eta < 0$	0/0	3.71e-06/3.71e-06	1.13e-05/1.13e-05	8.75e-06/8.75e-06	0/0
JES η interc. total $\eta > 0$	0/0	9.92e-08/9.92e-08	2.54e-05/2.54e-05	9.14e-07/9.14e-07	0/0
JES η interc. total stat.	0.000449/-0.000449	0.000147/-0.000147	2.99e-05/2.99e-05	2.02e-05/2.02e-05	0/0
JES effective NP stat. 1	5.72e-05/5.72e-05	3.17e-05/3.17e-05	3.32e-05/3.32e-05	4.01e-05/4.02e-05	7.02e-05/-7.01e-05
JES effective NP stat. 2	0.000349/-0.000349	0.000131/-0.000131	4.71e-07/4.71e-07	7.15e-06/7.15e-06	8.92e-06/8.92e-06
JES effective NP stat. 3	0/0	9.32e-06/9.32e-06	8.13e-07/8.13e-07	6.92e-06/6.92e-06	1.05e-05/1.05e-05
JES effective NP stat. 4	0/0	1.05e-05/1.05e-05	5.57e-07/5.57e-07	7.89e-06/7.89e-06	6.28e-06/6.28e-06
JES effective NP stat. 5	0/0	1.3e-06/1.3e-06	1.13e-06/1.13e-06	0/0	1.05e-05/1.05e-05
JES effective NP stat. 6	5.22e-05/5.22e-05	3.28e-05/3.28e-05	4.28e-06/4.21e-06	1.86e-05/1.86e-05	2.86e-05/-2.86e-05
JES effective NP mixed 1	0.000349/-0.000349	1.36e-05/1.37e-05	2.05e-06/2.08e-06	1.11e-05/-1.1e-05	1.76e-05/-1.75e-05
JES effective NP mixed 2	0.000349/-0.000349	3.78e-05/-3.79e-05	6.08e-05/-6.08e-05	2.16e-05/-2.16e-05	2.62e-05/-2.62e-05
JES effective NP mixed 3	0/0	1e-05/1e-05	4.71e-07/4.71e-07	1.03e-07/1.03e-07	7.55e-06/7.55e-06
JES effective NP modelling 1	0.00269/-0.00269	0.000361/-0.000361	0.00282/-0.00282	0.00249/-0.00249	0/0
JES effective NP modelling 2	5.22e-05/5.22e-05	9.8e-05/9.8e-05	6.7e-05/6.7e-05	6.99e-05/6.99e-05	7.15e-05/7.15e-05
JES effective NP modelling 3	0.000349/-0.000349	3.28e-05/3.28e-05	7.34e-05/7.33e-05	1.73e-05/1.73e-05	8.47e-05/-8.45e-05
JES effective NP modelling 4	0/0	5.61e-06/5.61e-06	3.36e-07/3.36e-07	2.99e-06/2.99e-06	4.77e-06/4.77e-06
JES pile-up offset μ	0.00201/-0.00201	0.000287/-0.000287	0.000246/-0.000247	0.000119/-0.000119	0/0
JES pile-up offset NPV	0.00203/-0.00203	0.000335/-0.000335	0.0026/-0.0026	5.15e-05/5.14e-05	0/0
JES pile-up p_T term	0.000348/-0.000348	4.51e-05/-4.51e-05	9.38e-05/-9.37e-05	1.67e-05/-1.67e-05	1.85e-05/-1.83e-05
JES pile-up ρ topology	0.00373/-0.00373	0.000365/-0.000365	0.00279/-0.00279	0.000184/-0.000184	0.00042/-0.00042
b -JES response	0.000195/-0.000195	7.34e-05/7.33e-05	1.73e-05/1.73e-05	0/0	0/0
JES flavour composition (CR $Z + \gamma$)	0.00434/-0.00434	0.00447/0.00447	0.00281/0.00281	0.00396/0.00396	0.00646/0.00646
JES flavour response (CR $Z + \gamma$)	0.00276/0.00276	0.00038/0.00038	0.00307/0.00307	0.00228/0.00228	0.00221/0.00221
JES effective NP detector 1	0.000351/0.000351	3.23e-05/3.23e-05	3.05e-05/3.05e-05	1.9e-05/1.9e-05	2.39e-05/2.39e-05
JES effective NP detector 2	0/0	1.63e-06/1.63e-06	4.57e-06/4.37e-05	2.76e-06/2.76e-06	2.91e-06/2.91e-06
JES single particle high- p_T	0/0	0/0	0/0	0/0	0/0
JES punch through	0/0	9.92e-08/9.92e-08	0/0	1.23e-07/1.23e-07	2.33e-07/2.33e-07
JER data vs. MC	0.00574/-0.00574	0.000251/-0.000251	0.000498/-0.000498	-0.00351/0.00351	0.00185/-0.00184
JER effective NP 1	-0.00368/0.00368	-0.00144/0.00144	-0.00164/0.00164	-0.00245/0.00245	-0.00035/0.00035
JER effective NP 2	-0.00376/0.00376	-4.44e-05/-4.45e-05	0.00123/-0.00123	-0.00236/0.00236	-0.000287/0.000287
JER effective NP 3	-0.003842/0.003843	0.000109/-0.000109	0.000892/-0.000892	-0.00354/0.00354	-0.000313/0.000313
JER effective NP 4	-0.003936/0.003936	-0.000147/0.000147	-0.000865/0.000865	-0.00111/0.00111	-0.000352/0.000352
JER effective NP 5	8.57e-05/-8.56e-05	0.000394/0.000394	-2.15e-05/2.15e-05	0.000333/0.000334	-0.000164/0.000164
JER effective NP 6	-0.00401/0.00401	0.000183/-0.000183	-0.000218/0.000218	6.04e-05/6.06e-05	-0.00029/0.00029
JER effective NP 7 (rest term)	-0.00383/0.00383	-0.000218/0.000218	-0.000869/0.000869	-0.000145/0.000145	-0.000267/0.000267
P_T^γ reweighting ($Z + \gamma$ -jets)	0/0	0/0	0.618/-0.448	0/0	0/0
P_T^γ reweighting ($Z + \gamma$ -jets)	0/0	0/0	0/0	6.61e-08/-6.01e-09	0/0
P_T^γ reweighting ($W + \gamma$ -jets)	0/0	0/0	0/0	0.116e-05/-0.114e-05	0/0
μ_R, μ_F ($W + \gamma$ -jets)	0/0	0/0	0/0	-5.18e-08/-3.3e-08	0/0
normalisation: $W + \gamma$ -jets, HF	0/0	0/0	0/0	0.303/-0.309	0/0
μ_R, μ_F ($t\bar{t} + \gamma$)	0/0	0/0	0/0	8.47e-08/1.88e-08	0/0
$\sigma^{\text{theory}}(t\bar{t} + \gamma)$	0/0	0/0	0/0	0/0	0.00454/0.00454
y CR $Z + \gamma$ bin 0	0.146/0.146	0.348/0.348	0.738/0.738	0.149/0.149	0.637/-0.0637
y CR $Z + \gamma$ bin 1	0.269/0.269	0.272/0.272	0.158/0.158	0.352/0.352	0.515/0.515
y CR $Z + \gamma$ bin 2	0.136/0.136	0.146/0.146	0.0293/0.0293	0.0605/0.0605	0.101/0.101
y CR $Z + \gamma$ bin 3	1.16e-06/1.16e-06	0.0826/0.0826	0.0161/0.0161	0.0289/0.0289	0.0561/0.0561
y CR $Z + \gamma$ bin 4	0.449/0.449	0.151/0.151	0.0578/0.0578	0.0476/0.0476	0.141/0.141
SF($Z + \gamma$ -jets)	0/0	0/0	0/0	0.127/-0.127	0/0
SF($W + \gamma$ -jets)	0/0	0/0	0/0	0.0859/-0.0859	0/0

Table 74: Relative effect of each systematic uncertainty (post-fit) on the yields in the SR for $\text{N} \neq \text{T}$ binning using different $\ell\ell$ regions (1).

	Signal ($t\bar{t}$, RH)	$e \rightarrow \gamma$ fake	$j \rightarrow \gamma$ fake	Z+jjets	W+jjets	other prompt
Luminosity	0.0196/-0.0196	0.0196/-0.0196	0.0196/-0.0196	0.0/-0.0	0.0/-0.0	0.0196/-0.0196
Pile-up	0.0167/-0.0167	0.0193/-0.0193	0.0633/-0.0632	0.0305/-0.0304	0.0189/-0.0189	0.0222/-0.0222
JVT	0.00223/-0.00223	0.00044/-0.00044	0.00187/-0.00187	0.000757/-0.000757	0.000779/-0.000779	0.00215/-0.00215
$Sf(e \rightarrow \gamma)$	0.0/-0.0	-0.0329/(0.0331)	-0.133/-0.137	0.0/-0.0	0.0/-0.0	0.0/-0.0
Shower generator ($t\bar{t}$)	0.0/-0.0	-0.0341/(0.0341)	0.0426/-0.0425	0.0/-0.0	0.0/-0.0	0.0/-0.0
ME generator (single top)	0.0/-0.0	-0.00685/-0.00685	-0.00211/-0.00211	0.0/-0.0	0.0/-0.0	-0.0806/-0.0805
TW DS scheme	0.0/-0.0	0.00513/-0.00513	-0.144/-0.144	0.0/-0.0	0.0/-0.0	0.171/-0.157
$Sf(\text{photon ID})$	0.00631/-0.00631	0.0121/-0.0121	0.0131/-0.0131	0.0116/-0.0116	0.0115/-0.0115	-0.138/-0.138
$Sf(\text{photon iso})$	0.01097/-0.01097	0.0154/-0.0154	0.0149/-0.0149	0.0152/-0.0152	0.0143/-0.0143	0.0142/-0.0142
$Sf(\text{electron trigger})$	0.00103/-0.00103	0.00158/-0.00158	0.00126/-0.00126	0.000825/-0.000825	0.00107/-0.00107	0.00111/-0.00111
$Sf(\text{electron reco.})$	0.000526/-0.000526	0.000739/-0.000739	0.000635/-0.000635	0.000398/-0.000398	0.000476/-0.000476	0.000542/-0.000542
$Sf(\text{electron ID})$	0.00361/-0.00361	0.00527/-0.00527	0.00484/-0.00484	0.00256/-0.00256	0.00344/-0.00344	0.0039/-0.0039
$Sf(\text{electron iso.})$	0.000626/-0.000626	0.000648/-0.000648	0.000491/-0.000491	0.000348/-0.000348	0.00044/-0.00044	0.000475/-0.000475
$Sf(\text{muon trigger stat.})$	0.000891/-0.000891	0.000521/-0.000521	0.00134/-0.00134	0.00123/-0.00123	0.00084/-0.00084	0.000857/-0.000857
$Sf(\text{muon trigger syst.})$	0.000333/-0.000333	0.00199/-0.00199	0.00357/-0.00357	0.00373/-0.00373	0.003/-0.003	0.00327/-0.00327
$Sf(\text{muon ID stat.})$	0.000253/-0.000253	0.000163/-0.000163	0.00027/-0.00027	0.000331/-0.000331	0.000269/-0.000269	0.000267/-0.000267
$Sf(\text{muon ID syst.})$	0.00144/-0.00144	0.000926/-0.000926	0.000172/-0.000172	0.000175/-0.000175	0.000147/-0.000147	0.00146/-0.00146
$Sf(\text{muon iso. stat.})$	0.00014/-0.00014	8.87e-05/-8.87e-05	0.000127/-0.000127	0.00699/-0.00699	0.00313/-0.00313	0.00042/-0.00042
$Sf(\text{muon iso. syst.})$	0.00116/-0.00116	0.000707/-0.000707	0.000108/-0.000108	0.000153/-0.000153	0.00021/-0.00021	0.00115/-0.00115
$Sf(\text{muon TTVA stat.})$	0.000111/-0.000111	6.67e-05/-6.67e-05	0.0013/-0.00111	0.00013/-0.00013	0.000108/-0.000108	0.000109/-0.000109
$Sf(\text{muon TTVA syst.})$	4.84e-05/-4.84e-05	2.71e-05/-2.71e-05	5.4e-05/-5.4e-05	4.5e-05/-4.5e-05	5.28e-05/-5.28e-05	4.89e-05/-4.89e-05
EGamma resolution all	0.00956/-0.00956	0.00841/-0.00841	0.0135/-0.0135	0.0133/-0.0133	0.00875/-0.00875	0.00431/-0.00431
EGamma scale all	0.0159/-0.0159	0.00971/-0.00971	0.0196/-0.0196	0.0125/-0.0125	0.00651/-0.00651	0.00641/-0.00641
Muon ID	0.00382/-0.00382	0.00936/-0.00936	0.00367/-0.00367	0.00699/-0.00699	0.00313/-0.00313	0.00681/-0.00681
Muon MS	0.00332/-0.00332	0.00103/-0.00103	0.00219/-0.00219	0.00651/-0.00651	0.00431/-0.00431	0.00543/-0.00543
Muon sagitta biasias	0.00229/-0.00229	0.000602/-0.000602	0.00217/-0.00217	0.00447/-0.00447	0.000988/-0.000988	0.000988/-0.000988
Muon sagitta ρ	0.00365/-0.00365	0.00194/-0.00194	0.0059/-0.0059	0.00755/-0.00755	0.0118/-0.0118	0.00218/-0.00218
Muon scale	0.000942/-0.000942	0.000692/-0.000692	0.00237/-0.00237	0.00431/-0.0043	0.00237/-0.00237	0.000793/-0.000793
ISR ($t\bar{t}$)	0.0/-0.0	0.0142/-0.0142	0.018/-0.018	0.0/-0.0	0.0/-0.0	0.0/-0.0
FSR ($t\bar{t}$)	0.0/-0.0	0.0173/-0.0173	0.0431/-0.0431	0.0/-0.0	0.0/-0.0	0.00134/-0.00134
ISR (single top)	0.0/-0.0	0.00193/-0.00193	0.0101/-0.0101	0.0/-0.0	0.0/-0.0	0.0192/-0.0192
FSR (single top)	0.0/-0.0	0.00541/-0.00541	0.0397/-0.0397	0.0/-0.0	0.0/-0.0	0.00406/-0.00406
PDF no. 1	0.00933/-0.00933	0.00105/-0.00105	0.00115/-0.00115	0.00147/-0.00147	0.000904/-0.000904	0.00058/-0.00058
PDF no. 2	0.00495/-0.00495	0.00169/-0.00169	0.00237/-0.00237	0.00449/-0.00449	0.00158/-0.00158	0.00268/-0.00268
PDF no. 3	0.0119/-0.0119	0.0159/-0.0159	0.00145/-0.00145	0.00884/-0.00884	0.00699/-0.00699	0.00378/-0.00378
PDF no. 4	0.00337/-0.00337	0.00335/-0.00335	0.00377/-0.00377	0.00378/-0.00378	0.00251/-0.00251	0.00363/-0.00363
PDF no. 5	0.00847/-0.00847	0.00107/-0.00107	0.000663/-0.000663	0.000983/-0.000983	0.006648/-0.006648	0.00334/-0.00334
PDF no. 6	0.00961/-0.00961	0.00137/-0.00137	0.00185/-0.00185	0.000249/-0.000249	0.00427/-0.00426	0.00602/-0.00602
PDF no. 7	0.0104/-0.0104	0.00211/-0.00211	0.00215/-0.00215	0.00862/-0.00862	0.00645/-0.00645	0.00521/-0.00521
PDF no. 8	0.0102/-0.0102	0.000797/-0.000797	0.00105/-0.00105	0.00274/-0.00274	0.000662/-0.000662	0.00377/-0.00377
PDF no. 9	0.00431/-0.00431	0.003572/-0.003572	0.00356/-0.00356	0.002771/-0.002771	0.000633/-0.000633	0.0013/-0.0013
PDF no. 10	0.0113/-0.0113	0.00176/-0.00176	0.00213/-0.00213	0.000524/-0.000524	0.000923/-0.000923	0.00497/-0.00497
PDF no. 11	0.00195/-0.00195	0.000784/-0.000784	0.00104/-0.00104	0.00209/-0.00209	0.00984/-0.00984	0.00118/-0.00118
PDF no. 12	0.0127/-0.0127	0.00153/-0.00153	0.00129/-0.00129	0.00167/-0.00167	0.00289/-0.00289	0.00662/-0.00662
PDF no. 13	0.0112/-0.0112	0.00214/-0.00214	0.00156/-0.00156	0.00271/-0.00271	0.000803/-0.000804	0.00521/-0.00521
PDF no. 14	0.00782/-0.00781	0.000887/-0.000887	0.00118/-0.00118	0.00141/-0.00141	0.000283/-0.000283	0.00288/-0.00288
PDF no. 15	0.0109/-0.0109	0.000443/-0.000443	0.00674/-0.00674	0.001671/-0.001671	0.000277/-0.000277	0.004471/-0.004471
PDF no. 16	0.00673/-0.00673	0.00124/-0.00124	0.000748/-0.000748	0.00133/-0.00133	0.000923/-0.000923	0.00374/-0.00374
PDF no. 17	0.0167/-0.0167	0.00316/-0.00316	0.00219/-0.00219	0.006151/-0.006151	0.0024/-0.0024	0.00862/-0.00862
PDF no. 18	0.0127/-0.0127	0.00797/-0.00798	0.00104/-0.00104	0.000921/-0.000921	0.003371/-0.003371	0.00167/-0.00167
PDF no. 19	0.000916/-0.000916	0.00155/-0.00155	0.00162/-0.00162	0.000902/-0.000902	0.000479/-0.000479	0.00129/-0.00129
PDF no. 20	0.00947/-0.00947	0.00141/-0.00141	0.0006351/-0.0006351	0.000662/-0.000662	0.000222/-0.000222	0.00384/-0.00384
PDF no. 21	0.00904/-0.00904	0.000443/-0.000443	0.00149/-0.00149	0.000959/-0.000959	0.000277/-0.000277	0.00386/-0.00386
PDF no. 22	0.00757/-0.00757	0.00146/-0.00146	0.000996/-0.000996	0.00177/-0.00177	0.000353/-0.000353	0.00438/-0.00438
PDF no. 23	0.0116/-0.0116	0.00168/-0.00168	0.00166/-0.00166	0.000339/-0.000339	0.006644/-0.006644	0.00589/-0.00589
PDF no. 24	0.0124/-0.0124	0.00166/-0.00166	0.00102/-0.00102	0.00151/-0.00151	0.0014/-0.0014	0.00338/-0.00338
PDF no. 25	0.00805/-0.00805	0.00178/-0.00178	0.00134/-0.00134	0.00318/-0.00318	0.000743/-0.000743	0.002884/-0.002884
PDF no. 26	0.00901/-0.00901	0.00174/-0.00174	0.00136/-0.00136	0.00347/-0.00347	0.00104/-0.00104	0.004489/-0.004489
PDF no. 27	0.0104/-0.0104	0.00173/-0.00173	0.00117/-0.00117	0.0004101/-0.0004101	0.00126/-0.00126	0.00471/-0.00471
PDF no. 28	0.0132/-0.0132	0.00476/-0.00476	0.00294/-0.00294	0.00137/-0.00137	0.00217/-0.00217	0.0084/-0.0084
PDF no. 29	0.0105/-0.0105	0.000799/-0.000799	0.00128/-0.00128	0.000681/-0.000681	0.00214/-0.00214	0.00472/-0.00472
PDF no. 30	0.0199/-0.0199	0.00544/-0.00544	0.00129/-0.00129	0.000201/-0.000201	0.000405/-0.000405	0.0099/-0.0099
μ_R , μ_F (single top)	0.0/-0.0	0.00327/-0.00327	0.0139/-0.0139	0.0/-0.0	0.0/-0.0	0.00882/-0.00882
μ_R , μ_F (W+jets)	0.0/-0.0	0.00126/-0.00126	0.0171/-0.0166	0.0/-0.0	0.0/-0.0	0.0/-0.0
μ_R , μ_F (Z +jets)	0.0/-0.0	0.0864/-0.0825	0.0295/-0.0295	0.0/-0.0	0.0/-0.0	0.00528/-0.00528
μ_R , μ_F (diboson)	0.0/-0.0	0.00672/-0.00672	0.00247/-0.00247	0.0/-0.0	0.0/-0.0	0.0005172/-0.0005172
$\sigma^{\text{theory}}(t\bar{t})$	0.0/-0.0	0.03/-0.03	0.033/-0.033	0.0/-0.0	0.0/-0.0	0.0118/-0.0118
$\sigma^{\text{theory}}(\text{single top})$	0.0/-0.0	0.00544/-0.00544	0.00129/-0.00129	0.0/-0.0	0.0/-0.0	0.00882/-0.00882
$\sigma^{\text{theory}}(\text{W jets})$	0.0/-0.0	4.49e-05/-4.48e-05	0.00164/-0.00164	0.0/-0.0	0.0/-0.0	0.0/-0.0
$\sigma^{\text{theory}}(\text{Z jets})$	0.0/-0.0	0.0181/-0.0181	0.00163/-0.00163	0.0/-0.0	0.0/-0.0	0.000172/-0.000172
E_T^{miss} soft-term reso. para.	-0.002589/-0.002589	-0.0168/-0.0168	-0.00605/-0.00605	-0.0349/-0.0348	-0.00459/-0.00459	-0.00203/-0.00203
E_T^{miss} soft-term reso. perp.	-0.00494/-0.00494	-0.0311/-0.0311	-0.013/-0.013	-0.0016/-0.0016	-0.0016/-0.0016	-0.000171/-0.000171
E_T^{miss} soft-term scale	0.00817/-0.00817	0.000817/-0.000817	0.00587/-0.00587	0.00616/-0.00616	0.00276/-0.00276	

Table 75: Relative effect of each systematic uncertainty (post-fit) on the yields in the SR for the right-handed $t\bar{t}$ -coupling using data in all regions (II).

Signal ($t\gamma\gamma$, RH)	$e \rightarrow \gamma$ fake		$j \rightarrow \gamma$ fake		$\text{Not reviewed}_{W+\gamma+\text{jets}}$		$\text{Not reviewed}_{W+\gamma+\text{jets}}$	
	on/off	in/out	on/off	in/out	on/off	in/out	on/off	in/out
Heavy flavour fraction ($W+\text{jets}$)	0/0	-0.00105 / 0.00105	0.0925 / -0.0926	0/0	0/0	0/0	0/0	0/0
Heavy flavour fraction ($Z+\text{jets}$)	0/0	-0.00809 / -0.00805	-0.0581 / 0.0607	0/0	0/0	0/0	0/0	0/0
Heavy flavour fraction (diboson)	0/0	-0.000138 / 0.000138	0.000455 / 0.000455	0.00147 / -0.0147	0.0174 / -0.0174	0.0081 / -0.0081	0.012 / -0.012	0.000184 / -0.000184
$SF(b\text{-tag eigenvar. B1})$	0.0106 / -0.0106	0.0129 / -0.0129	0.00149 / 0.00149	0.00156 / 0.00156	0.00129 / 0.00129	0.00881 / -0.00881	0.00167 / -0.00167	0.00113 / -0.0113
$SF(b\text{-tag eigenvar. B2})$	0.0105 / -0.0105	0.0103 / -0.0103	0.0116 / -0.0116	0.00827 / 0.00827	0.00449 / -0.00449	0.00149 / -0.00149	0.000584 / -0.000584	0.00112 / -0.00112
$SF(b\text{-tag eigenvar. B3})$	0.0149 / 0.00149	0.001 / 0.001	0.00101 / 0.00101	0.00228 / 0.00228	0.000412 / 0.000412	0.00112 / 0.00112	0.00112 / 0.00112	0.000584 / -0.000584
$SF(b\text{-tag eigenvar. B4})$	0.00105 / 0.00105	0.000817 / 0.000817	0.000107 / 0.00107	0.000202 / 0.00217	0.00012 / 0.00102	4.32e-05 / 4.32e-05	0.000154 / -0.000154	0.000154 / -0.000154
$SF(b\text{-tag eigenvar. B5})$	0.00105 / 0.00105	0.000161 / 0.000161	0.000217 / 0.000217	0.000147 / 0.00147	0.00016 / -0.0016	1.03e-05 / 1.03e-05	1.51e-05 / 1.51e-05	0.000154 / -0.000154
$SF(b\text{-tag eigenvar. B6})$	0.000249 / 0.000249	2.7e-05 / 2.7e-05	2.32e-05 / 2.32e-05	4.98e-05 / 4.98e-05	2.3e-05 / 2.3e-05	0.00024 / 0.00024	0.00024 / 0.00024	0.000154 / -0.000154
$SF(b\text{-tag eigenvar. B7})$	5.61e-06 / 5.61e-06	3.96e-06 / 3.96e-06	7.71e-06 / 7.71e-06	1.02e-05 / 1.02e-05	2.31e-06 / 2.31e-06	5.15e-06 / 5.15e-06	5.15e-06 / 5.15e-06	0.000154 / -0.000154
$SF(b\text{-tag eigenvar. B8})$	8.46e-07 / 8.46e-07	6.5e-07 / 6.5e-07	6.5e-07 / 6.5e-07	2.7e-06 / 2.7e-06	5.75e-07 / 5.75e-07	4.54e-07 / 4.54e-07	4.54e-07 / 4.54e-07	0.000154 / -0.000154
$SF(b\text{-tag eigenvar. B9})$	0.00186 / -0.00186	0.00545 / -0.00545	0.00222 / -0.00222	0.0175 / -0.0175	0.00627 / -0.00627	0.0327 / -0.0327	0.000245 / -0.000245	0.000245 / -0.000245
$SF(b\text{-tag eigenvar. C1})$	0.0036 / -0.0036	0.002 / -0.002	0.00131 / -0.00131	0.000622 / -0.000622	0.000987 / -0.000987	0.0238 / -0.0238	0.00029 / -0.000289	0.00029 / -0.000289
$SF(b\text{-tag eigenvar. C2})$	0.00112 / 0.00112	0.000622 / 0.000622	0.00227 / -0.00227	0.0216 / -0.0217	0.0455 / -0.0456	0.0475 / -0.0476	9.08e-05 / 9.08e-05	9.08e-05 / 9.08e-05
$SF(b\text{-tag eigenvar. C3})$	0.000249 / 0.000249	2.26e-07 / -2.18e-07	0.00227 / -0.00227	0.00293 / -0.00293	0.0358 / -0.00358	0.00226 / -0.00226	1.46e-05 / 1.46e-05	1.46e-05 / 1.46e-05
$SF(b\text{-tag eigenvar. light 1})$	2.54e-08 / 2.54e-08	0.00258 / 0.00258	0.00105 / 0.00105	0.000931 / 0.000931	0.00119 / 0.00119	0.00141 / 0.00141	3.17e-05 / 3.17e-05	3.17e-05 / 3.17e-05
$SF(b\text{-tag eigenvar. light 2})$	2.54e-08 / 2.54e-08	0.00384 / 0.00384	0.000686 / 0.000686	1.41e-05 / 1.41e-05	3.26e-06 / 3.26e-06	1.16e-05 / 1.16e-05	1.16e-05 / 1.16e-05	1.16e-05 / 1.16e-05
$SF(b\text{-tag eigenvar. light 3})$	2.54e-08 / 2.54e-08	1.95e-05 / 1.95e-05	1.53e-05 / 1.53e-05	0.00104 / 0.00104	0.00234 / 0.00234	0.00162 / 0.00162	1.26e-05 / 1.26e-05	1.26e-05 / 1.26e-05
$SF(b\text{-tag eigenvar. light 4})$	2.54e-08 / 2.54e-08	1.95e-05 / 1.95e-05	1.53e-05 / 1.53e-05	0.00101 / -0.0101	0.0262 / -0.0262	0.00273 / -0.00273	0.0108 / -0.0108	0.00162 / 0.00162
$SF(b\text{-tag extrapolation})$	3.85e-05 / 3.85e-05	0.00258 / 0.00258	0.00101 / -0.0101	3.87e-07 / -2.82e-07	0/0	0.000175 / 0.000175	-6.72e-08 / -3.95e-09	-6.72e-08 / -3.95e-09
$SF(b\text{-tag extrapolation, from charm})$	0.0135 / -0.0135	0.0135 / -0.0135	0.0135 / -0.0135	0.000723 / 0.000723	0.000104 / 0.000104	0.000842 / 0.000842	0.000768 / 0.000768	0.000768 / 0.000768
JES η interc. modelling	1.34e-07 / -1.01e-07	3.87e-07 / -2.82e-07	0/0	0.000104 / 0.000104	0.000416 / 0.000416	0.000432 / 0.000432	0.000183 / 0.000183	0.000183 / 0.000183
JES η interc. non-closure $\eta < 0$	0.00167 / 0.00167	0.000795 / 0.000795	0.000387 / -0.00387	0.00077 / -0.0077	0.000708 / 0.000708	0.0039 / -0.0039	0.00319 / -0.00319	0.00319 / -0.00319
JES η interc. non-closure $\eta > 0$	9.71e-05 / 9.71e-05	0.000547 / -0.00547	0.000149 / 0.00149	0.000149 / 0.00149	0.000172 / 0.000172	0.000188 / 0.000188	0.0012 / 0.0012	0.0012 / 0.0012
JES effective NP stat. 1	0.000376 / 0.000376	0.000258 / 0.000258	0.000225 / 0.000225	0.000973 / 0.000973	0.000708 / 0.000708	0.00156 / 0.00156	0.00248 / 0.00248	0.00248 / 0.00248
JES effective NP stat. 2	0.000161 / 0.00161	0.000161 / 0.00161	0.000151 / 0.00151	0.000151 / 0.00151	0.000339 / 0.000339	0.000125 / 0.000125	0.000512 / 0.000512	0.000512 / 0.000512
JES effective NP stat. 3	0.00111 / 0.00111	0.000973 / 0.000973	0.000105 / 0.000105	0.000821 / 0.000821	0.000219 / 0.000219	0.000112 / 0.000112	0.000252 / 0.000252	0.000252 / 0.000252
JES effective NP stat. 4	0.00251 / 0.00251	0.00108 / 0.00108	0.00346 / 0.00346	0.00503 / 0.00503	0.00183 / 0.00183	0.000534 / 0.000534	0.000344 / 0.000344	0.000344 / 0.000344
JES effective NP stat. 5	0.00167 / 0.00167	0.000795 / 0.000795	0.000824 / 0.000824	0.000297 / 0.000297	0.000349 / 0.000349	0.00145 / 0.00145	0.000237 / 0.000237	0.000237 / 0.000237
JES effective NP stat. 6	0.00143 / 0.00143	0.000839 / 0.000839	0.000103 / 0.00103	0.000308 / 0.000308	0.000879 / 0.000879	0.000291 / 0.000291	0.000291 / 0.000291	0.000291 / 0.000291
JES effective NP mixed 1	0.00485 / 0.00485	0.000859 / 0.000859	0.000514 / 0.000514	0.000221 / 0.000221	0.000655 / 0.000655	0.000204 / 0.000204	0.000512 / 0.000512	0.000512 / 0.000512
JES effective NP mixed 2	0.00485 / 0.00485	0.000225 / 0.000225	0.000225 / 0.000225	0.000389 / 0.000389	0.003444 / 0.003444	0.000275 / 0.000275	0.00129 / 0.00129	0.00129 / 0.00129
JES effective NP mixed 3	0.000575 / 0.000575	0.0139 / -0.0139	0.0129 / -0.0129	0.0237 / -0.0237	0.0132 / -0.0132	0.00778 / -0.00778	0.0111 / -0.0111	0.000252 / 0.000252
JES pile-up ρ modelling 1	0.0277 / -0.0277	0.00444 / -0.00444	0.00422 / -0.00422	0.0113 / -0.0113	0.00303 / -0.00303	0.0013 / -0.0013	0.0244 / -0.0244	0.0244 / -0.0244
JES pile-up ρ topology	0.0277 / -0.0277	0.0026 / 0.0026	0.00505 / 0.00505	0.00397 / 0.00397	0.00397 / 0.00397	0.00344 / 0.00344	0.00344 / 0.00344	0.00344 / 0.00344
b-JES response	0.00351 / 0.00351	0.0184 / 0.00184	0.00193 / 0.00193	0.000349 / 0.000349	0.000349 / 0.000349	0.00145 / 0.00145	0.00131 / 0.00131	0.00131 / 0.00131
JES flavour composition (SR)	0.00656 / 0.00656	0.000859 / 0.000859	0.000889 / 0.000889	0.000221 / 0.000221	0.000655 / 0.000655	0.000662 / 0.000662	0.00769 / -0.00769	0.00769 / -0.00769
JES effective NP modelling 4	0.00875 / -0.00875	0.006056 / -0.006056	0.00351 / -0.00351	0.0154 / -0.0154	0.0154 / -0.0154	0.034 / -0.034	0.0157 / -0.0157	0.0157 / -0.0157
JES pile-up offset μ	0.0212 / -0.0212	0.0128 / -0.0128	0.0128 / -0.0128	0.0351 / -0.0351	0.0155 / -0.0155	0.0113 / -0.0113	0.0157 / -0.0157	0.0157 / -0.0157
JES pile-up offset NP	0.00575 / 0.00575	0.000259 / 0.000259	0.00166 / 0.00166	0.00538 / 0.00538	0.00298 / 0.00298	0.00218 / 0.00218	0.00095 / 0.00095	0.00095 / 0.00095
JES effective NP modelling 1	0.000798 / 0.000798	0.000768 / 0.000768	0.000938 / 0.000938	0.000221 / 0.000221	0.000403 / 0.000403	7.21e-05 / 7.21e-05	0.000225 / 0.000225	0.000225 / 0.000225
JES single particle high- p_T	2.54e-08 / 2.54e-08	4e-07 / 4e-07	9.77e-06 / 9.77e-06	0/0	0.00182 / 0.00182	0.00152 / 0.00152	5.44e-05 / 5.44e-05	5.44e-05 / 5.44e-05
JES punch through	0/0	0.0247 / -0.0247	0.0285 / -0.0285	0.0207 / -0.0207	0.0276 / -0.0276	-0.00933 / 0.00933	0.00899 / -0.00899	0.00899 / -0.00899
JER effective NP 1	0.0123 / -0.0123	0.0171 / -0.0171	0.0207 / -0.0207	0.0168 / -0.0168	0.0168 / -0.0168	0.00444 / 0.00444	0.00926 / 0.00926	0.00926 / 0.00926
JER effective NP 2	0.0122 / -0.0122	0.0116 / -0.0116	0.0184 / -0.0184	0.00962 / -0.00962	0.00585 / -0.00585	-0.00444 / 0.00444	0.00495 / -0.00495	0.00495 / -0.00495
JER effective NP 3	0.0051 / -0.0051	0.00751 / -0.00751	0.0076 / -0.0076	0.012 / -0.012	0.0157 / -0.0157	0.00444 / 0.00444	0.00381 / 0.00381	0.00381 / 0.00381
JER effective NP 4	0.00116 / -0.00116	0.000499 / -0.000498	0.00324 / -0.00324	0.0166 / -0.0166	0.0137 / 0.0138	-0.00069 / 0.00069	0.00474 / -0.00474	0.00474 / -0.00474
JER effective NP 5	0.00292 / -0.00292	0.00142 / -0.00142	0.00646 / -0.00646	0.0119 / -0.0119	0.0142 / -0.0142	0.00286 / -0.00286	0.000229 / 0.000229	0.000229 / 0.000229
JER effective NP 6	0.00062 / -0.00062	0.00213 / -0.00213	0.00651 / -0.00651	-0.000345 / 0.000345	0.00184 / -0.00184	0.00344 / -0.00344	0.000344 / -0.000344	0.000344 / -0.000344
JER effective NP 7 (rest term)	0.00353 / -0.00353	0/0	0.921 / -0.921	0.921 / -0.921	0/0	0/0	0/0	0/0
$SF(j \rightarrow \gamma)$	0/0	0/0	0/0	0/0	0/0	0/0	0/0	0/0
P_T^Y reweighting ($Z\gamma\gamma$ -jets)	0/0	0/0	0/0	0/0	1.28e-05	-1.28e-05	0/0	0/0
μ_R, μ_F ($t\bar{t} \rightarrow \gamma$ -jets)	0/0	0/0	0/0	0/0	0/0	0/0	0/0	0/0
Heavy flavour fraction ($Z\gamma\gamma$ -jets)	0.00188 / -0.00188	0.0011 / -0.011	0.0113 / -0.0113	0.0157 / -0.0157	0.0157 / -0.0157	0.0113 / 0.00113	0/0	0/0
P_T^Y reweighting ($W\gamma\gamma$ -jets)	0/0	0/0	0/0	0/0	0/0	0/0	0/0	0/0
μ_R, μ_F ($W\gamma\gamma$ -jets)	0.00191 / -0.00191	0.00363 / -0.00363	0.00186 / -0.00186	0.0012 / -0.0012	0.000569 / -0.000569	0.000501 / 0.000501	0.00501 / 0.00501	0.00501 / 0.00501
$\sigma^{\text{theory}}(t\bar{t} \rightarrow \gamma)$	0.00361 / -0.00361	0.00381 / -0.00381	0.00381 / -0.00381	0.00151 / -0.00151	0.000975 / -0.000975	0.00576 / -0.00576	0.00576 / -0.00576	0.00576 / -0.00576
γ SR bin 0	0.00269 / 0.00269	0.00028 / 0.00028	0.00168 / 0.00168	0.00212 / -0.00212	0.00121 / -0.00121	0.0137 / -0.0137	0.0137 / -0.0137	0.0137 / -0.0137
γ SR bin 1	0.00321 / -0.00321	0.00142 / -0.0						

Table 76: Relative effect of each systematic uncertainty (post-fit) on the yields in the CR $W+\gamma+jets$ using data+all regions (I).

	Signal ($t\bar{c}$, RH)	$e \rightarrow \gamma$ fake	$j \rightarrow \gamma$ fake	$Z \rightarrow \gamma$ jets	$W \rightarrow \gamma$ jets	other prompt γ
Luminosity	0.0196/-0.0196	0.0196/-0.0196	0.0196/-0.0196	0.0/0	0.0/0	0.0196/-0.0196
File-up	0.0137/-0.0137	0.0137/-0.0137	0.0441/-0.0444	0.00503/-0.00503	0.0243/-0.0242	0.0204/-0.0204
JVT	0.00115/-0.00115	0.000764/-0.000764	0.00954/-0.00954	0.00049/-0.00049	0.00957/-0.00957	0.00184/-0.00184
SF($e \rightarrow \gamma$)	0/0	0.0893/-0.0851	0/0	0/0	0/0	0/0
Shower generator ($t\bar{t}$)	0/0	-0.0127/-0.0128	-0.0091/-0.00912	0/0	0/0	0/0
ME generator ($t\bar{t}$)	0/0	0.00186/-0.00186	0.00241/-0.00241	0/0	0/0	0/0
Shower generator (single top)	0/0	-0.0031/-0.0031	-0.000906/-0.000906	0/0	0/0	-0.0729/-0.0729
ME generator (single top)	0/0	0.000891/-0.000891	-0.000522/-0.000522	0/0	0/0	0.198/-0.178
TW DS scheme	0/0	-0.000373/-0.000373	-0.000606/-0.000606	0/0	0/0	-0.122/-0.122
SF(photon ID)	0.0064/-0.00664	0.0113/-0.0113	0.014/-0.014	0.0125/-0.0125	0.0117/-0.0117	0.0113/-0.0113
SF(photon iso.)	0.0108/-0.0108	0.0152/-0.0152	0.0052/-0.0052	0.046/-0.046	0.0142/-0.0142	0.014/-0.014
SF(electron trigger)	0.00114/-0.00114	0.00204/-0.00204	0.00119/-0.00119	0.00139/-0.00139	0.00124/-0.00124	0.00121/-0.00121
SF(electron rec.)	0.000642/-0.000642	0.000912/-0.000912	0.000459/-0.000459	0.000576/-0.000576	0.000558/-0.000558	0.000583/-0.000583
SF(electron iso.)	0.00394/-0.00394	-0.0033/-0.0033	0.0043/-0.0043	0.00442/-0.00442	0.00412/-0.00412	0.00412/-0.00412
SF(muon trigger stat.)	0.000769/-0.000769	0.000303/-0.000303	0.0007/-0.0007	0.000787/-0.000787	0.000851/-0.000851	0.000854/-0.000854
SF(muon trigger syst.)	0.000295/-0.000295	0.00115/-0.00115	0.00314/-0.00314	0.00289/-0.00289	0.00316/-0.00316	0.00306/-0.00306
SF(muon ID stat.)	0.000254/-0.000254	9.63e-05/-9.63e-05	0.000246/-0.000246	0.000258/-0.000258	0.000268/-0.000268	0.000257/-0.000257
SF(muon ID syst.)	0.00141/-0.00141	0.000553/-0.000553	0.00139/-0.00139	0.00141/-0.00141	0.00148/-0.00148	0.00147/-0.00147
SF(muon iso. stat.)	0.000139/-0.000139	5.44e-05/-5.44e-05	0.000148/-0.000148	0.000146/-0.000146	0.000146/-0.000146	0.000146/-0.000146
SF(muon iso. syst.)	0.000109/-0.000109	0.00041/-0.00041	0.00119/-0.00119	0.00115/-0.00115	0.00117/-0.00117	0.00114/-0.00114
SF(mun TTVA stat.)	0.000102/-0.000102	3.94e-05/-3.94e-05	0.00011/-0.00011	0.000104/-0.000104	0.000109/-0.000109	0.000106/-0.000106
SF(mun TTVA syst.)	3.90e-05/-3.90e-05	1.67e-05/-1.67e-05	5.68e-05/-5.68e-05	5.21e-05/-5.21e-05	5.07e-05/-5.07e-05	4.61e-05/-4.61e-05
EGamma resolution all	0.00566/-0.00566	0.00273/-0.0273	0.0172/-0.0172	0.00299/-0.00299	0.00114/-0.00114	0.00172/-0.00172
EGamma scale all	0.0122/-0.0122	0.0257/-0.0257	0.0156/-0.0156	0.00809/-0.00809	0.0081/-0.0081	0.0076/-0.0076
Muon ID	0.00333/-0.00333	0.000631/-0.000631	0.0151/-0.0151	0.00751/-0.00751	0.00909/-0.00909	0.00909/-0.00909
Muon MS	0.00261/-0.00261	0.000621/-0.000621	0.00649/-0.00649	0.00206/-0.00206	0.000732/-0.000732	0.00104/-0.00104
Muon sagitta resbias	0.00242/-0.00242	0.000619/-0.000619	0.00231/-0.00231	0.00111/-0.00111	0.000339/-0.000349	0.00278/-0.00278
Muon scale	0.00465/-0.00465	0.000531/-0.000531	0.0104/-0.010524	0.0275/-0.0275	0.00704/-0.00704	0.000946/-0.000945
ISR ($t\bar{t}$)	0/0	0.000251/-0.000251	0.000458/-0.000458	0.000252/-0.000252	0.000923/-0.000923	0.000649/-0.000649
FSR ($t\bar{t}$)	0/0	0.000863/-0.000863	0.00178/-0.00178	0/0	0/0	0/0
ISR (single top)	0/0	0.000856/-0.000855	0.000321/-0.000321	0/0	0/0	0/0
FSR (singl top)	0/0	0.000564/-0.000563	0.00176/-0.00176	0/0	0/0	0.00302/-0.00302
PDF no. 1	0.00851/-0.0085	0.000783/-0.000783	0.0412/-0.0412	0.00131/-0.0013	0.00129/-0.0129	0.00509/-0.00509
PDF no. 2	0.00442/-0.00442	0.00371/-0.00371	0.12/-0.119	0.00113/-0.00113	0.00114/-0.00114	0.00114/-0.00114
PDF no. 3	0.00971/-0.00971	0.00473/-0.00473	0.0451/-0.0451	0.0007/-0.007	0.00273/-0.00273	0.00314/-0.00314
PDF no. 4	0.02571/-0.02571	0.00371/-0.00371	0.0805/-0.0804	0.0016/-0.0016	0.00141/-0.00141	0.00495/-0.00495
PDF no. 5	0.00771/-0.00771	0.0238/-0.0238	0.11/-0.11	0.000779/-0.000779	0.00481/-0.00481	0.00552/-0.00552
PDF no. 6	0.00878/-0.00878	0.00108/-0.00108	0.0664/-0.0663	0.000162/-0.000162	0.00392/-0.00392	0.00552/-0.00552
PDF no. 7	0.0104/-0.0104	0.000527/-0.000527	0.0244/-0.0244	0.000272/-0.000272	0.00629/-0.00629	0.00629/-0.00629
PDF no. 8	0.0088/-0.0088	0.000335/-0.000336	0.0431/-0.0433	0.000365/-0.000365	0.00167/-0.00167	0.00451/-0.00451
PDF no. 9	0.003531/-0.003533	0.00113/-0.00113	0.06555/-0.06554	0.0031/-0.0031	0.0021/-0.0021	0.00587/-0.00587
PDF no. 10	0.0102/-0.0102	0.0021/-0.0021	0.0711/-0.0711	0.0022/-0.0022	0.0061/-0.0061	0.00109/-0.00109
PDF no. 11	0.00108/-0.00108	0.00161/-0.00161	0.0941/-0.0938	0.00194/-0.00194	0.00412/-0.00412	0.00966/-0.00966
PDF no. 12	0.00658/-0.00658	0.00316/-0.00316	0.103/-0.102	2.21e-05/-2.23e-05	0.00694/-0.00694	0.00481/-0.00481
PDF no. 13	0.00241/-0.00241	0.00073/-0.00073	0.0281/-0.0283	0.000127/-0.000127	0.0046/-0.0046	0.000444/-0.000444
PDF no. 14	0.00124/-0.00124	0.00124/-0.00124	0.0834/-0.0839	0.00107/-0.00107	0.00518/-0.00518	0.00455/-0.00455
PDF no. 15	0.00973/-0.00973	0.000898/-0.000898	0.0575/-0.0575	0.000262/-0.000262	0.00399/-0.00399	0.00587/-0.00587
PDF no. 16	0.000582/-0.000582	0.000582/-0.000582	0.05555/-0.05555	0.000568/-0.000568	0.004051/-0.0040405	0.004051/-0.0040405
PDF no. 17	0.0161/-0.0161	0.00256/-0.00255	0.0727/-0.0727	0.00187/-0.00187	0.00714/-0.00714	0.00966/-0.00966
PDF no. 18	0.0118/-0.0118	0.00167/-0.00167	0.0824/-0.0823	0.000127/-0.000127	0.00744/-0.00744	0.00668/-0.00668
PDF no. 19	0.00103/-0.00103	0.013/-0.013	0.0645/-0.0645	0.000101/-0.000101	0.000453/-0.000453	0.000444/-0.000444
PDF no. 20	0.00836/-0.00836	0.00164/-0.00164	0.0661/-0.0666	0.000459/-0.000459	0.00041/-0.00041	0.000335/-0.000335
PDF no. 21	0.00723/-0.00723	0.000376/-0.000377	0.0629/-0.0628	0.000109/-0.000109	0.00315/-0.00315	0.00502/-0.00502
PDF no. 22	0.0096/-0.0096	0.002/-0.002	0.0958/-0.0957	0.000329/-0.000328	0.0041/-0.0041	0.00615/-0.00615
PDF no. 23	0.0134/-0.0134	0.00736/-0.00736	0.0792/-0.0791	0.000725/-0.000724	0.00333/-0.00333	0.00523/-0.00523
PDF no. 24	0.0116/-0.0116	0.00145/-0.00145	0.0655/-0.0649	0.000405/-0.000405	0.00388/-0.00388	0.00668/-0.00668
PDF no. 25	0.00742/-0.00742	0.00101/-0.00101	0.0745/-0.0744	0.000836/-0.000835	0.00414/-0.00414	0.00449/-0.00449
PDF no. 26	0.00798/-0.00798	0.000961/-0.000961	0.0802/-0.0808	0.00157/-0.00157	0.00455/-0.00455	0.00535/-0.00535
PDF no. 27	0.0096/-0.0096	0.002/-0.002	0.0802/-0.0802	0.000329/-0.000328	0.0041/-0.0041	0.00615/-0.00615
PDF no. 28	0.0134/-0.0134	0.00578/-0.00578	0.0688/-0.0687	0.00987/-0.00987	0.00111/-0.00111	0.00674/-0.00674
PDF no. 29	0.00953/-0.00952	0.00152/-0.00152	0.0707/-0.0706	0.00109/-0.00109	0.00378/-0.00378	0.00575/-0.00575
PDF no. 30	0.0186/-0.0186	0.00129/-0.00129	0.0661/-0.0666	0.000579/-0.000579	0.00288/-0.00288	0.00103/-0.00103
μ_R , μ_F (single top)	0/0	0.00132/-0.00132	0.0302/-0.0286	0/0	0/0	0.00698/-0.00698
μ_R , μ_F ($W+jets$)	0/0	0.00827/-0.00827	0.0146/-0.0147	0/0	0/0	0/0
μ_R , μ_F ($Z+jets$)	0/0	0.13/-0.121	0.0416/-0.0407	0/0	0/0	0/0
μ_R , μ_F (diboson)	0/0	0.00543/-0.00543	0.0121/-0.0121	0/0	0/0	0/0
$\sigma_{\text{theory}}(t\bar{t})$	0/0	0.00199/-0.00199	0.00194/-0.00194	0/0	0/0	0/0
$\sigma_{\text{theory}}(W+jets)$	0/0	0.00228/-0.00228	0.00664/-0.00664	0/0	0/0	0.00118/-0.00118
$\sigma_{\text{theory}}(Z+jets)$	0/0	7.78e-05/-7.8e-05	0.0423/-0.0423	0/0	0/0	0/0
$\sigma_{\text{theory}}(diboson)$	0/0	0.0327/-0.0327	0.00465/-0.00465	0/0	0/0	0/0
$\sigma_{\text{theory}}(W+jets)$	0/0	0.00048/-0.00048	0.000528/-0.000528	0/0	0/0	0.00598/-0.00598

Table 77: Relative effect of each systematic uncertainty (post-fit) on the yields in the CR $W+\gamma+jets$ coupling using data in all regions (II). Not reviewed, for internal circulation only

Signal ($t\gamma$, RH)	$e \rightarrow \gamma$ fake	$j \rightarrow \gamma$ fake	$Z+\gamma+jets$	$W+\gamma+jets$	other prompt γ
E_T^{miss} soft-term reso. para.	-0.0027 / 0.0027	-0.0352 / 0.0351	0.0078 / -0.0078	-0.0417 / 0.0416	-0.00508 / 0.00507
E_T^{miss} soft-term reso. perp.	-0.00158 / 0.00158	-0.032 / 0.032	-0.0113 / 0.0113	-0.0317 / 0.0316	-0.00277 / 0.00277
E_T^{miss} soft-term scale	0.00485 / -0.00485	0.033 / -0.0343	0.0115 / -0.0115	0.0384 / -0.0384	0.0069 / -0.0069
$SF(b\text{-tag eigenvar. B1})$	0.00454 / -0.00454	0.00557 / -0.00567	0.00749 / -0.00749	0.000355 / -0.000355	0.000132 / -0.000133
$SF(b\text{-tag eigenvar. B2})$	0.00745 / 0.00745	0.000467 / 0.000467	7.51e-05 / 7.51e-05	3.11e-05 / 3.11e-05	1.62e-05 / 1.62e-05
$SF(b\text{-tag eigenvar. B3})$	0.00453 / -0.00453	0.00332 / -0.00332	0.000534 / -0.000534	0.000176 / -0.000176	6.9e-05 / -6.9e-05
$SF(b\text{-tag eigenvar. B4})$	0.00458 / 0.00458	0.00183 / 0.00183	5.5e-05 / 5.5e-05	5.93e-06 / 5.93e-06	0.000366 / 0.000366
$SF(b\text{-tag eigenvar. B5})$	0.000437 / 0.000437	0.000339 / 0.000339	3.43e-05 / 3.43e-05	1.98e-05 / 1.98e-05	1.05e-06 / 1.05e-06
$SF(b\text{-tag eigenvar. B6})$	0.000102 / 0.00102	6.47e-05 / 6.47e-05	1.09e-05 / 1.09e-05	1.12e-05 / 1.12e-05	1.16e-06 / 1.16e-06
$SF(b\text{-tag eigenvar. B7})$	8.24e-06 / 8.24e-06	1.03e-05 / 1.03e-05	9.14e-07 / 9.14e-07	6.26e-06 / 6.26e-06	9.32e-08 / 9.32e-08
$SF(b\text{-tag eigenvar. B8})$	2.52e-06 / 2.52e-06	1.36e-06 / 1.36e-06	8.42e-07 / 8.42e-07	6.86e-07 / 6.86e-07	3.48e-06 / 3.48e-06
$SF(b\text{-tag eigenvar. B9})$	3.39e-07 / 3.39e-07	1.56e-07 / 1.56e-07	1.07e-07 / 1.07e-07	1.15e-07 / 1.15e-07	2.42e-09 / -2.42e-09
$SF(b\text{-tag eigenvar. C1})$	0.00114 / -0.00114	0.00024 / -0.00024	0.000146 / -0.000146	0.000251 / -0.000251	0.000163 / -0.000163
$SF(b\text{-tag eigenvar. C2})$	0.00163 / -0.00163	0.000149 / -0.000149	8.97e-05 / -8.99e-05	0.00016 / -0.00016	0.000359 / -0.000359
$SF(b\text{-tag eigenvar. C3})$	0.000484 / 0.00484	5.07e-05 / 5.07e-05	1.94e-05 / 1.94e-05	5.97e-05 / 5.97e-05	5.84e-05 / 5.84e-05
$SF(b\text{-tag eigenvar. light 1})$	0.000116 / -0.000116	0.000421 / -0.000421	0.000439 / -0.000439	0.000437 / -0.000437	0.000263 / -0.000263
$SF(b\text{-tag eigenvar. light 2})$	6.98e-06 / 6.98e-06	2.91e-05 / 2.91e-05	4.77e-05 / 4.77e-05	3.72e-05 / 3.72e-05	1.06e-05 / 1.06e-05
$SF(b\text{-tag eigenvar. light 3})$	1.56e-06 / 1.56e-06	8.44e-06 / 8.44e-06	1.11e-05 / 1.11e-05	4.16e-06 / 4.16e-06	3.61e-06 / 3.61e-06
$SF(b\text{-tag eigenvar. light 4})$	1.57e-06 / 1.57e-06	4.38e-06 / 4.38e-06	7.06e-06 / 7.06e-06	6.48e-06 / 6.48e-06	5.18e-06 / 5.18e-06
$SF(b\text{-tag extrapolation})$	2.08e-05 / 2.08e-05	6.15e-06 / 6.15e-06	5.37e-06 / 5.37e-06	2.63e-06 / 2.63e-06	1.29e-05 / 1.29e-05
$SF(b\text{-tag extrap. from charm})$	1.17e-07 / 1.17e-07	2.2e-06 / 2.2e-06	2.96e-06 / 2.96e-06	4.33e-05 / 4.33e-05	2.42e-09 / -2.42e-09
JES η interc. modelling	0.0136 / -0.0136	0.0206 / -0.0245	0.0206 / -0.0206	0.0115 / -0.0115	0.00886 / -0.00886
JES η interc. non-closure high- E_T	0 / 0	1.26e-05 / -1.25e-05	2.48e-09 / -8.68e-09	6.67e-06 / -6.74e-06	8.35e-07 / -8.36e-07
JES η interc. non-closure $\eta < 0$	0.000869 / 0.000869	0.000597 / 0.000597	0.00204 / 0.00204	0.000765 / 0.000765	0.00141 / 0.00141
JES η interc. non-closure $\eta > 0$	0.00386 / 0.00386	0.000509 / 0.000243	0.000221 / 0.000221	0.00264 / 0.000264	0.000374 / 0.000374
JES η interc. total stat.	0.000509 / -0.000509	0.00053 / -0.00093	0.000876 / -0.000876	0.000375 / -0.000375	0.000939 / -0.000939
JES effective NP stat. 1	0.00139 / 0.00139	0.00354 / 0.00354	0.00243 / 0.00243	0.00125 / 0.00125	0.000337 / 0.000337
JES effective NP stat. 2	0.00042 / 0.0042	0.000841 / 0.000838	0.00691 / 0.00691	0.000248 / 0.000248	0.000628 / 0.000628
JES effective NP stat. 3	0.000864 / 0.000864	0.000841 / 0.000841	0.00167 / 0.00167	0.00076 / 0.00076	0.000202 / 0.000202
JES effective NP stat. 4	0.00132 / 0.00132	0.00294 / 0.00294	0.0018 / 0.0018	0.000844 / 0.000844	0.000248 / 0.000248
JES effective NP stat. 5	0.000982 / 0.000982	0.00144 / 0.00144	0.00192 / 0.00192	0.0006 / 0.0006	0.000739 / 0.000739
JES effective NP stat. 6	0.000928 / 0.000928	0.0016 / 0.0016	0.00211 / 0.00211	0.0007 / 0.0007	0.000269 / 0.000269
JES effective NP mixed 1	0.00199 / 0.00199	0.00563 / 0.00563	0.00183 / 0.00183	0.00167 / 0.00167	0.000529 / 0.000529
JES effective NP mixed 2	0.00212 / 0.00212	0.00154 / 0.00154	0.00447 / 0.00447	0.000616 / 0.000616	0.00112 / 0.00112
JES effective NP mixed 3	0.00102 / 0.00102	0.00184 / 0.00184	0.000541 / 0.000541	0.000634 / 0.000634	0.000364 / 0.000364
JES effective NP modelling 1	0.0255 / -0.0255	0.0313 / -0.0313	0.0267 / -0.0259	0.0152 / -0.0152	0.025 / -0.025
JES effective NP modelling 2	0.0281 / 0.0281	0.00607 / 0.00607	0.00461 / 0.00461	0.00512 / 0.00512	0.0062 / 0.0062
JES effective NP modelling 3	0.00194 / 0.00194	0.00539 / 0.00539	0.00271 / 0.00271	0.00123 / 0.00123	0.00393 / 0.00393
JES effective NP modelling 4	0.00733 / 0.00733	0.00654 / 0.00654	0.00201 / 0.00201	0.000487 / 0.000487	0.000332 / 0.000332
JES pile-up offset μ	0.0108 / -0.0108	0.0189 / 0.0189	0.0239 / -0.0239	0.0102 / -0.0102	0.00203 / -0.00203
JES pile-up offset NPV	0.00369 / -0.00369	0.00859 / -0.00859	0.00841 / -0.00841	0.00925 / -0.00925	0.00137 / 0.00137
JES pile-up PT term	0.0007 / 0.0007	0.00067 / 0.00067	0.00375 / -0.00375	0.000607 / -0.000607	0.00067 / -0.00067
JES pile-up ρ topology	0.0257 / -0.0256	0.0311 / -0.0311	0.0295 / -0.0295	0.0114 / -0.0114	0.0244 / -0.0244
b -JES response	0.0146 / -0.0146	0.0044 / -0.0044	0.025 / -0.025	0.00867 / -0.00867	0.0013 / -0.0013
JES flavour composition (CR $W+\gamma+jet$)	0.0291 / -0.0291	0.0423 / -0.0423	0.0407 / -0.0407	0.0308 / -0.0308	0.0704 / -0.0704
JES flavour response (CR $W+\gamma+jet$)	0.0154 / -0.0154	0.0291 / -0.0291	0.0303 / -0.0303	0.0174 / 0.0174	0.00362 / 0.00362
JES effective NP detector 1	0.0017 / 0.0017	0.00607 / 0.00607	0.00381 / 0.00381	0.00163 / 0.00163	8.89e-05 / 8.89e-05
JES effective NP detector 2	0.000414 / 0.000414	0.000496 / 0.000496	0.000356 / 0.000356	0.000356 / 0.000356	0.000251 / 0.000251
JES single particle high- p_T	0 / 0	2.86e-05 / 2.86e-05	0 / 0	0 / 0	0 / 0
JES punch through	0 / 0	7.12e-05 / 7.12e-05	2.37e-07 / 2.37e-07	6.29e-06 / 6.29e-06	2.22e-05 / 2.22e-05
JER data vs. MC	0.00995 / -0.00994	0.00176 / -0.00176	0.0277 / -0.0276	0.0136 / -0.0136	-0.00326 / -0.00326
JER effective NP 1	0.0179 / -0.0179	0.021 / -0.021	0.0603 / -0.0603	0.0293 / -0.0293	0.0167 / -0.0167
JER effective NP 2	0.00626 / -0.00626	0.021 / -0.021	0.0484 / -0.0483	0.0254 / -0.0253	0.00762 / -0.00762
JER effective NP 3	0.000614 / -0.000614	0.00753 / -0.00753	0.0538 / -0.0538	0.0155 / -0.0165	0.00557 / -0.00557
JER effective NP 4	-0.000646 / 0.000646	0.000667 / -0.000667	0.00112 / -0.00112	0.00474 / -0.00474	0.006631 / -0.006631
JER effective NP 5	-0.000764 / 0.000764	0.000884 / -0.000883	-0.000707 / 0.000707	-0.00308 / 0.00308	0.00379 / -0.00378
JER effective NP 6	-0.000607 / 0.000608	8.68e-05 / -8.69e-05	0.00256 / -0.00256	-0.00548 / 0.00548	0.00325 / -0.00325
JER effective NP 7 (rest term)	0.00058 / -0.00058	0.0164 / -0.0164	0.0281 / -0.0281	0.00106 / -0.00106	0.00498 / -0.00498
SF($j \rightarrow \gamma$)	0 / 0	0 / 0	0.921 / -0.46	0 / 0	0 / 0
P_T^γ reweighting ($Z+\gamma+jets$)	0 / 0	0 / 0	0 / 0	6.09e-08 / 1.03e-08	0 / 0
μ_R, μ_F ($Z+\gamma+jets$)	0 / 0	0 / 0	0 / 0	0.0831 / -0.0837	0 / 0
P_T^γ reweighting ($W+\gamma+jets$)	0 / 0	0 / 0	0 / 0	0 / 0	-7.26e-09 / 4.84e-09
μ_R, μ_F ($W+\gamma+jets$)	0 / 0	0 / 0	0 / 0	0 / 0	0 / 0
normalisation: $W+\gamma+jets$, HF	0 / 0	0 / 0	0 / 0	0.0663 / -0.0665	0 / 0
$\sigma_{\text{theory}}(t\bar{t} + \gamma)$	0.31 / 0.31	0.678 / 0.678	0.752 / 0.752	0.756 / 0.756	0.747 / 0.747
γ CR $W+\gamma+jet$ bin 0	0.0983 / 0.0983	0.137 / 0.137	0.0864 / 0.0864	0.0314 / 0.0314	0.123 / 0.123
γ CR $W+\gamma+jet$ bin 1	0.0567 / 0.0567	0.044 / 0.044	0.0399 / 0.0399	0.0234 / 0.0234	0.0263 / 0.0263
γ CR $W+\gamma+jet$ bin 2	0.0502 / 0.0502	0.0332 / 0.0332	0.0384 / 0.0384	0.0177 / 0.0177	0.0272 / 0.0272
γ CR $W+\gamma+jet$ bin 3	0.063 / 0.063	0.036 / 0.036	0.0284 / 0.0284	0.0165 / 0.0165	0.0201 / 0.0201
γ CR $W+\gamma+jet$ bin 4	0.0856 / 0.0856	0.0305 / 0.0305	0.0111 / 0.0111	0.0179 / 0.0179	0.0198 / 0.0198
γ CR $W+\gamma+jet$ bin 5	0.136 / 0.136	0.0273 / 0.0273	0.0124 / 0.0124	0.0127 / 0.0127	0.0174 / 0.0174
γ CR $W+\gamma+jet$ bin 6	0.2 / 0.2	0.0167 / 0.0167	0.031 / 0.031	0.0107 / 0.0107	0.0147 / 0.0147
γ CR $W+\gamma+jet$ bin 7	0 / 0	0 / 0	0 / 0	0 / 0	0 / 0
γ CR $W+\gamma+jets$	0 / 0	0 / 0	0 / 0	0 / 0	0 / 0
$SF(W+\gamma+jets)$	0 / 0	0 / 0	0 / 0	0 / 0	0 / 0
$SF(W+\gamma+jets)$	0 / 0	0 / 0	0 / 0	0 / 0	0 / 0

Not reviewed, for internal circulation only

Table 78: Relative effect of each systematic uncertainty (post-fit) on the yields in the CR $Z + \gamma$ for the right-handed $t\gamma$ coupling using data in all regions (I).

	Signal ($t\gamma$, RH)	$e \rightarrow \gamma$ fake	$j \rightarrow \gamma$ fake	$Z \gamma$ +jets	$W \gamma$ +jets	other prompt γ
Luminosity	0.0196/-0.0196	0.0196/-0.0196	0.0196/-0.0196	0.0/0	0.16/-0.156	0.0196/-0.0196
Pile-up	0.219/-0.219	0.0264/-0.0264	0.0377/-0.0377	0.0351/-0.035	0.00173/-0.00173	0.0262/-0.0261
IVT	0.0026/0.0026	0.00954/0.00954	0.008841/0.008841	0.000585/0.000585	0.0037/0.0037	0.0037/0.0037
SF($e \rightarrow \gamma$)	0/0	0.0893/-0.0851	0/0	0/0	0/0	0/0
Shower generator ($t\bar{t}$)	0/0	-0.0018/-0.00188	-0.007/-0.00702	0/0	0/0	0/0
ME generator ($t\bar{t}$)	0/0	0.0053/-0.0053	0.00514/-0.00514	0/0	0/0	0/0
Shower generator (single top)	0/0	-0.00347/-0.00347	0.00284/-0.00284	0/0	0/0	-0.0335/0.0335
ME generator (single top)	0/0	-0.00201/-0.00201	0.00145/-0.00145	0/0	0/0	-0.0574/-0.0556
TW DS scheme	0/0	-0.00253/-0.00253	0.00142/-0.00142	0/0	0/0	-0.00811/-0.00811
SF(photon ID)	0.0105/-0.0105	0.012/-0.012	0.0152/-0.0152	0.0128/-0.0128	0.0117/-0.0117	0.0109/-0.0109
SF(photon iso.)	0.0152/-0.0152	0.0154/-0.0154	0.0153/-0.0153	0.0148/-0.0148	0.0116/-0.0111	0.0138/-0.0138
SF(electron trigger)	0.000417/0.000417	0.00023/0.00023	0.000242/0.000242	0.000234/0.000234	0.000234/0.000234	0.000152/0.000152
SF(electron reco.)	0.0022/0.0022	0.0013/0.0013	0.000872/0.000872	0.000936/0.000936	0.00145/0.00145	0.00103/0.00103
SF(electron ID)	0.0181/-0.0181	0.00983/-0.00983	0.00749/-0.00749	0.00749/-0.00749	0.0151/-0.0151	0.00736/-0.00736
SF(electron iso.)	0.00287/0.00287	0.0012/0.0012	0.00836/0.00836	0.00077/0.00077	0.00205/0.00205	0.000904/0.000904
SF(muon trigger stat.)	0.000112/0.000112	0.000396/0.000396	0.000444/0.000444	0.000528/0.000528	0.000447/0.000447	0.000519/0.000519
SF(muon trigger syst.)	0.000352/0.000352	0.000871/0.000871	0.00126/0.00126	0.00126/0.00126	0.00119/0.00119	0.000626/0.000626
SF(muon ID stat.)	0.000257/0.000257	0.000453/0.000453	0.000633/0.000633	0.000663/0.000663	0.000558/0.000558	0.000358/0.000358
SF(muon ID syst.)	0.00155/0.00155	0.0027/0.0027	0.00471/0.00471	0.00372/0.00372	0.00182/0.00182	0.00371/0.00371
SF(muon iso. stat.)	0.000171/0.000171	0.000297/0.000297	0.00026/0.00026	0.000336/0.000336	0.00033/0.00033	0.00033/0.00033
SF(muon iso. syst.)	0.00136/0.00136	0.00187/0.00187	0.00254/0.00254	0.00273/0.00273	0.00162/0.00162	0.00254/0.00254
SF(muon TTV stat.)	0.000117/0.000117	0.000178/0.000178	0.000229/0.000229	0.000261/0.000261	0.000128/0.000128	0.000251/0.000251
SF(muon TTV syst.)	7.32e-05/7.32e-05	7.59e-05/7.59e-05	0.000101/0.000101	0.000129/0.000129	6.25e-05/6.25e-05	0.000105/0.000105
EGamma scale all	0.217/-0.217	0.00436/-0.00436	0.0236/-0.0236	0.00178/-0.00178	0.0691/-0.0692	0.0186/-0.0186
EGamma scale all	0.0633/-0.0633	0.00811/-0.00811	0.0278/-0.0278	0.00958/-0.00958	0.0692/-0.0692	0.00406/-0.00406
Muon ID	0/0	0.00819/-0.00819	0.004571/-0.004571	0.00693/-0.00693	0.0361/-0.0361	0.00456/-0.00456
Muon MS	0/0	0.000766/-0.000766	0.009921/-0.009921	0.000746/-0.000746	0.0561/-0.0561	0.000627/-0.000627
Muon sagitta residuals	0/0	0.000517/-0.000517	0.00461/-0.00461	0.000145/-0.000145	0/0	0.000291/-0.000291
Muon sagitta ρ	0/0	0.00119/-0.00119	0.00121/-0.00121	0.000144/-0.000144	0.000199/-0.000199	0.000489/-0.000489
Muon scale	0/0	0.000885/0.000885	0.00182/0.00182	0.00011/0.00011	0/0	0.00063/0.00063
ISR ($t\bar{t}$)	0/0	0.00743/-0.00743	0.00312/-0.00312	0/0	0/0	0/0
FSR (single top)	0/0	0.000152/-0.000152	0.000114/-0.000114	0/0	0/0	0/0
FSR (single top)	0/0	0.00486/-0.00486	0.000165/-0.000165	0/0	0/0	0/0
PDF no. 1	0.0175/-0.0175	0.0329/-0.0329	0.00164/-0.00164	0.00123/-0.00123	0.00192/-0.00192	0.00433/-0.00433
PDF no. 2	0.0058/-0.0058	0.0296/-0.0296	0.00156/-0.00156	0.00173/-0.00173	0.0128/-0.0128	0.00418/-0.00418
PDF no. 3	0.00887/-0.00887	0.00208/-0.00208	0.0073/-0.0073	0.00635/-0.00635	0.0241/-0.0241	0.00345/-0.00345
PDF no. 4	0.00321/-0.00321	0.0144/-0.0144	0.00475/-0.00475	0.00361/-0.0036	0.0143/-0.0143	0.00338/-0.00338
PDF no. 5	0.0152/-0.0152	0.0118/-0.0118	0.00871/-0.00871	0.000807/-0.000807	0.00112/-0.00112	0.00393/-0.00393
PDF no. 6	0.0181/-0.0181	0.00799/-0.00799	0.00039/-0.00039	0.000253/-0.000253	0.00155/-0.00155	0.0047/-0.0047
PDF no. 7	0.0135/-0.0135	0.00694/-0.00694	0.00664/-0.00664	0.00283/-0.00283	0.00772/-0.00772	0.00756/-0.00756
PDF no. 8	0.0132/-0.0132	0.0039/-0.0039	0.00542/-0.00542	0.000706/-0.000706	0.00428/-0.00428	0.00518/-0.00518
PDF no. 9	0.0105/-0.0105	0.00652/-0.00652	0.00478/-0.00478	0.00275/-0.00275	0.0127/-0.0127	0.00383/-0.00383
PDF no. 10	0.0164/-0.0164	0.0116/-0.0116	0.0161/-0.0116	0.00184/-0.00184	0.0046/-0.0046	0.006/-0.006
PDF no. 11	0.00735/-0.00734	0.0184/-0.0184	0.001/-0.001	0.00257/-0.00257	0.0163/-0.0163	0.00155/-0.00155
PDF no. 12	0.0138/-0.0138	0.0185/-0.0185	0.00324/-0.00324	0.000245/-0.000245	0.00401/-0.00401	0.00362/-0.00362
PDF no. 13	0.0212/-0.0212	0.0106/-0.0106	0.00232/-0.00232	0.00172/-0.00172	0.00348/-0.00348	0.00589/-0.00589
PDF no. 14	0.0181/-0.0181	0.00648/-0.00648	0.006551/-0.006551	0.0016/-0.0016	0.0041/-0.0041	0.00313/-0.00313
PDF no. 15	0.0201/-0.0202	0.0161/-0.0161	0.00161/-0.00161	0.00103/-0.00103	0.0046/-0.0046	0.0049/-0.0049
PDF no. 16	0.0225/-0.0225	0.00259/-0.00259	0.000551/-0.000555	0.000537/-0.000537	0.00165/-0.00165	0.00243/-0.00243
PDF no. 17	0.0275/-0.0274	0.01/-0.01	0.00326/-0.00326	0.000301/-0.000301	0.00416/-0.00416	0.0106/-0.0106
PDF no. 18	0.0243/-0.0243	0.0101/-0.0101	0.000449/-0.000448	3.4e-05/-3.4e-05	0.00162/-0.00162	0.00647/-0.00647
PDF no. 19	0.00552/-0.00552	0.00366/-0.00366	0.000799/-0.000799	0.000377/-0.000377	0.00269/-0.00269	0.00314/-0.00314
PDF no. 20	0.0179/-0.0179	0.00851/-0.00851	0.000465/-0.000465	0.000166/-0.000166	0.00583/-0.00583	0.00432/-0.00432
PDF no. 21	0.0173/-0.0173	0.00536/-0.00536	0.00103/-0.00103	0.00126/-0.00126	0.00421/-0.00421	0.00392/-0.00392
PDF no. 22	0.0167/-0.0167	0.00283/-0.00283	0.00191/-0.00191	0.00127/-0.00127	0.00473/-0.00473	0.00405/-0.00405
PDF no. 23	0.0192/-0.0192	0.00846/-0.00846	0.000809/-0.000809	0.000392/-0.000392	0.00573/-0.00573	0.00494/-0.00494
PDF no. 24	0.0186/-0.0186	0.00871/-0.00871	0.00023/-0.00023	0.000505/-0.000505	0.00251/-0.00251	0.00695/-0.00695
PDF no. 25	0.0155/-0.0155	0.0106/-0.0106	0.000753/-0.000753	0.000783/-0.000783	0.00199/-0.00199	0.00368/-0.00368
PDF no. 26	0.0171/-0.0171	0.0142/-0.0142	0.00234/-0.00234	0.00141/-0.00141	0.00384/-0.00384	0.0045/-0.0045
PDF no. 27	0.0187/-0.0187	0.00979/-0.00979	0.000567/-0.000567	0.000301/-0.000301	0.00242/-0.00242	0.00356/-0.00356
PDF no. 28	0.01417/-0.01417	0.0116/-0.0116	0.00101/-0.00101	0.00127/-0.00127	0.00473/-0.00473	0.00783/-0.00783
PDF no. 29	0.0193/-0.0193	0.00703/-0.00703	0.000536/-0.000536	0.00198/-0.00198	0.00534/-0.00534	0.00503/-0.00503
PDF no. 30	0.0208/-0.0208	0.0105/-0.0105	0.00138/-0.00138	0.000636/-0.000636	0.00419/-0.00419	0.0128/-0.0128

Not reviewed, for internal circulation only

Table 79: Relative effect of each systematic uncertainty (post-fit) on the yields in the CR $Z + \gamma$ for the right-handed $t\bar{c}\gamma$ coupling using data in all regions (II).

	Signal ($t\bar{c}\gamma$, RH)	$e \rightarrow \gamma$ fake	$j \rightarrow \gamma$ fake	$Z \gamma + \text{jets}$	$W \gamma + \text{jets}$	other prompt γ
μ_R, μ_F (single top)	0/0	0.000119/-0.000119	0.000102/-0.000102	0/0	0/0	0.00273/-0.00273
μ_R, μ_F (W -jets)	0/0	0/0	0/0	0/0	0/0	0/0
μ_R, μ_F (Z -jets)	0/0	0.014/-0.0139	0.162/-0.15	0/0	0/0	0/0
μ_R, μ_F (diboson)	0/0	0.019/-0.0473	0.019/-0.0119	0/0	0/0	0.00449/-0.0045
$\sigma_{\text{theory}}(t\bar{t})$	0/0	0.00106/-0.000106	0.00203/-0.000203	0/0	0/0	0/0
$\sigma_{\text{theory}}(\text{single top})$	0/0	0.000187/-0.000187	6.84e-05/-6.84e-05	0/0	0/0	0.00386/-0.00386
$\sigma_{\text{theory}}(W\text{-jets})$	0/0	0/0	0/0	0/0	0/0	0/0
$\sigma_{\text{theory}}(Z\text{-jets})$	0/0	0.000903/-0.000904	0.0469/-0.0469	0/0	0/0	0/0
$\sigma_{\text{theory}}(\text{diboson})$	0/0	0.0571/-0.0572	0.00652/-0.000652	0/0	0/0	0.0069/-0.0069
JES η interc. modelling	0/0	0.000302/-0.000302	0.000227/-0.000227	0.000712/-0.000712	9.76e-05/-9.74e-05	0/0
JES η interc. non-close E_T	0/0	0/0	0/0	0/0	0/0	0/0
JES η interc. non-close $\eta < 0$	0/0	3.68e-06/3.68e-06	1.13e-05/1.13e-05	8.75e-06/8.75e-06	0/0	7.98e-06/7.98e-06
JES η interc. non-close $\eta > 0$	0/0	1.04e-07/1.04e-07	0/0	9.13e-07/9.13e-07	0/0	5.41e-07/5.41e-07
JES η interc. total stat.	0/0	0.000147/-0.000147	2.54e-05/-2.55e-05	5.58e-05/-5.59e-05	0/0	5.19e-05/5.19e-05
JES effective NP stat. 1	0/0	3.17e-05/3.17e-05	2.98e-05/2.98e-05	2.02e-05/2.02e-05	0/0	2.32e-05/2.32e-05
JES effective NP stat. 2	0/0	0.000132/0.000132	3.46e-05/3.46e-05	4.04e-05/4.04e-05	0/0	7.07e-05/7.07e-05
JES effective NP stat. 3	0/0	7.1e-06/7.1e-06	4.69e-07/4.69e-07	7.15e-06/7.15e-06	0/0	8.94e-06/8.94e-06
JES effective NP stat. 4	0/0	9.32e-06/9.32e-06	8.36e-07/8.36e-07	6.91e-06/6.91e-06	0/0	1.05e-05/1.05e-05
JES effective NP stat. 5	0/0	1.05e-05/1.05e-05	5.91e-07/5.91e-07	7.89e-06/7.89e-06	0/0	6.32e-06/6.32e-06
JES effective NP stat. 6	0/0	1.19e-05/1.19e-05	1.32e-06/1.32e-06	9.15e-06/9.15e-06	0/0	1.04e-05/1.04e-05
JES effective NP mixed 1	0/0	1.37e-05/1.37e-05	2.14e-06/2.14e-06	1.11e-05/1.11e-05	0/0	1.77e-05/1.77e-05
JES effective NP mixed 2	0/0	3.81e-05/3.81e-05	6.13e-05/6.13e-05	2.18e-05/2.18e-05	0/0	2.64e-05/2.64e-05
JES effective NP mixed 3	0/0	1e-05/1e-05	4.69e-07/4.69e-07	1.03e-05/1.03e-05	0/0	7.53e-06/7.53e-06
JES effective NP modelling 1	0/0	0.000361/-0.000361	0.000282/-0.000282	0.000249/-0.000249	0/0	0.000367/-0.000366
JES effective NP modelling 2	0/0	9.79e-05/9.79e-05	6.72e-05/6.72e-05	7.05e-05/7e-05	0/0	7.15e-05/7.15e-05
JES effective NP modelling 3	0/0	3.22e-05/3.22e-05	3.43e-06/3.43e-06	7.39e-05/-7.38e-05	0/0	2.89e-05/2.89e-05
JES effective NP modelling 4	0/0	5.6e-06/5.6e-06	3.58e-07/3.58e-07	2.99e-06/2.99e-06	0/0	4.77e-06/4.77e-06
JES pile-up offset μ	0/0	0.000292/-0.000292	0.00025/-0.00025	0.00012/-0.000121	0/0	0.000171/-0.000171
JES pile-up offset NPV	0/0	0.000341/-0.000341	0.000264/-0.000264	5.23e-05/-5.24e-05	0/0	0.000219/-0.000219
JES pile-up offset p_T term	0/0	4.53e-05/-4.52e-05	9.41e-05/-9.41e-05	1.68e-05/-1.68e-05	0/0	1.85e-05/-1.84e-05
JES pile-up ρ topology	0/0	0.000367/-0.000367	0.00281/-0.00281	0.000185/-0.000185	0/0	0.000422/-0.000422
b-JES response	0/0	5.83e-05/-5.83e-05	7.39e-05/-7.38e-05	8.52e-05/-8.52e-05	0/0	8.52e-05/8.52e-05
JES flavour composition (CR $Z\gamma\gamma$)	0/0	0.000417/0.000417	0.00281/0.00281	0.000396/0.000396	0.00023/0.00023	0.000646/0.000646
JES flavour response (CR $Z\gamma\gamma$)	0/0	0.000252/0.000252	0.00038/-0.00038	0.000307/0.000307	0.000228/0.000228	0.000221/0.000221
JES effective NP detector 1	0/0	3.23e-05/3.23e-05	3.05e-05/3.05e-05	1.9e-05/1.9e-05	0/0	2.4e-05/2.4e-05
JES effective NP detector 2	0/0	1.65e-06/1.65e-06	4.37e-05/4.37e-05	2.76e-06/2.76e-06	0/0	2.96e-06/2.96e-06
JES single particle high- p_T	0/0	0/0	0/0	0/0	0/0	0/0
JES punch through	0/0	1.04e-07/1.04e-07	0/0	1.23e-07/1.23e-07	0/0	2.29e-07/2.29e-07
JER data vs. MC	0/0	0.000252/-0.000252	0.000499/-0.000499	-2.08e-05/2.08e-05	-0.00352/0.00352	0.000185/-0.000185
JER effective NP 1	-0.00403/0.00403	-0.00015/0.00015	-0.00017/0.00017	-0.000254/0.000254	-0.00314/0.00314	-0.000364/0.000364
JER effective NP 2	-0.00393/0.00393	-4.41e-05/4.41e-05	0.00123/-0.00123	-0.00023/-0.00023	-0.000286/0.000286	-0.000286/0.000286
JER effective NP 3	-0.00868/0.00868	0.00011/-0.00011	0.000898/-0.000898	-0.000357/0.000357	-0.00312/0.00312	-0.00315/0.00315
JER effective NP 4	-0.00401/0.00401	-0.000147/0.000147	-0.000861/0.000861	-0.00011/0.00011	-0.00351/0.00351	-0.00309/0.00309
JER effective NP 5	-0.00398/0.00398	8.48e-05/-8.49e-05	-0.000136/0.000135	-5.97e-05/5.97e-05	-0.00038/-0.00038	-0.000162/0.000162
JER effective NP 6	-0.00402/0.00402	0.00018/-0.00018	-0.000215/0.000215	-0.000089/0.000899	-0.00015/0.00015	-0.000276/0.000276
JER effective NP 7 (test term)	-0.00403/0.00403	-0.000225/0.000226	0.919/-0.459	0/0	-0.00314/0.00314	0/0
$P_\gamma^{\gamma\gamma}$ reweighting ($Z\gamma\gamma$ +jets)	0/0	0/0	0/0	1.8e-08/-1.5e-08	0/0	0/0
$P_\gamma^{\gamma\gamma}$ reweighting ($Z\gamma\gamma$ +jets)	0/0	0/0	0/0	0.0922/-0.0929	0/0	0/0
normalisation: $W\gamma\gamma$	0/0	0/0	0/0	-4.71e-08/3.77e-08	0/0	0/0
μ_R, μ_F ($t\bar{t}\gamma$ +jets)	0/0	0/0	0/0	0/0	0/0	0/0
μ_R, μ_F ($t\bar{t}\gamma$)	0/0	0/0	0/0	9.43e-08/-4.71e-08	0/0	0/0
$\sigma_{\text{theory}}(t\bar{t}\gamma)$	0/0	0/0	0/0	0/0	0.00454/0.00454	0/0
γ CR $Z\gamma\gamma$ bin 0	0.151/0.151	0.348/0.348	0.738/0.738	0.714/0.714	0.49/0.49	0.344/0.344
γ CR $Z\gamma\gamma$ bin 1	0.312/0.312	0.273/0.273	0.158/0.158	0.0293/0.0293	0.0605/0.0605	0.0961/0.0961
γ CR $Z\gamma\gamma$ bin 2	0.131/0.131	0.146/0.146	0.0286/0.0286	0.0161/0.0161	0.0289/0.0289	0.0663/0.0663
γ CR $Z\gamma\gamma$ bin 3	1.19e-06/1.19e-06	0.0826/0.0826	0.0578/0.0578	0.0477/0.0477	0.148/0.148	0.0558/0.0558
SF($Z\gamma\gamma$ +jets)	0/0	0/0	0/0	0.1/-0.1	0/0	0/0
SF($W\gamma\gamma$ +jets)	0/0	0/0	0/0	0.0755/-0.0755	0/0	0/0

1898 Y Studies of a fit when separating the MC uncertainties

1899 The fit is performed when separating all statistical uncertainties of each bin in each region for each
 1900 process from each other in order to track down large pulls on statistical uncertainties of certain bins to a
 1901 single process. Subsequently, in each bin 6 NPs for the statistical uncertainties of the different processes
 1902 considered in the fit are introduced, resulting in $6 \times (8 + 8 + 5) = 126$ NPs. The fit is performed using data
 1903 in all regions. The observed limits on the branching ratio are given in Table 80 that are similar to those
 1904 of the default setup shown in Table 35. In Figures 309, 310, 311, and 312, the pull values representing
 1905 the statistical uncertainties of the bins are shown for the different signal couplings. As the outcomes
 1906 and the limits are compatible with those using the default setup, it is concluded that the default setup is
 1907 sufficient.

Table 80: 95 % C.L. upper limits on the branching ratio $\mathcal{B}(t \rightarrow q\gamma)$ with $q = u, c$ for the different signal couplings when treating each statistical uncertainty of each process in each bin in each region independently.

Signal coupling	tuy , left-handed	tuy , right-handed	$tc\gamma$, left-handed	$tc\gamma$, right-handed
$\mathcal{B}(t \rightarrow q\gamma) [10^{-5}]$	3.2	6.3	20.0	18.1

Not reviewed, for internal circulation only

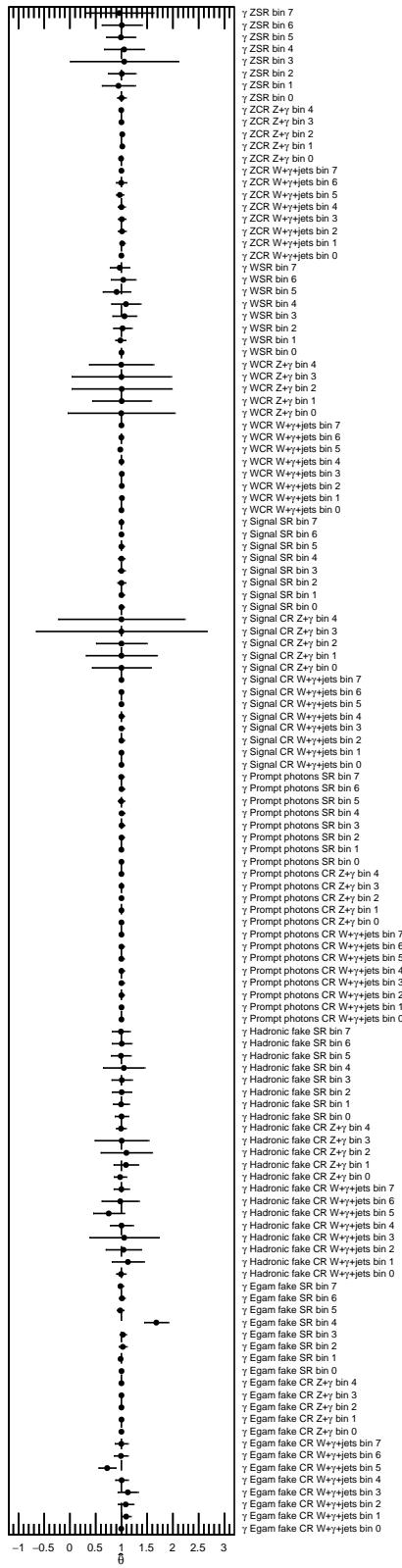


Figure 309: Pull values representing the statistics in each bin in each region for each process for the left-handed tuy coupling using data.

Not reviewed, for internal circulation only

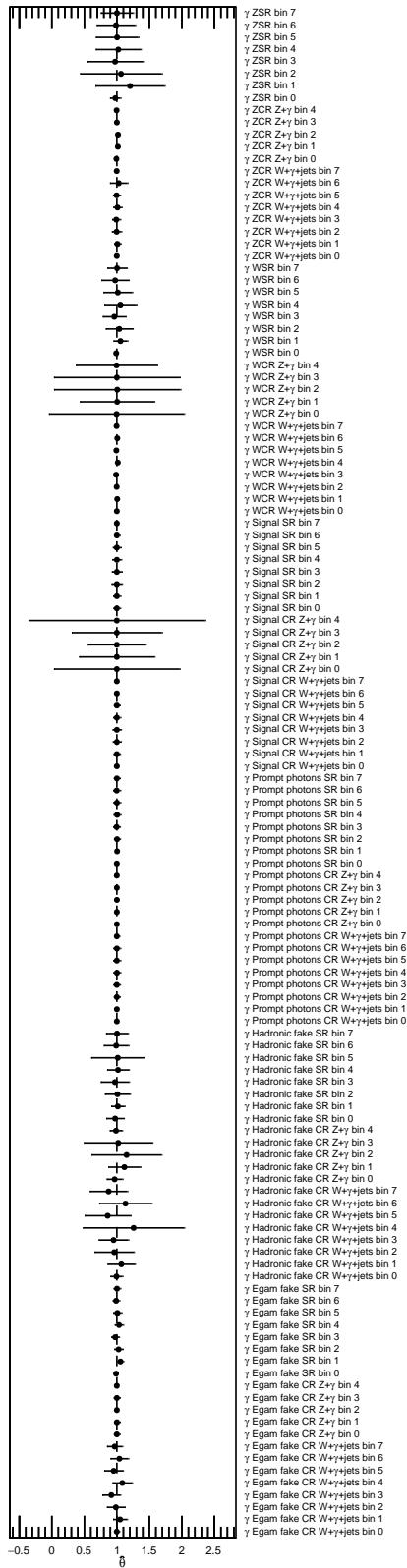


Figure 310: Pull values representing the statistics in each bin in each region for each process for the right-handed $t\bar{u}\gamma$ coupling using data.

Not reviewed, for internal circulation only

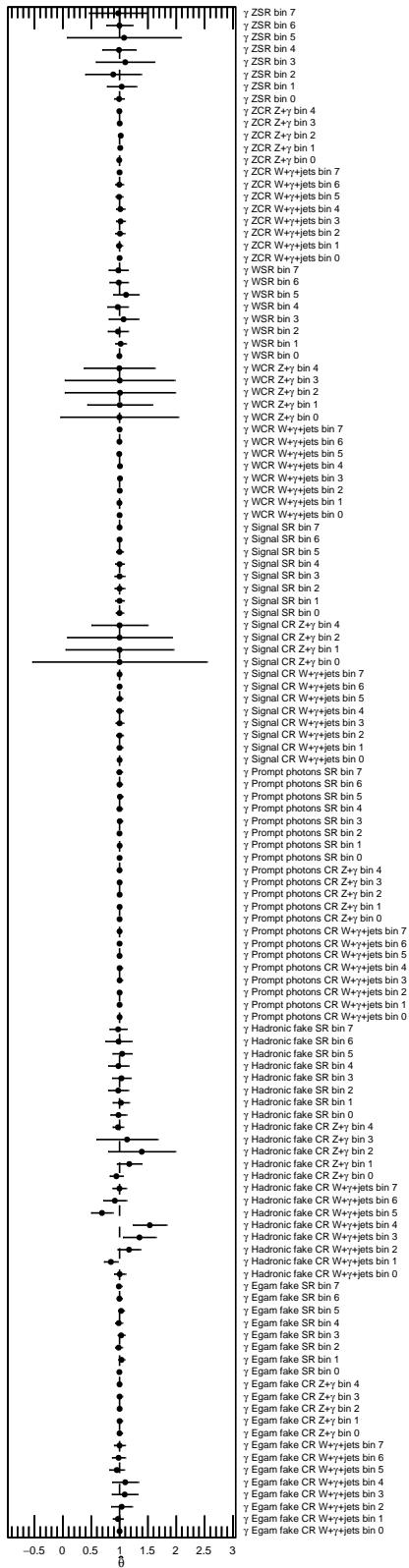


Figure 311: Pull values representing the statistics in each bin in each region for each process for the left-handed $t\gamma\gamma$ coupling using data.

Not reviewed, for internal circulation only

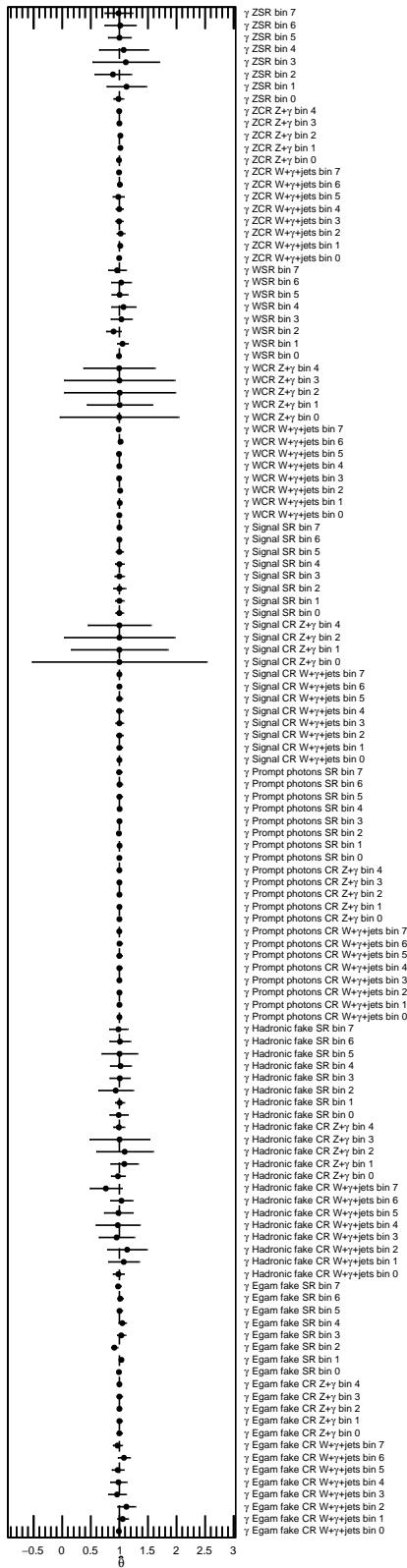


Figure 312: Pull values representing the statistics in each bin in each region for each process for the right-handed $t\gamma\gamma$ coupling using data.

Z Statistical fit for different signal samples using data in all regions

Z.1 Statistical fit using data in all regions for the right-handed $t\bar{u}y$ coupling

Not reviewed, for internal circulation only

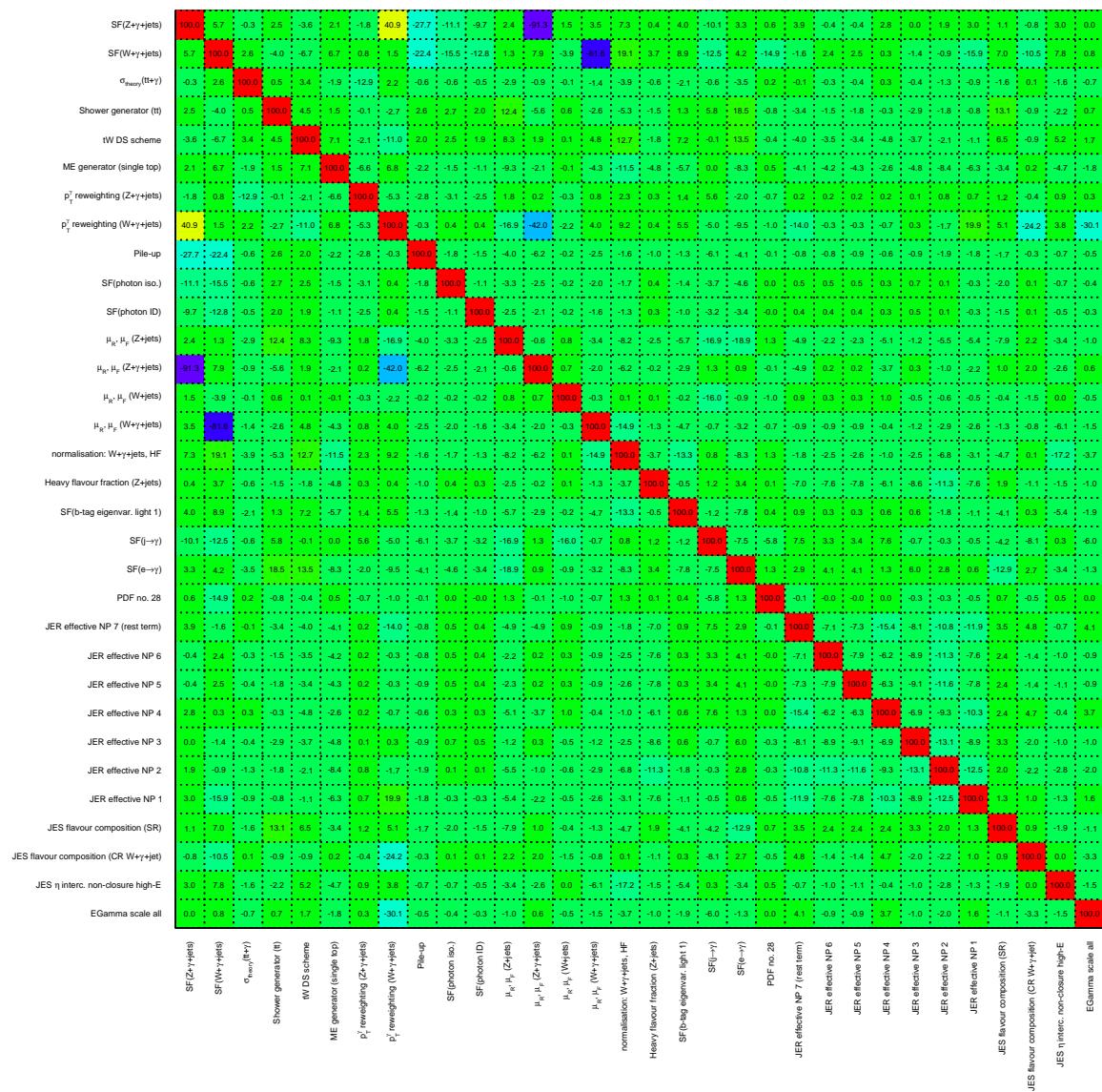


Figure 313: Correlation coefficients of all parameters with at least one coefficient above 10 % for the right-handed *tuy* coupling considered in the fit using data in all regions.

Not reviewed, for internal circulation only

Table 81: Yields for the different contributions in the different regions after the fit for the right-handed $t\gamma\gamma$ coupling. The statistical uncertainty and all systematic uncertainties are included.

Photon origin	SR		CR $W+\gamma+\text{jets}$			CR $Z+\gamma$		
$e \rightarrow \gamma$	4 880	\pm 500	8 400	\pm 1 400	250	\pm 34		
$j \rightarrow \gamma$	340	\pm 230	3 900	\pm 2 600	1 600	\pm 1 100		
$Z+\gamma+\text{jets}$	740	\pm 100	13 200	\pm 1 300	81 200	\pm 2 000		
$W+\gamma+\text{jets}$	1 780	\pm 370	99 800	\pm 3 400	6.0	\pm 1.9		
Other prompt photon	1 790	\pm 390	1 900	\pm 440	2 180	\pm 220		
Total SM	9 540	\pm 220	127 300	\pm 3 700	85 200	\pm 1 600		
Data	9 557		127 864		85 347			

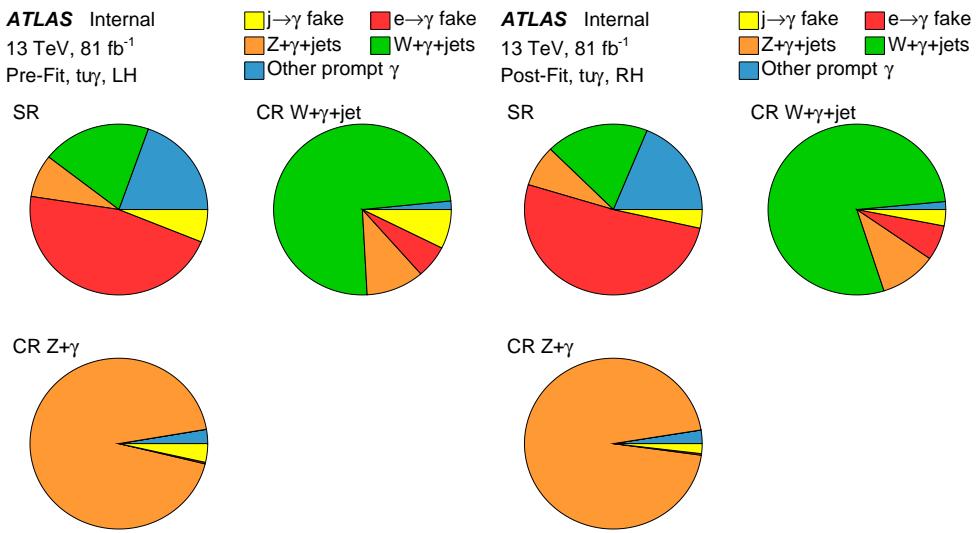


Figure 314: Pie charts showing the composition of the processes before (left) and after the fit using data in all regions (right) in the SR, CR $W+\gamma+\text{jets}$, and CR $Z+\gamma$.

Not reviewed, for internal circulation only

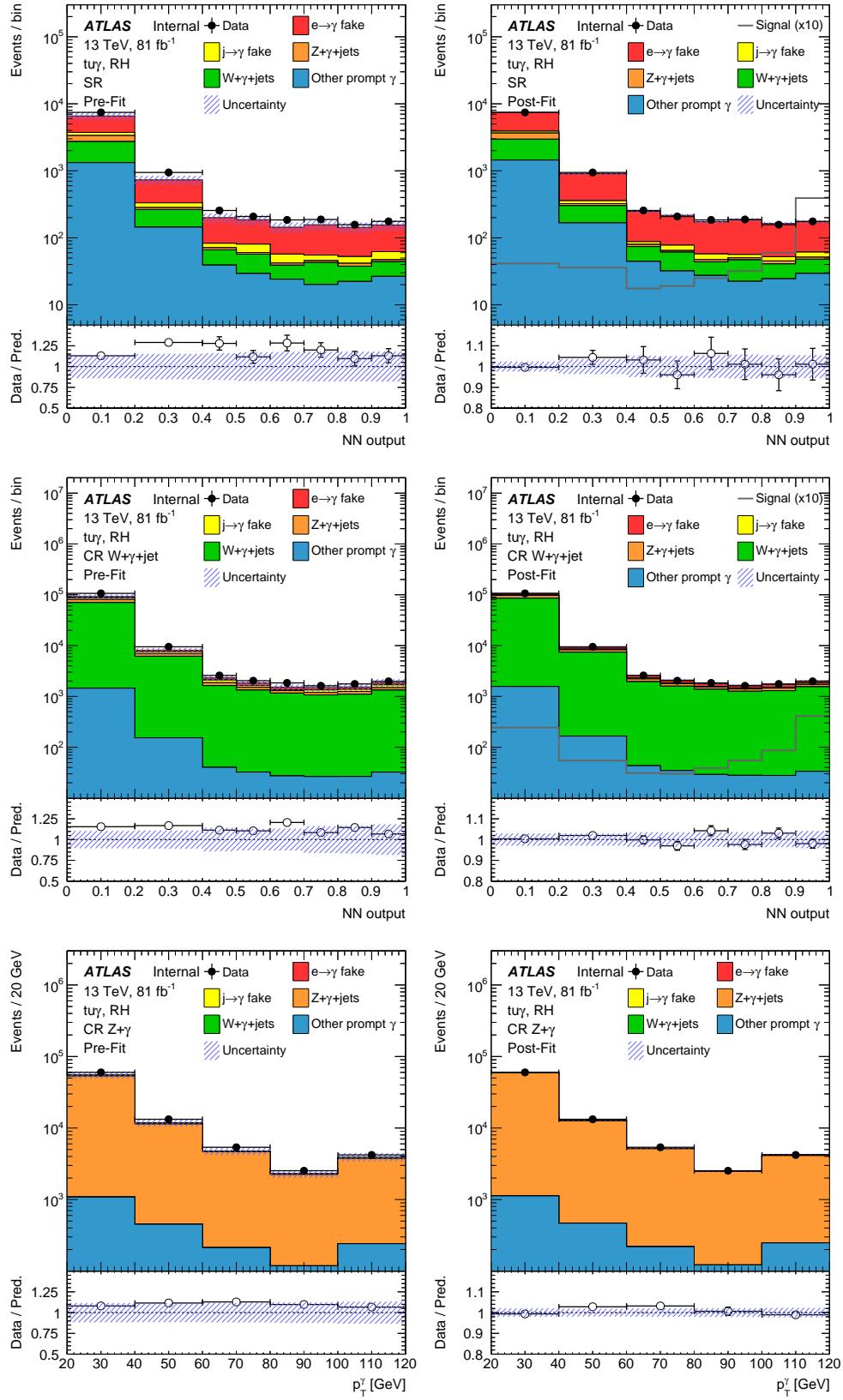


Figure 315: Pre- (left) and post-fit (right) distributions for the right-handed signal coupling tuy using data in all regions: NN output distribution in the SR (top), CR $W+\gamma+jets$ (middle) and the photon p_T spectrum in the CR $Z+\gamma$ (bottom). In the SR and CR $W+\gamma+jets$, the signal distribution scaled to the observed limit multiplied by 10 is included for the post-fit plots. Statistical and systematic uncertainties are included.

9th July 2019 - 11:54

Not reviewed, for internal circulation only

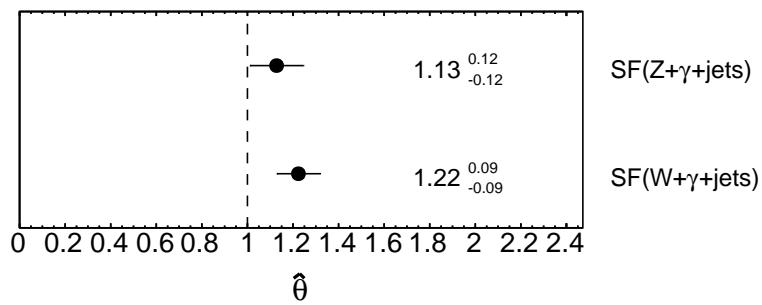


Figure 316: Normalisation factors for the $W+\gamma+\text{jets}$ and $Z+\gamma+\text{jets}$ process using the right-handed $t\gamma\gamma$ coupling using data in all regions.

Not reviewed, for internal circulation only

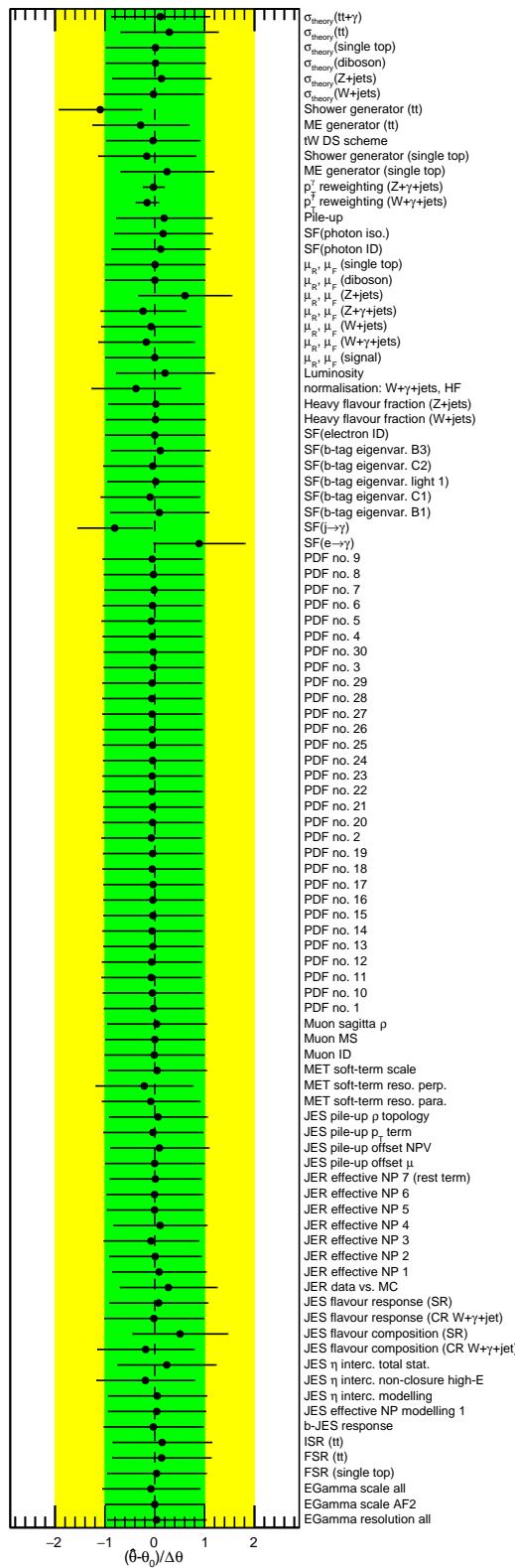


Figure 317: Pull values for the right-handed $t\gamma\gamma$ coupling for the different nuisance parameters considered in the fit using data in all regions.

Not reviewed, for internal circulation only

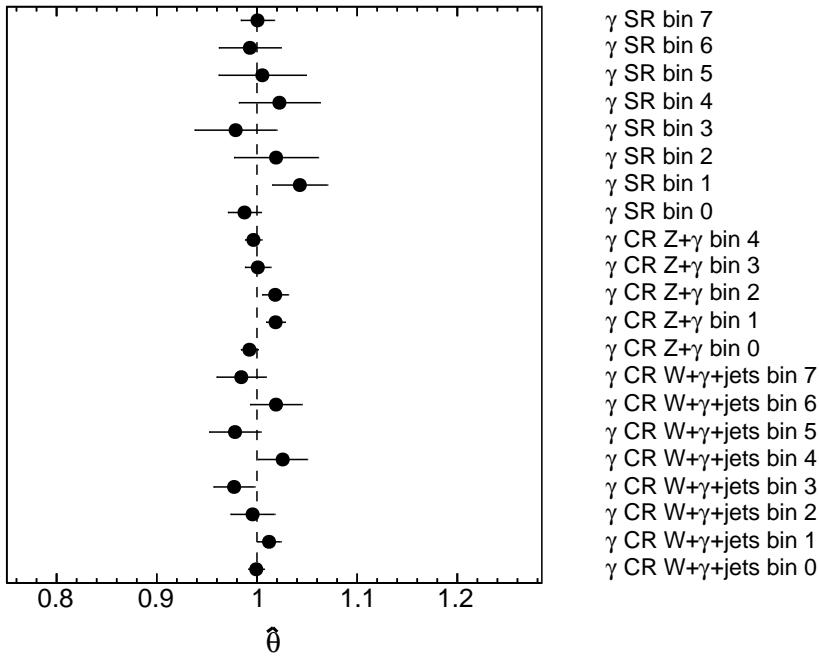


Figure 318: Normalisation factors γ for each bin in each region for the right-handed $t\bar{u}\gamma$ coupling using data in all regions.

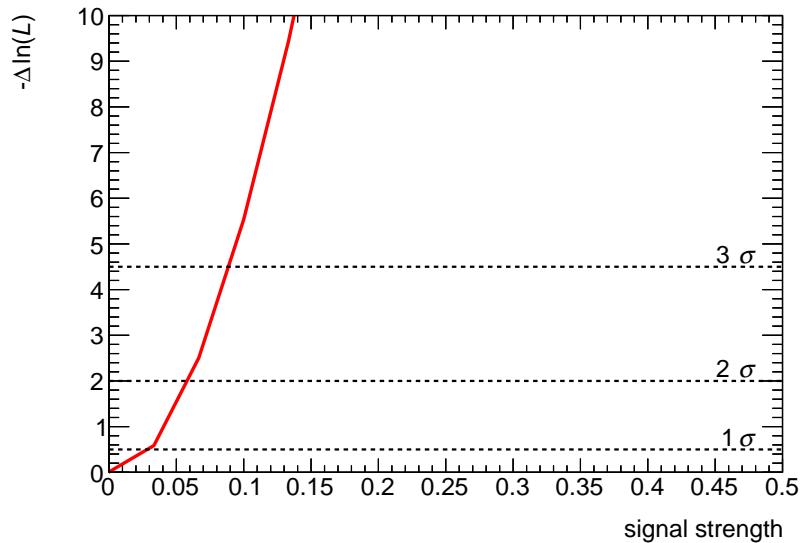


Figure 319: Distributions of the negative-log likelihood for the signal strength using data in all regions for the right-handed $t\bar{u}\gamma$ coupling. The one, two and three standard deviations are marked.

Not reviewed, for internal circulation only

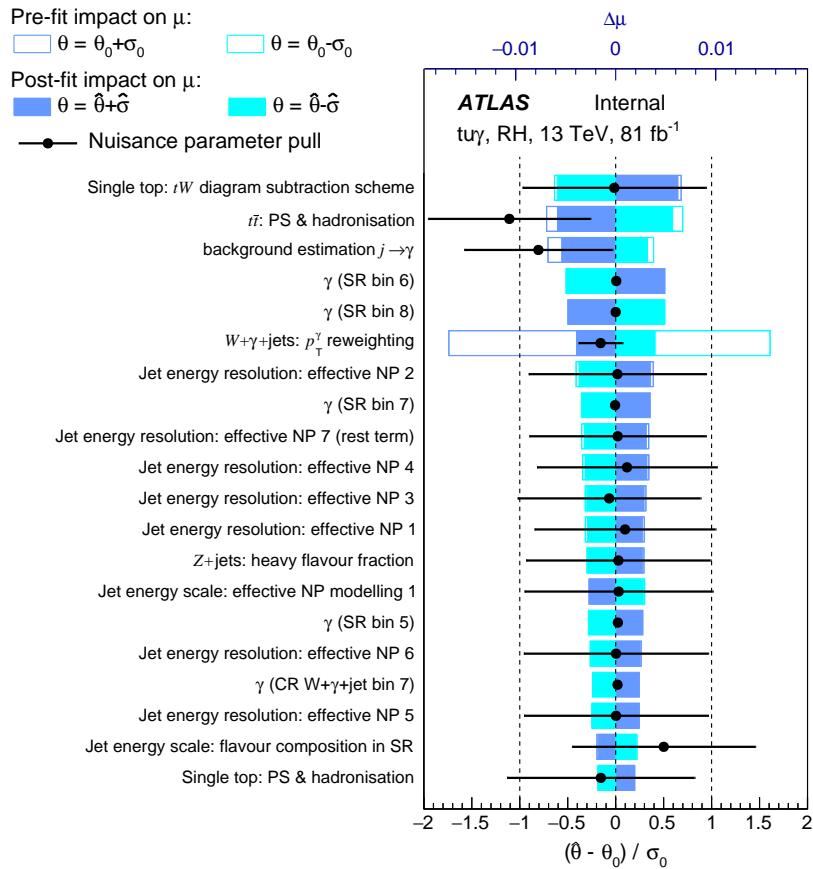


Figure 320: Ranking plot for the 20 nuisance parameters with the largest impact on the signal strength for the right-handed $tuya$ coupling using data in all regions and performing an S+B fit.

1910 **Z.1.1 Validation of fit result**

Not reviewed, for internal circulation only

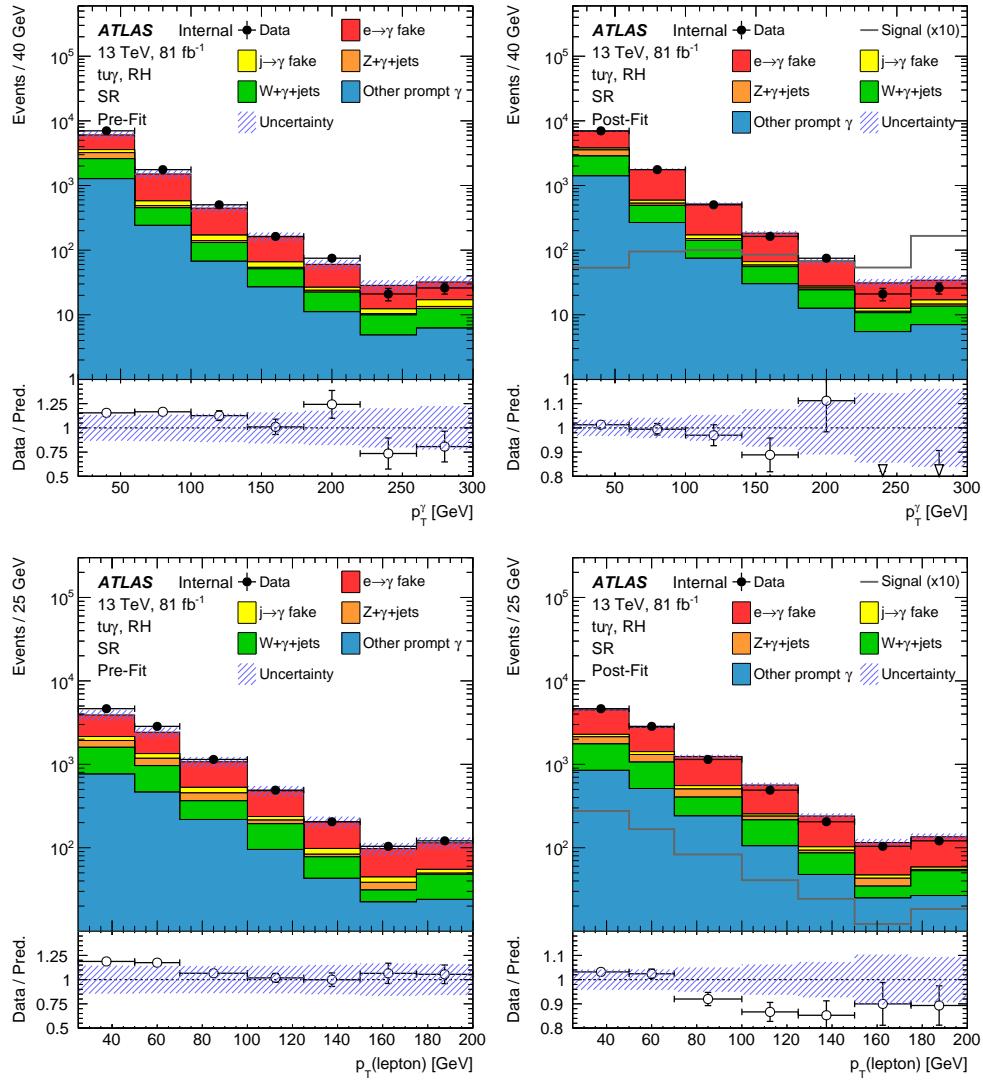


Figure 321: Pre- (left) and post-fit (right) distributions for the right-handed signal coupling $t\gamma\gamma$ using data in the SR: photon p_T (top), and lepton p_T (bottom). In the post-fit distributions, the signal distribution scaled to the observed limit multiplied by 10 is included. Statistical and systematic uncertainties are included.

Not reviewed, for internal circulation only

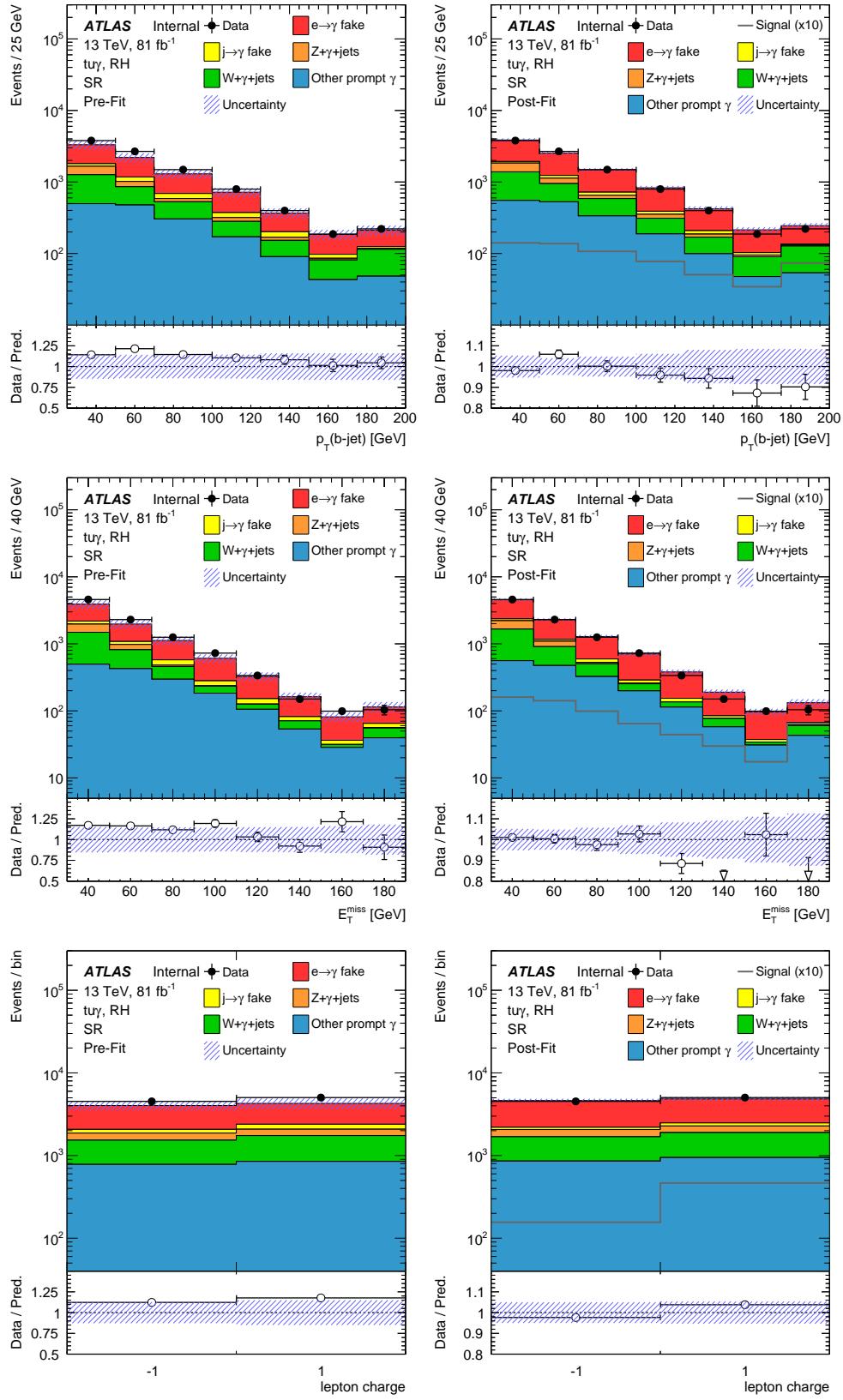


Figure 322: Pre- (left) and post-fit (right) distributions for the right-handed signal coupling tuy using data in the SR: jet p_T (top), missing transverse momentum E_T^{miss} (middle), and lepton charge (bottom). In the post-fit distributions, the signal distribution scaled to the observed limit multiplied by 10 is included. Statistical and systematic uncertainties are included.

9th July 2019 – 11:54

Not reviewed, for internal circulation only

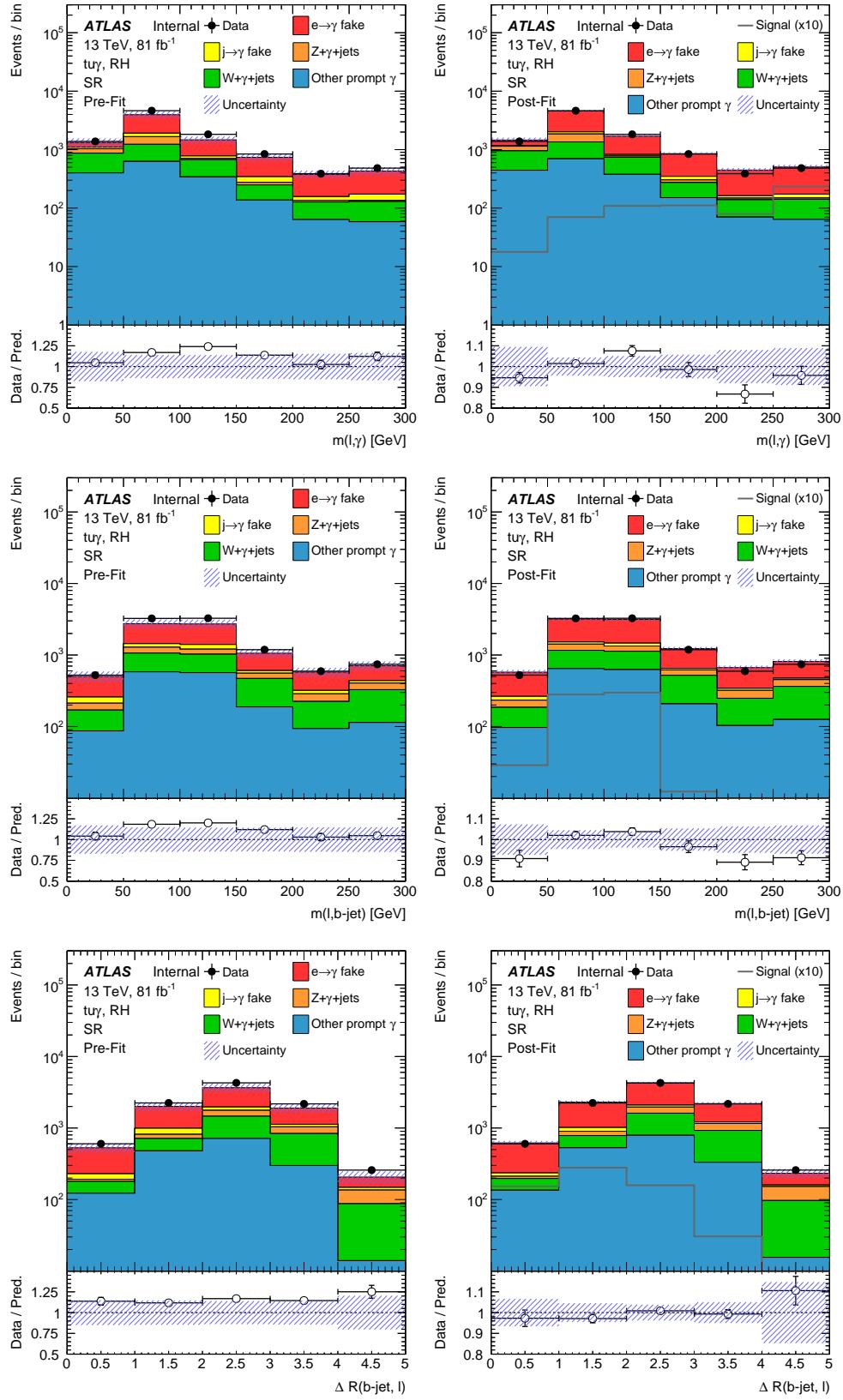


Figure 323: Pre- (left) and post-fit (right) distributions for the right-handed signal coupling tuy using data in the SR: invariant mass of the lepton-photon system $m(\ell\gamma)$ (top), invariant mass of the jet-lepton system $m(lj)$ (middle), and the distance between the jet and lepton $\Delta R(j, \ell)$ (bottom). In the post-fit distributions, the signal distribution scaled to the observed limit multiplied by 10 is included. Statistical and systematic uncertainties are included.

9th July 2019 - 11:54

416

Not reviewed, for internal circulation only

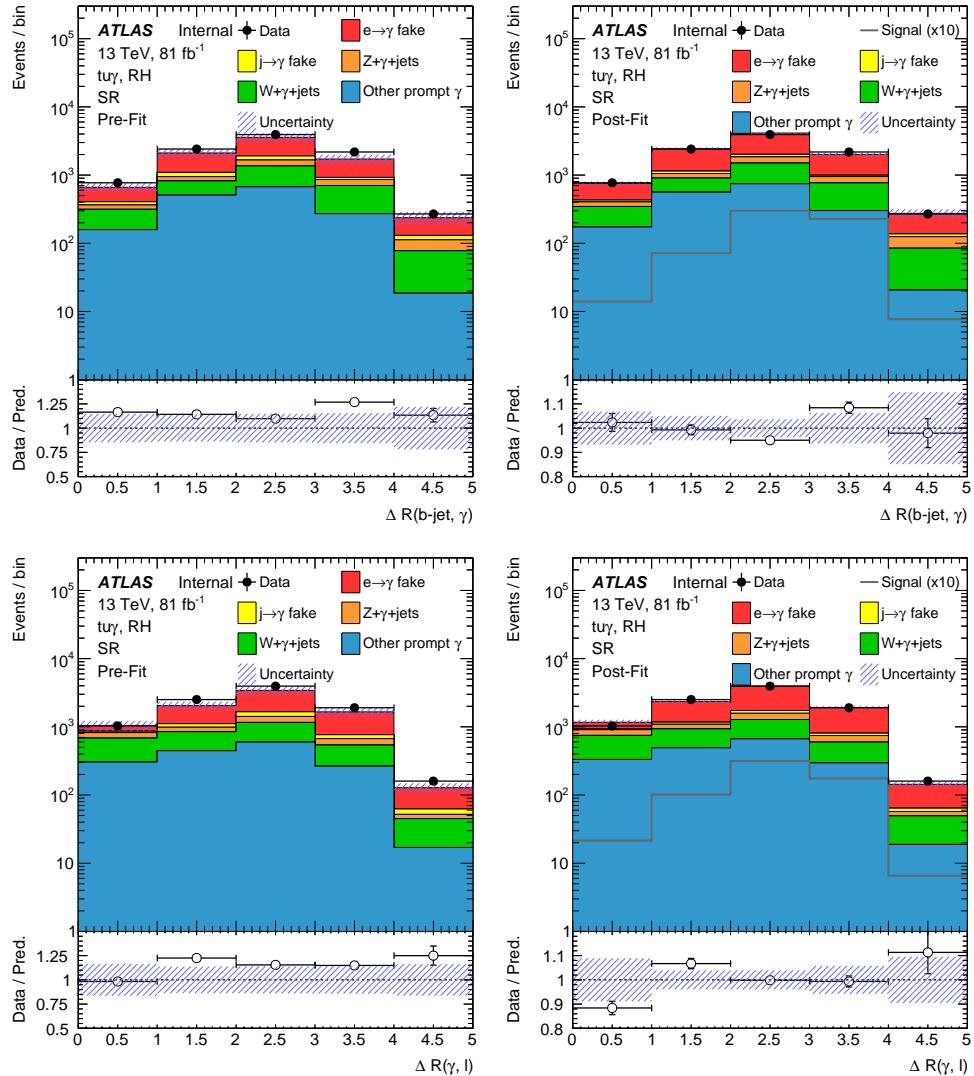


Figure 324: Pre- (left) and post-fit (right) distributions for the right-handed signal coupling tuy using data in the SR: the distance between the jet and photon $\Delta R(j, \gamma)$ (top), and the distance between the lepton and photon $\Delta R(\ell, \gamma)$ (bottom). In the post-fit distributions, the signal distribution scaled to the observed limit multiplied by 10 is included. Statistical and systematic uncertainties are included.

Table 82: Yields for the different contributions after the fit using the right-handed $t\gamma\gamma$ coupling in the VRs $SF(e \rightarrow \gamma)$ and combined background. The statistical uncertainty and all systematic uncertainties are included.

Photon origin	VR $SF(e \rightarrow \gamma)$		combined background VR		
$e \rightarrow \gamma$	267 000	\pm	29 000	42 900	\pm
$j \rightarrow \gamma$	690	\pm	220	5 600	\pm
$Z + \gamma + \text{jets}$	26 600	\pm	2 000	21 600	\pm
$W + \gamma + \text{jets}$	10 880	\pm	610	83 000	\pm
Other prompt photon	1 090	\pm	160	22 700	\pm
Total SM	306 000	\pm	30 000	176 000	\pm
Data	312 550			180 804	

Not reviewed, for internal circulation only

Not reviewed, for internal circulation only

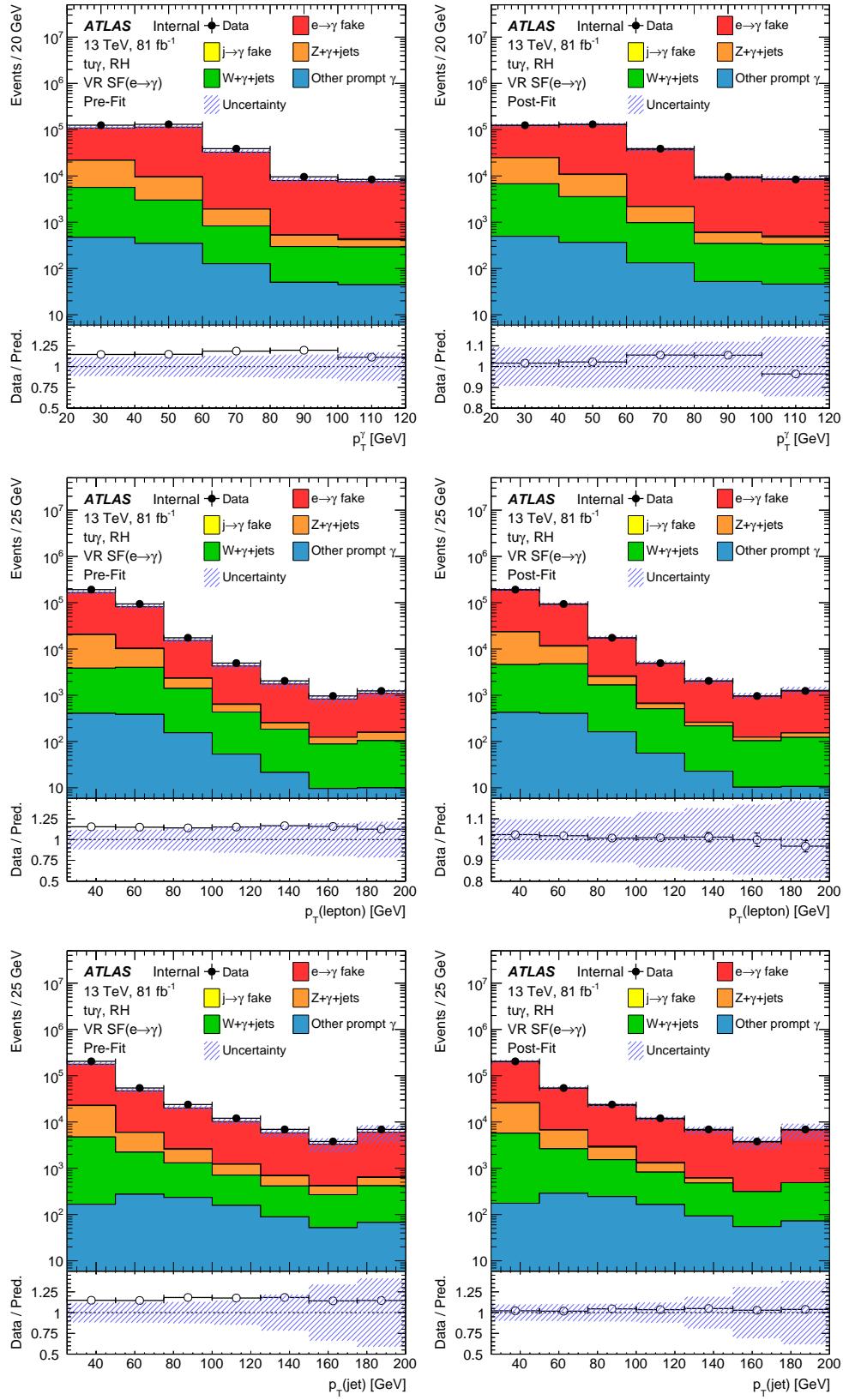


Figure 325: Pre- (left) and post-fit (right) distributions for the right-handed signal coupling tuy using data in the VR $SF(e \rightarrow \gamma)$: photon p_T (top), lepton p_T (middle), and jet p_T (bottom). Statistical and systematic uncertainties are included.

Not reviewed, for internal circulation only

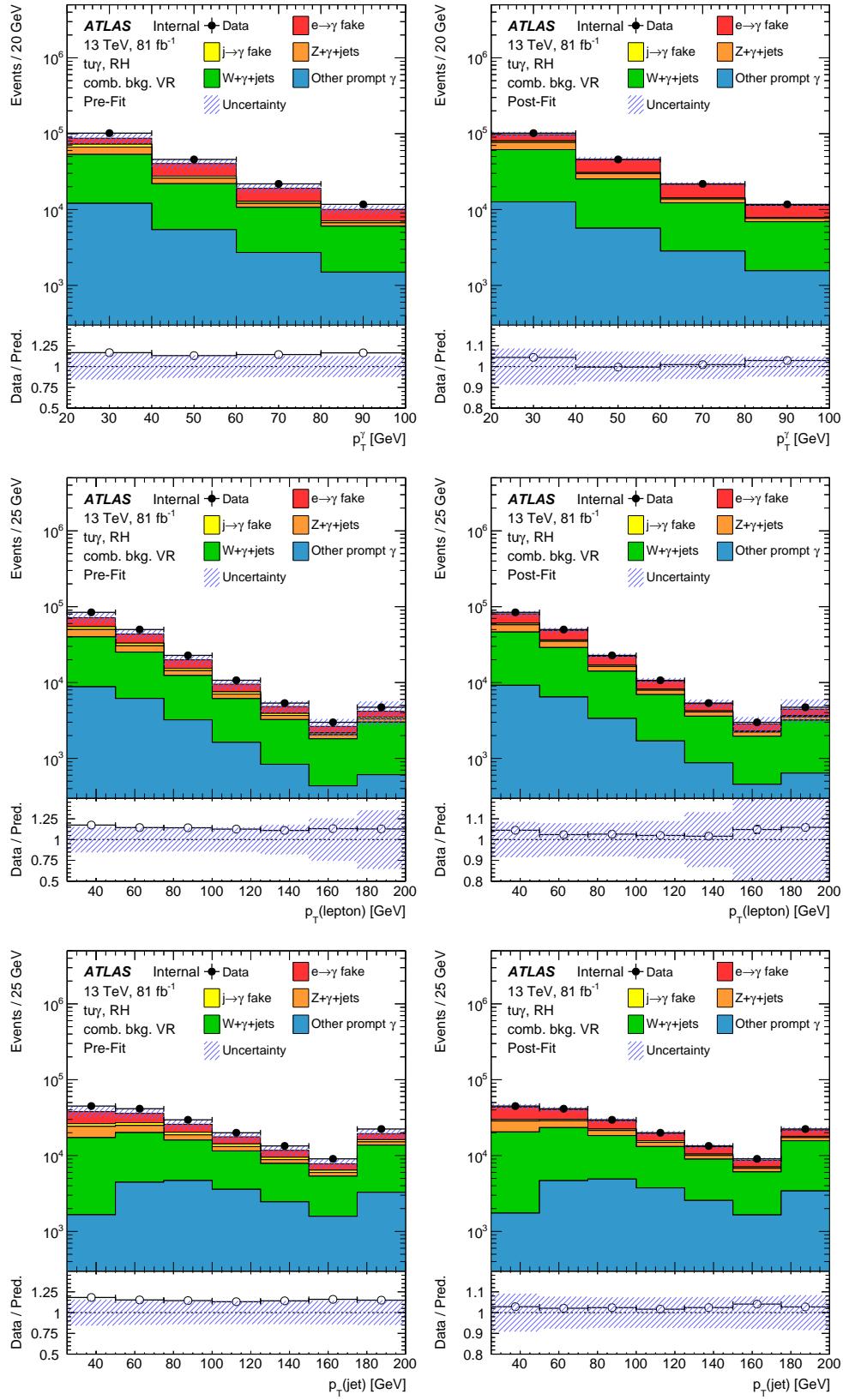


Figure 326: Pre- (left) and post-fit (right) distributions for the right-handed signal coupling tuy using data in the combined background VR: photon p_T (top), lepton p_T (middle), and jet p_T (bottom). Statistical and systematic uncertainties are included.

1911 Z.2 Statistical fit using data in all regions for the left-handed $t\gamma$ coupling

Not reviewed, for internal circulation only

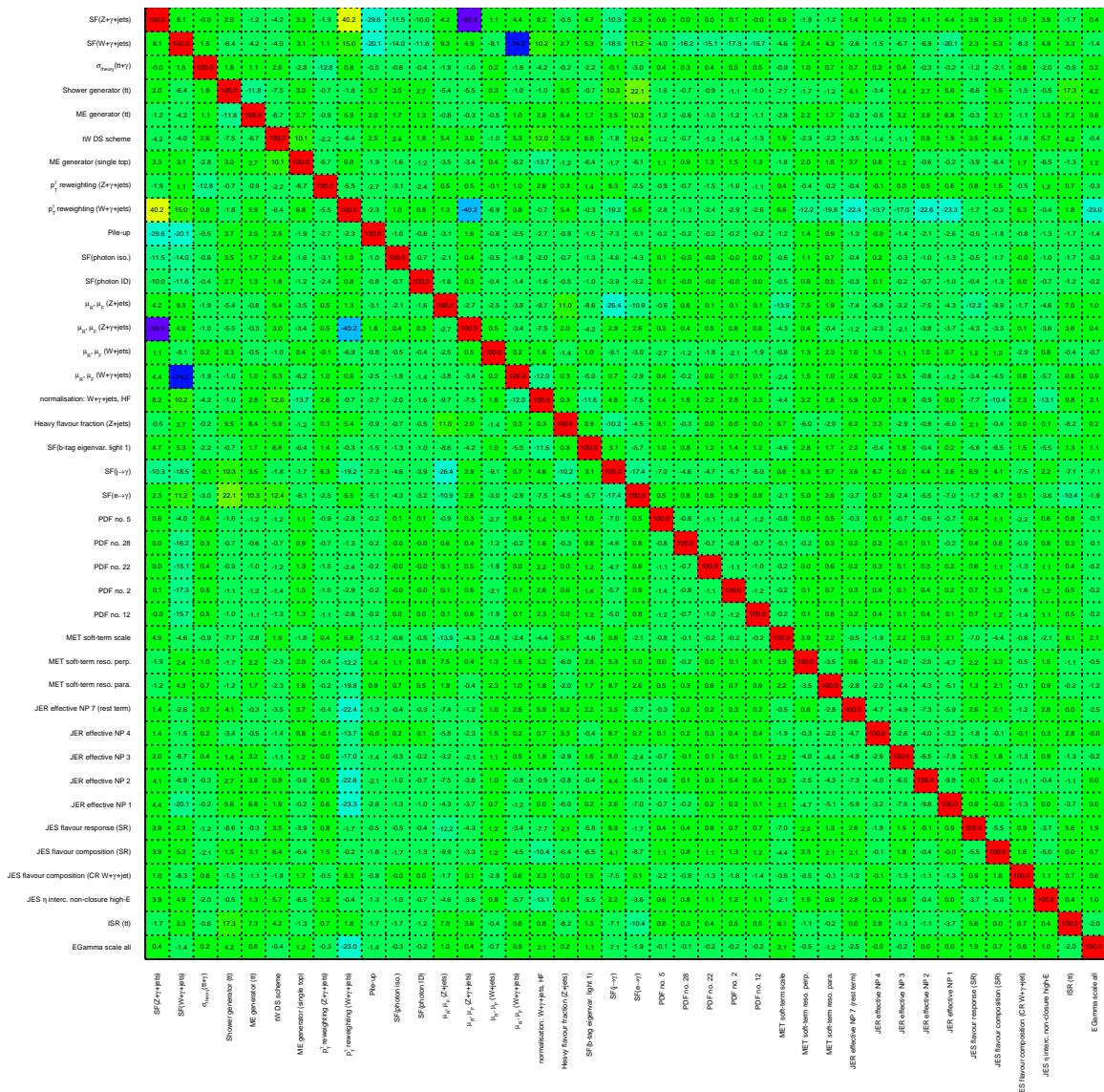


Figure 327: Correlation coefficients of all parameters with at least one coefficient above 10 % for the left-handed $t\gamma$ coupling considered in the fit using data in all regions.

Not reviewed, for internal circulation only

Table 83: Yields for the different contributions in the different regions after the fit for the left-handed $t\gamma\gamma$ coupling. The statistical uncertainty and all systematic uncertainties are included.

Photon origin	SR		CR $W+\gamma+\text{jets}$			CR $Z+\gamma$		
$e \rightarrow \gamma$	4 700	\pm 500	8 600	\pm 1 400	250	\pm 33		
$j \rightarrow \gamma$	420	\pm 240	5 900	\pm 3 500	2 100	\pm 1 000		
$Z+\gamma+\text{jets}$	770	\pm 110	13 600	\pm 1 400	81 200	\pm 2 100		
$W+\gamma+\text{jets}$	1 970	\pm 400	98 500	\pm 4 000	6.3	\pm 2.0		
Other prompt photon	1 730	\pm 380	1 900	\pm 440	2 160	\pm 220		
Total SM	9 590	\pm 240	128 500	\pm 4 100	85 700	\pm 1 700		
Data	9 557		127 864		85 347			

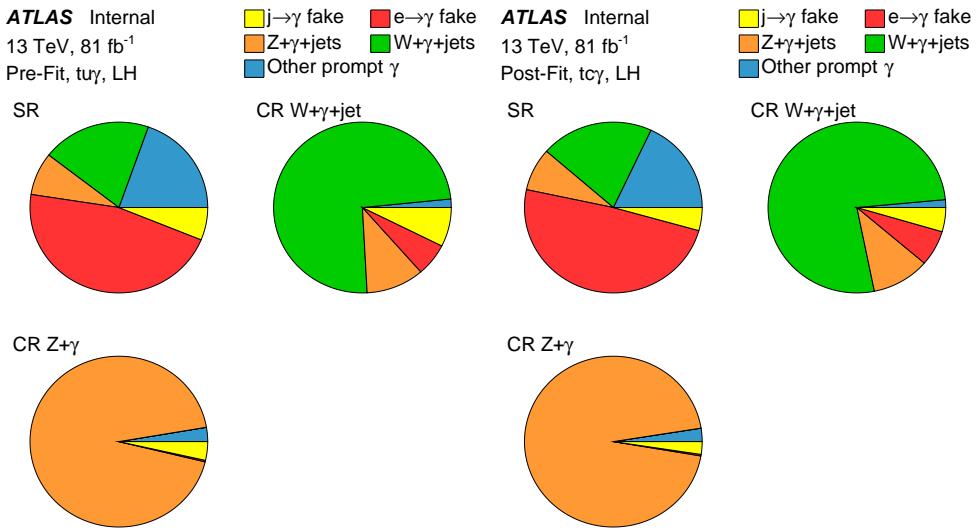


Figure 328: Pie charts showing the composition of the processes before (left) and after the fit using data in all regions (right) in the SR, CR $W+\gamma+\text{jets}$, and CR $Z+\gamma$.

Not reviewed, for internal circulation only

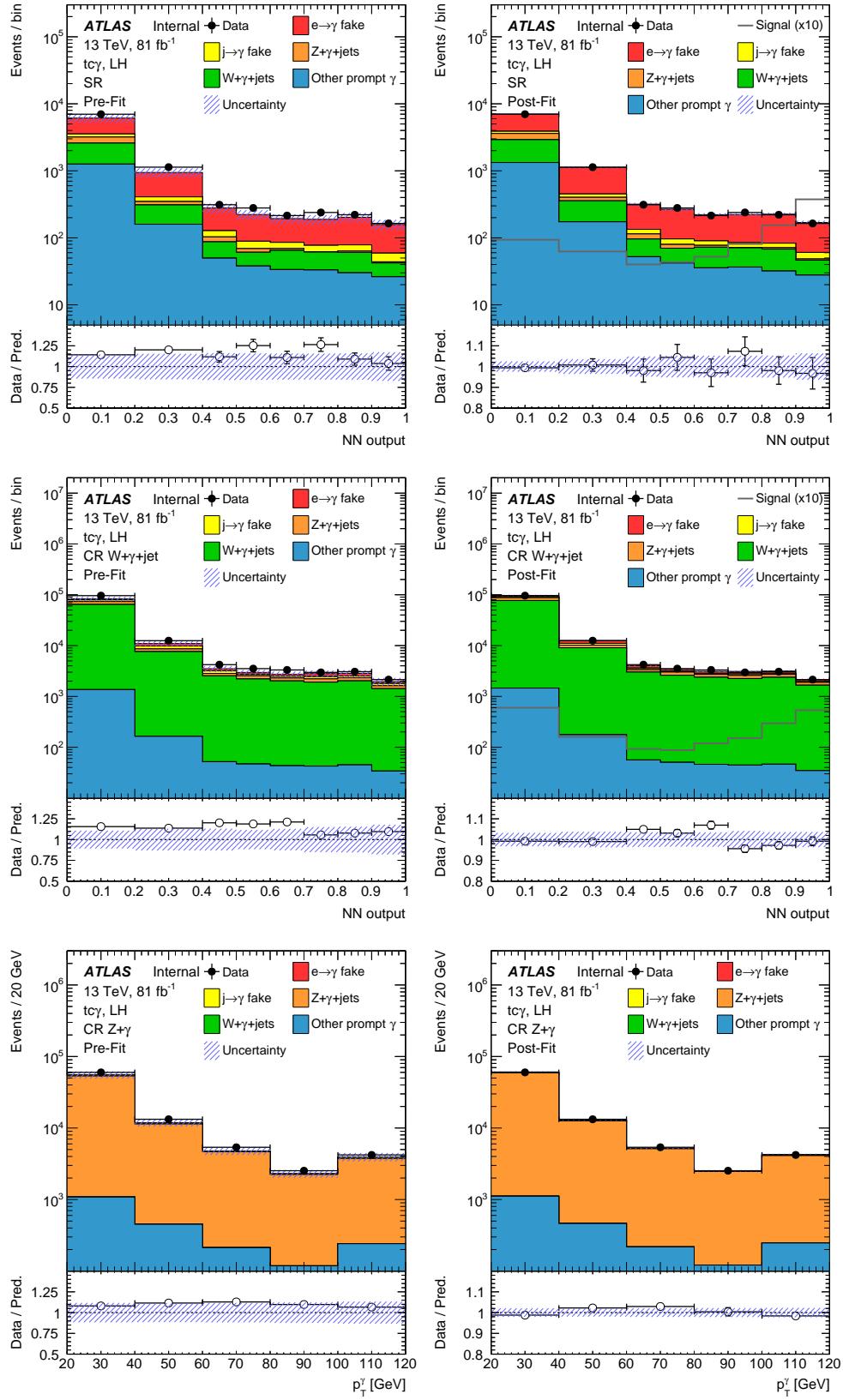


Figure 329: Pre- (left) and post-fit (right) distributions for the left-handed signal coupling $tc\gamma$ using data in all regions: NN output distribution in the SR (top), CR $W+\gamma+jets$ (middle) and the photon p_T spectrum in the CR $Z+\gamma$ (bottom). In the SR and CR $W+\gamma+jets$, the signal distribution scaled to the observed limit multiplied by 10 is included for the post-fit plots. Statistical and systematic uncertainties are included.

9th July 2019 - 11:54

[Not reviewed, for internal circulation only]

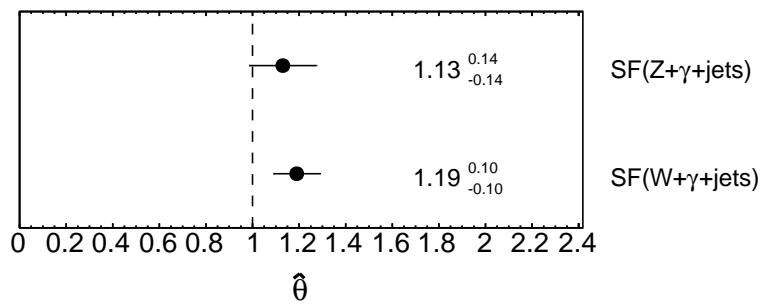


Figure 330: Normalisation factors for the $W+\gamma+\text{jets}$ and $Z+\gamma+\text{jets}$ process using the left-handed $t\bar{c}\gamma$ coupling using data in all regions.

Not reviewed, for internal circulation only

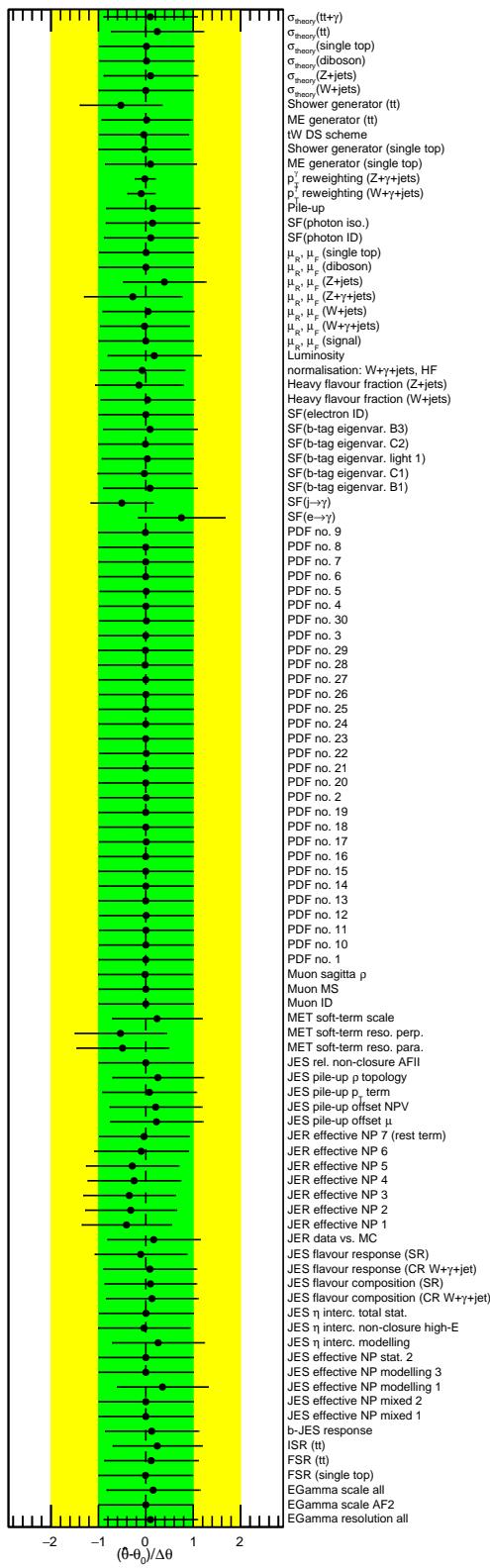


Figure 331: Pull values for the left-handed $tc\gamma$ coupling for the different nuisance parameters considered in the fit using data in all regions.

Not reviewed, for internal circulation only

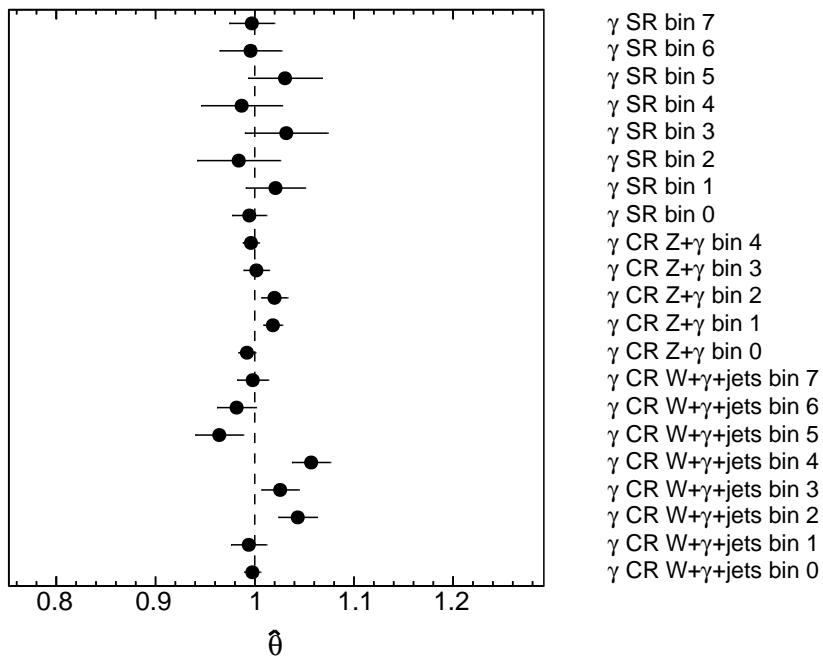


Figure 332: Normalisation factors γ for each bin in each region for the left-handed $t\bar{c}\gamma$ coupling using data in all regions.

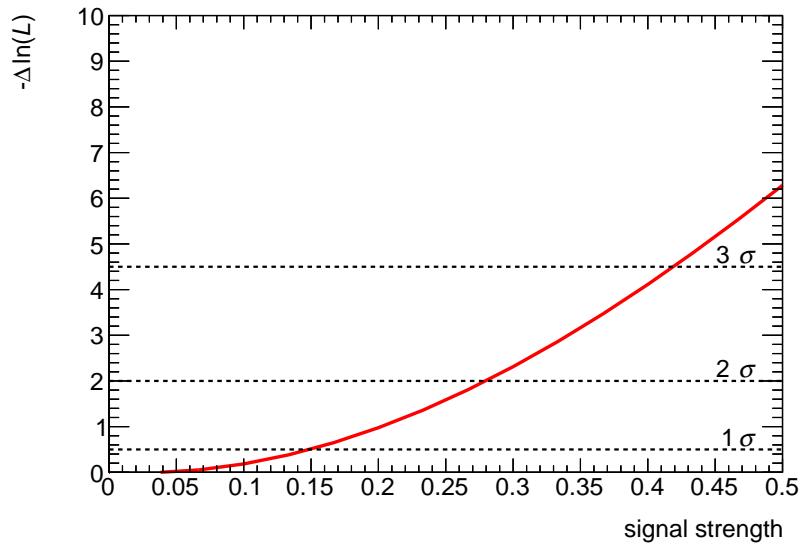


Figure 333: Distributions of the negative-log likelihood for the signal strength using data in all regions for the left-handed $t\bar{c}\gamma$ coupling. The one, two and three standard deviations are marked.

Not reviewed, for internal circulation only

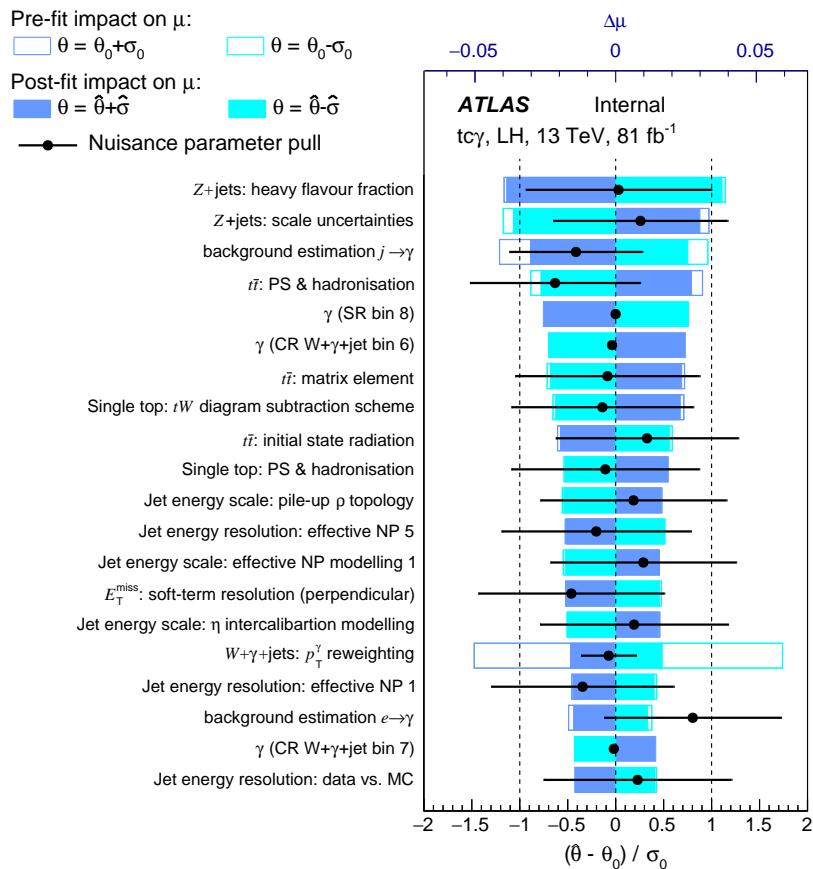


Figure 334: Ranking plot for the 20 nuisance parameters with the largest impact on the signal strength for the left-handed $t\gamma$ coupling using data in all regions and performing an S+B fit.

1912 Z.2.1 Validation of fit result

Not reviewed, for internal circulation only

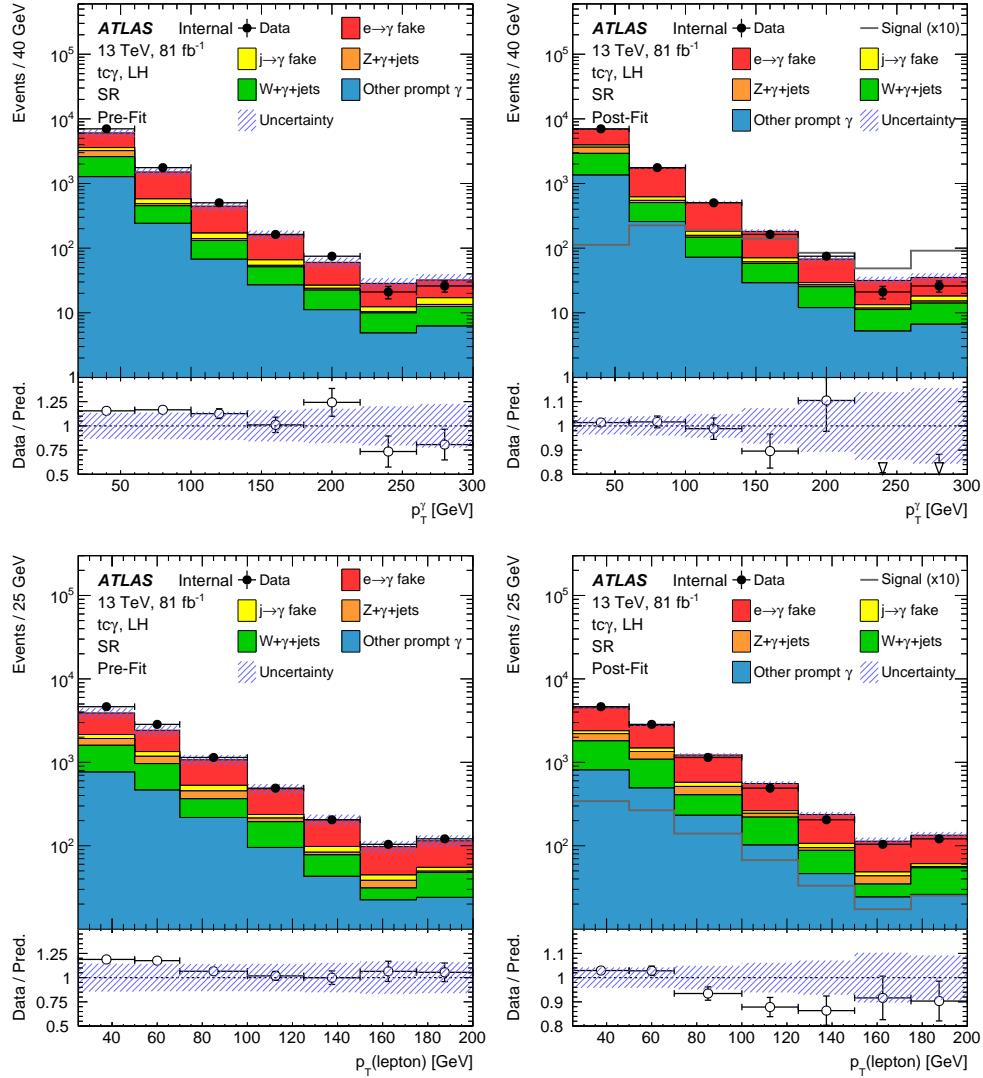


Figure 335: Pre- (left) and post-fit (right) distributions for the left-handed signal coupling $tc\gamma$ using data in the SR: photon p_T (top), and lepton p_T (bottom). In the post-fit distributions, the signal distribution scaled to the observed limit multiplied by 10 is included. Statistical and systematic uncertainties are included.

Not reviewed, for internal circulation only

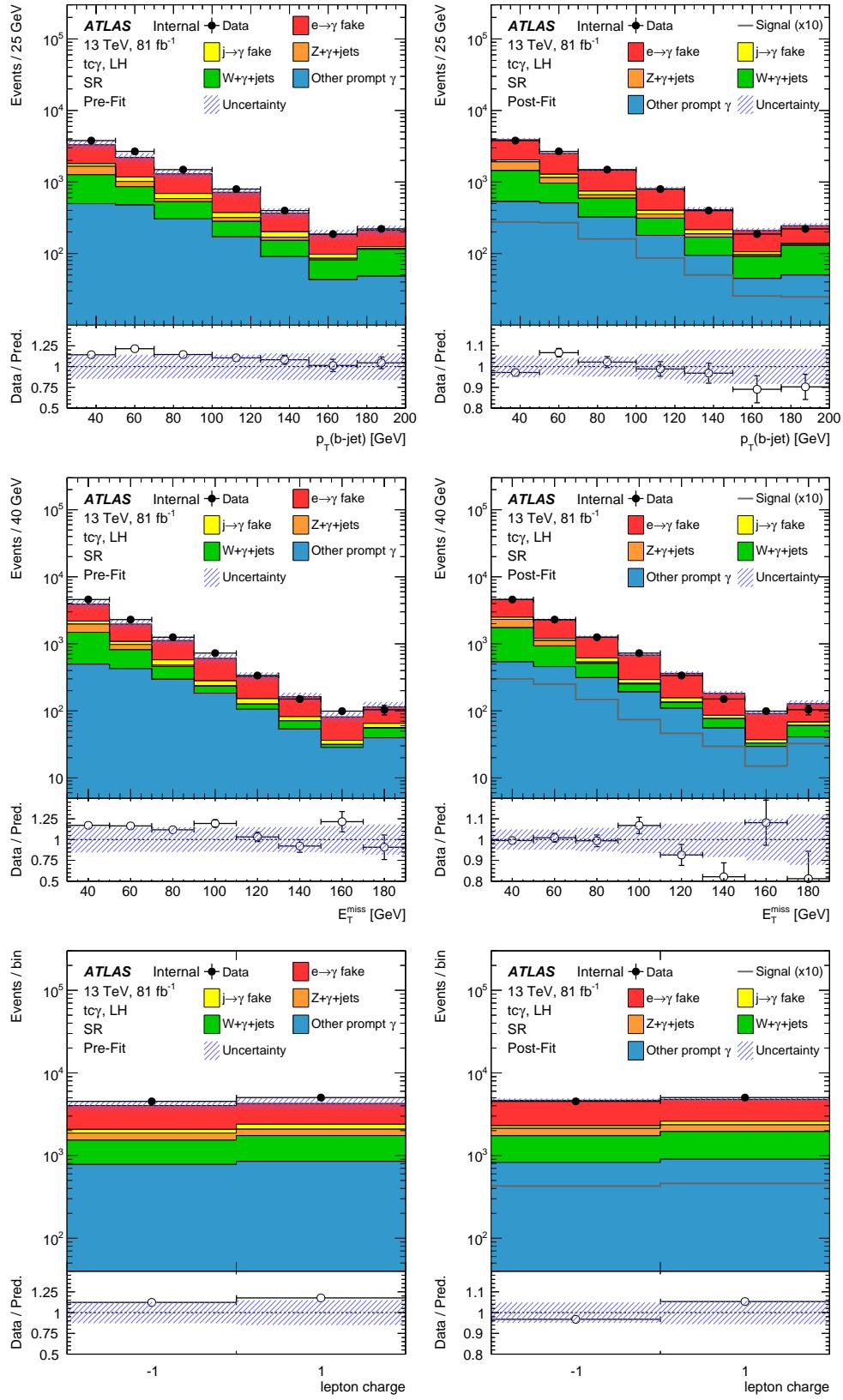


Figure 336: Pre- (left) and post-fit (right) distributions for the left-handed signal coupling $tc\gamma$ using data in the SR: jet p_T (top), missing transverse momentum E_T^{miss} (middle), and lepton charge (bottom). In the post-fit distributions, the signal distribution scaled to the observed limit multiplied by 10 is included. Statistical and systematic uncertainties are included.

9th July 2019 – 11:54

429

Not reviewed, for internal circulation only

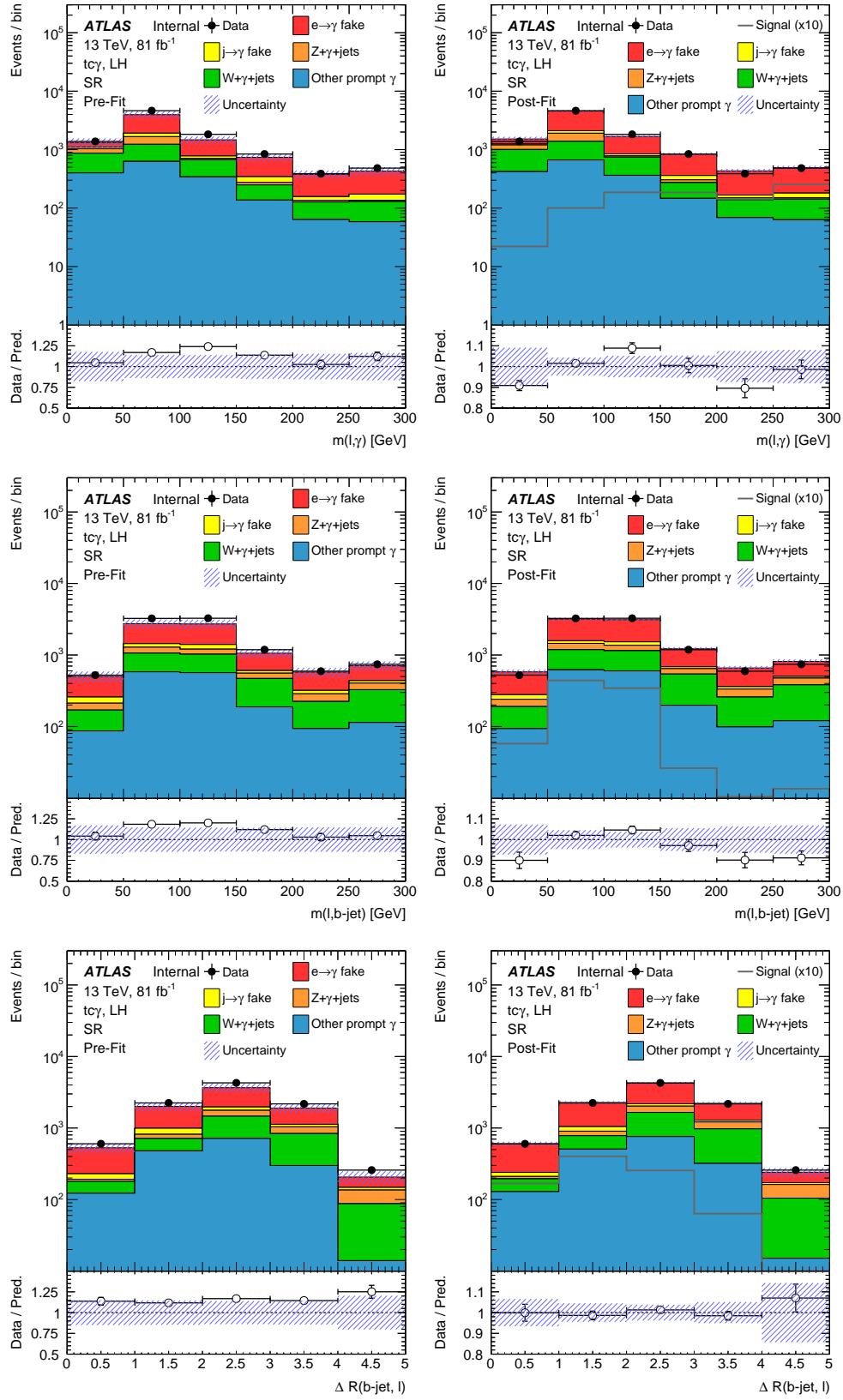


Figure 337: Pre- (left) and post-fit (right) distributions for the left-handed signal coupling $tc\gamma$ using data in the SR: invariant mass of the lepton-photon system $m(\ell\gamma)$ (top), invariant mass of the jet-lepton system $m(lj)$ (middle), and the distance between the jet and lepton $\Delta R(j, \ell)$ (bottom). In the post-fit distributions, the signal distribution scaled to the observed limit multiplied by 10 is included. Statistical and systematic uncertainties are included.

Not reviewed, for internal circulation only

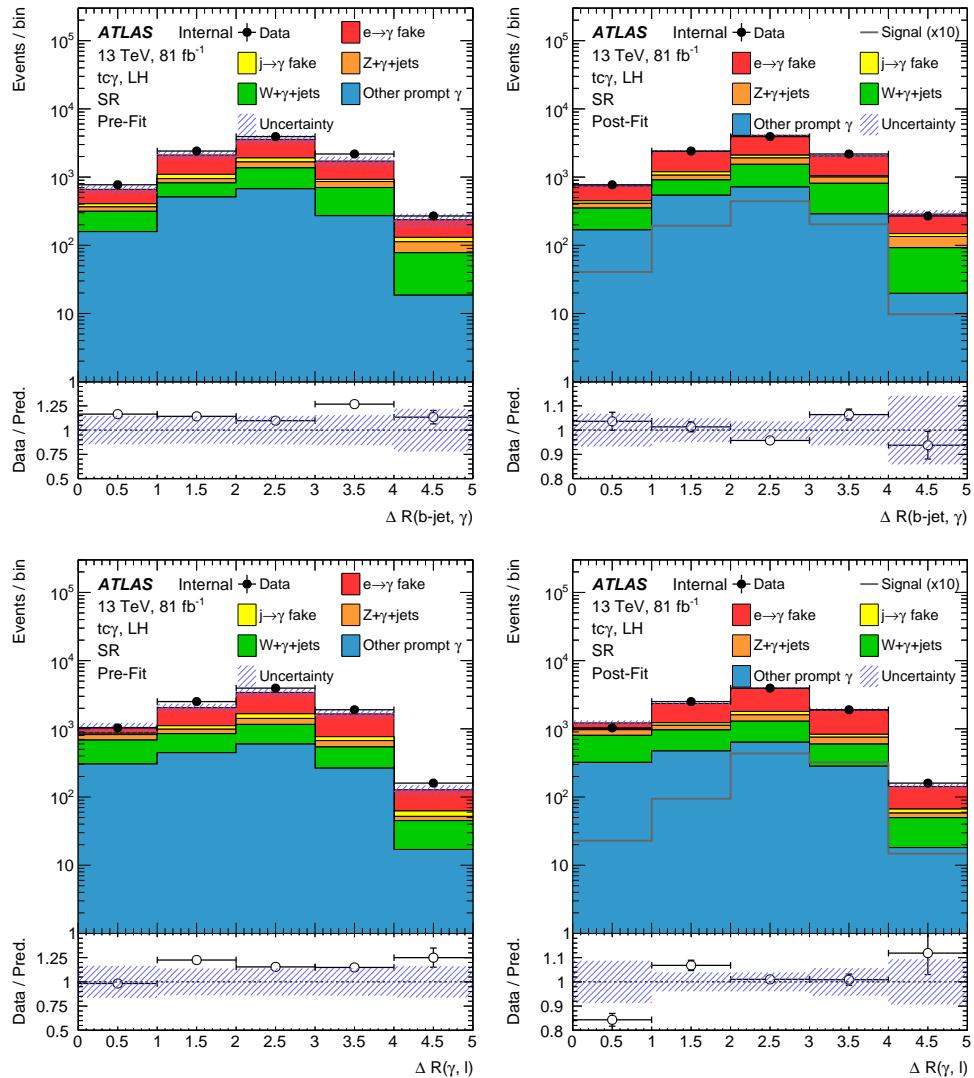


Figure 338: Pre- (left) and post-fit (right) distributions for the left-handed signal coupling $tc\gamma$ using data in the SR: the distance between the jet and photon $\Delta R(j, \gamma)$ (top), and the distance between the lepton and photon $\Delta R(\ell, \gamma)$ (bottom). In the post-fit distributions, the signal distribution scaled to the observed limit multiplied by 10 is included. Statistical and systematic uncertainties are included.

Table 84: Yields for the different contributions after the fit using the left-handed $t\gamma\gamma$ coupling in the VRs $SF(e \rightarrow \gamma)$ and combined background. The statistical uncertainty and all systematic uncertainties are included.

Photon origin	VR $SF(e \rightarrow \gamma)$		combined background VR		
$e \rightarrow \gamma$	266 000	\pm	29 000	40 900	\pm
$j \rightarrow \gamma$	690	\pm	210	6 800	\pm
$Z + \gamma + \text{jets}$	27 300	\pm	2 200	21 100	\pm
$W + \gamma + \text{jets}$	10 890	\pm	680	84 000	\pm
Other prompt photon	1 090	\pm	160	22 400	\pm
Total SM	306 000	\pm	30 000	176 000	\pm
Data	312 550			180 804	

Not reviewed, for internal circulation only

Not reviewed, for internal circulation only

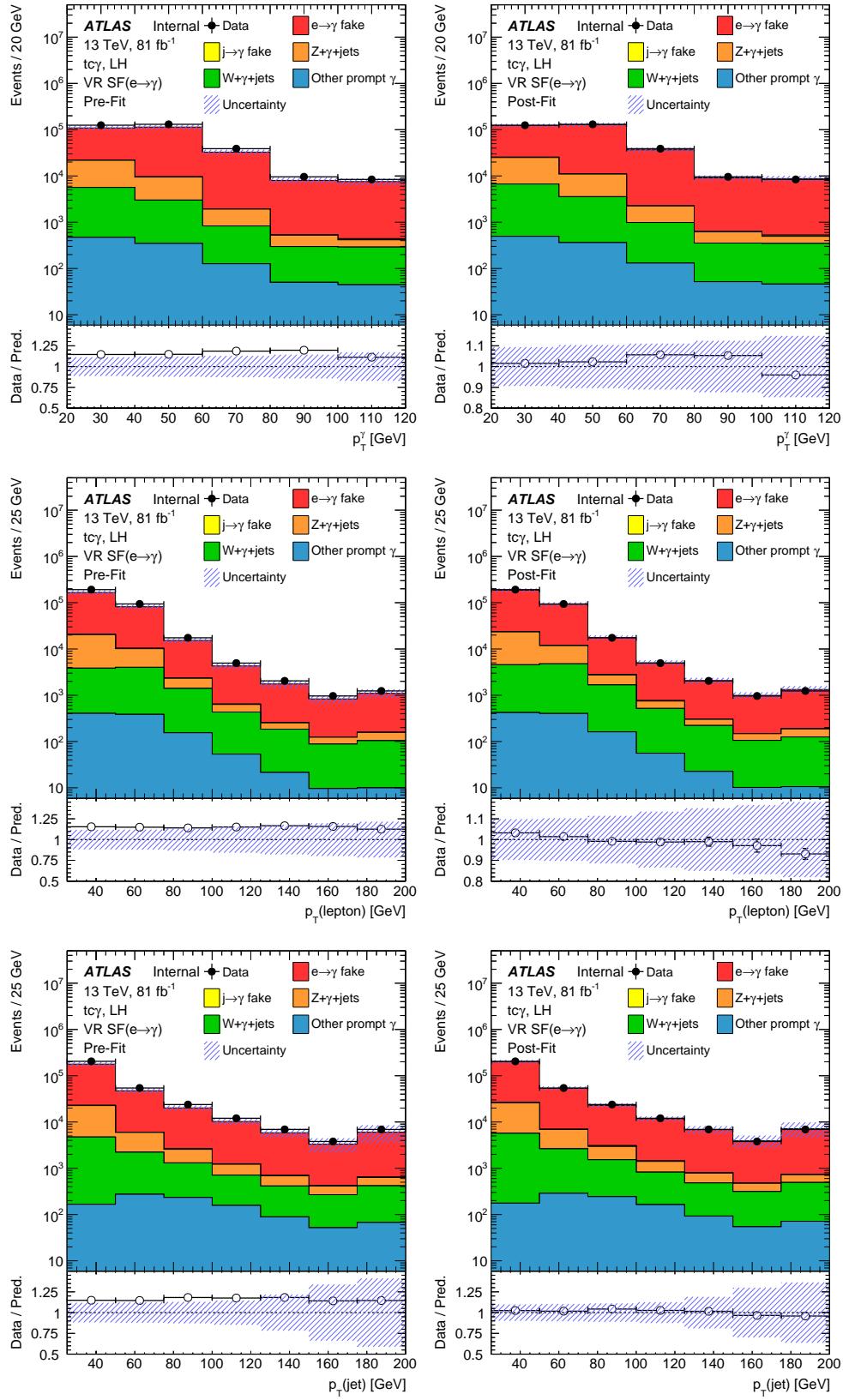


Figure 339: Pre- (left) and post-fit (right) distributions for the left-handed signal coupling $t\gamma$ using data in the VR $SF(e \rightarrow \gamma)$: photon p_T (top), lepton p_T (middle), and jet p_T (bottom). Statistical and systematic uncertainties are included.

Not reviewed, for internal circulation only

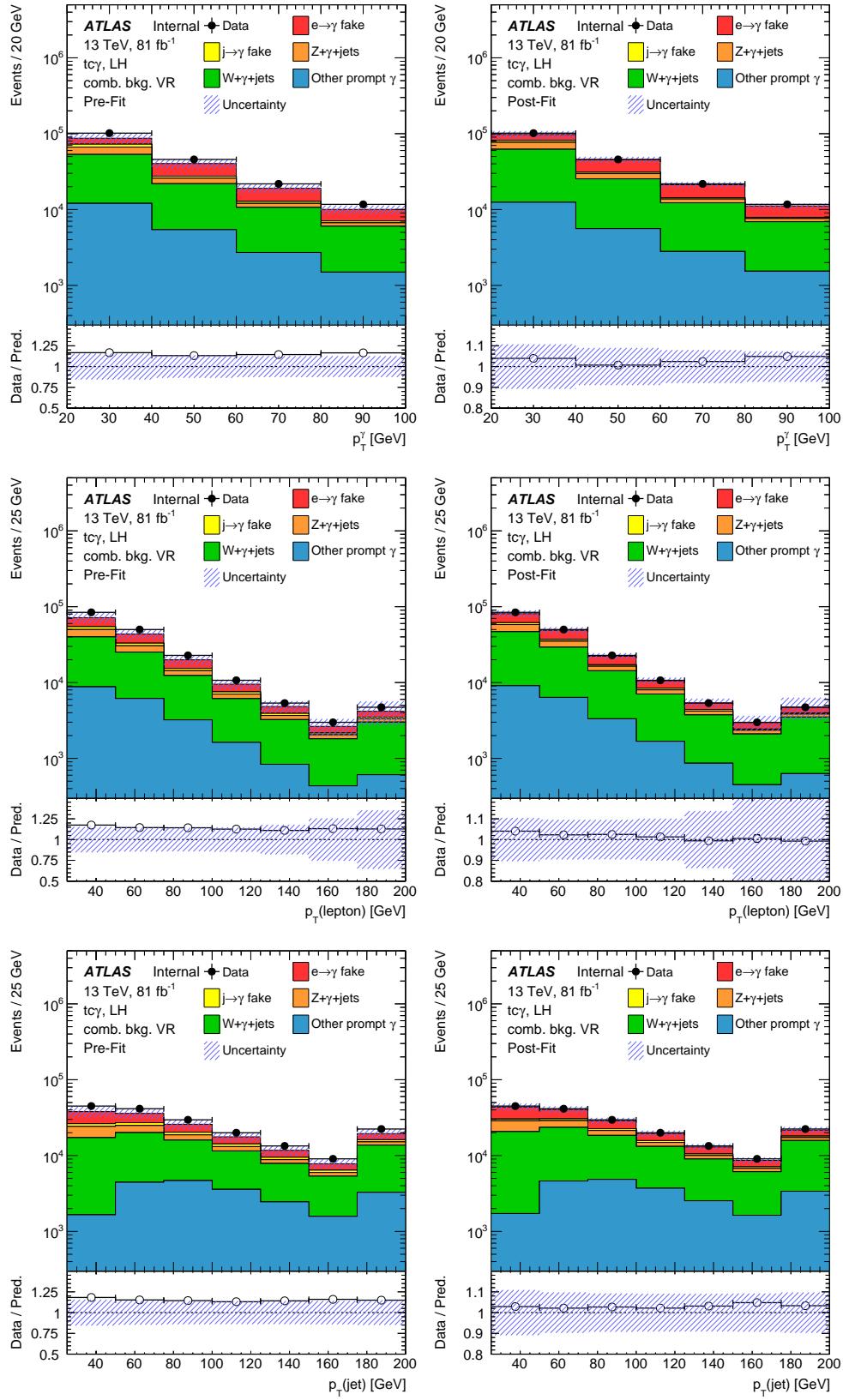


Figure 340: Pre- (left) and post-fit (right) distributions for the left-handed signal coupling $tc\gamma$ using data in the combined background VR: photon p_T (top), lepton p_T (middle), and jet p_T (bottom). Statistical and systematic uncertainties are included.

1913 Z.3 Statistical fit using data in all regions for the right-handed $t\gamma\gamma$ coupling

Not reviewed, for internal circulation only

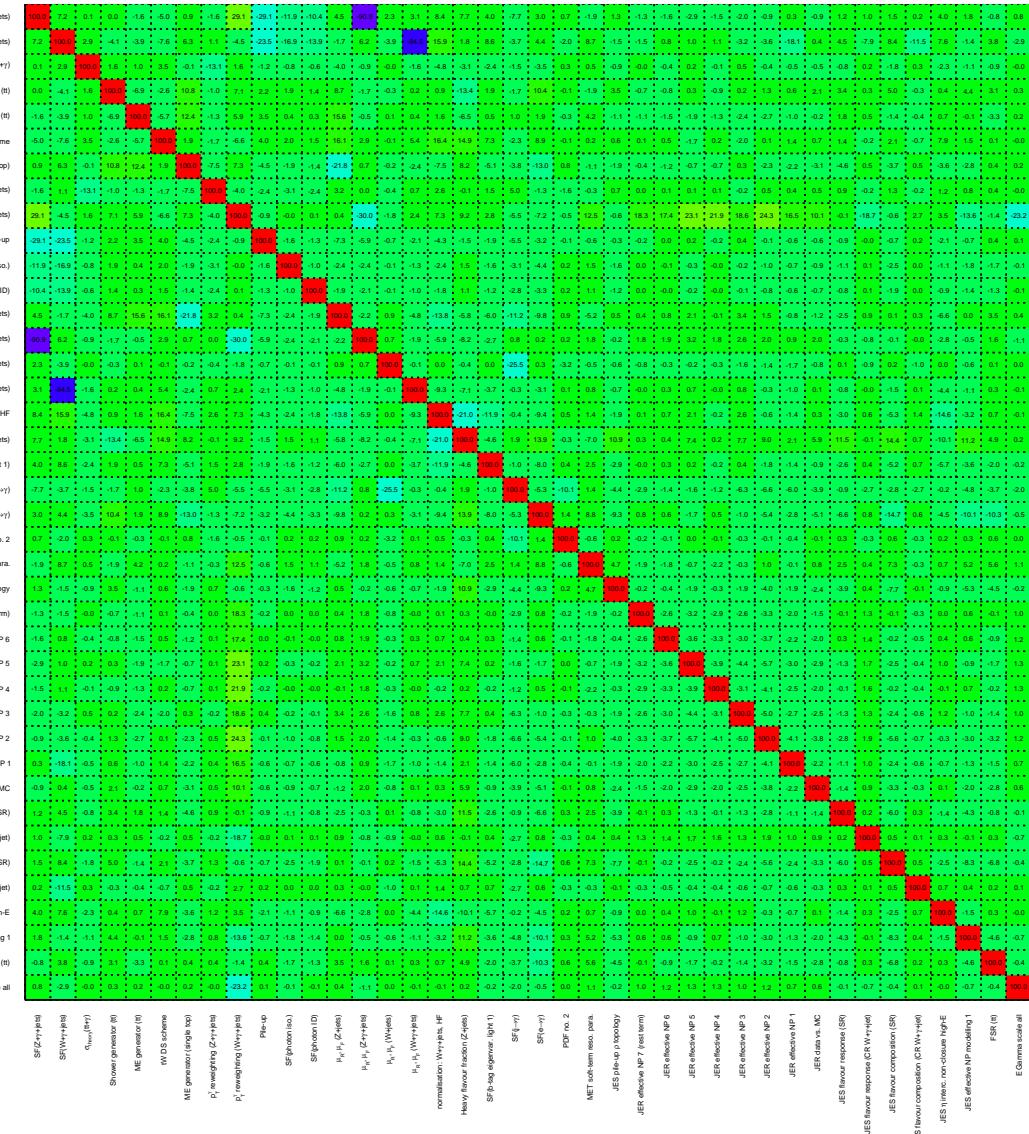


Figure 341: Correlation coefficients of all parameters with at least one coefficient above 10 % for the right-handed $t\gamma\gamma$ coupling considered in the fit using data in all regions.

Not reviewed, for internal circulation only

Table 85: Yields for the different contributions in the different regions after the fit for the right-handed $t\gamma\gamma$ coupling. The statistical uncertainty and all systematic uncertainties are included.

Photon origin	SR		CR $W+\gamma+jets$			CR $Z+\gamma$		
$e \rightarrow \gamma$	4 520	\pm 530	8 100	\pm 1 400	237	\pm 32		
$j \rightarrow \gamma$	280	\pm 190	3 100	\pm 1 900	1 390	\pm 950		
$Z+\gamma+jets$	750	\pm 110	13 300	\pm 1 300	81 300	\pm 1 900		
$W+\gamma+jets$	2 020	\pm 410	100 900	\pm 3 200	6.3	\pm 2.0		
Other prompt photon	1 930	\pm 450	2 090	\pm 510	2 200	\pm 220		
Total SM	9 500	\pm 240	127 500	\pm 3 600	85 100	\pm 1 600		
Data	9 557		127 864		85 347			

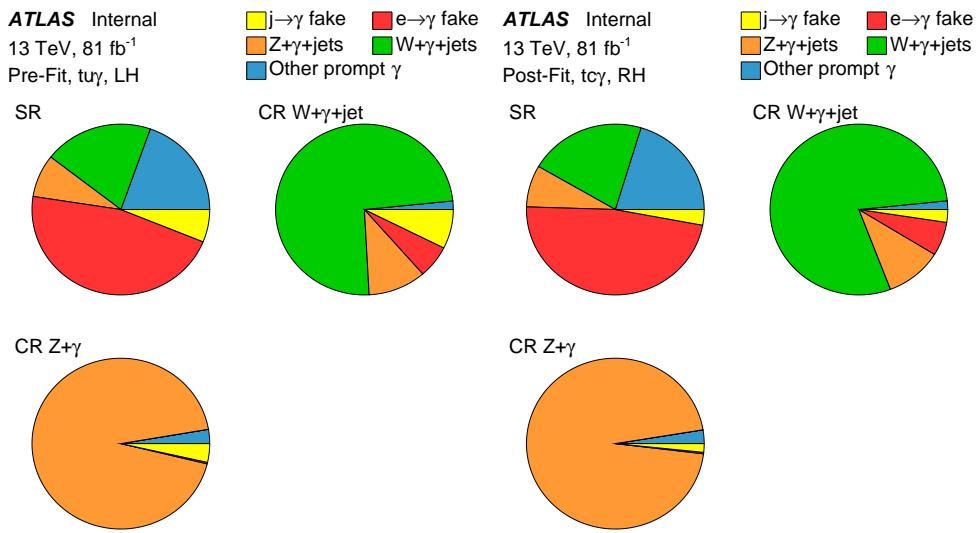


Figure 342: Pie charts showing the composition of the processes before (left) and after the fit using data in all regions (right) in the SR, CR $W+\gamma+jets$, and CR $Z+\gamma$.

Not reviewed, for internal circulation only

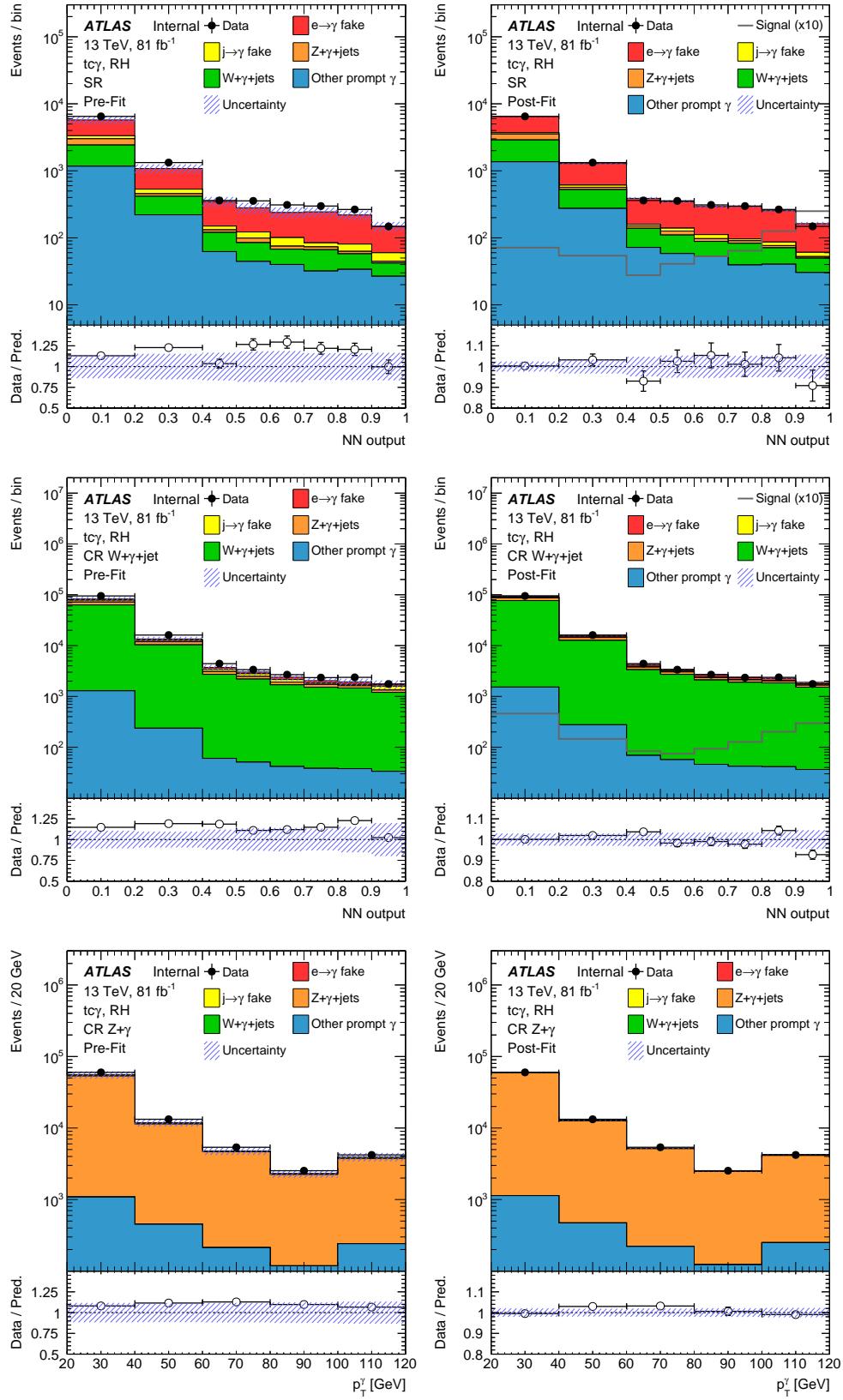


Figure 343: Pre- (left) and post-fit (right) distributions for the right-handed signal coupling $tc\gamma$ using data in all regions: NN output distribution in the SR (top), CR $W+\gamma+jets$ (middle) and the photon p_T spectrum in the CR $Z+\gamma$ (bottom). In the SR and CR $W+\gamma+jets$, the signal distribution scaled to the observed limit multiplied by 10 is included for the post-fit plots. Statistical and systematic uncertainties are included.
9th July 2019 - 11:54

Not reviewed, for internal circulation only

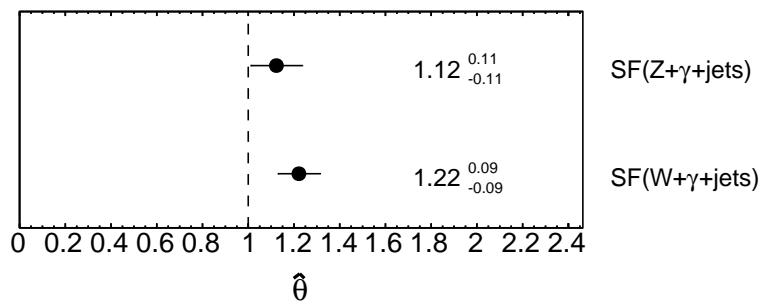


Figure 344: Normalisation factors for the $W+\gamma+\text{jets}$ and $Z+\gamma+\text{jets}$ process using the right-handed $t\gamma\gamma$ coupling using data in all regions.

Not reviewed, for internal circulation only

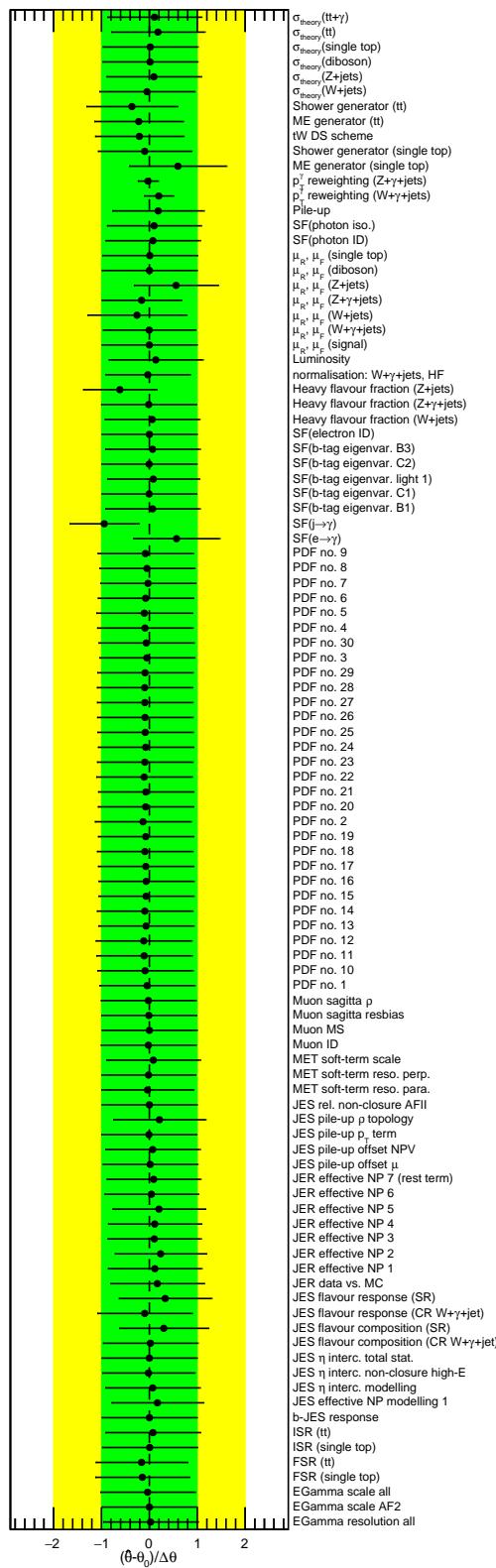


Figure 345: Pull values for the right-handed $tc\gamma$ coupling for the different nuisance parameters considered in the fit using data in all regions.

Not reviewed, for internal circulation only

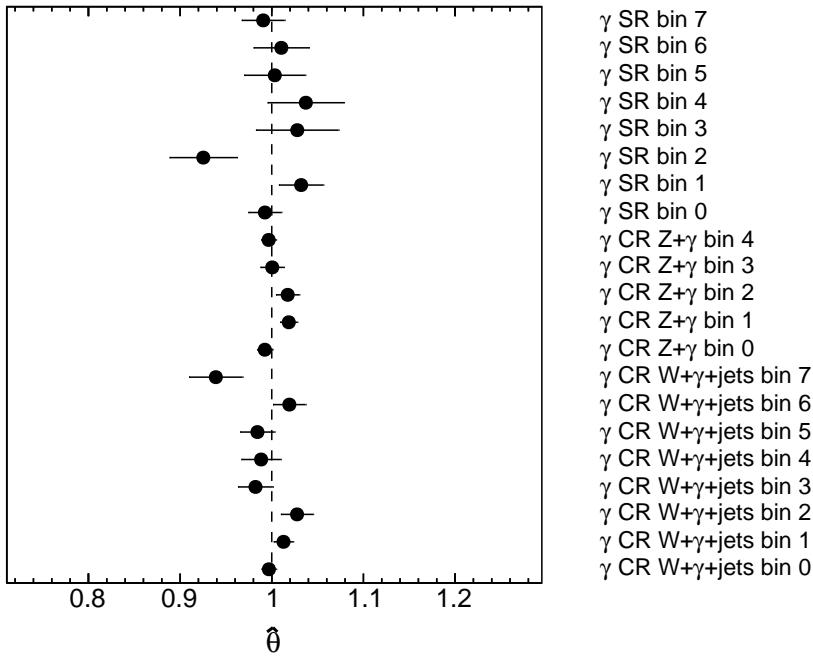


Figure 346: Normalisation factors γ for each bin in each region for the right-handed $t\gamma\gamma$ coupling using data in all regions.

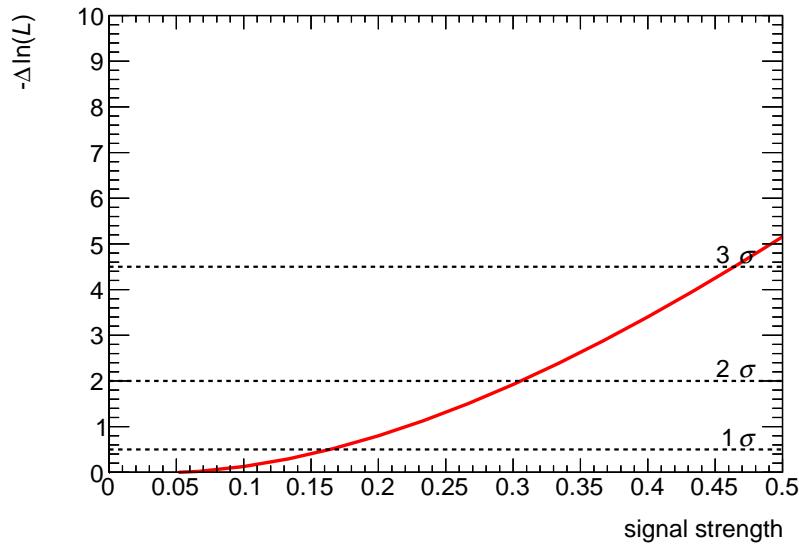


Figure 347: Distributions of the negative-log likelihood for the signal strength using data in all regions for the right-handed $t\gamma\gamma$ coupling. The one, two and three standard deviations are marked.

Not reviewed, for internal circulation only

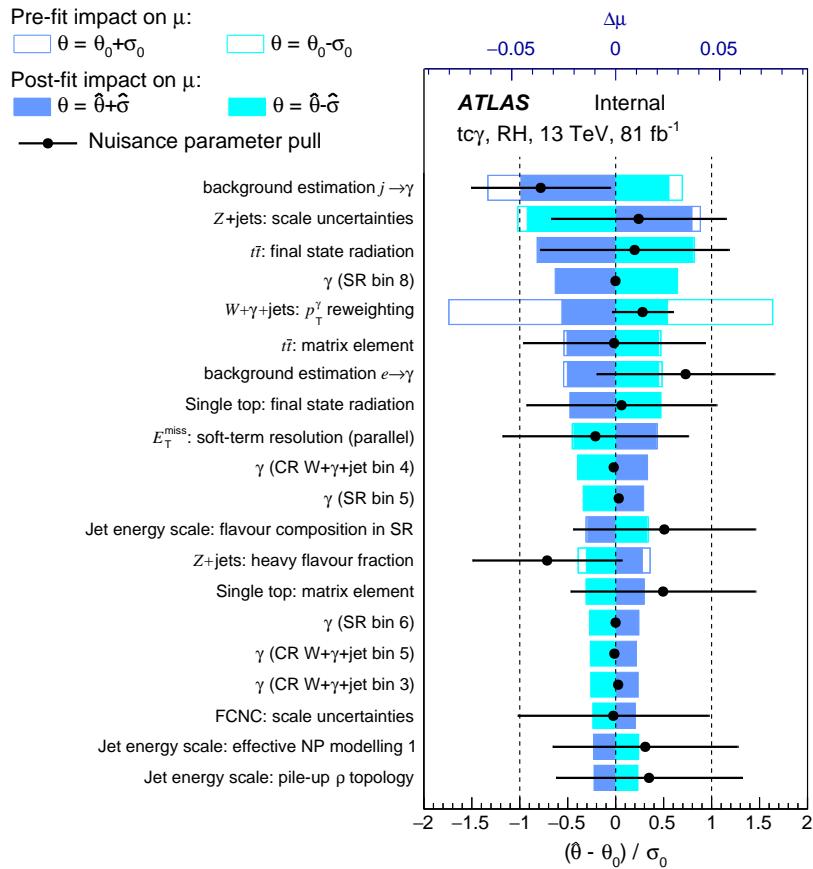


Figure 348: Ranking plot for the 20 nuisance parameters with the largest impact on the signal strength for the right-handed $tc\gamma$ coupling using data in all regions and performing an S+B fit.

1914 Z.3.1 Validation of fit result

Not reviewed, for internal circulation only

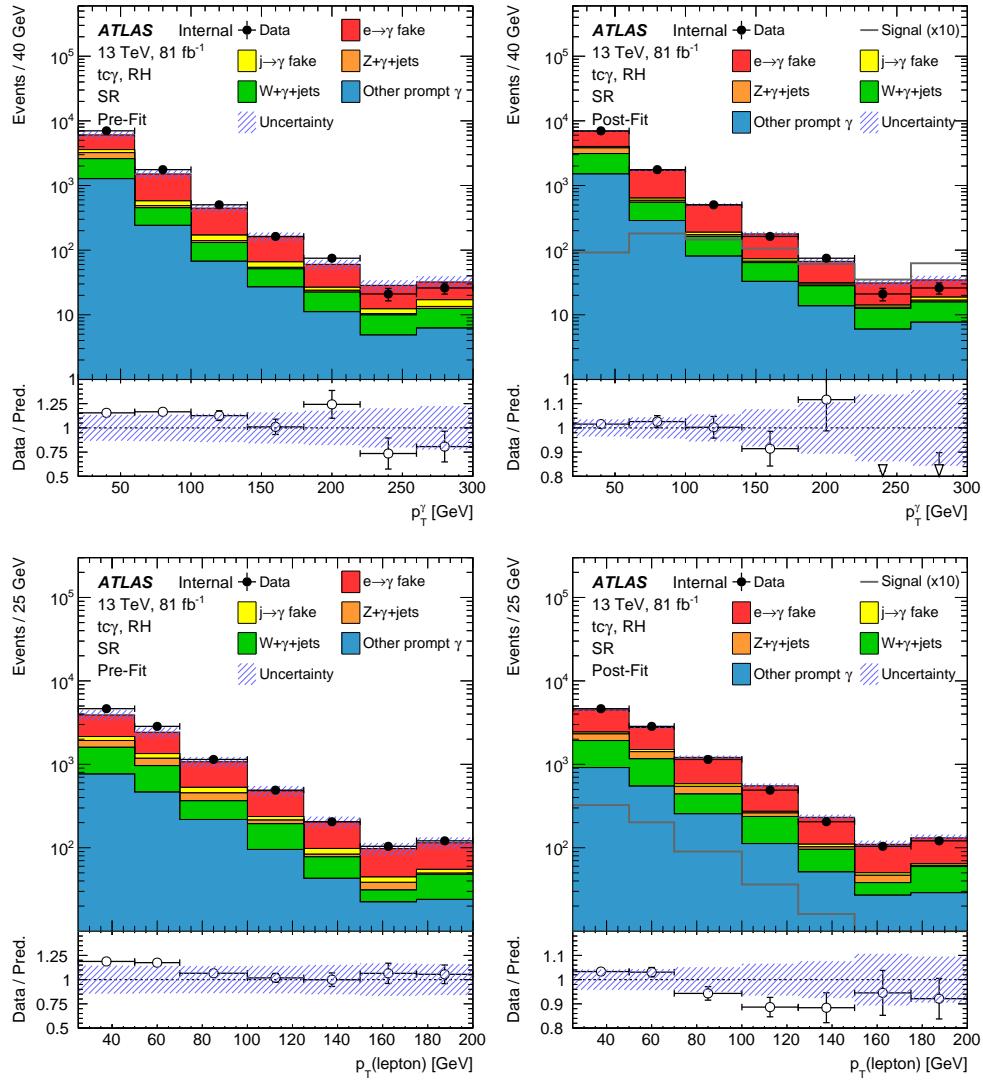


Figure 349: Pre- (left) and post-fit (right) distributions for the right-handed signal coupling $tc\gamma$ using data in the SR: photon p_T (top), and lepton p_T (bottom). In the post-fit distributions, the signal distribution scaled to the observed limit multiplied by 10 is included. Statistical and systematic uncertainties are included.

Not reviewed, for internal circulation only

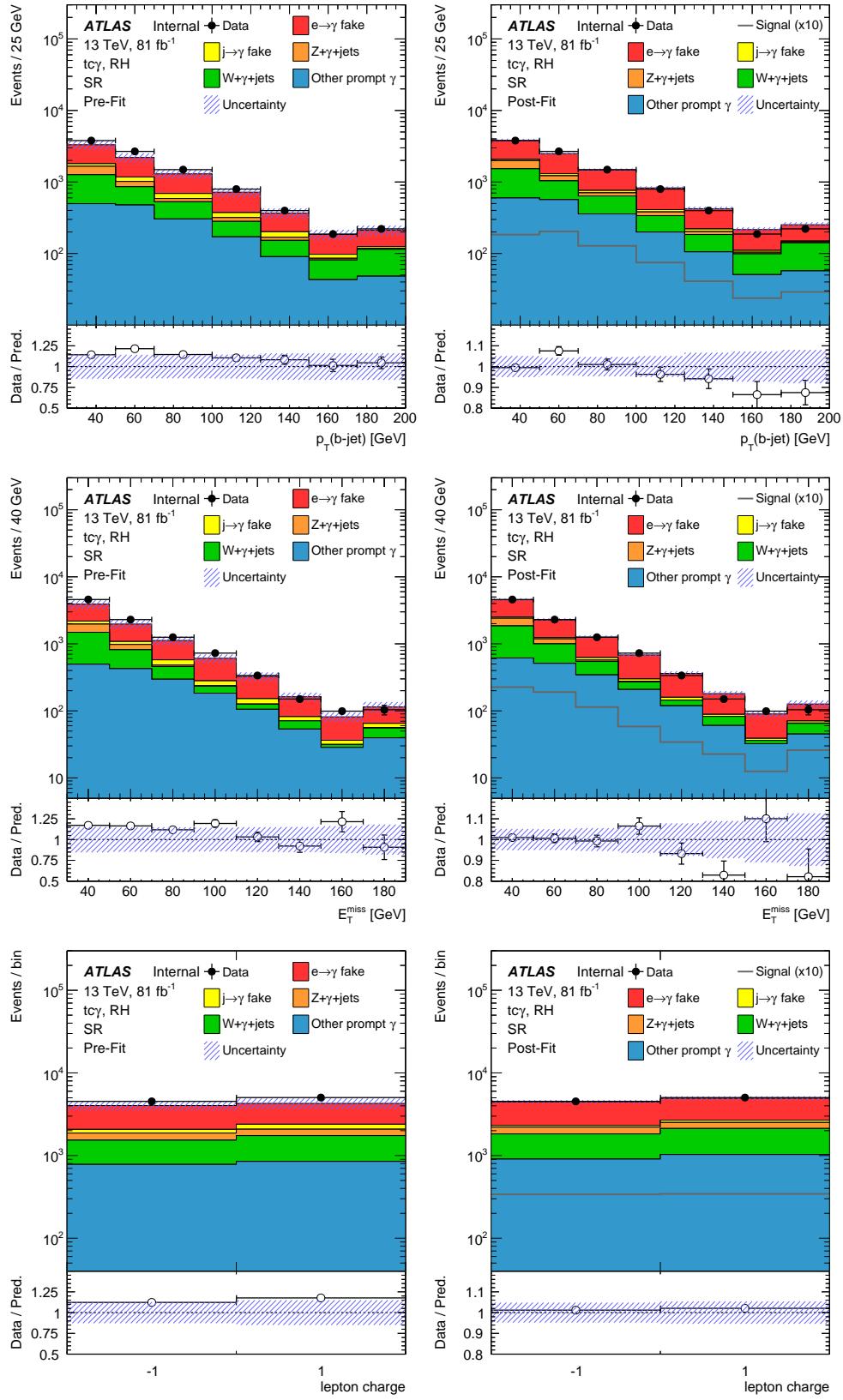


Figure 350: Pre- (left) and post-fit (right) distributions for the right-handed signal coupling $tc\gamma$ using data in the SR: jet p_T (top), missing transverse momentum E_T^{miss} (middle), and lepton charge (bottom). In the post-fit distributions, the signal distribution scaled to the observed limit multiplied by 10 is included. Statistical and systematic uncertainties are included.
9th July 2019 – 11:54

Not reviewed, for internal circulation only

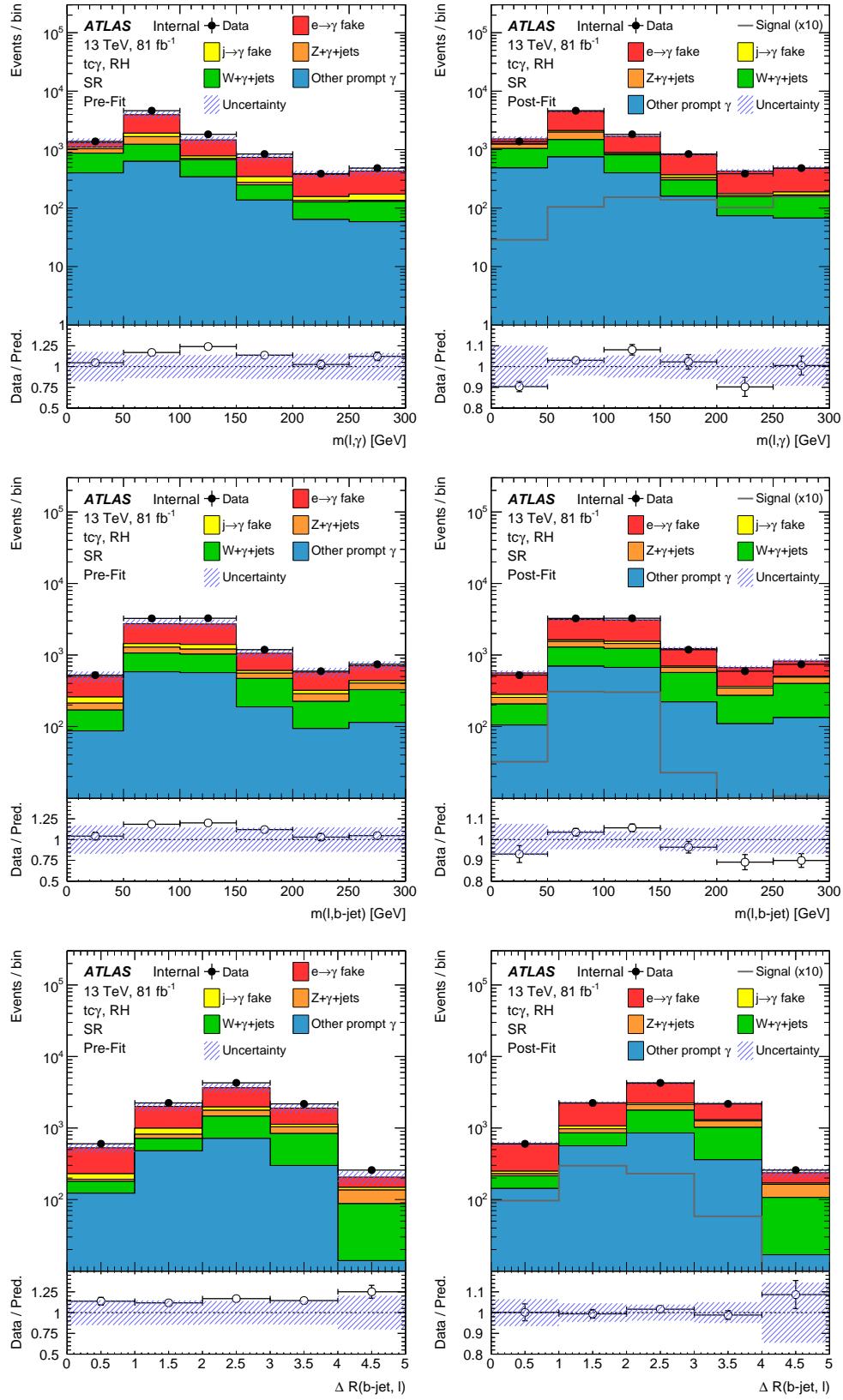


Figure 351: Pre- (left) and post-fit (right) distributions for the right-handed signal coupling $tc\gamma$ using data in the SR: invariant mass of the lepton-photon system $m(\ell\gamma)$ (top), invariant mass of the jet-lepton system $m(lj)$ (middle), and the distance between the jet and lepton $\Delta R(j, \ell)$ (bottom). In the post-fit distributions, the signal distribution scaled to the observed limit multiplied by 10 is included. Statistical and systematic uncertainties are included.

9th July 2019 – 11:54

444

Not reviewed, for internal circulation only

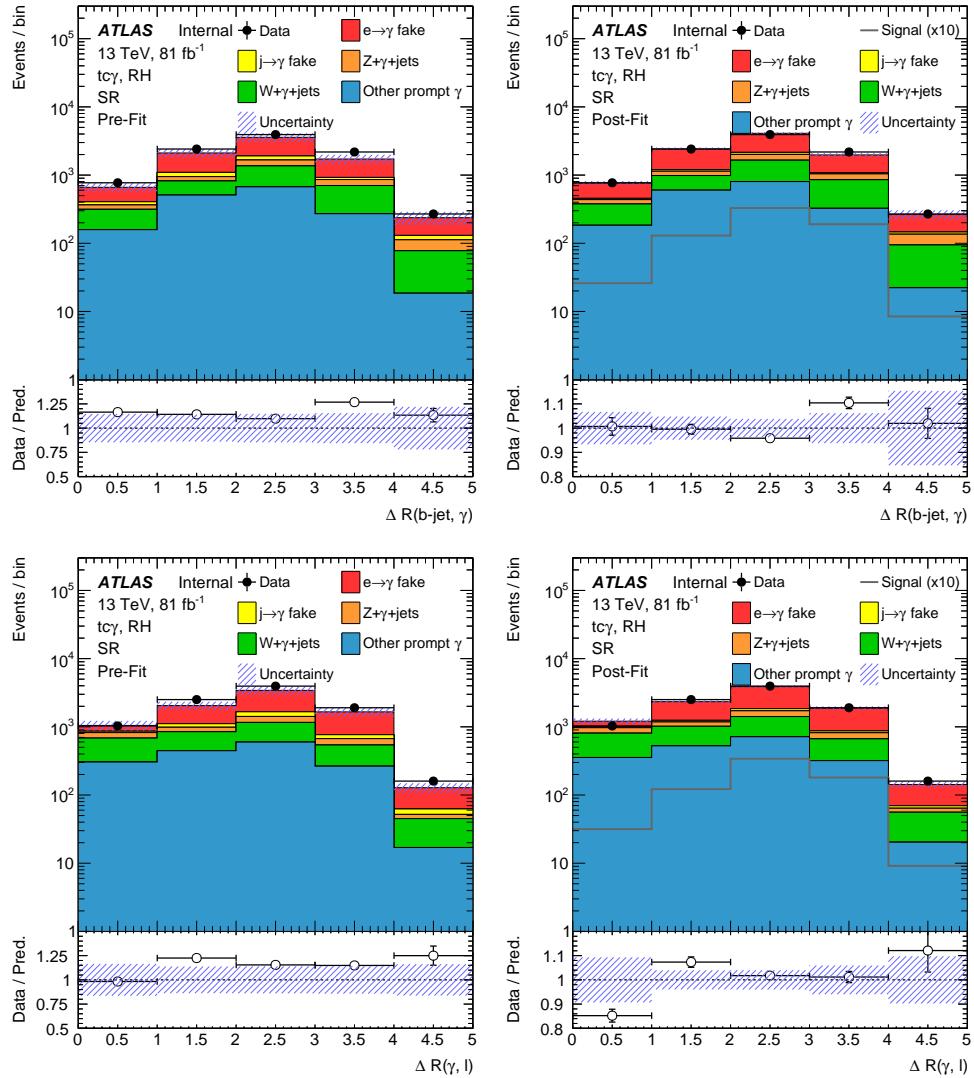


Figure 352: Pre- (left) and post-fit (right) distributions for the right-handed signal coupling $tc\gamma$ using data in the SR: the distance between the jet and photon $\Delta R(j, \gamma)$ (top), and the distance between the lepton and photon $\Delta R(\ell, \gamma)$ (bottom). In the post-fit distributions, the signal distribution scaled to the observed limit multiplied by 10 is included. Statistical and systematic uncertainties are included.

Table 86: Yields for the different contributions after the fit using the right-handed $t\gamma\gamma$ coupling in the VRs $SF(e \rightarrow \gamma)$ and combined background. The statistical uncertainty and all systematic uncertainties are included.

Photon origin	VR $SF(e \rightarrow \gamma)$		combined background VR		
$e \rightarrow \gamma$	258 000	\pm	28 000	42 600	\pm
$j \rightarrow \gamma$	600	\pm	200	4 400	\pm
$Z + \gamma + \text{jets}$	26 600	\pm	2 000	22 500	\pm
$W + \gamma + \text{jets}$	11 060	\pm	600	87 000	\pm
Other prompt photon	1 120	\pm	170	23 200	\pm
Total SM	297 000	\pm	29 000	180 000	\pm
Data	312 550			180 804	

Not reviewed, for internal circulation only

Not reviewed, for internal circulation only

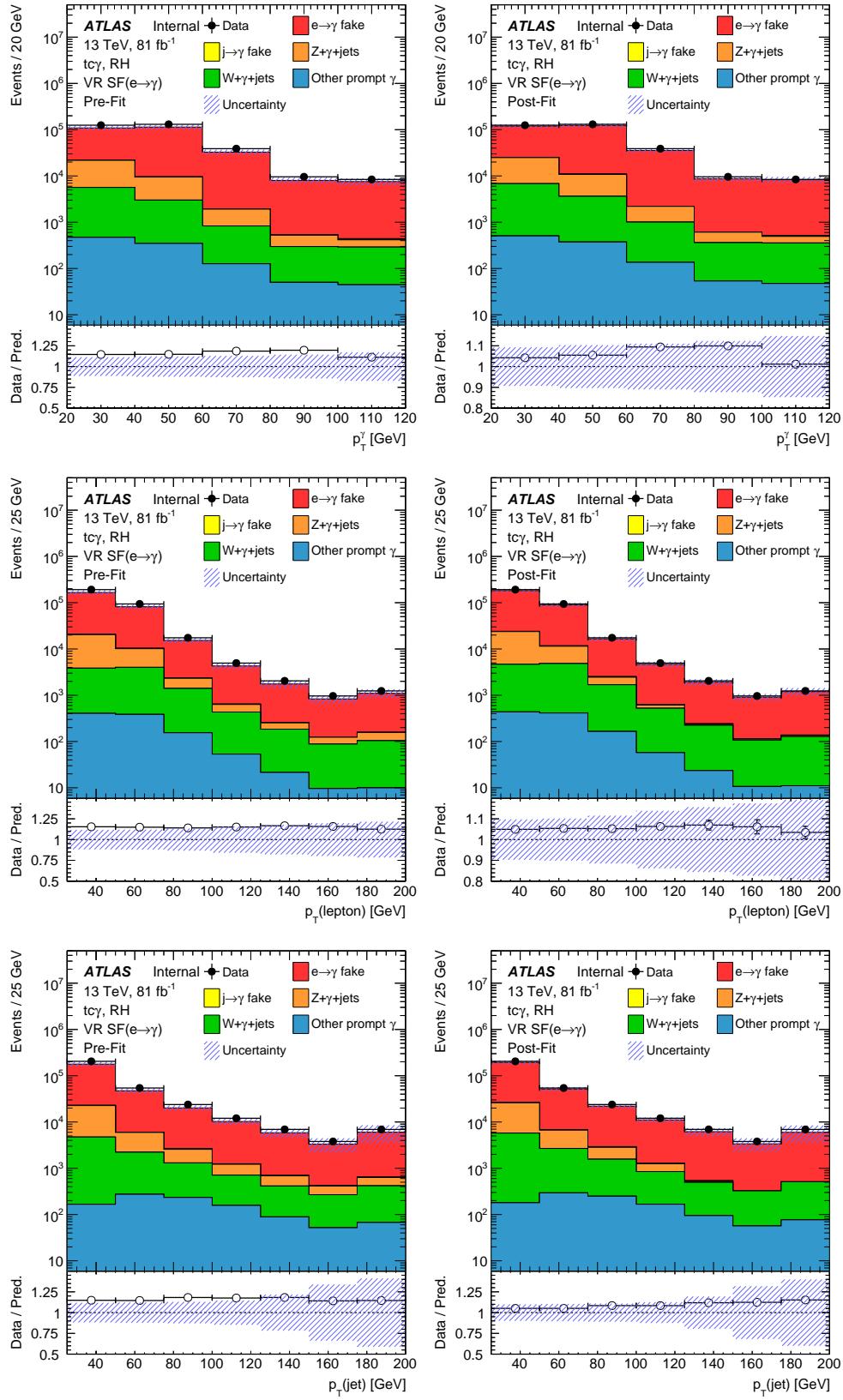


Figure 353: Pre- (left) and post-fit (right) distributions for the right-handed signal coupling $tc\gamma$ using data in the VR $SF(e \rightarrow \gamma)$: photon p_T (top), lepton p_T (middle), and jet p_T (bottom). Statistical and systematic uncertainties are included.

Not reviewed, for internal circulation only

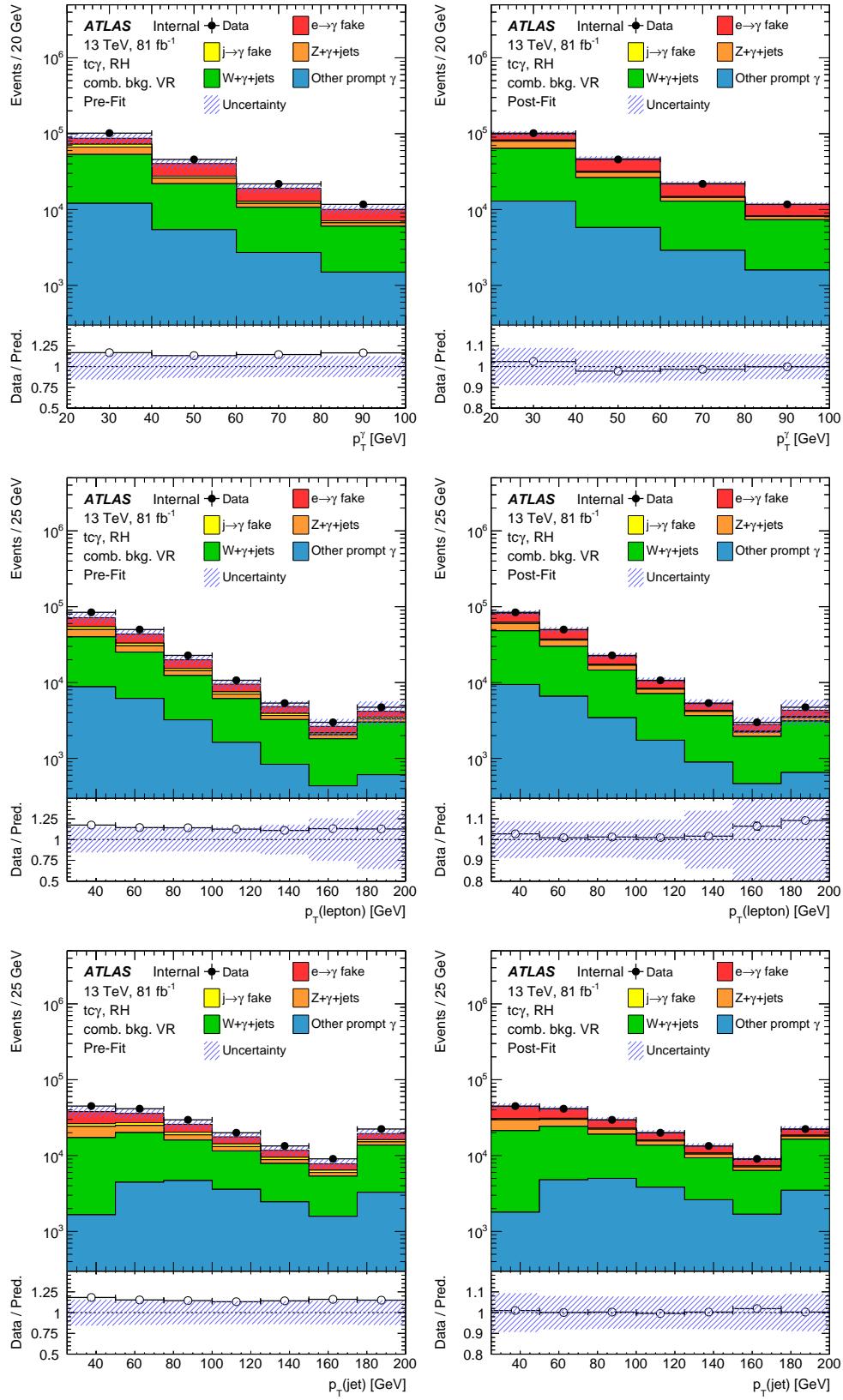


Figure 354: Pre- (left) and post-fit (right) distributions for the right-handed signal coupling $t\gamma$ using data in the combined background VR: photon p_T (top), lepton p_T (middle), and jet p_T (bottom). Statistical and systematic uncertainties are included.